

Volume 2



RADIOLOGY
Exam

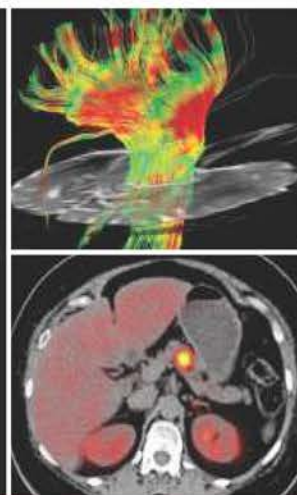
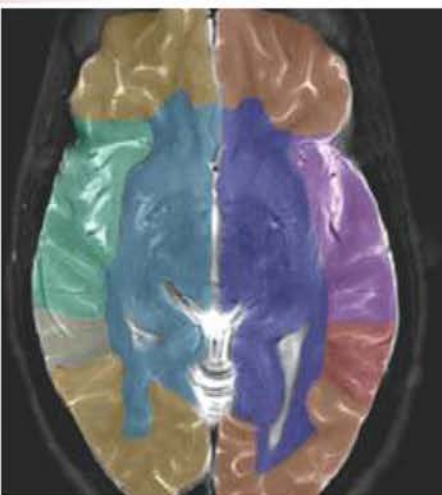
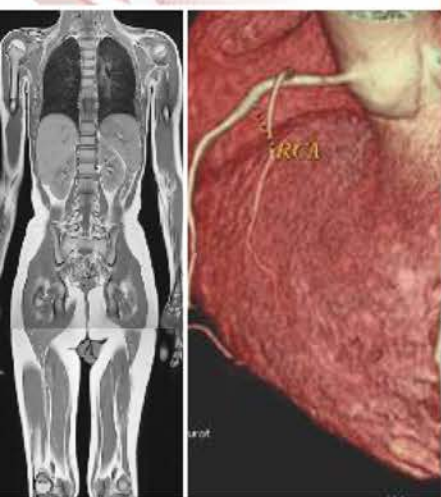
A Comprehensive

Volume 1



RADIOLOGY Exam Made Easy

A Comprehensive Case Based Approach to Radiologic Examination



- ▶ A complete stepwise aid for radiology board exams
- ▶ Precise structured guidelines for radiology case presentation
- ▶ Illustrative system-wise radiological anatomy
- ▶ Comprehensive coverage of over 200+ exam cases with an all-inclusive list of possible differential diagnoses
- ▶ 70 plus OSCE/ CORE exercises explained with high quality images and original illustrations
- ▶ An overview of the international certifying examinations such as FICR, MICR, EDIR



CBSPD Dedicated to Education
CBS Publishers & Distributors Pvt Ltd

- ▶ A complete stepwise aid for radiology board exams
- ▶ Precise structured guidelines for radiology case presentation
- ▶ Illustrative system-wise radiological anatomy
- ▶ Comprehensive coverage of over 200+ exam cases with an all-inclusive list of possible differential diagnoses
- ▶ 70 plus OSCE/ CORE exercises explained with high quality images and original illustrations
- ▶ An overview of the international certifying examinations such as FICR, MICR, EDIR



CBSPD Dedicated to Education
CBS Publishers & Distributors Pvt Ltd

C Amarnath



Volume 1

RADIOLOGY

Exam Made Easy

A Comprehensive Case Based Approach to Radiologic Examination

- A complete stepwise aid for radiology board examinations
- Precise structured guidelines for radiology case presentation
- Illustrative system-wise radiological anatomy
- Comprehensive coverage of over 200 examination cases with an all-inclusive list of possible differential diagnoses
- 70+ OSCE/CORE exercises explained with high quality images and original illustrations
- An overview of the international certifying examinations such as FICR, MICR, EDiR
- A complete handbook and reference for residents and young radiologists to guide them in their day-to-day radiological investigations and diagnoses



Volume 1

RADIOLOGY

Exam Made Easy

A Comprehensive Case Based Approach to Radiologic Examination

C Amarnath

MD, DNB, MNAMS, FRCR, FICR, FIMSA, MBA, PhD, EDiR, MICR, DiCRI

Professor and Head, Department of Radiodiagnosis

Stanley Medical College, Chennai

Senior Consultant, Scans World and Scans Point, Chennai



CBS Publishers & Distributors Pvt Ltd

New Delhi • Bengaluru • Chennai • Kochi • Kolkata • Lucknow • Mumbai
Hyderabad • Jharkhand • Nagpur • Patna • Pune • Uttarakhand

Disclaimer

Science and technology are constantly changing fields. New research and experience broaden the scope of information and knowledge. The authors have tried their best in giving information available to them while preparing the material for this book. Although, all efforts have been made to ensure optimum accuracy of the material, yet it is quite possible some errors might have been left uncorrected. The publisher, the printer and the authors will not be held responsible for any inadvertent errors, omissions or inaccuracies.

eISBN: 978-93-546-6948-4

Copyright © Authors and Publisher

First eBook Edition: 2024

All rights reserved. No part of this eBook may be reproduced or transmitted in any form or by any means, electronic or mechanical, including photocopying, recording, or any information storage and retrieval system without permission, in writing, from the authors and the publisher.

Published by Satish Kumar Jain and produced by Varun Jain for
CBS Publishers & Distributors Pvt. Ltd.

Corporate Office: 204 FIE, Industrial Area, Patparganj, New Delhi-110092

Ph: +91-11-49344934; Fax: +91-11-49344935; Website: www.cbspd.com; www.eduport-global.com;

E-mail: eresources@cbspd.com

Head Office: CBS PLAZA, 4819/XI Prahlad Street, 24 Ansari Road, Daryaganj, New Delhi-110002, India.

Ph: +91-11-23289259, 23266861, 23266867; Fax: 011-23243014; Website: www.cbspd.com;

E-mail: publishing@cbspd.com; eduportglobal@gmail.com.

Branches

-
- **Bengaluru:** Seema House 2975, 17th Cross, K.R. Road, Banasankari 2nd Stage, Bengaluru - 560070, Karnataka Ph: +91-80-26771678/79; Fax: +91-80-26771680; E-mail: bangalore@cbspd.com
 - **Chennai:** No.7, Subbaraya Street Shenoy Nagar Chennai - 600030, Tamil Nadu
Ph: +91-44-26680620, 26681266; E-mail: chennai@cbspd.com
 - **Kochi:** 36/14 Kalluvilakam, Lissie Hospital Road, Kochi - 682018, Kerala
Ph: +91-484-4059061-65; Fax: +91-484-4059065; E-mail: kochi@cbspd.com
 - **Mumbai:** 83-C, 1st floor, Dr. E. Moses Road, Worli, Mumbai - 400018, Maharashtra
Ph: +91-22-24902340 - 41; Fax: +91-22-24902342; E-mail: mumbai@cbspd.com
 - **Kolkata:** No. 6/B, Ground Floor, Rameswar Shaw Road, Kolkata - 700014
Ph: +91-33-22891126 - 28; E-mail: kolkata@cbspd.com

Representatives

-
- **Hyderabad**
 - **Pune**
 - **Nagpur**
 - **Manipal**
 - **Vijayawada**
 - **Patna**

*to
my beloved teachers*



Prof TS Swaminathan

Former Director
Barnard Institute of Radiology
Madras Medical College, Chennai



Prof N Kulasekaran

Former Director
Barnard Institute of Radiology
Madras Medical College, Chennai

Contributors

Abubacker Sulaiman

Professor and Head
Department of Radiology
Bhaarith Medical College
Selaiyur, Chennai

Amandeep Singh

Professor, Department of Radiodiagnosis
SGRD Institute of Medical Sciences and Research
Amritsar, Punjab

Anand N

Fortis Hospital
Chennai

Anbarasu A

Aran Diagnostic Imaging
Coimbatore

Ankur Shah

Gujarat Imaging Centre
Ahmedabad

Bagyam Raghavan

Apollo Hospitals
Chennai

Bindu Srinivasan

Research Volunteering
Department of Material Science and Engineering
University of North Texas, Texas

C Amarnath

Professor and Head, Department of Radiodiagnosis
Stanley Medical College
Chennai

Chirtrarasana P

Professor, Department of Radiodiagnosis
Stanley Medical College
Chennai

Devimeenal J

Professor, Department of Radiodiagnosis
Govt Kilpauk Medical College
Chennai

Emanuel R

Senior Consultant Radiologist, Bharat Scans
Chennai

Flora Nelson

Professor, Department of Radiodiagnosis
Govt Thoothukudi Medical College
Chennai

Gaurang Raval

Consultant Radiologist
NM Virani Wockhardt Hospital
Rajkot

Gaurav Shivgiri Goswami

Zydus Hospital
Ahmedabad

I Gurubharath

Professor, Department of Radiodiagnosis
Chettinad Medical College
Chennai

J Chezhian

Associate Professor, Department of Radiodiagnosis
Stanley Medical College
Chennai

Jayaraj Govindaraj

Apollo Hospitals
Chennai

K Gopinathan

Professor, Department of Radiodiagnosis
Govt Kilpauk Medical College
Chennai

K Sudha

Consultant Radiologist
Roentgen Scans World
Chennai

L Kayal

Professor, Department of Dental Surgery
Stanley Medical College
Chennai

M Indrani

Senior Consultant in Nuclear Medicine
Apollo Hospitals
Chennai

Muralikrishna L

Fortis Hospital
Chennai

N Chidambaranathan

Apollo Hospital
Chennai

Parveen Sulthana

Associate Consultant
Perth Radiological Clinic
Western Australia

Periyakaruppan AL

Govt Multi-Specialty Hospital
Omandurar Estate
Chennai

Philson J Mukkada

Associate Professor, Department of Radiology, ACS Medical College
Consultant Radiologist, Roentgen Scans World
Chennai

Rajendra N Solanki

Suyog imaging Center
Mehsana-Radiscan Diagnostics
Ahmedabad

Ravindran

Assistant Professor, Department of Radiodiagnosis
Institute of Child Health, Egmore
Chennai

S Babupeter

Professor, Department of Radiodiagnosis
Madras Medical College

Shelley Simon

Senior Consultant in Nuclear Medicine
Apollo Hospitals
Chennai

S Rajasekaran

Senior Consultant Radiologist
Chennai

V Sivakumar

Consultant Radiologist
Scansworld, Chamiers Road,
Chennai

Yuvalalakumaran

Professor, Department of Radiodiagnosis
Vinayaka Mission's Kirupananda Variyar Medical College and
Hospital, Salem

Foreword

I am pleased to write the Foreword to *Radiology Exam Made Easy*, a book that I believe will significantly contribute to the world of radiology. This project has been initiated and compiled by Dr C Amarnath, who has laboriously poured his heart, soul, and knowledge into this textbook with the sole purpose of imparting radiology knowledge to the upcoming generation.

Prof C Amarnath is well known in the radiology fraternity for his flair for teaching and a thoughtful approach to case reading sessions, and is dedicated to making them immensely exciting. He is not only a good teacher but also an able administrator. He was instrumental in leading the Department of Radiodiagnosis in Govt Stanley Medical College to great heights.

This book can be used religiously by residents as they enter the beautiful world of radiology to help them master the art and science of a perfect radiology reporting. The book is designed to make adding annotations, which could facilitate ready reckoning of cases and concepts. The book begins with the basic and most important overview of the radiology examination, and ultraprecise structured guidelines for radiology case presentation. This is followed by basic reporting templates, and a section on illustrated radiological anatomy including X-ray, CT scan, MRI and ultrasound of all the systems. It then moves on to a comprehensive coverage of more than 220 exam cases with an all-inclusive list of possible differential diagnoses. I am sure this book would serve as a strong stimulus and a useful guide to master the art of radiology case presentation.

My favourite section of the book is the OSCE/CORE exercises, explained with high quality images and original illustrations. Cases discussed in Question and Answer format throughout this book will provide an excellent arena for readers to test out their unique ideas and differentials. High yield *viva voce* materials covering radiological procedures, contrast agents, equipments, physics principles, etc., are described in such detail that these will surely widen the horizons of diagnostic capabilities of the readers. The indispensable and ever important field of emergency radiology is covered with a proactive approach. Keeping up with the role of international certifying exams in enhancing a radiologist's skillset today, an overview of FICR, MICR, EDiR has been presented along with sample papers to complete a perfect book.

I anticipate that this book will be used as a self-testing aid during examinations, and also as a revision tool. It contains a huge arsenal of cases, with an extensive reference collection of full interpreted images, addressed to students as well as consultants. It sets out to be an effective *learning catalyst* as it contains high yield cases and questions that a postgraduate could expect in an examination. With bulk of diagnoses today being made in radiology department, this book will definitely help you narrow down the differentials. We also hope this book would serve as an integral assistant in your daily practice.



Dr Hemant Patel

Past President, Indian Radiological and Imaging Association
Director, Gujarat Imaging Centre, Ahmedabad

Preface

Radiology Exam Made Easy—an exam preparatory manual focuses on crystal clear explanations about the various differential diagnoses from all systems with simple charts, tables, and classical cases to tide over the challenging phase of final year exams.

The content is derived from standard articles, textbooks, and the Stanley Radiology Museum's famed archives with inputs from experienced professors and consultants of radiology—all pieced together in a comprehensive, easy to read format. This book will supplement the information already learned, and enable that information to be used logically while approaching a case in clinical exams. I hope this book provides the sort of information that clinical radiologists will also find useful in their day-to-day practice.

The radiology curriculum consists of: 1. Basic radiology—the radiological anatomy, relevant clinical examination, physics relevant to radiology, and radiological techniques including protocols, 2. Essential radiology—accident and emergency imaging and 3. Core radiology—integrity of various systems in the body. The biggest strength of this project is the massive collection of cases curated diligently for the past 20 years. It is seen that a resident or young consultant radiologist refers to radiological anatomy 2–3 times in a day on an average. In this regard, this book will be really helpful as a one stop reference point.

Fear is nothing more than an obstacle that stands in the way of progress. With the view of vanquishing the fears of residents, this book will provide an easy and holistic approach to theory and practical board exams. Radiological anatomy is where our knowledge of human anatomy meets clinical practice. The third chapter of the book discusses and illustrates radiological anatomy as seen across all imaging modalities.

Case discussion section provides specific and realistic solutions that are needed to improve our practical skills in diagnostic radiology. It features over 220+ cases across all modalities from X-ray to PET CT/SPECT CT. In addition, self-test questions and guidelines on case presentation are included to assess and to boost confidence.

The rapidly growing field of interventional radiology may be intimidating for residents. To tackle this, the section on radiological procedures is specially drafted and is bound to spark an interest in interventional procedures.

Emergency radiology forms an integral part of any hospital's emergency team. To empower the radiologist to make rapid fire diagnoses, thus making huge impact on outcomes in emergency care. A section on international certifying exams provides an overview of design of EDiR, MICR and FRCR exams along with sample questions.

The key motive behind the creation of this book is to *replace the fear of unknown with curiosity*.

We hope this book will serve as a quick primary reference for residents to prepare for their examination and particularly useful in our clinical practice. We are always happy to hear your comments and suggestions.

The only thing to do with good knowledge is to pass it on; It's never of use to oneself.

C Amarnath

Acknowledgements

I extend my thanks to all the people who have worked so diligently and faithfully in shaping up this book. I would like to recognize all the professors and residents who have spent so much of their precious time in contributing their chapters to this book.

My sincere gratitude and respect go to my beloved teachers Prof TS Swaminathan, Prof N Kulasekaran, Prof JR Daniel, Prof K Manoharan, Prof S Vinayagam and Dr R Emmanuel. I would also like to thank my friends Dr AL Periyakaruppan, Dr K Gopinathan, Dr Philson J Mukkada and Dr V Sivakumar.

My colleagues in Stanley Medical College and Scans World have extended their valuable input and support throughout the period it took to bring out this book. I especially thank my colleagues Prof C Nellaiappan, Prof G Sathyan, Prof P Chirtrarasan, Prof J Chezhan, Prof V Sudhakar and Assistant Professors Dr K Sivakumar, Dr G Sakthivel Raja, Dr M Priya, Dr R Jayavarma and Dr S Usha.

I also thank my residents Dr K Arun Alex, Dr G Karthick Kiran, Dr R Karthick Rajan, Dr R Kiruthika, Dr A Ponshankar, Dr M Resnick Banu, Dr X Sebastian Antony, Dr G Anushya, Dr JS Krishnan, Dr Pragadesh Pandian, Dr Manasa, Dr Joel Kevin Raj, Dr Kharat Pandit Jeeja, Dr V Shilpa, Dr Sowmiya PK, Dr G Suresh, Dr T Pradeeba, Dr Thivakaran, Dr A Abdul Salam, Dr D Benin Reejan, Dr M Bharathiraja, Dr P Dineshbabu, Dr AS Kannan, Dr P Lavanya, Dr R Mythili, Dr V Prithviraj, Dr R Rajashree, Dr A Renita, Dr K Sadhana, Dr J Samkamel Sen, Dr TJ Vanathi, Dr P Lenin Prabhu, Dr Hariharan, Dr M Shyamala, Dr V Ramalakshmi, Dr V Dhanalakshmi, Dr R Kadalarasi, Dr R Raghavi, Dr S Sanjeev Prasad, Dr R Manikandan, Dr I Kittu, Dr M Rajkumar, Dr A Sahila Devi, Dr A Ameer Hussain, Dr CS Nischith, Dr K Roopini, Dr Hariharan S, Dr Hariharan M, Dr Vidhyalakshmi, GK, Dr Naveen S, Dr Logamani PK, Dr Magesh P, Dr Tamilselvi S, and Dr Kanchana J who helped me in compiling the cases and publishing my book. Not enough words would capture the part my son A. Anirudh has in being the driving force behind my achievements.

I will be failing in my duty if I do not place on record my sincerest thanks to all of my patients. Finally, I thank Dr M Nanda Kumar, Dr RS Satiish, and Dr RV Guhan for compiling and bringing the entire book together.

C Amarnath

Contents

| | |
|------------------------------------|------------|
| <i>Contributors</i> | <i>vii</i> |
| <i>Foreword by Dr Hemant Patel</i> | <i>ix</i> |
| <i>Preface</i> | <i>xi</i> |

| VOLUME 1 | |
|---|-----------|
| 1. Approach to Clinical Radiology Board Exams | 1–6 |
| 2. Radiology Case Presentation—General Guidelines | 7–50 |
| 3. Radiological Anatomy | 51–373 |
| 4. Imaging Approach for Radiology Cases | 374–1541 |
| 4.1–4.43 Central Nervous System | 374–685 |
| 4.44–4.65 Spine | 686–794 |
| 4.66–4.88 Head and Neck | 795–900 |
| 4.89–4.117 Chest | 901–1035 |
| 4.118–4.120 Breast | 1036–1054 |

| VOLUME 2 | |
|---|-----------|
| 4.121–4.134 Cardiovascular System | 1055–1125 |
| 4.135–4.164 Musculoskeletal System | 1126–1278 |
| 4.165–4.178 Gastrointestinal Tract | 1279–1343 |
| 4.179–4.187 General Abdomen Including Abdominal Wall, Peritoneum | 1344–1376 |
| 4.188–4.205 Hepatobiliary System | 1377–1450 |
| 4.206–4.223 Urinary and Reproductive System | 1451–1541 |
| 5. Objective Structured Clinical Examination (OSCE)/ Clinically Oriented Reasoning Evaluation (CORE) | 1542–1595 |
| 6. Applied Physics, Interventions, Drugs and Others | 1596–1784 |
| 6.1 Contrast Media in Radiology | 1596–1604 |
| 6.2 Emergency Drugs and Advanced Radiology Life Support | 1605–1612 |
| 6.3 Contrast and Special Procedures | 1612–1630 |
| 6.4 Radiological Physics—Instruments and Applications | 1631–1653 |

| | | |
|------|---|-----------|
| 6.5 | Nonvascular Interventions | 1654–1663 |
| 6.6 | Vascular Intervention: Essentials and Procedures | 1663–1694 |
| 6.7 | Occupational Hazards and Safety in Radiology | 1695–1704 |
| 6.8 | Governing Regulations—PCPNDT, AERB | 1705–1710 |
| 6.9 | Quality and Accreditation Standards in Radiology | 1710–1712 |
| 6.10 | Artifacts in Radiology | 1712–1720 |
| 6.11 | Pioneers in Radiology | 1720–1724 |
| 6.12 | Radiological Techniques and Protocols | 1724–1728 |
| 6.13 | Radiology Associations and Journals | 1728–1729 |
| 6.14 | Special Views in Radiology | 1730–1732 |
| 6.15 | Nuclear Medicine | 1732–1770 |
| 6.16 | Instruments and Hardwares in Radiology | 1770–1772 |
| 6.17 | Basic Biostatistics and Properties of Diagnostic Test | 1772–1779 |
| 6.18 | Recent Advances in Clinical Radiology | 1780–1784 |
| 7. | Essential Radiology—Trauma and Emergency | 1785–1807 |
| 8. | International Board Certifying Exams | 1808–1845 |
| 9. | Non-interpretation Skills in Radiology | 1846–1850 |
| 10. | Bibliography | 1851–1864 |
| | <i>List of Abbreviations</i> | 1865–1868 |
| | <i>Index</i> | 1869–1884 |

Approach to Clinical Radiology Board Exams

INTRODUCTION

'Rome was not built in a day'

We always look for shortcuts for success, but real success can be achieved only by hard work and true dedication to our work. At the same time, we should study smart and invest the available time wisely such that we could cover the vast syllabus. Understanding concept is worth the time instead of just cramming facts. Revision plays a key role so that all our valuable efforts may not be wasted. Presentation plays an important role as preparation so that we could effectively communicate our knowledge to the examiner.

1. Study Smart and Hard

A "strategy" for taking the exam was to simply revise everything before the big day. We spent hours upon hours highlighting everything in exam prep book. In retrospect, we could have saved tons of time by simply identifying the key subjects we did not really understand. The best advice usually comes from your seniors (every one of them—don't be happy with just asking one person) who recently took the exam.

Preparation involves

- Knowledge of the subject.
- Technique or approach.
- Knowledge of the exam itself.

Knowledge of the subject: This comes from your hard work of reading books, seeing more cases, attending various courses. Knowledge to pass is one aspect and knowledge to go out and practice is another aspect—both need to be acquired.

Technique or approach: This consists of various skills you need to tackle each component of the exams.

- Spotters:** The success in this component is entirely based on your knowledge, seeing more and more 'Aunt Minnie' type of cases.

- Cases writing:** Follow the standard case presentation proforma. Time is very important. Do not get bogged down by a difficult case, resulting in below par performance in an easy case due to lack of time. Unknown diagnoses can be handled by giving appropriate differential diagnosis.
- Viva:** FRCR Viva is a case presentation, using standard case presentation proforma. For MD/DNB exam viva, we have equipment/instruments.
- OSCE:** Some universities are introducing objective structured clinical examination (OSCE) components or in the process—don't be alarmed and in fact, these are easier components and more objective assessment is done and the examiners are silent observers.

Knowledge of the exam itself: Every university/national board exams are slightly different and you need to understand that; again the exams can vary slightly depending on the examiners as well. It is important that you need to look for information about the exams and be updated with the latest information from the university.

Studying for the exam is undoubtedly a daunting task. Not only can the sheer amount of material that one needs to learn seem overwhelming, but also the vast amount of resources available can be more of a burden than an asset. Residents often scramble to make time to go over every single review book out there, in an effort to have all of their bases covered. This strategy is not only nearly impossible but is likely to be counterproductive. Rather, one should focus on one comprehensive textbook while supplementing with question banks.

It seems daunting with all the resources out there. Don't be afraid to use many, but use them wisely. Ideally you should have read the standard textbooks once or twice during the first two and half years itself. Below is a rough plan:

4 months before the exam (first revision of the following books you have read before)

- Review standard textbooks of radiology
- Go through question banks.

- Make notes on what to write for each question, for a quick last minute revision
- Make small study groups among yourself and start doing case discussion/case presentation.

2 months before the Exam

- Continue above
- Review standard textbooks of radiology physics
- Case atlas for spotters
- Exercise spotter bank—you can practise spotter sets in exam pattern on daily basis/2–3 spotter sets per day.
- Case presentation practice in any radiology museum—you may present each case for 15 minutes without any break, others will help to improve the presentation, likewise practise 10 cases per day.
- Stanley Radiology Museum—permits all eager radiology postgraduates to utilise the radiology museum throughout the year for learning purpose.

< 1 month before the exam

- Final revision of standard textbooks
- Review facts/notes.
- Review questions.
- Practise drawing simple self-explanatory diagrams.

2. Stop Freaking Out!

Seriously, even though this seems like the biggest single moment of your life, it really isn't. This is just a test. Stress decreases your memory. To reduce stress, we recommended that students should just put things into perspective. Like I mentioned earlier, this is just a test! Even if you do not pass the first round, you still have family who loves you, friends that support you, and hopefully a roof over your head. Since passing a test will not affect any of these things, you need not make it gigantic impending thing. Take a few deep breaths in and out and begin to look at the exam as simply the culmination of your radiology education. Look, you have made it far so obviously you are capable of passing a test.

3. You Are What You Eat

Avoid foods with high amounts of sugar (including sugar soft drinks), fried foods, sugar substitutes and heavily processed foods (like white bread, pasta, and pizza). The effect these foods have on your brain is they can cause a condition commonly known as brain fog. Brain fog is best described as those times where everything in your head just seems muddy like you are trying to remember a word and no matter how hard you try you just cannot think of it. Avoid excess caffeine intake. Take fresh fruits

and vegetables. For best results, don't just clean up your diet the night before the big test but instead try a month or at least the week before.

4. Sleep

This is a huge one as well. What you might not realize is that if you are getting less than 7–8 hours of sleep a night, then your brain is probably not functioning optimally. We recommend trying to stick to a consistent bedtime schedule. Good sleep will improve your memory and concentrating capability. On the day before the exam, you must sleep for 7–8 hours, only then you can concentrate, recollect and perform well in exam. After a night of good sleep, go to the examination hall with a clear and fresh mind without any anxiety or over expectation.

5. Believe in Yourself

In this final step, we simply want you to stop for a second and take a moment to do a heart check. As I mentioned, you have made it this far. You put up with all the mean, unhelpful scenario of a medical curriculum, you passed all the required tests at your school, and you most of all put your life on hold for your radiology education. You can do this! Ok, so maybe you are not the best test taker in the world, or maybe you have zero confidence. We simply want you to take a few moments to reflect on all that you have achieved so far and begin to believe that you can do it!

1.1 APPROACH TO PRACTICAL EXAM WITHOUT TEARS

The practical examination system is different for MD, DNB, FRCR, EDiR and MICR candidates who often have to attend it in a different institution. Staying confident and not getting stressed is important for success. Feel confident about the portion of the syllabus you have covered instead of worrying about the things you didn't cover.

Before the Examination

Prepare answers to potential viva voce questions in advance and practice interactive sessions with seniors who have previously succeeded in the examination. It is imperative to study the viva voce books and actively participate in online radiology forums offering an extensive repository of radiology cases. The residents may participate in small study groups. It is advisable to present a case to senior faculty members, especially those who have been previous examiners; this will improve your presentation skills and confidence. It will

reduce your exam phobia. Utilise the local/neighbouring institutions, and their radiology museums.

In the Examination Hall

The candidate is expected to be well groomed and formally dressed to create a good first impression on the examiner and the candidate should reach the examination hall one hour before the exam which will calm the unnecessary nervousness. Avoid nervousness while presenting cases, to convey the content effectively to the examiner.

If a film is given for discussion, begin by describing the film without delay. Start with the modality, anatomical region, radiographic view, etc., and avoid staring at the film in silence. While describing a case, the candidate should, preferably, face the film instead of looking at the examiner. Only after completion of the case description and concluding the case, candidate should turn to face the examiners for further remarks and questions.

Always maintain eye to eye contact with examiner while answering questions. First start describing baseline modality, then proceed to higher modalities, so don't jump into higher diagnostic modalities, without describing the findings in the baseline modality. Choose the modality based on relevant clinical history provided.

During the discussion, listen keenly and understand the examiner's line of questioning. During the course of the examination, the examiner may drop hints if the candidate seems to be going down a wrong path. It is vital to catch such 'lifelines' and change one's line of thought, and answer accordingly.

Do not criticize the quality of film given. Avoid touching the film or using the tip of a pen as a pointer while describing findings of a case. When necessary, use a pointer (like a plastic ruler) rather than the finger. Never contradict/argue with the examiner.

Use correct terminology and definitions during case presentation and while answering specific questions. If the examiner says "plain radiograph", the candidate may use the same terminology. Use of the phrase "I don't remember" is preferable to "I do not know" when the candidate does not know the answer to a certain question. If the question was not clearly heard, politely request the examiner to repeat the question. Listen carefully; answer appropriately to the questions asked especially when the examiners are giving clues.

When the diagnosis is not known/when stuck in a case:

In situations when one fails to arrive at a diagnosis it may be useful to start thinking aloud, saying that one is looking at certain parts, e.g. I am now looking at the

lung, I am now looking at the cardiac shadow, etc. Try to pick up the findings while talking, instead of waiting to get the diagnosis. Even if you cannot come up with an aetiological diagnosis, it is possible that, while discussing with the examiner and listening intently to the guiding question, one will strike upon the diagnosis.

Checklist before attending practical exams:

- White over coat.
- Radiology exam kit.
- Hall ticket.
- Number badge and TLD badge.
- Dissertation/Logbook

Come relax and attend the exam.

1.2 TIPS FOR WRITING THEORY EXAM

Theory exams form an important part of the assessment of a candidate's knowledge (as well as imagination!). Expect the best, plan for the worst and prepare to be surprised... and to be prepared is half the victory. The other half depends on your presentation style and the evaluator.

Time Management

Totally we have 180 minutes, the first 5 minutes to be allotted to writing the registration number, page number and drawing margins in the answer sheet, then use the next five minutes for reading the questions and make sure to keep the last 15 minutes for verification of the answer sheet.

In MD exam pattern, there will be 25 min for each essay and 10 min for each short note, whereas for DNB (Diplomate in National Board) examinations there will be 15 mins for each short structured question. For each mark spend 1½ minutes writing, plan accordingly.

Question Type

Varies on a course and university basis. In most of the university examinations (MD) they have 2 long questions and 10 short notes, while in DNB examinations they have 10 short structured questions, each carrying 10 marks (Table 1.1). It is vital not to spend more time on the initial questions; otherwise you will run short of time for attempting rest of the questions.

Different universities have different marking schemes. Some universities allot 20 marks for each long note and 6 marks for each short note so that you have to spend 35 minutes for each long note and 8 minutes for each short note.

Table 1.1: Pattern of various examinations and sample for planning the exams

| Exam type | | Pattern | Marks | No. of questions | Pages | Duration (marks \times 1.6) |
|-----------|----------------|---------------------------------------|---------------------------|-------------------------------|-------|-------------------------------|
| DNB | | Long notes | 10 | 10 | 6–7 | 15 minutes each |
| MD | | Long notes | 15 | 2 | 10–12 | 25 minutes each |
| | | Short notes | 7 | 10 | 3–4 | 10 minutes each |
| FRCR 1 | Anatomy module | MCQs | 200 | 100 | – | 90 minutes |
| | Physics module | MCQs | 200 | 40 \times 5 (true or false) | – | 2 hours |
| FRCR 2A | | Single best answer questions (2 sets) | – | 120 | – | 3 hours (for each paper) |
| FRCR 2B | | Rapid reporting | – | 30 | – | 35 minutes |
| | | Long cases | – | 6 cases | – | 60 minutes |
| | | Viva (2 sessions) | 16 marks for each session | – | – | 30 minutes (each session) |

Answer Contents

For long answers, it is necessary to write 10 to 12 pages each with **diagrams/tables/boxes/classification** minimum of 2 to 3 per essay. For short notes—3 to 4 pages each, diagrams/tables minimum 1 per short note. Pay attention to writing the page number in the top and write 15–18 lines per page. Use spacing between words and underline important key points/sentences. Using **bullets, flow diagrams, diagrams, boxes/squares for highlighting the key points** is more vital if handwriting is not good (or) if you run out of time.

Use colour pens and sketches for diagrams, headings and **underlining important key points** and subtitles. **Answer all the questions and in the order** given in question paper. Write in medium size letters. There must be logical organization of the contents or the key points with one or two points in one paragraph. Writing more will not fetch more marks. The examiner looks for key points. If they are covered, you will get marks irrespective of the number of pages written. Writing controversial points is better avoided.

Good presentation in the examination is a skill and this differentiates a topper from a mediocre student (Table 1.2).

Some model theory exam answer papers given as follows for use of colour pencils/charts/diagrams (Fig. 1.1A to D).

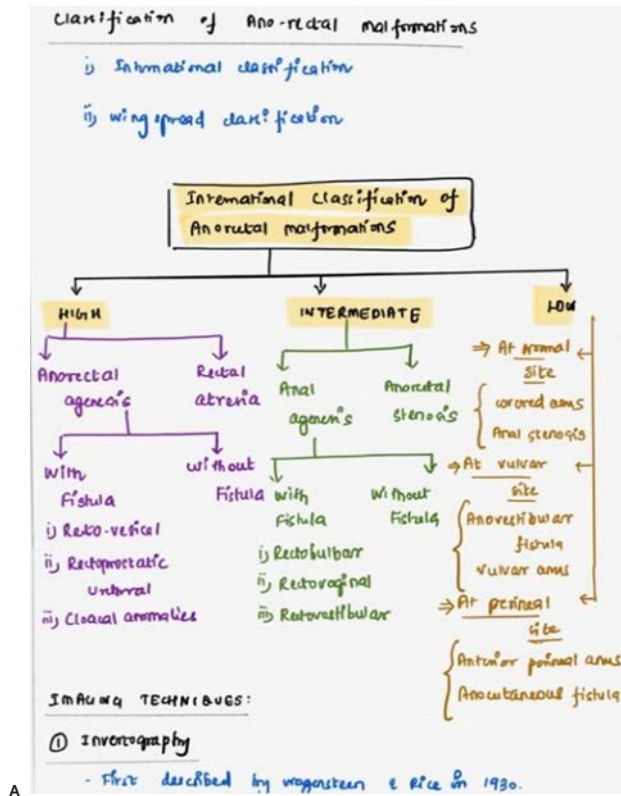
Scurvy Radiological Findings

- Generalized osteopenia
- **Cortical thinning:** “Pencil-point” cortex.
- Periosteal reaction due to subperiosteal hemorrhage

Table 1.2: Sample answer outline for theory questions

| |
|---|
| 1. Definition |
| 2. Demography |
| 3. Incidence |
| 4. Causes/anatomy/types /embryology |
| 5. Clinical features |
| 6. Location |
| 7. Pathophysiology |
| 8. Stages/manifestations |
| 9. Radiology: Plain X-ray, barium, USG, CT, MRI, DSA, intervention, PET/SPECT |
| 10. Diagnostic test |
| 11. Associated conditions/manifestations in other systems |
| 12. Differential diagnosis |
| 13. Complications |
| 14. Prognosis |
| 15. Management—further investigations and treatment. |

- **Scorbutic rosary:** Expansion of the costochondral junctions, may relate to the fracturing of the zone of provisional calcification during normal respiration. Similar to the rachitic rosary appearance seen in rickets.
- Haemarthrosis
- **Wimberger’s ring sign:** Circular, opaque radiologic shadow surrounding epiphyseal centers of ossification, which may result from bleeding.
- **Frankel’s line:** Dense zone of provisional calcification
- **Trümmerfeld zone:** Lucent metaphyseal band underlying Frankel’s line.



Segmental classifications.

⇒ **ASSOCIATED FEATURES**

- Skin retraction
- Nipple retraction
- Skin thickening
- Trabecular thickening
- Axillary lymphadenopathy
- Nipple discharge.

Final Assessment categories of BIRADS

| BIRADS | CATEGORY | MANAGEMENT | LIKELIHOOD OF CANCER |
|--------|---------------------------------|--------------------------|---|
| 0 | Need additional imaging | Additional imaging | N/A |
| 1 | Negative | Routine screening | 0% |
| 2 | Benign | Routine screening | 0% |
| 3 | Probably benign | Short interval follow up | >0% - <2% |
| 4 | Suspicious | Tissue diagnosis | HA >2% - <10% HB >10% - <50% HC >50% - <95% |
| 5 | Highly suggestive of malignancy | Tissue diagnosis | >95% |
| 6 | Known/Alleged proven | Surgery | N/A |

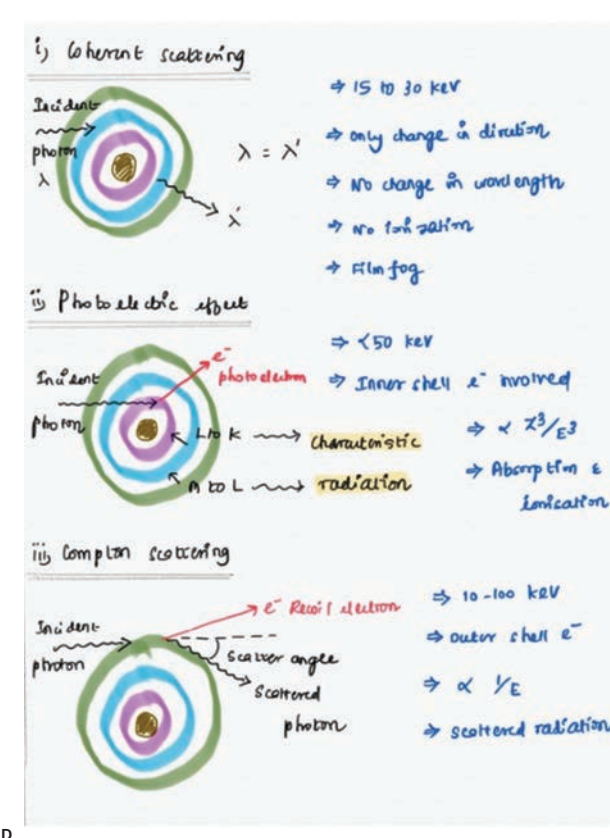
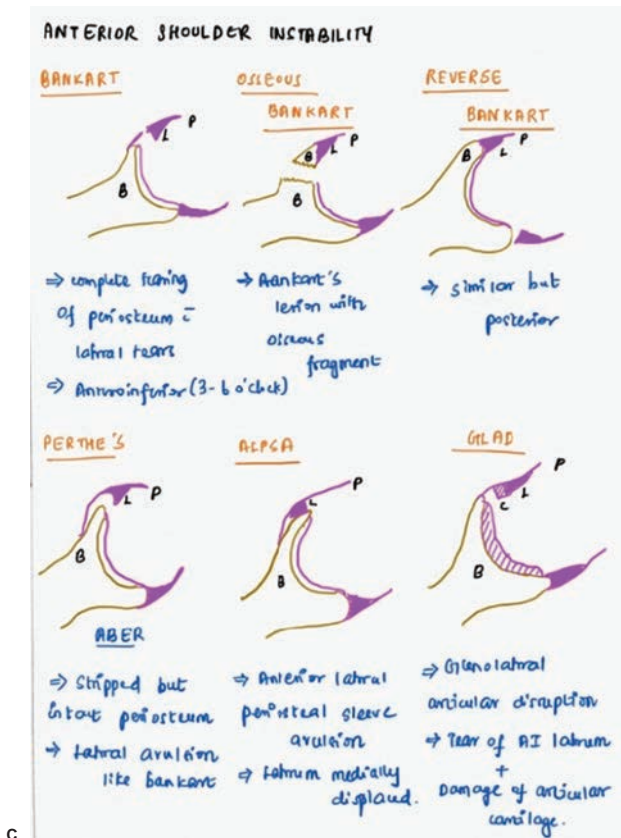


Fig. 1.1A to D: Sample answer sheets

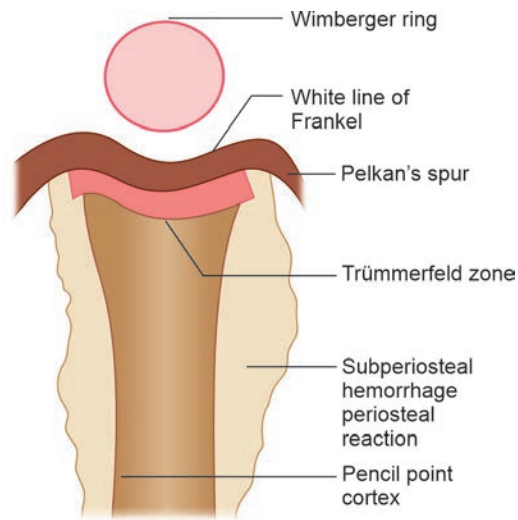


Fig. 1.2: Schematic diagram of scurvy findings

- **Pelkan spur:** Metaphyseal spurs which result in cupping of the metaphysis.

Diagrams are very important, in theory answersheets where we can show the important points in easy and efficient way (Fig. 1.2).



Volume 2

RADIOLOGY

Exam Made Easy

A Comprehensive Case Based Approach to Radiologic Examination

- A complete stepwise aid for radiology board examinations
- Precise structured guidelines for radiology case presentation
- Illustrative system-wise radiological anatomy
- Comprehensive coverage of over 200 examination cases with an all-inclusive list of possible differential diagnoses
- 70+ OSCE/CORE exercises explained with high quality images and original illustrations
- An overview of the international certifying examinations such as FICR, MICR, EDiR
- A complete handbook and reference for residents and young radiologists to guide them in their day-to-day radiological investigations and diagnoses



Volume 2

RADIOLOGY

Exam Made Easy

A Comprehensive Case Based Approach to Radiologic Examination

C Amarnath

MD, DNB, MNAMS, FRCR, FICR, FIMSA, MBA, PhD, EDiR, MICR, DiCRI

Professor and Head, Department of Radiodiagnosis

Stanley Medical College, Chennai

Senior Consultant, Scans World and Scans Point, Chennai



CBS Publishers & Distributors Pvt Ltd

New Delhi • Bengaluru • Chennai • Kochi • Kolkata • Lucknow • Mumbai
Hyderabad • Jharkhand • Nagpur • Patna • Pune • Uttarakhand

4.121 CARDIOVASCULAR SYSTEM

Case No. 121

Clinical history: A 28 years old female complaints of tachypnoea, tachycardia, and increased frequency of lower respiratory tract infection.

Radiological techniques and observation: Plain radiograph AP and lateral view, MRI axial view.

Figures 4.121.1 and 4.121.2 are plain radiograph frontal view showing trachea in midline. Diffuse cardiomegaly, obliteration of pulmonary bay indicating pulmonary plethora. Right cardiac shadow appears prominent. Costophrenic and cardiophrenic angles appear free. Visualised skeleton and soft tissue appear normal. On lateral view shows obliteration of the lower two-thirds of the retrosternal clear spaces—suggestive of right ventricle hypertrophy. Pulmonary artery appears enlarged, converge centrally—hilum convergent sign present. Incomplete doughnut sign seen suggestive of enlarged pulmonary artery. Visualised skeleton and soft tissue appear normal. Figure 4.121.3 is MRI showing atrial septal defect in fossa ovalis with communication between right atrium and left atrium. There is mild enlargement of the right atrium [RA] and right ventricle [RV] normal-sized left atrium [LA] and left ventricle [LV].

Interpretation: A: 28 years old female, C: Cardiomegaly, Obliteration of pulmonary bay, pulmonary plethora, B: Prominent right cardiac shadow, right ventricle hypertrophy obliterates the lower two-thirds of the retrosternal clear spaces, D: Atrial septal defect.

Principal diagnosis: Atrial septal defect.

Further investigations and management: ECG/ECHO/CTA/Cardiac MRI. Treatment—ASD has no effect on heart function *in-utero*, and newborns are asymptomatic. Surgically or percutaneously, the defect can be closed with an atrial septal occlusion device.

Discussion: Congenital heart disease approach evaluate five structures on the chest radiograph:

Acyanotic CHD with increased pulmonary vascularity
Common: Ventricular septal defect (VSD), atrial septal defect (ASD), patent ductus arteriosus (PDA), endocardial cushion defect (ECD), aortopulmonary septal defect, coronary arteriovenous fistulas, aortic sinus rupture, partial anomalous pulmonary venous connection (PAPVC), ALCAPA.

LVH causes retrocardiac clear space obliteration in lateral view of chest radiograph. In RVH, right ventricle obliterates the lower two-thirds of the retrosternal clear spaces.

Atrial septal defect (ASD) 2nd: Most common congenital cardiac anomaly

Types

- Ostium secundum type: Most common, 60%
- Ostium primum ASD: Coronary sinus type part of the ECD syndromes, 35%
- Sinus venosus defect 5%.

Associations

- Holt-Oram syndrome, Lutembacher syndrome (ASD and mitral stenosis) and Down syndrome.

Clinical presentation: Most patients are asymptomatic but as cardiac failure develops they may present with shortness of breath, palpitations and weakness. Chest auscultation reveals an ejection systolic murmur.

Radiographic features: Plain film—RA, RV and PA enlargement; no LA enlargement (different from VSD). The ascending aorta appears small (but in reality it is normal) because of the prominent pulmonary trunk and clockwise rotation of heart (RV enlargement). CT



Fig. 4.121.1



Fig. 4.121.2

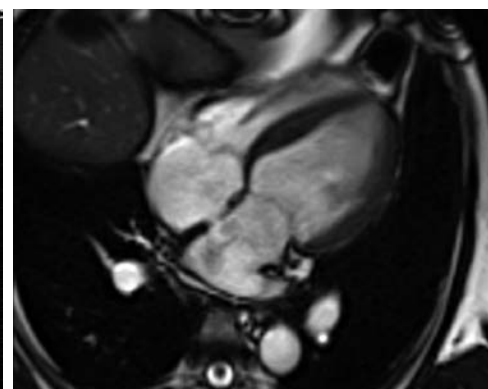


Fig. 4.121.3

Differential diagnosis: Left to right shunt

Ventricular septal defect (VSD): Second most common congenital cardiac anomaly. Types AV–5%, Conal–5%. Approximately 75% of minor VSDs close on their own within the first year of life; however, if a VSD has not closed by 10 years age, surgical patch closure is required.

X-rays reveal features of pulmonary arterial hypertension including left atrial enlargement, right and left ventricular enlargement, and constriction (pruning) of the pulmonary arteries. The septal defect can be seen directly with echocardiography. CTA/MRI also show additional functional information.



Fig. 4.121.4: Ventricular septal defect

Patent ductus arteriosus (PDA)
The L-R shunt because the pressure in the aorta is higher than in the pulmonary circulation.
Treatment: Medical—prostaglandin to keep ductus open. Indomethacin—to close the ductus. Endovascular-various closure devices, surgical-clipping.

Small PDA: Normal CXR, increased pulmonary vascularity, enlargement of the LA and LV, and Eisenmenger physiology may emerge in patients with long-term, severe illness. All of the preceding symptoms are observed in VSD; however, the following features suggest PDA: Unequal distribution of pulmonary arterial blood flow, particularly sparing of the left upper lobe, and aorta enlargement. Pulmonary angiography may reveal PDA as a slight linear density.



Fig. 4.121.5: Patent ductus arteriosus

Endocardial cushion defect (ECD): 40% of ECD patients have trisomy 21.
Types: Partial AV canal (ostium primum defect ± cleft in anterior mitral or septal tricuspid leaflets). Transitional AV canal (ostium primum defect, cleft in both AV valves, defect in superior IVS), complete AV canal and Gerbode defect (abnormal left-to-right shunt between the left ventricle and right atrium through a defect in the atrioventricular septum)

Radiographic features:
• Cardiomegaly
• Increased pulmonary vascularity
• Screen for other trisomy 21 findings: 11 ribs, multiple manubrial ossification centers
CT angiography shows shortening of the left ventricular inflow tract and elongation and narrowing of the left ventricular out-flow tract, which together produce the characteristic gooseneck sign.

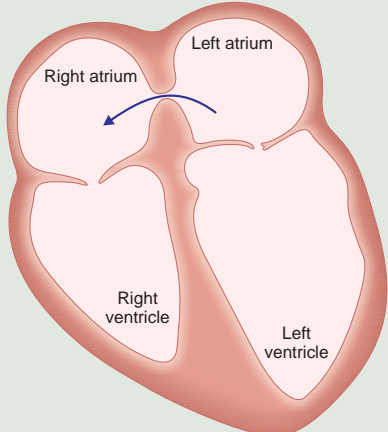


Fig. 4.121.6: Atrial septal defect

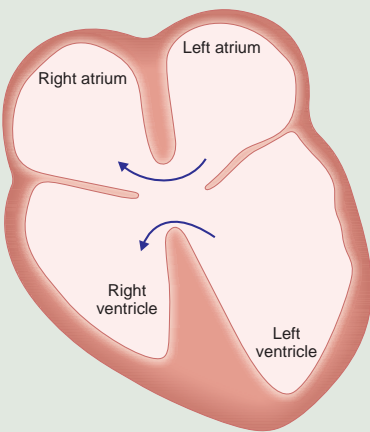


Fig. 4.121.7: Endocardial cushion defect

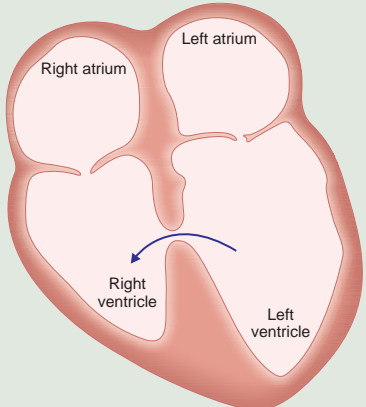


Fig. 4.121.8: Ventricular septal defect

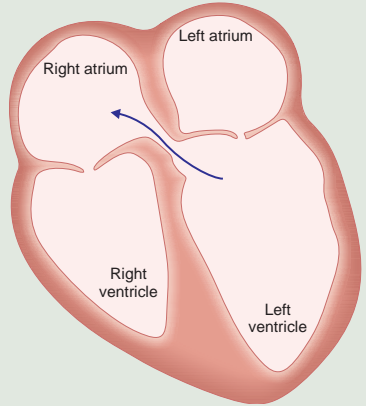
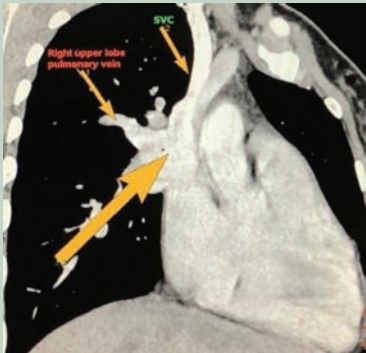
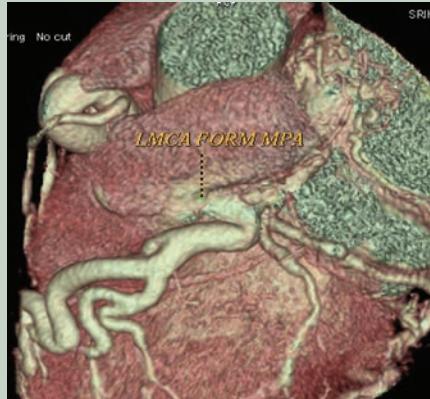


Fig. 4.121.9: Endocardial cushion defect/ Gerbode defect

| | | |
|---|---|---|
| <p>PAPVC (partial anomalous pulmonary venous connection) is an uncommon congenital cardiovascular disorder in which some, but not all, pulmonary veins drains into systemic circulation instead of the left atrium. Classification—supracardiac, cardiac, infracardiac types.</p> | <p>Chest radiographic features are particular to each subtype of PAPVC. Cardiomegaly can also be there CECT images show ASD with PAPVC right upper pulmonary vein draining into the right superior vena cava.</p> |  <p>Fig. 4.121.10: Partial anomalous pulmonary venous connection</p> |
| <p>Aortopulmonary septal defect (APSD) is a congenital condition in which there is improper connection between the pulmonary trunk and proximal aorta, in presence of separate aortic and pulmonary valves. Early surgical closure is indicated to prevent congestive heart failure and pulmonary hypertension.</p> | <p>Cardiomegaly and pulmonary plethora can be seen on a plain radiograph. The defect can be seen directly using echocardiography. Abnormal continuous forward flow on Doppler echocardiography in the pulmonary arteries shows the presence of an aortopulmonary connection. The defect can be seen directly using CT angiography.</p> | |
| <p>Coronary arteriovenous fistulas (CAVFs): Fistula between a coronary artery and right side of the cardiac circulation most commonly pulmonary artery. It represents left to right shunt. Treatment—generally symptomatic patients require closure via either transcatheter embolization or surgical ligation</p> | <p>Congestive heart failure and cardiomegaly are visible on chest radiographs. The gold standard for determining the origin, drainage, size, and course of CAVF is angiography. Electrocardiographically-gated CT cannot only identify the same CAVFs features as coronary artery angiography, but it also has the advantage of being non-invasive and conveniently accessible.</p> | |
| <p>Aortic sinus rupture or sinus of Valsalva aneurysm refers to abnormal dilatation of the sinus of Valsalva. It may be either congenital or acquired associated with Marfan's syndrome, Ehlers-Danlos, Takayasu arteritis. Treatment and prognosis: Surgical repair with a Bentall procedure could be performed.</p> | <p>X-ray—it is saccular and arises above the aortic annulus. Cardiac MRI/CT shows saccular aneurysm is seen arising from one of the sinuses (right coronary sinus most common). Transesophageal echocardiography is used to delineate origin of the aneurysm. The appearance is classically described as a “windsock” deformity. In color Doppler filling of the aneurysm may be observed and the use of contrast may allow visualization of the left-to-right shunt. The use of spectral Doppler allows quantification of flow velocity and direction rupture into a cardiac chamber mostly right ventricle causing left to right shunt.</p> | |
| <p>ALCAPA: Anomalous left coronary artery from the pulmonary artery also known as Bland-White-Garland (BWG) syndrome Left main coronary artery arises from pulmonary trunk rather from left coronary sinus. The LCA arises from the aorta in normal heart. The extent of collaterals determines the prognosis; however, most newborns present in the first year of life.</p> | <p>Normally, it supplies oxygen-rich blood to the left side of heart. In ALCAPA, the LCA originates from the pulmonary artery and it supplies oxygen-poor blood to the left side of heart. Cardiac CT shows anomalous left main coronary arterial origin from the posterior aspect of the pulmonary artery. Multiple intercoronary collateral arteries noted along the external surface of the heart. CT angiograms show anomalous origin of left coronary artery from the pulmonary artery</p> |  <p>Fig. 4.121.11: Anomalous left coronary artery from the pulmonary artery</p> |

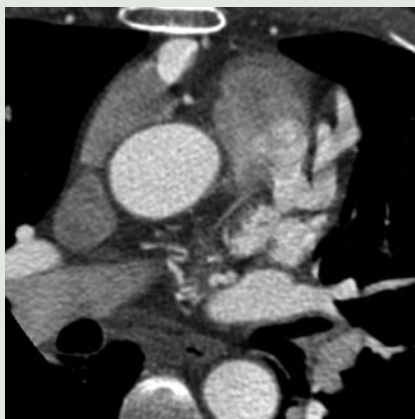


Fig. 4.121.12: Anomalous left coronary artery from the pulmonary artery

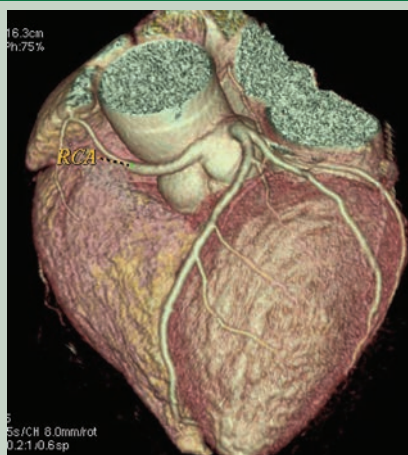


Fig. 4.121.13: Right coronary artery arising from left coronary cusp. Tortuous left coronary artery fistula draining into right atrium

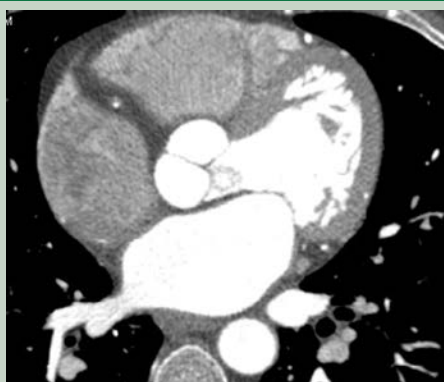


Fig. 4.121.14: Right coronary artery arising from left coronary cusp



Fig. 4.121.15: Right coronary artery arising from left coronary cusp

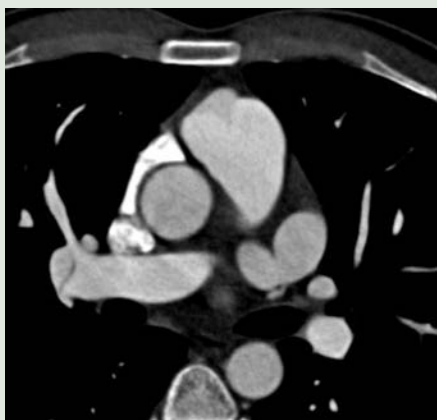


Fig. 4.121.16: Coronary artery fistula (right coronary artery dilated and drains into right atrium)

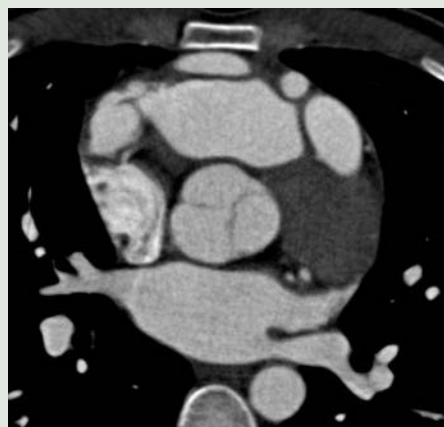


Fig. 4.121.17: Coronary artery fistula (right coronary artery dilated and drains into right atrium)



Fig. 4.121.18: Coronary artery fistula (right coronary artery dilated and drains into right atrium)

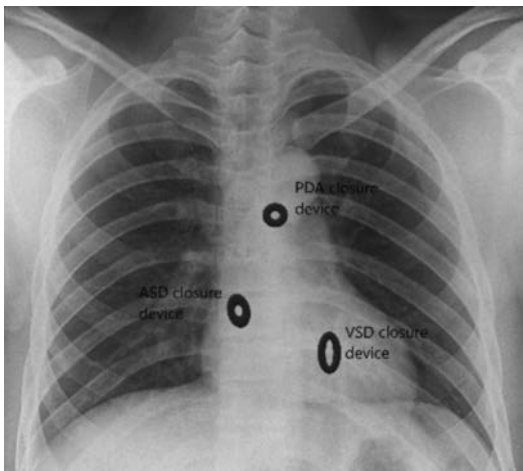


Fig. 4.121.19: Devices in heart

shows ASD most commonly ostium secundum type, communication between right atrium and left atrium.

CT angiography: It shows entry of contrast from left atrium to right atrium through the shunt in atrial septal defect. MRI shows added functional information (in addition to anatomy).

Checklist in Evaluation of Congenital Heart Diseases

In X-ray: 1.To look for chamber enlargement, 2. Plethoric or oligemic lung

In CT/MRI: 1. To look for thickness of ventricle wall, 2. Diameter of great vessels, 3. Flow rate across the great vessels, 4. Ventricular volume measurements, 5. Quantification of shunt, 6. Shunt reversal (Eisenmeger syndrome)

Causes for Pulmonary Arterial Hypertension

- 1. Pulmonary venous hypertension (PVH) is a complication of left heart failure (e.g. LVF, mitral valve disease) presenting with pulmonary oedema and pleural effusions.
- 2. Emphysema, interstitial lung disease, cystic fibrosis, LCH, LAM, and hypoventilation are examples of chronic lung disease.
- 3. Chronic thromboembolic pulmonary hypertension (CTEPH)—signs on CT include laminar thrombus (usually seen in larger arteries), intraluminal webs, pulmonary artery stenosis, peripheral lung scarring due to previous infarcts, mosaic attenuation in the lungs with smaller pulmonary arteries in the more lucent areas, and mosaic attenuation in bilateral lung fields with smaller pulmonary arterial diameter in the more lucent areas.
- 4. ASD, VSD, PDA, and partial anomalous pulmonary venous return are examples of chronic left-to-right shunts.
- 5. Systemic lupus erythematosus (SLE), Takayasu arteritis, vasculitis polyarteritis nodosa. In addition to the classic PA aneurysms, Behçet's disease and Hughes-Stovin syndrome can cause pulmonary artery stenosis/occlusions due to thrombosis/emboli.
- 6. Pulmonary veno-occlusive disease, which affects mostly teenagers and young adults. With interlobular septal thickening, pleural effusions, and ground-glass opacities, HRCT characteristics are comparable

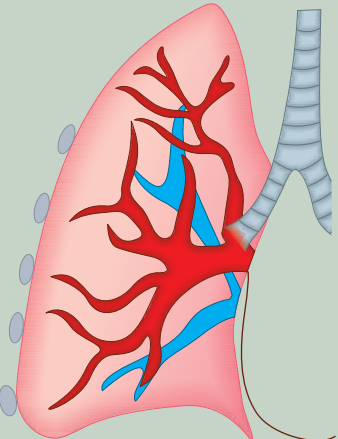
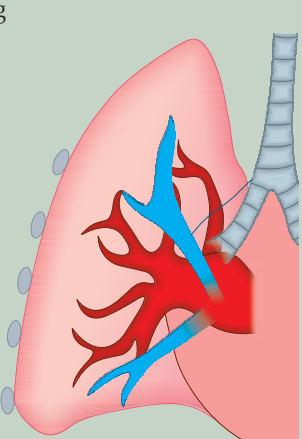
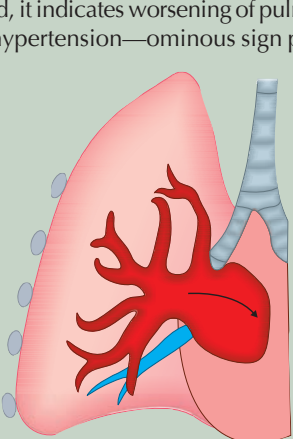
| Table 4.121.1: Grading of pulmonary arterial hypertension—radiological | | |
|---|--|---|
| Pulmonary arterial hypertension (PAH) | | |
| Mild: Mild dilatation of pulmonary artery—pleothoric lung | Moderate: Proximal ballooning of pulmonary artery with cardiomegaly and peripheral pruning | Severe: Reversal of flow in pulmonary artery (Eisenmenger syndrome), cardiomegaly reversed, it indicates worsening of pulmonary artery hypertension—ominous sign positive |
|  |  |  |
| Fig. 4.121.20: Pleothoric lung in mild PAH | Fig. 4.121.21: Moderate PAH | Fig. 4.121.22: Severe PAH |

Table 4.121.2: Grading of pulmonary arterial hypertension—clinical

| | <i>Systolic</i> | <i>Diastolic</i> | <i>Mean</i> |
|-----------------------|-----------------|------------------|-------------|
| Grade I: Mild | 30–50 | 20–25 | >30 |
| Grade II: Moderate | 50–70 | 26–35 | >40 |
| Grade III: Severe | 70–110 | 36–45 | >50 |
| Grade IV: Very severe | >110 | 46–55 | >60 |

to LVF, but with a normal left heart. The presence of centrilobular nodules is uncommon.

7. Pulmonary capillary haemangiomatosis, which affects mostly teenagers and young adults. On HRCT, there are a lot of ill-defined centrilobular nodules. Septal thickening between the lobes is uncommon. The left heart is normal.
8. Young adult women with idiopathic pulmonary arterial hypertension. Apart from those associated with pulmonary hypertension, there are usually no other imaging findings.
9. Chronic hypoxia due to the chest wall and upper airway (kyphoscoliosis, obesity without or with hypoventilation syndrome, e.g. Pickwickian syndrome)
10. Disorders of metabolism (glycogen storage disorders and Gaucher disease), sarcoidosis, connective tissue illnesses (such as scleroderma), fibrosing mediastinitis, portal hypertension, NF1, HIV, schistosomiasis, drugs/toxins, and others are some of the other reasons.

Criteria to rule out pulmonary arterial enlargement and pulmonary hypertension: On CXR elevated cardiac

apex due to right ventricular hypertrophy, enlarged right atrium, prominent pulmonary outflow tract, enlarged pulmonary arteries, pruning of peripheral pulmonary vessels. Pulmonary trunk diameter >29 mm measured in scan plane of its bifurcation at right angle to long axis lateral to ascending aorta. Diameter ratio of main pulmonary artery to aorta >1:1, right and left pulmonary arteries >18 mm in diameter measured in their intrapericardial portion 1 cm beyond origin. Right pulmonary artery more than 15 mm (women)/16 mm (men) and left pulmonary artery more than 18 mm suggest pulmonary hypertension.

Vascular signs of pulmonary hypertension: Widest short-axis diameter of pulmonary trunk ≥ 29 mm measured on transverse sections at level of PA bifurcation. Diameter ratio of distal pulmonary trunk to ascending aorta (measured at same level) >1. Diameter of main left and right pulmonary artery >16 mm, segmental artery-to-bronchus ratio >1 in 3 of 4 lobes (100% specific) “pruning” of peripheral pulmonary arteries \downarrow in caliber of smaller muscular arteries (vasoconstriction) + disproportionate increase in caliber of central fibrous arteries (sustained increase in flow by a factor of > 2).

Mediastinal and cardiac signs of pulmonary hypertension: Right heart hypertrophy + dilatation, RV myocardial thickness >4 mm, straightening of interventricular septum, right heart dilatation = ratio of RV: LV >11 at midventricular level on axial image, dilatation of tricuspid valve annulus, dilatation of IVC + coronary sinus.

Table 4.121.3: Chamber enlargement in congenital heart diseases (left to right shunt)

| <i>Left to right shunt</i> | <i>RA</i> | <i>RV</i> | <i>LA</i> | <i>LV</i> | <i>MPA</i> | <i>Aortic root</i> | <i>Lung</i> |
|---------------------------------|------------|------------|--------------|--------------|------------|--------------------|-------------|
| VSD | N | \uparrow | \uparrow | \uparrow | N | N | Plethoric |
| ASD | \uparrow | \uparrow | N | \uparrow | N | N | Plethoric |
| PDA | N | N | \uparrow | \uparrow | \uparrow | \uparrow | Plethoric |
| ALCAPA | N | \uparrow | \downarrow | \downarrow | N | N | Plethoric |
| PAPVC | \uparrow | \uparrow | N | N | N | N | Plethoric |
| Sinus of Valsalva aneurysm | N | \uparrow | N | N | \uparrow | \uparrow | Plethoric |
| Coronary arteriovenous fistulas | N | \uparrow | N | N | N | N | Plethoric |

4.122 CARDIOVASCULAR SYSTEM

Case No. 122

Clinical history: A 7 months old female child had complaints of cyanosis since birth and exertional breathlessness.

Radiological techniques and observation: Figure 4.122.1 is frontal radiograph of chest showing widened super mediastinum and the enlarged right atrium. Figures 4.122.2 to 4.122.6 are CECT Thorax in axial, coronal sections with MIP reformation respectively shows that left side dilated vertical vein, brachiocephalic vein above, and the dilated superior vena cava, all pulmonary venous connection noted in the right side draining directly into left vertical vein, which drains to left brachiocephalic vein. Thus, forming a figure of 8 appearance. Left lung field shows decreased pulmonary vasculature with increased attenuation than right side. No evidence of septal wall noted between the bilateral atria.

Interpretation: A—7 months old female child, C—direct visualisation of the anomalous pulmonary venous drainage on right side. B—classical snowman appearance is seen on frontal radiograph, D—TAPVC type 1.

Principal diagnosis: Considering the direct visualisation of anomalous pulmonary venous drainage, the diagnosis is total anomalous pulmonary venous drainage—type 1 supracardiac variant with atrial septal defect.

Treatment and prognosis: Surgical repair consists of creating a wide anastomosis between the posterior wall of the left atrium and pulmonary venous confluence.

Discussion: No drainage into the left atrium in TAPVR because all systemic and pulmonary venous blood reaches the right atrium. For survival, a right-to-left shunt is required, which is usually accomplished through a large patent foramen ovale/atrial septal defect. Return to the innominate vein or the superior vena cava through an ascending left vertical vein that drains to the innominate vein or the superior vena cava (type 1—supracardiac TAPVR). A descending vein that empties into the portal circulation infradiaphragmatically (type 2 infracardiac TAPVR). The coronary sinus is connected to the pulmonary vein confluence (type 3—cardiac TAPVR).



Fig. 4.122.1

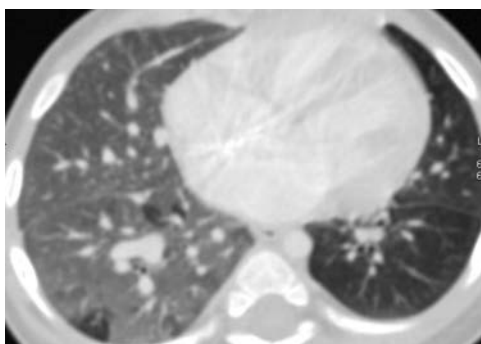


Fig. 4.122.2

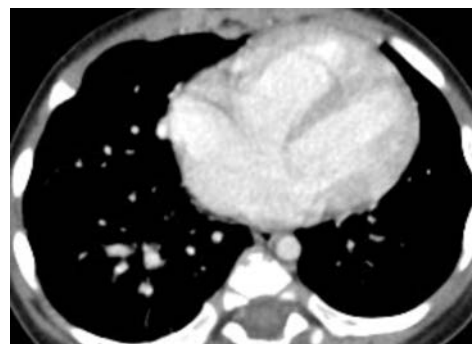


Fig. 4.122.3

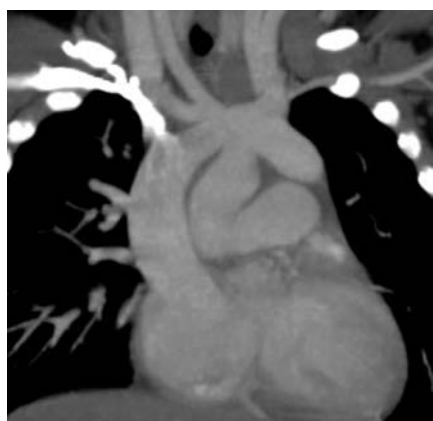


Fig. 4.122.4

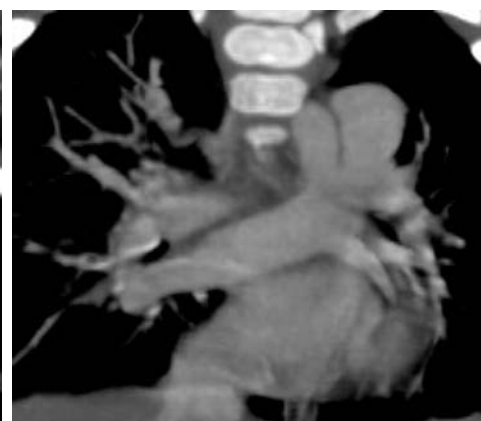
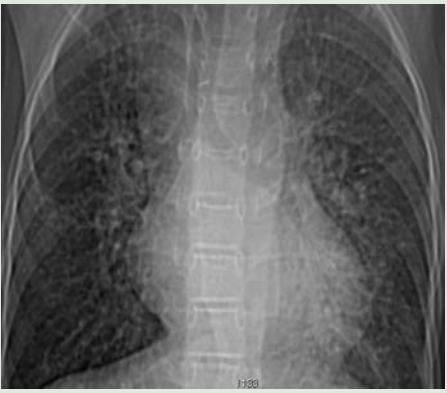

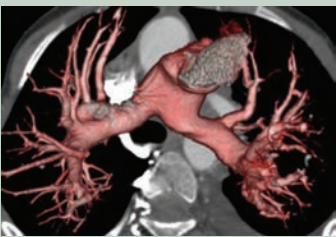
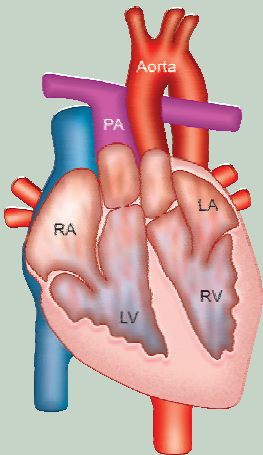
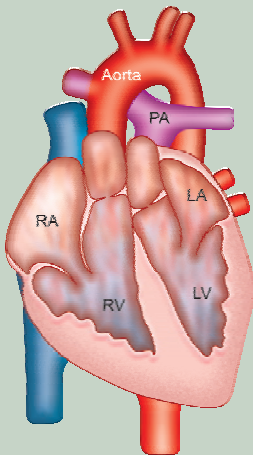
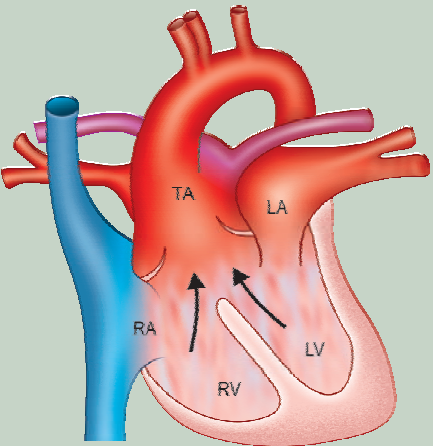


Fig. 4.122.5



Fig. 4.122.6

Table 4.122.1: Differential diagnosis for cyanotic heart disease

| | | | |
|---|--|---|--|
| <p>Transposition of great arteries: It is most common newborn cyanotic congenital cardiac anomaly presenting in the first day of life. Associated 10% with maternal diabetes and congenital coronary anomalies. Palliative procedure—Rashkind septoplasty. Definitive procedure—Mustard repair or Senning repair.</p> | | <p>Plain radiograph: The heart appears globular due to an abnormal convexity of the right atrial border and left atrial enlargement and therefore appears like an egg. The superior mediastinum appears narrow due to stress-induced thymic atrophy and hyperinflated lungs which give the picture of an egg suspended by a string on a chest radiograph, hence the name egg-on-a-string. Normal atrial and ventricular positions are preserved in D-TGA. The aorta is anteriorly and to the right of the pulmonary artery and comes from the right ventricle with a subaortic conus, while the left-sided pulmonary artery is seen posteriorly arising from the left ventricle with mitro-pulmonary fibrous continuity.</p> |  |
|  |  |  |  |
| <p>Fig. 4.122.7: D-TGA</p> | <p>Fig. 4.122.8: D-TGA</p> | <p>Fig. 4.122.9: L-TGA</p> | <p>Fig. 4.122.10: D-TGA</p> |
| <p>L-TGA—physiologically corrected, TGA—abnormal conal anatomy + abnormal positioning of the great vessels + ventricular inversion. As a result, with subaortic conus, the right ventricle is connected to the left atrium, and ascending aorta is anterior to the pulmonary artery on left side. Right-sided left ventricle is connected to the right atrium and the right-sided pulmonary artery with mitro-pulmonary fibrous continuity.</p> | | | |
| <p>Truncus arteriosus: Instead of a separate aorta and pulmonary trunk, this is a cyanotic congenital cardiac abnormality in which a single trunk provides both the pulmonary and systemic circulation.</p> | <p>Moderate cardiomegaly is frequently seen on chest radiographs, along with pulmonary plethora (due to collateral development) and a wider mediastinum. CT/CTA allows for direct visualisation of pathological anatomy. MRI—allows for direct visualisation of pathological anatomy. SSFP cine sequences can help with further functional evaluation.</p> |  | |
| | | <p>Fig. 4.122.11: Truncus arteriosus</p> | |

(Contd.)

Table 4.122.1: Differential diagnosis for cyanotic heart disease (Contd.)

Tetralogy of Fallot: 1 in 2000 babies. Most common neonatal cyanotic congenital heart disease. The combination of ventricular septal defect (VSD), right ventricular outflow tract obstruction (RVOTO), overriding aorta, and late right ventricular hypertrophy are seen. Surgical treatments used are shunt Waterston and Blalock-Taussig shunt.

Due to RVH and a concave pulmonary artery, a plain radiograph may reveal boot-shaped heart with an upturned cardiac apex. Reduced pulmonary arterial flow causes pulmonary oligoemia. CT reveals the complicated cardiovascular morphology, particularly the anatomical relation of the pulmonary and coronary arteries, as well as the identification of significant aortopulmonary collateral arteries (MAPCAs). The advantage of MRI is that it may provide both anatomical and functional information.

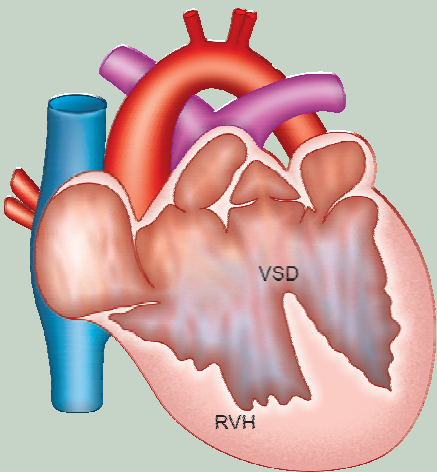


Fig. 4.122.12: Tetralogy of Fallot

Ebstein's anomaly: An aberrant tricuspid valve (septal and posterior leaflets) is shifted apically into the right ventricle, causing atrialization of the ventricle portions above the valve. We must search for more related pathology: ASD (particularly ostium secundum type), VSD, and tetralogy of Fallot are all examples of RVOT anomalies.

Severe right-sided cardiomegaly due to an elongated and enlarged right atrium, which may result in a raised apex, as seen on a plain radiograph. The heart is traditionally described as having a "box shape". CT/MRI findings include apical displacement of the tricuspid valve's septal and posterior leaflets, "atrialization" of the right ventricle, and tricuspid regurgitation.

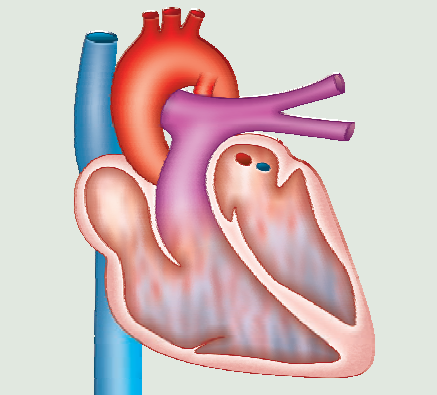


Fig. 4.122.13: Ebstein's anomaly

Single ventricle: A single or common ventricle is a ventricular chamber that receives both atrioventricular valves or one common atrioventricular valve.

CTA/MRI: Identification of the internal ventricular anatomy, the interrelation of the great vessels.

Pentalogy of Cantrell: Omphalocele ectopia cordis (abnormal heart location), diaphragmatic defect, pericardial defect or sternal cleft, cardiovascular abnormalities, ventricular septal defect (VSD), atrial septal defect (ASD), tetralogy of Fallot, and left ventricular diverticulum are the five key features.

Aberrant migration of the sternal anlage and myotomes during the early embryonic stage (6th to 7th week of pregnancy). Anomaly scans and MRIs are used to identify the abnormalities.



Fig. 4.122.14: Pentalogy of Cantrell

(Contd.)

Table 4.122.1: Differential diagnosis for cyanotic heart disease (Contd.)

The hypoplastic left heart syndrome: It is a cyanotic congenital heart defect that manifests as cardiac failure. One of the most prevalent causes of congestive heart failure in newborns, and the fourth most common cardiac defect to emerge within the first year of life. With a male predisposition, the frequency is 1 in 10,000 births.

The overall heart profile on a plain radiograph can be normal, or small / large. The prominent right atrial border indicates pulmonary venous congestion. CT/CT angiography/ Cardiac MRI: helps for direct view of the abnormalities as well as vascular structure. As a result of the compensatory effect, right-sided cardiac organs such as the right ventricle, right atrium, and pulmonary trunk are frequently enlarged.

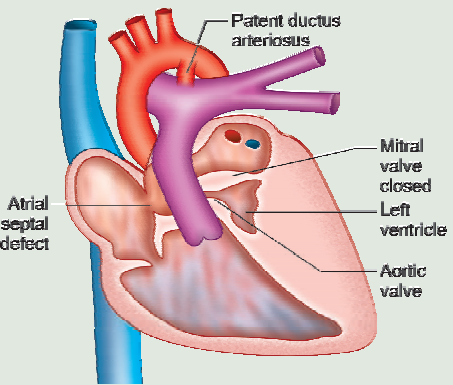


Fig. 4.122.15: Hypoplastic left heart syndrome

Tricuspid atresia = Tricuspid valve agenesis + right ventricular inlet agenesis. In order for circulation to be complete, an intra-atrial link through an ASD or a patent foramen ovale (PFO) is nearly always required.

Chest X-ray will show reduction in pulmonary vascularity (oligaemic appearance). The size of the heart might be normal or enlarged. CT and MRI allow for direct viewing of the anomaly, which usually reveals a fatty and/or muscular separation of the right atrium and right ventricle. In addition to anatomy, cine MRI can provide functional information.



Fig. 4.122.16: MAPCAs—aorta in red, MAPCA in green and yellow, pulmonary artery in purple

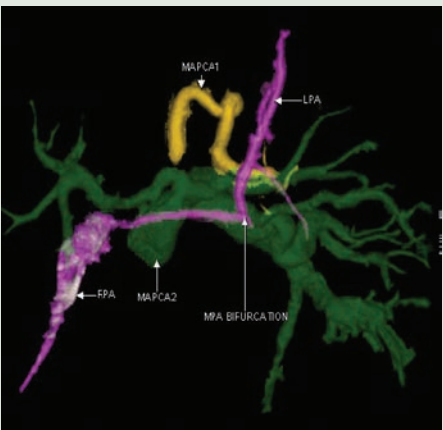


Fig. 4.122.17: MAPCAs—aorta in red, MAPCA in green and yellow, pulmonary artery in purple

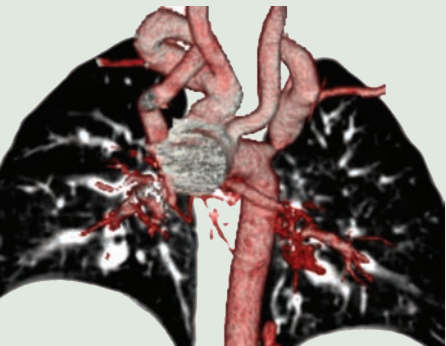


Fig. 4.122.18: MAPCAs—aorta in red, MAPCA in green and yellow, pulmonary artery in purple

MAPCA is major aortopulmonary collateral arteries. MAPCAs are long, convoluted foetal arteries that branch from the descending aorta and supply blood to the lungs via pulmonary arteries. Usually on the backside of the hilum, VSD and TOF are common in pulmonary atresia.

(Contd.)

Table 4.122.1: Differential diagnosis for cyanotic heart disease (Contd.)

On a frontal chest radiograph, the supracardiac variant (type I) can appear like a snowman, also known as the figure of 8 heart or cottage loaf heart. **Echocardiography**—blind ended left atrium with no connecting veins.
CT/MRA: Direct visualization of anomalous venous return.

The head of the snowman is produced by the dilated vertical vein on the left, the brachiocephalic vein on the top, and the superior vena cava on the right; the body of the snowman is made by the enlarged right atrium. Because of the higher flow volume, the right heart becomes more prominent with TAPVR, but the left atrium has normal size. Cardiomegaly is seen in types I and II.

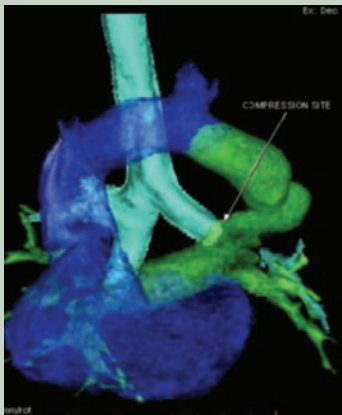


Fig. 4.122.19: Supracardiac type of TAPVC



Fig. 4.122.20: Supracardiac type of TAPVC

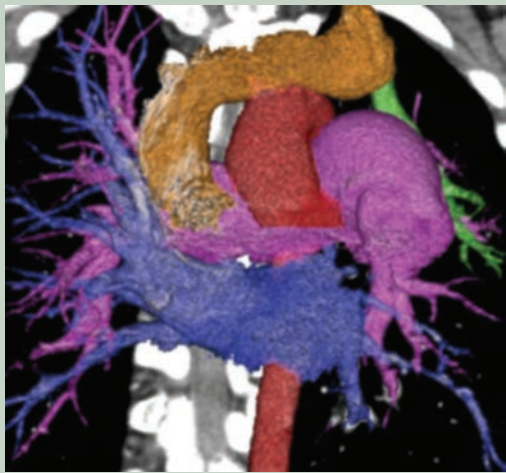


Fig. 4.122.21 Supracardiac type of TAPVC

Increased pulmonary vascularity: Total anomalous pulmonary venous return (TAPVR)—types I and II
Transposition of the great arteries. Single ventricle without pulmonary stenosis truncus arteriosus (types I, II and III)
Large AVSD

Decreased pulmonary vascularity: Tetralogy of Fallot, hypoplastic right heart syndrome, tricuspid atresia, hypoplastic right ventricle, pulmonary atresia/severe stenosis, Ebstein anomaly with ASD, double outlet right ventricle with pulmonary stenosis, pentalogy of Cantrell, Uhl anomaly, single ventricle with pulmonary stenosis

Table 4.122.2: Approach to cyanotic heart diseases

| Decreased pulmonary vascularity | | | | Increased pulmonary vascularity | |
|--|---|---|--|---|---|
| With right ventricular hypertrophy | With left ventricular hypertrophy | With combined ventricular hypertrophy | With neither ventricle predominance | With RVH | With LVH/combined ventricular hypertrophy |
| 1. Severe pulmonary stenosis with ASD 2. Pulmonary atresia with/without VSD 3. Tetralogy of Fallot | 1. Tricuspid atresia 2. Pulmonary atresia with hypoplastic right ventricle | 1. TGA with pulmonary stenosis 2. Truncus arteriosus with hypoplastic pulmonary arteries | Ebstein's anomaly (right atrial enlargement) | 1. Hypoplastic left heart syndrome 2. Double outlet single (right) ventricle 3. TAPVR 4. TGA | 1. Tricuspid atresia with transposition 2. Truncus arteriosus 3. TGA + VSD 4. Single ventricle |

Table 4.122.3: Relation of pulmonary artery to aorta in congenital transposition of great arteries


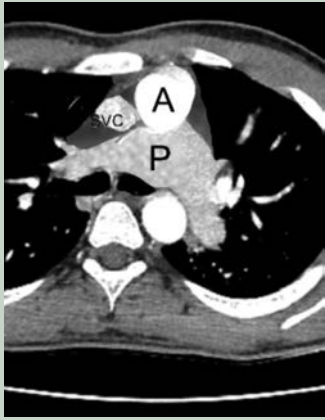
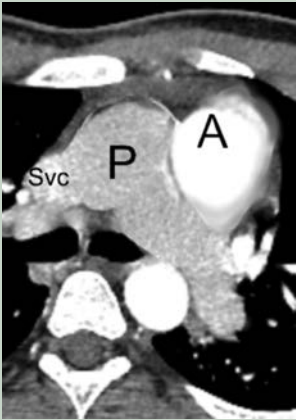
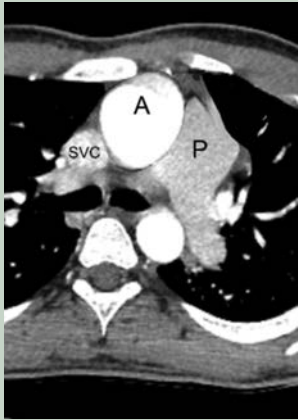
| <i>Normal—left anterior pulmonary artery, aorta posterior to PA</i> | <i>Dextro TGA—aorta anterior to pulmonary artery (right anterior aorta)</i> | <i>Levo TGA—congenitally corrected: Left anterior aorta</i> | <i>Classic double outlet RV—aorta and PA parallel to each other</i> |
|---|---|--|---|
|  |  |  |  |
| Fig. 4.122.22: Normal PAS arrangement (left anterior to right posterior) | Fig. 4.122.23: Dextro TGA | Fig. 4.122.24: Levo TGA | Fig. 4.122.25: Classic double outlet RV |

Table 4.122.4: Congenital cyanotic heart diseases (right to left shunt)

| <i>Right to left shunt</i> | <i>RA</i> | <i>RV</i> | <i>LA</i> | <i>LV</i> | <i>MPA</i> | <i>Aorta</i> | <i>Lung</i> |
|----------------------------|-----------|-----------|-----------|-----------|------------|--------------|-------------|
| TGA | ↑ | ↑ | ↑ | ↑ | N | N | Plethoric |
| TA | ↑ | ↓ | N | ↑ | ↓ | N | Oligemic |
| Truncus arteriosus | N | ↑ | N | ↑ | ↑ | ↑ | Plethoric |
| TAPVC | ↑ | ↑ | ↓ | N | ↑ | N | Plethoric |
| TOF | N | ↑ | N | N | ↓ | Overriding | Oligemic |
| Ebstein | ↑ | ↓ | N | N | ↓ | N | Oligemic |
| Hypoplastic left heart | N | N | ↓ | ↓ | N | ↓ | Oligemic |

4.123 CARDIOVASCULAR SYSTEM

Case No. 123

Clinical history: A 60-year-old man, known case of chronic kidney disease, presented with shortness of breath.

Radiological techniques and observations: Figures 4.123.1 and 4.123.2 are plain radiograph and axial CT images respectively. Frontal chest radiograph demonstrates diffuse enlargement of the cardiac outline, without any specific chamber enlargement/pulmonary artery changes. This global enlargement with narrow

vascular pedicle is mimicking money bag sign or water bottle sign, which refers to the cardiac silhouette shape on erect chest X-rays. No evidence of calcifications, a few patchy parenchymal opacities noted in the lung parenchyma.

Axial NECT thorax shows increased fluid collection (showing fluid attenuation) in the pericardial space, measuring 14 mm in this patient. No evidence of calcifications, a few patchy parenchymal opacities noted in the lung parenchyma. No pleural effusion.



Fig. 4.123.1



Fig. 4.123.2

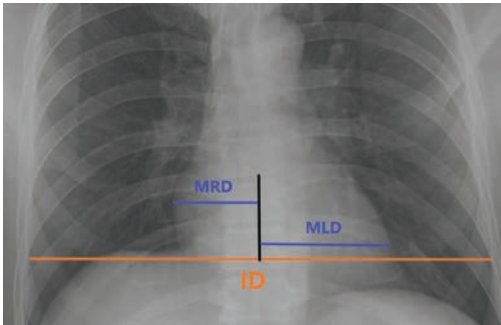


Fig. 4.123.3: Measurements on chest radiograph for cardiomegaly assessment

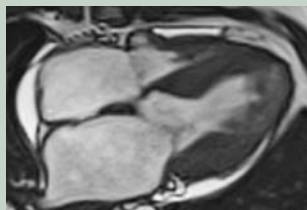
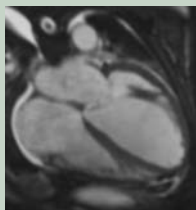






| Table 4.123.1: Differential diagnosis: For diffuse global cardiomegaly (nonspecific enlargement) | | |
|---|--|---|
| Dilated cardiomyopathy: Causes: Idiopathic, ischemic, familial, post-myocarditis, alcohol. Treatment: ACE inhibitors, ARB, beta blockers | Wall thickness within normal range, wall thinning present in ischemic cases. Increased LVESV, LVEDV. Decreased LV stroke volume, LVEF. Contrast MR: Delayed enhancement not usual in idiopathic dilated cardiomyopathy, regional sub-endocardial/transmural delayed enhancement occurs in ischemia. | |
| <div></div> <div>Fig. 4.123.4a: Dilated cardiomyopathy Fig. 4.123.4b: Hypertrophic cardiomyopathy</div> | | |
| Hypertrophic cardiomyopathy: In the absence of hemodynamic load, valvular heart disease causes myocardial hypertrophy. Causes: Familial, idiopathic | Hypertrophy involves the asymmetric septal, concentric, apical, midventricular, right ventricular wall. Treatment: To control heart rate beta-blockers. Other options include septal myectomy, septal ablation (arterial embolisation), and placement of an implantable cardioverter. | Increased LV wall thickness >12 mm Septal: Posterolateral wall thickness ratio >1.5 Normal LVEDV Normal or increased EF Contrast MR: Delayed enhancement in septum/junction of septum and anterior wall |
| Multivalvular heart disease: The combination of stenotic or regurgitant lesions occurring on ≥2 cardiac valves, and mixed VHD, i.e. the combination of stenotic and regurgitant lesions on the same valve Treatment—pharmacotherapy, valve replacement, reconstruction. | | |
| Other miscellaneous conditions: Anaemia, volume overload status | | |

Table 4.123.2: Radiographic findings in chamber enlargement of heart

| Chamber | Normal | | Enlargement | | |
|-----------------|---|--|---|---|--|
| | PA | Lateral | PA | Lateral | |
| Right atrium | <5.5 cm from midline to most lateral RA margin. <2.5 cm from right vertebral margin. Distance between the top of the arch and the junction of the SVC and the right atrium > distance between the latter and the right cardiophrenic angle. | - | >5.5 cm from midline to most lateral RA margin. >2.5 cm from right vertebral margin. Distance between the top of the arch and the junction of the SVC and the right atrium < distance between the latter and the right cardiophrenic angle. | - |  Fig. 4.123.5: RA enlargement |
| Left atrium | Normal carinal angle. Distance between left main stem bronchus and right lateral LA shadow <7 cm. | Normal bifurcation of bronchus. No indentation on esophagus | Double right heart border, double density sign. >75° splaying of carina, lifting of left main stem bronchus. >7 cm distance between left main stem bronchus and right lateral LA shadow | Walking man sign due to uplifting of left main bronchus. Posterior displacement and indentation of esophagus |  Fig. 4.123.6: LA enlargement  Fig. 4.123.7: LA enlargement—walking man sign |
| Right ventricle | MPA normal Cardiac apex maintained | Occupies the lower one-third of the retrosternal clear space | Large appearance of MPA. Upturned cardiac apex. | Occupies more than two-thirds of the retrosternal space |  Fig. 4.123.8: RV enlargement |
| Left ventricle | Cardiac apex—normal | Retrocardiac clear space maintained. Posterior cardiac margin projects <1.8 cm post to IVC measured at a point 2 cm above intersection of IVC with right hemidiaphragm | Rounding of the apex. Downturned cardiac apex. | Obliterating the retrocardiac clear space. Hoffman-Rigler rule: Posterior cardiac margin projects >1.8 cm post to IVC measured at a point 2 cm above intersection of IVC with right hemidiaphragm |  Fig. 4.123.9: LV enlargement |

(Contd.)

Table 4.123.2: Radiographic findings in chamber enlargement of heart (Contd.)

| Chamber | Normal | | Enlargement | | |
|---------|---|---------|--|---------|--|
| | PA | Lateral | PA | Lateral | |
| MPA | Normally in adults (>12 years) the pulmonary artery will be concave below the aortic knob. This is called pulmonary bay | | If pulmonary bay becomes convex, it denotes prominent pulmonary artery and MPA appears dilated if diameter above 29–33 mm. | |  <p>Fig. 4.123.10: A tangent line is drawn from aortic knob to left ventricle apex. The distance between the tangent and MPA falls in a range between 0 and 15 mm away from the tangent line</p> |
| AORTA | AP view—arch of aorta indenting on the left side of lower part of trachea. | | Diameter above Aortic root: 3.7 cm Ascending aorta: 3.6 cm Arch of aorta: 3.1 cm Descending aorta: 2.77 cm | | |

(For images refer to Radiological Anatomy, Chapter 3.3.K)

Table 4.123.3: Imaging findings in pericardial effusion

| Pericardial effusion | |
|--|--|
| Plain film <ul style="list-style-type: none"> • >250 ml is necessary to be detectable. • Oreo cookie sign on lateral view: Subpericardial fat stripe measures >10 mm (a stripe 1 to 5 mm can be normal). • Symmetrical enlargement of cardiac silhouette (water-bottle sign) • Postsurgical loculated pericardial effusion may mimic an LV aneurysm | Ultrasound <ul style="list-style-type: none"> • Study of choice • Echo-free space between epicardium and pericardium Cardiac tamponade |

Interpretation: A–60 years old male, C–increased fluid collection in the pericardial space, B–water bottle appearance on plain radiograph, D–Pericardial effusion

Principal diagnosis: Pericardial effusion.

Cardiomegaly: Global cardiomegaly leads to increased cardiothoracic ratio (>0.50). MRD = maximum transverse diameter to the right from midline. MLD = maximum transverse diameter to the left from midline. ID = internal diameter of the thorax drawn through the tip of the dome of the right diaphragm. Cardiothoracic ratio = $(MRD + MLD) \div ID$

Normal cardiothoracic ratios of various age groups: Newborn–<0.65, infants–<0.60, children–<0.55, adults–<0.5.

Further investigation: Echocardiography: When pericardial fluid reaches 50 ml, transthoracic echocardiography can reveal an anechoic separation of pericardial layers. The effusion will first emerge posteriorly in a supine patient, tracking anterior to the descending aorta and left atrium. The pericardial space is commonly inspected using the parasternal long-axis and subcostal four-chamber views.

Treatment: Asymptomatic conservative therapy is usually preferred. Pericardiocentesis can be used to drain the fluid if it is massive. To introduce a drain into the pericardial space, a Seldinger procedure is used, which is commonly done under ultrasound/echocardiographic guidance. Pericardial fenestration can be performed

in circumstances where effusions are recurring and symptomatic (e.g., malignancy).

Discussion: Early clinical manifestation will include dyspnea and reduced exercise tolerance, which will develop to severe diminished cardiac output and death in severe cases (e.g. cardiac tamponade). Idiopathic (virus-related, post-viral, or immune-related), inflammatory, systemic inflammatory disorders or connective tissue illnesses, systemic lupus erythematosus, rheumatoid arthritis, infection. Typical radiograph: On plain film, small pericardial effusions are frequently missed, cardiac shadow show globular enlargement, resulting in a water bottle appearance. The Oreo cookie sign appears on lateral CXR as a vertical opaque line (pericardial fluid) separating a vertical lucent line right behind the sternum (pericardial fat) anteriorly, from a vertical lucent line (epicardial fat) posteriorly.

CT: The thickness of a normal pericardium, as assessed on CT scans and MR imaging, is commonly taken to be 2 mm, with pathological being >3–4 mm. The purpose of a CT scan is to determine the aetiology of an effusion rather than to confirm the diagnosis. In ICU hospitalised patients, pericardial effusions are a common observation. The heart is surrounded by a fluid density substance.

Approach to cardiomegaly: Look for specific chamber enlargement, main pulmonary artery, arch of aorta, lung changes, pleural effusion.

Assessment of Cardiac Chamber Enlargement in Chest X-ray

The contour of the heart as visible on the frontal and lateral chest is referred to as cardiac silhouette. The cardiac silhouette size and shape can reveal important information about the underlying illness. The cardiac silhouette can be separated into right and left borders from the frontal projection: The right atrium, superior vena cava entering superiorly, and inferior vena cava often seen at its lower boundary comprise the right border. The left ventricle and left atrial appendage constitute the left border.

On the lateral projection, the right ventricle forms the anterior border, the left atrium (superiorly) forms the posterior border, and the left ventricle (inferiorly). In AP radiograph, the heart can appear artificially enlarged because the X-ray beam passes from anterior to posterior direction (for images refer to radiological anatomy, Chapter 3.3K).

4.124 CARDIOVASCULAR SYSTEM

Case No. 124

Clinical history: A 36-year-old female comes with history of breathlessness over the past 6 months getting worse on lying down. She gives history of episodes of sore throat with joint pain in childhood.

Radiological techniques and observation: Figure 4.124.1 is frontal chest radiograph of a skeletally mature female patient showing cardiomegaly with enlarged left atrium causing double density of the right heart border, splaying of carina, straightening of the left cardiac border. The aortopulmonary window is convex possibly due to enlarged pulmonary artery. The right side hilum shows dilatation of the pulmonary artery. The aortic knob is not visualized. The lung fields appear clear with prominent upper zone vessels. Both costophrenic angles appear normal without evidence of pleural effusion. The thoracic skeleton and soft tissues appear normal.



Fig. 4.124.1

Interpretation: A: 36-year-old female, C: Left atrial enlargement, B: Prominent pulmonary vessels suggest pulmonary hypertension and prominent upper zone vessels, cardiomegaly, D: Mitral stenosis with early pulmonary edema.

Principal diagnosis: Mitral stenosis probably of rheumatic etiology with features of pulmonary hypertension.

Differential diagnosis: Mitral stenosis is secondary to rheumatic disease in most of the cases.

Other etiologies include: Congenital mitral stenosis, infective endocarditis, carcinoid syndrome, Fabry's disease, Hurler's syndrome, Whipple's disease, left atrial myxoma.

Management: Further evaluation with transthoracic/transesophageal echocardiography to confirm the diagnosis. MR cine imaging with gradient-recalled echo (GRE) sequences can be used to identify degree of mitral valvular stenosis and any associated mitral regurgitation; estimate the gradient across the valve; and quantify ventricular volumes, mass, and function. Other valves especially the aortic valve should also be assessed for disease. Findings on CT include left atrial enlargement as well as calcification of the annulus. CT angiography is useful to evaluate coronary artery vasculature for preoperative workup in patients requiring surgical intervention for valve replacement or repair.

Medical management is directed toward alleviating symptoms and preventing complications like endocarditis and thromboembolism and arrhythmias. Surgical intervention is indicated in the symptomatic patient with moderate to severe stenosis ($<1.5 \text{ cm}^2$) or in the asymptomatic patient with evidence of pulmonary hypertension and moderate to severe stenosis. Surgical options include valve replacement or repair. Balloon valvuloplasty is preferred for high risk patients.

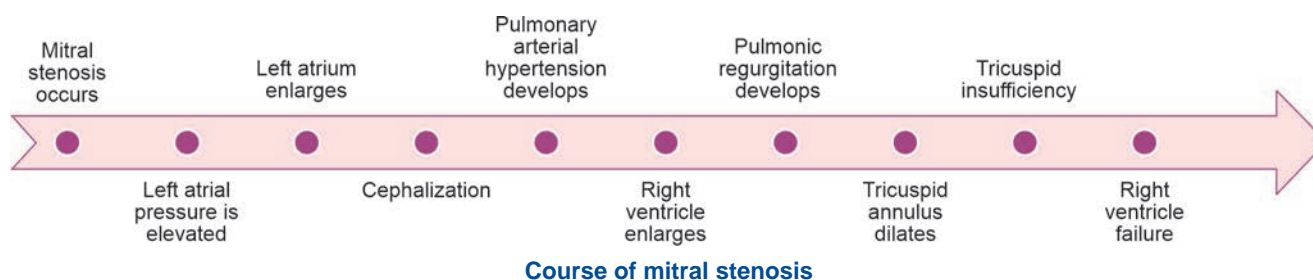


Table 4.124.1: Imaging features of other valvular heart diseases

| | |
|--|---|
| Mitral regurgitation Etiology Acute MR: MI, MVP, infective endocarditis Chronic MR: Dilated cardiomyopathy, RHD, infective endocarditis Treatment: Vasodilators, mitral valve replacement. | Plain film <ul style="list-style-type: none"> • “Big heart disease” (volume overload, cardiomegaly) • Enlarged chambers: LA + LV • PVH (usually less severe than in mitral) • Calcification of mitral annulus • Often coexistent with mitral stenosis |
| Aortic stenosis: M:F-4:1, old age Etiology: DM, hypertension, atherosclerosis causing aortic valve sclerosis, calcification Symptoms: Syncope, angina, dyspnea. Treatment: Pharmacotherapy, valve replacement | Plain film <ul style="list-style-type: none"> • Often difficult to detect abnormalities by plain film (usually no chamber enlargement) • Enlargement of ascending aorta (does not occur with supravalvular AS) • Calcification of aortic valve: Rare before age 40 • Echo • Multiple aortic valve echoes • Poststenotic dilatation of aorta • Doming of the aortic valve • LVH • Doppler: Velocity measurements |
| Aortic regurgitation Common in males >50 years, Etiology Root disease: Hypertension, congenital bicuspid aortic valve, connective tissue disorders (e.g. Marfan syndrome) Valvular: RHD calcific aortic valve disease, prolapse Treatment: Pharmacotherapy, valve replacement, reconstruction. | Plain film <ul style="list-style-type: none"> • Cardiomegaly • Dilated structures: LV, aorta Echo <ul style="list-style-type: none"> • Dilation of LV and aorta • Atypical valve leaflets • High-frequency vibrations of the anterior mitral Leaflet |
| Mitral stenosis (MS) In MS narrowing of the opening of the mitral valve between the left ventricle and the left atrium. Etiology: Mitral annular calcification, congenital mitral stenosis, infective endocarditis, cor triatriatum, radiation-induced heart disease | Plain film <ul style="list-style-type: none"> • Left atrial enlargement • Upper zone venous enlargement due to pulmonary venous hypertension • Pulmonary edema |
| Tricuspid stenosis: It is narrowing of the opening of the tricuspid valve between the right ventricle and the right atrium Etiology: Congenital tricuspid stenosis, carcinoid heart disease, nonbacterial thrombotic endocarditis, infective endocarditis, Fabry disease, cardiac amyloidosis | Plain film <ul style="list-style-type: none"> • Right atrial enlargement • Superior vena caval enlargement • Tricuspid valve calcification • Congestive heart failure features |
| Tricuspid regurgitation: In TR, abnormal backflow of blood into the right atrium during right ventricular contraction due to valvular leakage. It may be associated with aneuploidy | Antenatal ultrasound: The pulsed Doppler gate should be placed perpendicular across the tricuspid valve in the four-chamber view with the angle of insonation <20°. Jet velocity during regurgitation is at least 80 cm/sec. On color Doppler shows flow in the opposite direction with a different color compared to mitral valve flow with aliasing. |
| Pulmonary valve stenosis: The narrowing of the pulmonary valve orifice between the pulmonary trunk and the right ventricle | Plain film: Right ventricle and right atrial enlargement, prominent pulmonary trunk, left pulmonary artery is enlarged and congestive cardiac failure features. Increased haziness (due to increased vascularity) at the left lung base more than the right lung base is called Chen sign. |
| Pulmonary valve regurgitation also known as pulmonary valve insufficiency. Insufficiency causes backflow of blood from the pulmonary trunk into the right ventricle. | Plain film <ul style="list-style-type: none"> • Right ventricular enlargement • Prominent pulmonary trunk • Features of congestive heart failure |
| Tricuspid atresia (refer to Case 122) | |

| Table 4.124.2: Larry Elliot's grading of pulmonary venous hypertension | | |
|--|---|----------------------------|
| | CXR findings | PCWP |
| Stage 0 | Lower lobe predominance due to gravity | |
| Stage I | Upper lobe vein more prominent than lower lobe vein | 13–17 mm of Hg |
| Stage II | Interstitial edema, Kerley's B line | 18–25 mm of Hg |
| Stage III | Intra-alveolar edema, bilateral patchy opacities | 25 mm of Hg |
| Stage IV | Hemosiderosis ossification | Long standing hypertension |

Coronary artery anomalies

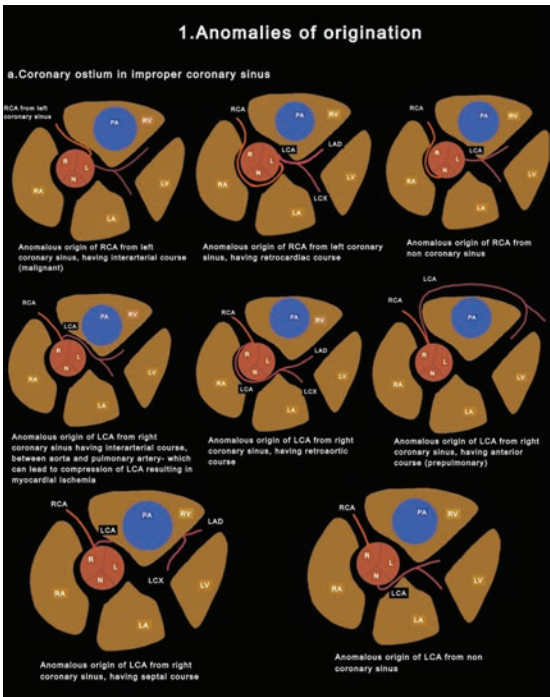


Fig. 4.124.2

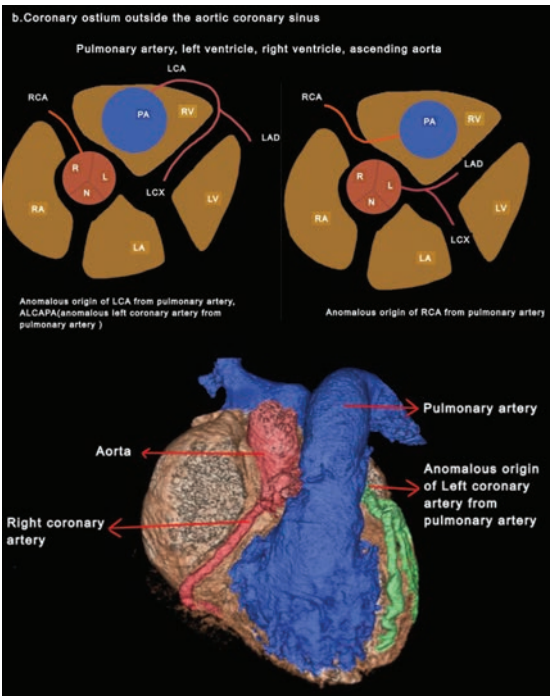


Fig. 4.124.3

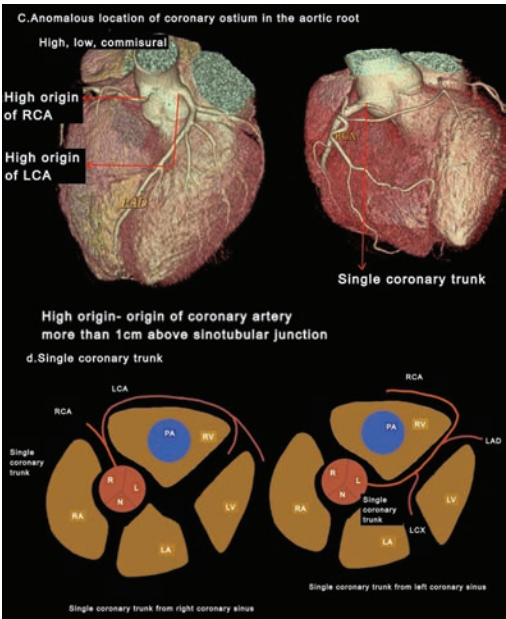


Fig. 4.124.4

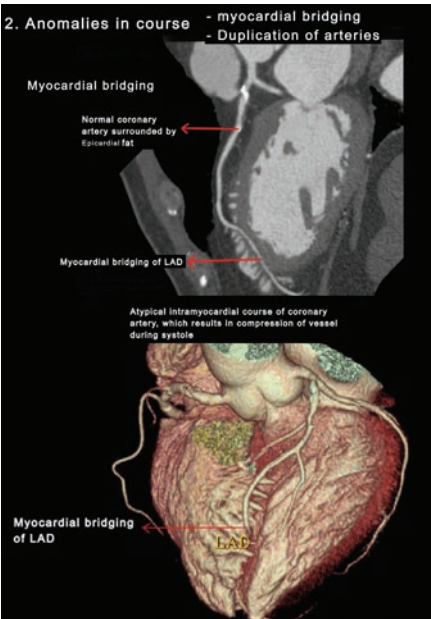


Fig. 4.124.5

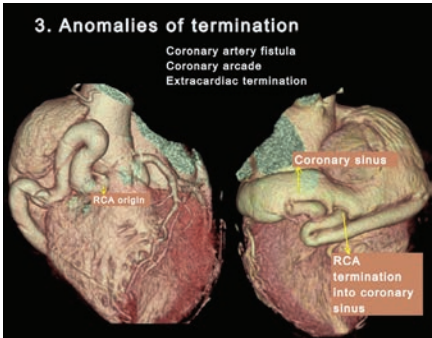


Fig. 4.124.6

4.125 CARDIOVASCULAR SYSTEM

Case No. 125

Clinical history: 45-year-old male, with complaints of altered bowel habits.

Radiological technique and observation: Figures 4.125.1 to 4.125.6 are CT of abdomen in soft tissue window, axial view at the level of liver respectively showing bilobed liver in the midline. Gall bladder is seen in the



Fig. 4.125.1



Fig. 4.125.2

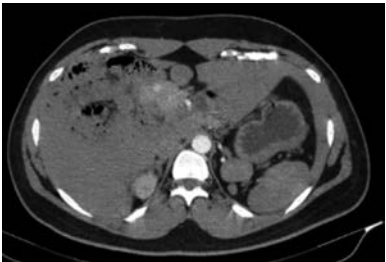


Fig. 4.125.3



Fig. 4.125.4



Fig. 4.125.5



Fig. 4.125.6



| Table 4.125.1: Differential diagnosis for left isomerism | | |
|--|---|---|
| Situs solitus | Thoracic and abdominal organs show normal position. Bronchial situs, visceral situs, atrial situs appear normal | |
| Situs inversus totalis | Inverted position of chest and abdominal organs. A total transposition of abdominal and thoracic viscera (mirror image of internal organs normal positioning). | <div><div><p>Fig. 4.125.7: Situs inversus totalis</p></div><div><p>Fig. 4.125.8: Situs inversus totalis</p></div></div> |
| Dextrocardia | Heart on the right side of chest | May occur with normal situs |
| Heterotaxy syndrome or situs ambiguus | Disturbance in the normal left-right distribution of thoracic and abdominal organs, which does not match the whole mirror image (situs inversus). Stomach, gall bladder in midline with bilobed liver | |
| Dextroposition of heart | Extrinsic circumstances, such as lung collapse or a massive pleural effusion, displaces heart to the right side. | |

Table 4.125.2: Morphological identification of cardiac chambers and bronchus

Bronchial situs identification

Right main bronchus: The relationship of the upper lobe bronchus (ULB) to the ipsilateral pulmonary artery is the most reliable marker of bronchial situs. A right lung has one with an eparterial bronchus. Eparterial bronchus is a major bronchus that passes above a pulmonary artery. In children, the angles are symmetrical, but in adults, the right main bronchus is steeper than the left. The right main bronchus is trilobed, short, and straight.



Fig. 4.125.9: Eparterial bronchus

Left main bronchus:

It is long, more horizontally oriented and hyparterial. Bilateral eparterial ULBs characterize right bronchial isomerism, whereas bilateral hyparterial ULBs characterize left bronchial isomerism. Other characteristics including the number of lobes, the ratio of left to right major bronchial lengths, and the branching pattern are less dependable. A left eparterial bronchus is the most common differential diagnosis for right isomerism.



Fig. 4.125.10: Hyparterial bronchus

Right atrium

Connections: superior and inferior vena cavae
Crista terminalis: It is a smooth thickened muscular structure which represents junction between sinus venosus and developing heart.
Right atrial appendages: Triangular or pyramidal shaped and broad-based; it contains pectinate muscles extending towards the atrioventricular valve

Left atrium

Connections: Pulmonary veins
Crista terminalis absent in left atrium
Left atrial appendages: Long slender finger-like
Contains pectinate muscles
Coronary sinus always runs inferoposteriorly to the left atrium

Morphologic right ventricle

Moderator band
Coarse trabeculae
Papillary muscles attached to both the free wall and the interventricular septum
Tricuspid AV valve
Septal and parietal bands

Morphologic left ventricle

Smooth septum
Thin, fine trabeculae
Only free wall show papillary muscles attachment
Bicuspid AV valve
Smooth superior septal surface

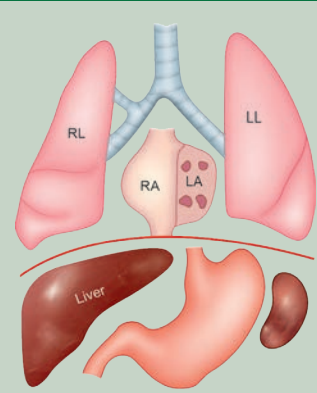


Fig. 4.125.11: Situs solitus

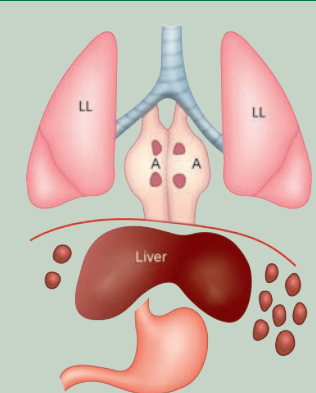


Fig. 4.125.12: Situs ambiguus with polysplenia (left isomerism)

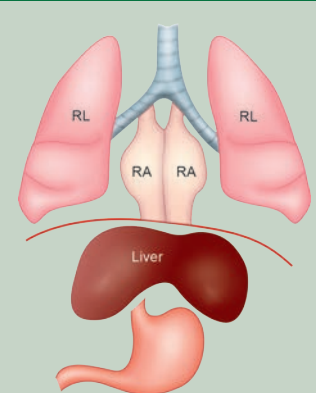


Fig. 4.125.13: Situs ambiguus with asplenia (right isomerism)

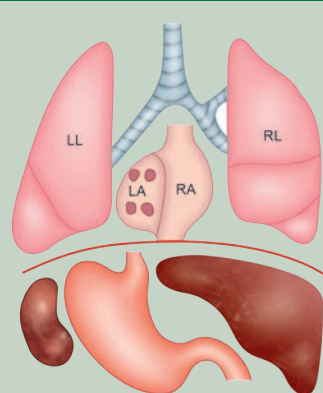


Fig. 4.125.14: Situs inversus totalis

midline. Splenic fossa appears empty. Multiple soft tissue dense round to ovoid structures noted in the bilateral hypochondrium—probably represent polysplenia. Polysplenia with no dominant (parent) spleen. Fundus of the stomach seen on left side. IVC is noted to the left of aorta.

Interpretation: A—45-year male, C—bilobed liver in the midline. Gall bladder is seen in the midline, B—polysplenia with no dominant (parent) spleen. IVC is noted to the left of aorta, D—situs ambiguus with left isomerism.

Principal diagnosis: Features of situs ambiguus with left isomerism.

Discussion: Heterotaxy syndrome, also known as situs ambiguus, is a condition in which the normal left-right arrangement of thoracic and abdominal organs does not exactly match to the complete mirror image (situs inversus)—stomach, gall bladder in the midline, bilobed liver.

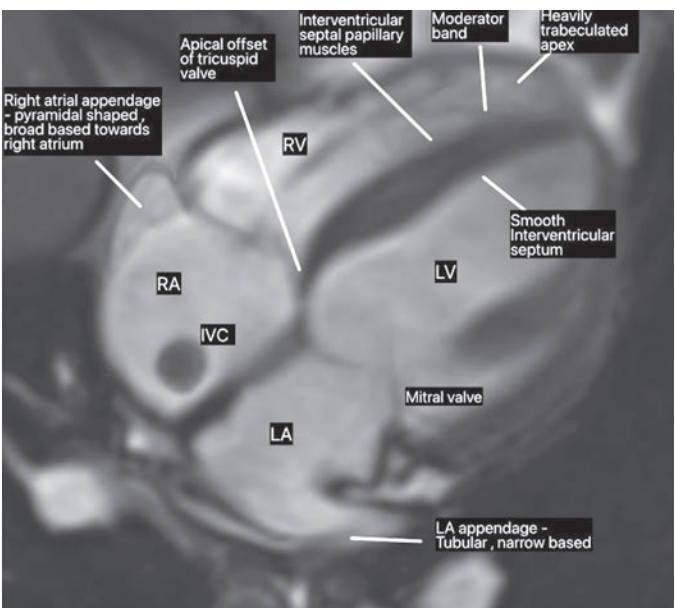
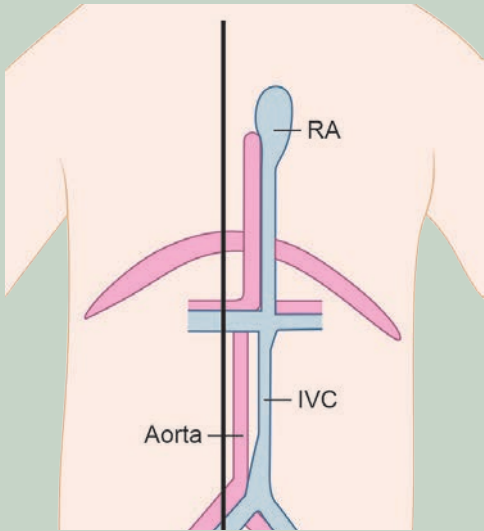
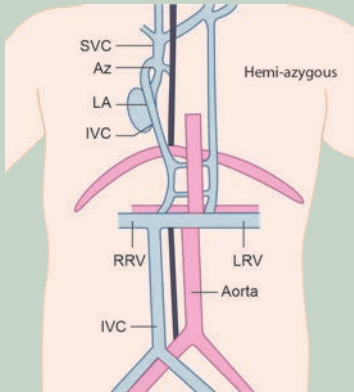


Fig. 4.125.15: Normal cardiac MRI

| Table 4.125.3: Anatomy in isomerisms | | |
|--------------------------------------|---|--|
| Morphology | Right isomerism/asplenia/bilateral right sidedness | Left isomerism/polysplenia/bilateral left sidedness |
| Cardiovascular system | Mesocardia /dextrocardia, single atrium with bilateral, single right ventricle right atrial appendages, right-sided aortic arch, double-outlet right ventricle, atrioventricular discordance, TGA, pulmonary stenosis and bilateral SVCs | Unbalanced ventricles, bilateral left atrial appendages, PAPVC, persistent left IVC draining into the left atrium, interrupted hepatic portion of IVC |
| Other malformations/dysfunction | Right-sided lungs on both sides and bronchi: Short bronchus, trilobed lungs, asplenia, symmetrical liver, right-sided stomach, intestinal malrotation | Polysplenia, bilateral left-sided lungs and bronchi: Long bronchus, bilobed lungs, midline liver, extra-hepatic biliary atresia/hypoplasia and extra-hepatic portal vein atresia |
| IVC and aorta | <div><p>The abdominal aorta and IVC are seen on the ipsilateral side of the midline with bilateral SVC and left-sided IVC in right isomerism.</p><p>Fig. 4.125.16: Right isomerism</p></div> | <div><p>IVC disruption at the suprarenal level with continuation as an azygous or hemi-azygous vein with the abdominal aorta and IVC on opposing sides of the midline characterises typical left isomerism. Left isomerism is also associated with persistent left SVC draining into the right atrium (RA), bilateral left pulmonary artery arrangement, and an interrupted hepatic component of the IVC.</p><p>Fig. 4.125.17: Left isomerism</p></div> |

The incidence is unknown, however, it is thought to be anywhere between 1 in 8,000 and 25,000 live births. The immotile cilia condition is linked to about 20–25 percent of cases (including Kartagener syndrome).

Clinical presentation: Patients may present with dextrocardia or a right-sided stomach bubble on a chest radiograph, or with symptoms related to heart abnormalities, intestinal blockage, or immunological weaknesses. For effective and efficient management, a thorough imaging assessment of each organ system is required to identify all rotational anomalies and their associated consequences. The severity of the isomerism and the existence of accompanying anomalies determine the symptoms. The most common symptom of right isomerism is cyanotic congenital heart disease. Because it is less related with severe congenital cardiac disease, left isomerism tends to manifest later in childhood or even adulthood. Intestinal malrotation with midgut volvulus can also be seen.

The structure of the atrial appendage determines whether the isomerism is right or left. The thoracoabdominal visceral laterality is abnormal, and it is frequently accompanied by facial and brain midline abnormalities. ZIC3, NODAL, CFC1, ACVR2B, LEFTY2, CITED2, and GDF1 are all human genes linked to heterotaxy syndrome.

Chest radiography: On chest radiography, the presence or absence of normal situs solitus can be evaluated. When

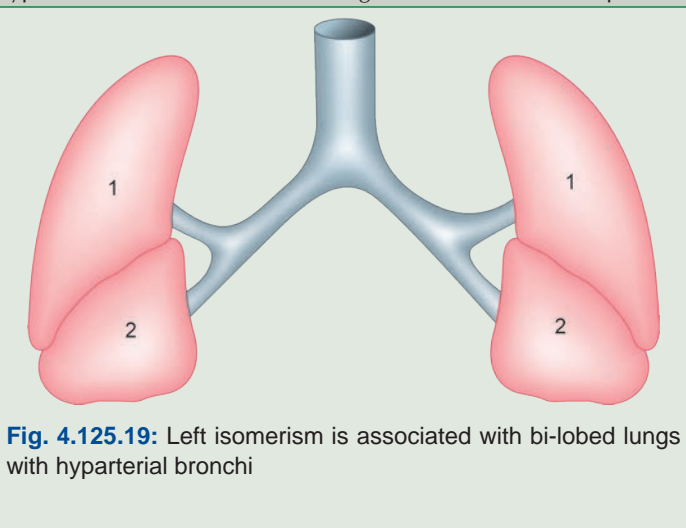
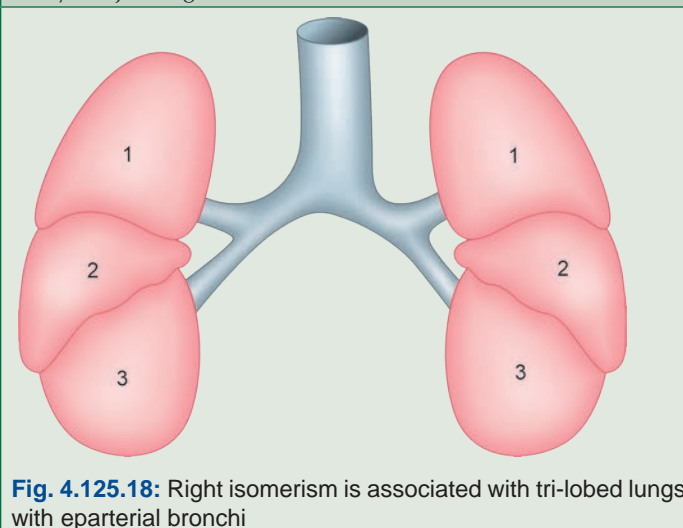
the aortic arch, heart apex, and stomach bubble are all on the left, it is called situs solitus. All of these structures are present on the right in situs inversus. Heterotaxy is implied in any other presentation. Isomerism is determined by the position of the pectinate muscle in reference to the atrioventricular junctions' vestibules. There are four different atrial appendage configurations. Atrioventricular septal defect (AVSD) or a double-outlet right ventricle can also cause right isomerism.

Abdominal USG for presence/position of the spleen, position of liver and gallbladder, and to determine the position of the aorta and IVC. For cardiac catheterization it is necessary for delineation of aorta and IVC for surgical planning.

Intestinal malrotation is more common with right than left isomerism. Barium meal with follow through can show the duodenal and jejunal locations, which do not cross the midline in heterotaxy.

Prognosis: Heterotaxy syndrome is a type of congenital heart disease that can be fatal. Despite recent breakthroughs in medical and surgical treatment, the long-term outlook is still uncertain. Right isomerism has a 5-year survival rate of 30 to 74 percent, whereas left isomerism has a higher 5-year survival rate of 65 to 84 percent due to the less complex accompanying cardiac abnormalities.

Bronchopulmonary anatomy is consistent with atrial appendage structures and reinforces the diagnosis of heterotaxy—bronchial anatomy is key. Major lung fissures can be identified on conventional CT as hypovascular lucent bands or on high-resolution CT as sharp lines.



4.126 CARDIOVASCULAR SYSTEM

Case No. 126

Clinical history: Eight months old male child presented with dyspnoea, stridor and difficulty in swallowing.

Radiological techniques and observation: Figures 4.126.1 and 4.126.2 are esophagogram with barium contrast images—spot film frontal view shows impression on right side of barium-filled upper thoracic oesophagus and below an impression on the left side of the mid-thoracic oesophagus producing reverse S appearance. On lateral film anterior displacement of the trachea and oesophagus noted. No evidence of filling defect of the contrast, and abnormal dilatation/narrowing, no esophageal wall irregularities, no evidence of fistula, entry of contrast into fundus of stomach noted. Visualized skeleton appears normal. Figure 4.126.3 is CT aortogram axial MIP image showing right arch which is larger and more superior and the left arch which is smaller. The double aortic arch forms a vascular ring with compression of the proximal esophagus posteriorly as well as abutment and slight compression of the trachea. The double aortic arch unite posteriorly form the descending aorta. Volumetric 3D construction image showing right arch which is larger and more superior and the left arch which is smaller. Each side of the vascular ring gives off common carotid artery and subclavian artery.

Interpretations: A: Eight months old male child, C: Reverse S appearance of esophagus in spot film of esophagogram due to compression by double aortic arches, B: CT aortogram shows forming a vascular ring, D: Double aortic arch.

Principal diagnosis: Double aortic arch with vascular ring.

Vascular ring: Vascular ring is a congenital anomaly in which the aortic arch and its branches completely or incompletely encircle and compress the trachea or oesophagus or both.

Aortic arch anomalies: A large number of AA anomalies exist; however, only three are common:

- Left arch with an aberrant right subclavian artery (RSA) (asymptomatic)
- Right arch with an aberrant retroesophageal LSA (asymptomatic)
- Double arch (symptomatic)

Embryology: Aortic development begins during the 3rd week of gestation. Each primitive aorta consists of a ventral and a dorsal segment. The two ventral aortae fuse to form the aortic sac, and the two dorsal aortae fuse to form the midline descending aorta. Six paired primitive, or pharyngeal, aortic arches develop between the ventral and dorsal aorta.

Proximal segment forms aortic sac. Middle segment forms the left 4th aortic arch. Distal segment forms the dorsal aorta.

Double Aortic Arch

Double aortic arch is a congenital abnormality of aortic arch system. Failure of normal regression of the 4th arch results in double aortic arch. Two aortic arches form a complete vascular ring causing tracheoesophageal compression. The two arches join for descending aorta mostly left side. Each arch will give subclavian and carotid artery.

Clinical features: Usually asymptomatic, dyspnoea, stridor, recurrent pneumonia and dysphagia (less

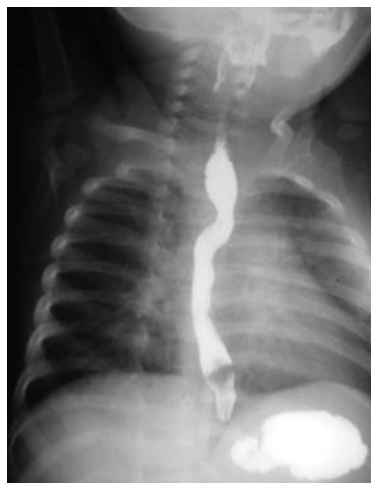


Fig. 4.126.1



Fig. 4.126.2

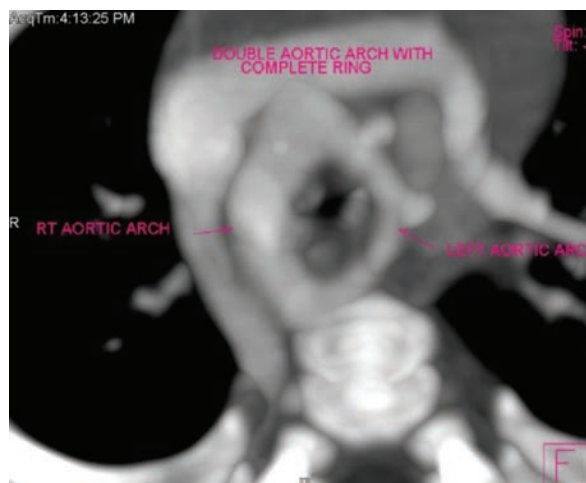


Fig. 4.126.3

Table 4.126.1: Differential diagnosis for aortic arch anomalies



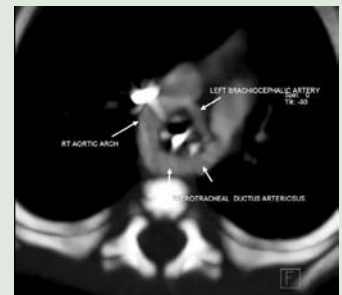

| | | |
|--|---|--|
| <p>Left aortic arch with aberrant right</p> <p>Subclavian artery: Also known as arteria lusoria, are one of the commonest of the aortic arch anomalies.</p> <p>Clinical presentation: They are often asymptomatic, but around 10% of people may complain of tracheo-esophageal symptoms, almost always as dysphagia, termed dysphagia lusoria</p> | <ul style="list-style-type: none">• Left aortic arch• Abnormal course of right subclavian artery. Its relationship with oesophagus is variable <p>Posterior to esophagus—80% Between esophagus and trachea—15% Anterior to trachea—5% Posterior indentation of esophagus in oesophagogram.</p> |  <p>Fig. 4.126.4: Arteria lusoria</p> |
| <p>Right aortic arch with aberrant left subclavian artery:</p> <p>Most common variation of a right aortic arch, regression of the left fourth arch between the left common carotid and left subclavian arteries, usually with persistence of the left sixth arch.</p> | <ul style="list-style-type: none">• Right arch• Retroesophageal indentation• Diverticulum of Kommerell: Aortic diverticulum at origin of aberrant subclavian artery |  <p>Fig. 4.126.5: Right aortic arch with aberrant left subclavian artery</p> |
| <p>Right aortic arch with diverticulum of Kommerell:</p> <p>Right aortic arch with mirror image branching: second most common form of a right-sided aortic arch, strongly associated with CHD in up to 98% of cases, including tetralogy of Fallot, truncus arteriosus, tricuspid atresia, and transposition of the great arteries with pulmonary valve stenosis.</p> | <ul style="list-style-type: none">• Right Aortic arch• No posterior indentation of esophagus |  <p>Fig. 4.126.6: Right aortic arch with mirror image branching</p> |
| <p>Aberrant left pulmonary artery from right pulmonary artery: Also known as pulmonary sling, represents an anatomical variant characterized by the left pulmonary artery arising from the right pulmonary artery and passing above the right main bronchus and in between trachea and esophagus to reach the left lung.</p> | <p>Barium esophagogram: Shows a indentation between trachea and esophagus above the level of the carina, usually seen as an anterior indentation over the esophagus. It may lead to compression and focal stenosis of the trachea.</p> <p>CT/MRI:The main bronchi have horizontal courses (i.e. low T-shaped carina), and vascular anatomy is normally well delineated on CT or MR angiography. Atelectasis may be seen in the upper lobes.</p> |  <p>Fig. 4.126.7: Pulmonary sling</p> |
| <p>Cervical aortic arch: Development of the cervical arch from the second or third primitive arches with regression of the fourth arch and failure of normal caudal descent of an otherwise normal fourth aortic arch. An aortic arch extending abnormally high in the neck, occurring more commonly on the right.</p> | | |
| <p>Aortic coarctation: Aortic narrowing in the region of the isthmus. M:F = 4:1</p> <p>Two types:</p> <ul style="list-style-type: none">• Localized or adult or postductal or juxta-ductal type• Tubular hypoplasia or infantile or preductal or diffuse | <p>Chest X-ray shows figure of 3 sign (pre-stenotic dilatation, indentation at the coarctation, post-stenotic dilatation), Roesler sign (inferior rib notching)</p> <p>Barium study: Oesophagus will show reverse 3 sign or E sign.</p> <p>CT: Narrow segment will be visualised</p> <p>Coexistent cardiac anomalies are common.</p> | |
| <p>Further management: The CT aortogram findings are discussed with paediatric thoracic intervention team for further management</p> | | |

Table 4.126.2: Approach based on pattern of vascular compression of oesophagus and trachea

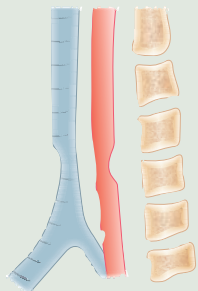


Fig. 4.126.8: Anterior tracheal indentation + large posterior esophageal impression

- A. Anterior tracheal indentation + large posterior esophageal impression:
- 1. Double aortic arch
 - 2. Right aortic arch with aberrant left subclavian artery + left ductus/ligamentum arteriosus
 - 3. Left aortic arch with aberrant right subclavian artery + right ductus/ligamentum arteriosus (extremely rare).

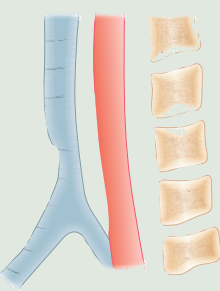


Fig. 4.126.9: Anterior tracheal indentation

- B. Anterior tracheal indentation:
- 1. Compression by innominate artery with origin more distal along aortic arch.
 - 2. Compression by left common carotid artery with origin more proximal arch,
 - 3. Common origin of innominate and left common carotid artery (bovine arch).

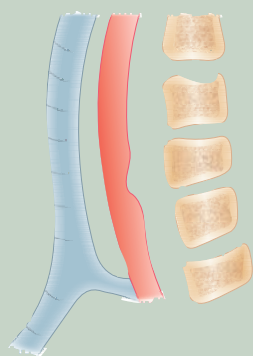


Fig. 4.126.10: Small posterior esophageal impression

- C. Small posterior esophageal impression: Dysphagia lusoria
- 1. Left aortic arch aberrant right subclavian artery
 - 2. Right aortic arch with aberrant left subclavian artery

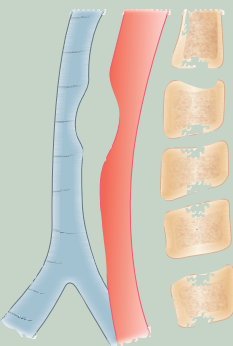


Fig. 4.126.11: Posterior tracheal indentation + anterior esophageal impression

- D. Posterior tracheal indentation + anterior esophageal impression:
- 1. Aberrant left pulmonary artery (pulmonary sling)

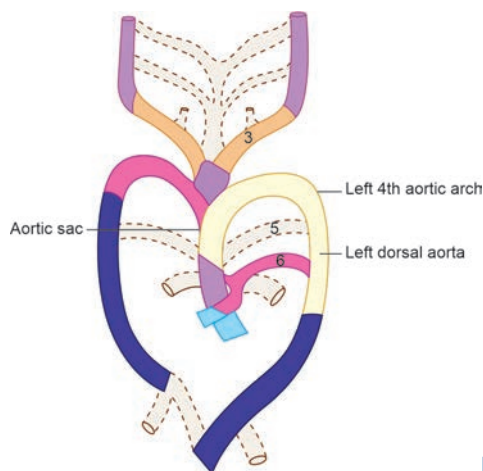


Fig. 4.126.12: Fetal aortic arches

common than respiratory symptoms, more common after starting baby on solids). Presentation usually within 6 months of age.

Diagnosis

Chest X-ray: Right aortic arch may deviate trachea to left due to normal left arch. Ill-defined aortic arch is often observed. Compression of air-filled trachea may be visible. Sometime may present with signs of pneumonia.

Barium swallow: Oesophagus shows left and right indentations on the posteroanterior view and large posterior indentation seen in lateral view.

Echocardiography: Useful for diagnosing vascular ring and for excluding intracardiac defects.

CT and MRI: With contrast useful diagnostic tool. Reveals position, relationship of arches to trachea and bronchi.

Aortic angiography and cardiac catheterization: Evaluate the hemodynamic and anatomy of associated congenital cardiac defects. Contrast is injected into ascending aorta through catheter, aortography is used to delineating anomalous arch vasculature.

Tracheography and bronchoscopy: Not routinely done, useful to delineate the site and severity of tracheal compression due to vascular ring.

Treatment: Medical—asymptomatic patients need no surgical treatment. Treatment of pulmonary infection.

Surgical indication: Stridor, apnoeic spells, recurrent pulmonary infection, respiratory distress.

Procedure: Open division of vascular ring through left thoracotomy, division of smaller of the two arches is done.

4.127 CARDIOVASCULAR SYSTEM

Case No. 127

Clinical history: 58 years female with acute onset of chest pain radiating to back and deep abdominal pain. ECG—Within normal limits, BP: 130/80 mmHg, pulse: 88/min.

Radiological techniques and observations: Figures 4.127.1 to 4.127.7 show CT aortic angiogram with oral contrast, in axial and reformatted coronal sections show intimal flap (straight arrow) in the descending thoracic and abdominal aorta, extending up to the bilateral common iliac arteries. The smaller lumen

appear denser, oval in shape—probably the true lumen. On comparison, the larger lumen appears less dense, crescentic in shape—probably the false lumen. The false lumen is seen wrapping around the true lumen (beak sign). Visualised portions of arch of aorta appear normal. No evidence of wall thickening (wall thickening may be due to atherosclerosis or vasculitis like Takayasu arteritis). No evidence of thrombosis in the false lumen. Celiac trunk, SMA, IMA and left renal artery (curved arrow) arising from the true lumen and right renal artery (dotted arrow) arising from the false lumen. Moderate

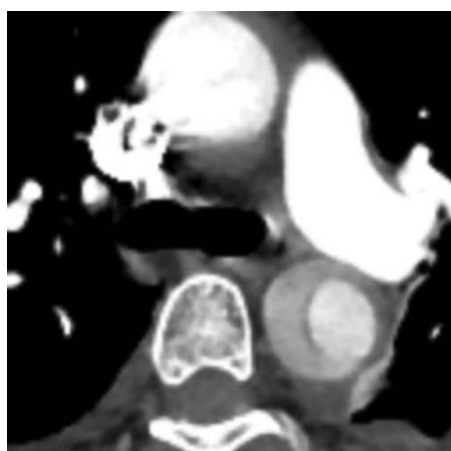


Fig. 4.127.1



Fig. 4.127.2

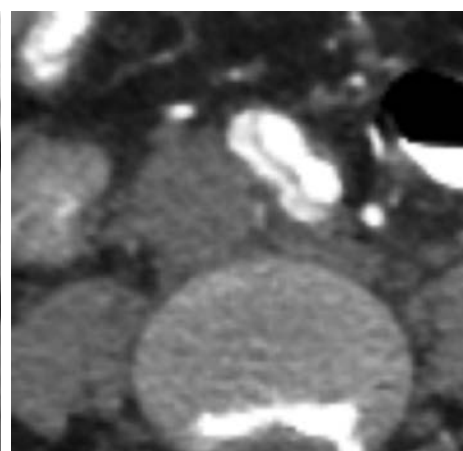


Fig. 4.127.3



Fig. 4.127.4



Fig. 4.127.5

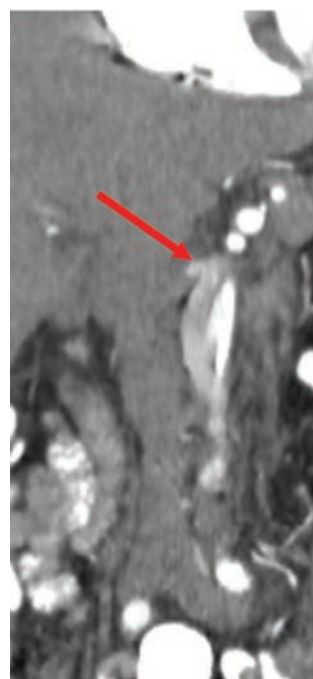


Fig. 4.127.6

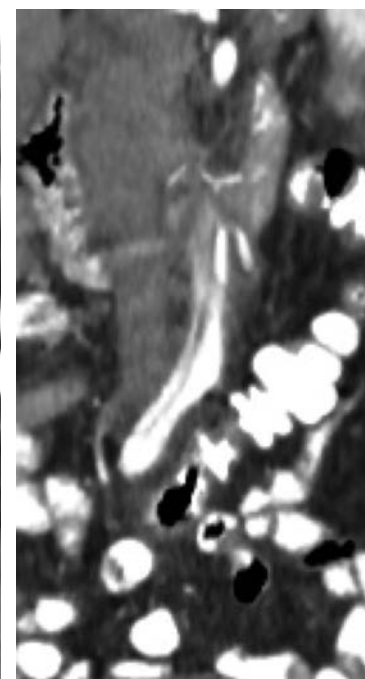


Fig. 4.127.7



Fig. 4.127.8: Extension of the dissection flap into iliac arteries

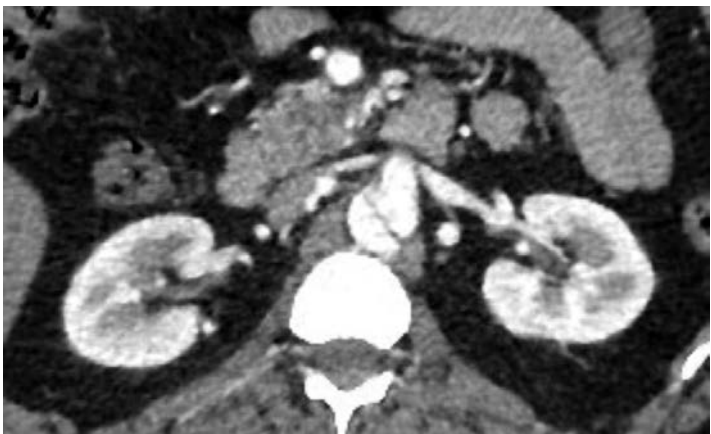

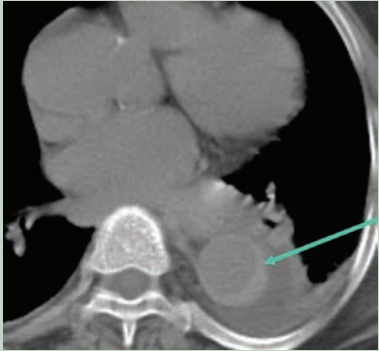
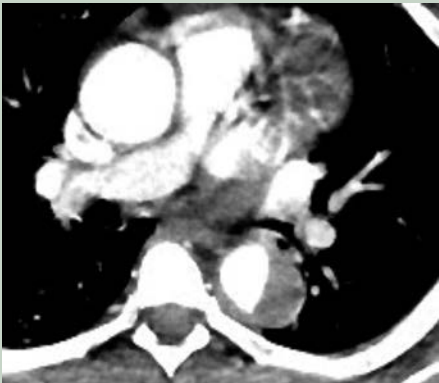
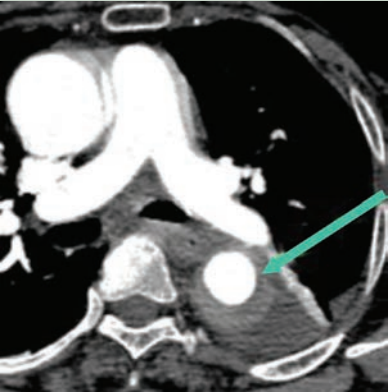


Fig. 4.127.9: Extension of the dissection flap into renal arteries

| Table 4.127.1: Difference between aortic dissection and intramural hematoma | |
|--|---|
| Aortic dissection | Intramural hematoma |
| NECT shows inward displacement of mural calcification. CT angiogram shows an intimomedial flap separating the true lumen from the false lumen. | A crescenting hyperattenuating mural blood collection in the NECT. |
|  |  |
| Fig. 4.127.10: Aortic dissection | Fig. 4.127.12: Intramural hematoma |
|  |  |
| Fig. 4.127.11: Aortic dissection | Fig. 4.127.13: Intramural hematoma |

| Table 4.127.2: Difference between true and false lumen | | |
|--|---------------|-----------------------|
| Features | False lumen | True lumen |
| Size | Larger lumen | Smaller lumen |
| Configuration | Crescentric | Round or oval |
| Flap curvature | Convex | Concave |
| Doppler signal | Sluggish | Dense |
| Wrap around | + | - |
| Beak sign | + | - |
| Cobwebs | + | - |
| Thrombus | + | - |
| Outer wall calcifications | - | + |
| Origin of branch artery | Usually renal | Celiac axis, SMA, IMA |

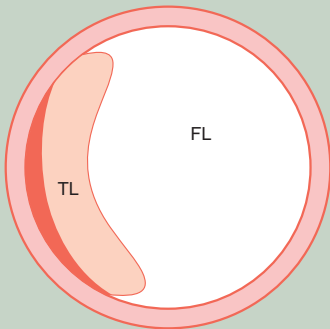


Fig. 4.127.14: False lumen

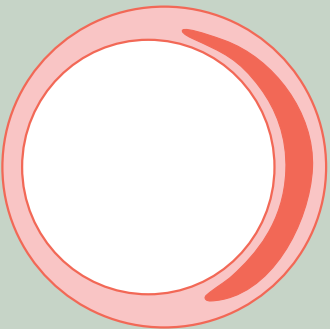


Fig. 4.127.15: True lumen



Fig. 4.127.16: Svensson class I aortic dissection showing both true lumen and false lumen

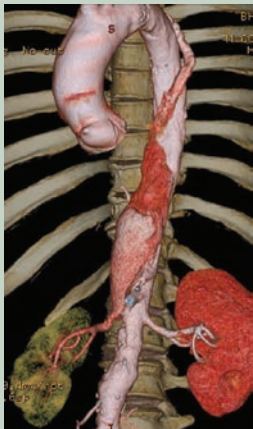


Fig. 4.127.17: False lumen supplying the right kidney

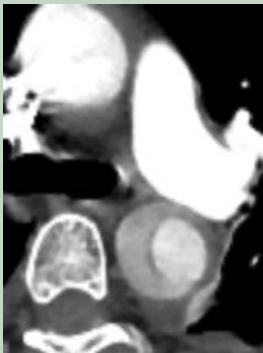


Fig. 4.127.18: Beak sign: Acute angle between dissection flap and outer wall—most useful sign. Outer wall calcification is present in true lumen.

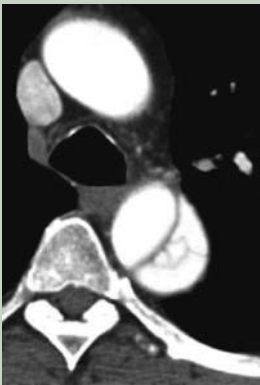


Fig. 4.127.19: Collagenous media—remnants/cobwebs—seen in the false lumen only.



Fig. 4.127.20: The true lumen is brighter and smaller. Thrombus formation is within the false lumen

| Table 4.127.3: Svensson classification of variants of aortic dissection | |
|---|--|
| Class | Description |
| I | Classical dissection with true and false lumen |
| II | Intramural haematoma or haemorrhage |
| III | Subtle dissection without haematoma |
| IV | Penetrating atherosclerotic aortic ulcer |
| V | Iatrogenic or traumatic dissection |

stenosis of the origin of celiac trunk noted, with post-stenotic dilatation. No stenosis of the SMA, IMA and left renal artery. No evidence of pericardial effusion, pleural effusion. Visualised left kidney appears normal. Visualised bones appear normal.

Interpretation: A: 58 years old female, B: Intimal flap in the descending thoracic and abdominal aorta, extending up to the bilateral common iliac arteries, C: The false lumen wrapping around the true lumen. D: Thoracic and abdominal aortic dissection.

Principal diagnosis: Thoracic and abdominal aortic dissection with right renal artery arising from the false lumen: Stanford type B and DeBakey type IIIB classification.

Differential diagnosis: Periarteritis/IgG4 diseases (refer to case 129)

Management: Patient to be immediately referred to the cardiothoracic surgery department for endovascular repair with TEVAR (thoracic endovascular aortic repair).

Brief discussion about the condition: Aortic dissection results in the separation of two lumens by an intimal flap. The false lumen represents the space created by the splitting of the aortic wall; the true lumen represents the native aortic lumen. **Angiographic Features:** Key diagnostic finding is the intimal flap. Intimal flap or false and true lumens are detectable in 85–90%. Delayed opacification of false lumen, compression of true lumen by false lumen, occlusion of branch vessels, soft tissue companion shadow adjacent aorta (hematoma, thrombosed false lumen) are seen. Abnormal catheter position, inability to opacify the true lumen (catheter in false lumen) may be present. False lumen is located anterolateral in ascending aorta and posterolateral in descending aorta. **CT features:** Same hallmark findings as angiography—intimal flap and two lumens (true and false lumen). CT is more accurate in detection of: 1) Thrombosed false channels, 2) Periaortic hematoma and 3) Pericardial/pleural blood. CT is not accurate in evaluation of coronary arteries or great vessels, aortic valve, entry or exit sites. Dynamic contrast—enhanced helical CT is the technique of choice. Pre-contrast scan (to detect wall hematoma), dynamic contrast-enhanced helical CT (to detect intimal flap) and delayed contrast-enhanced helical CT (occasionally needed). **Role of CT:** Triage patients with equivocal clinical findings and surveillance of chronic dissections. **MRI features:** Conventional spin echo is excellent for detecting intimal flaps and wall hematoma. Phase-contrast gradient echo detects differential flow velocities in true and false lumens. Cine MR sequences allow detection of aortic insufficiency.

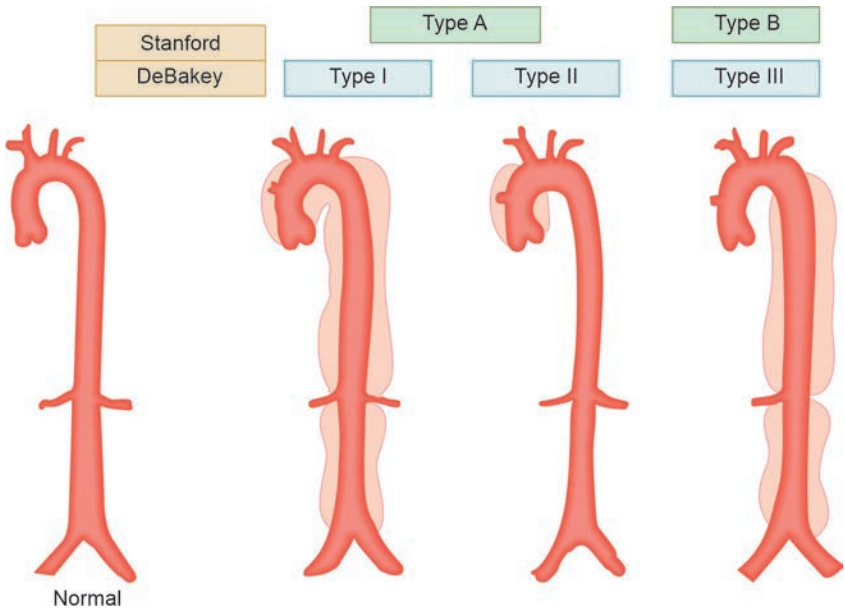


Fig. 4.127.21: Aortic dissection classification

Treatment options in aortic dissection: Stanford type A dissections are treated surgically via sternotomy with the objective of reconstructing the aortic true lumen and preventing further expansion of the false lumen, often requiring aortic reconstruction with a prosthetic graft. Surgical intervention is extensive and may require coronary artery re-implantation and restoration of aortic valve competence with intra-operative utilization of hypothermic circulatory arrest and cardiopulmonary bypass. Adjunctive endovascular techniques have been employed more recently to treat type A dissection with introduction of branched endograft.

Endovascular interventions have also been used for “retro-A dissections”; dissections with an entry tear distal to the left subclavian origin, in which the false lumen extends retrograde into the ascending aorta. The objective of taking this course would be to cover the primary dissection entry point to prevent further retrograde propagation or re-entry.

Medical therapy alone can often treat uncomplicated type B aortic dissections. At one year, the INSTEAD (investigation of stent grafts in aortic dissection) trial found no significant difference in mortality between patients who had medical therapy plus endovascular stent-graft insertion and those who received medical therapy. Nonetheless, for uncomplicated dissections, pre-emptive thoracic endovascular intervention [thoracic endovascular aortic repair (TEVAR)] is increasingly being employed to avoid late sequelae including aneurysmal false lumen degeneration and delayed rupture [thoracic endovascular aortic repair (TEVAR)]. For complicated type B aortic dissections, endovascular repair has become the principal modality of treatment, given the excess mortality of open repair. Placement of a stent-graft to cover the primary tear in anatomically suitable candidates maintains patency of the true lumen and in ideal cases causes depressurization and subsequent thrombosis of the false lumen. Previous indications for open surgical repair, including aneurysmal expansion, refractory pain, and malperfusion are now indications for endovascular intervention, given better expediency and safety. Mortality estimate for TEVAR recipients in cases of complicated dissection with end-organ malperfusion or rupture was 10.8% at 30 days and 29.4% at 1 year, similar to mortality rates for medically treated patients with uncomplicated dissection.



Fig. 4.127.22: Post-TEVAR follow-up CT angiogram reconstruction image

Dissection flap fenestration: Image depiction of a Rösch-Uchida needle used to traverse the dissection flap from the true to the false lumen (fenestration) with intravascular ultrasound (IVUS). The direction of the needle puncture is determined using real time IVUS guidance at the level of the needle tip, which is directed through the dissection flap, generally from the smaller true to the larger false lumen (A). After advancing the catheter over the stylet into the false lumen, the stylet is removed and a wire is placed into the false lumen (B). A 16 mm angioplasty balloon is centered across the flap and inflated to widen the fenestration and promote flow from false-to-true lumen (C), thus creating a fenestration (D). This procedure increases true lumen perfusion and perfusion pressure while incidentally promoting flow in the false lumen. The principal role of dissection flap fenestration is to help restore perfusion to branches compromised by dynamic obstruction. In certain cases, it is performed to arrest the process of retrograde false lumen thrombosis, which, if untreated, can lead to devastating visceral and spinal malperfusion through occlusion of vessels originating in part or completely from the false lumen.

4.128 CARDIOVASCULAR SYSTEM

Case No. 128

Clinical history: 65-years-old gentleman presented with complaints of chest pain.

Imaging technique and observation: Figures 4.128.1 and 4.128.2 are plain radiograph chest PA and lateral projection showing widened mediastinum prominent aortic knob and increased thickness of left aortopulmonary window with mild deviation of trachea to the right. Lateral border of descending thoracic aorta seen. No evidence of cardiomegaly. No evidence of pleural effusion. No evidence of lung consolidation. No evidence of lytic lesion in ribs and thoracic vertebra. No evidence of superior and inferior rib notching.

Plain CT chest shows vascular outpouching noted in anterior wall of arch and descending thoracic aorta with a few specks of intimal calcification.

Figure 4.128.3 is CT aortic angiogram image demonstrating saccular aneurysm in thoracic aorta just distal to the origin of left subclavian artery. Aneurysm shows large luminal thrombosis. No evidence of aortic dissection/rupture. No evidence of pleural effusion. No evidence of erosion scalloping of anterior vertebral body.

Interpretation: A: 65 years old gentleman, lesion in thoracic aorta, C: Saccular aneurysm with large luminal thrombosis, B: No evidence of aortic dissection or rupture, D: Thoracic aortic aneurysm with thrombosis. (difficult to differentiate from penetrating atherosclerotic ulcer from saccular aneurysm).

Principal diagnosis: Thoracic aortic aneurysm with thrombosis.

Treatment of thoracic aortic aneurysm:

- Mild to moderate aneurysmal dilatation can usually be treated conservatively and monitored.

- When the diameter reaches 5–6 cm intervention is usually considered as the risk of rupture is significantly elevated. Treatment options include: Open repair: Thoracic aortic aneurysm repair. Endovascular repair: Thoracic Endovascular Aortic Repair (TEVAR)—stent graft should be considered when an asymptomatic descending aortic TAA reaches 5.5 cm. A higher threshold (6 cm) is suggested for open repair given its greater risks. Risk of rupture of aortic aneurysm: 4–4.9 CM–0.3%/5–5.9 CM – 1.7%/>= 6 CM – 3.6%. Pre-requisites for TEVAR: Proximal neck of at least 15 to 25 mm from the origin of the left subclavian artery, Distal neck of at least 15 to 25 mm proximal to origin of the celiac artery, adequate vascular access, absence of severe tortuosity, calcification or atherosclerotic plaque in the aortic or pelvic vasculature.

Discussion: Common site of thoracic aorta aneurysm is ascending aorta (70%).

Causes of aortic aneurysms: Atherosclerosis, inflammatory/aortitis, rheumatoid arthritis (RA), ankylosing spondylitis, Takayasu arteritis, giant cell arteritis (GCA); infection, tuberculosis and syphilis, genetic syndromes, Marfan's syndrome, Ehlers–Danlos syndrome, trauma/post-surgery, drug-induced (Ciprofloxacin).

Shapes of aortic aneurysms: Saccular aneurysm, Fusiform aneurysm.

Normal size of aorta: Ascending thoracic aorta up to 5 cm, descending thoracic aorta up to 4 cm.

Abdominal aorta up to 3 cm.

The spectrum of acute aortic syndrome includes, aortic dissection, aortic intramural hematoma, penetrating atherosclerotic ulcer, aortic aneurysmal rupture, traumatic aortic injury.



Fig. 4.128.1

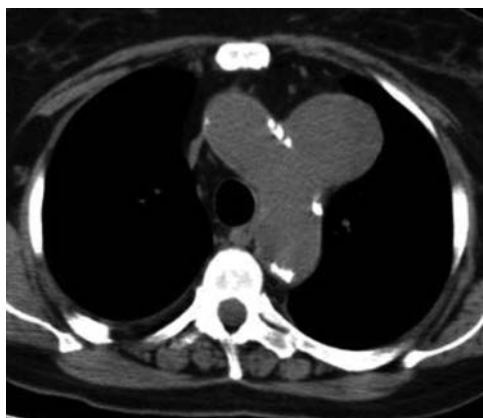


Fig. 4.128.2



Fig. 4.128.3

Table 4.128.1: Differential diagnosis for focal aortic contour bulging



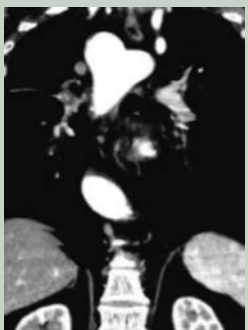
| | | |
|--|--|---|
| Penetrating atherosclerotic ulcer: Typically seen in older male patients with a history of hypertension. Common location is mid to distal thoracic aorta. | It is an ulcerating atherosclerotic lesion that penetrates the intima and progresses into the media, exposing the media to pulsatile arterial flow and subsequent haematoma formation. DSA – contrast-filled pouch like protrusion of aortic lumen. |  |
| Aortic dissection: Most common form of acute aortic syndrome. Stanford and DeBakey classification commonly used for grading systems. | Blood enters the medial layer of the aorta wall by a penetrating ulcer in the intima and tracks along the media, forming a cleavage plane (false lumen) between the inner two-thirds and outer one-third. |  |
| Aortic intramural hematoma: It is an atypical form of aortic dissection due to hemorrhage into the wall from the vasa vasorum without an intimal tear. | Crescentic thickening of the aortic wall > 7 mm. High attenuation crescent sign—focal attenuating (60–70 HU) regions of eccentrically thickened aortic wall on non-contrast CT. No intimal flap seen. | |
| Kommerell diverticulum: It mainly refers to the bulbous morphology of the origin of an aberrant left subclavian artery in the context of a right-sided aortic arch. | Barium swallow-impression can be seen from the left side of esophagus simulating a double aortic arch. CT shows bulbous enlargement of the proximal subclavian artery at its origin from the aortic arch posterior to the esophagus. Treatment: TEVAR/surgery |  |
| Aortic spindle: The proximal descending thoracic aorta has aortic spindles, which represent an anatomical variation. | It has a circumferential smooth bulging, occurring just distal to the aortic isthmus. Differential diagnoses include aortic pseudoaneurysm, ductus diverticulum, and thoracic aortic aneurysm. | |
| Traumatic aortic injury | Traumatic aortic injury can result from both penetrating and blunt chest injuries. Motor vehicles accidents are one of the main causes of TAI. | |



Fig. 4.128.7: Aortic aneurysm

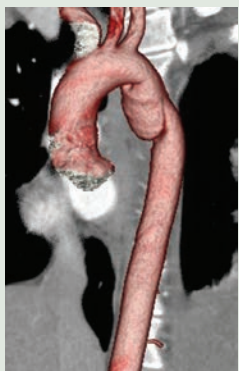


Fig. 4.128.8: Aortic arch pseudoaneurysm

Triple rule out CT angiography: This protocol includes aortic dissection, pulmonary embolism (PE), coronary artery disease (CAD).

Findings predictive of impending rupture of aortic aneurysm: Increased aneurysm size on serial imaging (rate of 10 mm or more per year). Very large abdominal aortic aneurysm >7 cm. Thrombus fissuration. Discontinuity in calcification. Hyperattenuating crescent sign—well defined peripheral crescent of increased attenuation within the thrombus of a large abdominal aortic aneurysm. Contained rupture of an aortic aneurysm. Draped aorta sign in which the posterior wall of the aorta is not seen distinctly from adjacent structures.

Traumatic aortic injury (TAI): It can result from both penetrating and blunt chest injuries. Motor vehicles accidents are one of the main causes of TAI.

Etiology: Blunt trauma—motor vehicle collisions (~70%) and crush injuries (~20%), penetrating trauma—gunshot injuries more than stabbing. Thoracic aortic injury is most common type of traumatic aortic injury and is a critical life-threatening, life ending event.

M/c Location in thoracic aorta—at aortic isthmus

M/c Location in abdominal aorta—at the level of the inferior mesenteric artery.

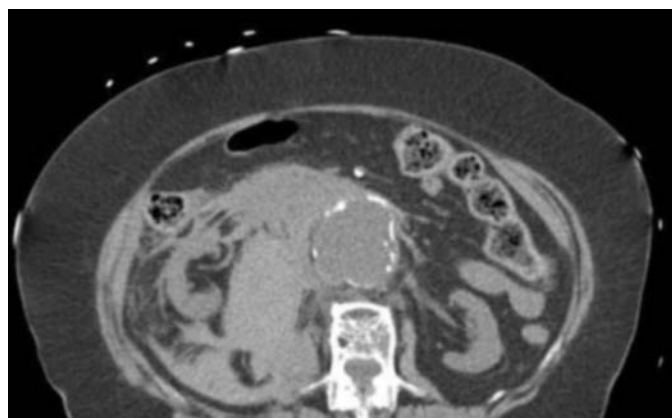


Fig. 4.128.9: Impending rupture of aortic aneurysm

Plain radiograph: Signs of mediastinal hematoma are: Widened mediastinum (more than 8 cm when supine, or more than 6 cm when upright) with thickened left apical cap, indistinct or abnormal aortic contour, deviation of trachea or NGT to the right, loss of the aortopulmonary window, widened paraspinal stripe and paratracheal stripe.

CT aortogram: Investigation of choice, direct signs are intraluminal filling defect (intimal flap or clot) and abnormal aortic contour (mural hematoma).

Table 4.128.2: Presley Trauma Center: CT grading for traumatic aortic injury (TAI)

| Grade | Subgrade | CT Findings |
|--|----------|---|
| Grade I Normal aorta Treatment: Non-operative | Ia | Normal thoracic aorta No mediastinal hematoma |
| | Ib | Normal thoracic aorta Mediastinal hematoma (para-aortic) |
| Grade II Minimal aortic injury Treatment: Delayed repair | IIa | Small <1 cm pseudoaneurysm Intermediate <1 cm intimal flap or thrombus No mediastinal hematoma |
| | IIb | Small <1 cm pseudoaneurysm Intermediate <1 cm intimal flap or thrombus Mediastinal hematoma (para-aortic) |
| Grade III Confined thoracic aortic injury Treatment: Urgent repair (aortic stent graft or open repair) | IIIa | >1 cm regular well-defined pseudoaneurysm Intimal flap or thrombus No ascending aorta, arch or great vessel involvement Mediastinal hematoma |
| | IIIb | >1 cm regular well-defined pseudoaneurysm Intimal flap or thrombus Ascending aorta, arch or great vessel involvement Mediastinal hematoma |
| Grade IV Total aortic disruption Treatment: Urgent repair | IV | Irregular poorly-defined pseudoaneurysm Intimal flap or thrombus Mediastinal hematoma |

4.129 CARDIOVASCULAR SYSTEM

Case No. 129

Clinical history: A 20 years old female presented with the complaints of bilateral upper limb pain aggravated during work. On examination there was feeble bilateral upper limb pulse. History of fever—low grade in nature not associated with chills and rigors. Hypertension with elevated ESR is also seen.

Radiological techniques and observations: Figures 4.129.1 to 4.129.3 are ultrasonography with four-vessel Doppler study of the neck showing long, smooth,

homogeneous and circumferential echogenic thickening of the right common carotid artery wall with 30–40% luminal narrowing. On transverse section, this finding is termed the macaroni sign. No evidence of post acoustic shadowing, No evidence of eccentric soft tissue plaque. Doppler study of left CCA and left vertebral artery shows reversal of flow in left vertebral artery. The flow in left proximal subclavian artery could not be assessed.

Figures 4.129.4 to 4.129.8 are CT cross-sectional imaging and CT angiogram images showing smooth circumferential wall thickening in the right CCA which

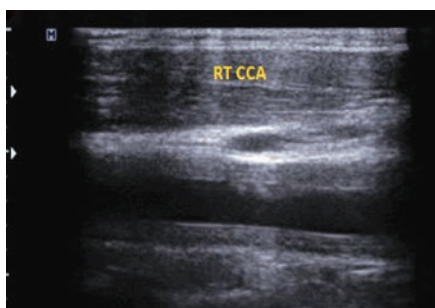


Fig. 4.129.1



Fig. 4.129.2



Fig. 4.129.3

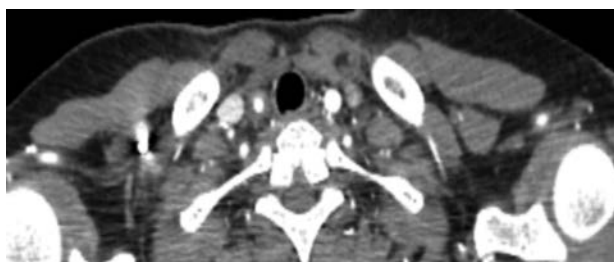


Fig. 4.129.4



Fig. 4.129.5

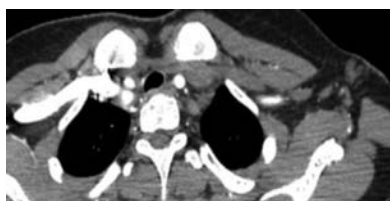


Fig. 4.129.6

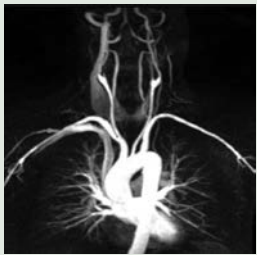
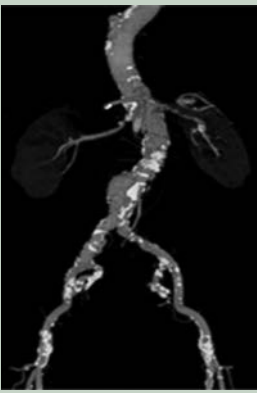
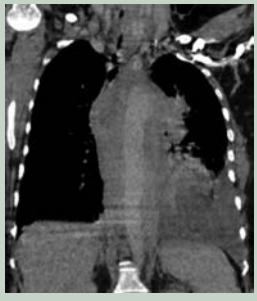
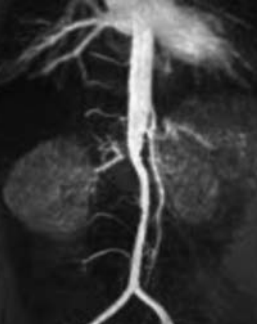


Fig. 4.129.7



Fig. 4.129.8

Table 4.129.1: Differential diagnosis for Takayasu arteritis

| | | |
|---|--|--|
| <p>Giant cell arteritis</p> <p>Giant cell arteritis has a similar aetiology and imaging features to TA; however, persons above 50 years are at high risk to develop giant cell arteritis. The external and internal carotid arteries are the most commonly affected in giant cell arteritis.</p> | <p>USG: Increased diameter of the superficial temporal artery and hypoechoic wall thickening (halo sign).</p> <p>CT: Wall thickening, calcification.</p> <p>Angio: Aneurysm, occlusion.</p> |  <p>Fig. 4.129.9: Giant cell arteritis</p> |
| <p>Atherosclerotic plaques: They are more common above 45 years.</p> <p>Three patterns are observed:</p> <ol style="list-style-type: none"> Atherosclerosis: Large and medium-sized arteries. Mönckeberg medial calcific sclerosis: Muscular arteries. Arteriolosclerosis: Small arteries and arterioles | <p>Atheromatous plaque, discontinuous wall thickening with calcifications</p> <p>Involves large and medium-sized arteries more frequently.</p> <p>Complications: Atheromatous ulcer, dissection, intra-mural hematoma, occlusion of the lumen.</p> <p>Some TA patients have calcification in the ascending aorta, but it is uncommon in atherosclerosis.</p> |  <p>Fig. 4.129.10: Atherosclerotic plaques</p>  <p>Fig. 4.129.11: Atherosclerotic plaques</p> |
| <p>Polyarteritis nodosa is more common in people 30–50 years old, and it affects males more than females. It also affects patients with hepatitis B more frequently. The principal sites of disease are the gastrointestinal and renal arteries.</p> | <p>CT angiography images show the splenic, superior mesenteric and bilateral renal arteries are all affected, while the aorta is disease free. Multiple small aneurysm formation in the involved vessels can be observed.</p> | |
| <p>Midaortic syndrome is a rare condition that affects children and teenagers. The abdominal aorta and its primary branches progressively over time, leading to aortic stenosis.</p> <ul style="list-style-type: none"> High blood pressure (most common) Claudication that comes and goes Failure of the kidneys | <p>Any region of the abdominal aorta can be observed on CT angiography, but the interrenal segment, which includes the beginnings of the renal arteries, is always constricted. Swollen splanchnic collaterals (e.g. inferior mesenteric artery, Riolo's arc, Drummond's marginal artery) are common. The aorta and the iliac arteries bifurcation areas are not affected.</p> |  <p>Fig. 4.129.12: Midaortic syndrome</p> |

Contd.

Table 4.129.1: Differential diagnosis for Takayasu arteritis (Contd.)

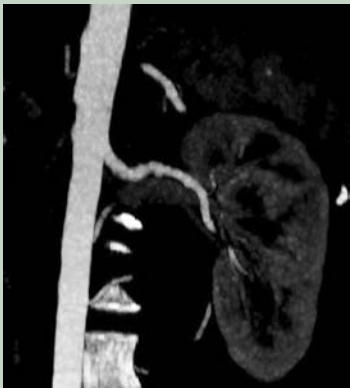
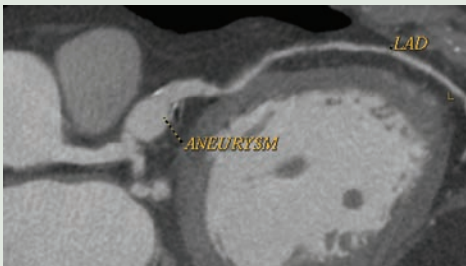
| | | |
|---|--|--|
| <p>Fibromuscular dysplasia: It is characterized by an idiopathic, non-inflammatory, and non-atherosclerotic angiopathy of small and medium-sized arteries. Most common in young women between the age of 30–50 years. Renal artery is the most common location, next common is extra cranial internal carotid and vertebral arteries.</p> | <p>DSA is the gold standard. Symptomatic cases respond well to angioplasty. The characteristic finding is alternating stenoses and dilatations, causing a string of beads appearance seen in medial type. There is focal concentric, long-segment tubular stenosis or diverticular outpouching present in intimal and adventitial type. Cross-sectional imaging (CT and MRI) allows assessment of end-organ ischemic damage.</p> |  <p>Fig. 4.129.13: Fibromuscular dysplasia</p> |
| <p>IgG4 diseases/periaortitis</p> <p>IgG4-related disease can impact the cardiovascular system, particularly the coronary arteries and pericardium, as well as the walls of large and medium-sized vessels including the aorta and subclavian artery. The vessel wall thickening on CT scans is uniformly improved.</p> <p>T1: hypo/T2: Hyperintense on MRI, and T1+C (Gd) on T1+C (Gd) exhibits intense vessel wall enhancement.</p> <p>FDG: FDG uptake is abnormally high in some areas of the PET/CT fusion image, indicating active inflammation. PET is a powerful tool for determining the metabolic activity of a mass and identifying other areas of inflammation. Inflammatory processes can be visualised with combined PET/CT, which can assist identify IgG4-related CVD from atherosclerosis.</p> |  <p>Fig. 4.129.14: Kawasaki disease with left anterior descending artery aneurysm</p> | |

Table 4.129.2: Approach to vasculitis

| | | |
|-------------------------------|--|---|
| Aorta | Wall thickening and enhancement | IgG4 related Periaortitis, Takayasu arteritis (active stage), giant cell arteritis (active stage), Cogan syndrome |
| | Aneurysm | Behçet's disease, Takayasu arteritis, Giant cell arteritis |
| | Stenosis | Chronic stage of aortitis |
| Temporal artery | Giant cell arteritis | |
| Coronary artery | Kawasaki, IgG4 related periaortitis, Takayasu arteritis, eosinophilic polyangiitis | |
| Coeliac, SMA and renal artery | Polyarteritis nodosa | |
| | Fibromuscular dysplasia segmental arterial mediolysis | |

is causing 75% luminal narrowing. No evidence of calcification.

There is concentric wall thickening involving arch of aorta and left subclavian artery at its origin. Left subclavian artery shows complete occlusion for a length of 22 mm. Left vertebral artery is reformed through circle of Willis from right vertebral artery indicating

steal phenomenon. There is concentric wall thickening involving descending thoracic aorta causing 50% luminal narrowing.

There is concentric wall thickening involving abdominal aorta at the level of renal artery and extends till the L2 level. Left renal artery is not visualized from the ostium for a length of 7 mm—complete occlusion.

Table 4.129.3: 2012 International Chapel Hill consensus conference update

| | |
|--|---|
| Large vessel vasculitis <ul style="list-style-type: none"> • Takayasu arteritis • Giant cell arteritis | Medium vessel vasculitis <ul style="list-style-type: none"> • Polyarteritis nodosa • Kawasaki disease |
| Small vessel vasculitis <ul style="list-style-type: none"> • Anti-neutrophil cytoplasmic antibody (ANCA)-associated vasculitis • Microscopic polyangiitis • Granulomatosis with polyangitis (eosinophilic granulomatosis with polyangiitis (formerly Churg-Strauss syndrome) | Immune-complex small vessel vasculitis <ul style="list-style-type: none"> • Anti-glomerular-basement-membrane (anti-GBM) disease • Cryoglobulinemic vasculitis • IgA vasculitis (formerly Henoch-Schönlein purpura) • Hypocomplementemic urticarial vasculitis (anti-C1q vasculitis) |
| Variable vessel vasculitis <ul style="list-style-type: none"> • Behçet's disease • Cogan syndrome | Vasculitis associated with systemic disease <ul style="list-style-type: none"> • Lupus vasculitis • Rheumatoid vasculitis • Sarcoid vasculitis |

Table 4.129.4: Difference between Mönckeberg medial sclerosis and atherosclerosis

| | |
|--|--|
| <i>Mönckeberg medial sclerosis (medial calcification)</i> | <i>Atherosclerosis (intimal calcification)</i> |
| Occurs in territorial branches | Occurs in systemic arteries |
| Early calcification | Slow and late calcification |
| Not associated with inflammation | Associated with inflammatory process |
| On USG the circumferential calcification gives string of bead appearance | Calcification may be eccentric/circumferential/discontinuous |
| No evidence of luminal narrowing | Echogenic plaque noted to occlude the lumen |

Interpretation: A—young female, lesion in aorta and its branches, C—smooth circumferential thickening of aortic arch and its branches, descending aorta, abdominal aorta, B—stenosis of abdominal and thoracic aorta, left subclavian artery, right CCA and bilateral renal arteries D—Takayasu arteritis.

**Fig. 4.129.15:** Mönckeberg medial sclerosis

Principal diagnosis: Takayasu arteritis type V (Numano's new angiographic classification)

Mönckeberg's vascular sclerosis: It is a rare and low prevalence disease of unknown cause in which small and medium size arteries suffer calcification of the media layer. Primary damage to elastic fibres which occurs in medial calcification; leads to accumulation of hydroxy apatite crystals.

Further management: With a remission rate of up to 60%, corticosteroids have been regarded the mainstay of treatment for TA. Balloon angioplasty and stenting/ bypass surgery is the most prevalent palliative treatment for patients with symptomatic stenotic or occlusive lesions. Aneurysmal enlargement with a danger of rupture, stenotic or occlusive lesions leading to critical organ ischaemia, and uncontrolled hypertension due to renal artery stenosis are all surgical indications. Because of the high rate of restenosis, interventional management is generally not suggested until clinical remission has been reached.

Short localised stenotic lesions without activated inflammation are thought to have good outcomes after interventional treatment. Long-term follow-up with CTA or MRA should be commenced following surgery or percutaneous angioplasty with or without endovascular

stenting to monitor the patency and complications of diseased arteries, stents, or bypass vessels.

Numano's new angiographic classification of Takayasu arteritis.

Type I—affects only the branches of the aortic arch.

Type IIa—affects ascending aorta, aortic arch and its branches.

Type IIb—affects ascending aorta, aortic arch and its branches, and thoracic descending aorta.

Type III—affects the descending thoracic aorta, the abdominal aorta and/or the renal arteries. The ascending aorta, the aortic arch and its branches are not affected.

Type IV—affects only the abdominal aorta and/or renal arteries.

Type V—combined features of type IIb and IV.

Sharma Criteria for Diagnosis of Takayasu Arteritis

Major criteria: Left and right mid-subclavian artery lesion, characteristic signs and symptoms of at least one month duration. **Minor criteria:** A high rate of erythrocyte sedimentation, tenderness in the carotid artery, hypertension, aortic regurgitation/annuloaortic ectasis, stenosis of the pulmonary artery, lesion of the left mid-common carotid artery, lesion of the distal brachiocephalic trunk, lesion of the descending thoracic aorta, lesion of the abdominal aorta, and lesion of

the coronary artery. Presence of either one of 2 major criteria; 1 major criterion and 2 minor criteria; or 4 minor criteria—indicates high risk for TA.

Marked intimal proliferation and fibrosis lead to occlusion and narrowing of aorta and involved arteries; Aneurysms may also be found. Age: 90% <30 years (in distinction to all other arteritis types). More common in females.

Imaging: Smooth long-segment stenoses of arch vessels (most common), stenosis and occlusion of aorta (may mimic coarctation), thickening of aortic wall, pulmonary artery involvement, 50% abdominal coarctation and proximal renal artery stenoses. Only minor calcification is seen.

Relation between SAPHO Syndrome and Takayasu Arteritis

Synovitis-acne-pustulosis-hyperostosis-osteitis (SAPHO) syndrome is characterized by cutaneous and osteoarticular manifestations. SAPHO predominantly in the adult population and CRMO in the pediatric population. CRMO involves the extremities more commonly while SAPHO syndrome involves the axial skeleton with major focus on the costo-sternoclavicular region. Most common skin lesions in SAPHO include palmoplantar pustulosis and severe acne. Plain



Fig. 4.129.16: SAPHO syndrome, X-ray of the pelvis showed an ill-defined lytic area with surrounding dense sclerosis involving the right greater trochanter with extension into the inter-trochanteric region and the adjacent neck of femur

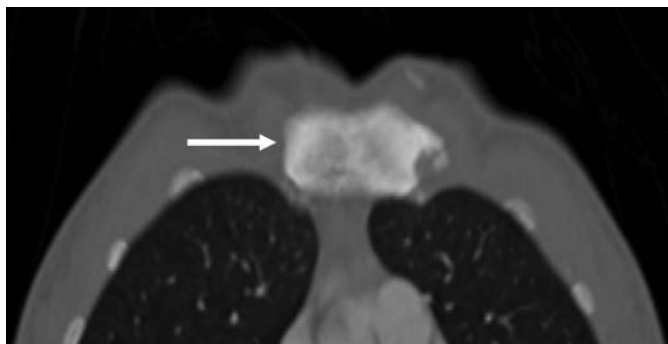


Fig. 4.129.17: SAPHO syndrome, CT chest showed an ill-defined lytic area with surrounding dense sclerosis involving the sternum



Fig. 4.129.18: SAPHO syndrome, CT lumbar spine showed multiple ill-defined lytic areas with surrounding dense sclerosis involving lumbar vertebral bodies

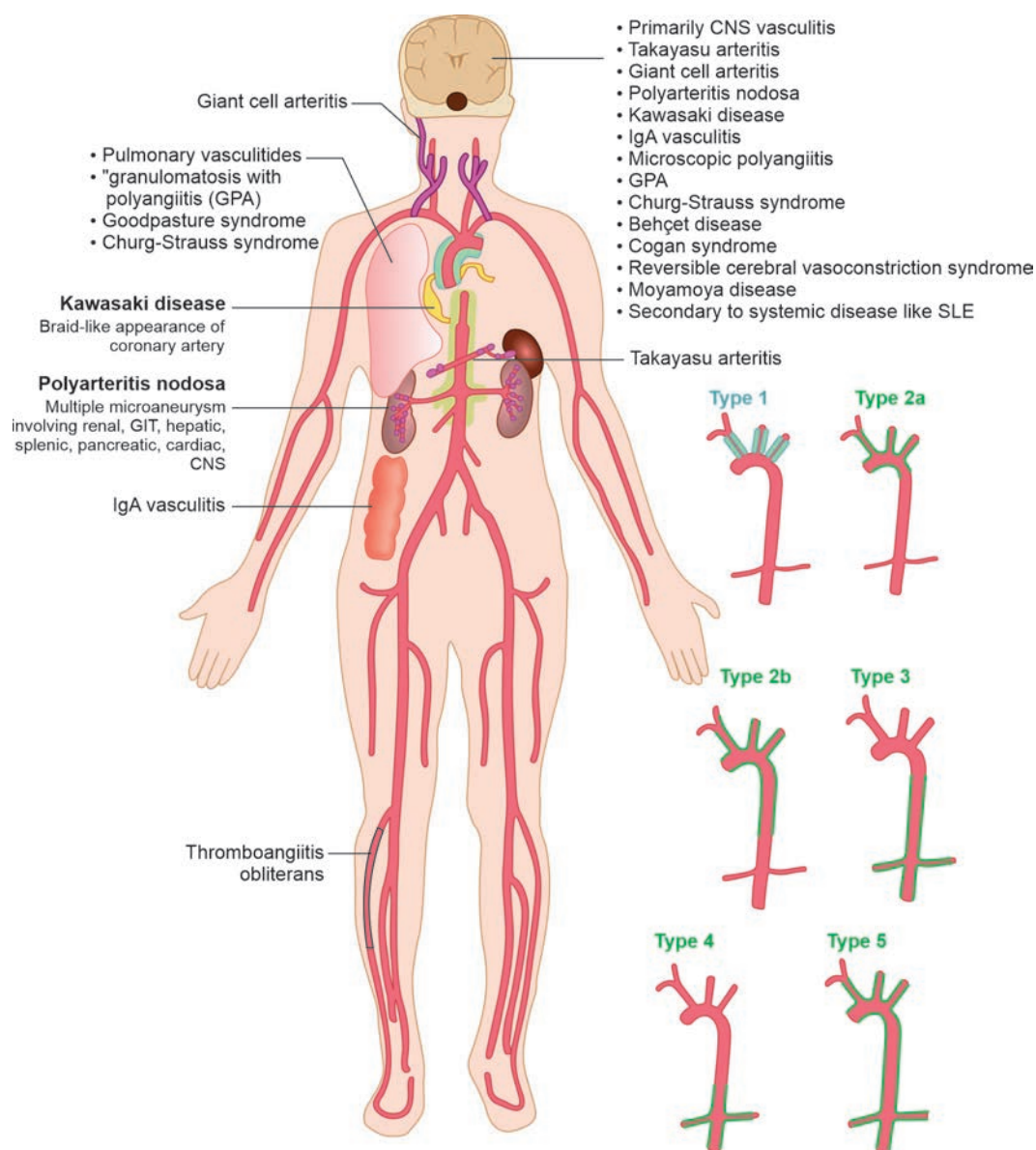


Fig. 4.129.19: Various arteritis and their sites

radiography shows expanded bone with sclerosis, osteolysis, periosteal reaction, hyperostosis and osteitis. Joint arthritis with decreased joint space and erosions are common. Paravertebral ossification, sacroilitis are also seen involving the vertebral column. Benhamou diagnostic criteria help in the diagnosis of SAPHO syndrome. It involves at least one of the 4 inclusion criteria and all of the exclusion criteria.

Inclusion criteria: Severe acne, palmo-plantar pustulosis, hyperostosis with or without dermatosis.

Exclusion criteria: Septic osteomyelitis, infectious chest wall arthritis, infectious palmoplantar pustulosis, palmoplantar keratoderma, diffuse idiopathic skeletal

hyperostosis, osteoarticular manifestations of retinoid therapy.

There are very few case reports depicting the association of SAPHO syndrome in middle aged women with Takayasu arteritis. The time interval between the SAPHO syndrome and the onset of Takayasu arteritis has been variable with duration ranging between 8 months to 12 years. Our patient had a time interval of 5 months. Treatment options include NSAIDs, antimicrobials (azithromycin, doxycycline, sulfamethoxazole/trimethoprim, clindamycin), anti-rheumatic drugs (colchicine, corticosteroids, biphosphonates) and disease-modifying agents (methotrexate, sulfasalazine, infliximab).

4.130 CARDIOVASCULAR SYSTEM

Case No. 130

Clinical history: 40-year-old male smoker with history of bilateral lower limb claudication (right > left)

Radiological techniques and observations: Figures 4.130.1 to 4.130.3, colour Doppler imaging with spectral waveforms of right common iliac artery, right posterior tibial artery and left posterior tibial artery respectively. Right common iliac artery shows normal flow with normal triphasic wave pattern. Right posterior tibial artery shows flow with biphasic pattern (parvus tardus appearance). Left PTA shows very minimal flow with monophasic wavepattern. Vessel wall appears to be normal. No evidence of any collections or calcifications in visualized field. Further imaging with CT angiography is done.

Figures 4.130.4 to 4.130.6 are CT angiogram limited axial section and coronal section at level of bilateral thigh and MIP images revealing occlusion of bilateral superficial femoral artery. Multiple dilated corkscrew collaterals are noted in right thigh. Further sections (not provided) revealed complete occlusion of bilateral profunda femoris, partial occlusion of left popliteal artery and complete occlusion of right popliteal artery.

Bilateral anterior tibial artery and posterior tibial artery were thinned out and reformed by muscular arteries with intermittent flow. Bilateral peroneal artery and dorsal pedis artery showed thin intermittent flow. CT angiogram MIP images confirm the diagnosis. There is no evidence of any soft tissue collection/hematoma. Visualised bone appears to be normal bilaterally.

Interpretations: A: 40-year-old male smoker, peripheral arteries of bilateral lower limb, C: Multilevel occlusions, B: Multiple dilated corkscrew collaterals, D: TAO with vascular occlusion.

Principal Diagnosis: Thromboangiitis Obliterans with Vascular Occlusion

Differential diagnosis

1. Atherosclerosis—commonly seen in old age (>45 years). No evidence of any superficial thrombophlebitis. Hypertension and coronary artery disease will be common association. Large vessels are involved.
2. Thromboangiitis obliterans—age group <45 years and strong association with smoking. There will be associated superficial thrombophlebitis. Hypertension and coronary artery disease will be uncommon.

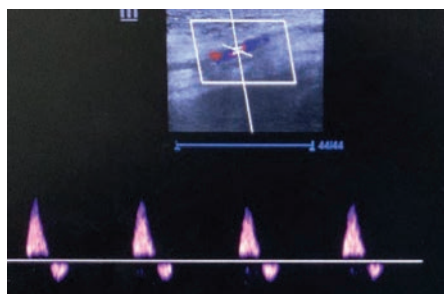


Fig. 4.130.1: Right common iliac artery

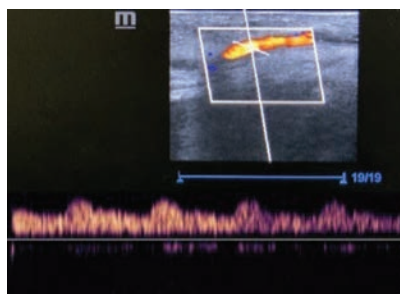


Fig. 4.130.2: Right posterior tibial artery

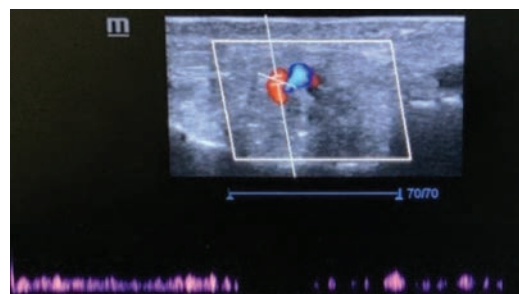


Fig. 4.130.3: Left posterior tibial artery

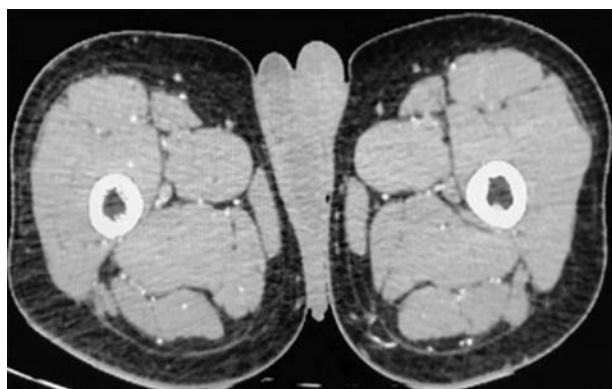


Fig. 4.130.4



Fig. 4.130.5

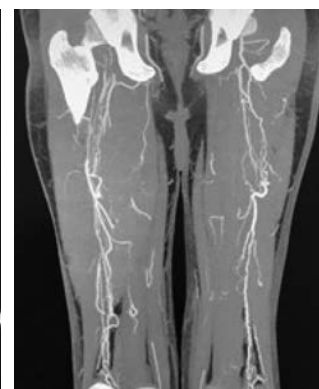


Fig. 4.130.6

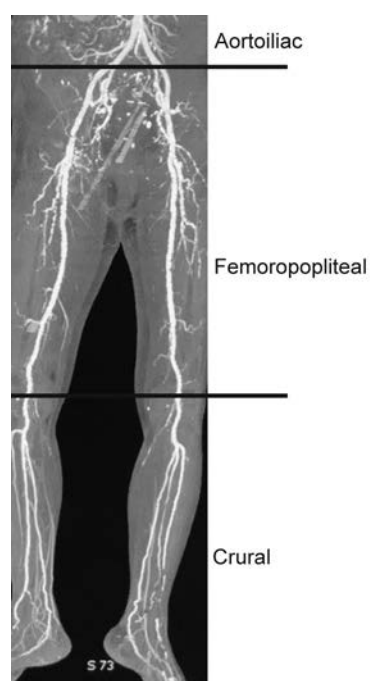


Fig. 4.130.7: Level of peripheral arterial disease into 3 categories

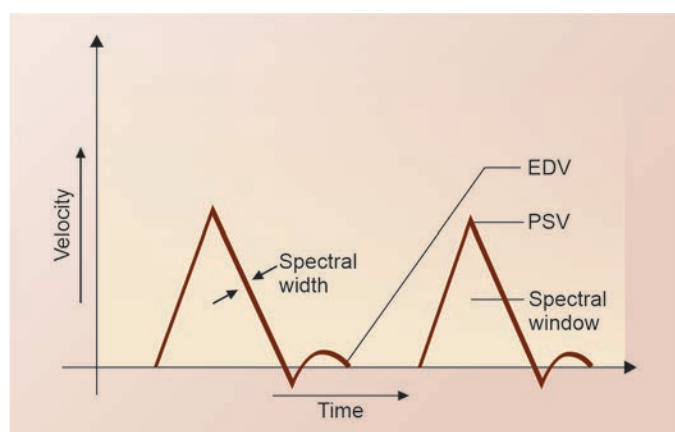


Fig. 4.130.8: Normal triphasic flow

Disease is infrapopliteal/infrabronchial. Medium and small sized vessels are involved.

3. Vasculitis—inflammation of blood vessels and ischaemia to organs supplied by it. Most common vasculitis affecting lower limb is giant cell arteritis (GCA) and Takayasu arteritis. It is imperative that GCA can be considered in differential diagnosis of unexplained lower extremity claudication, especially in patients with a few risk factors for atherosclerotic disease.

Brief discussion about the condition: Thromboangiitis obliterans: It is a segmental progressive non-atherosclerotic inflammatory disease of medium and

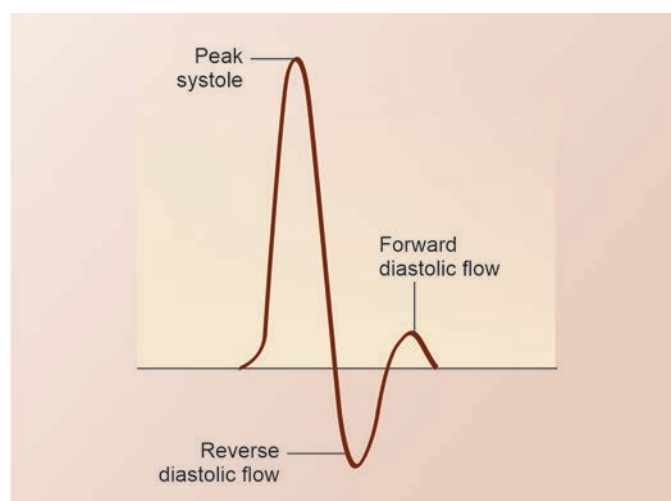


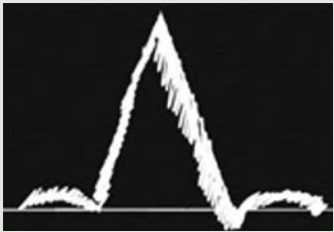

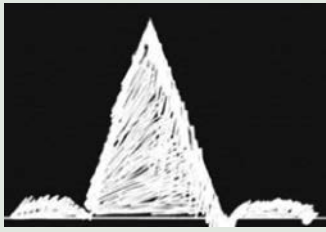

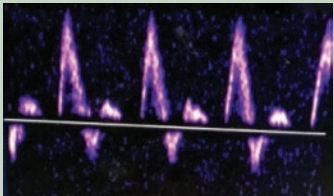
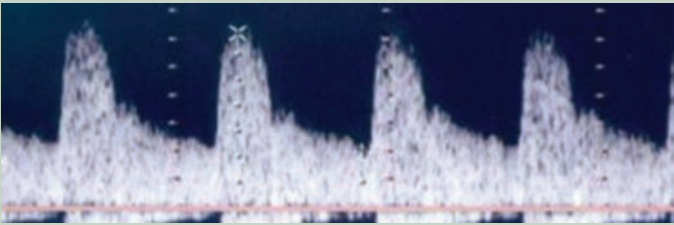
Fig. 4.130.9: Normal triphasic flow pattern

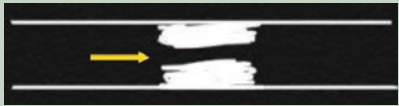
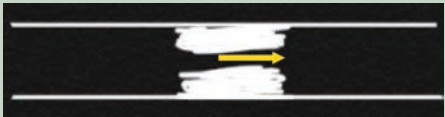
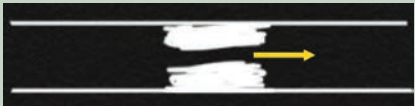
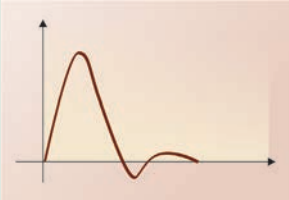
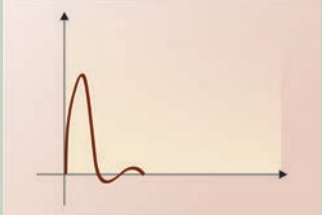
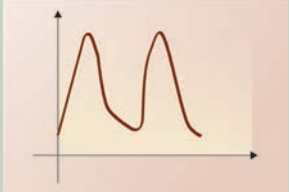
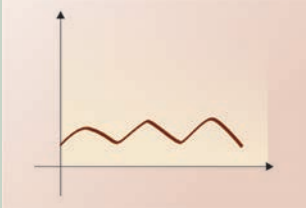
small-sized vessels with superficial thrombophlebitis which is more common in lower limbs than upper limbs. Most commonly seen in young/middle aged males with history of smoking and tobacco usage. Risk factors include:

1. Smoking
2. Hormonal influence/familial factors.
3. Hypersensitivity to cigarette
4. Altered autonomic functions
5. Lower socioeconomic group
6. Recurrent minor feet injury

Pathogenesis of the condition: Smoke (carbon monoxide and nicotinic acid)—vasospasm and hyperplasia of intima—thrombosis of vessels—obliteration of vessels—segmental panarteritis. Small and medium sized vessels (plantar, tibial, radial) are most commonly involved. Artery vein and nerve are involved together. Nerve involvement due to blockage of vasa nervosa causes rest pain. Arterial involvement leads to claudication pain. If collaterals (typically corkscrew collaterals) are developed that maintains flow to ischaemic area, it is known as compensatory peripheral vascular disease. If collaterals are also blocked due to smoking, then it is called decompensatory peripheral vascular disease or critical limb ischaemia. Here arterial lumen is blocked, but wall is not thickened as in case of atherosclerosis. Clinical features include claudication pain, rest pain and ulcerations with gangrene. It may also present as Raynaud's phenomenon.

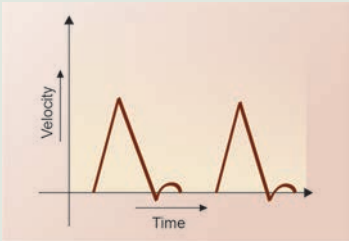
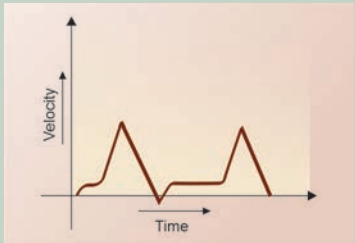
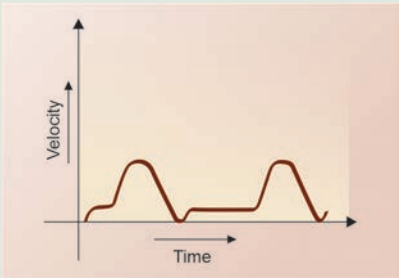
In PAD (peripheral arterial disease), the level of the lesion is grouped into three categories: 1. Aortoiliac, 2. Femoropopliteal and 3. Crural (tibiopedal). The infrarenal portion of the abdominal aorta, common iliac arteries, internal iliac arteries, and external iliac arteries,

| Table 4.130.1: Spectral waveform changes with arterial occlusion | | | |
|--|--|--|---|
| Normal artery | Mild occlusion | Moderate occlusion | Severe occlusion |
| Normal triphasic waveform with clear spectral window | Spectral widening/spectral broadening—increase in spectral width | Spectral filling-in. Filling-in of normal spectral window | Poor definition of spectral borders with forward and reverse flow above and below base line |
|  |  |  |  |
| Fig. 4.130.10: Spectrum in normal artery pattern | Fig. 4.130.11: Spectrum in mild to moderate narrowing | Fig. 4.130.12: Spectrum in moderate narrowing | Fig. 4.130.13: Spectrum in severe occlusion |
|  |  | | |
| Fig. 4.130.14: Spectrum in normal triphasic waveform | Fig. 4.130.15: Spectral broadening and spectral filling is due to occlusive peripheral arterial disease | | |

| Table 4.130.2: Changes in waveform depending on site of examination | | |
|--|--|---|
| Prestenotic | Stenotic | Poststenotic |
|  |  |  |
| Fig. 4.130.16: Prestenotic | Fig. 4.130.17: Stenotic | Fig. 4.130.18: Poststenotic |
|  | | |
| Fig. 4.130.19: Normal | | |
|  |  |  |
| Fig. 4.130.20: Narrow systolic peak | Fig. 4.130.21: Raised PSV and EDV | Fig. 4.130.22: Parvus tardus waveform |

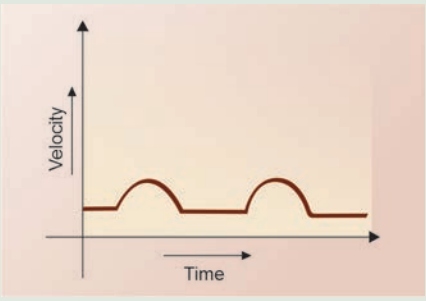
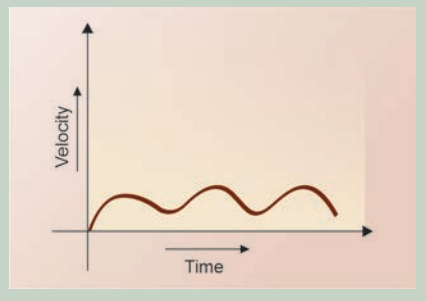
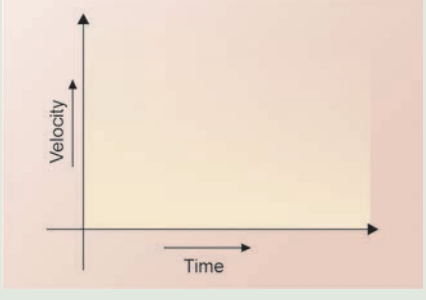
Contd.

| Table 4.130.2: Changes in waveform depending on site of examination (Contd.) | | |
|---|--|--|
| Prestenotic | Stenotic | Poststenotic |
| Proximal to the lesion normal flow pattern can be seen in many cases (stenosis <50%). In other cases (stenosis>50%) high resistance waveform with narrow systolic peak (since forward flow occur for a very short period) and very little diastolic flow. | Peak systolic velocity (PSV) is elevated. End diastolic volume (EDV) also increases proportionally with degree of stenosis. Peak systolic velocity is the first measurement to become abnormal. PSV, EDV and systolic–diastolic ratio are important parameters. PSV at stenosis divided by PSV proximal to stenosis >2 when combined with spectral broadening or filling in corresponds to >50% luminal narrowing. | Normal waveform is seen if stenosis is less than 50%, if more than 50%, flow is dampened with decreased flow volumes and decreased velocities due to proximal obstruction. Slowed systolic acceleration, taking longer time to reach peak, small systolic amplitude and rounding of systolic peak–parvus tardus pattern. Reason for this waveform is vasodilatation distal to occlusion, and reduced resistance. |
| PSV—decreased or normal | PSV—increased | PSV—decreased |
| EDV—slightly decreased or normal | EDV—increased | EDV—decreased |

| Table 4.130.3: Changes in waveform with severity of occlusion in post-stenotic site | | |
|---|--|---|
| Normal lumen | Normal triphasic waveform with normal spectral window. EDV—zero |  Fig. 4.130.23: Waveform pattern in normal lumen |
| Mild to moderate narrowing | Raised EDV with preserved diastolic reversal. Decreased velocity, widening of systolic complex, dampened waveform, spectral broadening and spectral filling. |  Fig. 4.130.24: Waveform pattern in mild to moderate narrowing |
| Moderate to severe narrowing | Raised EDV with absent diastolic reversal. Decreased velocity, widening of systolic complex, dampened waveform, spectral broadening and spectral filling. |  Fig. 4.130.25: Waveform pattern in moderate to severe narrowing |

Contd.

Table 4.130.3: Changes in waveform with severity of occlusion in post-stenotic site (Contd.)

| | | |
|-------------------------|---|---|
| Tight stenosis | Contiguous diastolic flow. Decreased velocity, widening of systolic complex, dampened waveform, spectral broadening and spectral filling. |  <p>Fig. 4.130.26: Waveform pattern in tight stenosis</p> |
| Near complete occlusion | Parvus tardus pattern. Decreased velocity, widening of systolic complex, dampened waveform, spectral broadening and spectral filling. |  <p>Fig. 4.130.27: Waveform pattern in near complete occlusion</p> |
| Complete occlusion | No evidence of flow |  <p>Fig. 4.130.28: Waveform pattern in complete occlusion</p> |

all proximal to the inguinal ligament or deep circumflex iliac artery, are all affected by aortoiliac illness. The common femoral arteries, profunda femoral arteries and superficial femoral arteries all become popliteal arteries as they reach the adductor canal and stop at the origin of the anterior tibial arteries in femoropopliteal disease. The anterior tibial, posterior tibial, peroneal, dorsalis pedis, and plantar arteries are all affected by crural disease. Plaques tends to form at bifurcation or bends associated with repetitive external stress. Most common site is popliteal trifurcation > femoral bifurcation. Infrarenal abdominal aorta, iliac bifurcations, carotid bifurcations, superficial femoral arteries as they exit hunters canal and ostia of coronary, renal and mesenteric arteries are all common sites of plaque formation.

Doppler waveform: Doppler spectra is a time velocity waveform that represents intravascular blood flow velocities during cardiac cycle. Time is represented along horizontal axis and velocity along vertical axis. Normal peripheral arterial waveform has three, four or occasionally five components. First there is rise in acceleration and pressure of blood flow at onset of systole. Then there is a short period of reversal as pressure wave is reflected from constricted distal arterioles. This is followed by further short forward flow due to elastic compliance of main arteries in diastole and Intensity or brightness of spectral waveform represents number of red blood cells that are reflecting ultrasound beam at beach velocity. Width of spectral line (spectral width) represents range of velocities within the vessel. Normal

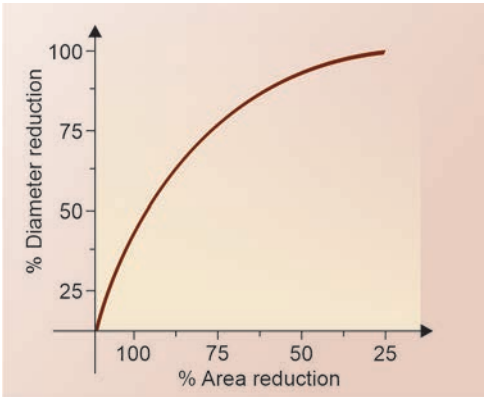


Fig. 4.130.29: Relationship between diameter stenosis and area stenosis

black zone between spectral line and zero velocity base line is called spectral window. PSV–peak systolic velocity and EDV–end diastolic velocity.

As occlusion progresses, post-stenotic resistance decreases due to vasodilatation leading to above mentioned type of Doppler waveforms. In case of IUGR uterine artery normal waveform (low resistance) shifts to high resistance waveform as grading of IUGR progresses. This leads to reversal of appearance of waves seen in peripheral arterial occlusion (normal uterine artery—low resistance flow corresponding to post-stenotic arterial waveform in severe occlusion to IUGR—high resistance flow corresponding to normal peripheral arterial triphasic pattern) (Table 4.130.4).

Relationship between diameter stenosis and area stenosis: Degree of area reduction $\pi r^2(\pi(3.14) \times \text{radius square})$ is greater than area of diameter reduction unless there is either no stenosis or 100% stenosis. This is given by the equation.

Penile Doppler: Procedure—high frequency probe is used. Patient is placed in supine position, penis positioned in anatomic position along anterior abdominal wall. Drugs: 60 mg papaverine is injected intracavernosally. Another alternative is 10–15 µg of prostaglandin E1 or

phentolamine. Insulin syringe is used to inject the drug into lateral aspect of midshaft of penis.

Measurements: Major parameters include peak systolic velocity and end diastolic velocity pre-injection and post injection. Other minor parameters include diameter of cavernosal artery, flow signals of deep dorsal vein. Normal peak systolic velocity of cavernosal artery post injection must be more than 35 cm/sec and end diastolic velocity must be less than 3–5 cm/sec.

Varicocele: Incompetence or absent valves in internal testicular vein predisposed to stasis or retrograde blood flow resulting in dilatation of pampiniform plexus. This is the cause of majority of varicoceles. More commonly seen on left side due to long course of left renal vein which drains directly to left renal vein. They manifest as dilated serpiginous channels more than 2 mm (at rest) and more than 3 mm (at Valsalva) in head of epididymis and spermatic cord. There can be flow reversal/reflux with Valsalva’s manoeuvre. Grading of varicocele is as follows.

CT angiography: CTA is required the use of iodinated CM for vascular imaging. Injection rates vary per protocol, but are commonly between 4 and 6 ml/s when supplied intravenously with a dual channel power injector. The amount of iodinated media used depend on the patient and protocol followed, with an abdominal CTA with runoffs requiring 100 to 120 ml. The dose is reduced to 80 ml for people with a low BMI. When a saline chaser is administered after the CM media has been injected, the vasculature is enhanced more and the CM dose is reduced.

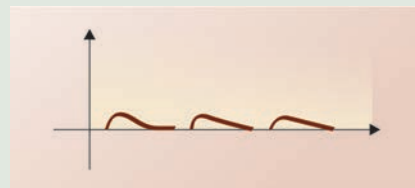
MR angiography: Vasovist, a higher relaxivity blood-pool agent, has been introduced, expanding the diagnostic armamentarium of the radiologist by providing new prospects in the field of peripheral MRA. Vasovist’s increased relaxivity and longer intravascular residence time result in better first-pass image quality and the ability to gather more steady-state MRA data.

| Table 4.130.4: Percentage of area reduction (A) = percentage of diameter reduction (D) × (2–(D/100)) | | | | | | |
|--|-----------------|-----|-----|-----|-----|----------------|
| %Diameter reduction | 0% | 25% | 50% | 75% | 90% | 100% |
| %Area reduction | Zero percentage | 44% | 75% | 94% | 99% | 100 percentage |

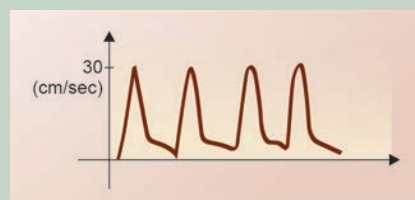
| | | | | | | |
|----------------------|------|-----|-----|-----|-----|------|
| % Diameter reduction | 0% | 25% | 50% | 75% | 90% | 100% |
| | | | | | | |
| % Area | Zero | 44% | 75% | 94% | 99% | 100 |

Table 4.130.5: Appearance of Doppler waveforms correlates with status of erection which has five stages

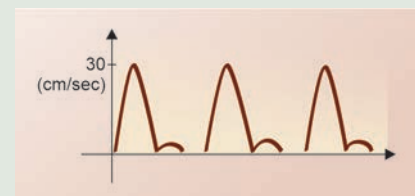
Flacid (prior to injection): Dampened systolic flow, monophasic profile with relatively small diastolic component.

**Fig. 4.130.30:** Waveform prior to injection

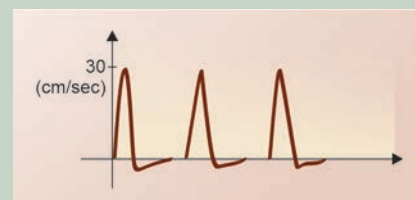
Initial latent (filling phase): Brisk increase in both diastolic and systolic flow (30 cm/sec) in cavernosal artery. Antegrade flow in both systole and diastole which reflects low resistance flow in sinusoidal spaces

**Fig. 4.130.31:** Waveform in initial latent phase

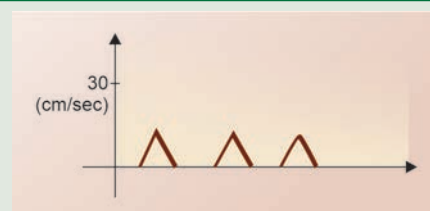
Tumescent: More blood flows to corpora cavernosa, intracavernosal pressure increases, diastolic notch appears at end systole and diastolic flow diminishes. Systolic flow remains brisk (30 cm/sec).

**Fig. 4.130.32:** Waveform in tumescent phase

Full erection: Intracavernosal pressure rises more than arterial pressure during diastole and hence diastolic reversal is observed. Maximal PSV (with narrowing of systole) occurs in normal cases at this stage. Diastolic flow reversal is reliable indicator of intact veno-occlusive mechanism or no venous leak.

**Fig. 4.130.33:** Waveform in full erection

Rigid erection: Intracavernosal pressure approximates arterial systolic pressure (reduced systolic velocity) with decrease in PSV and absence of diastolic component.

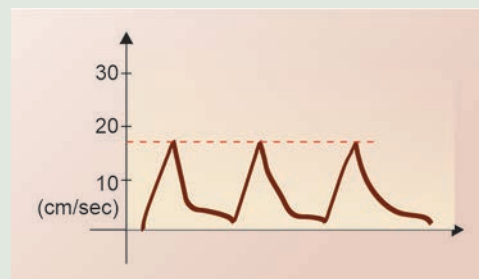
**Fig. 4.130.34:** Waveform in rigid erection**Table 4.130.6: Diagnostic criteria for erectile dysfunction**

| Doppler parameter | Diagnostic criterion |
|---|--|
| Peak systolic velocity of cavernosal artery | Indicator of arterial reflux—normal >35 cm/sec, gray zone—25–35 cm/sec and abnormal is less than 25 cm/sec. |
| End diastolic velocity of cavernosal artery | Normal is <3–5 cm/sec, venous leak is >5 cm/sec |
| Deep dorsal vein | Normal is less than 3 cm/sec, increase is >10 cm/sec. It is used as an adjuvant for venous leaks. |
| Compliance/Diameter of cavernosal artery | Normally it should increase as response to pharmacological stimulus. Minimal increase must be at least 60–75%. |

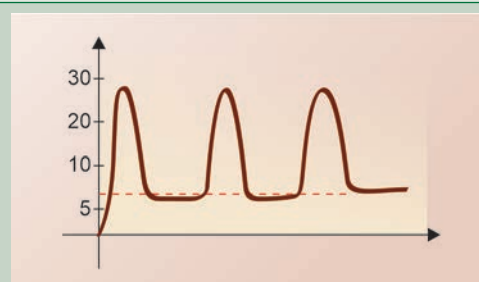
Erectile dysfunction: Vasculogenic erectile dysfunction is analysed by Doppler study. It can be either arterial or venous.

Table 4.130.7: Doppler-based types of erectile dysfunction

Arteriogenic erectile dysfunction: Impairment of arterial inflow into cavernosum due to various reasons. PSV is the most accurate indicator. Arterial ED is defined when PSV is less than 25 cm/sec. Asymmetric velocities in side–side comparison of PSV of right and left cavernosal artery is considered abnormal if difference is more than 10 cm/sec.

**Fig. 4.130.35:** Waveform in arteriogenic erectile dysfunction

Venogenic erectile dysfunction: Impaired veno-occlusive mechanism leading to venous leak. Persistent EDV more than 5 cm/sec during all phases of erection suggestive of venous ED. Patients with normal arterial inflow (PSV > 25 cm/sec) with weak erections are very likely to have venous leakage. Absence of diastolic reversal is suggestive of veno-occlusive dysfunction and venous leak. It should be emphasized that veno-occlusive diseases are diagnosed only when PSV is normal (> 25 cm/sec)

**Fig. 4.130.36:** Waveform in venogenic erectile dysfunction**Table 4.130.8: Approach to erectile dysfunction (PSV and EDV in cm/sec/DDV—deep dorsal vein/CA—cavernosal artery)**

| | <i>Normal</i> | <i>Neurogenic</i> | <i>Arterial dysfunction</i> | <i>Venous incompetence</i> | <i>Psychohenic</i> |
|------------------------------|-------------------------------------|-------------------|-----------------------------|----------------------------|---------------------|
| Pre-injection | Flaccid | Flaccid | Flaccid | Flaccid | Flaccid |
| Post-injection arterial (CA) | PSV > 25 EDV < 5 (both arteries) | No erection | PSV < 25 Normal diastole | PSV > 25 | PSV > 25 EDV < 5 |
| Post-injection venous (DDV) | < 5 cm/sec | No erection | < 5 cm/sec | > 10 cm/sec (both veins) | < 5 cm/sec |

Table 4.130.9: Varicocele grading

| |
|--|
| Grade I: No dilated intrascrotal veins/reflux in spermatic cord veins of inguinal region during Valsalva |
| Grade II: Prominent veins at upper pole of testis/reflux at upper pole veins during Valsalva |
| Grade III: No major dilatation in supine position/dilated veins upto lower pole of testis only on standing position/Reflux at lower pole veins during Valsalva |
| Grade IV: Dilated veins even in supine position/reflux during Valsalva |
| Grade V: Dilated veins/reflux without Valsalva maneuver |

Endovascular treatment: The various endovascular methods for revascularization in PVD include percutaneous transluminal balloon angioplasty (PTA) and stenting, intra-arterial thrombolysis, thrombectomy, atherectomy, ultrasound angioplasty, laser angioplasty,

cryoplasty, radiation and gene transfer therapy. Cryoplasty, coated balloons, new-generation stents and stent grafts show promise in preventing restenosis after treatment of the condition.

Stents are classified as balloon and self-expandable. Balloon-expandable stents are crimped on a balloon and deployed during inflation. The single greatest advantage of these stents is their ability to be deployed precisely at the site of stenosis. Self-expanding stents, on the other hand, have an inherent memory instilled during the manufacturing process to expand to a predetermined diameter and are flexible. They are commonly used in all major peripheral vessels.

Covered stents represent a separate class of stents and have a polytetrafluoroethylene (PTFE) covering. These devices are predominantly used in applications such as the treatment of aneurysms, pseudoaneurysms,

Table 4.130.10: Percutaneous transluminal angioplasty and stenting

Percutaneous transluminal angioplasty and stenting: The majority of PTA is done with balloon catheters. A guidewire is used to traverse the pathological region and a balloon catheter is then traced over the wire and positioned across it. The occlusion opens as a result of plaque fracture, intimal separation, and media stretching during inflation and deflation. A vessel's response to angioplasty may be hampered by acute elastic recoil or a flow-limiting sub-intimal flap, both of which can be efficiently addressed with the use of a metal tubular mesh (stent). Elective stenting improves patency rates in specific places such as the renal ostia and the beginnings of the internal carotid arteries. The best results of PTA are achieved in stenotic lesions that are short, concentric and noncalcific.

**Fig. 4.130.37:** Percutaneous transluminal angioplasty and stenting**Table 4.130.11: Difference between neurogenic claudication and vascular claudication**

| Findings | Neurogenic claudication | Vascular claudication |
|----------------------------|--|---|
| Pain type and location | Radiculopathy manifests as lower extremity aching, burning and paraesthesias usually in a specific dermatome. Spinal pseudoclaudication (due to spinal canal stenosis) manifests as weakness and starts soon after standing up, relieved with bending forward. | Calf tightness and cramping with definite claudication distance |
| Radiation | Proximal to distal | Distal to proximal |
| Exacerbation | Lumbar extension | All lower extremity exercise |
| Walking distance | Variable | Constant |
| Relief | Lumbar flexion and rest | Cessation of lower extremity exercise |
| Backpain | Common | Rare |
| Lower extremity appearance | Normal | Vascular changes including hair loss |
| Pulses in lower extremity | Normal | Diminished |
| Lumbar range of motion | Diminished, painful | Normal |
| Treatment | Symptomatic medical management with NSAIDs and physiotherapy | Medical and endovascular treatment |

traumatic arterial perforations and arteriovenous fistulas (AVFs). Their role in cases of complete occlusion is being evaluated. Drug-eluting stents are the latest in stent technology aimed at overcoming the problems of in-stent restenosis. The ones that are commonly used are coated with paclitaxel and sirolimus.

Intra-arterial thrombolysis and mechanical thrombectomy: Traditionally, balloon embolectomy has been the treatment of choice for patients with an

acute arterial embolism. However, because surgical thrombectomy is less successful in acute on chronic limb ischemia, intra-arterial thrombolysis is an attractive alternative. Good results have been obtained with the use of intra-arterial urokinase and t-PA. The recent deluge of devices also shows promise when used concurrently with thrombolysis. The commonest used device continues to be a large diameter catheter for aspiration.

Table 4.130.12: Patterns of arterial spectral waveforms

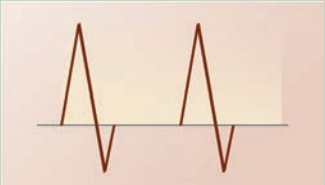



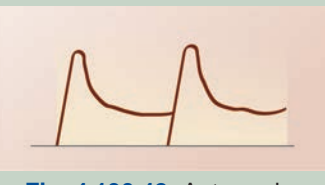
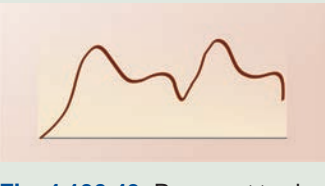



| Type | Spectral waveform | Description | Interpretation |
|------|--|---|--|
| 1 |  <p>Fig. 4.130.38: Normal triphasic flow</p> | Antegrade, very high pulsatile, very high resistant, tetrainflectional, triphasic flow with no late diastolic forward flow and $RI = 1$. | |
| 2 |  <p>Fig. 4.130.39: High resistant, tetrainflectional, triphasic flow</p> | Antegrade, high pulsatile, high resistant, tetrainflectional, triphasic flow with $EDV = 0$ and $RI \leq 1$. | Peripheral extremity arteries at rest |
| 3 |  <p>Fig. 4.130.40: Tetrainflectional, triphasic flow</p> | Antegrade, high pulsatile, high resistant, tetrainflectional, triphasic flow with $EDV = 5$ to 10 cm/sec, $RI > 0.7$ | |
| 4 |  <p>Fig. 4.130.41: Biphasic flow pattern</p> | Antegrade, moderate pulsatile, low resistant, bi-inflectional, biphasic flow pattern, $EDV = 10$ cm/sec, $RI 0.6$ to 0.7 . | Chronic atherosclerotic plaque with stenosis causing absent diastolic reversal due to collateral circulation in distal vessels. Normally seen in fasting state in superior and inferior mesenteric arteries. |
| 5 |  <p>Fig. 4.130.42: Antegrade, moderate pulsatile, low resistant, monoinflectional, biphasic flow</p> | Antegrade, moderate pulsatile, low resistant, monoinflectional, biphasic flow, $RI < 0.5$. | Normally seen in renal arteries, umbilical artery, uterine artery in pregnancy, internal carotid arteries, and postprandial state in superior and inferior mesenteric arteries. |
| 6 |  <p>Fig. 4.130.43: Parvus et tardus</p> | Antegrade, low pulsatile, low resistant, bi-inflectional, biphasic flow. (Parvus et tardus) | Chronic severe arterial stenosis causing prolonged systolic acceleration with small systolic peak. |

Table 4.130.12: Patterns of arterial spectral waveforms (Contd.)

| Type | Spectral waveform | Description | Interpretation |
|------|---|--|---|
| 7 |  <p>Fig. 4.130.44: Antegrade, very low resistant, monophasic flow</p> | Antegrade, very low resistant, monophasic flow. | Severe acute arterial stenosis—post-trauma. |
| 8 |  <p>Fig. 4.130.45: Trickle of antegrade monophasic flow</p> | Occasional trickle of antegrade monophasic flow. | Severe acute arterial stenosis—post-trauma. |
| 9 |  <p>Fig. 4.130.46: Absent flow</p> | Absent flow. | Complete acute arterial occlusion |

4.131 CARDIOVASCULAR SYSTEM

Case No. 131

Clinical history: 40 years old male with dyspnea and orthopnea

Radiological investigations and observations: Figures 4.131.1 and 4.131.2 are frontal radiograph chest in PA and lateral shows trachea in midline and right heart border is more than 5.5 cm from interspinous line indicating mild right atrial enlargement. In addition to that there is thin peripheral calcification noted along the left cardiac border, apex possibly the calcification in the pericardium. Bilateral costophrenic and cardiophrenic angle free. Rest of the lung fields appear normal. There is mild superior mediastinal widening noted.

With this my principal diagnosis is constrictive pericarditis.

Other differentials for pericardial calcification include: 1. Infection tuberculosis, 2. Asbestosis, 3. Following trauma/cardiac surgery, 4. Renal failure

Causes for biatrial enlargement include: 1. Restrictive cardiomyopathy, 2. Rheumatoid heart disease, 3. Constrictive pericarditis

Next line of investigations includes cardiac echo, CT may be done for look for calcification and then dynamic cardiac MRI pericardial thickening, enhancement, septal

bounce in inspiration free breath sequence also to rule out restrictive cardiomyopathy.

Figures 4.131.3 and 4.131.4 are CT axial sections in bone window and mediastinal window with contrast showing extensive calcification in the pericardium is evident with atrial enlargement. Bilateral pleural thickening right more than left with right pleural calcification. Ventricle appear tubular. With these findings, principal diagnosis is calcific constrictive pericarditis.

Figures 4.131.5 to 4.131.8 are dynamic contrast enhanced MRI images, which show pericardium is thickened to >4 mm. MRI is better than CT at differentiating between pericardial fluid and thickened pericardium.

In inspiration normally septum move towards the right ventricle. Free breathing cine MRI demonstrates septal flattening and septal bounce. Septal bounce (paradoxical interventricular septal movement during early diastole (i.e. initial septal movement towards and then away from the left ventricle) is a specific and relatively sensitive sign of ventricular interdependence due to constrictive pericarditis help to distinguish constrictive pericarditis from restrictive cardiomyopathy.

Interpretation: A: 40 years old, pericardium, C: Pericardial calcification—atrial enlargement and



Fig. 4.131.1

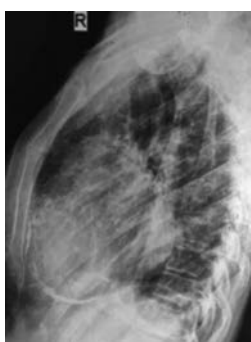


Fig. 4.131.2

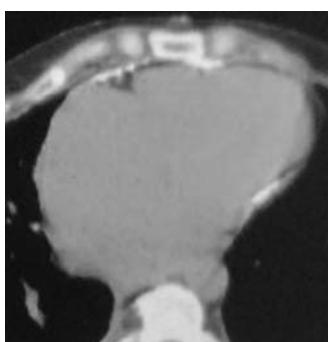


Fig. 4.131.3

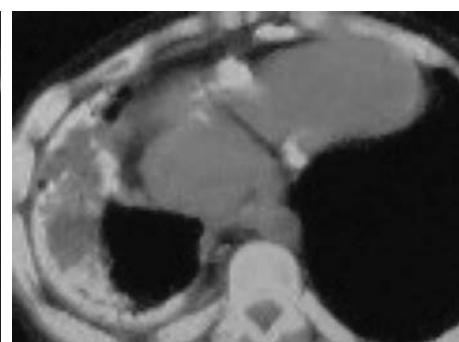


Fig. 4.131.4

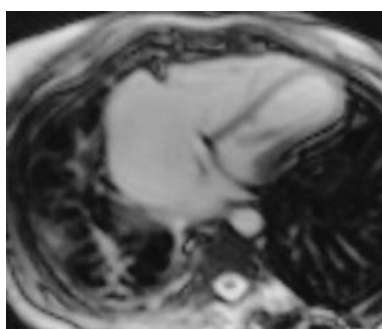


Fig. 4.131.5

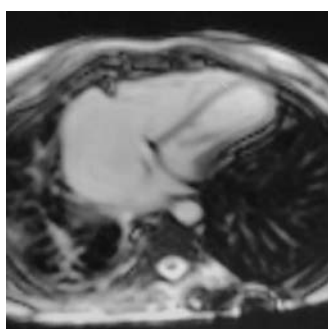


Fig. 4.131.6

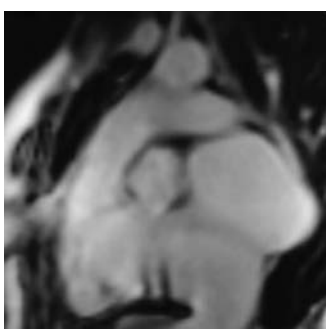


Fig. 4.131.7

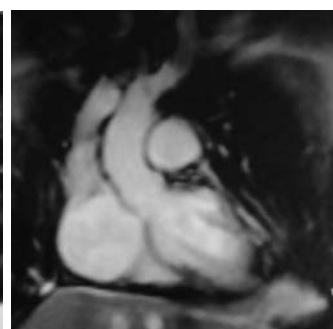


Fig. 4.131.8

tubular-shaped ventricles with septal bounce in MRI, D: Constrictive pericarditis.

Principal diagnosis: Constrictive pericarditis

Management: Pericardiectomy

Calcification in heart: Calcification in mitral/mitral valve—mitral stenosis; myocardial calcification—infarction; pericardial calcification—constrictive pericarditis; ventricular calcification—endomyocardial fibrosis which may result in aneurysm; coronary artery calcification.

Discussion: Constrictive pericarditis.

Constrictive pericarditis is due to progressive pericardial fibrosis, which impedes diastolic ventricular expansion. It is a nonspecific reaction to various conditions, such as infectious pericarditis, connective tissue disease, neoplasm, trauma, long-term renal dialysis, cardiac surgery, and radiation therapy.

- Thickening does not necessarily indicate constrictive disease
- Calcification suggests likelihood of constrictive physiology
- At times isolated to the right side of the heart
- Associated findings: Tubular ventricular configuration and congestive heart failure

Diagnostic clue

- Pericardial thickening in combination with heart failure. Thickness greater than 4 mm indicates pericardial thickening (normal 1–3 mm)
- Associated signs of hepatic venous congestion, enlargement of atria, dilated superior/inferior vena cava and hepatic veins, ascites, pleural effusions and pericardial effusion, with tubular small ventricles.
- **Location:** Thickening may be isolated over right atrium, right ventricle or right trioventricular groove

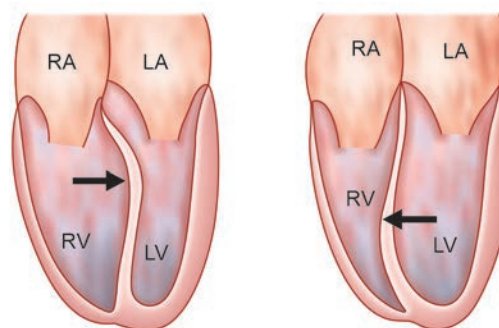


Fig. 4.131.9: Septal bounce in constrictive pericarditis (left), normal (right)

- May see prominent leftward convexity or sigmoid-shaped septum

Salient features

- Pulmonary venous hypertension
- Normal heart size or mild cardiomegaly
- Left atrial enlargement may be discernible.
- Flattened cardiac contours are pathognomonic but infrequently observed
- Calcification of the cardiac margin, especially the atrioventricular and interventricular grooves
- There are four different presentations of constrictive pericarditis: Acute inflammatory, effusive constrictive, adhesive, and chronic fibrous

Cardiac valves in chest X-ray: In chest radiography PA view, imaginary line drawn from right cardiophrenic angle to left atrial appendage: Aortic valve lies above the line, mitral valve below the line.

In lateral radiograph, line drawn from apex to base of heart—pulmonary and aortic valves are above the line where mitral and tricuspid below and through the line.

Cardiac pacemakers (Refer to OSCE)

Table 4.131.1: Types of constrictive pericarditis

| Acute inflammatory constrictive | Effusive constrictive | Chronic fibrous constrictive | Adhesive constrictive (very rare) |
|--|---|--|---|
| 1. Pericardial thickness ~4 mm 2. ±Effusion 3. Early contrast enhancement of pericardium | 1. Pericardial thickness ~4 mm 2. Effusion 3. ±Adhesions between parietal and visceral pericardium 4. Early contrast enhancement of parietal and visceral pericardium. | 1. Pericardial thickness ~4 mm 2. No effusion 3. No early contrast enhancement 4. Enhancement of thickened pericardium on delayed (10–15 mm after gadolinium) inversion recovery gradient | 1. Pericardial thickness >4 mm echo MR images 2. Adhesions between visceral and parietal pericardium 3. Adhesions between pericardium and other surrounding mediastinal tissues |

4.132 CARDIOVASCULAR SYSTEM

Case No. 132

Clinical history: A 29-year-old male, complaints of abdominal swelling, pedal edema with palpitation.

Radiological techniques and observation: Figures 4.132.1 to 4.132.5 are cardiac MRI images in axial and sagittal sections in phase sensitive inversion recovery (PSIR) sequences have been provided. Situs solitus with levocardia. Dilated atrium and ventricle noted. Mild pericardial effusion. No evidence of significant pericardial thickening seen. No evidence of septal bounce. Inter-atrial septum appears intact with normal thickness. No evidence of fatty replacement. Dynamic

perfusion imaging shows no evidence of perfusion defects in both ventricles. Non-enhancing hypointense lesion in ventricular cavity at the anterior wall of left ventricle (LV) near the apex with perfusion defect—thrombus. Delayed contrast enhancement study shows mild endocardial enhancement along the basal and mid LV cavity and intense enhancement along the endocardium in the apical and apex of right ventricle (RV) and LV. No evidence of mid ventricular/transmural enhancement. Mild to moderate right pleural effusion and mild left pleural effusion. Pneumonitis in the superior segment of left lower lobe lung. Subsegmental atelectasis in the basal segments of left lower lobe.

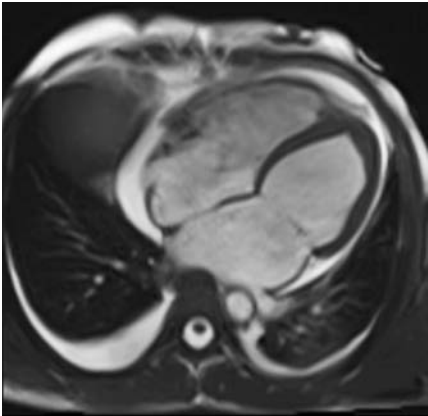


Fig. 4.132.1

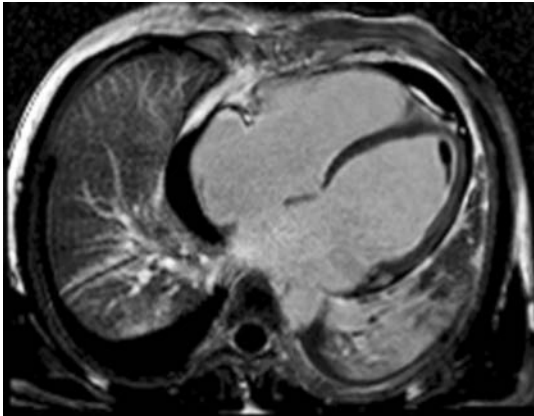


Fig. 4.132.2



Fig. 4.132.3

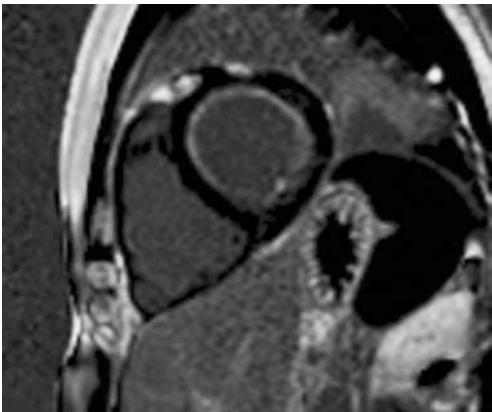


Fig. 4.132.4

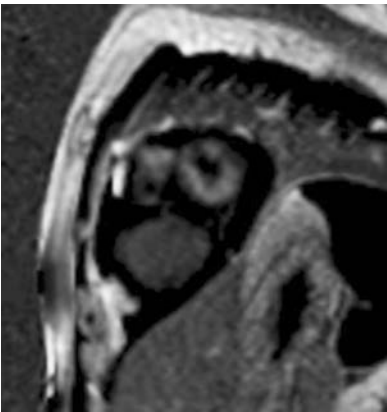


Fig. 4.132.5

| Table 4.132.1: Management in endomyocardial fibrosis | |
|---|--|
| Medical therapy: Within two years, one-third to one-half of individuals with advanced illness die. Although rate management can provide symptomatic relief, atrial fibrillation is a poor prognostic predictor. Heart failure is difficult to manage, and diuretics are only helpful in the early stages of the condition, losing effectiveness as the ascites progresses. | Surgery Endocardial resection—endocardectomy with valve replacement or repair is a procedure used to resect the myocardium in patients with severe heart failure. The immediate postoperative mortality rate is substantial, ranging from 15 to 30%. |

Table 4.132.2 Criteria for diagnosis and assessment of the severity of EMF

| Criteria | Score |
|--|-------|
| Major criteria | |
| Endomyocardial plaques thickness >2 mm | 2 |
| Thin (≤ 1 mm) endomyocardial patches affecting >1 ventricular wall | 3 |
| Obliteration of the right ventricular / left ventricular apex | 4 |
| Thrombi or spontaneous contrast without severe ventricular dysfunction | 4 |
| Right ventricular apex retraction (right ventricular apical notch) | 4 |
| Dysfunction of AV valve due to valvular apparatus adhesion | 1–4 |
| Minor criteria | |
| Thin endomyocardial patches that are confined to 1 ventricular wall | 1 |
| Restrictive flow pattern observed across mitral or tricuspid valves | 2 |
| Diastolic opening of pulmonary valve | 2 |
| Diffuse thickening involving anterior mitral leaflet | 1 |
| Enlarged atrium with normal-sized ventricle | 2 |
| M-movement of the interventricular septum and flat posterior wall | 1 |
| Higher density in moderator or other intraventricular bands | 1 |
| When two main criteria or one major criterion plus two minor criteria were present, a definitive diagnosis of endomyocardial fibrosis was made. Mild endomyocardial fibrosis is indicated by a total score of 8; moderate disease is indicated by a score of 8 to 15; and severe disease is indicated by a total score of >15. | |
| The severity of atrioventricular regurgitation is used to assign a score. | |
| M-movement of the interventricular septum is a movement pattern seen on M-mode echocardiography that is hypothesised to be caused by obliteration or constriction of the left ventricular apex in combination with mitral regurgitation. | |

Interpretation: A: 29 years, myocardium, C: Cardiac MRI images show, thrombus in ventricular cavity at the anterior wall of left ventricle (LV) near the apex, B: Delayed contrast enhancement study shows mild endocardial enhancement along the basal and mid LV cavity and intense enhancement along the endocardium in the apical and apex of right ventricle (RV) and LV, D: Endomyocardial fibrosis.

Principal diagnosis: Restrictive cardiomyopathy—possibly endomyocardial fibrosis (Loeffler endocarditis) than cardiac amyloidosis.

Differential diagnosis: 1. Ischemic cardiomyopathy, 2. Non-ischemic cardiomyopathy
Hypertrophic cardiomyopathy, dilated cardiomyopathy, arrhythmogenic right ventricular dysplasia, myocarditis, Takotsubo cardiomyopathy.

Treatment: The disease is associated with a high rate of morbidity and mortality, with a two-year median survival rate after diagnosis. Chronic heart failure, arrhythmia, and thromboembolism are all common causes of death.

Discussion: Endomyocardial fibrosis (EMF) is an idiopathic condition that manifests as restrictive cardiomyopathy. It is most common in the world's tropical and subtropical climates. Children and teenagers

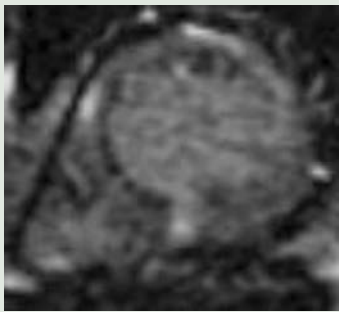
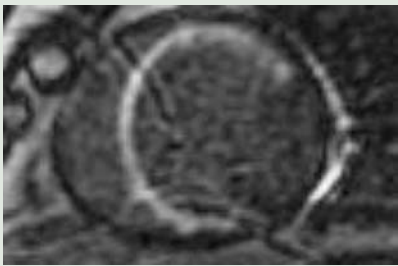
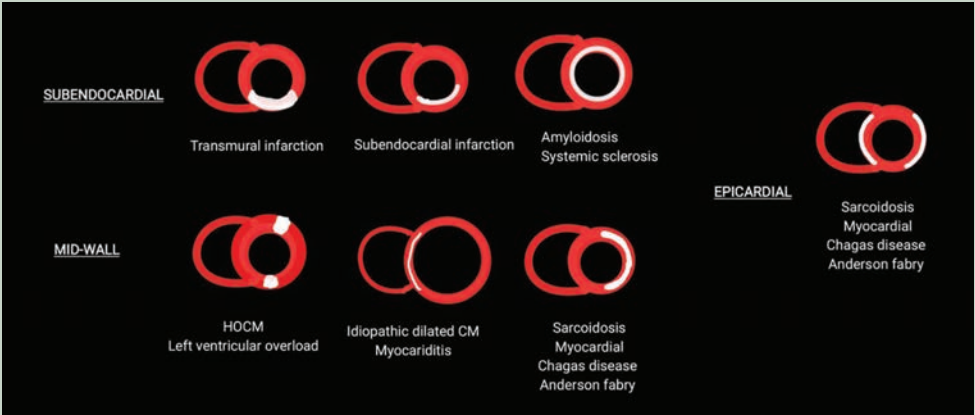
may have a stronger preference. It can happen as a result of idiopathic high eosinophilic condition, causing Loeffler endocarditis. Endomyocardial fibrosis was diagnosed when two main criteria or one major criterion plus two minor criteria were present: Instances with scores of 8 or less were classified as mild, cases with scores of 8 to 15 as moderate, and cases with scores of 15 or more as severe.

Imaging findings: Apical fibrosis of one or both ventricles is seen on echocardiography. Apical thrombi are frequently present, tethering the atrioventricular (AV) valve papillary muscles, resulting in mitral and/or tricuspid regurgitation. Atrial hypertrophy of enormous proportions. Doppler recordings of mitral valve inflow show a restrictive filling pattern.

X-ray of the chest cardiomegaly is a condition that ranges in severity from mild to severe. Patients with right-sided involvement have right atrial enlargement, patients with left-sided involvement have left atrial enlargement, and those with biventricular involvement have biatrial enlargement. Left-sided involvement with pulmonary venous congestion: Calcification of the endocardium.

On coronary angiography, varied degrees of AV valve regurgitation with the apex of the affected ventricle obliteration is evident.

Table 4.132.3: Spectrum of late gadolinium enhancement (LGE) are normal, focal, multi-focal and extensive LGE

| | |
|---|---|
|  |  |
| <p>Fig. 4.132.6: Multifocal LGE myocarditis</p> | <p>Fig. 4.132.7: Extensive LGE LAD, RCA territory infarct</p> |
|  | |
| <p>Fig. 4.132.8: Approach to late gadolinium enhancement (LGE)</p> | |
| <p>Absent LGE: Athlete's heart/non-ischemic cardiomyopathy (with ventricular fibrillation)/myocardial necrosis/stunned and hibernating myocardium.</p> | |

Late Gadolinium Enhancement on Cardiac MRI

- 1. Myocardial infarction—the distribution is sub-endocardial or full thickness and in a recognized coronary artery territory.
- 2. Cardiomyopathy—such as due to sarcoid, myocarditis, HCM, DCM or ARVD. The distribution is not that of infarction and is often mid-myocardial or subepicardial. The finding of myocardial scar tissue in this way tends to be associated with a worse prognosis.
- 3. Diffuse late enhancement—can be seen with extensive cardiac amyloid infiltration.

The fibrofatty replacement of the RV myocardium is the hallmark of arrhythmogenic right ventricular cardiomyopathy (ARVC), a hereditary cardiomyopathy. In at least 15% of patients, the left ventricle is also implicated. Patients have progressive RV failure and ventricular arrhythmias, which can lead to sudden cardiac death, especially in children and teenagers.

According to the ARVC task force, criteria from 2010 have been updated.

MRI findings that match a key requirement for “global or regional dysfunction and structural changes”: RV akinesia, dyskinesia, or dyssynchronous RV contraction in a regional area and one of the following: RV end-diastolic volume to BSA ratio: 110 ml/m² (male) or 100 ml/m² (female) or a 40 percent RV ejection fraction.

Findings on MRI that are consistent with a minor criterion for “global or regional dysfunction and structural alterations”: RV akinesia, dyskinesia, or dyssynchronous RV contraction in a regional area and one of the following RV end-diastolic volume to BSA ratio of 100 to 110 ml/m² (male) or 90 to 100 ml/m² (female); or RV ejection percentage of 40 to 45%.

Cardiac MRI: The Basic Sequences

- ECG-gated spin echo (SE) or fast-spin echo (FSE) (turbo spin echo [TSE])
- ECG-gated db-HASTE (double IR-half-Fourier single-shot turbo-spin echo)

Uses: To identify extraluminal aortic pathology, intramural hematoma, or dissection.

Table 4.132.4: Difference between various cardiomyopathies

| | |
|--|--|
| Hypertrophic cardiomyopathy: Development of inappropriate hypertrophy of myometrium develop in the absence of hemodynamic stress, valvular heart disease. Causes: Familial, idiopathic Imaging: <ul style="list-style-type: none"> • Hypertrophy involves the asymmetric septal, concentric, apical, midventricular, right ventricular wall. • Increased LV wall thickness >12 mm • Septal: Posterolateral wall thickness ratio > 1.5 • Normal LV EDV • Normal or increased EF • CMR: Delayed enhancement in septum/junction of septum and anterior wall. | Dilated cardiomyopathy: <ul style="list-style-type: none"> • Dilation and diminished contraction of left or both ventricles. Causes: Idiopathic, ischemic, familial, post-myocarditis, alcohol. Imaging: <ul style="list-style-type: none"> • Wall thickness within normal range, wall thinning present in ischemic cases • Increased LV ESV, LV EDV • Decreased LV stroke volume, LVEF • CMR: Delayed enhancement not usual in idiopathic dilated cardiomyopathy, regional sub-endocardial/transmural delayed enhancement occurs in ischemia. |
| Restrictive cardiomyopathy: <ul style="list-style-type: none"> • Amyloidosis, hemochromatosis, and sarcoidosis are the most common causes of restrictive cardiomyopathy, respectively. • Amyloid deposits in the myocardium induce aberrant diastolic function, which includes biatrial enlargement, left ventricle concentric thickening, and impaired systolic performance in both ventricles. • CMR: Delayed enhancement imaging reveals enhancement along the subendocardial perimeter, extending into the adjacent myocardium in varying degrees. • There is circumferential subendocardial enhancement that extends into the myocardium next to it. DD: Constrictive pericarditis | Constrictive pericarditis: Causes <ul style="list-style-type: none"> • TB (most common cause) • Other infections (viral, pyogenic) • Cardiac surgery • Radiation injury Radiographic Features Calcifications are a common occurrence. Constrictive pericarditis affects 50% of patients with calcification. Pericardial calcification affects 90% of patients with constrictive pericarditis. In the atrioventricular grooves, pericardial calcification is more prevalent. Pericardial thickening more than 4 mm; Pleural effusion, PVH, elevated RV pressure: dilated SVC and azygos. |
| Spongiform cardiomyopathy, commonly known as left ventricular non-compaction (LVNC), is a condition characterised by hypertrophic ventricular trabeculations and deep interventricular recesses. Cardiac transplantation is the only way to cure left ventricular non-compaction. | Non-compaction of the left ventricle is not diagnosed by chest radiography. Left ventricular non-compaction was previously diagnosed by echocardiography. Echocardiographic criteria for left ventricular non-compaction. <ul style="list-style-type: none"> • Bilayered mural appearance of the left ventricle • Inner hypoechoic layer of the left ventricular wall representing the endocardium is hypertrabeculated and referred to as the non-compacted. Outer “compacted” layer, representing the epicardium increased thickness of the NC layer with an NC/C ratio >2.3 consistent with the diagnosis • Regional increase in left ventricular trabeculation • Pronounced intertrabecular “crypts” or recesses • Left ventricular dysfunction and intraventricular thrombus Cardiac MRI (CMR) has a better contrast resolution than echocardiography and it is the modality of choice for the diagnosis of spongiform cardiomyopathy. The best diagnostic clue is a ratio of non-compacted telediastolic myocardium to compacted telediastolic myocardium of more than 2.3:1 |

Cardiac gating: TR = R–R interval for SE or FSE; gating not absolutely needed for HASTE

- Can be performed breath-hold (fast imaging) or multiple averages non-breath-hold (NBH)
- HASTE can be used in arrhythmias

Cine gradient echo imaging (GRE): FASTCARD

True fast imaging with steady-state precession (FISP)

Uses: To determine flow, motion, aortic valvular disease

Cardiac gating: Choose temporal resolution based on TR and R-R interval

Velocity encoded cine imaging (Vinnie)

- **Uses:** To quantify flow at stenoses to estimate pressure gradient or collateral blood flow

3D spoiled GRE (with interpolation)

- **Uses:** Aortography or pulmonary angiography
- Preferably breath-hold (ungated)

- Single or double dose (0.1–0.2 mmol/kg) Gd-contrast
- Timing based on test dose or fluoroscopic triggering

Cardiac MRI: Advanced tools

1. *Myocardial perfusion*: Baseline and stress dynamic multislice segmented GRE or echo planar imaging (EPI) during bolus infusion of Gd optional adenosine or perfusion stress
2. *Myocardial tagging*: Wall motion and thickening analysis, stress and strain, wall velocity optional dobutamine stress test for wall motion abnormalities
3. *Myocardial viability*: Enhancement on delayed post-contrast images. Inversion recovery spoiled gradient echo for nulling of normal myocardium
4. *Coronary MRA* (intravascular or extravascular contrast agents)
5. *Coronary flow* (phase contrast flow quantification) Optional adenosine for flow reserve measurements
6. Real-time MR fluoroscopy

Post-processing tools:

- Maximum intensity projection/maximum perfusion reserve index (MIP/MPRI)/volume rendering of Gd-MRA

- Ventricular function: Calculating EFs, stroke volumes from cine GRE LV volume = $(A1 \times Z) + (A2 \times Z) + \dots + A_n$ = cross-sectional area of slice n, Z = slice thickness. If Z = 1 cm, then LV volume = $A1 + A2 + A3 + \dots$

EDV (end diastolic volume) = sum all short axes at maximum, **ESV** (end systolic volume) = sum all short axes at minimum. **SV** (stroke volume) = EDV – ESV, **EF** = (EDV – ESV)/EDV = SV/EDV

- Flow quantification from velocity-encoded phase contrast GRE
- Wall motion abnormalities: Thickening, stress/strain maps, velocity maps
- Perfusion: Analysis of enhancement profiles

Pitfalls in cardiothoracic MRI:

- Right atrial pseudomass: Protrusion along posterior wall of right atrium between SVC and IVC, caused by normal structures such as eustachian valve, Chiari network.
- Differentiation: Mass or thrombus.
- Metallic artifacts
- Pseudosubclavian stenosis on Gd-MRA of thoracic aorta

Table 4.132.5: MRI sequences and planes used in evaluation of cardiac shunts

| Sequence | Planes | Information |
|---|--|--|
| Scouts | Transverse, sagittal, coronal | Localizing |
| HASTE | Transverse | Define anatomy, plan for subsequent views |
| Cine steady-state free precession | Vertical long axis, three chambers, short-axis stacks, four-chamber stacks | Evaluate function, volumes, mass |
| Velocity-encoded phase-contrast | | |
| Velocity encoding = 200 cm/s | Ascending aorta, main pulmonary artery | Assess flow and estimate Qp:Qs = pulmonary-to-systemic flow ratio. |
| Velocity encoding = 50 cm/s, en face | Orthogonal to septal defect | Assess shunt volume |
| MR angiography | Coronal | Evaluate vasculature, detect anomalous drainage |
| 3D Whole-heart SSFP (This is also a good sequence to use in patients with renal dysfunction who cannot receive IV contrast material) | Transverse | Assess cardiovascular anatomy, detect anomalous drainage, assess coronary artery anatomy |

Optimal Planes for Imaging Cardiac Structures and Chambers

| Structure or chamber | Imaging planes |
|-----------------------|---|
| Left ventricle | Four-chamber view, horizontal long- and short-axis views, and LVOT view |
| Right ventricle | Right-sided horizontal long-axis view, short-axis view, and RVOT view |
| Left atrium | Horizontal long-axis view, LVOT view, and four-chamber view |
| Right atrium | Axial, coronal, and right-sided horizontal long-axis planes |
| Aorta | Oblique sagittal plane |
| Main pulmonary artery | Sagittal plane of the RVOT view |
| Coronary arteries | Three-point planes |

| Table 4.132.6: CMR techniques for IHD | | | |
|--|---------------------------|------------------------------------|-------------------------|
| <i>Cine MRI (rest/stress)</i> | <i>T2-MRI</i> | <i>Perfusion MRI (rest/stress)</i> | <i>DE-MRI</i> |
| Contractile function | Myocardial edema | Myocardial blood flow | Myocardial necrosis |
| Systolic function/ Ischemia/ viability | Infarct age/ area at risk | Myocardial ischemia | Infarct size/ viability |

- Inaccurate timing
- Poor ECG-gating

Comprehensive MR Approach for Dysfunctional Myocardium

MRI: Regional wall motion abnormality (hypokinesis, akinesis, or dyskinesis) or myocardial thinning (5.5 mm at end-diastole) on cine cardiac MRI suggest left ventricular myocardial ischemia or infarction. Subendocardial or transmural late gadolinium enhancement is then used to measure scar load. Those dysfunctional or thinned patches in which hyperenhancement impacts 50% wall thickness identified as hibernating myocardium that may improve in function or thickness after revascularization. Dobutamine stress MRI can also be used to assess viability, as dobutamine stress enhances the contractility of hibernating (viable) myocardium. While nonviable myocardium remains dysfunctional.

4.133 CARDIOVASCULAR SYSTEM

Case No. 133

Clinical history: A 65-year-old male, came with complaint of chest pain and palpitation, pre- and post-treatment status.

Radiological techniques and observation: Figures 4.133.1 to 4.133.3 are cardiac MRI post-contrast short axis view, interval CT angiography pre- and post-treatment images. Pretreatment: CT coronary angiogram axial section curved reformatted images show soft plaque near the origin of the left main coronary artery causing 70–80% stenosis. There is atheromatous soft plaque in left anterior descending artery for the length of approximately 2–3 cm causing 70–75% stenosis. Cardiac MRI post-contrast short axis view of base of heart shows subendocardial enhancement in the anterior wall left ventricle and interventricular septum (Fig. 4.133.1).

Post-treatment: CT coronary angiogram axial section shows coronary stent in left anterior descending (LAD) artery. Contrast flow noted within the stent. There is no significant luminal narrowing (Fig. 4.133.3).

Interpretation: A: 69 years old, C: CT angiography images show, soft plaque near the origin of the left main coronary artery. There is atheromatous soft plaque in left anterior descending artery cardiac MRI showing infarct in the anterior wall of left ventricle and interventricular septum, B: Post-treatment CT coronary angiogram axial section shows coronary stent in left anterior descending (LAD) artery. Contrast flow noted within the stent without significant luminal narrowing D: Ischaemic heart disease.

Principal diagnosis: Ischemic heart disease.

Treatment: Lifestyle modification, drugs—aspirin, beta blockers, calcium channel blockers, nitroglycerin,

angiotensin-converting enzyme inhibitors and angiotensin II receptor blockers. Surgical treatment Includes stenting and CABG.

Discussion: Ischaemic heart disease is a condition in which the heart's blood supply is compromised. The term "ischaemia" refers to a "reduced blood supply." Because there is no alternate blood supply for the heart muscle, a blockage in the coronary arteries lowers the delivery of blood to the heart muscle.

Radiographic features: Triple rule out in CT scan is done to rule out aortic dissection, pulmonary embolism, coronary artery diseases (CAD).

CTA (indications): Acute chest pain in patients with a low-to-intermediate pretest probability of CAD, evaluation of coronary artery anatomy and bypass grafts, coronary artery calcium scoring. **Haemodynamically** significant stenosis are those >70% for all coronary arteries, except the left main coronary artery where >50% stenosis is considered significant. Echocardiography shows new regional wall motion abnormalities, tardokinesis, post-systolic thickening. MRI finding in MI: In the acute phase of infarction, myocardial edema can be seen as T2 weighted high signal regions. These segments of the myocardium are called "myocardium at risk". Myocardial scar tissue can be identified using late gadolinium enhancement images and is useful in differentiating infarction (subendocardial or transmural) from non-infarcted myocardium or other non-ischemic cardiomyopathies and infiltrative disease. MRI also shows hypokinesia/akinesia of myocardium, subendocardial or transmural infarct, absent chordae tendineae, aneurysmal bulging. **Severity assessment:** The recently proposed NCCT grading scale for stenosis severity assesses the degree of luminal diameter stenosis.

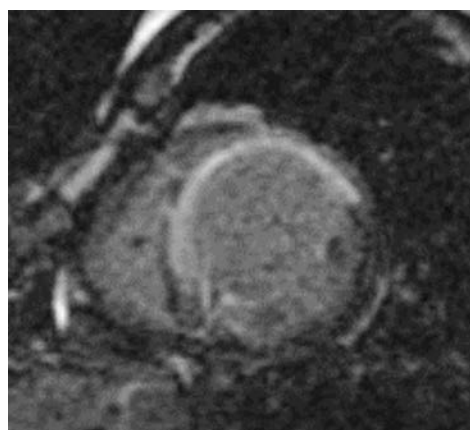


Fig. 4.133.1

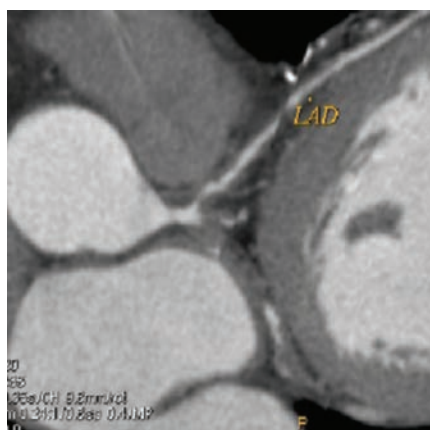


Fig. 4.133.2

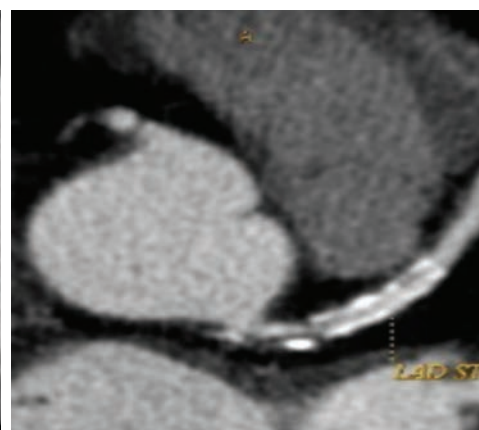


Fig. 4.133.3

Table 4.133.1: Differential diagnosis for acute chest pain

| | |
|---|--|
| Pulmonary embolism (refer to case 99) | |
| Aortic dissection (refer to case 127) | |
| Myocarditis is a general term referring to inflammation of the myocardium. Types of myocarditis are fulminant, acute, chronic active, and chronic persistent. | <p>Imaging features</p> <p>CECT: Delayed myocardial enhancement with iodinated contrast.</p> <p>MRI: Cine SSFP shows regional or global wall motion abnormalities and pericardial effusion.</p> <p>MR contrast: Early gadolinium enhancement shows regional vasodilatation and increased blood volume due to the inflammation in myocarditis. Late gadolinium enhancement shows delayed myocardial enhancement in myocarditis it is an indication of irreversible myocardial necrosis and fibrosis.</p> |
| Takotsubo cardiomyopathy is a disorder marked by brief aberrant cardiac wall motion that is not limited to a single coronary artery zone. Seen in postmenopausal women, and it generally occurs as a result of unanticipated emotional/physical stress. Broken heart syndrome is another name for it. | The left ventricular apex shows systolic “ballooning” on echocardiography. Four unique patterns of dyskinesia and ballooning are observed on cardiac MRI: Apical, biventricular, mid-ventricular, and basal. Takotsubo cardiomyopathy is distinguished from anterior STEMI by the absence of late enhancement on delayed contrast sequences. |
| Pericarditis is inflammatory process involving the pericardium. Males > females. Treatment: Colchicine, aspirin or ibuprofen corticosteroids. | <p>Imaging features</p> <p>ECHO: Pericardial thickening, pericardial effusion, cardiac tamponade.</p> <p>CECT: Enhancement of the thickened pericardium</p> <p>MRI: Increased pericardial thickness over 4 mm.</p> <p>T2 black-blood images show edema of the visceral and parietal pericardium.</p> <p>T1+c: late gadolinium enhancement (LGE) of pericardium are seen.</p> |
| Acute cholecystitis (refer to case 197) | |
| Ischaemic cardiomyopathy is described as left-ventricular dysfunction as a result of a continuous loss of oxygen caused by coronary artery disease. When a coronary artery is closed, the infarction always starts subendocardially and advances towards the epicardium, and all patients with ischemic cardiomyopathy show delayed enhancement in a classic ‘CAD’ pattern. | <p>Due to myocyte membrane breakdown in acute infarctions, MRI contrast enters the injured myocardial cells.</p> <p>The retention of contrast material in the vast interstitial space between the collagen fibres in the fibrotic tissue causes late enhancement in chronic infarctions.</p> |

Table 4.133.2: Radiopharmaceuticals for cardiac nuclear study

| <i>Single photon emission computed tomography (SPECT)</i> | <i>Positron emission tomography (PET) or PET/CT</i> |
|--|---|
| 1. 201thallium (201Tl, 3–4 mCi) | 82Rb (10–40 mCi) by generator |
| 2. 99mTc methoxyisobutyl - sestamibi (cardiolite, mibi, 25 mCi), | 11c-FFA (30 mCi) by cyclotron |
| 3. 99mTc 1,2bis [bis (2-ethoxyethyl) phosphinoethane-tetrofosmin (myoview, 25 mCi) | 13NH ₃ (15–25 mCi) by cyclotron |
| 4. Teboroxime | |

Table 4.133.3: Methods of stress testing

| <i>Physical exercise</i> | <i>Pharmacologic stress</i> |
|--------------------------|--|
| Treadmill bicycle | Vasodilators: Adenosine, lexiscan (regadenoson, A2A adenosine receptor agonist), dipyridamole, catecholamines: Dobutamine |

| Table 4.133.4: Difference between thallous chloride and Tc-sestamibi | | |
|--|---------------------------|---|
| Radionuclide properties | Thallous chloride | Tc-sestamibi |
| Chemistry | +1 cation, hydrophilic | +1 cation, lipophilic |
| Shelf life | 6 days | 6 hours |
| Photon energy | 68–80 keV | 140 keV |
| Uptake | Active: NA, K-ATPase Pump | Passive diffusion (if intact membrane potentials) |
| Extraction fraction | 85% | 66% |
| Heart uptake | 4% | 1.2% |
| Redistribution | Redistributes | Fixed |

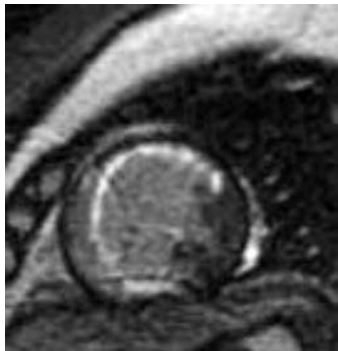


Fig. 4.133.4: LAD and RCA infarct

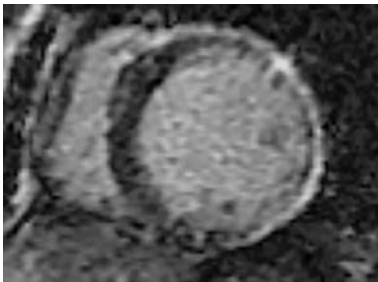


Fig. 4.133.5: LCX infarct

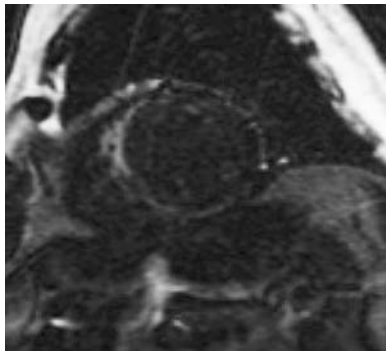


Fig. 4.133.6: LAD infarct

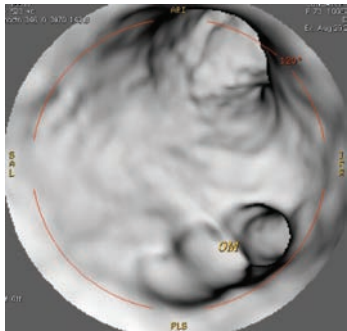


Fig. 4.133.7: Virtual coronary scopy

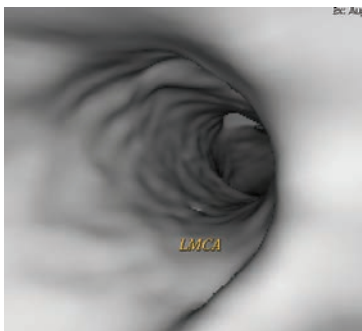


Fig. 4.133.8: Virtual coronary scopy

0% = no visible stenosis, 1–24% = minimal stenosis, 25–49% = mild stenosis, 50–69% = moderate stenosis, 70–99% = severe stenosis, 100% = occlusion. Coronary calcium scoring (Agatston score) – (Refer to OSCE)

Coronary lesions classification by ACC/AHA is a system use to classify coronary arterial calcific plaque burden. It is classified as coronary artery disease—reporting and data system—(Refer to OSCE)

Cardiovascular scintigraphy (indication)

- Coronary artery disease
- Myocardial perfusion scintigraphy (201 thallium/ 99mTc agents/82 rhenium)

- Myocardial viability (201 thallium/18F FDG-PET)
 - Acute myocardial infarction (99mTc agents)
 - Myocarditis, transplant rejection
 - 67 gallium imaging (myosin Ab imaging)
- Evaluation of EF, stroke vol, chamber size, wall motion (MUGA / first pass/ myocardial perfusion).
- Perfusion imaging in patients with a bundle branch block during exercise or dobutamine-induced stress may reveal a reversible or persistent septal perfusion deficit. The exact cause of these apparent septal defects is unknown; however, the decrease in septal blood flow seen at higher heart rates could be due to asynchronous

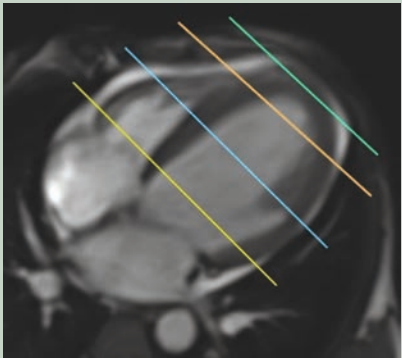
| Table 4.133.5: Left ventricular segmentation | | | | | |
|--|---------------------|----|-------------------|---|-----------------|
| 1 | Basal anterior | 7 | Mid-anterior | 13 | Apical anterior |
| 2 | Basal anteroseptal | 8 | Mid-anteroseptal | 14 | Apical septal |
| 3 | Basal inferoseptal | 9 | Mid-inferoseptal | 15 | Apical inferior |
| 4 | Basal inferior | 10 | Mid-inferior | 16 | Apical lateral |
| 5 | Basal inferolateral | 11 | Mid-inferolateral | 17 | Apex |
| 6 | Basal anterolateral | 12 | Mid-anterolateral |  | |

Fig. 4.133.9: Planning for cardiac MRI from 4-chamber view to get 2-chamber view

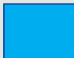


-  Left anterior descending artery
-  Right coronary artery
-  Left circumflex artery

Fig. 4.133.10: Color coding for coronary arteries used in this case

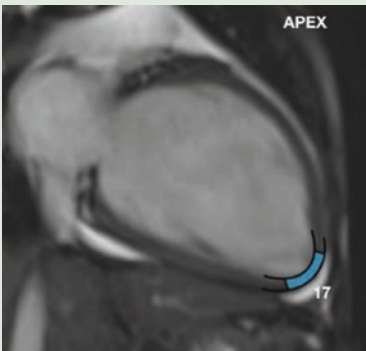


Fig. 4.133.11: Apex of heart in vertical long axis view

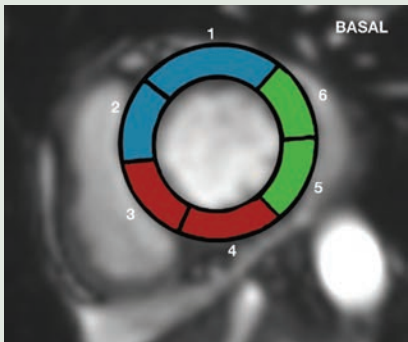


Fig. 4.133.12: Horizontal short axis view with color coded arteries respect to bull's eye model – 1 (basal)

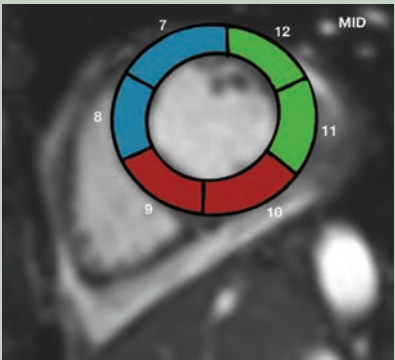


Fig. 4.133.13: Horizontal short axis view with color coded arteries respect to bull's eye model – 2 (mid)

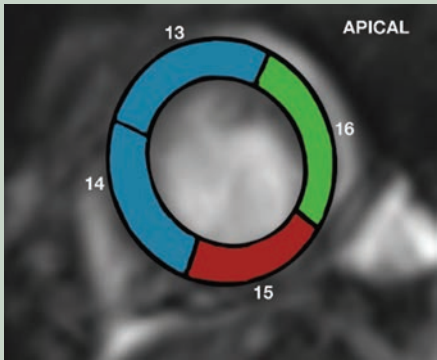


Fig. 4.133.14: Horizontal short axis view with color coded arteries respect to bull's eye model – 3 (apical)

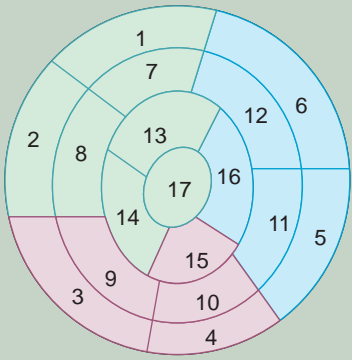


Fig. 4.133.15: Bull's eye model

Table 4.133.6: Interpreting stress MRI

| Rest study | Stress study | Conclusion |
|------------|-------------------------------------|---------------------|
| No defect | No defect | No ischemia |
| No defect | Defect | Ischemia |
| Defect | Same defect | Infarct/hibernation |
| Defect | Larger defect or different location | Ischemia + infarct |

septal contraction caused by a disrupted activation sequence in patients with bundle branch block and incomplete diastole relaxation of the septum.

Quantitation of Extent and Severity of CAD (before or after cardiac catheterization)

Rest and stress myocardial perfusion imaging with left ventricular ejection fraction (LVEF) and wall motion study is performed

- Severity of ischemia: Mild, moderate, severe
- Extent of ischemia: Percent of total wall found ischemic
- Vessel(s) involved: Single, two, multiple, LAD/LCX/RCA
- Function: Wall motion, volumes, EF (global and regional)

Visual analysis of perfusion SPECT: 0-normal uptake, 1-mildly reduced uptake, 2-moderately reduced uptake, 3-severely reduced uptake, and 4-no uptake.

Interpretation and reporting: Myocardium divided into 17 segments on the basis of 3, short axis and a long axis slice, perfusion graded from 0 (normal perfusion) to 4 (no uptake), SSS—summed stress score—stress perfusion abnormality, SRS—summed rest score—extent of infarction, SDS—summed difference score—stress induced ischemia.

Nuclear medicine: First pass radionuclide ventriculography (RVG)—IV injected radioactive tracer passes through right chambers—lungs—left chambers

- Tc 99m DTPA preferred, RAO projection
- 2–5 cycles summed for RV phase, 5–7 for LV phase
- Time activity curves generated—quantitative analysis

PET in Cardiology

In cardiology, PET has become the ‘gold standard’ for non-invasive evaluation of stunned (ischemic) myocardium

- Differentiation of ischemic heart muscle from infarcted myocardium
- Absolute quantification of myocardial blood flow

Table 4.133.7: Interpreting and reporting findings at myocardial perfusion imaging—general guidelines

| |
|---|
| Perfusion defect size |
| Small (<10% of total left ventricular volume) |
| Moderate (10–20% of total left ventricular volume) |
| Large (20–40% of total left ventricular volume) |
| Extensive (>40% of total left ventricular volume) |
| Perfusion defect severity (semiquantitative segmental scoring) |
| Mild (<40% decrease from database norm; score of 1 or 2) |
| Moderate (40–60% decrease from database norm; score of 2) |
| Severe (>60% decrease from database norm; score of 3) |
| Absent perfusion (no activity; score of 4) |
| Perfusion defect location |
| Cardiac wall (anterior, septal, inferior, lateral, or apical) |
| Expected coronary artery involvement |
| Perfusion defect reversibility indicators |
| Cross-hatching of the perfusion defect on the stress image—based polar map |
| Improvement by 2 points or more in the semiquantitative segmental score, or an absolute segmental score of 0 or 1, on rest images |
| Risk for future hard cardiac events |
| Low risk (summed stress score, 4–7) |
| Intermediate risk (summed stress score, 8–12) |
| High risk (summed stress score, >12) |
| Extracardiac findings (radiotracer activity in adjacent tissues or organs) |

Advantages of PET

- Higher spatial resolution
- Improved attenuation correction
- Quantification regional blood flow
- Blood flow reserve by PET—early identification of CAD
- Higher sensitivity and specificity (95%) for detection of CAD
- Two sets of resting images to detect viable and hibernating myocardium (Table 4.133.9).

Stress 18 FDG PET-MPI

Most commonly used protocol: Oral loading of 50–70 gm of glucose stimulating insulin secretion and increasing FDG uptake into normal myocardium to near maximal. Euglycemic insulin clamping is an alternative technique and is more complex but guarantees more stable and controlled metabolic conditions. FDG uptake into normal and ischemic but viable myocardium is enhanced and negative FDG uptake is considered to indicate scar tissue.

Table 4.133.8: Stepwise interpretation of cardiac MRI using perfusion sequences

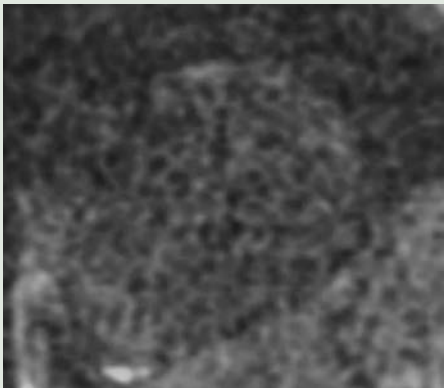


Fig. 4.133.16: Step 1—precontrast

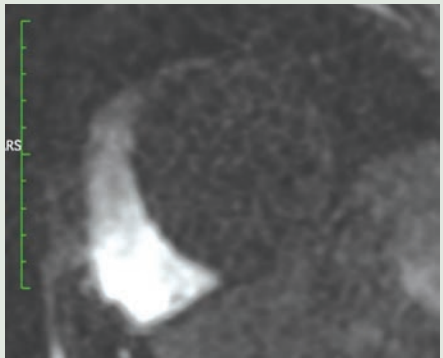


Fig. 4.133.17: Step 2—started filling of right ventricle

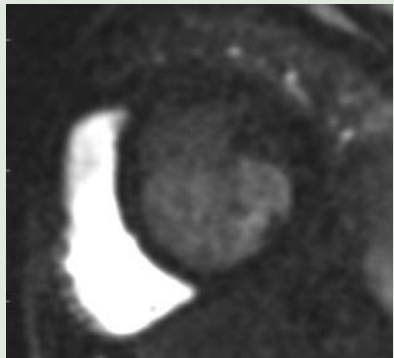


Fig. 4.133.18: Step 3—complete filling of right ventricle and pulmonary vessels

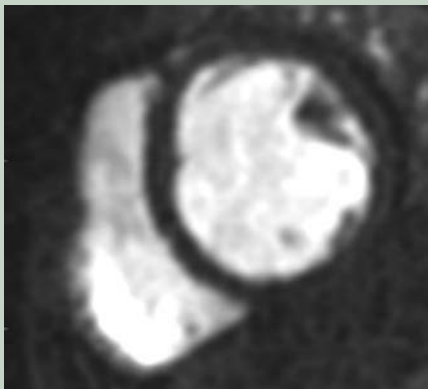


Fig. 4.133.19: Step 4—complete filling of both ventricle—myocardium appears dark

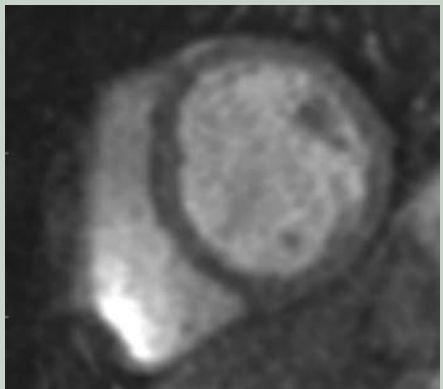


Fig. 4.133.20: Complete filling of both ventricle, myocardium appears white due to coronary circulation

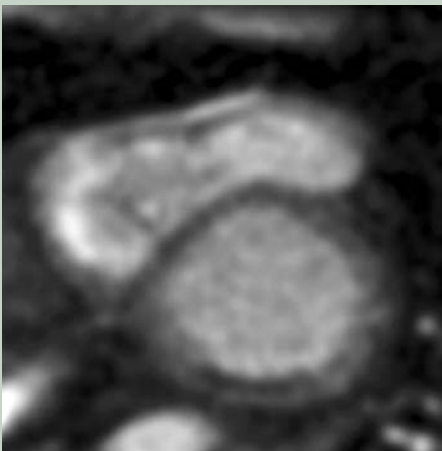


Fig. 4.133.21: infarcted area appears dark (LCX)

Reporting template in coronary CT

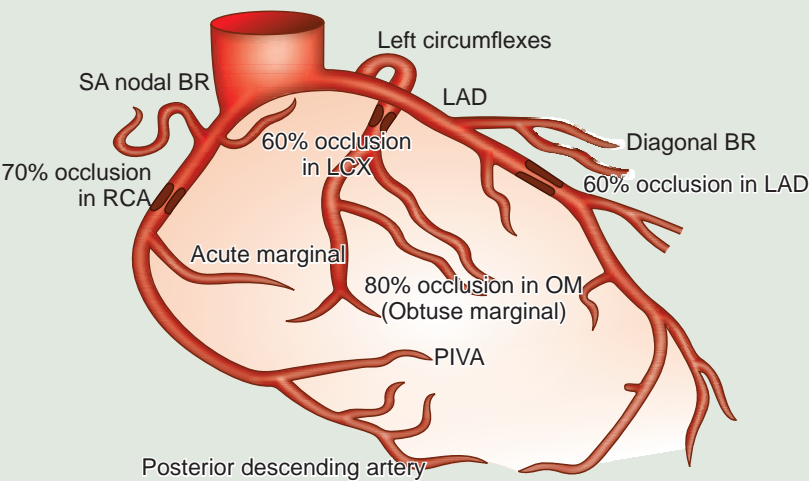


Fig. 4.133.22: Reporting template in coronary CT

(Contd.)

Table 4.133.8: Stepwise interpretation of cardiac MRI using perfusion sequences (Contd.)

Reporting template in cardiac MRI

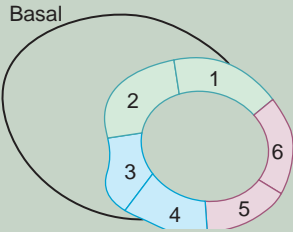
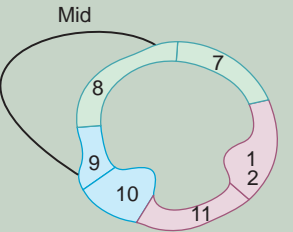
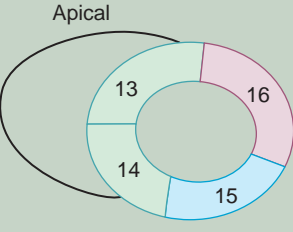
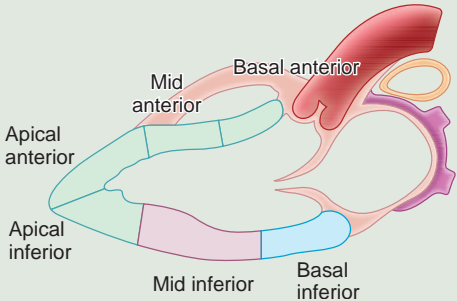
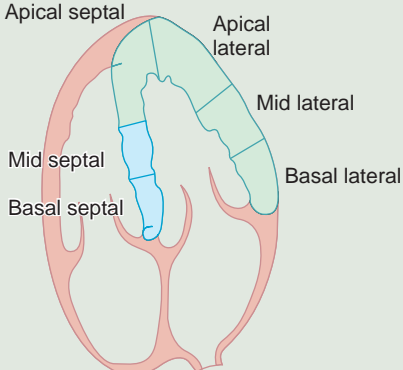

| | | |
|---|--|---|
|  <p>Fig. 4.133.23: Short axis view—basal</p> |  <p>Fig. 4.133.24: Short axis view—mid</p> |  <p>Fig. 4.133.25: Short axis view—apical</p> |
|  <p>Fig. 4.133.26: Vertical long axis view</p> |  <p>Fig. 4.133.27: Horizontal long axis view</p> |  <p>Fig. 4.133.28: Apex</p> |

Table 4.133.9: Difference between N13 ammonia or O-15 water PET-MPI and Rubidium 82 PET-MPI

| <i>N13 ammonia or O-15 water PET MPI (myocardial perfusion imaging)</i> | <i>Rubidium-82 PET MPI (myocardial perfusion imaging)</i> |
|---|---|
| <ul style="list-style-type: none">• Widely used for the last 2 decades• Has 10 mins half life• Needs a onsite cyclotron• Takes 100–120 mins for the procedure• Both rest and stress images can be gated• Good quality of gated and ungated images• Cumbersome and time taking• Some normal volunteers show mild defect in lateral wall of LV in N-13 ammonia retention | <ul style="list-style-type: none">• Rb-82 is a monovalent cation with a ultra short half life of 75 seconds• Can be done without a onsite cyclotron• Serial evaluations of regional myocardial perfusion can be made at intervals as short as 5 mins• First pass extraction at rest is 50–60% via Na, K-ATPase pump similar to thallium 201 and less than N-13• Uptake is a function of both blood flow and myocardial cell integrity |

Novel myocardial perfusion tracer-PET perfusion tracers have half-lives that are very short. This limits their applicability for exercise stress—flurpiridaz f-18—new PET-MPI radiopharmaceutical—in phase III clinical trial—has a long half life 110 min, binds to mitochondrial complex with high affinity—has an extraction ratio of

>90%. It can be used during exercise stress testing unlike other traditional pet tracers. F-18 FDG is an excellent probe to target macrophage infiltration as a marker of plaque inflammation. Myocardial perfusion and viability assessment help to identify candidates who would benefit from revascularization.

Table 4.133.10: Viability imaging for ischemic heart disease

| | |
|--|---|
| Thallium-201 SPECT Single injection for stress and resting phase, redistribution occurs, excessive radiation dose. | Technetium-99m MIBI SPECT Separate injections for stress and resting phase without redistribution, less radiation dose |
| FDG-PET (for viability) Because myocardial uses glucose for metabolism when it is under the influence of ischemia, it uses fatty acids for energy under normal circumstances. Non-viable myocardium will not show any uptake | Cardiac MR perfusion imaging <ul style="list-style-type: none"> • No ionizing radiation exposure • Dynamic imaging with gadolinium for perfusion • Delayed imaging for viability assessment |
| CT myocardial perfusion imaging <ul style="list-style-type: none"> • Single phase or dynamic perfusion imaging during stress +/- rest • Coronary arteries can be assessed at the same time | |

Table 4.133.11: Imaging features on CMR based on viability and its management

| Myocardial status | Perfusion | | Wall motion | | | De-MRI (Delayed MRI) | Treatment |
|----------------------------|-----------|--------|-------------|-----------------|------------------|-------------------------|----------------------------|
| | Rest | Stress | Rest | Low dose/stress | High dose/stress | | |
| Normal | Normal | Normal | Normal | ↑ | ↑↑ | Normal | No treatment/ follow-up |
| Inducible Ischemia | Normal | ↓ | Normal | ↑ | ↑↑ | Normal | Revascularisation |
| Stunned | Normal | ↓ | ↓ | ↑ | ↑↑ | Normal | Revascularisation |
| Hibernating | ↓ | ↓↓ | ↓ | ↑ | ↑↑ | Normal | Revascularisation |
| Sub-endocardial infarction | ↓ | ↓↓ | ↓ | ↓ | ↓↓ | Hyperenhance LGE | Revascularisation +/- |
| Transmural infarction | ↓ | ↓↓ | ↓ | ↓ | ↓↓ | Hyperenhance LGE | No revascularisation |

Table 4.133.12: Imaging findings for ischemic heart disease on DSE, SPECT, PET, CMR

| DSE (dobutamine stress echocardiography) | SPECT | PET | CMR (cardiac MR) |
|--|--|--|---|
| Subjective | Objective | Objective | Subjective |
| No radiation | Radiation | Radiation | No radiation |
| Cannot quantify | Relative quantitation of myocardial flow | Absolute quantitation of flow | Cannot quantify |
| Lower cost, easy availability | Most commonly used | Requires cyclotron, not readily available | Upcoming |
| Poor image in COPD and obesity | Study protocol extends one or two days, artifacts. | Gold standard for viability assessment, least artifacts. | Not possible if pacemaker, motion artifacts |

4.134 CARDIOVASCULAR SYSTEM

Case No. 134

Clinical history: 62 yers male presenting with dyspnea, chest pain \times 9 months and fever on and off \times 1 month. Radiological technique: Figure 4.134.1—scanogram with Fig. 4.134.2—plain and Fig. 4.134.3—contrast enhanced CT and Figs 4.134.4 and 4.134.5—MR images have been provided.

Observations: Scanogram shows multiple macronodules of varying sizes in bilateral lung fields with cardiomegaly.

CT shows well-defined non-enhancing multicystic lesion noted in the interventricular septum. Minimal enhancement of the cyst wall noted. Interatrial septum, the chambers of the heart, valves and great vessels appear normal. No evidence of any calcifications in the lesion. Cardiomegaly noted. No evidence of pericardial effusion. Visualized bilateral lung fields show similar cystic lesions.

In MR black blood T2 weighted sequences, the lesions appear hyperintense with fluid-fluid levels.

Interpretation: A: 62 years old, heart, C: Well-defined non enhancing T2 hyperintense multicystic lesions with daughter cysts in both interventricular septum of heart and bilateral lungs, B: No evidence of any calcifications in the lesion. Cardiomegaly noted. No evidence of pericardial effusion. D: Hydatid disease of heart and lung.

Principal diagnosis: Hydatid disease of heart and lung.

Differential diagnosis:

- Cystic tumor of atrioventricular node.
- Metastases: Most common cardiac tumor
Peicardial 70%, epicardial (34%), myocardial (32%)
(melanoma/lymphoma/leukemia) endocardial (5%)
Most common metastases are lung, breast, kidney and ovarian.

Others: Pleural mesothelioma, malignant melanoma, lymphoma and leukemia, pancreatic adenocarcinoma, gastric carcinoma, colonic carcinoma, mixed germ cell testicular tumor.

Lipoma: Rare, affects all ages. CT, MRI – fat characteristics, does not enhance. Surgical excision.

Next line of investigation:

1. Echo—to assess cardiac functioning.
2. Cardiac MRI—for better delineation of lesion.
 - Cine GRE—helpful in demonstrating tumour motion.
 - Perfusion MRI/CE-MRI
3. Coronary angiography—to assess the relationship with coronary vessels.

Management: Start the patient on Albendazole. Surgical excision under cardiopulmonary bypass is the treatment of choice. During surgery, measures should be taken to prevent perioperative embolization of germinative membrane.

Specific signs of cardiac hydatid: Multivesicular nature, membrane detachment, cyst wall calcification and daughter cysts.

Common areas of cardiac hydatid involvement: Left ventricle (60%) > Right ventricle (10%), Interventricular septum rare—4%.

Common route of invasion:

1. Invasion of myocardium through coronary artery circulation.
2. Pulmonary vein from rupture of pulmonary cysts.

Complications: Intracardiac rupture: Pulmonary embolism, systemic arterial embolization, anaphylaxis and sudden death, rupture into pericardial cavity—cardiac tamponade.



Fig. 4.134.1

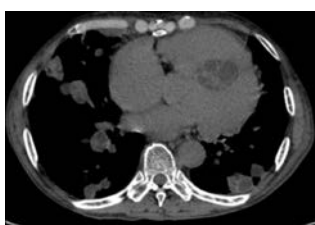


Fig. 4.134.2

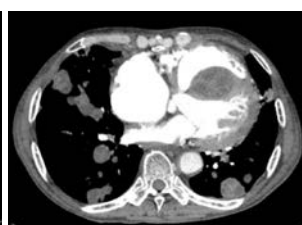


Fig. 4.134.3

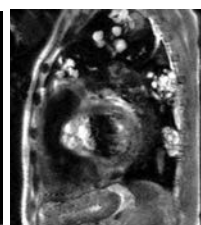


Fig. 4.134.4

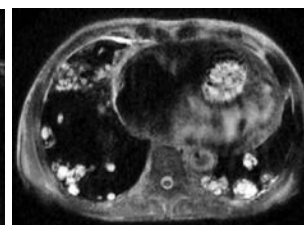


Fig. 4.134.5

Table 4.134.1: Difference between myxoma and thrombus

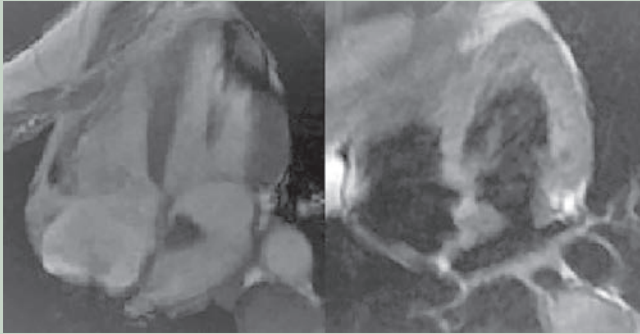
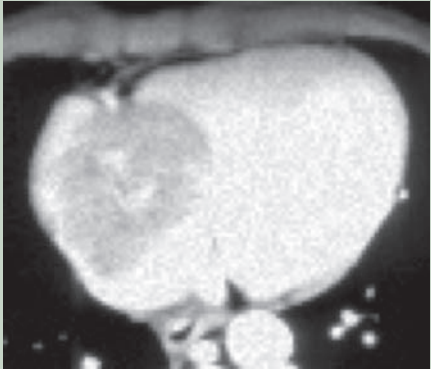


| <i>Myxoma</i> | <i>Thrombus</i> |
|---|---|
|  <p>Fig. 4.134.6: Myxoma</p> <ul style="list-style-type: none"> • Most commonly in left atrium • Single lesion, pedicle • CECT—heterogeneous enhancement • Necrosis/haemorrhage/cysts present • MR—T1/T2 isointense, bloom on GRE—high iron content • MR perfusion—enhancement present. |  <p>Fig. 4.134.7: CLOT</p> <ul style="list-style-type: none"> • Most common—left atrial appendage • Laminated appearance, irregular or lobulated borders, microcavitations • Absence of a pedicle • CT—homogeneous attenuation • CECT—does not enhance • MR—nulled at T1 values >600. Thrombus cannot recover from saturation. |

Table 4.134.2: Imaging fat in heart

| | |
|--|--|
| <p>Lipomas—smooth—contoured, encapsulated, fatty masses.</p> <p>Liposarcoma—irregular, multilobular morphology with almost complete absence of identifiable fat.</p> | <p>Lipomatous hypertrophy—wedge-shaped or diffuse fatty thickening of the interatrial septum.</p> |
|--|--|

Table 4.134.3: Paediatric cardiac tumors

| | |
|---|--|
| <p>Rhabdomyoma</p> <p>Infants and children</p> <p>Usually small and multiple</p> <p>Hyperechoic on ECHO</p> <p>Ca⁺⁺ rare.</p> <p>MR—T1: iso, T2: hyper</p> <p>Associated with tuberous sclerosis</p> <p>Spontaneous tumor regression +</p> <p>In utero—non-immune hydrops and fetal death</p> | <p>Fibroma</p> <p>Children</p> <p>Usually solitary</p> <p>Mural Ca⁺⁺: 25% with hypokinetic myocardium.</p> <p>CECT: Enhancement +</p> <p>T1: iso, T2: hypo</p> <p>Most common resected paediatric cardiac tumor.</p> <p>Cause of death—invasion or compression of cardiac conduction system.</p> |
| <p>Hemangioma</p> <p>All age groups, asymptomatic.</p> <p>ECHO: Hyperechoic lesions</p> <p>CECT: Intensely enhancement +</p> <p>MRI: Like hepatic hemangiomas (T1—intermediate and T2—hyperintense)</p> <p>Coronary arteriography: Vascular blush, particularly in the capillary and arteriovenous types of hemangiomas, which exhibit rapid blood flow.</p> <p>Cavernous hemangiomas: Very slow flow and therefore do not typically enhance at angiography.</p> <p>Rx: Surgical excision.</p> | <p>Paraganglioma</p> <p>Extremely rare neoplasms, adults</p> <p>Arise from intrinsic cardiac paraganglial (chromaffin) cell—atria.</p> <p>Symptoms and biochemical—similar to pheochromocytoma</p> <p>CECT—markedly enhancing lesion involving the left atrium</p> <p>MRI T1 hypointense T2 very hyperintense</p> <p>Caution with contrast—hypertensive crises.</p> <p>Surgical excision with cardiopulmonary bypass.</p> |

| Table 4.134.4: Malignant cardiac tumors | |
|---|---|
| Angiosarcoma | Lymphoma |
|  |  |
| <p>Fig. 4.134.8: Angiosarcoma</p> <ul style="list-style-type: none">• Malignant, rare• Most common in right atrium• CT demonstrates—broad-based tumor attachment, myocardial, pericardial, and mediastinal invasion; as well as extension into the great vessels and pulmonary metastases.• Cardiac sarcomas enhance heterogeneously, with non-enhancing areas typically corresponding to necrosis• The mean survival is from 3 months to 1 year• Aggressive surgery: Local recurrence and metastatic disease occur frequently and early, usually within 1 year. Heart transplantation.• Chemotherapy and radiation therapy—not beneficial | <p>Fig. 4.134.9: Lymphoma</p> <ul style="list-style-type: none">• Greater frequency in immunocompromised patients, particularly in association with the acquired immunodeficiency syndrome.• Mean age 60 years, most common in right atrium• Echocardiography—hypoechoic• NCCT—hypoattenuating, CECT—heterogeneous enhancement• MRI imaging demonstrates poorly marginated and heterogeneous lesions• T1WI: Hypointense relative to cardiac muscle and T2 isointense• Rx: Chemotherapy, poor prognosis |

| Table 4.134.5: Approach to cardiac tumors (Fig. 4.134.10) | | | | | | |
|---|--|--------------------------|---------------------|----------------------------------|------------------------------|--|
| Right atrium | Left atrium | Right ventricle | Left ventricle | Interatrial septum | Valves | Pericardium |
| Angiosarcoma Lymphoma | Myxoma—F. ovalis, thrombus—LAA, Paraganglioma—roof, Leiomyosarcoma—posterior | Angiosarcoma Teratoma | Fibroma Thrombus | Lipoma Lipomatous hypertrophy | Fibroelastoma Vegetations | Primary pericardial mesothelioma, lymphoma, metastasis |

| Table 4.134.6: Nature of cardiac hydatid in right and left | |
|--|-------------------------|
| Right sided | Left sided |
| Tendency to expand and rupture more frequently | Rupture less frequently |
| Grow subendocardially | Grow subepicardially |

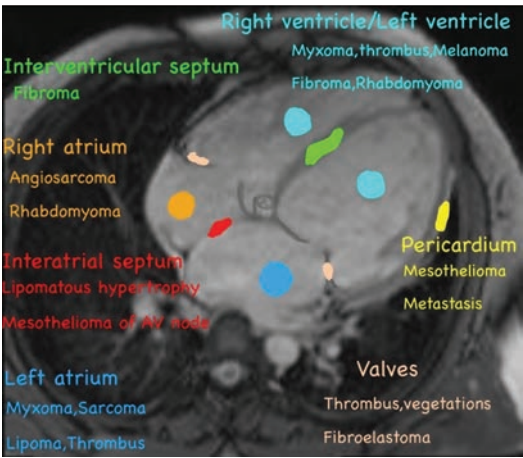


Fig. 4.134.10: Cardiac masses

4.135 MUSCULOSKELETAL SYSTEM

Case No. 135

Clinical history: A 3 years old child with milestone regression, dysmorphic facies and abdominal distension.

Radiological techniques and observation: Figure 4.135.1 is AP radiograph chest showing paddle-shaped ribs with reduced intercostal spaces. Figure 4.135.2 is lateral radiograph of skull showing macrocephaly and J-shaped sella. Figure 4.135.3 is AP radiograph pelvis showing hypoplasia of base of ilia showing inferior beaking with enlargement of the acetabulum and coxa valga. Figures 4.135.4 and 4.135.5 are lateral radiograph of DL spine showing kyphosis, platy spondyly with hypoplastic dorsolumbar vertebra and middle beaking

which is seen in most of the vertebra. Figure 4.135.6 is hand radiograph showing proximal pointing of metacarpals with maintained middle constriction.

Interpretation: A: 3 years old child, C: Proximally pointed metacarpals with maintained middle constriction, inferior beaking of iliac wings, J-shaped sella, oar-shaped ribs, diffuse platyspondyly with middle beaking, D: Mucopolysaccharidosis. Since middle constriction in metacarpals are maintained and there is middle beaking in vertebrae: Morquio disease.

Principal diagnosis: Mucopolysaccharidosis: Morquio disease.

MRI spine screening should be done to rule out other manifestations.



Fig. 4.135.1



Fig. 4.135.2



Fig. 4.135.3

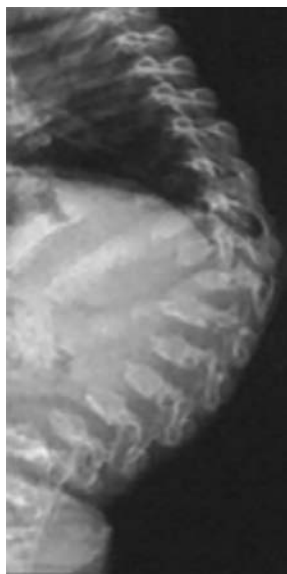


Fig. 4.135.4



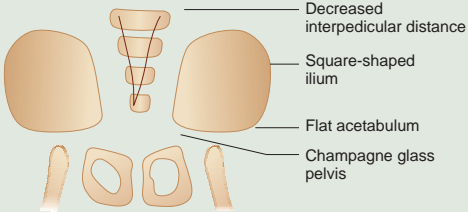
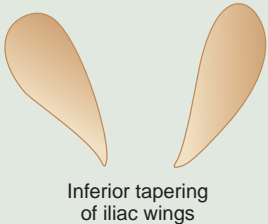

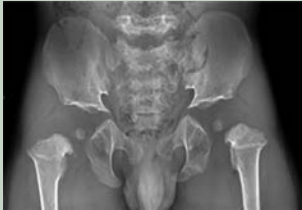
Fig. 4.135.5



Fig. 4.135.6

| Table 4.135.1: Manifestations of MPS | |
|--------------------------------------|---|
| Intracranial manifestations | Enlarged perivascular spaces (refer to case 37), white matter lesions, hydrocephalus, cortical atrophy, cervical spinal canal stenosis |
| Skull | J-shaped sella: Flattened tuberculum sella |
| Hands and feet | V-shaped deformity of the distal ulna and radius (hypoplastic), hypoplastic and irregularly shaped carpal and tarsal bones, proximal pointed metacarpals and metatarsals, Bullet-shaped phalanges |
| Pelvis | Dysostosis multiplex—hip dysplasia, rounded iliac wings, inferior tapering of the ilium, poorly developed acetabulum. Underdeveloped medial femoral epiphysis, coxa valga. Proximal humeral notch, long narrow femoral neck, fraying and flaring of metaphyses |
| Chest | Paddle-shaped/oar-shaped ribs: Ribs widened anteriorly and tapered posteriorly |
| Otorhinolaryngological imaging | Thickened tympanic membrane, poor pneumatisation of sphenoidal bone, opacification of mastoid and middle ear cavity, flattened and deformed mandibular condyles, poor pneumatisation of mastoid sinus and impacted teeth |
| Spine | Compression of the spinal cord at the C1–C2 joint (seen predominantly in MPS IV and VI). Atlanto-axial subluxation due to transverse ligament laxity, dural thickening resulting from collagen and GAG deposits, odontoid hypoplasia/aplasia, anterior soft tissue mass of odontoid (made of unossified fibrocartilage and reactive changes) and posterior arch of C1 indentation. Platyspondyly. Inferior beaking: Hurler; middle beaking: Morquio. Kyphoscoliosis |

| Table 4.135.2: Pearls on Hurler’s, Morquio syndrome, platyspondyly and vertebral beaking | | | |
|--|---|-------------------------|---|
| <i>Hurler</i> | <i>Morquio syndrome</i> | <i>Platyspondyly</i> | <i>Vertebral beaking</i> |
| Mentally retarded | Mentally normal | Gaucher disease | Hurler syndrome—anterior inferior beaking |
| Early corneal clouding | Late (after 10 years) | Metatrophic dysplasia | Morquio syndrome—anterior middle beaking |
| Some vertebra | Most of the vertebra involved | Osteogenesis imperfecta | Achondroplasia |
| Inferior beaking | Middle beaking | Morquio syndrome | Down syndrome |
| Middle constriction lost | Middle constriction of metacarpals maintained | Thanatophoric dysplasia | Cretinism |
| | | | Neuromuscular diseases |

| Table 4.135.3: Difference between achondroplasia and MPS | |
|--|---|
| <i>Achondroplasia</i> | <i>MPS</i> |
| Squaring of ilium (tombstone) with horizontal acetabular roof. Trident pelvis (champagne glass pelvis) Lumbar spine: Interpedicular distance gets narrowed | Inferior beaking of ilium (hibiscus petal shaped), increased acetabular angles and constricted iliac bone base. Posterior vertebral scalloping, gibbus deformity, bullet-shaped vertebra. Platyspondyly with beaking (middle/inferior). |
|  Fig. 4.135.7: Achondroplasia |  Fig. 4.135.9: MPS |
|  Fig. 4.135.8: Achondroplasia |  Fig. 4.135.10: MPS |

Management: Confirm the diagnosis with glycosaminoglycans level in urine and enzyme assay. Enzyme replacement therapy and hematopoietic stem cell transplant.

Differentials for J-shaped sella (MPS)

1. Neurofibromatosis
2. Hydrocephalus
3. Achondroplasia
4. Pituitary mass
5. Optic chiasma glioma.

Discussion: Mucopolysaccharidosis (MPS) (dysostosis multiplex) is inherited metabolic disease and member of the group of lysosomal storage disorders. Degradation of mucopolysaccharides, also known as glycosaminoglycans is the characteristic feature. There are 7 types of MPS (I, II,

III, IV, VI, VII, and IX), that has multiple subtypes based on enzyme deficient and the clinical severity.

1. MPS I. MPS IH: Hurler syndrome (most severe)
2. MPS II: Hunter syndrome. Neuropathic (severe), non-neuropathic (mild)
3. MPS III: Sanfilippo syndrome.
4. MPS IV: Morquio syndrome.
5. MPS VI: Maroteaux-Lamy syndrome.
6. MPS VII: Sly syndrome.
7. MPS IX: Natowicz syndrome

Causes of atlantoaxial subluxation: Congenital—Os odontoideum, Down syndrome, Morquio syndrome, spondyloepiphyseal dysplasia, osteogenesis imperfecta, Marfan syndrome, NF1; acquired—rheumatoid arthritis, psoriatic arthritis, reactive arthritis.

4.136 MUSCULOSKELETAL SYSTEM

Case No. 136

Clinical history: Five years old male child with history of decreased height and shortening of limbs since birth.

Radiological techniques and observations: Figures 4.136.1–4.136.5 are plain radiograph of anteroposterior view of abdomen, pelvis, bilateral femur and lateral radiograph of thoracolumbar spine, skull shows shortened iliac bone with squaring and pelvis appears champagne glass shape. Horizontal orientation of acetabular roof, the interpedicular distance in the lumbar spine decreases progressively from L1 to L5. There is posterior scalloping of the vertebral body and it appears bullet shaped. There is symmetrical shortening of the femur with widened metaphysis. The distal femoral epiphyses show inverted V-shaped appearance (Chevron sign). Lateral radiographs show diffuse shortening of vertebral body height and increased height of the disc space. No evidence of pubic diastasis. Overall length of the spine appears normal. Lateral radiograph of skull shows relatively large cranial vault with small skull base, frontal bossing with the depressed nasal bridge (midfacial retrusion). Plain radiograph AP view of chest, abdomen with bilateral upper limb shows, symmetrical shortening and bowing of the bilateral humerus with thickening. Chest is bell shaped. Ulnar appears shortened compared to radius. Plain radiograph of bilateral hand and wrist shows widening of gap between middle and ring finger (Trident hand). There is shortening and thickening of the phalanx distal phalanx appears small and pointed. There is no evidence of destruction of bone/osteopenia. The clavicle appears normal.

Interpretation: A: 5 years old male child, C: Symmetrical shortening of bilateral iliac bones with squaring

and champagne glass shaped pelvis, shortening of bilateral femur, bilateral humerus more pronounced in proximal and upper limb (rhizomelic dwarfism), B: Progressive narrowing of interpedicular distance from L1 to L5. Bell-shaped chest, frontal bossing and midface hypoplasia. Widened gap between middle and ring finger (trident hand), small and pointed distal phalanx. D: Achondroplasia.

Principal diagnosis: Achondroplasia (symmetrical shortening of limb more in upper extremities and proximal long bones, trident hand, posterior scalloping of vertebrae, champagne glass pelvis, decreasing interpedicular distance in lumbar spine).

1. Skeletal Dysplasia

Skeletal dysplasia is a heterogeneous group of more than 450 disorders characterised by abnormalities of cartilage and bone growth and development resulting in abnormal shape and size of skeleton and disproportionate long bones, spine and skull. Skeletal dysplasias can be classified based on genetic, biological and radiological manifestation. 92% of dysplasia have genetic aberrations, and can be classified based on genetic abnormalities (revised in 2019).

Osteochondrodysplasia is an abnormality of bone/cartilage/growth/texture. It is usually due to genetic mutation and continues to evolve throughout life. Dysostosis are malformations of individual/multiple bones in combination. It is usually due to abnormal blastogenesis *in utero* and phenotypically static.

There are multiple grouping system of skeletal dysplasia based on different characteristics. Since there are significant overlaps between different entities and



Fig. 4.136.1



Fig. 4.136.2

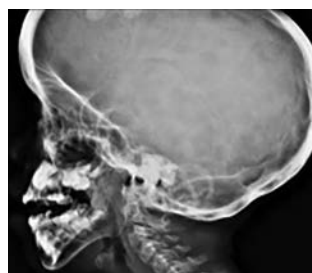


Fig. 4.136.3






Fig. 4.136.4







Fig. 4.136.5

Table 4.136.1: Differential diagnosis for achondroplasia

| Condition | Imaging findings |
|--|---|
| Achondrogenesis: Autosomal recessive lethal chondrodystrophy characterised by Triad, 1. Severe short limb dwarfism 2. Lack of vertebral calcification 3. Large head with decreased calvarial ossification Prevalence 2.3 per 100000. Prognosis is lethal <i>in utero</i> . Often confused with thanatoporic dwarfism. | Type-1 Parenti-Fraccaro disease Complete lack of ossification of calvarium, spine and pelvis, absent sacrum and pubic bone, extremely short long bones, thin rib with multiple fractures. Type-2 Langer-Saldino Defective enchondral ossification alone, non-ossification of lower lumbar vertebrae and sacrum, short and stubby horizontal ribs without fractures. |
| Pseudoachondroplasia Part of osteochondroplasia, prevalence is 4 in 1000000, mutation of COMP (Cartilage Oligomeric Matrix Protein) gene in chromosome 19. Age of presentation 2–4 years. Gait disturbance and joint laxity. Normal skull and face. Complication—premature osteoarthritis. | <div></div> <p>Fig. 4.136.6: Pseudoachondroplasia Fig. 4.136.7: Pseudoachondroplasia</p> <p>Skull—normal, spine—persistent oval-shaped vertebral bodies, odontoid dysplasia, disc space widening</p> <p>Extremities: Short long bones with flared metaphysis. Small irregular flared epiphysis with delayed development. Medial beaking of femoral neck. Genu valgum/varum. Pelvis—widened triradiate cartilage.</p> |
| Thanatophoric dysplasia: It is the sporadic lethal skeletal dysplasia characterised by severe rhizomelia, incidence is 6.9 in 100000 births. Severe respiratory distress (early in life), hypotonic infants, protrubent abdomen, extended abdomen, extended arms and abducted externally rotated thighs. | <p>OB USG—Short limb dwarfism with extremely short and bowed telephone receiver like femurs, extremely small hypoplastic thorax, macrocrania with frontal bossing, clover leaf skull (14%), diffuse platyspondyly, polyhydramnios and protruded abdomen. Plain radiograph: Head is large with short skull base with prominent frontal bone, trilobed clover leaf skull. Chest: Narrow chest, short horizontal ribs, spine—generalised platyspondyly with H or U-shaped vertebra plana, increased intervertebral space height, pelvis—small and squared off iliac bones, flat acetabulum, narrow sacrosciatic notch.</p> <div></div> <p>Fig. 4.136.8: Thanatophoric dysplasia</p> |




(Contd.)

Table 4.136.1: Differential diagnosis for achondroplasia (Contd.)

| Condition | Imaging findings | |
|---|---|--|
| <p>Osteogenesis imperfecta: Connective tissue disorder leading to micromelic dwarfism. Mutation in COLA1 and COLA2 leading to defective synthesis of collagen I. Four types are: Type I—autosomal dominant, Type II—autosomal recessive/sporadic, Type III—autosomal recessive, Type IV—autosomal dominant. Type II is lethal. Clinical traid are blue sclera, abnormal dentition and skeletal fragility. In Type IV OI sclera is normal. Complication is multiple fractures and deformity. Multiple fractures often transverse in lower extremities are hallmark also seen with excessive callus. Shepherd crook deformity and protrusio acetabuli are seen in femur.</p> | <p>Diffuse decrease in bone density, pencil thin cortex, multiple fractures. Six types A to F based on, a) Vertebral contours, b) bowing of long bones, c) Trefoil-shaped pelvis, d) Cystic changes in long bones epiphysis and metaphysis, e) Thickness of long bone cortices, f) Thickness of rib cortices. Platybasia, basilar impression and vertebral body appear like biconcave lens.</p> |  <p>Fig. 4.136.9: Osteogenesis imperfecta</p> |
| <p>Chondrodysplasia punctuata (autosomal recessive lethal form) type of epiphyseal dyplasia which shows punctuate or stippled calcification in multiple epiphysis. The recessive type is lethal and child dies within 1 year of life. Characterised by symmetric proximal limb shortening, joint contractures, mental retardation, cataract, optic atrophy and skin changes. In most cases there are coronal clefts in vertebral body, but stippling is absent in recessive type and spinal deformity is not as severe as dominant Conradi-Hünemann syndrome.</p> | <p>Appearance of stippled epiphysis within 1st year of life. In recessive type stippling primarily seen in hips, shoulders, knees and wrist. Symmetric shortening of the limbs particularly proximal and upper extremities. The metaphysis are flared. The long bones are bowed.</p> |  <p>Fig. 4.136.10: Chondrodysplasia punctuata</p>  <p>Fig. 4.136.11: Chondrodysplasia punctuata</p> |
| <p>Epiphyseal dysplasia multiplex: Disorder with abnormalities of epiphyses usually manifests in childhood and lead to severe degenerative changes. Autosomal dominant. Waddling gait, premature joint degeneration and short stature, tibiotalar slant. The carpal and tarsal bones are hypoplastic. Long tubular bones of hands are short and thick. The femoral head and condyles are flattened. Associated with scoliosis, osteochondritis dissecans and SCFE.</p> | <p>Delayed development of epiphysis and mottled with irregular mineralisation during 2nd or 3rd year of life. The involvement is bilateral and symmetrical with hips, knees and ankles most commonly involved.</p> |  <p>Fig. 4.136.12: Epiphyseal dysplasia multiplex</p> |

(Contd.)

Table 4.136.1: Differential diagnosis for achondroplasia (Contd.)

| Condition | Imaging findings | |
|---|--|---|
| <p>Chondroectodermal dysplasia also known as the Ellis-van Creveld syndrome is a rare autosomal recessive acromesomelic dwarfism. Clinical features are absent or hypoplastic brittle spoon-shaped nails, dysplastic tooth, scant hair, genital malformation, accelerated skeletal maturation with normal spine. Death occurs within 1 month of life in 30–50% cases. DD-Asphyxiating thoracic dysplasia.</p> <p>Upper extremity-drumstick forearm (swelling of proximal ulna and distal radius). Lower extremity: Mesomelic shortening, slanting proximal tibial metaphysis, medial tibial diaphyseal exostosis, excessive shortening of fibula. Supernumerary carpal bones and post-axial polydactyly.</p> | <p>Skull: Wormian bones, cleft lip Chest: Narrow thorax in AP and transverse, cardiomegaly, short horizontal ribs and anterior osseous expansion, elevated clavicles. Pelvis-Small flattened ilium, trident-shaped acetabulum with indentation roof and bony spur (pathognomic). Extremities: Thickening and shortening of all long bones, absence of terminal phalanx, and mesomelia (shortening of forearms) and legs medial tibial exostosis.</p> |  <p>Fig. 4.136.13: Chondroectodermal dysplasia post-axial polydactyly</p>  <p>Fig. 4.136.14: Chondroectodermal dysplasia</p> |
| <p>Spondyloepiphyseal dysplasia congenita Sporadic/autosomal dominant Disproportionate dwarfism with spine and hip involvement more than extremities, flat facies, short neck, deafness, cleft palate and waddling gait. Complications: Retinal detachment, secondary arthritis.</p> | <p>Epiphyseal irregularities vertebral bodies—ovoid vertebral bodies and severe platyspondyly vertebral body appears bulbous (pear shape), hypoplasia of odontoid process, progressive kyphoscoliosis, narrowing of disc space. Pelvis: Broad iliac bases, flat acetabular roof. Chest-bell shaped, pectus carinatum. Extremities—slightly shortened limbs, coxa vara and genu valgum, multiple accessory epiphysis in hands and feet.</p> |  <p>Fig. 4.136.15: Spondyloepiphyseal dysplasia congenita</p> |
| <p>Campomelic dysplasia Sporadic/autosomal recessive dwarfism a/w, a. Hydrocephalus (23%) b. Congenital heart disease (30%): VSD, ASD c. Hydronephrosis Pretibial dimple. Death usually occurs <5 months of age.</p> | <p>Chest and spine: Hypoplastic scapula, narrow bell-shaped chest, hypoplastic vertebral bodies and non-mineralised pedicles. Pelvis-Vertically narrowed iliac bones, wide symphysis, narrow iliac bones with small wings, shallow acetabulum. Extremities: Dislocation of hips and knees, anterior bowing of long bones, hypoplastic fibula, clubfoot.</p> | |

(Contd.)

| Table 4.136.1: Differential diagnosis for achondroplasia (Contd.) | |
|---|---|
| Condition | Imaging findings |
| Asphyxiating thoracic dysplasia also known as Jeune syndrome, is an autosomal recessive type of rare short limb skeletal dysplasia, which is primarily characterized by a constricted long narrow thoracic cavity, cystic renal dysplasia and characteristic skeletal features. Complication—development of pulmonary hypoplasia, renal failure from cystic renal disease and hepatic cirrhosis. | Radiographic features , thorax—short narrow elongated chest shape (can be bell-shaped) may be seen as a narrow fetal thorax antenatally high riding clavicles (“handlebar clavicles”) irregular costochondral junctions. Others—dysplastic acetabula with flat acetabular roof trident acetabula short and flared iliac bones ischial and pubic bones with medial and lateral spurs. Short broad phalanges short distal limbs (acromelic dwarfism) polydactyly (often pre-axial); 14% coned epiphyses. |



Fig. 4.136.16: Asphyxiating thoracic dysplasia



Fig. 4.136.17: Asphyxiating thoracic dysplasia

| Table 4.136.2: Comparison between achondroplasia group | | | | | |
|--|---|--|---|---|--|
| Body part | Achondrogenesis | Achondroplasia (homozygous) | Achondroplasia (heterozygous) | Hypochondroplasia | Pseudoachondroplasia |
| Skull and facial bone | Large head with decreased ossification | Enlarged calvaria, shortened skull base and small face | Enlarged calvaria, shortened skull base, frontal bossing, midface hypoplasia | Normal | Normal |
| Spine (interpedicular distance) | Lack of ossification of spine | Progressive reduction. Hypoplastic vertebral bodies | Progressive reduction | Narrowing | Normal |
| Pelvis | Absent sacrum and pubic bone | Squaring of ilium, flat acetabular roof | Squaring of ilium, flat acetabular roof (champagne glass pelvis) | Flat acetabular roof | Widened triradiate cartilage |
| Chest | Short and thin ribs with multiple fractures | Short ribs with flared ends | Short anteriorly flared concave ribs | Normal | Normal |
| Extremities | Extremely short long bones without bowing | Severe rhizomelic shortening | Rhizomelic shortening Chevron sign, trident hand and trumpet appearance (long bone) | Rhizomelic shortening with mild flaring | Short long bones with flared metaphysis. medial beaking of femoral neck. |

Table 4.136.3: Difference between pseudoachondroplasia and achondroplasia

| <i>Pseudoachondroplasia</i> | <i>Achondroplasia</i> |
|---|--|
| Skull: Normal | Prominent head with prognathism |
| Spine: Platyspondyly is seen | Increased disc height, platyspondyly not usually seen |
| Interpedicular distance is normal | Interpedicular distance is decreased along lumbar spine caudally |
| No posterior scalloping | Posterior scalloping of vertebrae and vertebrae is bullet shaped |
| Epiphyses and metaphysis is abnormal | Only metaphyses are abnormal |
| Trident hand and champagne glass pelvis is absent | Trident hand and champagne glass pelvis is present |

Table 4.136.4: Radiological classification of osteochondrous dysplasia (according to Panda A, et al 2014)

| <i>Group I: Epiphyseal dysplasia</i> | <i>Group II: Metaphyseal dysplasia</i> | <i>Group III: Osteopenic dysplasia</i> |
|--|---|---|
| Chondrodysplasia punctata Multiple epiphyseal dysplasia Dysplasia epiphysealis hemimelica Spondyloepiphyseal dysplasia Thanatophoric dysplasia | Asphyxiating thoracic dysplasia Chondroectodermal dysplasia Achondroplasia Hypochondroplasia Hypophosphatasia | Mucopolysaccharidoses and Mucopolipidosis Osteogenesis imperfecta Ehlers-Danlos syndrome Massive osteolysis of Gorham |
| <i>Group IV: Sclerosing dysplasia</i> | <i>Major involvement of spine</i> | <i>Group V: Miscellaneous</i> |
| Osteopetrosis Osteopoikilosis Osteopathia striata Melorheostosis Pyknodysostosis Progressive diaphyseal dysplasia Infantile cortical hyperostosis Camurati-Engelmann disease Craniotubular dysplasia | Spondyloepiphyseal dysplasia Diastrophic dwarfism Spondylometaphyseal dysplasia Spondyloepimetaphyseal dysplasia Pseudoachondroplasia | Cleidocranial dysplasia |

Table 4.136.5: Classification based on lethal dysplasias

| <i>Relatively common lethal dysplasia</i> | <i>Rare lethal dysplasia</i> |
|--|---|
| Thanatophoric dysplasia Achondrogenesis Osteogenesis imperfecta Type 2 | Congenital hypophosphatasia Campomelic dysplasia Chondrodysplasia punctata—rhizomelic and non-rhizomelic Homozygous achondroplasia Short rib polydactyly syndrome |

multiple variants in a single entity, devising a single classification system including all the skeletal dysplasias is difficult (Tables 4.136.4 and 4.136.5).

Based on involvement of axial skeleton (dwarfism-shortening of trunk)



- Decreased height of spine:** Spondyloepiphyseal dysplasia, spondylometaphyseal dysplasia, spondyloepimetaphyseal dysplasia, metatrophic dysplasia, Morquio's syndrome, achondrogenesis, Dyggve-Melchior-Clausen syndrome, Kniest dysplasia.
- Small chest with short ribs:** Asphyxiating thoracic dysplasia, achondrogenesis, campomelic dysplasia,

thanatophoric dysplasia, homozygous achondroplasia, Ellis-van Creveld syndrome.

Radiographic Approach to Skeletal Dysplasia

Skeletal survey: Skull (AP and lateral) to include atlas and axis, spine (AP), pelvis (AP), one upper limb (AP), one lower limb (AP), hand (bone age) AP, feet (AP) are required to diagnose or exclude skeletal dysplasia in a suspected child. In cases with epiphyseal irregularity or stippling radiographs of bilateral upper and lower limbs are recommended. Similarly, serial radiographs are recommended to assess the evolution of disease and complication.

| Table 4.136.6: Classification based on limb shortening | |
|--|--|
| Skeletal dysplasia causing rhizomelic limb shortening —shortening of proximal limb, humerus and femur. | Achondroplasia—eterozygous, hypochondroplasia, pseudo-achondroplasia. Rhizomelic type of chondrodysplasia punctata, spondyloepiphyseal dysplasia, congenita, thanatophoric dwarfism, diastrophic dysplasia, Jansen metaphyseal dysplasia. |
| Skeletal dysplasia causing mesomelic limb shortening short middle segments, e.g. radius, ulna, tibia, fibula. | Langer and Nievergelt dysplasia, Léri-Weill syndrome (also made lung deformity seen), Robinow syndrome, Reinhardt syndrome. |
| Langer type is autosomal recessive dysplasia characterised by mental impairment | Radiographic features are, mesomelic shortening of limbs, hypoplasia of ulna and fibula, hypoplasia of mandible with short condyles. Widening with mild to moderate bowing of diaphysis. |
| Nievergelt type autosomal dominant dysplasia severe mesomelic shortening of lower limbs | Radiographic features are shortening of all long bones marked in tibia and radius, marked thickening of tibia and fibula in central portion and club foot. Widening with mild to moderate bowing of diaphysis, hypoplasia of fibula with absent lateral malleolus. Made lung deformity of wrist |
| Skeletal dysplasia causing acromelic limb shortening short distal segments, e.g. metacarpals, phalanges | Asphyxiating thoracic dysplasia, pyknodysostosis |
| Skeletal dysplasia causing micromelic limb shortening: All bones of the limbs are shortened. | Achondrogenesis, fibrochondrogenesis, Kniest dysplasia, dys-segmental dysplasia, Roberts syndrome |
| Combined-acromesomelic dysplasia | Ellis-van Creveld syndrome, type Nievergelt of mesomelic dysplasia type, Robinow of mesomelic dysplasia, type Werner of mesomelic dysplasia |

| Table 4.136.7: Differential diagnosis based on bone density | |
|--|---|
| Increased(sclerosing) | Decreased(osteopenic) |
| Osteopetrosis Pyknodysostosis Cleidocranial dysplasia Osteopoikilosis Osteopathia striata Melorheostosis Camurati-Engelmann disease Craniotubular dysplasia | Osteogenesis imperfecta Achondrogenesis |
|  |  |
| Fig. 4.136.18: Osteopetrosis | Fig. 4.136.19: Osteogenesis imperfecta |

1. Spine



Fig. 4.136.21: Platyspondyly



Fig. 4.136.22: Lumbar interpedicular narrowing

Fig. 4.136.20: Vertebral body pathologies in osteochondral dysplasia

Table 4.136.8: Spectrum of spine abnormalities in skeletal dysplasia

Short trunk—platyspondyly: Morquio's syndrome, spondylo-epiphyseal dysplasia congenita, spondyloepimetaphyseal dysplasia, thanatophoric dysplasia, pseudochondroplasia, metatrophic dysplasia, recessive type of chondrodysplasia punctuata, Ehlers-Danlos syndrome

Coronal clefting: Chondrodysplasia punctuata, Kniest dysplasia, mesomelic dysplasia, metatrophic dysplasia.










Fig. 4.136.23: Platyspondyly

Fig. 4.136.24: Platyspondyly

Fig. 4.136.25: Coronal clefting

(Contd.)

| Table 4.136.8: Spectrum of spine abnormalities in skeletal dysplasia (Contd.) | |
|---|---|
| <p>Posterior scalloping of vertebral body: Achondroplasia (spinal canal stenosis), Hurler syndrome, Morquio's syndrome, Marfan's syndrome, Ehler-Danlos syndrome</p>  | <p>Inter-pedicular distance narrowing (spinal canal stenosis): Achondroplasia, spondyloepiphyseal dysplasia.</p>  |
| <p>Fig. 4.136.26: Posterior scalloping of vertebral body</p> | <p>Fig. 4.136.27: Achondroplasia</p> |
| <p>Middle beaking Morquio's syndrome</p>  | <p>Inferior beaking Hurler syndrome</p>  |
| <p>Fig. 4.136.28: Morquio's syndrome</p> | <p>Fig. 4.136.29: Hurler syndrome</p> |
| <p>Spinal canal narrowing—short pedicle: Achondroplasia</p>  | <p>Wedge-shaped upper lumbar vertebra: Achondroplasia</p>  |
| <p>Fig. 4.136.30: Achondroplasia</p> | <p>Fig. 4.136.31: Achondroplasia</p> |
| <p>Humping: Platyspondyly with heaping up and hyperostosis on the posterior two-thirds of endplates giving a hump-shaped vertebra. Spondyloepiphyseal dysplasia congenita.</p>  | <p>Scoliosis/kyphosis Lumbar angular kyphosis—gibbus deformity, lumbosacral lordosis-achondroplasia. Scoliosis—pseudoachondroplasia. Angular kyphosis/gibbus deformity, exaggerated lumbar lordosis, kyphoscoliosis—mucopolysaccharidosis (MPS).</p> |
| <p>Fig. 4.136.32: Spondyloepiphyseal dysplasia congenita</p> | |

(Contd.)

Table 4.136.8: Spectrum of spine abnormalities in skeletal dysplasia (Contd.)

Bullet—achondroplasia



Fig. 4.136.33: Gibbus deformity

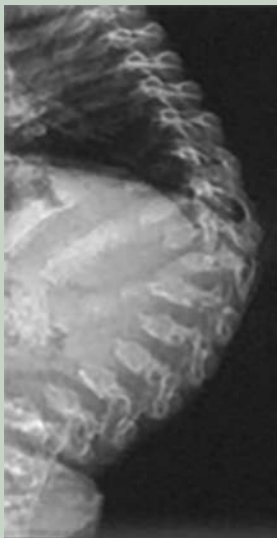


Fig. 4.136.34: Gibbus deformity



Fig. 4.136.35: Bullet—achondroplasia

Absent sacrum: Achondrogenesis, atlantoaxial subluxation—mucopolysaccharidosis (MPS) (Morquio's, Hurler syndrome)

A step by step approach will make it easier to narrow down the differentials and diagnose a skeletal dysplasia. Following features are to be looked in a skeletal survey.

1. Bone mineralisation—differentiating sclerosing, osteopenic dysplasia.
2. Axial bone involvement—skull, spine (Dwarfism-shortening), thorax
3. Appendicular bone—pattern of shortening (Acro, meso, rhizo, micro)—location of abnormality (epiphysis, metaphysis, diaphyseal)
4. Other features—fractures, bowing, stippling, polydactyly
5. General examination and clinical features.

2. Chest

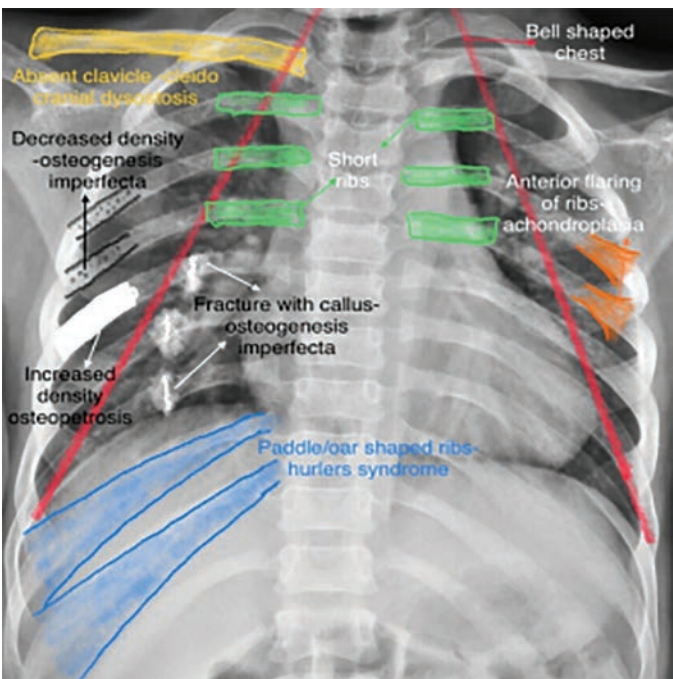


Fig. 4.136.36: Various chest abnormalities in osteochondral dysplasia

Table 4.136.9: Spectrum of chest skeletal abnormalities in skeletal dysplasia

Short ribs with polydactyly

Asphyxiating thoracic dysplasia (Jeune’s syndrome) (pre-axial polydactyly),
Short rib polydactyly syndrome (Saldino-Noonan, Majewski),
Chondroectodermal dysplasia (post axial polydactyly), Ellis-van Creveld syndrome.



Fig. 4.136.37: Asphyxiating thoracic dysplasia

Short ribs

Campomelic dysplasia
Thanotophoric dysplasia
Homozygous achondroplasia, mesomelic dwarfism
Spondyloepiphyseal dysplasia
Achondrogenesis, hypophosphatasia



Fig. 4.136.38: Thanotophoric dysplasia

Clavicle: Absence of outer end of clavicle, cleidocranial dysostosis, pyknodysostosis



Fig. 4.136.39: Absence of outer end of clavicle

Bell-shaped chest: Asphyxiating thoracic dysplasia, cleidocranial dysplasia, osteogenesis imperfecta



Fig. 4.136.40: Bell-shaped chest







Beaded ribs, multiple fractures—osteogenesis imperfecta (OI)



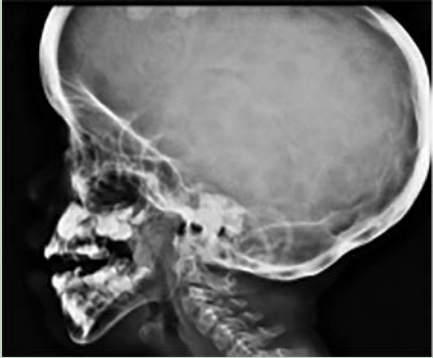
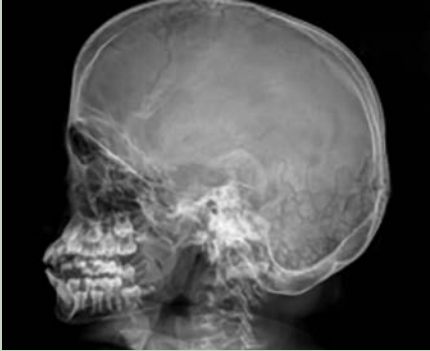
Fig. 4.136.41: Osteogenesis imperfecta

Small or hypoplastic scapula—campomelic dysplasia

3. Skull

| Table 4.136.10: Spectrum of skull abnormalities in skeletal dysplasia | |
|---|---|
| <p>Large head—macrocephaly Achondroplasia (frontal bossing, midface hypoplasia), Thanotophoric dysplasia, mucopolysaccharidoses (with J-shaped sella, frontal bossing) Achondrogenesis (flat forehead and nasal bridge).</p>  | <p>J-shaped sella: Hurler syndrome</p>  |
| <p>Fig. 4.136.42: Macrocephaly</p> | <p>Fig. 4.136.43: Hurler syndrome</p> |
| <p>Small head—microcephaly: Dyggve-Melchior-Clausen syndrome Large fontanelles, wide sutures: Cleidocranial dysostosis, pyknodysostosis</p>  | <p>Thickening of skull: Osteopetrosis, MPS (Morquio, Hurler syndrome), pyknodysostosis</p>  |
| <p>Fig. 4.136.44: Wide sutures</p> | <p>Fig. 4.136.45: Thickening of skull</p> |
| <p>Wormian bones: Cleidocranial dysostosis (normal bone density), pyknodysostosis (increased bone density), osteogenesis imperfecta (decreased bone density).</p>  | <p>Mandible: Micrognathia with obtuse angle of mandible—pyknodysostosis</p>  |
| <p>Fig. 4.136.46: Wormian bones</p> | <p>Fig. 4.136.47: Micrognathia Micrognathia—achondrogenesis</p> |

(Contd.)

| Table 4.136.10: Spectrum of skull abnormalities in skeletal dysplasia (Contd.) | |
|---|--|
| <p>Frontal bossing, midface hypoplasia—achondroplasia</p>  | <p>Thin calvaria—osteogenesis imperfecta</p>  |
| <p>Fig. 4.136.48: Frontal bossing, midface hypoplasia in achondroplasia</p> | <p>Fig. 4.136.49: Thin calvaria in osteogenesis imperfecta</p> |
| <p>Clover leaf skull, large calvaria: Thanotophoric dysplasia</p> | <p>Craniotubular dysplasia (density maintained limbs—defects in tubulation. Medullary cavity +)</p> |
| <p>Craniosynostosis scaphocephaly: MPS (Morquio, Hurler syndrome)</p> | <p>Basilar impression, platybasia: Osteogenesis imperfecta</p> |

4. Appendicular Skeleton

1. Pelvis with hip

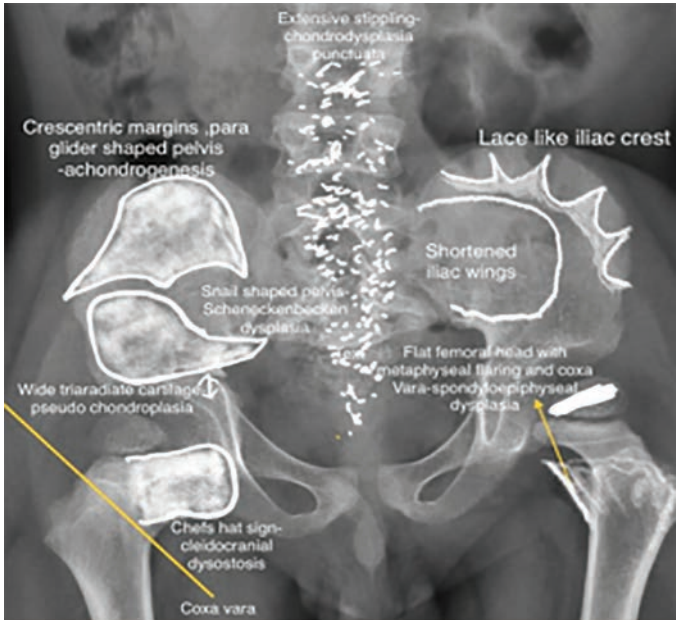


Fig. 4.136.50: Findings in osteochondral dysplasia in pelvis

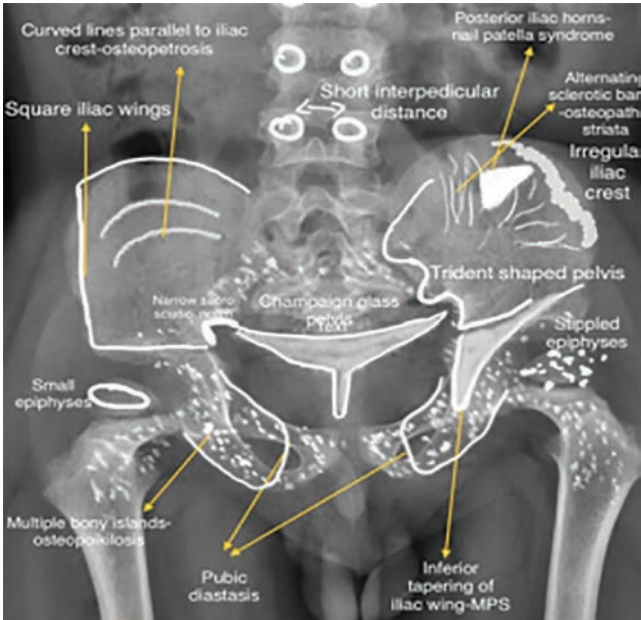


Fig. 4.136.51: Findings in osteochondral dysplasia in pelvis

Table 4.136.11: Spectrum of pelvis abnormalities in skeletal dysplasia

Square iliac wing: Tombstone (flattened acetabuli)
Achondroplasia
Thanatophoric dysplasia



Fig. 4.136.52: Square iliac wing

Trident pelvis: Achondroplasia
Jeune asphyxiating thoracic dysplasia
Ellis-van Creveld syndrome
Thanatophoric dysplasia

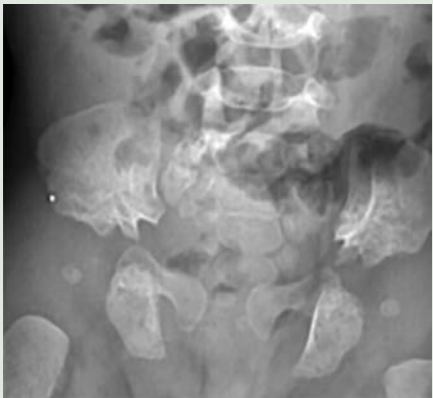


Fig. 4.136.53: Trident pelvis

Lacy iliac crest
Dyggve Melchior-Clausen syndrome,
Smith-McCort syndrome,
Enchondromatosis.



Fig. 4.136.54: Lacy iliac crest

Pubic diastasis/small pubic bones
Cleidocranial dysostosis,
Spondyloepiphyseal dysplasia congenita,
Achondrogenesis.



Fig. 4.136.55: Small pubic bones

Oblique acetabulum, hypoplastic inferior ilii with flaring of wings:
Mucopolysaccharidosis Morquio's, Hurler syndrome

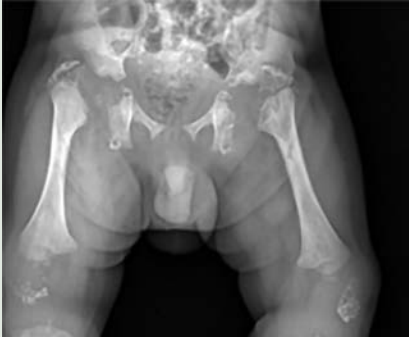




Fig. 4.136.56: Oblique acetabulum, hypoplastic inferior ilii with flaring of wings



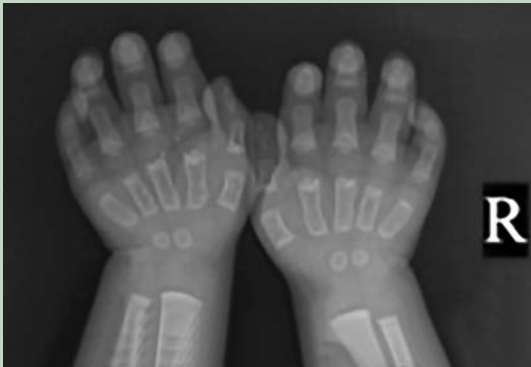
Irregular flattened femoral head
Multiple epiphyseal dysplasia,
Spondyloepiphyseal dysplasia tarda.
DD: Perthes' disease, Meyer's dysplasia.







Fig. 4.136.57: Irregular flattened femoral head

| Table 4.136.11: Spectrum of pelvis abnormalities in skeletal dysplasia (Contd.) | |
|---|---|
| <p>Calcific stippling of the sacrum and epiphyses around hip joint: Chondrodysplasia punctata Rhizomelic chondrodysplasia punctata.</p>  <p>Fig. 4.136.58: Chondrodysplasia punctata</p> | <p>Delayed appearance and fusion of femoral head epiphyses Pseudoachondroplasia Spondyloepiphyseal dysplasia congenita Multiple epiphyseal dysplasia. DD: Congenital dysplasia of hip.</p>  <p>Fig. 4.136.59: Pseudoachondroplasia</p> |
| <p>Champagne glass appearance of pelvis, small sacroiliac notch—achondroplasia.</p>  <p>Fig. 4.136.60: Champagne glass appearance of pelvis, small sacroiliac notch in achondroplasia</p> | <p>Small femoral head Spondyloepiphyseal dysplasia congenita Pseudoachondroplasia</p> |
| <p>Elephant ears shaped iliac bone: Down syndrome, achondroplasia.</p> | <p>Iliac horns: Nail patella syndrome</p> |
| <p>Coxa valga—MPS—Hurler syndrome</p> | <p>Coxa vara: Pseudoachondroplasia, osteogenesis imperfecta, cretinism, Paget’s disease, craniocleidodysostosis.</p> |

2. Long bones—pattern of shortening, associated features

| Table 4.136.12: Spectrum of long bone abnormalities in skeletal dysplasia | |
|--|--|
| <p>Rhizomelia Achondroplasia—heterozygous Hypochondroplasia, pseudoachondroplasia Rhizomelic type of chondrodysplasia punctata Spondyloepiphyseal dysplasia, congenita, thanatophoric dwarfism, diastrophic dysplasia, Jansen metaphyseal dysplasia.</p>  | <p>Mesomelia Langer and Nievergelt dysplasia, Leri-Weill syndrome (also made lung deformity seen), Robinow syndrome, Reinhardt syndrome.</p>  |
| <p>Acromelia Asphyxiating thoracic dysplasia Pynknodysostosis.</p>  | <p>Micromelia Achondrogenesis, fibrochondrogenesis Kniest dysplasia, dys-segmental dysplasia, Roberts syndrome.</p> |
| <p>Limb bone agenesis Proximal: Femoral hypoplasia—unusual face syndrome. Distal: Mesomelic dysplasia, femoral hypoplasia—unusual face syndrome. Complete (amelia): Osteogenesis imperfecta type II.</p> | <p>Phocomelia Thalidomide embryopathy, Holt-Oram syndrome, TAR syndrome.</p> |

(Contd.)

| Table 4.136.12: Spectrum of long bone abnormalities in skeletal dysplasia (Contd.) | |
|---|--|
| <p>Bent bones</p> <p>Rhizomelic Amelia, osteopetrosis, campomelic dysplasia, short rib polydactyly, cleidocranial dystostosis, Ellis-van creveld syndrome.</p> <p>Mesomelic Osteogenesis imperfecta type I and III</p>  | <p>Fractured bones Multiple fractures with different stages of healing, osteogenesis imperfecta (pencil thin cortex) (DD: NAI).</p>  |
| <p>Fig. 4.136.64: Bent bones in bilateral femur</p> | <p>Fig. 4.136.65: Fractures bones in bilateral femur</p> |
| <p>Exostosis: Multiple hereditary exostosis (limb length discrepancy) Ellis-van Creveld syndrome.</p>  | <p>Pseudoarthrosis Osteogenesis imperfecta, neurofibromatosis.</p>  |
| <p>Fig. 4.136.66: Multiple hereditary exostosis (limb length discrepancy)</p> | <p>Fig. 4.136.67: Pseudoarthrosis of tibia in neurofibromatosis</p> |

Location of abnormality—epiphyseal

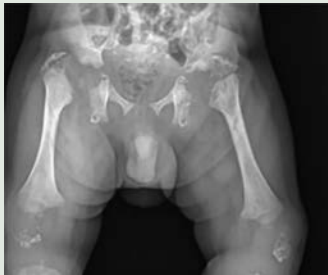
| Table 4.136.13: Spectrum of epiphyseal abnormalities in skeletal dysplasia | |
|--|---|
| <p>Stippled/fragmented epiphyses Chondrodysplasia punctata, multiple epiphyseal dysplasia, spondyloepiphyseal dysplasia</p>  | <p>Other non-dysplastic causes of stippled epiphyses Normal variant, avascular necrosis, hypothyroidism, hypoparathyroidism Down's syndrome, trisomy 18, fetal warfarin syndrome, homocystinuria (distal radius + ulnar epiphyses), Zellweger cerebrohepatorenal syndrome.</p> |

Fig. 4.136.68: Fragmented epiphyses

Metaphyseal




| | |
|--|--|
| <p>Erlenmeyer flask deformity—metaphysis Pyle's disease (metaphyseal dysplasia) Achondroplasia, Schmid type of metaphyseal chondrodysplasia, McKusick type of metaphyseal dysplasia, Hypophosphatasia</p>  | <p>Chevron deformity—metaphyseal flaring: Achondroplasia</p>  |
|--|--|

Fig. 4.136.69: Pyle's disease

Fig. 4.136.70: Chevron deformity

Table 4.136.14: Diaphyseal abnormalities in skeletal dysplasia

| | |
|---|---|
|  | <p>Fig. 4.136.71: Camurati-Engelmann disease</p> |
|---|---|

3. Hand

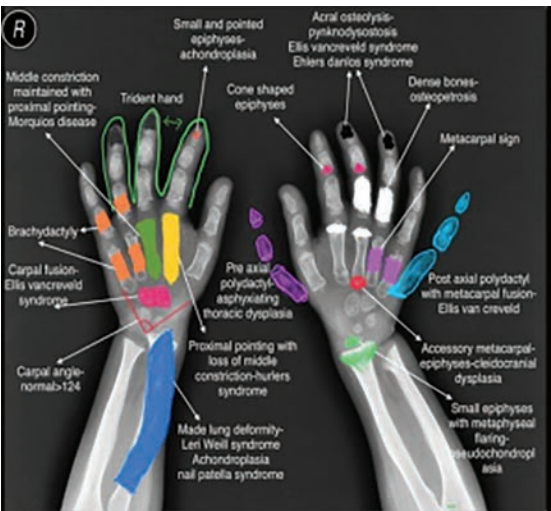


Fig. 4.136.72: Pathologies in bilateral hand radiograph in osteochondral dysplasias

Table 4.136.15: Spectrum of hand pathologies encountered in skeletal dysplasia

Polydactyly: Ellis-van Creveld syndrome, short rib polydactyly syndrome, asphyxiating thoracic dysplasia.



Fig. 4.136.73: Polydactyly

Metacarpal sign: Shortening of 4th +/- 5th metacarpal

Metacarpal sign (shortening of 4th and 5th metacarpal)
Multiple epiphyseal dysplasia, melorheostosis.



Fig. 4.136.75: Shortening of 4th and 5th metacarpal in melorheostosis

Madelung deformity

Léri-Weill syndrome, achondroplasia, Nail patella syndrome.



Fig. 4.136.77: Madelung deformity

Trident hand splayed, deviated towards ulna, short and broad fingers: Achondroplasia



Fig. 4.136.79: Trident hand

Short metacarpal and phalanx

Achondroplasia, asphyxiating thoracic dysplasia, Ellis-van Creveld syndrome, thanatophoric dysplasia, pseudochondroplasia.



Fig. 4.136.74: Short metacarpal and phalanx

Acral osteolysis

Pyknodystosis, Ellis-van Creveld syndrome, Ehlers-Danlos syndrome.



Fig. 4.136.76: Acral osteolysis in pyknodystosis

Proximal pointing of metacarpals (bullet)—MPS—(Morquio's, Hurler syndrome).

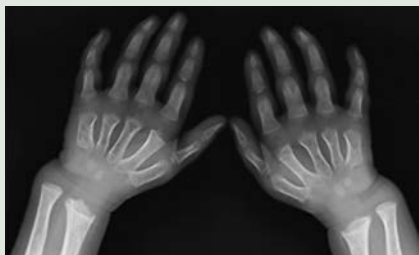


Fig. 4.136.78: Bullet-shaped metacarpals

Slanting of articular surface of radius and ulna—Morquio's



Fig. 4.136.80: Slanting of articular surface of radius and ulna in Morquio's syndrome

Table 4.136.16: Types of disproportion seen in skeletal dysplasia

| <i>Upper to lower segment ratio(normal)</i> | <i>Short trunk dwarfism</i> | <i>Short limb dysplasia</i> | <i>Spine assess for</i> |
|---|---|--|---|
| <ul style="list-style-type: none"> • 1.7 newborn • 1.0 ages 2–8 years • 0.95 adult | <ul style="list-style-type: none"> • Metatrophic dysplasia • Spondyloepiphyseal dysplasia • Morquio's syndrome | <ul style="list-style-type: none"> • Achondroplasia • Metaphyseal chondrodysplasia | <ul style="list-style-type: none"> • Scoliosis • Kyphosis • Lordosis |

Table 4.136.17: Clinical features in skeletal dysplasia

| Mental retardation | Dental deformities | Disproportionately large head: | Congenital cataract | Myopia | Renal involvement |
|---------------------------|---------------------------|---|----------------------------|---------------|---------------------------------|
| Chondrodysplasia punctata | Cleidocranial dystostosis | Achondroplasia Thanatophoric dysplasia | Chondrodysplasia punctata | SED congenita | Asphyxiating thoracic dysplasia |

Table 4.136.18: Radiographic findings of common dwarfing dysplasia

| <i>Dysplasia</i> | <i>Lethal</i> | <i>Skull and face</i> | <i>Spine</i> | <i>Chest</i> | <i>Pelvis</i> | <i>Long bones</i> | <i>Hands and feet</i> |
|---------------------------------|---------------|--|--|---|--|--|---|
| Achondrogenesis | Yes | Large head, flat forehead and nasal bridge, cleft palate, micrognathia | Absent or poor ossification | Short and narrow bell-shaped chest | Small iliac wings, ischia poorly mineralised. | Severe micromelia, flipper-like limbs | Phalanges poorly mineralised |
| Achondroplasia (heterozygous) | No | Frontal bossing, midface hypoplasia, small skull base | Posterior scalloping, bullet-shaped vertebrae, decreased inter-pedicular distance, narrowed foramen magnum | Reduced AP diameter, flared rib ends | Champagne pelvis, flat acetabular roof | Rhizomelic shortening, metaphyseal cupping and fraying | Trident hands, metacarpals all equal in length |
| Asphyxiating thoracic dysplasia | Yes | Normal | Normal | Short horizontal ribs, narrow and elongated chest; handle bar clavicles | Small iliac wings, flat acetabular roof, acetabular spikes | Mild micromelia, cone-shaped epiphyses | Shortening phalanges metacarpals, metatarsals, polydactyly |
| Chondro-ectodermal dysplasia | No | Normal | Normal | Short | Small iliac wings, narrow sciatic notch, acetabular spikes | Rhizomelic and mesomelic shortening | Short phalanges polydactyly, carpal anomalies, dysplastic nails |
| Multiple epiphyseal dysplasia | No | Normal | Normal or minimally involved | Normal | Normal | Epiphyseal irregularity | Carpal and tarsal irregularity, brachydactyly |
| Pseudo chondroplasia | No | Normal | Tongue-like projections, biconcave shape | Normal | Delayed development of pubic bones and triradiate cartilage, acetabular spikes | | Short and broad |
| Spondylo-epiphyseal dysplasia | No | Normal | Variable platyspondyly, odontoid hypoplasia | Bell-shaped chests, flared ribs | Small iliac wings, flattened acetabular roofs, delayed ossification | | Normal |
| Thanatophoric dysplasia | Yes | Enlarged head, frontal bossing, flat nasal bridge, small skull base, clover leaf skull | Severe platyspondyly | Short horizontal ribs, narrow long chest | Small iliac wings, narrow sacrosciatic notch | | Short, broad hands and feet |

5. General Examination

General—facial features, hair quality, dental health, nails. Systemic features: Renal problems, cardiac abnormalities. Developmental history and family history.

Further Management

Multidisciplinary team comprising paediatrician, orthopaedician, paediatric surgeon and radiologist is formed. Genetic analysis is performed to confirm the diagnosis. There is often a danger of cervical cord compression due to narrowing of the foramen magnum. Treatment varies and is usually orthopedic, particularly to correct kyphoscolioses, as well as neurosurgical, to decompress the foramen magnum or

shunt hydrocephalus. Overall prognosis is good with near-normal life expectancy in heterozygous individuals. When homozygous, the condition is fatal due to respiratory failure. Early studies of growth hormone or statins are promising.

Brief Discussion about the Condition: Achondroplasia

Achondroplasia is the most common cause of short-limb dwarfism. Patients are of normal intelligence with normal motor function. However, they may have specific neurologic deficits.

Pathology: The disease results from a mutation in the fibroblast growth factor gene 3 (FGFR3) located on chromosome 4p16.3 which causes abnormal cartilage

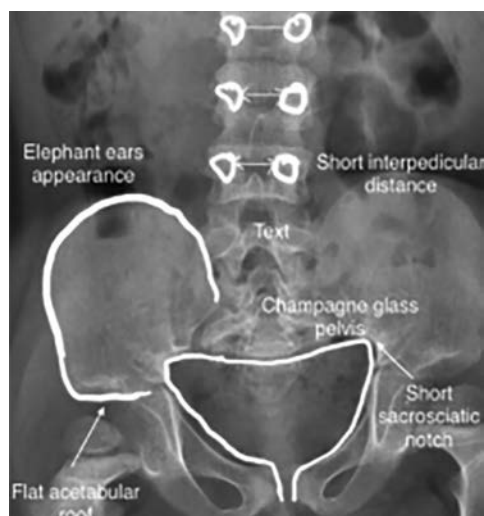


Fig. 4.136.81: Findings in achondroplasia on pelvis radiograph

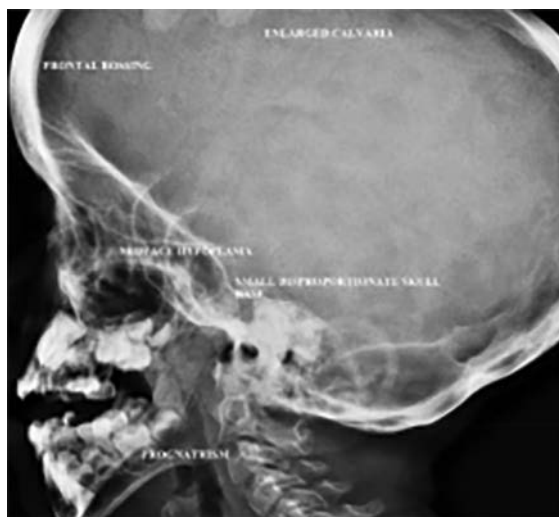


Fig. 4.136.82: Findings in achondroplasia on skull radiograph

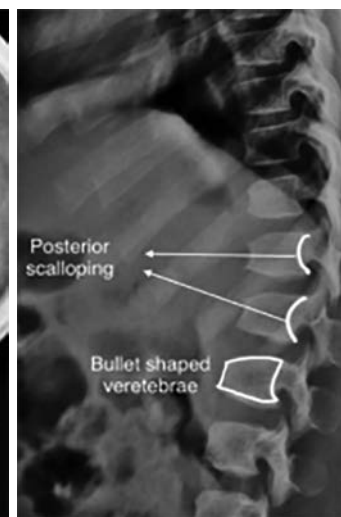


Fig. 4.136.83: Findings in achondroplasia on spine radiograph

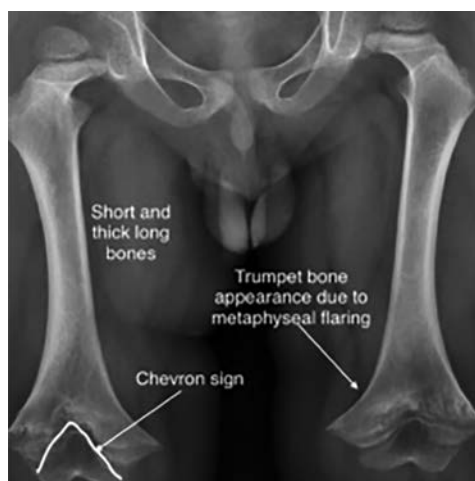


Fig. 4.136.84: Findings in achondroplasia on long bones

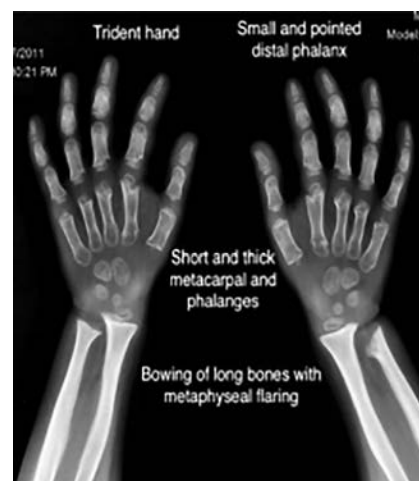


Fig. 4.136.85: Findings in achondroplasia on hand radiograph

formation. These are cell surface receptors comprised of an extracellular domain with three immunoglobulin-like regions, a transmembrane domain and an intracellular tyrosine kinase 19. The mutation to the FGFR3 gene in achondroplasia is a gain of function mutation with constitutive activation of an inhibitory signal. All bones that form by endochondral ossification are affected. Bones that form by membranous ossification are not affected, thus allowing the skull vault to develop normally.

Associations: SADDAN syndrome, severe achondroplasia with developmental delay and acanthosis nigricans.

Radiographic features: Almost all the bones of the skeleton are affected, and hence all parts of the body have bony changes with secondary soft tissue changes. Antenatally it is difficult to diagnose achondroplastic features until the 3rd trimester. **Antenatal ultrasound:** Antenatally detectable sonographic features include short femur length measurement often well below the 5th centile. The femur length (FL) to biparietal diameter (BPD) is taken as a useful measurement. Trident hand 2, 3 and 4 fingers appearing separated and similar in length. Protruding forehead: Frontal bossing and depressed nasal bridge. **Plain radiograph/CT/MRI:** Features on radiographs, CT and MRI are similar. Cranial—relatively large cranial vault with small skull base frontal bossing with the depressed nasal bridge (midfacial retrusion) narrowed foramen magnum cervico-medullary kink

relative elevation of the brainstem resulting in a large suprasellar cistern and vertically-oriented straight sinus, communicating hydrocephalus (due to venous obstruction at sigmoid sinus), large anterior fontanelle in infancy; may persist to 5 or 6 years of age. Spinal—posterior vertebral scalloping, progressive decrease in the interpedicular distance in the lumbar spine shows gibbus deformity with thoracolumbar kyphosis and also shows bullet-shaped/hypoplastic vertebra (not to be confused with Hurler syndrome), short pedicle, canal stenosis. Laminar thickening, widening of intervertebral discs, an increased angle between the sacrum and lumbar spine. Chest—anterior flaring of the ribs, anteroposterior narrowing of the ribs. Pelvis and hips—horizontal acetabular roof (decreased acetabular angle) small squared (tombstone or mickey mouse ear) iliac wings small trident pelvis, champagne glass type pelvic inlet and short sacroiliac notches. Limbs—metaphyseal flaring can give a trumpet bone type appearance, the femora and humeri are particularly shortened (rhizomelic shortening), long fibula, the fibular head is at the level of the tibial plateau, bowing to medial side of legs, the limbs may also appear thickened but are in fact normal in absolute terms; thickening is perceived due to reduced length, trident hand, chevron sign (inverted V-shape sign in distal epiphyses of femur), the metacarpal and metatarsal bones, and in some cases the proximal phalanges, are short and of similar length.

4.137 MUSCULOSKELETAL SYSTEM

Case No. 137

Clinical history: A 3-year-old female child referred from orthopaedic department with difficulties in walking and abnormal gait.

Imaging technique and interpretation: Figures 4.137.1 and 4.137.2 are radiograph showing hypoplastic left femoral capital epiphysis with lateral and superior subluxation of the femoral head, and a shallow acetabulum. There is delayed ossification of the head of left femur and the upper femoral epiphysis not seen in inferomedial quadrant as both the H (Hilgenreiner) and P (Perkin) lines are interrupted. Shenton line appears discontinuous. Figures 4.137.3 to 4.137.6 are MRI images done for further assessment of acetabular and proximal femoral morphology and to look for complications. Severe hypoplasia of left femoral head with superolateral subluxation and fibrofatty pulvinar hypertrophy. Acetabulum is shallow with non-visualization of femoral head within the acetabular cavity.

Interpretation: A: 3-year-old girl with abnormal gait; C: Severe hypoplasia of left femoral head with superolateral subluxation and shallow acetabulum. Interruption of H and P lines and Shenton line. There

is pulvinar fat hypertrophy and blunting of bony acetabulum; B: Superolateral subluxation of left femoral head, varus deformity and acetabular dysplasia; D: DDH.

Principal diagnosis: Developmental dysplasia of left hip (DDH).

Discussion: Previously called congenital hip dysplasia or congenital hip dislocation. Spectrum of conditions that range from irreducible dislocation of the hip at birth to neonatal hip instability. Fixed dislocation at birth is estimated at 1:1000 births and late dislocation, subluxation, and dysplasia at 0.4–0.6:1000 births. If one of the parents has had DDH, then the risk for the first child is 12%. Female predominance (6:1) and occurs from ligamentous laxity and abnormal position in utero. Other risk factors include: Oligohydramnios, breech presentation and firstborn status. Associated abnormalities include neuromuscular disorders, congenital torticollis, and skull and foot deformities. Simple conservative measures may reverse hip instability and reduce the incidence of secondary osteoarthritis of the hip later in life. A palpable hip “click” can be elicited when combined external rotation-abduction and internal rotation-adduction are alternately applied to the



Fig. 4.137.1



Fig. 4.137.2



Fig. 4.137.3

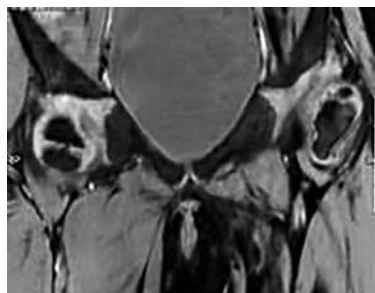


Fig. 4.137.4

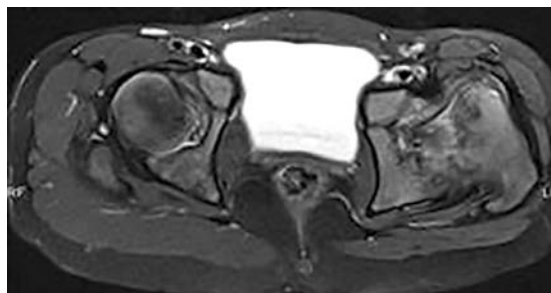

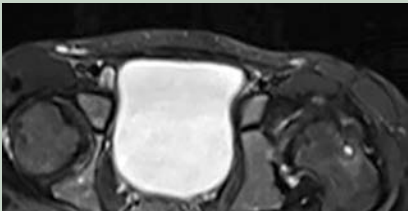




Fig. 4.137.5



Fig. 4.137.6

Differential diagnosis

| Table 4.137.1: Differential diagnosis for developmental dysplasia of hip | | |
|---|---|---|
| <p>Proximal femoral focal deficiency (PFFD): Congenital partial absence of the proximal end of the femur with shorting of the entire lower limb. The cause is uncertain but may be associated with exposure of thalidomide <i>in utero</i>. In severe cases the proximal femur, femoral head and neck, and acetabulum are absent. Associated with fibular hemimelia and absent patella.</p> | <p>MRI is a valuable tool in the assessment of PFFD patients and classification of disease severity and identifying small ossific components, irregular cartilaginous or fibrous tufts, and completely absent segment. Also, to assess the presence or absence of marrow edema pattern adjacent to pseudoarthrosis. GRE imaging is useful to depict the cartilage clearly. Aitken classification is most commonly used and classified as class A, B, C and D. Severe: Complete absence of one or both proximal femurs; Moderate: Absent segments of proximal femoral bone replaced by cartilaginous or fibrous tuft; Mild: Delayed proximal femoral ossification and pseudoarthrosis in the subtrochanteric region.</p> |  <p>Fig. 4.137.7: Proximal femoral focal deficiency</p> |
| <p>Post-septic hip (travelling acetabulum): Classified into 5 types. Type 1: Absent or minimal femoral head changes. Type 2: a) Deformity of femoral head with intact physis. b) Deformity of femoral head with premature physis closure. Type 3: Pseudoarthrosis of the femoral neck. Type 4: a) Complete destruction of the capital femoral epiphysis with stable neck. b) Complete destruction of the capital femoral epiphysis with instable small neck fragment. Type 5: Destruction of both femoral head and neck to the intertrochanteric line.</p> | |  <p>Fig. 4.137.8: Travelling acetabulum</p> |
| Legg-Calve-Perthes disease (Refer to case 156) | | |
| <p>Meyer dysplasia: It is a benign condition, also known as dysplasia epiphysealis capitis femoris. It is due to fragmentation and delayed ossification of femoral capital epiphyses that affects paediatric hips. It is considered more of a normal hip developmental variation rather than a true dysplasia. Age of presentation: 2–3 years. Usually asymptomatic. It can involve bilateral femur in half of the patients.</p> | <p>On radiography, the affected femoral epiphysis is smaller in size. There are often multiple nuclei of ossification, giving the epiphysis a “morulated appearance”. These then tend to fuse at around 5 years of age.</p> | <p>MRI shows multiple centers of ossification of the femoral head, with a normal signal intensity in all sequences and reduced height of cartilaginous epiphysis. Bone scan—normal.</p> |
| |  <p>Fig. 4.137.9: Meyer dysplasia</p> |  <p>Fig. 4.137.10: Meyer dysplasia</p> |

flexed hip of a newborn (Ortolani’s test and Barlow’s test). The pathophysiology of DDH is multifactorial, including shallow bony margin; delayed ossification of the acetabulum or femoral head; ligamentous laxity; and neuromuscular disease with shortening, weakness, or contractures. Hip flexion associated with breech presentation induces DDH by causing shortening of the psoas and decentring of the femoral head.

Treatment: A dysplastic hip can often be effectively treated by simple flexion–abduction bracing techniques,

such as the Pavlik harness device. Spontaneous improvement after 2 months following birth is unusual but can be influenced with treatment. Spica casting may be done when there is failure of the Pavlik harness to maintain reduction, usually after 4 months. Closed reduction: Usually for older patients; Open reduction (ORIF): Much older patients or if closed reduction is not successful.

Radiological features: Ultrasound allows visualization of the bony and cartilaginous acetabular margins, the

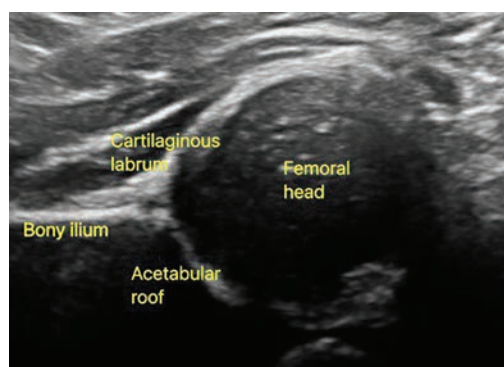


Fig. 4.137.11: Normal coronal B mode of hip joint

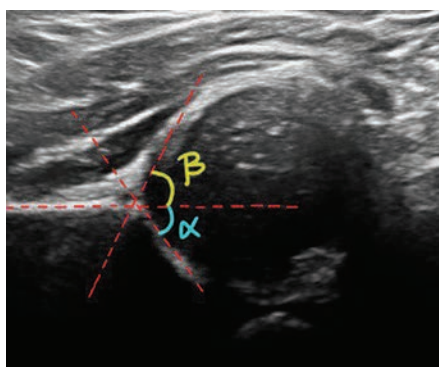


Fig. 4.137.12: Bony (α) and cartilaginous (β) roof angles

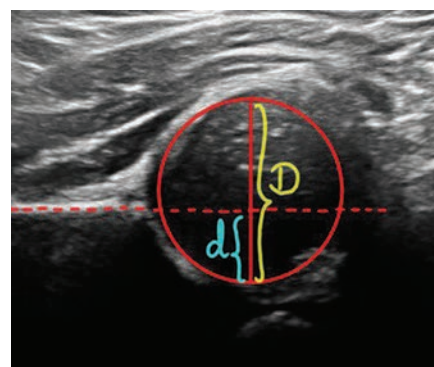


Fig. 4.137.13: Femoral head coverage

cartilaginous femoral head, the amount of femoral head coverage by the acetabulum, and with stress testing assessment of hip stability. The hip is scanned in the coronal plane, and the bony (α) and cartilaginous (β) roof angles are measured. The critical measurement is the cartilaginous (β) angle and is the basis for classifying the degree of dysplasia. Dynamic hip ultrasound may show no movement, slight movement, true subluxation, and frank dislocation. Following the application of the harness sonographic reassessment at 4- to 6-week intervals over 2–3 months are performed to monitor and document the therapeutic response.

D = Diameter of cartilaginous femoral head, d = Bony acetabular depth.

Femoral head coverage or $d/D = \text{acetabular depth} / \text{femoral head diameter} \times 100$. It is positively correlated with Graf alpha angle measured by ultrasound.

Alpha angle is the bony angle formed by vertical cortex of ileum and acetabular roof indicating the

degree of acetabular roof coverage. Beta angle is the cartilaginous angle formed by line through vertical ileum and cartilaginous acetabular labrum. With superolateral femoral head displacement, the labrum is elevated, thereby increasing the beta angle.

Plain radiograph: To assess symmetry and defining the relationship of the proximal femur to the developing pelvis. The ossification of the superior femoral epiphyses should be symmetric. Delay of ossification is a sign of developmental dysplasia of the hip. Classical findings are Putti's triad: An absent or small proximal femoral capital epiphysis, lateral displacement of the femur, and a shallow acetabulum with an increased inclination of the acetabular roof, usually $>30^\circ$. Disruption of Shenton's line (arc) and/or the iliofemoral line may show interruption of the expected smooth arcuate contour if there is sufficient superior and lateral subluxation of the femur. Other findings may include shortened varus femoral neck with varus angulation, delayed closure of

Table 4.137.2: Classifications of hip joint by ultrasound

| Morphologic hip ultrasound classification | | | | Terjesen femoral head coverage | |
|---|--|-------------------------------|---------------------------------------|--------------------------------|---|
| Type | Description | Bony Angle (α°) | Cartilaginous angle (β°) | Femoral head coverage | Inference |
| 1A | Normal hip | >60 | <55 | $>50\%$ | Normal |
| 1B | Normal hip, transitional form | >60 | >55 | 49–40% | Possible dysplasia in newborn |
| 2A | Physiologically immature (<3 months old) | 50–59 | >55 | 49–40% | Dysplasia in infant greater than 4 months |
| 2B | Delayed ossification (>3 months old) | 50–59 | >55 | 39–10% | Subluxation |
| 2C | Deficient bony acetabulum; femoral head concentrically located | 43–49 | 70–77 | $<10\%$ | Dislocation |
| 2D | Deficient bony acetabulum; femoral head subluxed | 43–49 | >77 | | |
| 3 | Dislocated | <43 | >77 | | |
| 4 | Severe dysplasia with inverted labrum | | | | |

| Table 4.137.3: Lines and angles in pelvis radiograph |
|---|
| Hilgenreiner line: The Hilgenreiner line is a line drawn horizontally through the inferior aspect of both triradiate cartilages. It should be horizontal but is mainly used as a reference for the Perkin line and measurement of the acetabular angle. |
| Perkin line: The Perkin line is drawn perpendicular to Hilgenreiner line, intersecting the lateral most aspect of the acetabular roof. The upper femoral epiphysis should be seen in the inferomedial quadrant (i.e. below Hilgenreiner line, and medial to Perkin line). |
| Acetabular angle: A transverse line is drawn through the right and left triradiate cartilages at the pelvic rim. A second oblique line which extends along the acetabular roofs is then constructed. The angle of intersection is measured. Average 20°, Minimum 12°, Maximum 29°. An increased acetabular angle is frequently associated with acetabular dysplasia and congenital hip dislocation. A decreased acetabular angle is seen in Down's syndrome. |
| Shenton line (ARC): The Shenton line is drawn along the inferior border of the superior pubic ramus and should continue laterally along the inferomedial aspect of the proximal femur as a smooth line. If there is a superolateral migration of the proximal femur due to DDH then this line will be discontinuous. |
| Center-edge angle of Wiberg: A vertical line is drawn through the center point of the femoral head. Another line is constructed through the femoral head center to the outer upper acetabular margin. The angle formed is then measured. Average 36°, minimum 20°, maximum 40°. A shallow angle may be related to underlying acetabular dysplasia, which has been linked to the onset of degenerative joint disease. It provides a measure of coverage of the femoral head. |
| The line of Klein describes a line along the superior edge of the neck of the femur. It is useful in detecting early slipped upper femoral epiphysis in adolescents. The line should normally intersect the lateral part of the superior femoral epiphysis. If the line of Klein fails to intersect the epiphysis during the acute phase, it is called Trethowan sign. |
| The iliopectineal line is seen in the AP view of the pelvis and serves to evaluate the anterior acetabular column. The iliopectineal line is a curvilinear line running from the iliosacral joint along the medial border of the iliac wing and the superior border of the superior pubic bone up to the symphysis and delineates the inner margin of the pelvic ring. Disruption of the iliopectineal line is a sign for an anterior column fracture, superior pubic ramus or an anterior pelvic arch fracture. In severe protrusio acetabuli, the acetabular fossa can sometimes be seen extending medially in relation to the iliopectineal line. In Paget disease, hypophosphatasia or neoplastic conditions this line can be thickened. |



Fig. 4.137.14: Lines and angles in pelvis

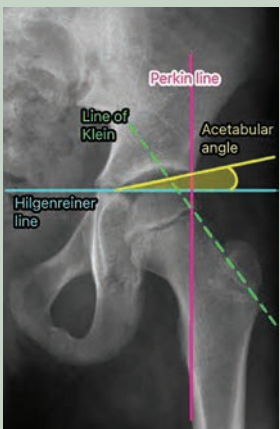


Fig. 4.137.15: Lines and angles in pelvis

the ischiopubic synchondrosis, and triradiate cartilages. Long standing dislocation manifests as a shallow acetabulum and a large, flattened femoral head with superior and lateral displacement. The head is at risk for complicating avascular necrosis. Neo- or pseudo-acetabulum is formed on the posterosuperior surface of the iliac wing.

Imaging with MRI and CT is performed to assess for associated sequelae or for surgical planning. CT—to assess the extent of proximal femoral ossification, characterize osseous anatomy for surgical planning, and identify the location and extent of pseudoarthroses.

MRI: Used for evaluating hip anatomy once femoral head and acetabular ossification centers have developed; these ossification centers hinder adequate visualization of acetabular structures on US by approximately 3 to 4 months of age. To assess for avascular necrosis and for presurgical planning. Complications related to DDH, including labral tears, labral detachment, focal cartilaginous lesions, and ligamentum teres injury can be seen in MRI. In addition, patients with DDH are often found to have characteristic anatomic variations including labral hypertrophy, capsular thickening and laxity and hypertrophy of the fibrofatty pulvinar.

4.138 MUSCULOSKELETAL SYSTEM

Case No. 138.1

Clinical history: A 12-year-old female with history of trauma.

Radiological technique and observations: Radiograph of left knee joint provided with CT sections of left distal femur in bone window and soft tissue window.

Figures 4.138.1.1 well-defined lytic lesion with thin sclerotic margin noted in distal metadiaphyseal region, located eccentrically in the cortical region of left femur. Figures 4.138.1.2 to 4.138.1.4 are axial CT image shows break in the cortical integrity with preserved soft tissues and narrow zone of transition. No periosteal reaction and no extension into the medullary cavity noted. No obvious chondroid/osteoid/fibrous matrix noted. No soft tissue involvement/mass lesion.

Interpretation: A: 12 years old female, C: Well-defined lytic lesion with thin sclerotic margin located eccentrically in the cortical region of metadiaphysis of the bone with cortical break, B: No extra osseous soft tissue component and no periosteal reaction likely to be a benign lesion D: Non-ossifying fibroma

Principal diagnosis: Non-ossifying fibroma.

Brief discussion: Non-ossifying fibromas (NOF) are the most common type of non-neoplastic fibrous bone lesion and are a larger version (>2 cm) of a fibrous cortical defect; both are encompassed by the term fibroxanthoma or metaphyseal fibrous defect. NOFs are relatively prevalent in children and teenagers, seen between 10 and 15 years. It is estimated that 30–40% of all normal children are affected. M:F = 2:1. They are rarely noticed after the age of 30, as they heal on their own and are eventually filled in by bone. The vast majority of NOFs have no symptoms. Larger lesions are painful and weaken the bone at risk of pathological fracture. Multiple

NOF can have NF-1 and Jaffe-Campanacci syndrome association.

Plain radiograph/CT: NOFs are Multiloculated eccentric lucent cortical lesion showing sclerotic rim, seen in the metaphysis. Initially, they are adjacent to the physis, with increases in age, they grow away from the physis. They have no periosteal reaction/cortical breach/associated soft tissue mass. The MR appearance of a lesion varies depending on when it is imaged, as well as the stage of development and healing. The lesion shows strong or intermediate T2 signal at first, with a low signal rim around it that corresponds to the sclerotic border. The signal on all sequences decreases as it grows and begins to ossify. Variable contrast enhancement is seen. Nuclear medicine: The appearance of a lesion on a bone scan depends on its stage: NOF is rarely associated with increased activity. During NOF healing, there is mild to moderately enhanced activity, which corresponds to mild hyperaemia and osteoblastic activity.

Treatment: The majority of NOFs do not require therapy or a biopsy (as it does not touch lesion). If the fracture is significant (more than 50% of the parent bone's diameter), prophylactic curettage and bone grafting may be necessary to avert a pathological fracture.

DD for don't touch lesion

- Benign lesions:** Focal cortical dysplasia, non-ossifying fibroma, osteopoikilosis, cortical desmoid, small single focus of fibrous dysplasia, pseudotumor-haemophilia, intra-osseous ganglion, enchondroma in short tubular bone, simple bone cyst, enostosis (bone island), bone infarct, synovial herniation pit.
- Normal variants:** Os odontoideum, dorsal defect of patella, pseudocyst of humerus.
- Post-traumatic:** Myositis ossificans, geode or subchondral cyst, costochondritis (Tietze syndrome)



Fig. 4.138.1.1

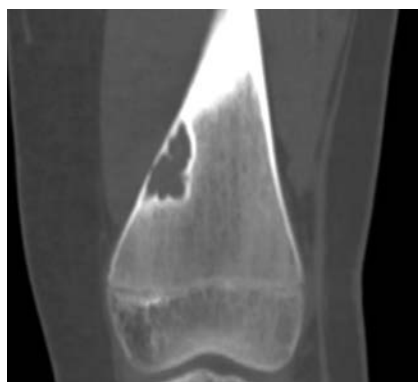


Fig. 4.138.1.2

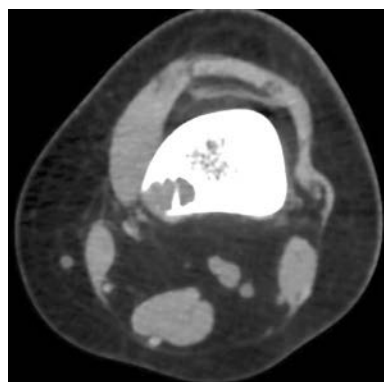


Fig. 4.138.1.3

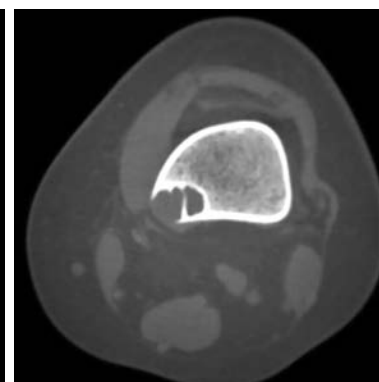


Fig. 4.138.1.4

Table 4.138.1.1: Differential diagnosis for pediatric metadiaphyseal lesion



| | | |
|---|---|---|
| <p>Fibrous cortical defect: Occur in children (usually 2–15 years), and male predilection 2:1. Typically occur in the metaphysis or metadiaphyseal junction. They are typically located in the distal femur or proximal or distal tibia (<2 cm).</p> | <p>Plain radiograph and CT show lucent intracortical defects, outlined by a thin rim of sclerosis without medullary involvement and no periosteal reaction. MRI- T1: Hypointense; T2: Variable, depending on the phase of healing.</p> <p>Nuclear medicine (bone scan)- they are negative; however, mild hyperemia and moderate bone uptake are present during healing. If extensive uptake or hyperemia is present, then an alternative diagnosis or superimposed fracture should be considered.</p> |  <p>Fig. 4.138.1.5: Fibrous cortical defect</p> |
| <p>Cortical desmoid: They are also known as distal femoral cortical defects or Bufkin lesion. They are benign self-limiting “do not touch” lesion and affect adolescents with male predilection.</p> | <p>Typically seen as a saucer-shaped radiolucent cortical irregularity involving the posteromedial aspect of distal femoral metaphysis at adductor magnus tendon attachment. MRI: T1—hypointense; T2—hyperintense; may show enhancement post-contrast.</p> |  <p>Fig. 4.138.1.6: Cortical desmoid</p> |
| <p>Fibrous dysplasia: (Refer to case 147): Common in medullary cavity</p> | | |
| <p>Langerhans cell histiocytosis (Refer to case 153)</p> | | |
| <p>Aneurysmal bone cyst (Refer to case 139)</p> | | |
| <p>Benign fibrous histiocytoma: They are rare tumors, typically presents between 20 and 50 years. No sex predilection. They are lytic, loculated lesions with narrow zone of transition and with no matrix mineralization. They occur in an eccentric subarticular location similar to GCT but with a well-defined sclerotic margin indicating slower growth. They occur on either side of the knee in 1/3rd of cases. Treatment is surgical resection.</p> | | |

Table 4.138.1.2: Differential diagnosis for metaphyseal lesions

| Cortical lesions | Medullary lesions | Aggressive metaphyseal lesions | Others |
|--|--|--------------------------------|--|
| Non-ossifying fibroma Fibrous cortical defect Osteoid osteoma Osteoblastoma Osteochondroma | Fibrous dysplasia Enchondroma Simple bone cyst Giant cell tumor | Osteosarcoma Chondrosarcoma | Aneurysmal bone cyst Chondromyxoid fibroma Osteomyelitis Metastasis |

Table 4.138.1.3: Size characteristics of similar type benign metaphyseal lesions

| | |
|---|-----------------------------|
| Fibrous cortical defect <2 cm | Non ossifying fibroma >2 cm |
| Osteoid osteoma <2 cm | Osteoblastoma >2 cm |
| In osteochondroma, cartilage cap >1.5 cm indicates malignant transformation (a few studies prefer >2 cm as cut-off) | |

Table 4.138.1.4: Differential diagnosis to be considered in all single/multiple bone lesions

| Whenever single or multiple bone lesions, always consider | | |
|--|--|--|
| In pediatrics | In adults | Non-tumoral bone conditions |
| <ul style="list-style-type: none"> • Langerhans cell histiocytosis • Osteomyelitis • Metastasis/neuroblastoma • Leukemia/lymphoma • Ewing's sarcoma/ osteosarcoma | <ul style="list-style-type: none"> • Myeloma (plasmacytoma) • Metastasis • Lymphoma | <ul style="list-style-type: none"> • Brown tumour • Osteomyelitis • Hydatid cyst • Hemophilic pseudotumour |

Case No. 138.2

Clinical history: An 18-year-old male with pain in the left hip, mainly nocturnal pain relieved by taking aspirin.

Radiological technique and observations: Figure 4.138.2.1 is radiograph of bilateral hip joints with proximal femur shows a subtle cortically placed radiolucent nidus within the medial aspect of left femoral neck with reactive sclerosis of bone surrounding the nidus. Solid periosteal reaction with cortical thickening noted. No evidence of cortical break. Figures 4.138.2.2 and 4.138.2.3 are CT bone window in coronal and axial section confirms the focally lucent nidus (size around 1 cm) within surrounding reactive cortex. No evidence of any other lesion. Figures 4.138.2.4 to 4.138.2.6 are MRI T1 coronal and axial sections and STIR axial section images showing the nidus clearly with mild marrow edema and surrounding cortical sclerosis. No evidence of soft tissue component.

Interpretation: A: 18-year-old male; C: Cortically placed radiolucent nidus within medial aspect of left femoral neck with surrounding reactive bone sclerosis and solid periosteal reaction; B: No extra osseous soft tissue component and no cortical break; D: Osteoid osteoma (nidus size 1 cm)

Principal diagnosis: Osteoid osteoma

Brief discussion about the condition: Osteoid osteomas are benign bone forming tumors that predominantly occurs in young patients between the ages of 10 and 25 years. Most common in long bones of limbs (50% in femur and tibia). There is a predilection for the upper end of the femur, particularly the neck and trochanters. In the vertebra, predominantly affects posterior elements. The classic clinical presentation is of a gradual onset of increasingly severe, deep, aching localised bone pain, which however, only 65% of patients have the classic presentation of night pain relieved by aspirin. Localized swelling and point tenderness are frequently noted. Limitation of motion, painful limp, stiffness, and weakness of nearby joints may be noted. Painful, rigid scoliosis resulting from a lesion located on the concave side of the curve is the classic clinical presentation of a lumbar (most common) or thoracic osteoid osteoma. When a cervical vertebra is involved, torticollis and secondary contracture of the sternocleidomastoid muscle may be noted. Lesions in the spinous processes do not produce torticollis or scoliosis, but rather localized pain and spinal stiffness. There are three specific anatomic locations for osteoid osteoma: Cortical (most common), cancellous (intramedullary), and subperiosteal.

Radiological features: The radiographic appearance of a well-developed lesion is a characteristic lucent nidus with surrounding florid perifocal reactive sclerosis. This



Fig. 4.138.2.1

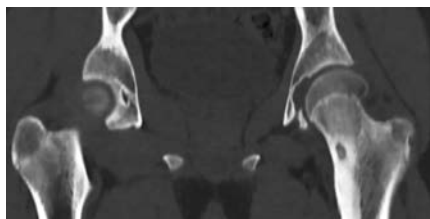


Fig. 4.138.2.2

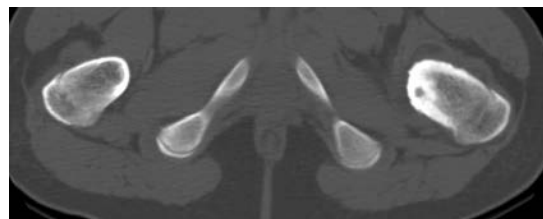


Fig. 4.138.2.3

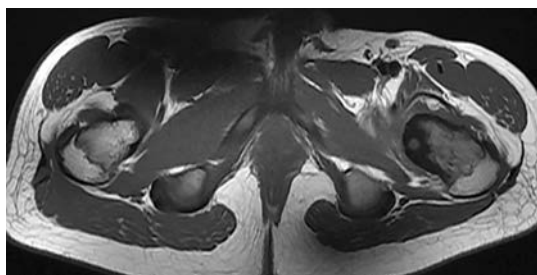


Fig. 4.138.2.4

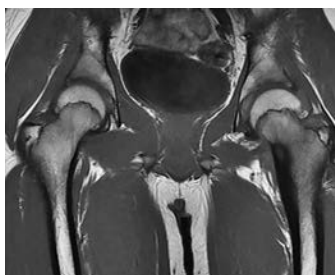


Fig. 4.138.2.5

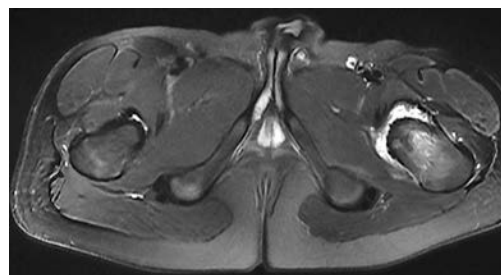


Fig. 4.138.2.6

Table 4.138.2.1: Differential diagnosis for osteoid osteoma

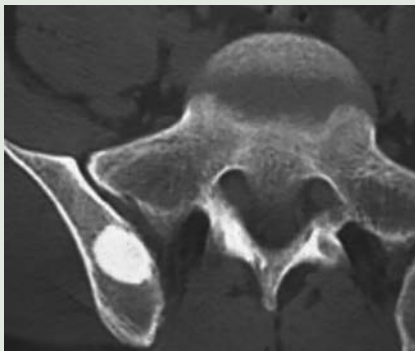


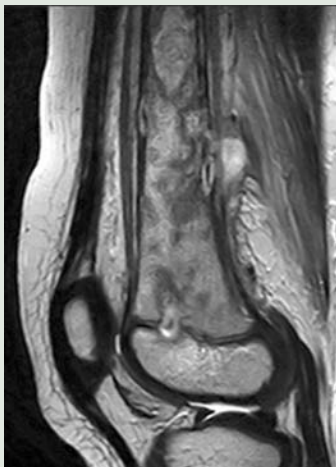
| | | |
|--|---|---|
| Bone island (Enostosis): It refers to a benign focus of cortical bone, located within marrow space. Pelvis, long bones, ribs and spine are most frequent locations. | They are usually ovoid homogeneously dense with long axis parallel to long axis of bone with a feathered border. No associated marrow edema or cortical destruction. Low signal intensity on all MRI sequences. |  |
| Fig. 4.138.2.7: Bone island | | |
| Chronic osteomyelitis: Long bones like femur and tibia are most common locations. Brodie abscess refers to subacute osteomyelitis with single focus of intraosseous abscess formation appearing as a lytic lesion with geographic sclerotic margins in metaphyseal location. | | On radiographs, appear as sclerotic bone with thickened cortex along endosteal and periosteal surfaces, periosteal new bone formation, soft tissue swelling +/- sequestrum. MRI shows marrow and soft tissue edema, abscess and sinus tracts. |
|  |  |  |
| Fig. 4.138.2.8: Chronic osteomyelitis | | Fig. 4.138.2.9: Chronic osteomyelitis |
| Fig. 4.138.2.10: Chronic osteomyelitis | | |
| Metastasis (osteoblastic): Refer to cases 142 and 154 | | |
| Paget's disease: Refer to case 142 | | |
| Lymphoma: Refer to cases 152 and 154 | | |
| Callus: Refers to bony and cartilaginous material forming a connecting bridge across a bone fracture during repair. Initially primary callus or soft callus is formed by cartilage, fibrous tissue and immature bone within the granulation tissue in fracture site. Ossification in primary callus may be seen on radiograph from 10 days to 2 weeks where it shows abundant, well-defined callus bridging the fracture site, with fracture lines becoming fuzzy. The callus fracture sign refers to the extension of fracture line beyond the cortex into the callus but not to the edge of the callus. It is a useful radiological predictor of progression to non-union and may represent insufficient mechanical stability at the fracture site. | | |

Fig. 4.138.2.7: Bone island

Fig. 4.138.2.8: Chronic osteomyelitis

Fig. 4.138.2.9: Chronic osteomyelitis

Fig. 4.138.2.10: Chronic osteomyelitis

is the typical appearance of a cortically placed osteoid osteoma. Intramedullary lesions that are intracapsular (such as those in the femoral neck) provoke much less reactive sclerosis because of the low rate of bone production from the intracapsular periosteum. Lesions in this location are much more difficult to detect because the lucent nidus is often the only abnormality visualized.

The nidus has <2 cm in diameter and typically ovoid; if >2 cm, it is called osteoblastoma.

In most cases of osteoid osteoma, plain roentgenograms are sufficient to demonstrate the lesion, providing the diagnosis in >75% of cases. CT may be helpful for localizing the nidus, especially where plain roentgenograms are equivocal. If the roentgenogram is negative but the

clinical history suggests a lesion, then a bone scan or MRI should be performed. In general, MRI is a reliable modality in the demonstration of the nidus. Bone scans will show a regional increase in uptake with an intense focal zone of uptake superimposed (double-density sign). This is particularly true with spinal lesions. If these studies are equivocal, angiography may be necessary to finally locate and provide the correct diagnosis. In angiography, the area of the lesion is highly vascularized, with an intensely homogeneous vascular blush appearing in the arterial phase and persisting late into the venous phase. This is the definitive means of distinguishing osteoid osteoma from a Brodie's abscess, which shows no such vascular blush within its necrotic cavity.

Treatment: In surgically accessible lesions a wide en bloc excision is the treatment of choice. It is not necessary to remove the reactive sclerosis, even though this may form the major part of the radiologic presentation. Vertebral body lesions are often treated with irradiation. Prognosis is good, with a little chance of recurrence when complete surgical excision of the nidus is accomplished. Percutaneous radiofrequency ablation under CT guidance is being used with increasing frequency. There are evidences that osteoid osteoma naturally resolves spontaneously with time and can be treated conservatively with NSAIDs.



Fig. 4.138.2.11: Osteosarcoma



Fig. 4.138.2.12: Intramedullary osteosclerosis, other sclerotic lesions include SAPHO, sickle cell anemia, Erdheim-Chester disease



Fig. 4.138.2.13: Chronic recurrent multifocal osteomyelitis (CRMO)

4.139 MUSCULOSKELETAL SYSTEM

Case No. 139

Clinical history: 8 years old boy with pain and swelling in distal femur.

Radiological techniques and observation: Figure 4.139.1 is plain radiograph AP view of knee showing a central lytic metaphyseal lesion with long axis parallel to length of bone and thin sclerotic margin. There is a pathologic fracture with cortical break as well as a “fallen bone” fragment and periosteal reaction is seen. Narrow zone of transition is noted. No specific matrix. No adjacent soft tissue noted. Epiphysis is normal.

Figure 4.139.2 is coronal T1W MR of the same patient showing a low signal lesion, signal nearly isointense to muscle. Figure 4.139.3 is the coronal T2-FS MR showing hyperintense lesion with fluid levels. Figure 4.139.4 is coronal T1 C + MR showing pronounced rim enhancement of the lesion.

Interpretation: A: 8 years old male, lesion in distal femur. C: Central lytic metaphyseal lesion with long axis parallel to length of bone and thin sclerotic margin. T1 hypointense, T2 hyperintense on MRI with peripheral rim enhancement. B: Pathologic fracture with cortical break as well as a “fallen bone” fragment. Periosteal reaction with narrow zone of transition. D: Simple bone cyst.

Principal diagnosis: Simple bone cyst (SBC) of distal femur with pathological fracture.

Brief discussion about the condition: Simple bone cysts, also known as unicameral bone cysts, are benign non-neoplastic lucent bony lesions that are most commonly observed in children and usually go unnoticed (age = 5–15 years). A pathological fracture is the most common consequence. They are usually intramedullary, and they are most common in the metaphysis of long bones, where they abut the growth plate. Common sites of SBC are the proximal humerus (50–60%), proximal femur (30%), and other long bones. SBCs can be seen uncommonly in adults at spine (typically the posterior elements), the pelvis (only 2%), the talus, calcaneus, or the iliac wing. On bone scintigraphy, they appear as photopenia foci (cold spot). A pathological fracture, on the other hand, would be seen as enhanced radioisotope activity.

Treatment

- Intralesional injections
- Resection, curettage and bone grafting
- Decompression/combined techniques
- Curettage, local adjuvant treatment and grafting

Complications

- Pathological fracture and growth disturbances.
- Recurrence after treatment.
- Embolization of the injected material such as steroid, bone marrow aspirate; local reactions to the material used to fill the cyst cavity.
- Exaggerated inflammatory response following the use of recombinant bone morphogenic protein in patients with recalcitrant SBCs.



Fig. 4.139.1



Fig. 4.139.2



Fig. 4.139.3

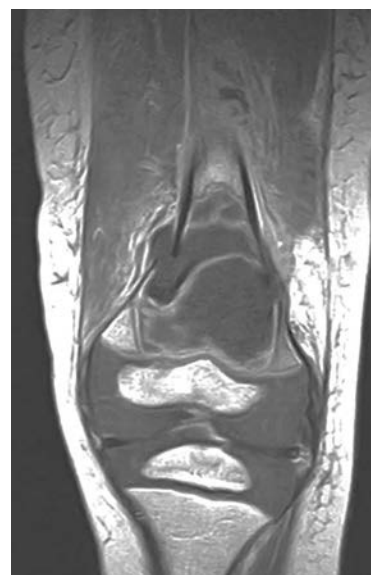





Fig. 4.139.4

Table 4.139.1: Differential diagnoses for SBC

| | | |
|--|--|---|
| <p>Aneurysmal bone cyst: Age—10–20 years (75% occur before epiphyseal closure). Sites—ends of long bones (70–80%), especially in the lower limbs. Also, flat bones and vertebral appendages.</p> | <p>Arises in unfused metaphysis or in metaphysis and epiphysis after fusion. Well-defined lucency with thin but intact cortex. Marked expansion (ballooning) with narrow zone of transition. Multiloculated lesion with septations and fluid–fluid level(s) on CT and MRI. Thin internal strands of bone/trabeculation. ± New bone in the angle between original cortex and the expanded part. In the spine they involve the posterior elements. May rarely arise from the surface of bone in a subperiosteal location. T1 + C – septations may enhance. Bone scan: Doughnut sign: Increased uptake peripherally with a photopenic center.</p> |  <p>Fig. 4.139.5: Aneurysmal bone cyst—clue is normal epiphysis</p> |
| <p>Haemophilic pseudotumor is complication of hemophilia presenting as progressive cystic swelling seen in < 2% of hemophiliacs. They develop in the muscles of the pelvis and lower extremity, or in bone following intraosseous bleeding. Pathological fractures can also be present.</p> | <p>(a) Intraosseous—a well-defined medullary lucency with a sclerotic margin. It may breach the cortex. ± Periosteal reaction and soft-tissue component. (b) Subperiosteal—periosteal reaction with pressure resorption of the cortex and a soft-tissue mass.</p> |  <p>Fig. 4.139.6: Haemophilic pseudotumor (subperiosteal)</p> |
| <p>Fibrous dysplasia (Refer to case 147)</p> | | |
| <p>Enchondromas (Refer to case 151)</p> | | |
| <p>Intraosseous ganglia are small radiolucent lesions usually reported incidentally in the epiphysis and subchondral region without degenerative arthritis.</p> | <p>They are uni-/multilocular cysts with a fibrous lining and gelatinous substance inside. A well-defined solitary lytic lesion with a sclerotic edge is typical. There is no evidence of communication with the joint. Increased radiotracer uptake is visible on bone scans (in 10 percent).</p> |  <p>Fig. 4.139.7: Intraosseous ganglia</p> |
| <p>Eosinophilic granuloma: LCH (Refer to case 153): It frequently involves axial skeleton than appendicular skeleton. Vertebral involvement is mostly seen in children. Well-defined lucency in the medulla ± thin sclerotic rim. ± Endosteal scalloping. True expansion is uncommon except in ribs and vertebral bodies. ± Overlying periosteal reaction. Multilocular lucency, without expansion, in the pelvis. Punched-out lucencies in the skull vault with a little or no surrounding sclerosis. May coalesce to give a 'geographical skull'. Destructive lesions in the skull base, mastoids, sella or mandible ('floating teeth'). Vertebra plana with intact intervertebral discs.</p> | | |

Contd.

Table 4.139.1: Differential diagnoses for SBC (Contd.)


| | | |
|---|--|---|
| Chondromyxoid fibroma Age—10–30 years. Sites—proximal tibia (50%); also, femur and ribs. | Metaphyseal ± extension into epiphysis, but never only in the epiphysis. Round or oval, well-defined lucency with a sclerotic rim. Eccentric expansion. Internal calcification is uncommon, occasional septation. |  |
| Giant cell tumor (Refer to case 140) | | |
| Telangiectatic osteosarcoma (Refer to case 150) | | |
| Desmoplastic fibroma: They are rare, locally aggressive benign neoplasm. Seen between 1st and 3rd decade of life. No sex predilection. They usually arise in the metaphyseal region of long bones (femur, humerus, tibia and radius), then mandible and ilium. They arise as either subperiosteal or intraosseous tumors and are large at presentation. Two patterns can be seen—an ill-defined moth-eaten or permeative lesion and an expanding, trabeculated lesion. En bloc resection in the current treatment of choice. | | |
| Osteomyelitis (Refer to case 149) | | |

Fig. 4.139.8: Chondromyxoid fibroma**Table 4.139.2: Difference between solid and cystic lucent bone lesions**

| <i>Solid lucent lesions</i> | <i>Cystic lucent lesions</i> |
|--|---|
| Osteoblastic (osteoid osteoma, osteoblastoma, telangiectatic, osteosarcoma) | Simple bone cyst, aneurysmal bone cyst |
| Cartilaginous (enchondroma, chondroblastoma, chondromyxoid fibroma, chondrosarcoma) | Various bone cysts (synovial, degenerative), intraosseous lipoma |
| Fibrous and histiocytic (non-ossifying fibroma, fibrous dysplasia, osteofibrous dysplasia, desmoplastic fibroma, fibrosarcoma, malignant fibrous histiocytoma) | Brown tumor of hyperparathyroidism, vascular lesions, hydatid cyst |
| Lymphoma | Hemophilic pseudotumor |
| Myeloma (plasmacytoma) | Intraosseous ganglion |
| Ewing sarcoma, metastatic (from lung, breast, gastrointestinal tract, kidney, thyroid), giant cell tumor, reparative giant cell granuloma, Langerhans cell histiocytosis, Paget disease (osteolytic phase—osteoporosis circumscripta) | Bone abscess |
| Lucent is a descriptive way to describe how the bone appears less thick (is more clear/translucent—the alternative meaning of the word lucent, has bright /light meaning) on radiograph; it does not state about the underlying disease process. | Lytic refers to the occurrence of a specific pathological process characterised by bone lysis/destruction. A lytic lesion is always lucent, but a lucent lesion does not have to be lytic; for instance, it could be cystic. |

4.140 MUSCULOSKELETAL SYSTEM

Case No. 140

Clinical history: A 34 years female with knee pain.

Radiological techniques and observation: Figures 4.140.1 and 4.140.2 are frontal and lateral radiographs of knee joint respectively show an eccentrically located well-defined expansile lytic lesion without sclerotic margin in metaepiphyseal region of proximal tibia with narrow zone of transition, with juxta-articular involvement and endosteal scalloping without any evidence of cortical break. No evidence of obvious specific matrix/periosteal reaction/soft tissue involvement. No evidence of skip lesions. With this principal diagnosis is giant cell tumor. Further MRI is needed to characterise the lesion, to assess the medullary involvement and articular extension. Figures 4.140.3 to 4.140.5 are MRI images in T1 coronal, STIR sagittal and coronal views respectively showing the lesion to be T1 hypointense and predominantly STIR hyperintense with no evidence of cortical break or periosteal reaction. There is no evidence of fluid-fluid levels and no evidence of surrounding edema. Minimal joint effusion noted. No evidence of neurovascular structure invasion.

Interpretation: A: 34 years old female, lesion involving proximal tibia; C: Expansile eccentric epiphyseal lytic lesion; B: Narrow zone of transition, subarticular involvement, no definite matrix; D: Giant cell tumor.

Principal diagnosis: Giant cell tumor.

Brief discussion about the condition: GCT—also known as osteoclastomas are benign bone tumor with sheets of neoplastic ovoid mononuclear cells and osteoclast type

of giant cells. Age group—20 to 40 years (only 3% occur before epiphyseal closure). Most common site around knee (50–60%) > distal radius > sacrum > vertebral body. Abuts articular surface; Cortical ridges or internal septa seen producing a multilocular appearance and fluid levels on CT or MRI. Pathological fracture may be present. MRI—low to intermediate signal solid component which enhances on post-contrast, thus differentiating from ABC. Nuclear medicine—most GCTs demonstrate increased uptake especially around periphery with a central photopenic region—doughnut sign. Rarely malignant GCT (5–10%)—to sarcomas (osteosarcoma, fibrosarcoma or undifferentiated pleomorphic sarcoma)

- Primary malignant—within benign GCT
- Secondary malignant (most common)—secondary to radiotherapy treatment of benign GCT
- Lung metastasis is common—but have excellent prognosis—“benign metastasing giant cell tumour”

Management:

- Referral to orthopedician and multidisciplinary approach to manage the case.
- Marginal resection, curettage, filled with bone graft
- Wide resection to limit recurrence with arthroplasty and osteochondral graft (not preferred in young age)

Enneking staging: Based on tumor grade, local spread and metastatic disease of malignant skeletal tumors.

Stage 1: Indolent radiographic and histologic appearance

Stage 2: More aggressive radiographic appearance (expanded but intact periosteum)

Stage 3: Aggressive growth with soft tissue but histologically benign; distant metastasis.



Fig. 4.140.1



Fig. 4.140.2



Fig. 4.140.3

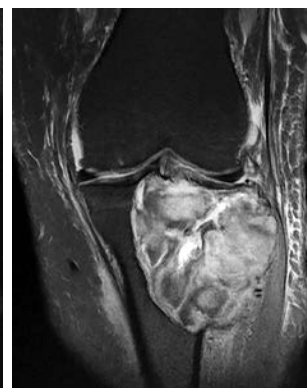


Fig. 4.140.4

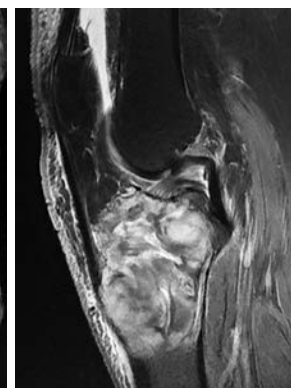


Fig. 4.140.5

Table 4.140.1: Differential diagnosis for GCT**Aneurysmal bone cyst** (Refer to case 139)**Clear cell chondrosarcoma:**

Age—3rd to 5th decade, with men being affected twice as often as women (M:F ~ 2:1). The lesion is most commonly found on an epiphyseal level (conventional chondrosarcoma, which is usually metaphyseal-diaphyseal). Proximal femur (55–60%), proximal humerus, distal femur, or proximal tibia are the tubular long bones most commonly seen.

Clear cell chondrosarcomas are lytic and expansile on radiographs, with a low reported incidence of calcified matrix. Endosteal irregularity is a common occurrence. There is no periosteal response. Once pathologic fracture occurs, soft tissue expansion and cortical break are seen. MRI-T1—homogeneous intermediate signal intensity; T1+ contrast—show heterogeneous enhancement; T2—heterogeneous signal intensity.

Geode cyst—also known as subchondral cyst; this is due to intraosseous synovial fluid intrusion through the exposed articular plate or secondary to trabecular fractures. Associated with degenerative joint disease, rheumatoid arthritis, calcium pyrophosphate dihydrate crystal deposition disease (CPPD), avascular necrosis.

Well-defined ovoid/round lytic lesion in epiphysis often with sclerotic margin in subarticular location with underlying arthritis (degenerative), associated joint space narrowing and osteophytes.

**Fig. 4.140.6:** Subchondral cyst**PVNS** (Refer to case 160)**Table 4.140.2: Differential diagnosis for epiphyseal lesions**

| <i>Epiphyseal lytic lesions in adults</i> | <i>Epiphyseal lesions in children</i> | <i>Expansile lytic lesions (blow out lesions)</i> |
|--|---|--|
| GCT, geode, clear cell chondrosarcoma, PVNS, metastasis, myeloma | Chondroblastoma Osteomyelitis LCH | Giant cell tumor, brown tumor, fibrous dysplasia, aneurysmal bone cyst, multiple myeloma, metastasis, chondrosarcoma, plasmacytoma |

Table 4.140.3: Difference between benign and malignant GCT

| <i>Benign GCT</i> | <i>Malignant GCT</i> |
|--|---|
| Eccentric, expansile epiphyseal lytic lesion with non-sclerotic margin, narrow zone of transition and sharply-defined margins, thinned out cortex. | Aggressive expansile eccentric lytic lesion with cortical destruction and surrounding soft tissues, wide zone of transition |

4.141 MUSCULOSKELETAL SYSTEM

Case No.141

Clinical history: A 16-years-old male presented with the complaints of pain in the knee after trivial trauma.

Radiological techniques and observation: Figures 4.141.1–4.141.3 are radiograph knee skyline view, AP and lateral view respectively showing single well-defined, multilobulated lytic lesion in the patella, with no specific (osteoid, chondroid, osseofibrous, fatty) matrix. Endosteal scalloping noted with internal separations and narrow zone of transition. There is no evidence of cortical breach/periosteal reaction/soft tissue component. There is no evidence of extension across the joint. No skip lesion/no other similar lesions. Since the patella is considered as an epiphyseal equivalent, differential diagnosis of epiphyseal lesions is considered here. With these imaging findings differential diagnosis for a 16 years old male will be chondroblastoma, Brodie's abscess, eosinophilic granuloma, intraosseous lipoma.

For further characterization CT is needed to look for matrix and to look for cortical breach.

Figures 4.141.4 to 4.141.5 are CT in bone window axial section confirming the radiograph findings and it shows ring and arc calcification. No periosteal reaction.

Suspicious cortical break noted in the anterior surface of patella without surrounding soft tissue mass.

MRI is needed to look for joint involvement, intramedullary extension, skip lesions and neurovascular bundle invasion. Figures 4.141.6 to 4.141.8 are T1 sagittal images, PD axial and sagittal images showing a well-defined PD hyperintense and T1 hypointense lesion in the patella with fluid-fluid level noted inside the lesion. No evidence of cortical breach, no joint extension, no soft tissue component and neurovascular invasion.

Interpretation: A: 16 years old male, lytic lesion in the patella; C: Single well defined, with no specific matrix B: Shows endosteal scalloping with internal separations and narrow zone of transition. No evidence of cortical breach/periosteal reaction/soft tissue component/extension across the joint. D: Chondroblastoma.

Principal diagnosis: Chondroblastoma

Brief discussion about the condition: Chondroblastomas—also called Codman's tumor. Most frequently affects those 10–25 years old; M > F (nearly 2:1). 90% are medullary; 10% are cortical. 77% of the lesions occur in the knee, hip, and shoulder. Joint discomfort, muscular wasting, soreness, and swelling/local bulk are all



Fig. 4.141.1



Fig. 4.141.2



Fig. 4.141.3

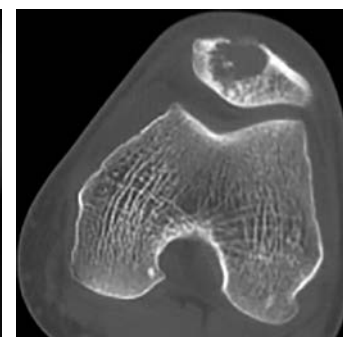


Fig. 4.141.4

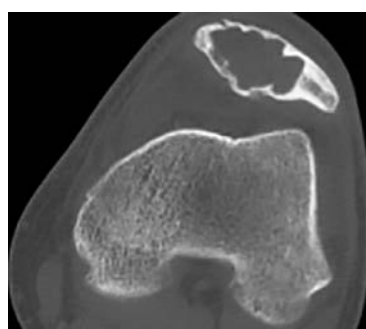


Fig. 4.141.5

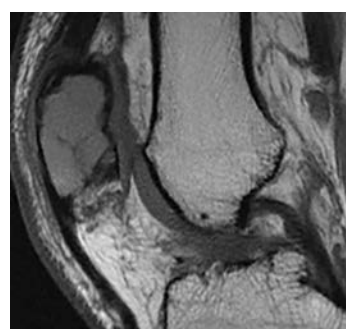


Fig. 4.141.6

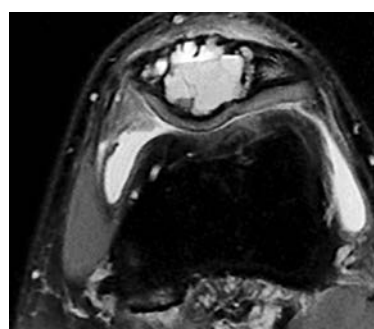


Fig. 4.141.7

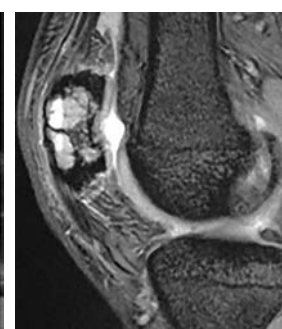


Fig. 4.141.8

Table 4.141.1: Differential diagnosis for epiphyseal lesions in pediatric age group

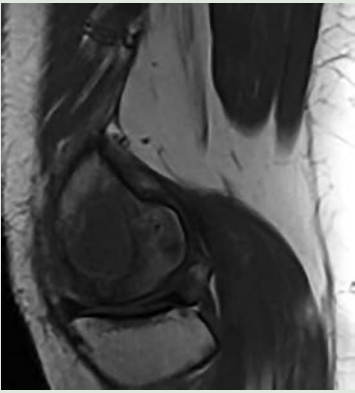
| | | |
|---|--|---|
| Brodie abscess/osteomyelitis: Subacute osteomyelitis with single focus of intraosseous abscess formation. Affects children before epiphyseal fusion. | Radiographs: Lytic lesion with geographic sclerotic margins, metaphyseal location. MR: Well-defined intraosseous abscess with peripheral enhancement. The penumbra sign represents a rim of vascularized granulation tissue around a bone abscess cavity that has a higher T1 signal intensity than the cavity itself. |  |
| Langerhans cell histiocytosis (Refer to case 153) | | |
| Chondroblastoma (Present case) | | |
| Epiphyseal lesions in adult age group | | |
| Giant cell tumor (Refer to case 140) | | |
| Geode (Refer to case 140) | | |
| Clear cell chondrosarcoma (Refer to case 140) | | |
| Aneurysmal bone cyst (Refer to case 139) | | |

Fig. 4.141.9: Brodie abscess

possible clinical manifestations. Chondroblastoma releases prostaglandins, which cause discomfort, and it can also cause synovial response due to its epiphyseal position. Malignant transformation involving local and vascular invasion, as well as distant metastases, has been

observed in a limited percentage of instances. Secondly to underlying chondroblastoma, aneurysmal bone cysts might be found. The classic “chicken-wire calcification” is caused by calcium deposition surrounding the chondroblasts, which are polyhedral in shape.

Table 4.141.2: Salter and Harris classification of epiphyseal injuries




Fig. 4.141.10: Salter and Harris types 1, 2, 3




Fig. 4.141.11: Salter and Harris types 4, 5, 6




Fig. 4.141.12: Salter and Harris types 7, 8, 9

Plain radiograph: Chondroblastomas appear as well-defined lucent lesions with smooth or lobulated margins and a thin sclerotic rim that is seen eccentrically in the epiphysis of long tubular bones (e.g., femur, humerus, or tibia) or apophyses (e.g., greater trochanter of the femur, greater tuberosity of the humerus, acromion). They tend to expand to the metaphysis as they grow larger. Cortical breach is seen rarely. In 40–60% of cases, internal calcifications might be visible. They are about 1 to 10 cm in size, with the many case measures 3 to 4 cm at the time of diagnosis. One-third of individuals have a joint effusion. The presence of solid/layered periosteal reaction far from the lesion, is specific for chondroblastoma, among epiphyseal lesions. CT scan shows the connection between the growth plate and the articular surface. Internal calcification (calcified matrix seen in up to 50% of cases), solid periosteal response (seen in up to 50% of cases), and cortical breach are also more visible. Scalloping of the endosteum can be visible. MRI helps to identify transphyseal or transcortical extension, as well as reveals concomitant bone marrow and soft tissue edema. The margins of these lesions are well-circumscribed and lobulated. T1 denotes an intermediate signal; T2 denotes a varied signal; STIR denotes a strong signal; T1 C+ denotes a heterogeneous moderate enhancement. Fluid-fluid levels are seen due to an associated aneurysmal bone cyst.



Fig. 4.141.13: Chondroblastoma

Management: Treatment typically consists of curettage and packing of the resulting cavity with either bone or bone cement (polymethylmethacrylate). Radiofrequency ablation has also been used.

Complications: Pathological fractures and rarely, malignant transformation and pulmonary metastasis.

Salter and Harris classification of epiphysis injuries: Includes 5 types (Table 4.141.2) and additionally added types which are uncommonly used includes 6, 7, 8, 9.

4.142 MUSCULOSKELETAL SYSTEM

Case No. 142.1

Clinical history: A 60-year-old female patient with lower back ache.

Radiological procedures and observations: Figure 4.142.1.1 is X-ray pelvis radiograph in AP projection is showing increased cortical thickening and sclerosis of iliopectineal lines (pelvic brim sign). There are coarse trabecular opacities with enlargement in the bilateral iliac wings, left pubic rami, ischium, right head of femur. Areas of sclerosis and cortical thickening noted in the L3 lumbar vertebrae (ivory vertebra). Pathological fracture noted in the left intertrochanteric region of femur with proximal femoral screw fixation.

Figures 4.142.1.2 to 4.142.1.5 are limited sections CT axial with coronal, sagittal reformations of lumbar spine and pelvis in bone window showing increased cortical thickening and sclerosis encasing the L3 vertebral margins. Flattening of normal concavity of anterior margin of L3 vertebral body noted. Coarse trabecular thickening noted involving L3 vertebra and bilateral iliac

bones. Figures 4.142.1.6–4.142.1.9 are limited sections of axial, coronal, sagittal T2 lumbar spine showing heterointensity involving the L3 vertebral body with intervertebral disc space narrowing at L3–L4 level causing disc bulge. No evidence of abnormal marrow signal. Spinal canal is normal. No evidence of cord compression.

Interpretation: A—60-year-old female, lesion in the L3 vertebral body and pelvis; C—coarse trabeculations, cortical thickening and sclerosis; B—bony enlargement; D—Paget's disease.

Principal diagnosis: Paget's disease

Brief discussion: Paget disease of the bone is a common, chronic bone disorder characterized by excessive abnormal bone remodelling. It is common and can affect up to 4% of individuals over 40 and up to 11% over the age of 80. There may be a slight male predilection. Localized discomfort and tenderness, higher focal temperature due to hyperemia (hypervascularity), increased bone size, bowing deformities, kyphosis of



Fig. 4.142.1.1

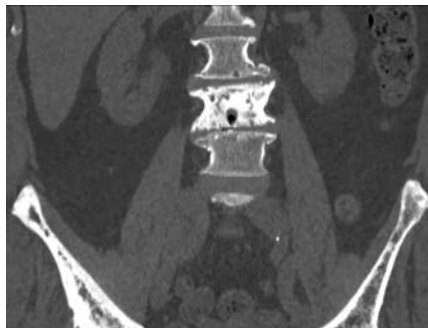


Fig. 4.142.1.2

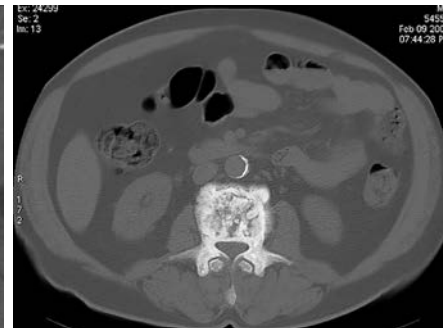


Fig. 4.142.1.3



Fig. 4.142.1.4



Fig. 4.142.1.5

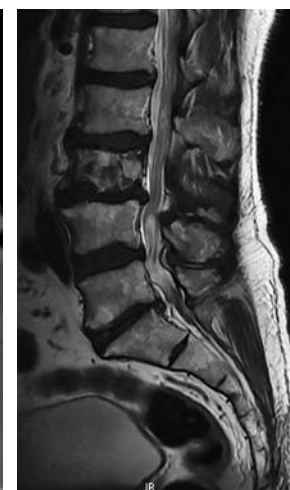


Fig. 4.142.1.6

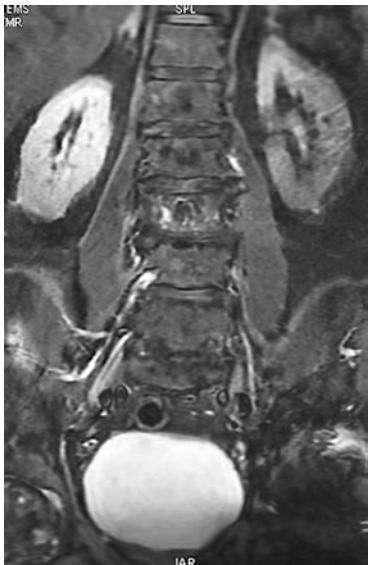


Fig. 4.142.1.7

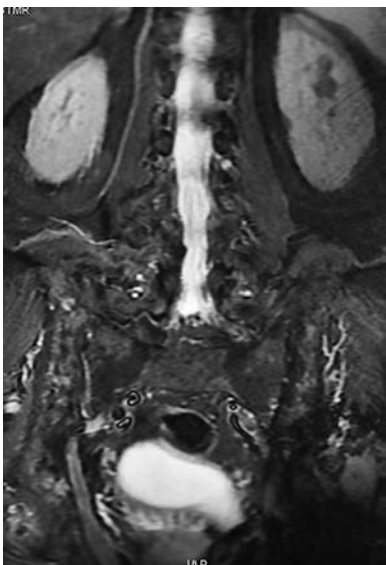


Fig. 4.142.1.8

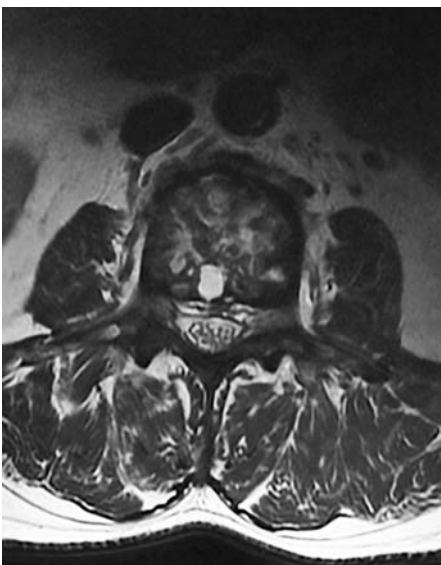


Fig. 4.142.1.9

Differential diagnosis

Table 4.142.1.1: Differential diagnosis for Paget's disease

Osteoblastic metastasis (Refer to case 154): In the pelvis, osteosclerosis in Paget disease can mimic osteoblastic metastasis. The presence of asymmetric or unilateral distribution, accentuated trabecular pattern, and enlargement of the involved bone are typical features of Paget disease. Osteoblastic metastasis can simulate the cotton-wool appearance of osteosclerotic lesions of Paget disease.

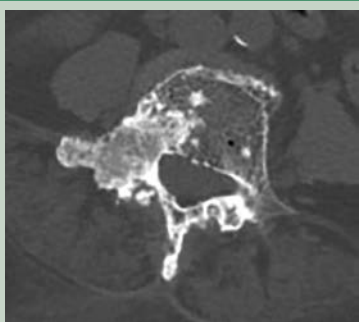


Fig. 4.142.1.10: Osteoblastic metastasis

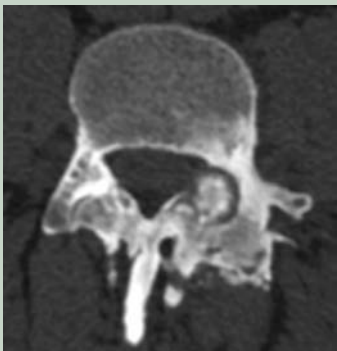

Vertebral hemangiomas: The most prevalent benign spinal neoplasms are hemangiomas. They are frequently asymptomatic and are discovered by chance on imaging for other reasons due to their distinctive features. Vertebral hemangiomas are often identified by their corduroy fabric / jail bar appearance. The enlarged spinal trabeculae cause a polka-dot / salt and pepper appearance on axial CT. Extrasosseous components are better visible on MRI, and the hemangioma components are depicted as fat and water. In both T1 and T2 scans, thickened trabeculae appear as low signal regions. Due to its fat component, T1 hyperintensity is seen. T1/T2 hyperintense with increased signal intensity on T2 (because of water content) Significant enhancement on T1 post-contrast owing to high vascularity



Fig. 4.142.1.11: Vertebral hemangiomas (corduroy)



Fig. 4.142.1.12: Vertebral hemangiomas (polka-dot)

| | | |
|---|---|---|
| Osteoid osteoma: Refer to case 138.2 |  |  |
| | Fig. 4.142.1.13: Osteoid osteoma | Fig. 4.142.1.14: Osteoid osteoma |
| Familial expansile osteolysis is a rare autosomal-dominant bone dysplasia that in its early stage may resemble Paget disease. It is seen at fourth decades. No sex predilection known. | Progressive osteoclastic resorption is accompanied by medullary expansion of bone, producing both generalized and local bony changes. Pain, pathologic fracture of disintegrated bone, skeletal deformity, loss of dentition, and deafness are features of the disease. | |
| Rare differentials include: Familial idiopathic hyperphosphatasia (“juvenile” Paget disease), fibrogenesis imperfecta ossium, axial osteomalacia (rare condition associated with a coarsened trabecular pattern on radiographs simulating Paget disease). | | |

the spine, and restricted range of motion are some of the symptoms that may be present. Polyostotic disease is more common than mono-ostotic disease. The spine, pelvis (frequently asymmetric), skull, and proximal long bones are the most common sites of involvement.

Pathology: The cause is unknown, however, it is an osteoclast-related disease. It has been proposed that viral infection (paramyxovirus) has propensity for genetic susceptibility. Markers-elevated serum alkaline phosphatase, normal calcium and phosphorus levels, increased urine hydroxyproline.

There are three stages to the process: Early destructive stage (incipient active, lytic): Osteoclastic activity

predominates; Osteoblastic and osteoclastic activity in the intermediate stage (active, mixed); Inactive, sclerotic/ blastic stage.

Radiographic features: Osteolytic/lucent areas are seen in early phase which are later followed by bone expansion with a coarse trabecular pattern is seen on radiographs. Sclerotic changes are seen in late phases.

Skull: Osteoporosis circumscripta (stage one): extensive, well-defined lytic lesions involving the inner aspect of the outer table of the skull with a preserved inner table. Mixed lytic and sclerotic lesions of the skull—cotton wool appearance. Diploic widening affects both the inner and outer calvarial tables, with the former being more



Fig. 4.142.1.15: Cotton wool appearance of skull

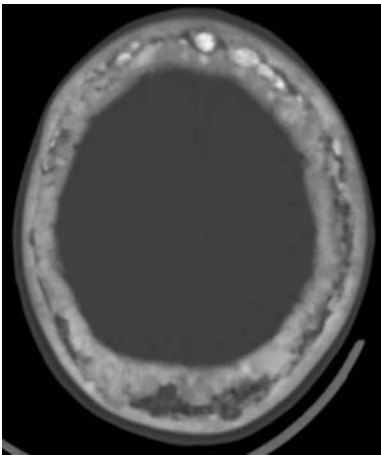


Fig. 4.142.1.16: Cotton wool appearance of skull



Fig. 4.142.1.17: Osteoporosis circumscripta



Fig. 4.142.1.18: Fibrous dysplasia

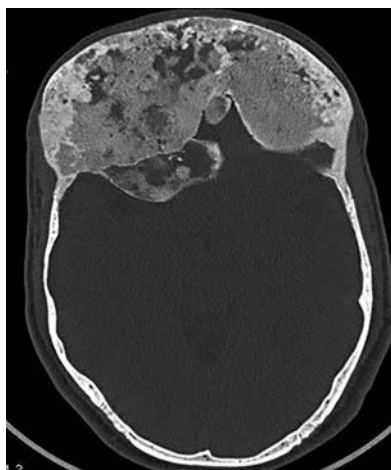


Fig. 4.142.1.19: Fibrous dysplasia

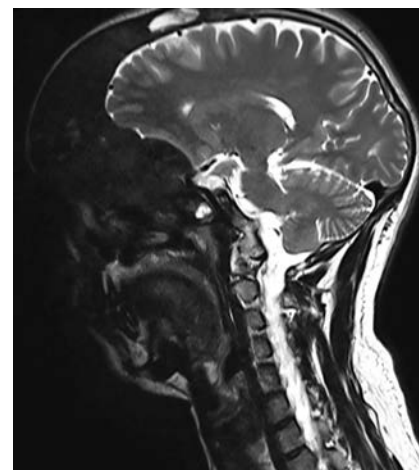


Fig. 4.142.1.20: Fibrous dysplasia

severely impacted. Platypasia with basilar invagination with the appearance of the skull falling on facial bones, as if wearing a Tam o' Shanter hat.

Paget disease of the spine typically appears with cortical thickening and sclerosis encasing the vertebral borders, giving the appearance of a picture frame on radiographs in mixed-phase. Flattening of the typical concavity of the anterior edge of the vertebral body on lateral radiographs also contributes to the rectangular appearance. Vertical trabecular thickening is more coarse than intraosseous hemangiomas, which have a more delicate pattern. Pelvis: Obliteration of Köhler's teardrop, acetabular protrusion, bony expansion of pubic rami and ischium is due to cortical thickening and sclerosis of the iliopectineal (arcuate line) and ischiopubic lines. These are frequently asymmetric, and they appear more frequently on the right side.

Blade of grass or candle flame sign: Begins as a subchondral area of lucency with tip of V-shaped osteolysis extending towards the diaphysis; lateral bowing of the femur, anterior curvature of the tibia.

MRI: The overall signal characteristics vary, most likely reflecting the normal progression of the illness process at various stages. Patterns of involvement includes: a) The most prevalent pattern, which corresponds to long-term illness, is a strong signal intensity in Pagetic bone that is similar to that of fat; b) Speckled appearance: T1 hypointense and T2 hyperintense signals suggest the presence of compact bone or fibrous tissue—second most common pattern: Probably corresponds to granulation tissue, hypervascularity, and edema seen in early mixed active disease; c) Low signal intensity on both T1 and T2 images; suggesting the existence of compact bone

or fibrous tissue—least common pattern: Seen in late sclerotic stage. Usually, fatty marrow signal is seen in all sequences.

Bone scintigraphy: Tc-99m-MDP is a very sensitive but non-specific bone scintigraphy technique. It is beneficial to characterise the disease's broad scope and dissemination. Increased uptake in all stages of the disease, albeit uptake may be normal in the burnt-out sclerotic quiescent phase. Mickey Mouse sign: On posterior planar imaging, uptake in the vertebral body and posterior elements form an inverted triangular pattern resembling the Mickey Mouse silhouette: heart/clover sign and T/champagne glass sign. Diffuse mandibular uptake generating a bearded look is a Lincoln sign.

Complications: Weakening of bones results in deformity and pathological fractures, risk for osteoarthritis, hearing loss—sensorineural type and conductive type, vestibulocochlear nerve compression in the internal auditory canal, bone mineral density loss in cochlear capsule, middle ear ossicles fixation, neural compression cranial nerve paresis, basilar invagination may occur in advanced cases with hydrocephalus or brainstem compression, secondary development of tumors, high output congestive cardiac failure, when bone involvement >15%—rapid bone formation/resorption can lead to left-to-right shunting and decreased peripheral resistance, hyperparathyroidism, extramedullary hematopoiesis.

Management: Treated with bisphosphonates to reduce the bone turnover, to promote healing of osteolytic lesions and improve bone pain. Analgesics and non-hormonal anti-inflammatory drugs for pain management.

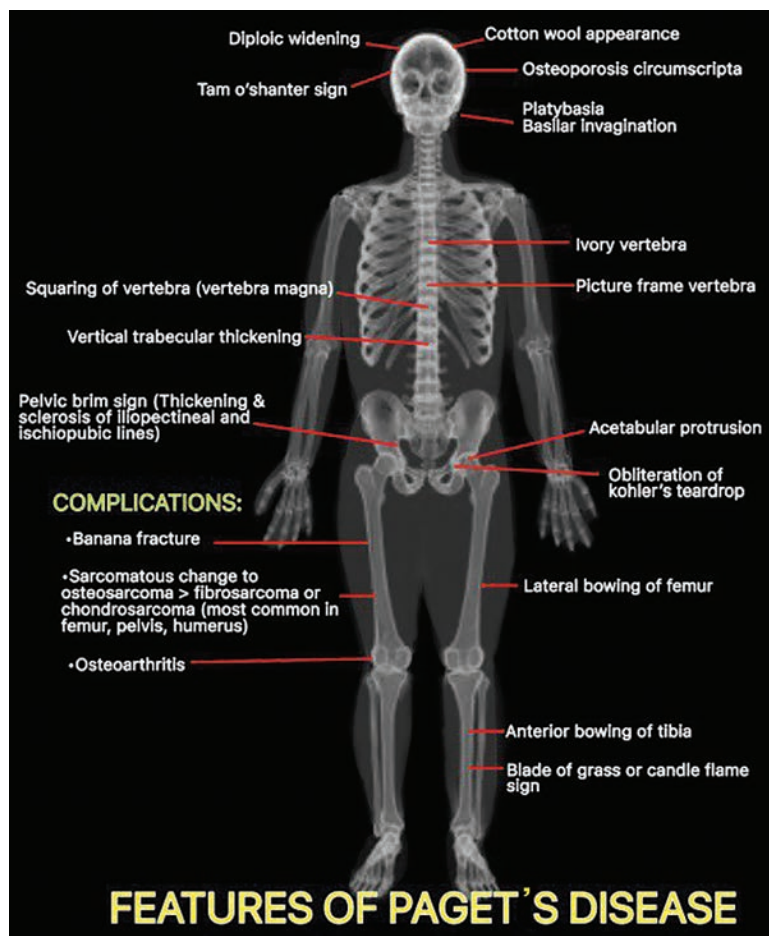


Fig. 4.142.1.21: Manifestations of Paget's disease

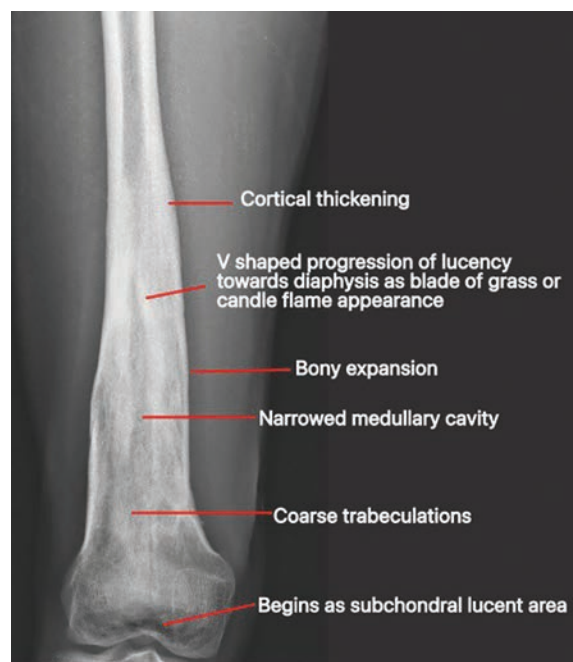


Fig. 4.142.1.22: Paget's disease of long bone

Case No. 142.2

Clinical history: A 31-year-old male, presented with varied musculoskeletal complaints, anemia and bone pain with history of surgery.

Radiological technique and observations: Figures 4.142.2.1 to 4.142.2.8 are AP radiograph of pelvis and bilateral hip joint with corresponding limited axial, coronal and sagittal CT sections respectively showing increased bony sclerosis and marrow expansion noted in bilateral femur and pelvis. Iliofemoral bypass graft is placed in right side. Severe sacroiliac joint erosions are noted. Left femoral head appears deformed with secondary osteoarthritic changes in left hip joint.

Interpretation: A—31-year-old male, lesion in pelvis; C—sclerosis of bony cortex and expansion of marrow; B—secondary osteoarthritis of left hip joint; D—sickle cell disease.

Principal diagnosis: Sickle cell anemia

Brief discussion about the condition: Normal human hemoglobin A contains 4 globin chains: $2\alpha + 2\beta$ chains.

Hb SS: Abnormal β chains twist (polymerization) leads to RBC (red blood cell) distortion which is exaggerated with deoxygenation leading to irreversible sickling (banana-shaped RBCs). Sickled RBCs occlude vessels leading to infarction and are quickly removed leading to anemia. Typically detected on newborn screening. Painful crisis of bone in 50% by age 5. Acute chest syndrome is the 2nd most common cause of hospitalization.

Acute chest syndrome: New pulmonary opacity on chest radiograph + ≥ 1 additional symptom (such as fever, cough, sputum production, tachypnoea, dyspnoea, or hypoxia) in setting of sickle cell disease (SCD). It is most common in patients aged 2–4 years; incidence decreases with age. ACS is the most common cause of premature death in patients with SCD. Upper and middle lobe opacities more common in children. Lower lobe disease more common in adults. Opacity may not appear until 2–3 days after symptoms develop, referred to as “Radiographic Lag”. Pleural effusion is common (50%). Can see perfusion defect in V/Q scan which may mimic pulmonary embolism. Treatment includes oxygen,

antibiotics, pain control, IV fluids, incentive spirometry and blood transfusions.

Sickle cell dactylitis: Infarction involving diaphysis of tubular bones in the hands and feet is common in newborns and young children. Sickle cell dactylitis/hand-foot syndrome, is a type of infarction caused by the presence and persistence of red marrow. Sickle cell dactylitis is frequent between the ages of 6 months and 2 years, but it is uncommon after that due to the red marrow in hand and feet regress with maturity. Tender and swollen hands and feet, reduced mobility, and fever are common clinical symptoms in children. Patchy regions of lucency with periosteal reaction might be seen on radiographs.

What will you look for in a single IVU image, in a suspected case of sickle cell anemia?

Renal papillary necrosis as evidenced by Ball on 'T' sign, lobster claw or signet ring sign, avascular necrosis/sclerosis of femoral heads, small spleen (autosplenectomy) identified by lateralization of stomach bubble, splenomegaly in acute cases, gall stones, cholecystectomy clips in right upper quadrant (if postsurgical), H-shaped or biconcave vertebrae, enlarged visualised ribs due to marrow expansion.

Further investigations and management: Hemoglobin electrophoresis; Sickle cell crisis: Oxygen, hydration, pain management and blood transfusion; prophylactic penicillin + pneumococcal and *Haemophilus influenzae* vaccines to prevent infection.



Fig. 4.142.2.1



Fig. 4.142.2.2

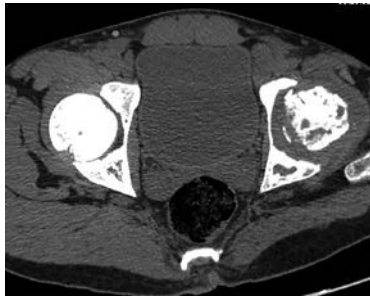


Fig. 4.142.2.3

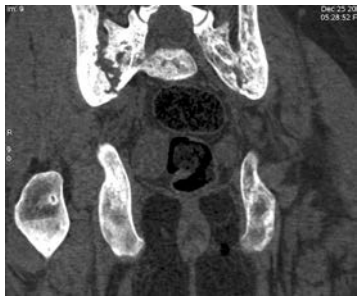


Fig. 4.142.2.4



Fig. 4.142.2.5

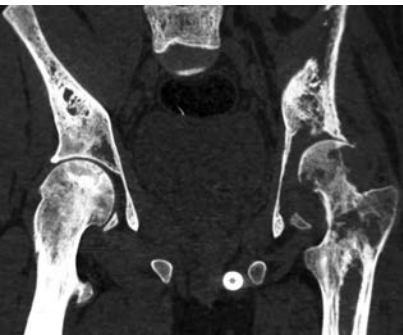


Fig. 4.142.2.6

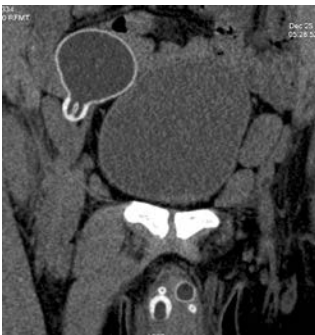


Fig. 4.142.2.7

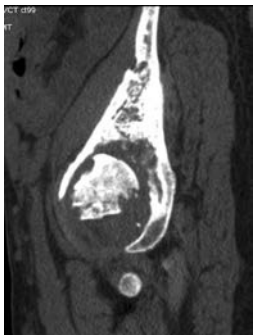


Fig. 4.142.2.8

| Table 4.142.2.1: Differential diagnosis for sickle cell anemia | |
|--|---|
| Thalassemia: Abnormal synthesis of beta chains of haemoglobin. Classified clinically and pathologically into three types as major, minor and intermediate. Changes of bone marrow expansion similar to SCD. | <ul style="list-style-type: none">• Avascular necrosis less common than in SCD• Hypopneumatisation of the frontal, maxillary, and sphenoid sinuses, filled with marrow containing bone• Ribs: Rib-within-a-rib appearance, noted particularly in the middle and anterior portions of the ribs exaggerated H-shaped vertebra and “hair on end” skull diploe. |
| Langerhans cell histiocytosis (Refer to case 153) | |
| Leukemia: The first peak occurs between the ages of 3 and 7, with a second peak occurring after 40 years. | Bone involvement can be seen. A metaphyseal radiolucent band. Other radiological findings include subperiosteal new bone formation and osteolytic lesions involving the medullary cavity and cortex. |
| Other hemolytic anemias | Hereditary spherocytosis (slight diploic widening, gallstones). Pyruvate Kinase deficiency (wide diploic space, gallstones). Glucose-6-phosphate dehydrogenase deficiency (bone changes absent) |

Table 4.142.2.2: Pathological and imaging correlation in sickle cell anemia

| S. No. | Cause/pathology | Radiological features |
|--------|-----------------------------------|---|
| 1. | Extramedullary hematopoiesis | <ul style="list-style-type: none"> Expanded diploic space; hair on end appearance (10%) Paraspinal/intraspinal masses (intermediate signal intensity on both T1-weighted and T2-weighted MR) |
| 2. | Intramedullary Marrow hyperplasia | Widening of medullary spaces and cortical bone thinning, which can lead to pathologic fractures. |
| 3. | Thrombosis and infarction | 6 months–2 years: Dactylitis Adults and children: Cortical thickening, medullary infarct Splenic infarct/auto-splenectomy |
| 4. | Epiphyseal infarction | <ul style="list-style-type: none"> Avascular necrosis of hip > humerus Epiphyseal shortening with cup deformity of metaphysis |
| 5. | Growth effects | H-shaped vertebra/fish mouth vertebra/tibiotalar slant deformity |
| 6. | Infection | <ul style="list-style-type: none"> Osteomyelitis (sclerosis with areas of lucencies, cortical break, periosteal reaction, soft tissue collection: Salmonella sp. M/C) Septic arthritis (Synovial thickening, edema, enhancement and fluid collection) |
| 7. | RBC breakdown | Gall stones |
| 8. | Nuclear medicine | Bone infarction vs. osteomyelitis <ul style="list-style-type: none"> Infarction: Tc-99m MDP bone scan shows ↑ activity; Tc-99m Sulfur colloid marrow scan shows ↓ activity Osteomyelitis: Bone scan shows ↑ activity; Sulfur colloid marrow scan shows normal activity |

**Fig. 4.142.2.9:** Anemic hand

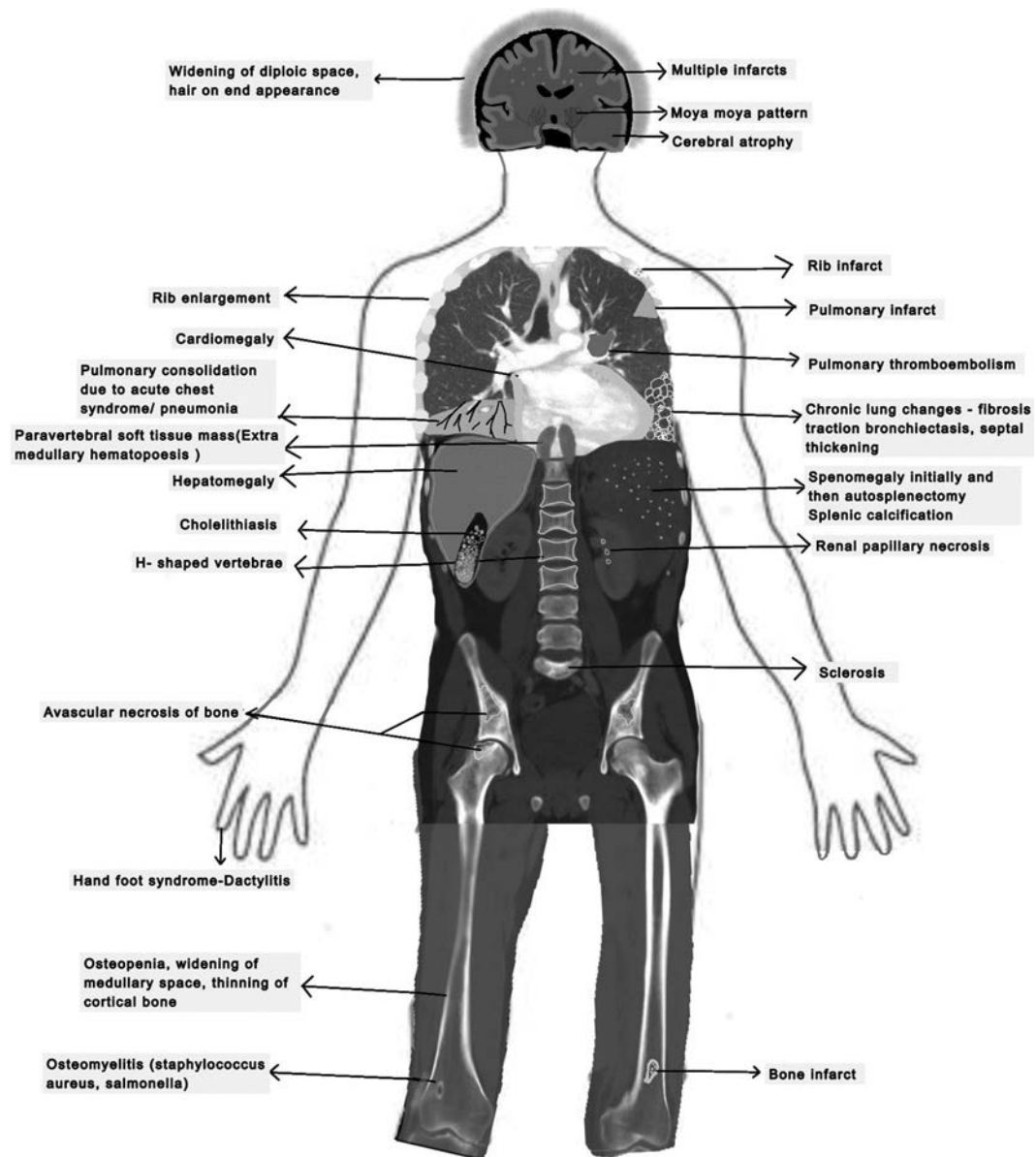


Fig. 4.142.2.10: Manifestations of sickle cell anemia

4.143 MUSCULOSKELETAL SYSTEM

Case No. 143

Clinical history: 42-year-old male patient with complaints of chronic hip pain.

Radiological techniques and observations: Figure 4.143.1 is radiograph of pelvis AP view showing multiple expansile lytic lesions with narrow zone of transition, involving the right iliac bone, right ischium, right pubis, sacrum, lower lumbar vertebra and visualised portions of right femur. The lesion is seen involving the long axis of the femur. No specific matrix, no periosteal reaction noted. Coarse trabeculae, cortical thinning and endosteal scalloping noted. Pathological fracture noted in the upper 1/3rd of femoral diaphysis. Multiple ill-defined soft tissue lesions noted in the right thigh, in muscular plane, with areas of tiny calcifications. Left

femur and pelvic bones appear normal. Figure 4.143.2 is chest radiograph PA view showing well-defined, round-shaped, homogeneous radiopaque mass lesion in upper and mid-zone of left lung. Superior, inferior and medial borders are well defined, lateral margin makes acute angle with the chest wall. Clear interface between the lesion and the adjacent lung parenchyma noted. No evidence of intralesional calcification/cavity/fat/air bronchogram/air fluid level. Remaining part of the left lung and right lung appears normal. No underlying rib erosions. Cardiac silhouette appears normal. Bilateral costophrenic and cardiophrenic angles are free. Visualised bones and soft tissue appear normal.

Figures 4.143.3 to 4.143.5 are non-enhanced CT pelvis, axial sections showing multiple expansile lytic lesions in the right ilium, right ischium, sacrum and visualised



Fig. 4.143.1



Fig. 4.143.2

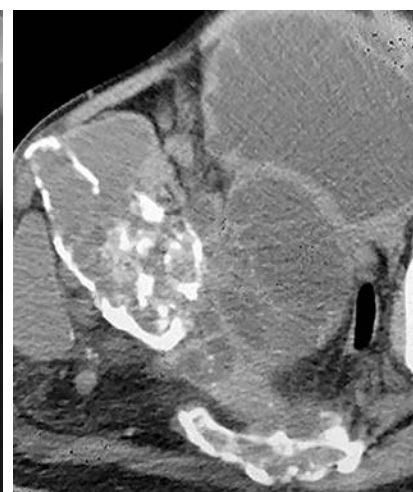


Fig. 4.143.3



Fig. 4.143.4



Fig. 4.143.5

Table 4.143.1 Differential diagnosis for lytic iliac bone lesion





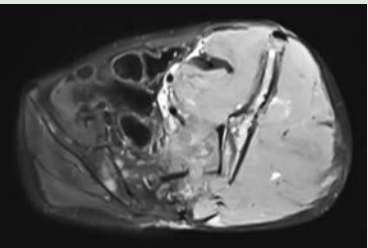
| | | |
|---|--|---|
| <p>Fibrous dysplasia (refer to case 147): Non neoplastic condition with defect in osteoblastic differentiation and maturation, with the replacement of normal bone with large fibrous stroma and islands of immature woven bone.</p> | <p>Lesion is usually smooth and homogenous with endosteal scalloping and cortical thinning. The cortex is usually intact. Other features include ground-glass matrix, well circumscribed lesions, no periosteal reaction and rind sign. The proximal right femur and right ilium shows diffusely abnormal irregular trabecular pattern with areas of increased and decreased osseous density and ground-glass opacity.</p> |  <p>Fig. 4.143.6: Fibrous dysplasia</p> |
| <p>Aneurysmal bone cyst: Benign expansile tumor-like bone lesions of uncertain etiology, composed of numerous blood-filled channels, and mostly diagnosed in children and adolescents.</p> | <p>Radiographs demonstrate sharply defined, expansile osteolytic lesions, with thin sclerotic margins. CT and MRI are able to demonstrate the characteristic fluid-fluid levels. Bone scan shows Doughnut sign- increased uptake peripherally with a photopenic center. Expansile lytic lesion involving the metaphysis of proximal right femur. Epiphysis appears relatively spared.</p> |  <p>Fig. 4.143.7: Aneurysmal bone cyst</p> |
| <p>Metastasis: Common primaries causing osteolytic metastases are renal, lung, breast, thyroid, GI tract, urothelial, ovarian, melanoma, chordoma and paraganglioma.</p> | <p>Bone scan: Tracer avidity in regions of bone production at margins of tumor, not directly by lytic tumor. FDG PET has better specificity but lower sensitivity for detecting malignant bone metastases when compared with bone scan.</p> |  <p>Fig. 4.143.8: Metastasis</p> |
| <p>Giant cell tumor (refer to case 140) They almost invariably occur when the growth plate has closed and are therefore typically seen in early adulthood. A mild female predilection. Seen in flat bones and pelvis is one of the commonest sites. 1. Occurs only with a closed growth plate. 2. Abuts articular surface: 84–99% come within 1 cm of the articular surface. 3. Well-defined with non-sclerotic margin (though <5% may show some sclerosis) 4. Eccentric, if large this may be difficult to assess.</p> | | |
| <p>Ewing's Sarcoma (refer to case 149)</p> |  <p>Fig. 4.143.9: Ewing's sarcoma</p> |  <p>Fig. 4.143.10: Ewing's sarcoma</p> |
| <p>Langerhans cell histiocytosis (refer to case 153).</p> | | |
| <p>Haemophilic pseudotumor (refer to case 139).</p> | | |
| <p>Others: Brown tumour, chondrosarcoma</p> | | |

Table 4.143.2: Difference between multiple lytic and expansile bone lesions

| <i>Multiple lytic bone lesions</i> | <i>Non-tumor conditions causing expansile lesion</i> |
|---|---|
| Fibrous dysplasia, enchondroma, eosinophilic granuloma, metastases, myeloma, hyperparathyroidism (brown tumor), infection | Hyperparathyroidism, hydatid disease, hemophilic pseudotumor, osteomyelitis |

portions of right femur with soft tissue within the bone marrow and endosteal destruction. Cortical break noted in the superomedial aspect of the right ilium. Multi loculated septated cystic lesions are seen in the pelvic cavity, right iliacus muscle and upper part of right thigh involving all the three muscular compartments of thigh. A few calcifications noted in the wall of the cystic lesion. Multilobulated cystic lesions noted in the right lateral abdominal wall and right paravertebral region.

Interpretation: A—42 years male, lesion involving right ilium, right ischium, sacrum and visualised portions of right femur; C—predominant cystic lesions with septations in the bones and soft tissues; B—multiloculated septated cystic lesions seen in the pelvic cavity, right iliacus muscle and upper part of right thigh involving all the three muscular compartments of thigh and homogeneous round lesion in left lung; D—the possibilities include: a) Lung primary with bone metastasis; b) Bone primary with lung metastasis; c) Both are same lesions (metastases, systemic diseases); d) Both are different lesions.

Principal diagnosis: Hydatid disease involving the right pelvic bone and right femur with adjacent soft tissue component and pulmonary hydatid cyst.

Further investigation: USG abdomen to look for hydatid cyst in the liver. Serological tests are done. Indirect hemagglutination test and enzyme-linked immunosorbent assay are the most widely used methods for detection of anti-Echinococcus antibodies (immunoglobulin G [IgG]). Histopathology is confirmatory. Sometimes, however, the diagnosis is established only after surgery.

Management: Patient to be referred to orthopaedic department for planning the management. Oral Albendazole is one of the most commonly used agents

in the treatment of hydatid disease. Treatment of osseous hydatidosis is closer to oncologic therapy than to the usual surgical treatment of visceral hydatid cysts using combined chemotherapy and reconstructive procedures. Because of the poor results with medical treatment, osseous hydatidosis must be treated by a radical operation with wide excision, adapted to each localization. In the main, the prognosis of osseous hydatidosis remains poor, especially with spinal and pelvic localizations, which are the most frequent ones. The prognosis and treatment of osseous hydatidosis belong in the same category as a locally malignant lesion.

Brief discussion: Hydatid disease is the infection of bone by the parasitic tapeworm. There are two main species of the Echinococcus, granulosus and alveolaris/multilocularis. *Echinococcus granulosus* is more common, the dog is the main host. A less common sylvatic form has wolf as the main host. *Echinococcus multilocularis* is less common, but more invasive and fox is the main host. Echinococcus is rare, accounting for less than 5% of cases of hydatidosis. Most common sites: Lungs, liver. In the bones spine and pelvis are commonest sites.

Classic appearance is multiple cysts (bundle of grapes appearance) with daughter cysts.

Uni or multiloculated intraosseous cysts which may expand the bone and extend into adjacent soft tissues are seen. MR T1WI: Fluid has variable signal intensity from low to bright; depends on protein content. MR C+: Enhancement of cyst periphery and septa.

Puncture Aspiration Injection Reaspiration (PAIR) procedure: Percutaneous treatment of the hydatid cyst emerged as an alternative to surgery with low morbidity and mortality rates. The PAIR technique involves puncture of the cyst wall, aspiration of cyst contents, instillation and re-aspiration of the scolicidal agent (hypertonic saline, 95% ethanol, povidone iodine).

4.144 MUSCULOSKELETAL SYSTEM

Case No. 144

Clinical history: A 12 years old boy, who came with complaints of left leg pain for 2 years.

Radiological technique and observation: Figures 4.144.1 and 4.144.2 are AP and lateral radiograph of left leg provided. It shows well-defined longitudinally oval lobulated bubbly cortical based lytic diaphyseal lesion with sclerotic margin of left tibia with endosteal scalloping and mild anterior bowing of tibia. There is narrow zone of transition, no medullary involvement, no evidence of definitive matrix, no periosteal reaction, no evidence of cortical break/pathological fracture, no soft tissue swelling. No evidence of nidus noted. Figures 4.144.3 to 4.144.6 are MRI leg with STIR, T1 coronal and T1, STIR axial images respectively showing intra-cortical lytic lesions appearing hypointense on T1 and intermediate to hyperintense on STIR with endosteal scalloping and mild anterior bowing of tibia noted. No evidence of surrounding edema. No evidence

of periosteal reaction. No medullary encroachment. Adjacent neurovascular bundles appear normal.

Interpretation: A: 12 years old child with tibial lesion; C Well-defined longitudinally oval lobulated bubbly cortical based lytic diaphyseal lesion with sclerotic margin of left tibia; B: Endosteal scalloping and anterior bowing of tibia; D: Osteofibrous dysplasia.

Principal diagnosis: Osteofibrous dysplasia (Ossifying fibroma of Kempson-Campanacci).

Management: Conservative management—Do not touch lesion/touch me not lesion. Biopsy is reserved for aggressive lesions. Surgery is reserved for aggressive large lesions.

Moth-eaten bone in an adult: Infective: Acute osteomyelitis; Neoplastic: Metastases, multiple myeloma, leukaemia, lymphoma of bone, long-bone sarcomas (Ewing's sarcoma, osteosarcoma, chondrosarcoma, fibrosarcoma and malignant fibrous histiocytoma), Langerhans' cell histiocytosis.



Fig. 4.144.1



Fig. 4.144.2

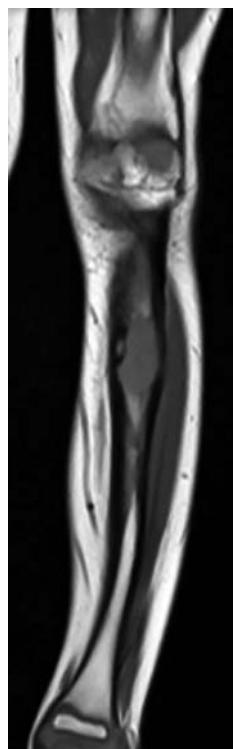


Fig. 4.144.3

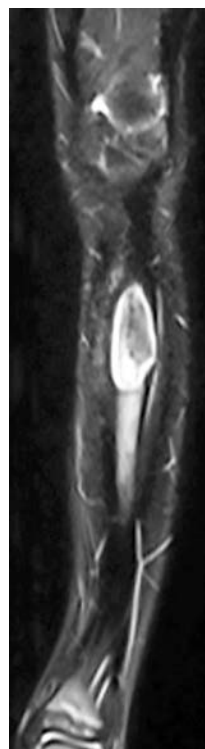


Fig. 4.144.4

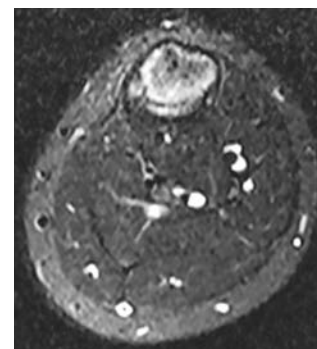


Fig. 4.144.5

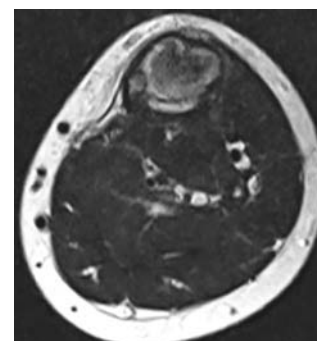






Fig. 4.144.6

Table 4.144.1: Differential diagnosis for osteofibrous dysplasia






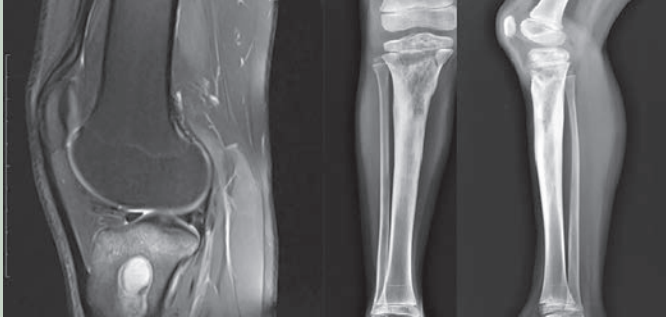


| Condition | Clinical and radiological features | Osteofibrous dysplasia (comparison) |
|--|---|--|
| Osteofibrous dysplasia/ossifying fibroma | 1st /2nd decade, males; 90% in tibia Diaphyseal, especially involving the middle to distal third of the shaft and typically involving the anterior cortex, intracortical osteolysis, with anterior bowing. | 12 years male All findings are consistent |
| Fibrous dysplasia | Age 20–30 years, M = F. Diaphyseal. Ground-glass lucency. Intramedullary location. 70% single lesion. | <20 years age Intracortical location |
| Non-ossifying fibroma (NOF) | <20 years, male, eccentric metaphyseal lesion, size more than 3 cm. If multiple (associated with NF1, fibrous dysplasia, Jaffe-Campanacci syndrome); Size less than 3 cm-Fibrous cortical defect (FCD) | Diaphyseal lesion |
| Adamantinoma, OFD-like adamantinoma | Multiple non-ossifying fibromas. Age 20–50 years, Males more common. 10–15 cm size. Characteristic location: Midanterior cortex of tibial diaphysis. Low grade malignant tumour with features similar of OFD but with aggressive medullary involvement cortical break. | No medullary involvement No cortical break |
| Ewing sarcoma | Age <20 years, males, centric, permeative type of destruction with excessive soft tissue swelling and periosteal reaction. Diaphyseal lesion. | Eccentric No soft tissue swelling No periosteal reaction |
| Neurofibromatosis | Pseudoarthrosis of tibia. Anterior bowing. | No other feature to say NF |
| Eosinophilic granuloma | <20 years age, more common in males, pain and soft tissue swelling, centric location, diaphyseal /metaphyseal location. | No soft tissue swelling Eccentric location |
| Chondromyxoid fibroma | Age 20–30 years. Metaphyseal, eccentric lucent, well-defined, slightly expansile lesion with endosteal sclerosis; it is oriented along the long axis of the host bone. | Diaphyseal lesion |

Table 4.144.2: Tibial lesions differential diagnosis

| | | | |
|---|---|--|---|
|  <p>Fig. 4.144.7: Fibrous dysplasia</p> |  <p>Fig. 4.144.8: NOF</p> |  <p>Fig. 4.144.9: FCD</p> |  <p>Fig. 4.144.10: Adamantinoma</p> |
|---|---|--|---|

(Contd.)

Table 4.144.2: Tibial lesions differential diagnosis (Contd.)

| | | | | |
|--|---|---|---|--|
|  |  |  |  |  |
| Fig. 4.144.11: Paget's disease | Fig. 4.144.12: Osteoid osteoma | Fig. 4.144.13: Enchondroma | Fig. 4.144.14: Ewing's sarcoma | Fig. 4.144.15: Pseudoarthrosis NF-1 |
|  | |  | |  |
| Fig. 4.144.16: Tibial osteomyelitis | | Fig. 4.144.17: Chronic recurrent multifocal osteomyelitis | | Fig. 4.144.18: Idiopathic intramedullary osteosclerosis |

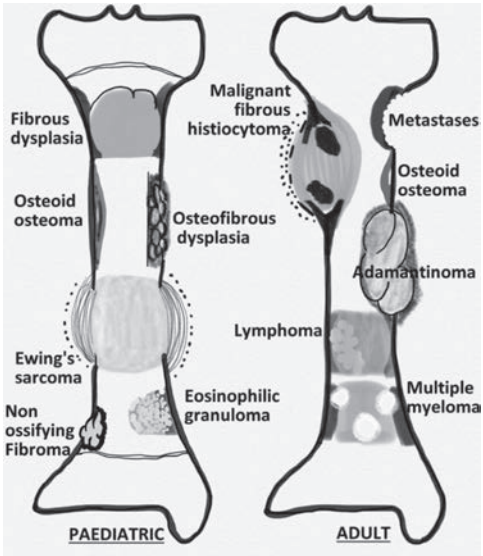


Fig. 4.144.19: Tibial diaphyseal lytic lesions

4.145 MUSCULOSKELETAL SYSTEM

Case No. 145

Clinical history: 20-years-old female who is a known case of chronic renal failure with complaints of pain in left forearm.

Radiological techniques and observation: Figures 4.145.1 and 4.145.2 are plain radiograph AP and lateral views of left forearm shows a well-defined, purely lytic medullary lesions in the diaphysis of distal third of left radius. Narrow transition zone with cortical expansion and thinning with no obvious periosteal reaction and marginal sclerosis. There is no obvious osseous or cartilagenous matrix noted. There is no cortical break or associated soft tissue noted.

The patient can be further evaluated by cross sectional imaging like CT to narrow down the diagnosis.

Figures 4.145.3 and 4.145.4 are CT forearm sagittal reformatted and axial sections in soft tissue window show attenuation values of the solid component in the range of blood and fibrous tissue. Figures 4.145.5 to 4.145.8 are bone scintigraphy was done to further evaluate the characteristic of the lesion. Tc 99m pertechnetate scan shows multiple hot skeletal lesions—super scan.

Increased bony uptake and no uptake seen in the kidney.

Interpretations: A: 20 years old female; C: well-defined, purely lytic medullary lesions in the diaphysis of distal third of left radius, showing narrow zone of transition with cortical expansion and thinning; B: multiple hot

Table 4.145.1: Differential diagnosis for Brown tumour

| |
|--|
| Aneurysmal bone cyst (ABC) (Refer to case 139) |
| Fibrous cortical defect (Refer to case 138) |
| Non-ossifying fibromas (NOF) (Refer to case 138) |
| Enchondromas (Refer to case 151) |

skeletal lesions on super scan; D: Brown tumor due to secondary hyperparathyroidism.

Principal diagnosis: Secondary hyperparathyroidism with brown tumor.

Management: Surgical management along with adjuvant treatment to maintain low parathormone levels. Patient referred to orthopaedic surgeon and endocrinologist.

Discussion: Hyperparathyroidism is the effect of excess parathyroid hormone in the body. It can be primary, secondary, or tertiary (Table 4.145.2).

Tertiary hyperparathyroidism: Autonomous parathyroid adenoma caused by the chronic overstimulation of hyperplastic glands in renal insufficiency.

Associations: Multiple endocrine neoplasia type I (MEN1), multiple endocrine neoplasia type IIA (MEN2a), familial hypocalciuric hypercalcemia, familial isolated primary hyperparathyroidism, hyperparathyroidism-jaw tumor syndrome.

Diagnostic workup for parathyroid disorders:

- **Blood investigations:** Increased calcium levels and parathormone suggests hyperparathyroidism.



Fig. 4.145.1



Fig. 4.145.2

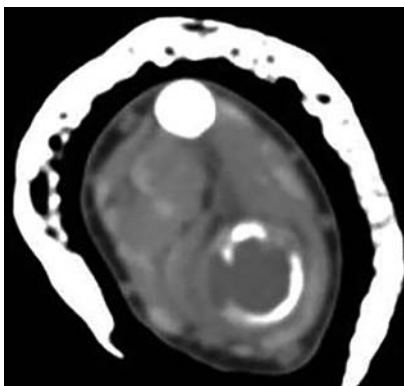


Fig. 4.145.3

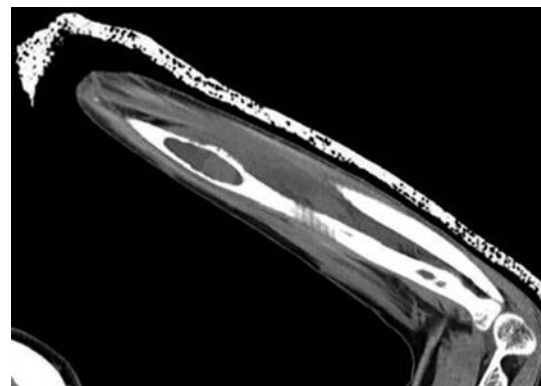


Fig. 4.145.4



Fig. 4.145.5



Fig. 4.145.6



Fig. 4.145.7

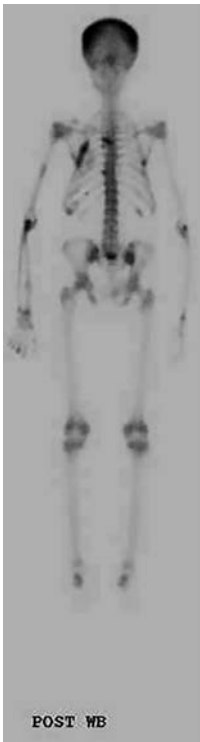


Fig. 4.145.8

| Table 4.145.2: Difference between primary and secondary hyperparathyroidism | |
|---|--|
| <p>Primary hyperparathyroidism Caused by parathyroid adenoma (~80%) Multiple parathyroid adenomas (4%) Parathyroid hyperplasia (10–15%) Parathyroid carcinoma (1–5%)</p> | <p>Secondary hyperparathyroidism Caused by chronic hypocalcaemia with renal osteodystrophy being the most common cause (others include malnutrition, vitamin D deficiency) which results in parathyroid hyperplasia.</p> |
| <p>Skeletal manifestations <i>Subperiosteal bone resorption:</i> Classically affects the radial aspects of the proximal and middle phalanges of the 2nd and 3rd fingers, Medial aspect of tibia, femur, humerus, lamina dura: floating teeth (not specific). <i>Subchondral resorption:</i> Lateral end of the clavicles, symphysis pubis, sacroiliac joints <i>Subligamentous resorption:</i> Ischial tuberosity, trochanters, inferior surface of calcaneus and clavicle. <i>Intracortical resorption:</i> Cigar/oval-shaped or tunnel-shaped radiolucency in the cortex. Physeal resorption, endosteal resorption, terminal tuft erosion (acro-osteolysis), Rugger jersey spine, salt and pepper sign in the skull (pepper pot skull), chondrocalcinosis, Browns tumor (solitary or multiple expansile lytic lesions without any soft tissue mass/cortical destruction in mandible, clavicle, ribs and pelvis).</p> | <p><i>Findings in secondary (and tertiary) hyperparathyroidism</i> are often associated with the osteosclerosis of renal osteodystrophy and the osteomalacia of vitamin D deficiency. Features include subperiosteal bone resorption (symmetrical and bilateral), osteopenia, osteosclerosis, soft tissue calcification, chondrocalcinosis, renal stones and nephrocalcinosis, Rugger-Jersey spine, Superscan: generalized increased uptake on Tc-99m pertechnetate bone scan (focal uptake with adenoma); superior and inferior rib notching.</p> |

- **USG neck:** Most commonly used initial imaging modality. Homogeneous well-defined hypoechoic solid mass typically adjacent to thyroid gland, medial to common carotid artery. Doppler shows a characteristic extrathyroidal feeding vessel (typically a branch of inferior thyroid artery) entering the

parathyroid gland at one of the poles (polar vessel sign) and it tends to branch around the periphery of the gland before penetration. Internal vascularity commonly seen in peripheral location (characteristic arc or rim of vascularity).

Table 4.145.3: Spectrum of hyperparathyroidism imaging features

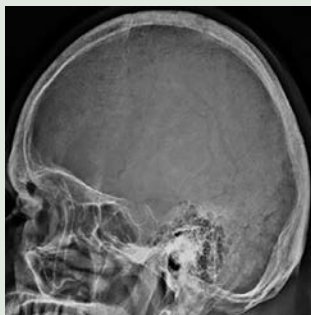




| | | |
|--|--|---|
|  |  |  |
| Fig. 4.145.9: Salt and pepper skull | Fig. 4.145.10: Rugger jersey spine | Fig. 4.145.11: Lateral end of clavicle resorption |
|  |  | |
| Fig. 4.145.12: Subperiosteal resorption with brown tumor | Fig. 4.145.13: Brown tumor | |

Table 4.145.4: Conditions causing superscan

| Diffuse metastatic diseases | Metabolic bone diseases | Miscellaneous |
|---|---|--|
| Prostatic carcinoma Breast cancer Transitional cell carcinoma Multiple myeloma Lymphoma | Renal osteodystrophy Hyperparathyroidism (often secondary hyperparathyroidism) Osteomalacia | Myelofibrosis/myelosclerosis Mastocytosis Widespread Paget's disease |

Table 4.145.5: Summary of imaging features in endocrine bone disorders

| Condition | Radiological features |
|--|---|
| Hypoparathyroidism (HP) due to reduced secretion of parathyroid hormone, results in hypocalcemia. There are a number of causes of hypoparathyroidism: Idiopathic, iatrogenic (post-parathyroidectomy or thyroidectomy) congenital absence of the parathyroid glands (DiGeorge syndrome), familial (autoimmune polyendocrine syndrome type 1) | Osteosclerosis is a prominent feature, anterior longitudinal ligament and paraspinal ligaments osteophyte formation, enthesopathy, especially around pelvis. Common features are dense metaphyseal bands, subcutaneous calcification, basal ganglia calcification HP>PPHP, growth arrest lines, thickened skull and abnormal dentition. |
| Pseudohypoparathyroidism (PHP): End-organ resistance to parathyroid hormone. Markers: Parathyroid hormone level: High, serum phosphate level: High, serum calcium level: low. Pseudopseudohypoparathyroidism (PPHP) has clinical and radiological characteristics that are similar to pseudohypoparathyroidism, but there are no changes in parathyroid hormone levels or calcium metabolism. PPHV is familial. Albright's hereditary osteodystrophy is a phenotype of PHP | Brachydactyly, short stature and premature physeal fusion, disproportionate short stature, metacarpal shortening, 1st, 4th, and 5th most common, metatarsal shortening, 3rd and 4th most common, short distal phalanges ± short middle phalanges, coned epiphyses of phalanges and metacarpals, metacarpals/metatarsals widening, short and broad-based, metaphyseal or more central, perpendicular to long axis of bone-exostosis, Bowing deformity, osteosclerosis/osteoporosis, can have associated hyperparathyroidism with radial aspect middle phalanges showing subperiosteal resorption. small round foci of soft tissue calcification around the joints and plaque like skin and subcutaneous tissues. |

(Contd.)

Table 4.145.5: Summary of imaging features in endocrine bone disorders (Contd.)

| Condition | Radiological features |
|---|---|
| Hypopituitarism: Reduced secretion of one or more of the pituitary gland's eight hormones. The secretion of one specific pituitary hormone was reduced by selective hypopituitarism. Most or all pituitary hormones were low secretion when panhypopituitarism was present. | Delayed skeletal maturation: Late appearance of epiphyses, late fusion of physes, slow rate of growth, osteopenia (childhood and adult disease). MRI: Small size adenohypophysis, partial or complete absence of visualization of the hypophyseal stalk, ectopic neurohypophysis. |
| Hyperpituitarism: Acromegaly: Onset of disease after physal closure, Gigantism: Onset of disease prior to physal closure. A pituitary adenoma is responsible for around 95% of cases. Other tumors of the pancreas, lungs, or adrenal glands that secrete growth hormone account for the remaining 5% of cases. Excessive usage of exogenous growth hormone in athletes can also cause this condition. | Enlargement of cartilage spaces: Joint space widening: Interphalangeal, metacarpophalangeal, metatarsophalangeal, knee. Widened intervertebral disc spaces, Prominent costochondral articulations. Bone formation: Periosteal surfaces, tendon and ligament attachments (enthesopathy), articular margins (osteophytes), capsular calcification/ossification. Cranial thickening, enlarged protuberances, hypertrophy of paranasal sinuses, Ossification of anterior vertebral body and disc space, Osteophytosis of hips, knee, spine, thickened diaphyses of long bones, Squaring metacarpal heads, phalangeal widening, outgrowths at base, Spade-like terminal tufts. Soft tissue enlargement: Especially hands and feet, thickened heel pad (>25 mm) is classic finding. Posterior vertebral scalloping: Common finding. |
| Hypothyroidism: Cretinism: Neonatal hypothyroidism; congenital hypothyroidism. Congenital hypothyroidism: Maternal iodine deficiency most common, major public health concern in underdeveloped countries. Juvenile, adolescent, adult onset hypothyroidism: Autoimmune (Hashimoto) thyroiditis most common; other causes include pituitary disorders, subacute (viral) thyroiditis, idiopathic. | Congenital hypothyroidism: Delayed skeletal maturation, Absent or small epiphyses; stippled epiphyses, Short thick bones, delayed closure of fontanelles. Juvenile and adolescent onset disease: Bone age delay of 1–2 years, slipped capital femoral epiphysis: Enlarged sella turcica. Labelled iodine scans a thyroid states: No uptake, Inborn errors of thyroid metabolism: Normal, Hashimoto thyroiditis: Increased uptake early → irregular patchy uptake midcourse → diminished uptake; ± hot or cold nodules in late disease. |
| Hyperthyroidism: Hyperthyroid states: Graves' disease, toxic nodular goitre. Perinatal form: Lethal type micromelia; markedly diminished bone density: skeleton may appear completely unmineralized. Perinatal form: Benign type. Skeletal changes show spontaneous resolution. Infantile form: Severe rachitic-like changes. Childhood form: Short stature, rickets-like changes, falsely widened—appearing sutures, and functional craniosynostosis. Adult form: Osteopenia, osteomalacia-like changes, Pseudofracture in lateral cortex proximal femur. Odontohypophosphatasia: Affects teeth only. Prenatal ultrasound: 3rd trimester excellent brain detail: ↓mineralization of skull allows ↑ through transmission, micromelia. Periosteal new bone formation: Spiculated, lacy appearance. Metacarpals, metatarsals most common. Radial aspect of metacarpals 1st through 4th. Ulnar aspect of 5th metacarpal. Middle and distal phalanges less common. Favours upper extremity with asymmetric distribution. | |
| Hypercortisolism: Cushing syndrome: Hypercortisolism from exogenous or endogenous causes ACTH independent: 1° adrenal disease, usually adenoma. Ectopic ACTH syndrome: Paraneoplastic syndrome, common cause is lung cancer; male >female. Cushing disease: ACTH dependent, usually from pituitary: Microadenoma; male < female. | Radiographs: Cloud-like densities. Periarticular: Within bursa, along extensor tendons; hips, shoulders, elbows, feet. Marrow deposits: Uncommon, ±periostitis. Other sites: Skin, retina, pulp stones in teeth. CT active phase: Multiple small cystic areas with peripheral mineralization, sedimentation phenomenon (fluid-calcium levels). CT inactive phase: Solid lobules of calcification. Bone scan: Uptake at sites of calcium deposition. MRT1WI: Heterogeneous hypointense/low SI. MR fluid-sensitive sequence: Active phase: Cystic areas bright; bright periphery 2° to foreign body reaction, edema in adjacent tissues, sedimentation with low signal. Inactive phase: Low signal foci with a little edema. |

- **CT:** Mainly to detect suspected ectopic glands. NECT helps distinguish hypodense parathyroid tissue from normally radiodense thyroid. 4D parathyroid CT—to precisely localise adenomas preoperatively. CECT—intense arterial enhancement and washout of contrast on delayed phase.
- **MRI:** Infrequently utilized.
- **Nuclear scan:** Tc-99m Sestamibi scan: Tracer is taken up by thyroid and parathyroids with rapid washout from thyroid and retention in parathyroids. Focal increased uptake on early and delayed images can be seen. Subtraction techniques: Tc-99m Sestamibi/

Tc-99m pertechnetate: Sestamibi taken up by both thyroid and parathyroid glands. Pertechnetate taken up only by thyroid gland. Subtraction studies remove thyroid uptake, and left with parathyroid uptake.

Super scan: It is an intense symmetric activity in the bones with diminished renal and soft tissue activity on a Tc 99m diphosphonate bone scan. A metastatic superscan tends to have uptake throughout the axial skeleton and proximal appendicular skeleton, often somewhat

heterogeneous. In contrast, a metabolic superscan tends to be more uniform and involve both the axial and more peripheral skeleton, including the distal extremities, calvarium, and mandible. The various causes are listed in Table 4.145.4.

For features of various arthritis and their distribution in X-ray hand, refer to case 4.157.

For features of various fractures in X-ray hand, refer to case 4.162.

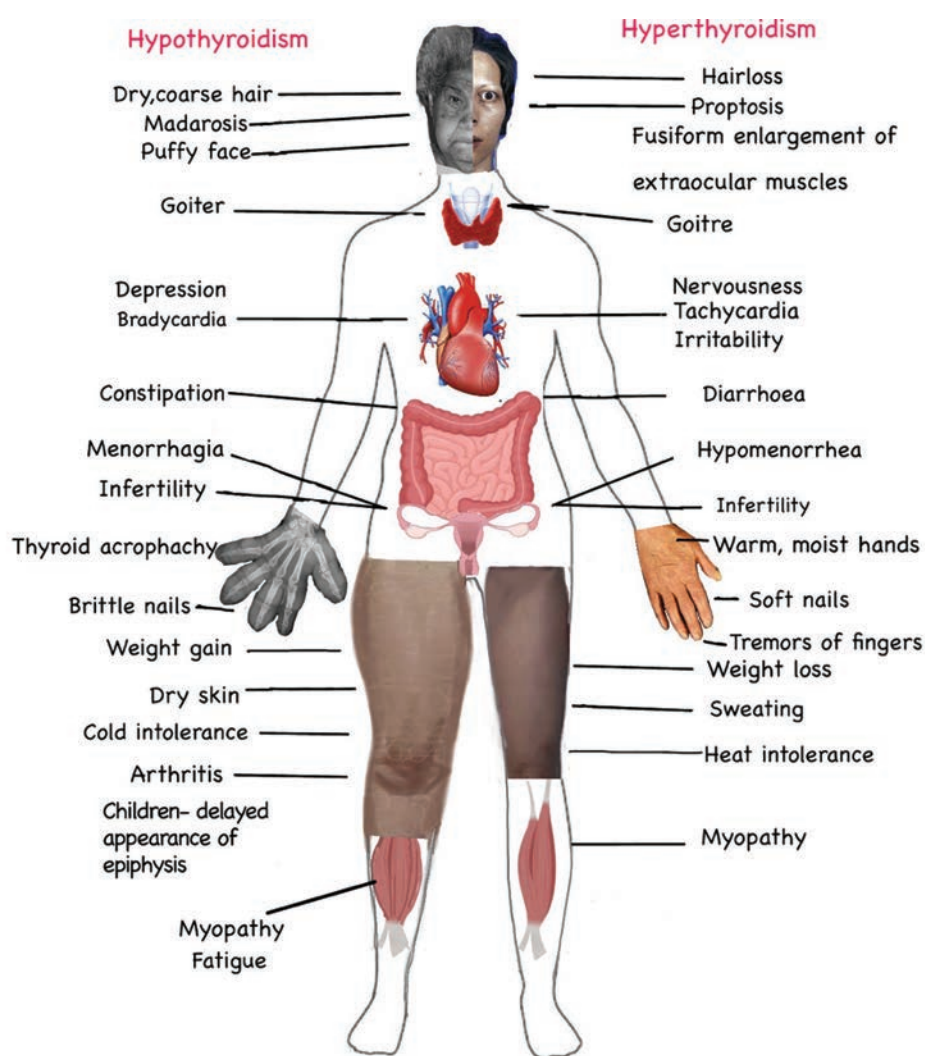


Fig. 4.145.14: Hypothyroidism and hyperthyroidism

X-ray Palmistry



Fig. 4.145.15: Features of hyperparathyroidism in X-ray hand



Fig. 4.145.16: Lytic lesions in X-ray hand



Causes of acral osteolysis : Other associated findings

1. Hyperparathyroidism-subperiosteal bone resorption involving the radial aspect of proximal and middle phalanges, soft tissue calcification, vascular calcification, cortical tunnelling, brown tumour
2. Scleroderma: soft tissue and periarticular calcification
3. Trauma, Frost bite, burns, Raynaud's phenomenon, Neurotrophic diseases such as leprosy
4. Sarcoidosis-Lace / honeycomb like lytic lesions
5. Psoriatic arthritis- pencil in cup deformity, sausage digits
6. Pyknodysostosis- dense bone

Fig. 4.145.17: Acral osteolysis in hand



Fig. 4.145.18: Systemic manifestations in X-ray hand



Fig. 4.145.19: Tumors in X-ray hand

4.146 MUSCULOSKELETAL SYSTEM

Case No. 146

Clinical history: 12-years-old male child, a k/c/o chronic kidney disease presents with complaints of pain over both hands and bilateral hip joint.

Radiological techniques and observation: Figures 4.146.1 is frontal radiograph of both hands of a 12 years old male child showing diffuse sclerosis of the visualized bones. No evidence of soft tissue swelling or calcification. No

evidence of lysis of the visualized bones. Figure 4.146.2 is frontal radiograph of pelvis showing diffuse sclerosis, mild widening of the physis with slipped right femoral capital epiphysis. No evidence of any lytic lesion noted in the pelvis.

Figure 4.146.3 is plain CT pelvis in bone window showing diffuse sclerosis with multiple lytic lesions consistent with brown tumor in the right iliac bone and ischium. No evidence of any soft tissue swelling noted.



Fig. 4.146.1



Fig. 4.146.2

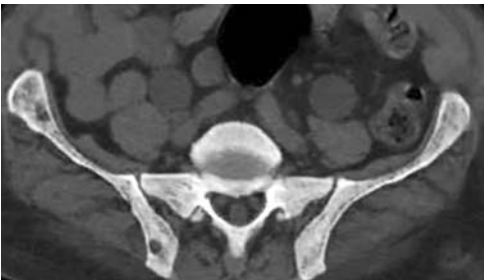


Fig. 4.146.3



Fig. 4.146.4

| Table 4.146.1: Differential diagnosis for diffuse sclerosis of bones | |
|--|---|
| Pediatrics | Adults |
| Myelosclerosis | Neoplastic: Osteoblastic metastasis (prostate and breast), lymphoma |
| Renal osteodystrophy | Paget’s disease |
| Pyknodystosis | Fluorosis |
| Osteopetrosis | Leukemia |

| Table 4.146.2: Difference between osteopetrosis and pyknodystosis | | |
|---|---|---|
| Features | Osteopetrosis | Pyknodystosis |
| | Albers-Schönberg disease/ Marble bone disease | Maroteaux-Lamy-Lysosomal storage disorder. |
| Hereditary | Infantile autosomal recessive and adult autosomal dominant type | Autosomal recessive type |
| Age group | Infancy (malignant form) to adulthood (benign form) | |
| Clinical features | Growth retardation +; failure to thrive, growth retardation, poor vision, multiple fractures, multiple cranial nerve palsies. | Short stature with dwarfism; delayed bone age. |
| Skull and face | Diffuse sclerosis of cranial vault with loss of diploic space. Hyperostosis of skull base Normal angled mandible with crowding of teeth. | Thick skull base with thin cranial vault, Wormian bones +, delayed closure of calvarial sutures—persistent posterior fontanelle. Hypoplastic facial bones with incomplete pneumatization of paranasal sinuses, obtuse angled mandible and micrognathia with mal-aligned tooth. |
| Extremities | Loss of corticomedullary differentiation (causing pancytopenia) with dense sclerotic bones giving a bone within bone appearance—spine, ilium (as growth occurs, cortical bone is not resorbed and remains visible within the larger bone). Erlenmeyer flask type deformity of the tubular bones. Alternating radiolucent metaphyseal bands. | Osteosclerosis with narrowed medullary cavity. Long bone fractures common. Acral osteolysis/ resorption/ band like lucency in terminal tuft (asymmetric and progressive). Phalangeal hypoplasia noted. Malformed radioulnar articulation and short hand. Hypoplastic/malformed clavicles (lateral end) |

(Contd.)







| Table 4.146.2: Difference between osteopetrosis and pyknodystosis (Contd.) | | |
|--|---|---|
| Features | Osteopetrosis | Pyknodystosis |
| Spine | Stenosis of neural and vascular foramen. Sandwich spine (thick end plate sclerosis). | |
| Abdomen | Severe hepatosplenomegaly due to extramedullary hematopoiesis | No hepatosplenomegaly |
| MRI | Bone appears T2 hypointense: Black bone disease; complete absence of marrow replaced by dense bones. Optic nerve atrophy noted. | Can see fracture lines as T2 hyperintensities |
| Treatment | Bone marrow transplant for cure and symptomatic treatment | Symptomatic management |
| |  |  |
| | Fig. 4.146.5: Osteopetrosis | Fig. 4.146.7: Pyknodystosis |
| |  |  |
| | Fig. 4.146.6a: Osteopetrosis | Fig. 4.146.8: Pyknodystosis |
| |  |  |
| | Fig. 4.146.6b: Osteopetrosis | Fig. 4.146.9: Pyknodystosis |

Figure 4.146.4 is X-ray spine showing diffuse sclerosis of superior and inferior end plates→Rugger jersey spine (thin end plate sclerosis).
Interpretation: A—12-year-old child with k/c/o of chronic kidney disease; C—diffuse sclerosis of the bones

of both hands and pelvis with brown tumor in the right iliac bone and ischium; B—widened physis and right slipped capital femoral epiphysis and rugger jersey spine; D—renal osteodystrophy.
Principal diagnosis: Renal osteodystrophy.

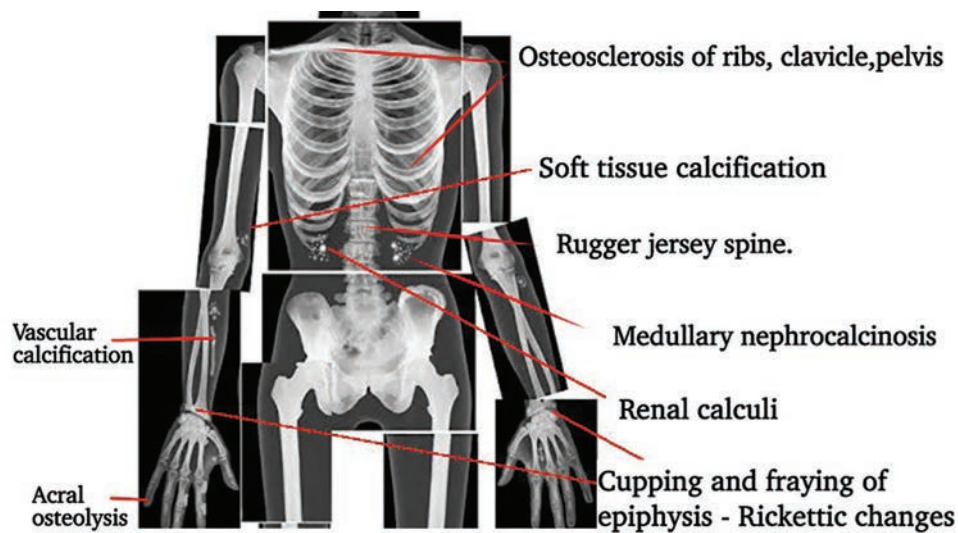




Fig. 4.146.10: Features of renal osteodystrophy

| Table 4.146.3: Difference between sandwich vertebra and rugger jersey spine | |
|--|--|
| <i>Sandwich vertebra</i> | <i>Rugger Jersey spine</i> |
| Diffuse end plate sclerosis with lucent centre of the vertebral body (thickness of sclerosis is more compared to the lucency). | The prominent endplate densities at multiple contiguous vertebral levels to produce an alternating sclerotic-lucent-sclerotic appearance |
|  |  |
| <p>Fig. 4.146.11: Sandwich vertebra</p> <p>Occurs in osteopetrosis</p> | <p>Fig. 4.146.12: Rugger jersey spine</p> <p>Occurs in hyperparathyroidism</p> |

| Table 4.146.4: Absorptiometry for bone marrow density | |
|---|--|
| Single-photon absorptiometry: Measures primarily cortical bone of appendicular bones, single-energy ¹²⁵ I radioisotope source. Site: Distal radius (wrist bone density), Os Calcis, Dose: 2.3 mrem | Dual-photon absorptiometry: Radioactive energy source with two photon peaks; should be reserved for patients <65 years of age because of interference from osteophytosis + vascular calcifications. Site: Vertebrae, femoral neck, Dose: 5–10 mrem |
| Single X-ray absorptiometry: Area projectional technique for quantitative bone density measurement. Site: Distal radius, calcaneus, Dose: low | Dual energy X-ray absorptiometry (DEXA): Most widely used and most precise technique. Quantitative digital radiography beams with two distinct energy levels allow identification of trabecular from cortical bone. Has replaced dual-photon absorptiometry and is produced by X-ray tube with higher radiation flux than radioisotope source. Site: Lumbar spine, femoral neck, whole body, forearm, Dose: < 3 rem. |

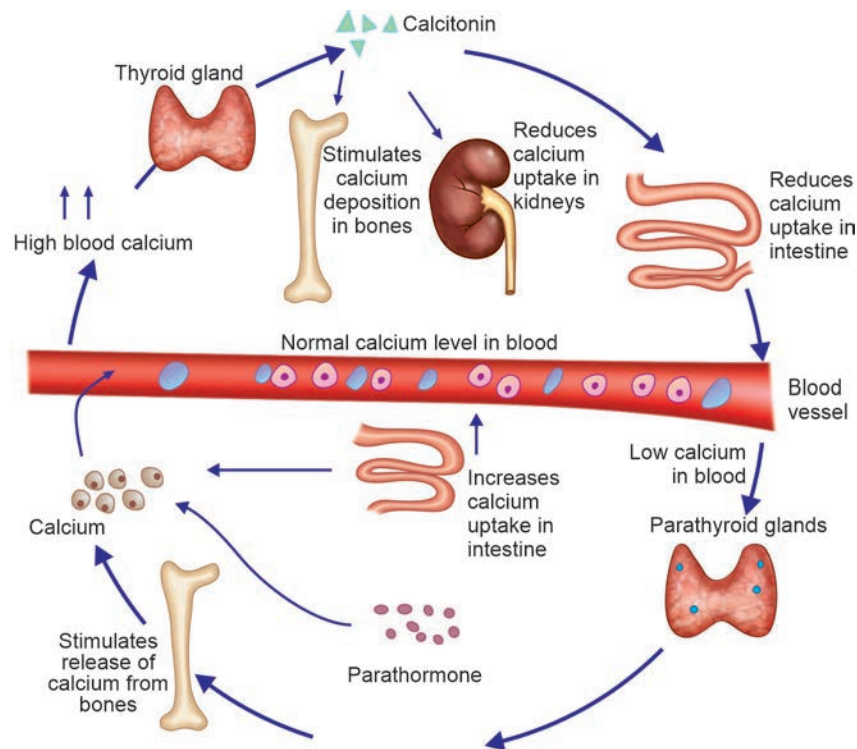


Fig. 4.146.13: Normal calcium cycle

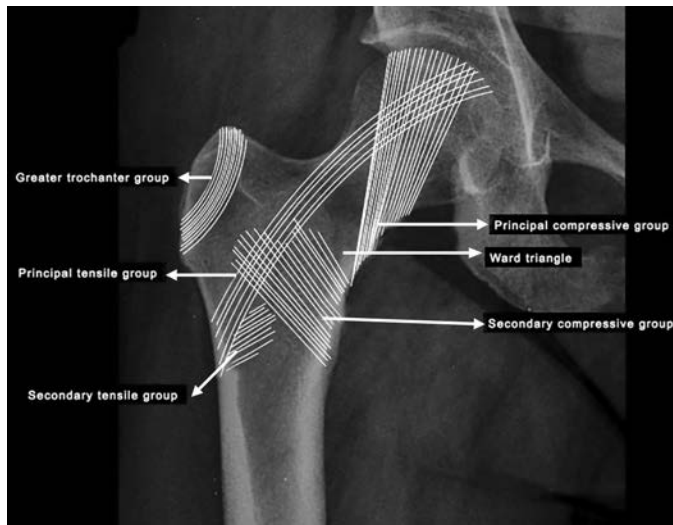


Fig. 4.146.14: Normal trabecular pattern in neck of femur and normal wards triangle

Brief discussion: Causes of renal osteo dystrophy—in children—end stage renal disease due to loss of renal parenchyma from structural abnormalities and in adults due to chronic glomerulonephritis and pyelonephritis.

This leads to impaired ability to form 1-25-dihydroxy vitamin D₃→low vit D (renal rickets) and excess phosphate →excess parathyroid→secondary hyperparathyroidism.



Fig. 4.146.15: Osteomalacia

Radiological features: → stimulates osteomalacia in adults, rickets in children, secondary hyperparathyroidism (refer to case 4.145) and osteosclerosis.

Metabolic Bone Disorders

Osteoporosis: It is a metabolic skeletal disease defined as a reduction of bone mineral density below a defined lower limit of normal.

Plain radiography: Increased radiolucency (at least 30 to 50% bone loss must be present), cortical thinning—pencil thinning (endosteal and intracortical resorption), altered trabecular pattern, fracture deformity with delayed healing and poor callus formation. (DDx: abundant

callus formation in osteogenesis imperfecta and Cushing syndrome).

Vertebral body: Trabecular changes—preferential resorption of horizontal trabeculae—pseudo-hemangiomatous appearance, washed out appearance, cortical thinning. Vertebra plana—pan cake or silver dollar, wedge—anterior body height 80% or < postvertebral body height, fish vertebra—biconcave, increased thoracic kyphosis, Schmorl’s nodes.

Pelvis and femora: Trabecular changes—increased radiolucency of wards triangle. Principle tensile

group first to be resorbed. Fracture following trivial trauma—most common sites proximal femur and pubic rami—intracapsular fracture femur neck—can precipitate avascular necrosis, Insufficiency fracture, Sacral fractures: 3 patterns seen on isotope bone scan H pattern- (butterfly/Honda sign)—bilateral vertical fractures through sacral ala connected by a transverse fracture through S2, S3 or S4, I pattern: Most common (70%)- single vertical fracture passing through the sacral ala, Arc pattern—linear/curvilinear transverse fracture passing horizontally across the sacrum.

Table 4.146.5: DEXA interpretation

| Diagnosis | T-score | Management | Follow-up |
|--------------|----------------|------------------------|-----------|
| Normal | >1 | Prevention | 3 years |
| Osteopenia | <-1 and > -2.5 | Prevention and therapy | 2 years |
| Osteoporosis | <-2.5 | Therapy | 1 year |

Table 4.146.6: Difference between scurvy and rickets

| Scurvy | Rickets |
|--|---|
| The radiological features are generalized osteopenia, cortical thinning: “Pencil-point” cortex, Periosteal reaction due to sub-periosteal hemorrhage, Scorbutic rosary: expansion of the costochondral junctions, may relate to the fracturing of the zone of provisional calcification during normal respiration, Similar to the rachitic rosary appearance is seen in rickets. Hemarthrosis may be seen. | Defective mineralization of growth plates affecting pediatric population. Presents with bone pain. X-ray: Physis—splaying—widening in long and short axis of metaphyseal ends. Cupping and fraying of metaphysis. Rachitic rosary—accumulation of osteoid at costochondral junction. Delayed ossification and skeletal maturation. |
| Wimberger’s ring sign: Circular, opaque radiologic shadow surrounding epiphyseal centers of ossification, which may result from bleeding, Frankel’s line: dense zone of provisional calcification, Trümmerfeld zone: Lucent metaphyseal band underlying Frankel’s line, Pelken spur: metaphyseal spurs which result in cupping of the metaphysis. | Deformities secondary to bone softening: 1. Craniotabes—flattening of posterior skull bones; 2. basilar invagination; 3. tri-radiate pelvis and acetabulo protrusion; 4. shepherd crook deformity (laterally bowed proximal femur); 5. sabre shin tibia. Bone scan—super scan with intense diffuse skeletal uptake. X-linked hypophosphatemic (vit D resistant) rickets: Normal serum calcium with often normal vitamin D levels. Early onset—in 1st few months of life. Adult—enthesopathy of pelvis, proximal femur. |

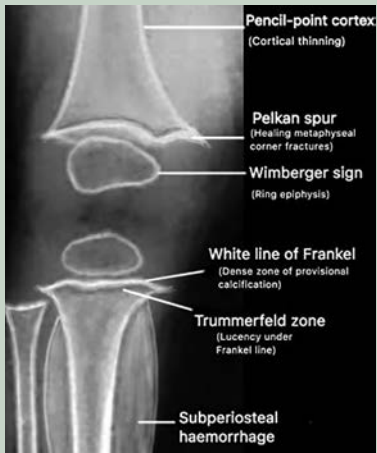


Fig. 4.146.16: Scurvy



Fig. 4.146.17: Rickets

Complications: Fractures at sites rich in labile trabecular bone (e.g. vertebrae, wrist) in postmenopausal osteoporosis, fractures at sites containing cortical + trabecular bone (e.g. hip) in senile osteoporosis.

Management: Vertebroplasty—percutaneous Injection of methyl meth acrylate (MMA)—needle is passed through the pedicles. Kyphoplasty—balloon used initially to decompress the fracture and correct some of the deformity, then the cement is injected.

Radiographs are insensitive prior to bone loss of 25–30%.

DEXA Data obtained: BMD (bone marrow density) value (g/cm^2), %BMD compared to young adults, %BMD compared to age-matched adults, T-score (SD of young-adult mean), Z-score (SD of age-matched mean). Quantitative computed tomography determines true volumetric density (mg/cm^3). High-turnover cancellous bone is important for vertebral strength and has high responsiveness. Low-turnover compact bone can be

measured separately, can be compared to external bone mineral reference. Phantom scanned simultaneously with patient to calibrate CT attenuation measurements, 10 mm thick section with gantry angle correction through center of vertebral body. Site—vertebrae (L1–L3), use: Assessment of vertebral fracture risk; measurement of age-related bone loss; follow-up of osteoporosis + metabolic bone disease.

Most sensitive technique—peripheral quantitative CT: Exact 3-dimensional localization of target volumes with multisection data acquisition capability covering a large volume of bone. Site—axial skeleton (lower dorsal + lumbar spine), proximal humerus, neck of femur, wrist, ribs.

Osteomalacia: Osteopenia with coarsened indistinct trabecular pattern, loss of cortical definition—thinned/ altered cortex, indistinct and blurred endosteal surface. Intra-cortical tunneling, looser's zone—high radionuclide uptake. Radiolucent transverse bands, triradiate pelvis.

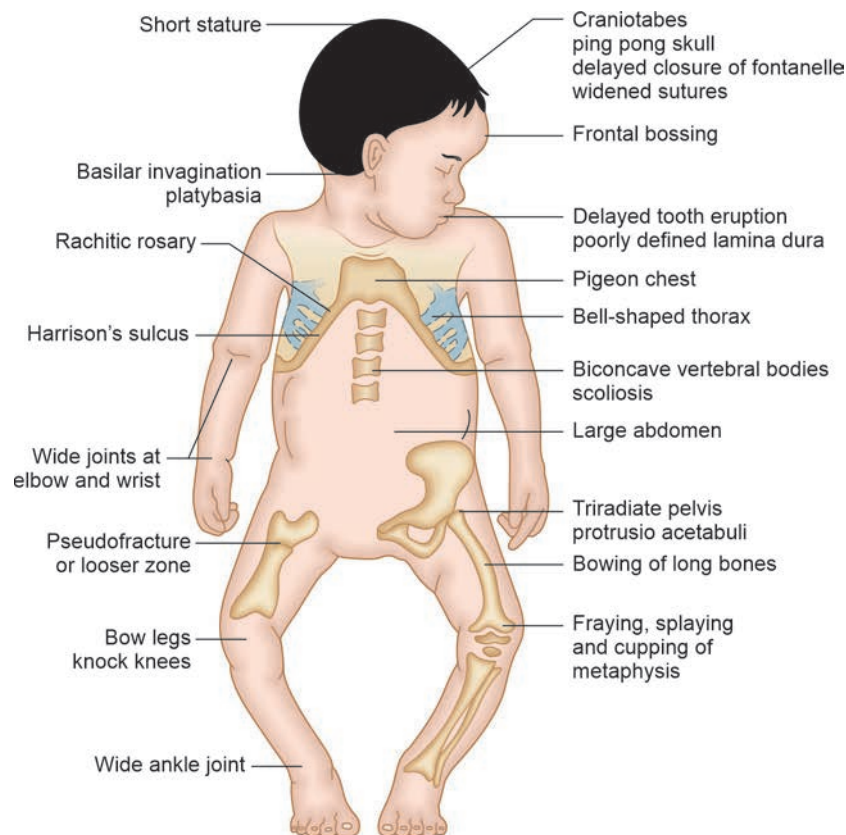


Fig. 4.146.18: Rickets manifestation

4.147 MUSCULOSKELETAL SYSTEM

Case No. 147

Clinical history: A 35-year-old asymptomatic female patient.

Radiological technique and observation: Figure 4.147.1 is plain radiograph of pelvis with both hip joint–AP view image showing lucent, sharply circumscribed lesions with sclerotic margin noted in the intertrochanteric region of right femur and left iliac bone just above the acetabulum with endosteal scalloping. No evidence of bone expansion/periosteal reaction/associated soft tissue components contiguous with the lesion/cortical break.

Figures 4.147.2 to 4.147.4 are CT pelvis—sagittal coronal, axial views in bone window image showing two, round, lucent, sharply circumscribed lesions with sclerotic borders noted in the intertrochanteric region of right femur and left iliac bone just above the acetabulum. The matrix of the lucency is smooth and relatively homogeneous appearance. No evidence cortical break/soft tissue components contiguous with the lesion.

Figures 4.147.5 and 4.147.6 are MRI pelvis—T2 coronal and axial images showing single well-defined T2 very bright lesion in intramuscular plane of right obturator externus muscle.

Interpretation: A: 35 years old female, lesion in intertrochanteric region of right femur and left iliac bone; B: Lesion with sharply demarcated sclerotic borders and ground-glass matrix; C: Intramuscular myxomas in right obturator externus muscle; D: Polyostotic fibrous dysplasia with Mazabraud syndrome.

Principal diagnosis: Polyostotic fibrous dysplasia with Mazabraud syndrome.

Liposclerosing myxofibrous tumor: Benign fibroosseous lesion, typified by propensity to occur in intertrochanteric region of femur (90%). Radiologically, it is seen as a mildly expansile, multilocular, geographic lucent lesion with sclerotic margin. Matrix calcification is seen in around 70% cases. Fat density is uncommon. Main differential is fibrous dysplasia which rarely has sclerotic rim.

Brief discussion: Fibrous dysplasia (FD)—usually described as long bone long lesion with intramedullary location. It is a non-neoplastic tumor-like congenital process, manifested as a localized defect in osteoblastic differentiation and maturation, with the replacement of normal bone with large fibrous stroma and islands of immature woven bone. Fibrous dysplasia has a varied radiographic appearance. If asymptomatic, it does not require treatment. It can affect any bone and



Fig. 4.147.1

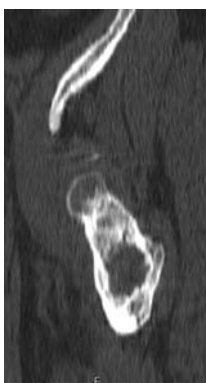


Fig. 4.147.2

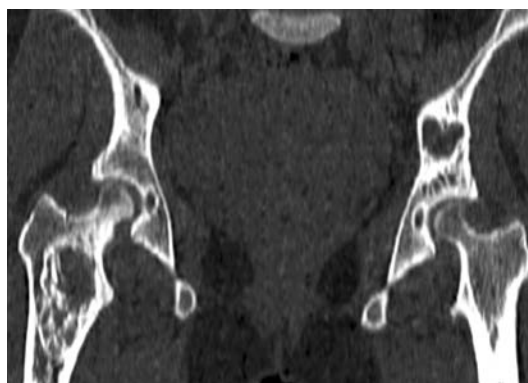


Fig. 4.147.3

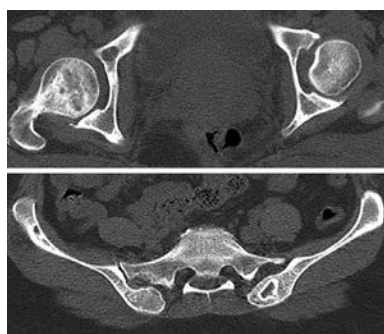


Fig. 4.147.4

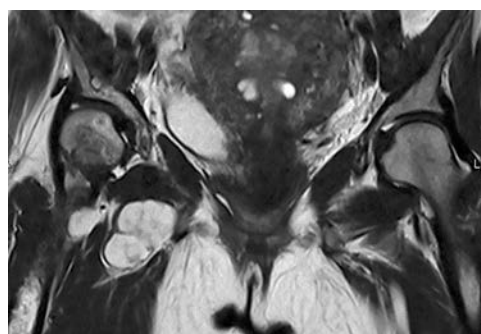


Fig. 4.147.5

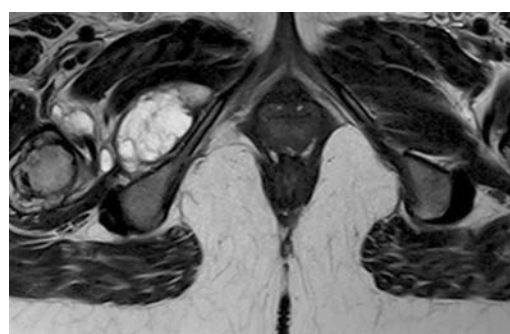


Fig. 4.147.6

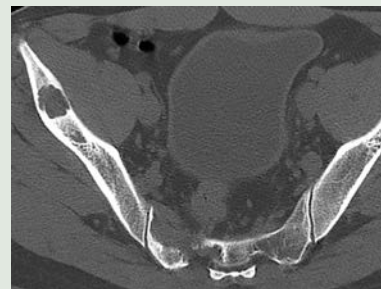
Table 4.147.1: Causes of multiple lytic lesions**Osteolytic bony metastasis**

From thyroid, breast, lung primary malignant lesions. Most common in >40 years. Most involve axial skeleton like skull, spine and pelvis. Rarely do mets occur distal to elbows or knees.

Most frequently occur where red bone marrow is found. May be expansile, Soap-bubbly (septated). Mets to spine frequently destroy posterior vertebral body including pedicle—"pedicle sign"

In general, mets appear as lytic bone lesions which have a little or no soft tissue mass associated with them.

Usually no periosteal reaction. May appear as moth-eaten, permeative or geographic lesions. Indistinct zones of transition, no sclerotic margins.

**Fig. 4.147.7: Osteolytic bony metastasis**

Multiple myeloma (refer to case 148)

Hyperparathyroidism (refer to case 145)

Multiple enchondromatosis: Develop from rests of growth plate cartilage. Endochondral ossification is seen at periphery.

Associated with two syndromes: Ollier's disease (multiple enchondromas) and Maffucci syndrome (multiple enchondromas, multiple hemangiomas of soft tissues and large soft tissue cavernous hemangiomas, Phleboliths). Usually solitary and metaphyseal in short tubular bones and <3 cm diameter.

Table 4.147.2: Difference between multiple lytic and sclerotic bone lesions

| <i>Multiple lytic lesions</i> | <i>Multiple sclerotic lesions</i> |
|-----------------------------------|--|
| <i>Pediatric age group</i> | <i>Pediatric age group</i> |
| 1. Histiocytosis X | 1. Fibrous dysplasia |
| 2. Metastatic neuroblastoma | 2. Osteomyelitis |
| 3. Fibrous dysplasia | 3. Eosinophilic granuloma |
| 4. Enchondromatosis | |
| 5. Rare: Multifocal osteomyelitis | |
| <i>Adults</i> | <i>Adults</i> |
| 1. Fibrous dysplasia | 1. Sclerotic metastasis |
| 2. Enchondroma | 2. Enostosis (bony island) |
| 3. Eosinophilic granuloma | 3. Calcified enchondromas |
| 4. Metastasis | 4. Paget's disease |
| 5. Multiple myeloma | 5. Sarcoma |
| 6. Hyperparathyroidism | 6. Myelofibrosis/mastocytosis |
| 7. Cystic angiomas | 7. Fibrous dysplasia |
| 8. Hydatid disease of bone | 8. Osteopoikilosis, osteopathica striata |

Table 4.147.3: Differential diagnosis for sclerotic lesions in bone

| | |
|--|--|
| Mnemonic: 5M'S to PROOF | |
| M etastasis | T uberous sclerosis |
| M yelofibrosis | P yknodysostosis, Paget disease |
| M astocytosis | R enal osteodystrophy |
| M elorheostosis | O steopetrosis |
| M etabolic (hypervitaminosis D, hypothyroidism, lead and phosphorous poisoning) | F luorosis |
| S ickle cell disease | |

can be divided into four subtypes, monostotic: Single bone; Polyostotic: Multiple bones; Craniofacial Fibrous dysplasia: Skull and facial bones alone; Cherubism: Mandible and maxilla alone (not true fibrous dysplasia).

Fibrous dysplasia is found predominantly in children and young adults, with ~75% of patients presenting before the age of 30 years (highest incidence between 3 and 15 years). In polyostotic form, patients usually

| Table 4.147.4: Lytic lesions of bone based on location | | |
|--|---------------------------------|----------------------------------|
| <i>Diaphyseal lytic lesion</i> | <i>Epiphyseal lytic lesions</i> | <i>Metaphyseal lytic lesions</i> |
| Simple bone cyst | Infection | Osteomyelitis |
| Fibrous dysplasia | Chondroblastoma | Metastasis |
| Enchondromas | Eosinophilic granuloma | Enchondromas |
| Metastasis | Brown tumor | Non-ossifying fibroma |
| Myeloma/plasmacytoma | Aneurysmal bone cyst | Osteosarcoma |
| Lymphoma | Giant cell tumor | |
| Osteomyelitis | Subchondral cyst | |
| Osteoid osteoma | | |
| Ewing sarcoma | | |
| Bone infarct | | |
| Langerhans cell histiocytosis | | |
| Adamantinoma | | |
| Osteofibrous dysplasia | | |
| Brown tumors | | |
| Hydatid cyst | | |

| Table 4.147.5: Difference between Mazabraud syndrome and McCune-Albright syndrome | |
|---|--|
| <i>Mazabraud syndrome</i> | <i>McCune-Albright syndrome</i> |
| A rare syndrome. | A genetic disorder. |
| Frequently seen in women. | Early childhood (range 0.3–9 years). |
| Usually present in middle age. | Typically, earlier in girls than in boys. |
| Usually polyostotic. | Polyostotic unilateral fibrous dysplasia. |
| Increased risk of osseous malignant transformation. | Precocious puberty, menarche at infancy, hypothyroidism, cutaneous pigmentation—coast of Maine, Café-au-lait spots seen. |
| Multiple soft tissue myxomas (intramuscular myxomas): Typically in large muscle groups. | |
| No skin presentation. | |

present by 10 years old. There is no recognized gender predilection.

Radiographic features:

Pelvis and ribs: Ribs are the most common site of monostotic fibrous dysplasia. Fibrous dysplasia is the most common cause of a benign expansile lesion of a rib, bubbly cystic lesions, fusiform enlargement of ribs, protrusio acetabuli. Extremities: may lead to premature fusion of growth plates leading to short stature, bowing deformities, shepherd of the femoral neck discrepant limb length.

Plain radiograph: The appearance of fibrous dysplasia is usually smooth and homogeneous with endosteal scalloping and cortical thinning. The borders are well defined and the cortex is usually intact but thinned due to the expansive nature of the lesion. Other features include: Ground-glass matrix, may be completely lucent (cystic)

or sclerotic, well-circumscribed lesions, no periosteal reaction, rind is seen. CT: Ground-glass opacities (56%), homogeneously sclerotic (23%), cystic (21%) with well-defined borders. Expansion of the bone, with intact overlying bone, endosteal scalloping may be seen.

MRI: MRI is not particularly useful in differentiating fibrous dysplasia from other entities as there is marked variability in the appearance of the bone lesions, and they can often resemble a tumor or more aggressive lesions. T1: Heterogeneous signal, usually intermediate T2: Heterogeneous signal, usually low, but may have regions of higher signal. T1 C+ (Gd): heterogeneous contrast enhancement. Nuclear Medicine: Demonstrates increased tracer uptake on Tc99 bone scans—best for polyostotic lesions (lesions remain metabolically active into adulthood). Management: Usually no treatment required as these are don't touch lesion.

4.148 MUSCULOSKELETAL SYSTEM

Case No. 148

Clinical history: 52-year-old male presented with anemia, bone pain and varied skeletal manifestations aggravated by exercise.

Radiological techniques and observations: Figures 4.148.1 and 4.148.2 are plain radiograph of skull AP and lateral view showing multiple, round, purely lytic, sharply circumscribed and more or less symmetrical punched out lesions noted scattered throughout the skull giving the appearance of “tear drop or rain drop”. The borders of the lesion show no sclerosis. Figure 4.148.3 is plain radiograph of the chest frontal view showing multiple sharply circumscribed lytic lesions in bilateral humerus. With these findings of multiple lytic lesion, differentials would be multiple myeloma and lytic bony metastases.

Interpretation: A: 52 years male; C—Skull shows multiple, round, purely lytic and more or less symmetrical lesions, multiple lytic lesions in bilateral humerus; B: Lesions giving appearance of tear drop or rain drop appearance in skull and sharply circumscribed; D: The multiplicity and symmetrical nature of these lesions still strengthens the diagnosis of myeloma.

Principal diagnosis: Multiple myeloma.

Further investigation and management: The next investigation for this patient is to perform a whole-body MR (WB-MR) or near-whole-body MR (T1 and STIR images most sensitive). If unable to perform whole-body MR, PET/CT may be used to define the extent of medullary/extramedullary disease. Bone marrow biopsy should be done, to evaluate the burden of the disease and staging. Treatment includes chemotherapy:

Dexamethasone ± melphalan ± antiangiogenesis (e.g. thalidomide) ± protease inhibitor (e.g., bortezomib) and autologous peripheral stem cell transplantation.

Brief discussion: Multiple myeloma: Most common primary malignancy of bone affecting the plasma cells in bone marrow (BM). Affects 40–80 years old with male predominance.

Radiographic findings show lytic lesions, diffuse osteopenia ± compression fractures. Rare manifestation: Sclerotic lesions [POEMS (polyneuropathy, organomegaly, endocrinopathy, M-protein, skin lesions) syndrome]. CT findings: Intramedullary soft tissue mass producing lytic lesions ± endosteal scalloping ± cortical breakthrough and soft tissue mass. PET/CT findings: Lesions show activity above background with ↑ detection of non-osseous lesions, rib, and scapular lesion. Bone scan: Myeloma is usually cold in bone scan, whereas metastasis is hot. MR findings: 3 Patterns: a) Micronodular (“variegated” or “salt and pepper”), b) Multifocal (usually ≥5 mm), c) Diffuse marrow infiltration. T1WI—diffuse or focal: Signal ≤ muscle/disc exhibiting a “variegated” or “salt and pepper” appearance. STIR: Untreated disease has ↑ signal intensity. T1WI C+ FS: Untreated disease enhances with contrast.

Normal marrow anatomy and function: It is important to understand the function and distribution of normal marrow to diagnose abnormalities and understand how best to image for marrow disease. In simplest terms, bone marrow consists of two components: Red marrow, yellow marrow. Red marrow is the haematopoietically active fraction of marrow that produces blood cells. Yellow marrow is haematopoietically inactive and composed mainly of fat cells, the purpose of which is uncertain.



Fig. 4.148.1



Fig. 4.148.2



Fig. 4.148.3

Table 4.148.1: Differential diagnosis for multiple myeloma

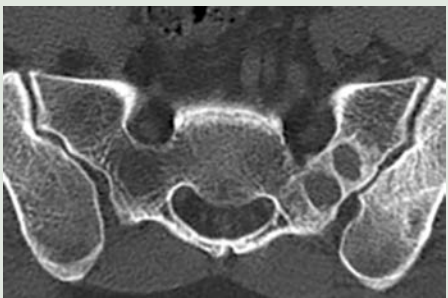

| | | |
|--|---|--|
| Lytic Metastasis Old age | Lung, thyroid and kidney are the most common primaries. Pedicles commonly involved. Mandible usually not involved. Hot bone scan (increased uptake). Not well circumscribed. ADC values higher than myeloma. |  |
| Fig. 4.148.4: Lytic metastasis in left ala of sacrum | | |
| Langerhans cell histiocytosis (Refer to case 153) | | |
| Hyperparathyroidism (Refer to case 145) | | |
| Lymphoma: Affects any age group, with peak incidence in 50–60 years. It is rare in children <10 years old. There is a slight male predominance. | The most common feature is a lytic pattern with permeative bone destruction and a wide zone of transition. Associated soft tissue masses are common. Bone marrow changes show T1 hypointense and T2 hyperintense areas. |  |
| Fig. 4.148.5: Lymphoma in left iliac bone | | |
| Leukemia: Peak age is between 3 and 7 years, with a second peak over 40 years. Bone lesions are seen. | One of the most important findings is a metaphyseal radiolucent band. Subperiosteal new bone growth and osteolytic lesions involving the medullary cavity and cortex are other radiographic findings. | |
| Osteoporosis (Refer to case 146) | | |



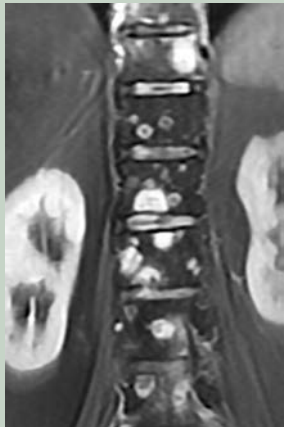
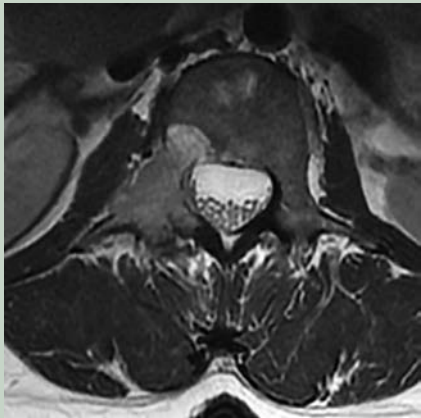
Table 4.148.2: Durie and Salmon plus staging

| Disease | Stage | Bone marrow | Radiograph | MRI | PET/CT |
|---------|-------|-------------------|-------------------|--------------------|--------------------|
| MGUS | - | <10% plasma cells | No lytic lesions | Normal | Normal |
| SMM | I | >10% plasma cells | No lytic lesions | Limited disease | Limited disease |
| MM | II | >10% plasma cells | <20 lytic lesions | 5–20 focal lesions | 5–20 focal lesions |
| | III | >10% plasma cells | >20 lytic lesions | >20 focal lesions | >20 focal lesions |

*MGUS–Monoclonal gammopathy of undetermined significance, SMM: Smoldering multiple myeloma, MM–multiple myeloma

Red and yellow marrow elements are supported by a system composed of reticulum cells, nerves, and vascular sinusoids. The trabecular bone serves as a framework to support the red and yellow marrow elements. When red marrow exists in a high enough concentration, it is evident on T1W and T2W images as intermediate signal intensity. On T1W images, it would be lower in signal intensity than yellow marrow and easy to identify. Because yellow and red marrow show intermediate signal intensity on T2W images, they can be difficult to distinguish from each other on this sequence. On


STIR or fat-suppressed T2W images, red marrow shows intermediate signal intensity that is more hyperintense than yellow marrow and similar in appearance to muscle. An important feature of normal red marrow is that it is always slightly higher in signal intensity than normal muscle or normal intervertebral disks on T1W images. It is never normal for marrow to have lower signal intensity than normal muscle or disk on the same T1W image. The reason red marrow is always slightly higher in signal intensity than muscle or disk on T1W images is because of the normal red marrow composition, where a

| Table 4.148.3: Difference between myeloma and metastasis | |
|---|---|
| <i>Myeloma</i> | <i>Metastasis</i> |
| Pedicles not involved | Pedicles commonly involved |
| Soft tissue mass is associated with bony lesion | As destructive process increases, soft tissue mass may develop |
| Mandible may be involved | Mandible usually not involved |
| Cold bone scan (no uptake) | Hot bone scan (increased uptake) |
| Numerous lesions | Less in number compared to myeloma |
| Uniform in size | Not uniform |
| Well circumscribed—punched out | Not well circumscribed |
| >3 contiguous vertebral involvement | Skip lesions |
| >5 lesions per vertebrae | Unlikely to have >5 lesions per vertebrae |
| Very low ADC values | Little higher than myeloma |
| Osteopenia, osteoporotic collapse | No osteopenia |
|  |  |
| Fig. 4.148.6: Myeloma | Fig. 4.148.8: Metastasis |
|  |  |
| Fig. 4.148.7: Myeloma | Fig. 4.148.9: Metastasis |

significant number of fat cells are scattered throughout the red marrow elements, contributing to the higher signal intensity. When red marrow becomes equal or lower in signal intensity than normal disk or muscle on T1W images, pathology should be suspected.

Yellow marrow (fatty or inactive marrow): The theory for the purpose of fat cells in yellow marrow is that they

provide surface or nutritional support for red marrow elements. The vascular supply to yellow marrow is sparse. Red marrow is not composed entirely of hematopoietic cells but always has a significant amount of fat cells scattered throughout the active cellular elements. Conversely, normal yellow marrow is never composed entirely of fat cells but has some small amount

| Table 4.148.4: Differentiation between malignant and benign vertebral collapse | | |
|--|---|--|
| Modality | Benign collapse | Malignant collapse |
| CT | No cortical destruction | Cortex is destroyed |
| | No paravertebral solid soft tissue mass (except abscess) | Epidural or focal paravertebral soft tissue mass |
| | Sharp fracture lines: Puzzle sign positive. | Unsharp fracture lines: Puzzle sign negative. |
| | Vacuum phenomenon—positive | Vacuum phenomenon: Negative. |
| | Posterior element less common | Posterior element more common |
| MRI | Retropulsed bone fragments | Expanded posterior vertebral contour |
| | Preserved normal marrow signal | Geographic replacement of normal marrow signal |
| | Regular margins | Irregular margins |
| | Linear horizontal hypointense T1/T2 band | Band sign—negative |
| | Fluid cleft sign—positive | Fluid cleft sign—negative |
| | Normal enhancement relative to adjacent vertebrae | Increased enhancement relative to adjacent vertebrae |
| | No restricted diffusion | Restricted diffusion—present. |
| | Loss of SI on opposed-phase | No loss of SI on opposed-phase |
| | Low ADC seen only in abscess, otherwise normal | Low ADC |
| PET | SUV–2 SDs below liver SUV | SUV–4 SDs above liver SUV |
| SPECT | Vertebral body and/or facet joint uptake | Vertebral body with pedicle and/or spinous process uptake |
| |  |  |
| |  |   |
| | <p>Fig. 4.148.10: Benign collapse</p> | <p>Fig. 4.148.12: Malignant collapse</p> |
| | <p>Fig. 4.148.11: Benign collapse</p> | <p>Fig. 4.148.13: Malignant collapse Fig. 4.148.14: Malignant collapse</p> |

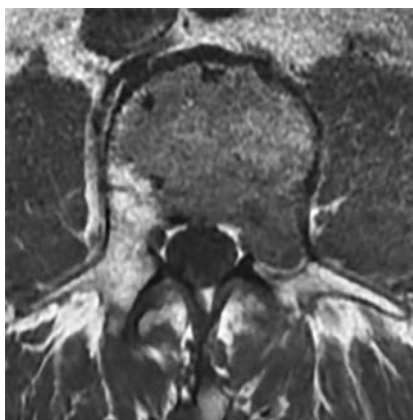


Fig. 4.148.15: T1 marrow infiltration—malignant



Fig. 4.148.16: Puzzle sign +ve (benign)



Fig. 4.148.17: Hip joint of adolescent showing yellow bone marrow

of active cellular elements present. Red marrow is the portion of marrow where the largest concentrations of active cellular elements exist, and yellow marrow is the portion of marrow where fat cells predominate. The fraction of yellow marrow increases with age as trabecular bone resorbs from osteoporosis and fat fills in the spaces created. On T1W MR images, yellow marrow has signal characteristics similar to subcutaneous fat, with relatively high signal intensity. The signal intensity follows that of subcutaneous fat, having a relatively intermediate signal intensity on T2W images and being completely suppressed and showing low signal intensity on fat-suppressed images. Fat signal in marrow is interrupted by groups of low signal intensity stress trabeculae. A thin, low signal intensity line where a physeal plate closed (the “physeal scar”) often is evident.

Marrow conversion: The amount and distribution of red and yellow marrow change with age and is completed by an individual’s middle twenties. At birth, nearly the entire osseous skeleton is composed of red marrow.

When epiphyses and apophyses ossify, they have red marrow within them only transiently, for a few weeks, before conversion to yellow marrow occurs. Conversion from red to yellow marrow proceeds from the extremities to the axial skeleton, occurring in the distal bones of the extremities (feet and hands) first and progressing finally to the proximal bones (humeri and femora). This process occurs in a roughly symmetric manner on each side in an individual.

Progression of conversion from red to yellow marrow within an individual long bone occurs in the following sequence: Epiphyses and apophyses first, then the diaphysis, followed by the distal metaphysis, and finally the proximal metaphysis. The rate of conversion may vary from one individual to another, but generalities have been established that are important to know. The reverse process of conversion can occur, called reconversion. This is a process of yellow marrow being reconverted to red marrow when there is increased demand for hematopoiesis.

Table 4.148.5: Approach to bone marrow abnormality in MRI

| <i>T1-signal</i> | <i>STIR</i> | <i>In-phase</i> | <i>Out-phase</i> | <i>Contrast</i> | <i>ADC</i> | <i>Condition</i> |
|------------------|-------------|-----------------|------------------|-----------------|----------------|-----------------------------------|
| ↑ | ↓ | ↑ | ↓ | - | - | Normal |
| ↑ | ↑ | ↑ | ↓ | - | - | Benign/hemangioma |
| ↓ | ↓ | ↓ | ↓ | - | - | Sclerosis |
| ↓ | ↓ | ↑ | ↓ | - | - | Red marrow* |
| ↓ | ↑ | ↑ | ↑ | ↑ Homogeneous | ↓ | Malignancy infiltrative disorders |
| ↓ | ↑ | ↑ | ↑ | ↑ Peripheral | ↑ (except ADC) | Infection |

*due to marrow reconversion seen in smokers, Vit D deficiency, obese, sickle cell anemia, high altitude, myelofibrosis, mastocytosis, thalassemia

4.149 MUSCULOSKELETAL SYSTEM

Case No. 149

Clinical history: A 12-year-old male who complains of pain and swelling in left thigh for 2 months.

Radiological techniques and observations: Figures 4.149.1–4.149.3 are plain radiograph of left hip, limited axial and coronal sections of CT in bone window images respectively. Plain radiograph reveals onion peel laminated type of periosteal reaction along lateral surface of left femur at diaphysis with wide zone of transition. No evidence of any obvious lytic or sclerotic areas noted in visualised bone. No evidence of any cortical break or any obvious soft tissue involvement. Coronal and Axial limited section of CT shows aggressive osseous destruction along the diaphysis of left femur giving a permeative appearance. There is evidence of cortical destruction with onion peel type of periosteal reaction

along both medial and lateral surfaces of femur. Codman triangle type of (interrupted) periosteal reaction is also visualised along the medial side of diaphysis of femur. Lesion is having a wide zone of transition. No evidence of soft tissue involvement seen in CT images.

Figures 4.149.4 and 4.149.5 are MR images STIR coronal and T1 post contrast axial sections respectively. STIR coronal MR image reveals ill-defined high intensity lesion along the diaphysis of left femur with adjacent soft tissue involvement. T1 post contrast image shows avid contrast enhancement of the lesion with adjacent soft tissue component. Figure 4.149.6 is Axial CT image in lung window showing multiple soft tissue dense well circumscribed variable sized round nodules scattered in bilateral lung fields suggestive of metastases.

Interpretations: A: 12 years old male with lesion along the diaphysis of left femur; C: Ill-defined high intensity



Fig. 4.149.1

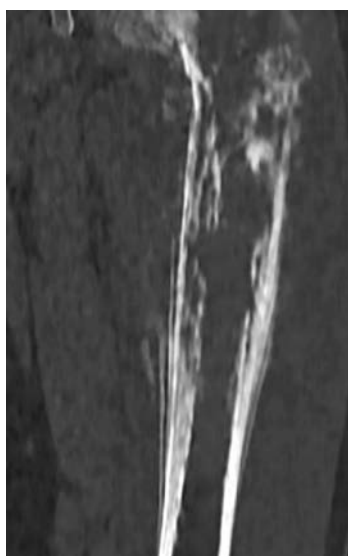


Fig. 4.149.2

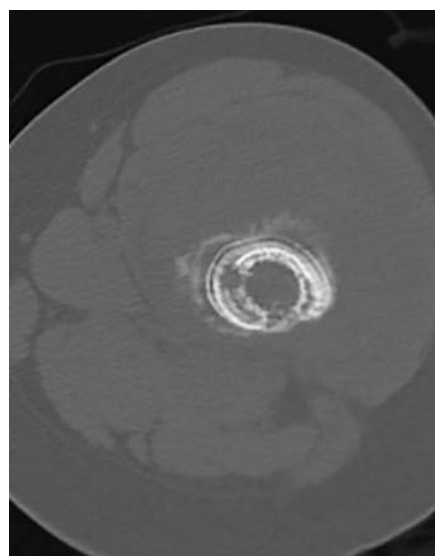


Fig. 4.149.3

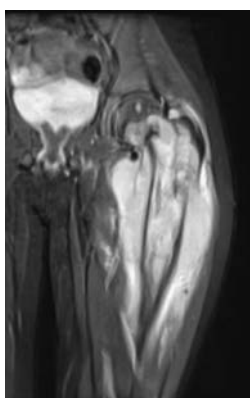


Fig. 4.149.4

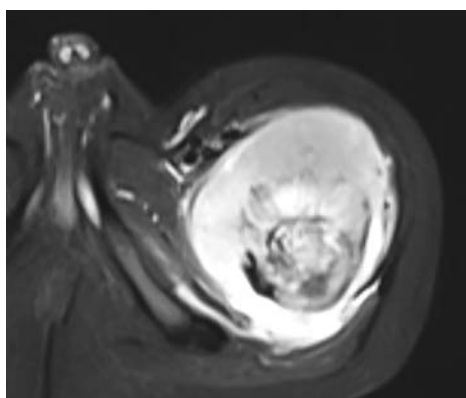
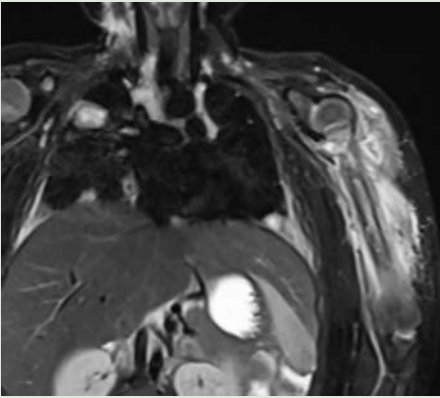



Fig. 4.149.5



Fig. 4.149.6

Table 4.149.1: Differential diagnosis for Ewing’s sarcoma

| | | | |
|--|--|--|---|
| Osteomyelitis: Clinical presentation, soft tissue involvement and CT findings are similar to Ewing’s sarcoma. Reactive osseous sclerosis may be similar to Ewing’s sarcoma. | Permeative reaction tend to be linear, thicker than in Ewing’s sarcoma. MR with contrast differentiates the two by the presence of thick-walled soft tissue and intramedullary abscess in osteomyelitis. |  |  |
| | | Fig. 4.149.7: Left humerus osteomyelitis with septic emboli in right lung | Fig. 4.149.8: Osteomyelitis (Brodie’s abscess) |

Osteosarcoma (Refer to case 150)

Langerhans cell histiocytosis (Refer to case 153)


| | | |
|--|--|---|
| Metastases: Renal cell carcinoma and thyroid papillary carcinomas can cause lytic metastases to bone. Adenocarcinoma mets are usually lytic. Breast cancer cause 34% lytic, 23% sclerotic and 43%mixed lesions. Prostate cancer also results in mixed metastases. | Location—bones with persistent red bone marrow. Lesion appears to be aggressive with soft tissue component. Fracture through lesser trochanter in adult—consider pathological until proven otherwise. Insufficiency fracture may mimic metastatic disease. PET-SUV reduction by 8.5 % following therapy is a strong predictor of response to therapy. |  |
| | | Fig. 4.149.9: Renal cell carcinoma lytic metastases |

Table 4.149.2: Difference between Ewing’s sarcoma and chronic osteomyelitis

| | |
|--|--|
| <i>Ewing’s sarcoma</i> | <i>Chronic osteomyelitis</i> |
| Diaphyseal location | Metaphyseal location |
| Very aggressive lytic lesion | Not aggressive |
| Onion peel periosteal reaction (Interrupted) | Moth eaten and osteoporotic areas (contiguous) |
| More of small round cell | Shows granulocytes |
| No cortical break | Cortical break will be seen |
| Soft tissue mass commonly present | Ulceration and sinuses of skin |

Table 4.149.3: Pathogenesis of osteomyelitis in various age groups



Fig. 4.149.10: **A:** <18 months. There are metaphyseal and transphyseal blood vessels allowing metaphyseal and epiphyseal origin of infections. **B:** Vascularisation of long bones in age group 18 months to 16 years. Separate epiphyseal and metaphyseal blood vessels. **C:** >16 years. Restoration of transphyseal blood vessels causing epiphyseal spread of infection

permeative type of lytic lesion with wide zone of transition and onion peel laminated type of periosteal reaction and codman triangle type periosteal reaction; B: Avid contrast enhancement of the lesion with adjacent soft tissue component and multiple soft tissue dense well circumscribed variable sized round nodules scattered in bilateral lung fields; D: Ewing sarcoma with lung metastases.

Principal diagnosis: Ewing sarcoma with lung metastases.

Which are the round cell tumors of bone?

They are referred to as the Ewing sarcoma family of tumors. They are Ewing sarcoma, extraosseous Ewing sarcoma, primitive neuroectodermal tumor (PNET) of bone and Askin's tumor.

Brief discussion: Ewing sarcoma arises from marrow stem cells. Marrow rich diaphysis are the most common sites. Incidence—most common in 10 to 25 years of age. Second commonest malignant non-hematopoietic bone tumor in children. The typical cytogenetic aberration, identified in 85–95% of lesions, is the non-random reciprocal translocation between chromosomes 11 and 22. Signs and Symptoms: Localized pain with swelling at the site of the lesion is a presenting complaint. Palpable soft tissue mass in more than one-third of patients. Fever, leucocytosis and increased ESR. Only malignant tumor of bone with symptoms simulating an infection.

Location: Long tubular bones and flat bones. Femur is the most common. Diaphysis is the most common location. Many cases with metadiaphyseal involvement are also reported. Tumor arises from medullary cavity, invades cortex, periosteum and spreads to soft tissue.

Radiological appearance: Bone destruction with a moth-eaten to permeative pattern is seen in 76–82% of lesions, and a wide zone of transition (poor margination) is seen in 96% of lesions.

- Diaphyseal lesion (usually in the lower extremity)
- Permeative in its appearance
- Wide zone of transition.
- Onion peel periosteal response (layers of reactive bones) is noted in only 25–50% of cases. Sunray type of periosteal reaction also seen. These radiating spicules have been referred to as the groomed or trimmed whiskers effect.
- Cortical saucerization is an early and characteristic sign.
- MRI—reveals marrow replacement (100%) and cortical destruction (92%), with an associated soft-tissue mass in 96% of cases. Ewing sarcoma are of intermediate signal intensity in both T1 and T2 with typical homogeneous appearance due to high cellularity.

Askin's tumor: Extraskeletal Ewing sarcoma or PNET located in thoracopulmonary region. It is a tumor of young population most commonly in females. A large unilateral pleural-based mass with or without pain is most common clinical presentation. Radiography shows a combination of pleural-based mass with pleural effusion. Pulmonary parenchymal disease can be seen in 25 percent cases. Ipsilateral hilar and mediastinal adenopathy and pneumothorax are other associated findings. Rib destruction is frequently associated with

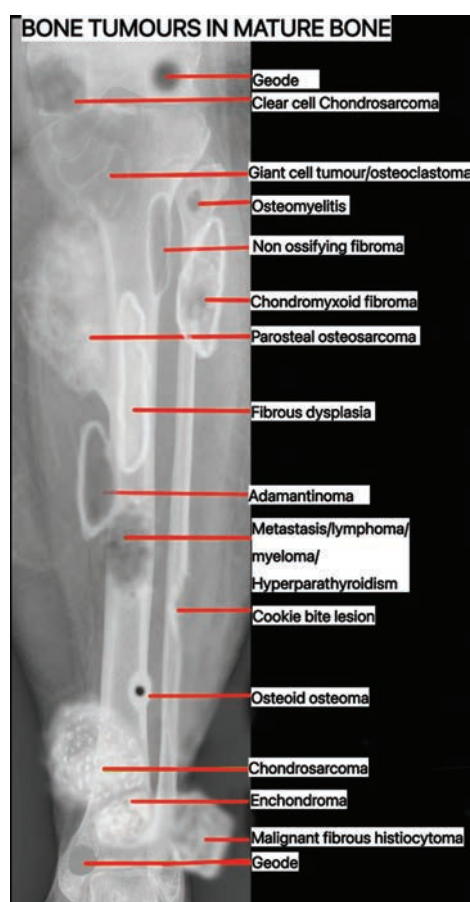


Fig. 4.149.11: Bone tumors in mature bone



Fig. 4.149.12: Bone tumors in immature skeleton

Askin tumor (63% of cases) and is associated with increased activity at bone scintigraphy.

Metastasis: Ewing's sarcoma is the most common primary malignant bone tumor to metastasize to bone (other tumor is osteosarcoma). The spine is a common site for metastasis. Multiple lesions in the one bone occur and are described as skip lesions, a phenomenon also seen in osteosarcoma. Secondary spread to the lungs is also a common occurrence, with the lung parenchyma and pleura being the favoured locations.

Treatment: After biopsy to confirm the diagnosis, therapy primarily involves initial use of neoadjuvant chemotherapy for the purpose of eliminating micrometastases and reducing the size of the primary tumor. Amputation is still used in lesions around the knee. Goal of surgical treatment is to achieve good local control. Radiation therapy along with neoadjuvant chemotherapy (4 to 8 cycles in 3 weeks interval) in early lesion. Future treatment—molecular therapeutics directed by cytogenic aberrations.

Post-treatment imaging: Imaging after institution of neoadjuvant therapy (chemotherapy, RT,

or both) is important to evaluate response to treatment. At radiography, common findings that are associated with a favorable response to therapy of osseous Ewing sarcoma at the tumor primary site include maturation of periosteal reaction, coarsening of the bone trabeculae, reconstitution of the cortex, increasing osseous sclerosis and progressive mineralization, and decrease in the size of the soft-tissue component of the lesion. These features of healing are typically complete by approximately 1 year after initiation of treatment, although reconstitution of the cortex may continue for 2 years. Unfortunately, these radiographic features of a favourable response to neoadjuvant therapy cannot be quantitated as to degree of tumor necrosis or used to predict treatment outcome. Evaluation of skip metastases requires assessment of the entire long bone at the primary site with MR imaging, bone scintigraphy, or FDG-PET. FDG-PET is more useful in evaluation of tumor response to treatment, with its ability to depict molecular changes before the morphologic abnormalities evaluated with cross sectional imaging.

4.150 MUSCULOSKELETAL SYSTEM

Case No. 150

Clinical history: A 17 years old male with left lower leg pain, swelling and fever on and off for the past 3 months.

Radiological technique and observation: Figures 4.150.1–4.150.4 shows dense sclerotic lesion with dense cloud like osteoid matrix with ill-defined margins roughly measuring 7 × 5 cm noted in the metaphysis of distal femur. The lesion shows a wide zone of transition. The lesion appears to involve both cortex and medulla. Cortical disruption noted. The lesion shows aggressive periosteal reaction with elevation of adjacent periosteum with Codman's triangle. Adjacent soft tissue involvement noted. No evidence of any skip lesions/pathological fracture. Adjacent knee joint appears normal.

Interpretation: A: 17 years old male with lesion in metaphysis of distal femur; C: Dense sclerotic bone lesion with osteoid matrix; B: Aggressive periosteal reaction, codman's triangle and soft tissue involvement; D: Conventional osteosarcoma.

Principal diagnosis: Conventional osteosarcoma involving distal femur.

Differential diagnosis: Sclerosing osteomyelitis—less likely as there is osteoid matrix in adjacent soft tissue.

Further investigations: CT—usually not indicated. To confirm the osteoid matrix.

MRI—local and locoregional staging: Extent of marrow (T1WI) and soft tissue involvement, lymph node involvement, invasion of epiphysis, joint involvement, neurovascular involvement and identify areas of viable tumor and mineralized matrix for biopsy, necrosis, skip lesions, fluid–fluid levels in telangiectatic variant.

CT chest: To look for hematogenous lung metastases—calcific metastases. Spontaneous pneumothorax—secondary to subpleural cavitating nodules may rupture to pneumothorax.

CT abdomen: To look for calcifying liver metastasis.

Bone scintigraphy/PET-CT: Systemic staging: To look for metastases. Sodium fluoride PET >> FDG-PET or bone scintigraphy in detection of skeletal metastasis.

Biopsy considerations

- Plane in conjunction with the surgical plane as needle track should be resected.
- Should cross only single compartment.
- Avoid contamination of the tissue needed for reconstructive surgery.
- Avoid mature bone matrix and necrotic regions.
- Should obtain both fine needle aspirate and core biopsy sample.

Management: Neoadjuvant chemotherapy and wide resection with postoperative chemoradiation.

Follow-up: Long-term surveillance to look for local recurrence and systemic metastases.

Discussion: Conventional osteosarcoma (OS).

- Most common non-haematologic primary bone tumor, second only to myeloma.
- Most common malignant bone tumor in adolescents.
- 85% of all types of osteosarcoma.
- *Clinical presentation:* 2nd decade (10–20 years), male > female, unremitting deep pain and mass.
- *Location:* Femur (40–45%) > Tibia (20%) > Humerus. 90% in metaphysis. Pysis is not a barrier, over 80% shows epiphyseal extension in children.



Fig. 4.150.1



Fig. 4.150.2



Fig. 4.150.3

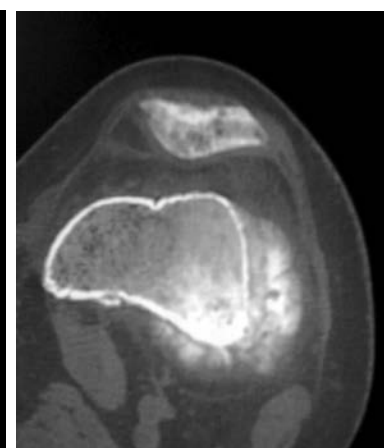


Fig. 4.150.4

Table 4.150.1: Bone tumor checklist

| | |
|-----|---|
| 1. | Age/ sex |
| 2. | Size, shape, margins and number of the lesion. |
| 3. | Location in the skeleton. |
| 4. | Lytic/sclerotic. |
| 5. | Pattern of bone destruction. |
| 6. | Presence and nature of visible tumor matrix. |
| 7. | Internal or external trabeculations. |
| 8. | Longitudinal epicenter: Epi/meta/diaphyseal location. |
| 9. | Transverse epicenter: Cortical/medullary location. |
| 10. | Zone of transition. |
| 11. | Periosteal reaction. |
| 12. | Cortical thinning/scalloping/break. |
| 13. | Joint involvement. |
| 14. | Soft tissue involvement. |
| 15. | Skip lesions and multiple bone involvement. |

Table 4.150.2: Amstutz classification for multifocal osteosarcomas

| | |
|-----------|--|
| Type I | Multiple synchronous bone lesions occurring within 5 months of diagnosis + patient ≤ 18 years of age. |
| Type II | Multiple synchronous bone lesions occurring within 5 months of diagnosis + patient ≥ 18 years of age. |
| Type IIIa | Early metachronous osteosarcoma occurring 5 to 24 months after diagnosis. |
| Type IIIb | Late metachronous osteosarcoma occurring > 24 months after diagnosis. |

- **Genetics:** Increased susceptibility in hereditary retinoblastoma and Li-Fraumeni syndrome.
- **MRI:** Osteoid low signal on all sequences, intense enhancement of marrow and soft tissue mass differentiates viable regions from low signal necrosis.
- **Management:** 80–90% mortality even if treated with wide resection alone. Pre-operative and post-operative chemoradiation indicated.

Table 4.150.3: Types of osteosarcoma

| | |
|--|---|
| • Primary osteosarcoma | Conventional, epithelioid, low grade central, small cell, fibro histiocytic, telangiectatic, gnathic, intracortical |
| • Primary multicentric OS | Synchronous and metachronous |
| • Primary surface OS | Parosteal, periosteal, de-differentiated periosteal and high-grade surface. |
| • Secondary OS | Malignant transformation of benign conditions like Paget's (mc), post-radiation sarcoma, fibrous dysplasia and dedifferentiated chondrosarcoma |
| • Metastatic OS | Lungs and bones |
| • Extra skeletal soft tissue OS | |
| <i>Type and demographics</i> | <i>Imaging features</i> |
| Epithelioid OS Uncommon subtype of conventional osteosarcoma that comprised of both typical osteosarcoma component and epithelioid cells. Often occurs in adolescent and children. | Presents clinically and radiographically like a conventional osteosarcoma. More aggressive. |
| Low grade central OS (well differentiated or sclerosing OS) Rare. M = F. 2nd–3rd decades. Metadiaphysis of long bones particularly femur and tibia. High incidence of recurrence. | Arising within osseous medullary cavity. Permeative poorly defined margins with some degree of cortical destruction. Minimal periosteal reaction. Small soft tissue mass. DD: Fibrous dysplasia-expanded lesion with thinned cortex. Langerhans cell histiocytosis—permeative, may have soft tissue mass. |
| Small cell OS Exceedingly rare tumor. Shows small round cells in histology. It may be confused with Ewing's sarcoma if the osteoid matrix is not included in the biopsy. | Mimics a round blue cell sarcoma—radiolucent lesion with permeative borders and a large soft tissue mass but with foci of osteoid or bone formation. It may extend well into the shaft with a pattern of permeative destruction. |
| Fibrohistiocytic OS Seen after 3rd decade. Giant cell rich osteosarcoma. | Radiolucent lesions with areas of bone formation resembling cotton balls or cumulus clouds. DD: Malignant fibrous histiocytoma—does not show areas of bone formation. |

(Contd.)

Table 4.150.3: Types of osteosarcoma (Contd.)

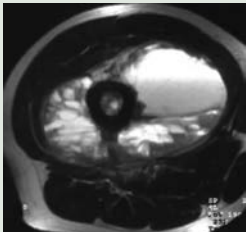
| | |
|---|--|
| <p>Telangiectatic OS (haemorrhagic OS) M > F Second and third decades of life. Treatment and prognosis similar to conventional OS.</p>  <p>Fig. 4.150.5: Telangiectatic OS</p> | <p>Osteolytic destructive lesion with or without matrix mineralization and complete absence of sclerotic changes. Aggressive periosteal reaction is present in most. Areas of T1 hyperintensity due to methemoglobin. On T2 heterogenous with fluid-fluid levels. Bone scan: “Doughnut sign” = peripherally increased uptake with central photopenia on bone scan = Typical</p> |
| <p>Multicentric OS</p> <ul style="list-style-type: none"> • Different histological subtyping of tumor pairs • Different response to chemotherapy • No detectable pulmonary metastases • No overt metastatic disease and • Presence of a syndromic predisposition helps to differentiate multicentric OS from metastatic OS. | <p>Two or more skeletal OS lesions seen in the same patient within 5 months of diagnosis (synchronous OS) or separated in time (metachronous OS). Metachronous OS further divided into early (tumor developing in less than 24 months from first OS diagnosis) and late (developing more than 24 months from first OS diagnosis) (Table 4.150.2)</p> |
| <p>Gnathic OS Primarily affects the mandible (horizontal ramus) and maxilla (alveolar ridge, sinus floor and palate). 6% of osteosarcomas. 60% in males. 30–40 years. Most of them secondary to Paget’s/FD/craniofacial radiotherapy. Mandibular OS has better prognosis than maxillary OS. Less malignant potential and better prognosis than other types.</p> | <p>60% osteoblastic/34% fibroblastic/<10% chondroblastic. Well-differentiated tumor with predominant cartilaginous component. Garrington sign is the thickening of the peri-odontal ligament/ membrane space of the involved teeth. Symmetric widening of the space can be seen early in the disease process due to infiltration of tumour cells.</p> |
| <p>Intracortical OS</p> <ul style="list-style-type: none"> • Rare • Mean age: 24 years • Male predominance | <p>The tumor involves cortex without extension into the medullary portion of the bone or soft tissues. Radiograph–radiolucent lesion with surrounding sclerosis. DD–osteoid osteoma or intracortical osteoblastoma.</p> |
| <p>Periosteal OS</p> | <p>Refer to Table 4.150.4</p> |
| <p>Parosteal OS</p> | <p>Refer to Table 4.150.4</p> |
| <p>Dedifferentiated OS</p> | <p>Most reported originally as conventional parosteal OS that after resection and multiple local recurrences undergo transformation to histologically high-grade sarcomas. On radiographs, mimics parosteal OS but with cortical destruction. Prognosis much worse than parosteal OS.</p> |
| <p>High grade surface OS (Juxtacortical OS)</p> | <p>High grade bone forming tumor arising from osseous surface. Underlying cortex may be partially destroyed. Perpendicular aggressive periosteal reaction. Adjacent soft tissue mass contains osteoid with invasion beyond apparent confines of matrix. Shows avid enhancement with contrast.</p> |
| <p>Secondary OS: Bone forming sarcoma arising in bone affected by underlying condition making it susceptible to sarcomatous degeneration. Paget sarcoma (0.7–0.9% of Paget’s)—median age is 64 years. Radiation sarcoma (0.03–0.8% of irradiated)—median latency period of 11 years following radiation. Dedifferentiated chondrosarcoma (10% dedifferentiate)—50 to 60 years. Others: Parosteal to conventional OS, bone infarct to OS (MFH >OS), fibrous dysplasia to OS (McCune-Albright syndrome), metallic implants to MFH>OS, chronic osteomyelitis, extremely poor prognosis</p> | <p>Paget sarcoma: Most common secondary OS (70–90%), mixed lytic sclerotic with a highly destructive pattern and cortical break. Decreased incidence in vertebra and increased incidence in humerus. Radiation sarcoma: Features of new bone destruction, osteoid matrix and soft tissue mass. Radiation osteonecrosis in 50%. Hypoplastic bone if irradiated as a child. Sites of frequent irradiation like shoulder girdle, iliac wing and long bones. Dedifferentiated chondrosarcoma: Superimposed destruction in one part of the lesion—new cortical breakthrough, soft tissue mass and osteoid. MFH >>OS.</p> |



Fig. 4.150.6: Periosteal and parosteal osteosarcoma



Fig. 4.150.7: Osteosarcoma

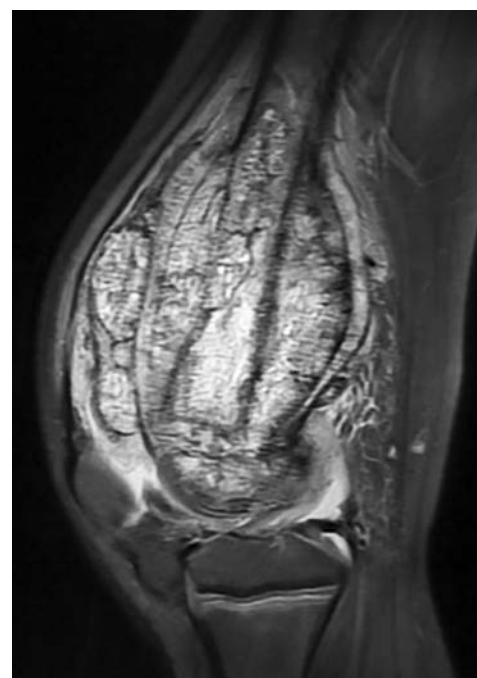


Fig. 4.150.8: Osteosarcoma—MRI

| Table 4.150.4: Difference between periosteal and parosteal osteosarcoma | |
|--|--|
| Periosteal osteosarcoma | Parosteal osteosarcoma |
| Intermediate grade OS | Low grade OS |
| Chondrogenic OS | Fibrogenic OS |
| Diaphysis or metadiaphysis location of tibia and femur. (ant. tibia) | Metaphyseal with preference for posterior cortex of distal femur |
| Generally <5 cm in length | Up to >10 cm at diagnosis |
| 2nd and 3rd decades | 3rd and 4th decades |
| Slight male predominance | Slight female predominance |
| Cortical thickening with osteoid matrix perpendicular to cortex | Tendency to wrap around with “cleft” |
| Periosteum elevated at proximal and distal ends of lesion | Partially circumferential, fusiform along length of bone, contiguous with cortex |
| Marrow involvement rare | Marrow involvement 40–50% |
| <2% of all osteosarcomas/25% of surface OS | 4–5% of all osteosarcoma / 65% of surface OS—most common |
| 85% five-year survival | 95% five-year survival |
| Prognosis poorer than parosteal osteosarcoma but better than conventional OS | Dedifferentiation into high grade OS (15–40%) with course similar to conventional OS |

- **Prognosis:** 1. Initial tumor stage, 2. Response to initial chemotherapy, 3. Completeness of resection.
- **Metastases:** Pulmonary (5–10% have pulmonary metastases at presentation) > osseous and nodal metastases.
- **Role of PET/CT as prognostic indicator:** High SUV and high total lesion glycolysis (TLG) associated with

worse disease-free survival and worst prognosis respectively.

Differentials

- **Ewing's sarcoma:** Diaphyseal with sclerosis only in bone, not in soft tissue.
- **Osteoblastoma:** Benign bone forming tumor commonly arising from posterior elements of spine.

Table 4.150.5: Difference between osteoid matrix and chondroid matrix

Osteoid matrix

Fluffy cotton-like or cloud-like densities



Fig. 4.150.9: Osteoid matrix

Chondroid matrix

Comma-shaped, punctate, annular, popcorn like with “ring and arc” appearance.

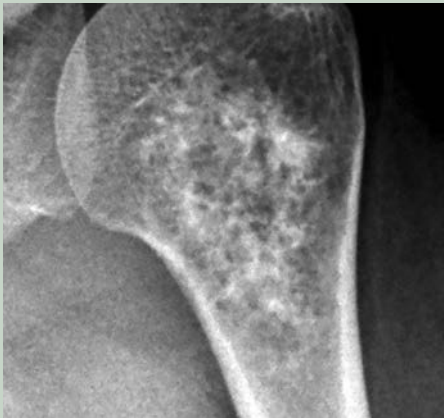


Fig. 4.150.10: Chondroid matrix



Fig. 4.150.11: Types of osteoid matrix

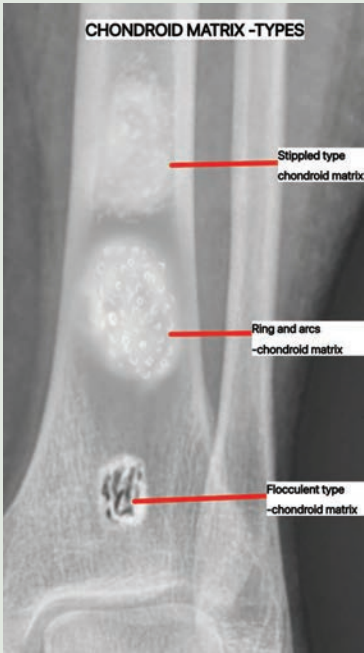


Fig. 4.150.12: Types of chondroid matrix

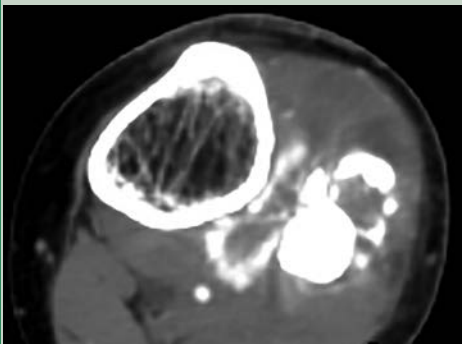


Fig. 4.150.13: Osteoid matrix—ivory type: New bone formation



Fig. 4.150.14: Osteoid: Cloud like

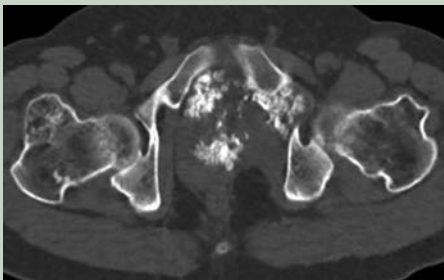


Fig. 4.150.15: Chondroid—rings and arcs—punctate calcification

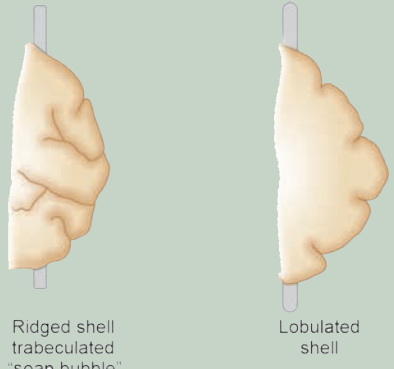

| Bilaterally symmetrical | Bilaterally asymmetrical |
|-------------------------------|--------------------------|
| Hypertrophic osteoarthropathy | Metastases |
| Pachydermoperiostitis | Osteomyelitis |
| Vascular insufficiency | Reiter's arthritis |
| Thyroid acropachy | Psoriatic arthropathy |
| Fluorosis | Osteoporosis |
| DISH | Osteomalacia |
| | Non-accidental injury |
| | Bleeding diathesis |
| | Sickle cell dactylitis |

Fig. 4.150.16: Differential diagnosis for bilateral symmetrical and asymmetrical periosteal reactions

- *Myositis ossificans*: Peripheral ossification with central lucency, with rest pain improves over time (osteosarcoma—central dense ossification and worsening of pain with time)

Tumors causing bone to bone metastasis: Ewing's sarcoma and osteosarcoma.

Primary osteosarcomatosis: Multiple osseous foci of tumors that appear within 5 months after the diagnosis of symptomatic, radiographically dominant tumor are classified as multifocal osteosarcoma or osteosarcomatosis.

| Table 4.150.6: Overview of periosteal reactions | | | |
|---|-----------------------------------|---|-------------------------------------|
| Continuous cortex destroyed | Continuous cortex present | Interrupted cortex present | Complex |
| 1. Smooth shell expanded cortex | Solid | Buttress | 1. Divergent Spiculated "Sun-burst" |
| 2. Lobulated shell | Single lamella | Codman's triangle | |
| 3. Ridged shell Trabeculated "soap bubble" | Lamellated "Onion skin" | Lamellated | |
| | Parallel Spiculated "Hair on end" | Parallel Spiculated | 2. Combined reactions |
| Cortex destroyed <ul style="list-style-type: none">• Expanded cortex• Lobulated shell• Ridged shell, trabeculated "soap bubble" For example: GCT, FCD, NOF, SBC, ABC, enchondroma, brown tumor, central chondrosarcoma, plasmacytoma, lytic metastases with thyroid/RCC primary. | |  <p>Ridged shell trabeculated "soap bubble"</p> <p>Lobulated shell</p> | |
| | | Fig. 4.150.17: Continuous periosteal reaction with destroyed cortex | |
| | |  | |
| | | Fig. 4.150.18: Continuous periosteal reaction with destroyed cortex | |

(Contd.)

Table 4.150.6: Overview of periosteal reactions (Contd.)

Cortex present

Solid (Continuous)

Long-standing benign process, e.g. post-traumatic, osteoid osteoma, osteoblastoma, eosinophilic granuloma, HPOA, DVT, fibrous dysplasia, osteofibrous dysplasia.

Buttress (Interrupted)

Beak-like interrupted solid periosteal new bone formation, e.g. saucerization by a non-mineralized tumor like periosteal chondroma where the periosteum reacts adjacent to saucerization. In expanding intramedullary process like ABC that breaks through an area of solid periosteal reaction.

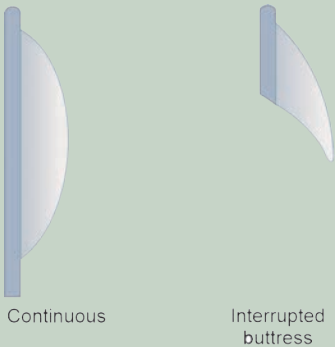


Fig. 4.150.19: Solid periosteal reaction with intact cortex



Fig. 4.150.20: Solid periosteal reaction with intact cortex

Single lamella (continuous): Uniformly dense single thin layer of new bone 1–2 mm from the cortical surface, e.g. premature infants up to 6 months. Early fracture healing, osteomyelitis, LCH, metastasis, chronic venous insufficiency.

Codman's triangle (interrupted)

When an aggressive bone lesion grows faster than the ossification of new periosteum, only the edge of the raised periosteum will ossify, e.g. osteosarcoma, metastasis, juxtacortical chondrosarcoma, MFH, Ewing's, active ABC and osteomyelitis

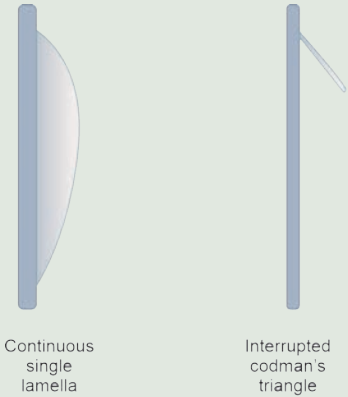


Fig. 4.150.21: Continuous and interrupted periosteal reaction



Fig. 4.150.22: Codman's triangle

Lamellated

“Onion skin”—multiple layers of new bone are formed concentrically around the cortex, e.g. Ewing’s sarcomas, chronic osteomyelitis and chondroblastomas.

Recent studies suggest that the multiple layers form because of modulation of sheets of fibroblasts in the adjacent soft tissue, which develop osteoblastic potential and give rise to sheets of new bone.

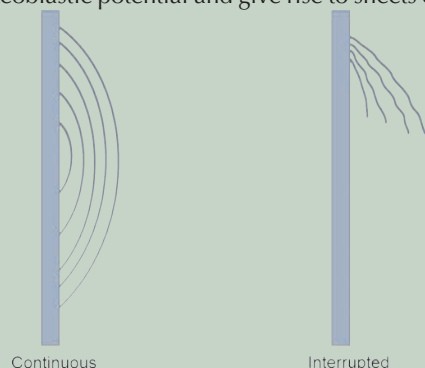


Fig. 4.150.23: Onion skin type of periosteal reaction



Fig. 4.150.24: Onion skin type of periosteal reaction

Parallel spiculated (hair on end)

Ossification of Sharpey’s fibers which attach the periosteum to the bone. Ewing’s sarcoma, osteosarcoma, metastasis, syphilis and Caffey’s disease. Focal sloping (velvet)—Chondrosarcoma.

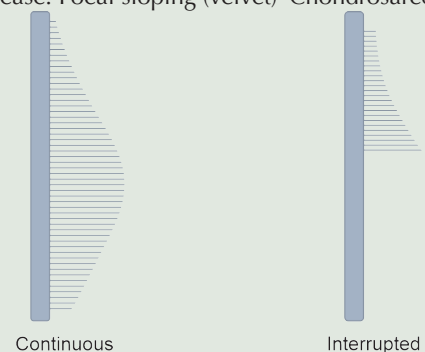


Fig. 4.150.25: Parallel spiculated periosteal reaction

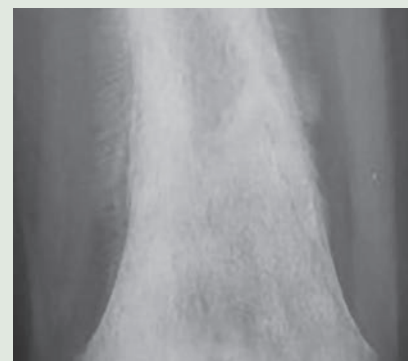


Fig. 4.150.26: Parallel spiculated periosteal reaction

Complex

Osteosarcoma, Ewing’s, Hemangioma, osteoblastic metastases (such as prostatic, bronchoalveolar, carcinoid, breast), osteoblastoma and tuberculosis.

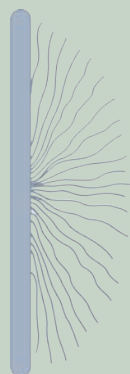


Fig. 4.150.27: Divergent spiculated sunburst type of periosteal reaction

Combined reactions

Disorganized with spicules in random orientation and appearance, e.g. osteosarcoma, metastasis, osteomyelitis, chondrosarcoma, Ewing’s sarcoma, stress fracture, MFH and spindle cell sarcoma.



Fig. 4.150.28: Complex periosteal reaction

Essential to differentiate from bone to bone metastases of osteosarcoma.

Periosteal reactions

- Aggressive expanding lesions like malignant bone tumours produce continuous type periosteal reaction with destroyed cortex and interrupted type Codman's triangle.
- Solid unilamellated uninterrupted periosteal reaction suggests benign etiology.

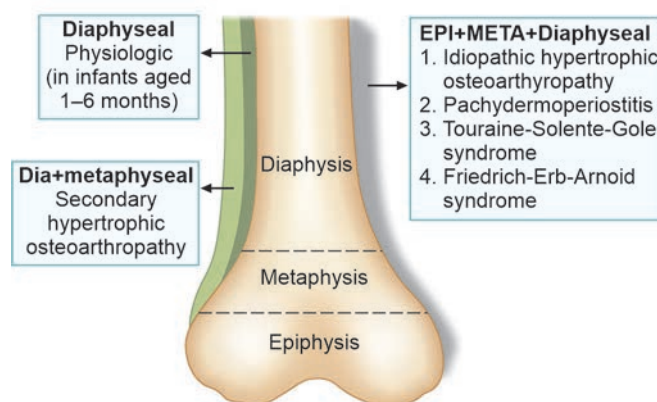


Fig. 4.150.29: Location of periosteal reaction

Table 4.150.7: Periosteal reaction in childhood

| | |
|---|---|
| <ul style="list-style-type: none"> • Benign: Physiologic (up to 35%): Symmetric involvement of diaphysis during first 1–6 months of life, nonaccidental trauma = battered child syndrome, infantile cortical hyperostosis: <6 months of age, hypervitaminosis A, scurvy, osteogenesis imperfecta, congenital syphilis • Malignant: Multicentric osteosarcoma, metastases from neuroblastoma + retinoblastoma, Acute leukemia | <p>Mnemonic: PERIOSTEAL SOCKS</p> <ul style="list-style-type: none"> • Physiologic, prostaglandin • Eosinophilic granuloma • Rickets • Infantile cortical hyperostosis • Osteomyelitis • Scurvy • Trauma • Ewing sarcoma • A-hypervitaminosis • Leukemia + neuroblastoma • Syphilis • Osteosarcoma • Child abuse • Kinky hair syndrome • Sickle cell disease |
|---|---|

Table 4.150.8: Enneking's system of classification of malignant musculoskeletal tumors

| Stage | Grade | Site | Metastasis |
|-------|-------|--------------------|--------------------------------|
| I-A | Low | Intracompartmental | None |
| I-B | Low | Extracompartmental | None |
| II-A | High | Intracompartmental | None |
| II-B | High | Extracompartmental | None |
| III | Any | Any | Regional or distant metastasis |

Table 4.150.9: American Joint Committee on Cancer System of staging bone tumors

| Stage | Grade | Size | Metastasis |
|-------|-------|-------|--------------------------|
| I-A | Low | <8 cm | None |
| I-B | Low | >8 cm | None |
| II-A | High | <8 cm | None |
| II-B | High | >8 cm | None |
| III | Any | Any | Skip metastasis |
| IV-A | Any | Any | Pulmonary metastasis |
| IV-B | Any | Any | Non-pulmonary metastasis |

4.151 MUSCULOSKELETAL SYSTEM

Case No. 151

Clinical history: A 48-year-old female presents with pain and swelling over the left shoulder joint for 3 months.

Radiological techniques and observation: Figure 4.151.1 is radiograph of left shoulder in frontal view showing a relatively well-defined sclerotic lesion noted in the metaphysis of the upper end of humerus involving the medullary region with areas of ring and arc calcification. Narrow transition zone without cortical break. No periosteal reaction or adjacent soft tissue involvement. There is no joint space narrowing. No similar lesion noted. Visualized other bones appear normal. Figures 4.151.2 to 4.151.4 are STIR axial and coronal views and T1 coronal view showing a well-defined heterointense lesion with mild cortical endosteal scalloping noted in the upper end of humerus, the low signal intensities correspond with the areas of calcification. Periosteal reaction noted in the STIR coronal view. No evidence of adjacent soft tissue swelling. No evidence of any other lesion noted. No evidence of joint effusion.

Interpretation: A: 48 years old female, intramedullary lesion in metaphysis of upper end of humerus; B: Well-defined sclerotic lesion; C: Areas of ring and arc calcification, narrow zone of transition without any cortical break; D: Low grade chondrosarcoma.

Principal diagnosis: Low grade chondrosarcoma.

Management: Wide resection involving the biopsy tract.

Differential diagnosis: With X-ray findings enchondroma, low grade chondrosarcoma and bone infarct are considered as differentials.

Brief discussion: Chondrosarcomas are malignant cartilaginous tumors that account for ~25% of all primary malignant bone tumors. Occurs in 4–5th decade of life. Presents with palpable lump, pain and pathological fracture. Chondrosarcomas can be either primary or secondary.

Most common sites → femur (lower end), proximal humerus, triradiate cartilage of pelvis, ribs, tibia, spine. Radiological features: Well-defined lytic lesion, intralesional calcification (rings and arcs), endosteal scalloping, cortical remodeling with periosteal reaction. CT → well-defined lytic lesion, cortical breach in 90% cases, soft tissue mass with matrix calcification.

MRI: T1 → iso to hypointense to muscle, T2 → very high intensity in non-mineralized portions. SWI → blooming of mineralized portion, T1 contrast → heterogenous moderate to intense contrast enhancement.

Nuclear scans: Increased uptake in bone scans in 80% of cases which is absent in enchondroma.

Treatment: Surgical curettage and bone graft, radio-frequency ablation (tumors <2.5 cm).

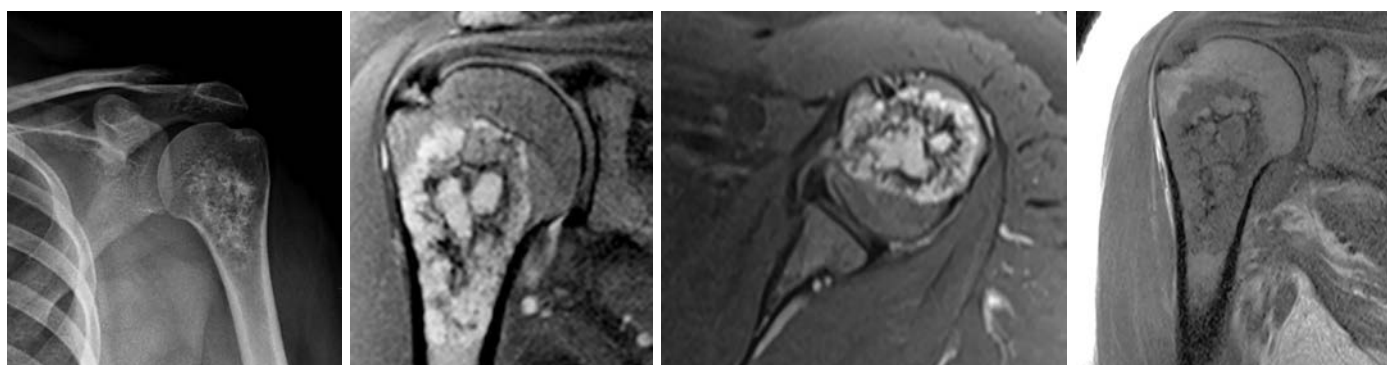


Fig. 4.151.1

Fig. 4.151.2

Fig. 4.151.3

Fig. 4.151.4

Table 4.151.1: Difference between primary chondrosarcoma and secondary chondrosarcoma

| Primary chondrosarcoma | Secondary chondrosarcoma (arising from pre-existing lesion) |
|------------------------|---|
| Conventional | Osteochondroma |
| Juxtacortical | 1. Solitary |
| Clear cell | 2. Multiple hereditary exostoses |
| Myxoid | Enchondroma—solitary, multiple |
| Mesenchymal | Ollier's (10%) |
| Extra skeletal | Maffucci (25%) |

Table 4.151.2: Difference between enchondroma and bone infarct


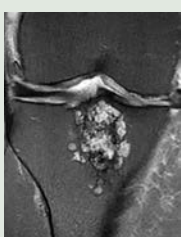
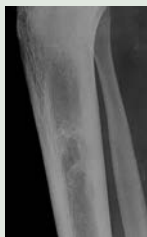
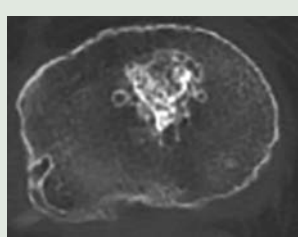
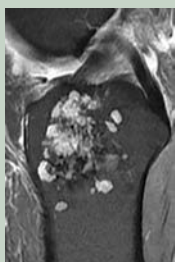
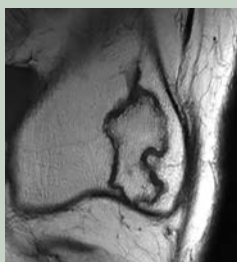
| Features | Enchondroma | Bone Infarct | |
|---|--|--|--|
| Pathology | A benign intramedullary cartilage forming tumor of the bone. Also known as chondroma. | Cell death of bone and marrow as a result of loss of blood supply: Osteonecrosis. Causes: Corticosteroid use, sickle cell disease, Gaucher disease, trauma, renal transplantation. | |
| Location | Metaphyseal region of short bones > long bones | Metaphyseal and diaphyseal regions of long bones> short bones | |
| Age | Peak incidence during 10–30 years | Any age group associated with risk factors like sickle cell disease, Gaucher disease, steroid use. | |
| Multiple lesions | Maffucci syndrome- associated with soft tissue AVM appearing as phleboliths in X-ray Ollier's disease | Sickle cell disease Gaucher disease | |
| X-ray | Typically they are small <5 cm lytic lesions. Well-defined lesion with ring and arc calcification (chondroid matrix) in the metaphyseal region of long bones. Endosteal scalloping +/- . Narrow zone of transition. No expansion of bone (exception short bones). No cortical break/ adjacent soft tissue/ periosteal reaction. | Diffuse/ serpiginous sclerotic lesion/lytic lesion with a sclerotic rim, mild periostitis and very minimal bone expansion noted in the medullary region of the metadiaphysis of long bones. Rarely shows cystic degeneration. | |
| MRI | T1WI: Low to intermediate signal intensity, predominant intermediate signal intensity suggests transformation to low-grade CS T2/STIR: Lobulated high signal typical of benign cartilage lesions. Matrix seen as low signal or signal void Post-contrast: Peripheral and septal, accentuating lobules | Double line sign in T2 and STIR sequences. Outer—hypointense rim—serpiginous sclerotic bone. Demarcation between the living and necrotic bone. Inner hyperintense region—granulation tissue/ inflammatory response of healing. Peripheral normal fatty tissue will be seen within the lesion. Internal signal may be variable depending upon the stages Fat—hyper on T1 and T2, suppressed on fat saturated sequence. Hemorrhagic—hyper on T1 and T2 without loss of signal on fat saturated sequence Edema—T1 hypo and T2 hyperintense. Fibrosis—hypo on T1 and T2. | |
| Bone scan | Increased uptake in 30% of cases | No uptake and appears photopenic on bone scan in blood pool phase | |
|   | |   | |
| Fig. 4.151.5: Enchondroma Fig. 4.151.6: Enchondroma | | Fig. 4.151.8: Bone infarct Fig. 4.151.9: Bone infarct | |
|  | |  | |
| Fig. 4.151.7: Enchondroma | | Fig. 4.151.10: Bone infarct | |

Table 4.151.3: Difference between enchondroma and chondrosarcoma

| Features | Enchondroma | Chondrosarcoma |
|----------------------------------|--|---|
| History and physical examination | <ol style="list-style-type: none"> 1. Younger patients 2. Seldom painful 3. Appendicular skeleton involved almost always (phalanx) 4. Size <5 cm | <ol style="list-style-type: none"> 1. Patient >25 years old 2. Inflammatory pain 3. In axial skeleton, a chondral tumor is a chondrosarcoma until otherwise proved 4. Size >5 cm |
| Imaging | <ol style="list-style-type: none"> 1. Normal intramedullary (except enchondroma protruberans) 2. No periosteal reaction 3. No endosteal scalloping/minimal 4. No changes on followup 5. No soft tissue masses <p>Bone scan → low/ absent uptake (Helps to differentiate between the low-grade chondrosarcoma from enchondroma).</p> | <ol style="list-style-type: none"> 1. Intramedullary 2. Periosteal reaction and associated microfractures. 3. Frequent endosteal scalloping. 4. Changes over time, such as calcifications disappearance, indicating malignant change 5. Soft tissue mass |
| Biopsy | <ol style="list-style-type: none"> 1. Typical encasement pattern 2. No endosteal scalloping 3. Multinodular aspect 4. Surrounded by lamellar bone 5. Does not invade bone marrow | <ol style="list-style-type: none"> 1. Invades haversian canals 2. Periosteal reaction with endosteal scalloping 3. Occasional necrotic 4. Invades bone marrow 5. Generally a single mass |

| Table 4.151.4: Summary of cartilage forming tumors | | | | |
|--|--|--|-----------------------------------|---|
| Types | Tumor types | Locations | Age | Morphology |
| Benign | Osteochondroma | Metaphysis of long tubular bones | 10–30 years | Bony excrescences with a cartilaginous cap; may be solitary/multiple and hereditary |
| | Chondroma | Small bones of hands and feet | 30–50 years | Well-circumscribed single tumors resembling normal cartilage; arise with medullary cavity of bone; uncommonly multiple and hereditary |
| | Chondroblastoma | Epiphysis with extension into the metaphysis, 75% long bones, eccentric location, MRI-inhomogeneously hyperintense on T2/STIR. | 10–25 years, M: F 2: 1 | Well-circumscribed geographic lytic lesion with sclerotic margin, eccentric, epiphyseal lesion, chondroid matrix with/ without calcification (cause for inhomogeneous signal in MR) no cortical break/ soft tissue swelling, 50% show periosteal reaction in metaphyseal region |
| | Bizarre parosteal osteochondromatous proliferation (BPOP)/ Nora lesion | Disordered mass of bone, cartilage, fibrous tissue, hands (55%), long bones (27%), feet (15%) | 30–40 years, mildly painful mass. | Pedunculated or sessile mass with/ without cleavage plane between the mass/ bone cortex. On CT cortex and medullary space from mass and bone are discontinuous. |
| Malignant | Chondrosarcoma | Bones of shoulder, pelvis, proximal femur and ribs | 40–60 years | Arise within medullary cavity and erode cortex; microscopically well-differentiated cartilage-like or anaplastic |

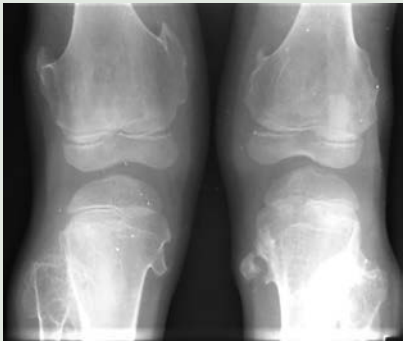


Fig. 4.151.11: Multiple osteochondromas/diaphyseal aclasis



Fig. 4.151.12: BPOP/Nora lesion



Fig. 4.151.13: Enchondroma hand



Fig. 4.151.14: Osteochondroma with malignant transformation

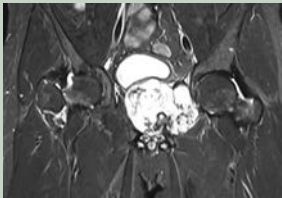


Fig. 4.151.15: Osteochondroma with malignant transformation

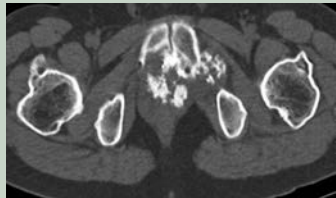


Fig. 4.151.16: Osteochondroma with malignant transformation

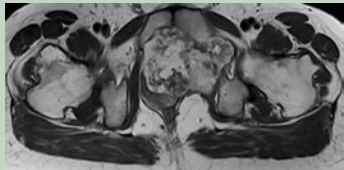


Fig. 4.151.17: Osteochondroma with malignant transformation

4.152 MUSCULOSKELETAL SYSTEM

Case No. 152

Clinical history: A 40-year-old female presented with painless swelling in upper aspect of left arm for the past five years. The swelling progressively increasing in size.

Radiological techniques and observation: Figures 4.152.1 to 4.152.6 are MRI of left shoulder with left humerus-STIR coronal, sagittal and axial and T1 coronal T1 images provided. It shows permeative lytic destructive lesion of shaft of the left humerus with pathologic fracture and overriding fracture ends noted. There is large adjacent STIR hyperintense soft tissue noted with multiple necrotic areas. Brachial vessels are pushed medially and partially encased. There is involvement of the ulnar nerve, medial nerve and radial nerve. Small lytic lesions seen in the head/ neck of the humerus. Multiple lymph nodes in left axilla.

Interpretation: A: 40 years old female, lesion of shaft of the left humerus; C: Permeative lytic destructive lesion; B: Large soft tissue involvement and pathological fracture; D: Malignant fibrous histiocytoma of left humerus.

Principal diagnosis: Malignant fibrous histiocytoma of left humerus.

Brief discussion: Malignant fibrous histiocytoma (MFH), which has more recently been classified as pleomorphic undifferentiated sarcoma (PUS). Malignant osseous neoplasm composed of fibroblasts and pleomorphic cells exhibiting storiform pattern. 2-5% of all primary malignant bone tumors.

Synonyms: Malignant histiocytoma, xanthosarcoma, malignant fibrous xanthoma, fibroxanthosarcoma.

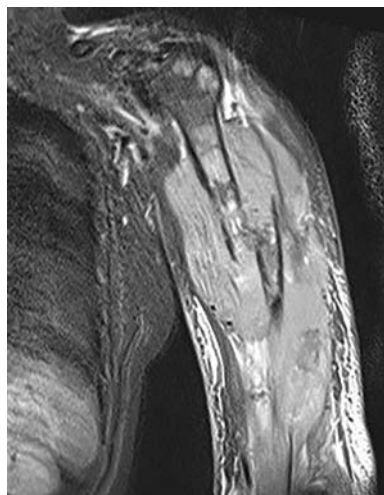


Fig. 4.152.1

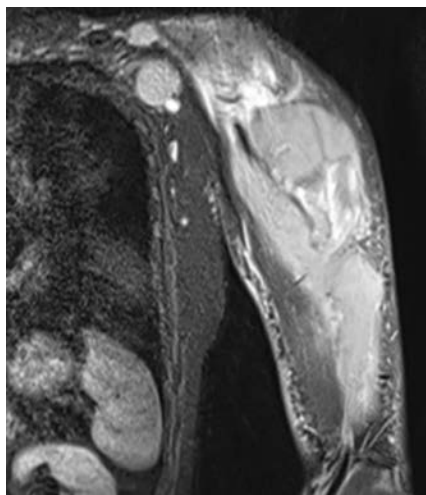


Fig. 4.152.2

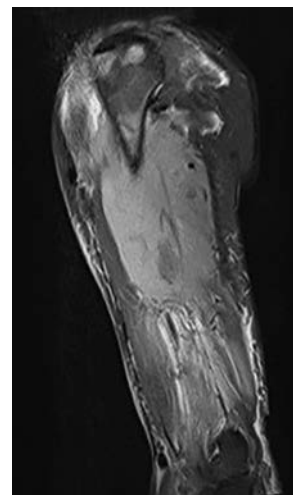


Fig. 4.152.3



Fig. 4.152.4

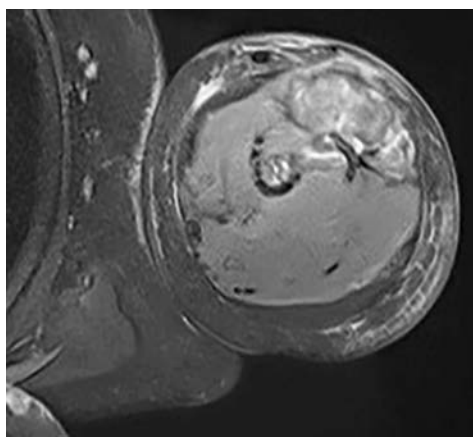


Fig. 4.152.5

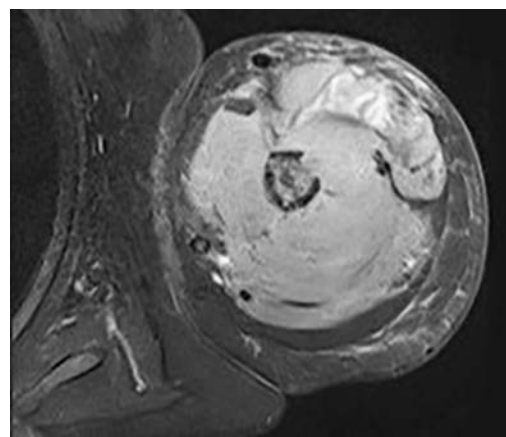
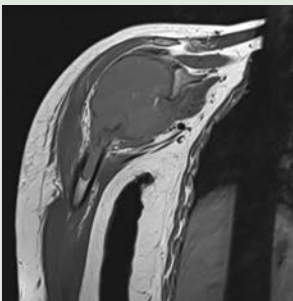
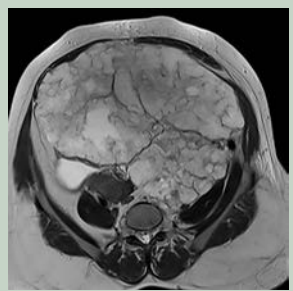

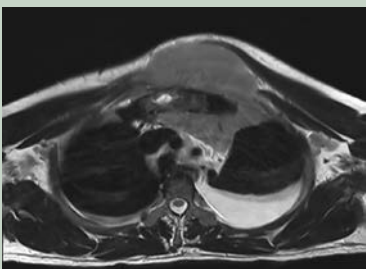


Fig. 4.152.6

Table 4.152.1: Differential diagnosis for malignant fibrous histiocytoma

| | | |
|---|---|--|
| <p>Fibrosarcoma: Lytic aggressive lesion of bone. Most common sites—distal femur, proximal femur, proximal tibia. 2nd to 6th decade—common. Equal incidence in male female.</p> | <p>X-ray: Aggressive destructive lesion, lytic, may contain sequestered bony fragments. Cortical breakthrough with soft tissue mass often present.</p> <p>MRI: T1-mass isointense to skeletal muscle. T2-hyperintense to muscle. Avid contrast enhancement.</p> <p>MFH more common than fibrosarcoma of bone. Differentiated histologically.</p> |  <p>Fig. 4.152.7: Fibrosarcoma</p> |
| <p>Chondrosarcoma: The typical presentation is in the 4th and 5th decades and there is a slight male predominance. Long bones (femur and tibia) being the most common locations.</p> | <p>X-ray: Lytic (50%) intralesional calcifications: (rings and arcs calcification)</p> <p>MRI: T1: Low to intermediate signal T2/STIR: High heterogeneous signal</p> <p>Compared to MFH, chondrosarcoma has</p> <ul style="list-style-type: none"> • Less aggressive behavior • Lobulated high signal on T2 images |  <p>Fig. 4.152.8: Chondrosarcoma</p> |
| <p>Osteosarcoma (Refer to case 150): Primary osteosarcoma typically occurs in young patients (10–20 years) with 75% taking place before the age of 20. Most commonly at the following sites—distal femur: 40%, tibia: 16%, humerus: 15%</p> | <p>X-ray: Wide zone of transition, permeative or moth-eaten appearance, aggressive periosteal reaction—sunburst type/ Codman triangle. Soft-tissue mass tumor matrix ossification/ calcification (ill-defined “fluffy” or “cloud-like”).</p> <p>MRI-T1-soft tissue non-mineralized component: Intermediate signal intensity, mineralized/ossified components: Low signal intensity, peritumoral edema: Intermediate signal intensity, scattered regions of haemorrhage will have a variable signal (see aging blood on MRI)</p> <p>enhancement: Solid components enhance.</p> <p>MRI-T2: Soft tissue non-mineralized component: High signal intensity mineralized/ossified components: low signal intensity, peritumoral edema: high signal intensity.</p> |  <p>Fig. 4.152.9: Osteosarcoma</p> |
| <p>Primary bone lymphoma</p> <p>Peak incidence seen in 50 to 60 years. Mostly affects male.</p> <p>Most common sites are pelvis and femur.</p> | <p>X-ray: Lytic, sclerotic, mixed pattern can be seen. The most common is a lytic permeative bone destruction showing wide transition zone.</p> <p>MRI – Bone marrow changes:</p> <p>T1: Low signal T2: High signal</p> <p>Associated soft tissue masses are common.</p> <p>Endosteal thickening of part of cortex if present, differentiate it from MFH</p> <p>Compared to lymphoma, MFH usually more destructive.</p> |  <p>Fig. 4.152.10: Primary bone lymphoma</p> |
| <p>Other differential diagnosis:</p> <ul style="list-style-type: none"> • Vascular sarcoma—highly aggressive, no matrix, often multifocal • Desmoplastic fibroma—more geographic, low T2 signal intensity is characteristic. | | |

Age: Wide range; higher incidence in patients >40 years. 10–15% occur in 2nd decade.

Primary MFH: Unknown

Secondary MFH: 28–43%: Prior osseous abnormality or treatment: Bone infarct, radiation, Paget disease, chondrosarcoma may transform to MFH, Fibrous dysplasia (extremely rare complication), fibroxanthoma (non-ossifying fibroma) (rare), chronic osteomyelitis (rare), liposclerosing myxofibrous tumor. Pain and swelling, occasionally for several months, pathologic fracture (20%) can be seen on presentation. Location: Long bones, central metaphysis or diaphysis (75%): Often extends from metaphysis to epiphysis or diaphysis–femur (30–45%) > tibia, fibula, humerus, 37% occur around knee, flat bones: Pelvis most common.

Radiographic findings: Mostly high grade at presentation, with lytic destructive pattern, with wide zone of transition. Generally no sclerotic margin, but if present is incomplete, cortical breakthrough and soft tissue mass, cortex generally not expanded, Periosteal reaction often absent; if present, aggressive.

CT: Useful for cortical destruction, but MRI is superior for intra- and extraosseous extent. In **secondary MFH**, may see evidence of underlying primary process.

MR findings–T1WI: Isointense to skeletal muscle, Fluid sensitive: Heterogeneous high signal, post-contrast: Gadolinium contrast enhancement is heterogeneous and nodular, often intense, and often more pronounced at periphery.

Bone scintigraphy: Helps identify metastatic disease, Tc-99m MDP—nonspecific increased activity throughout intraosseous portion of tumour (mechanism uncertain); Ga-67—higher sensitivity for both primary and (extra-osseous) metastatic lesions than Tc-99m

Malignant potential: Highly malignant. With propensity to metastasize and recur.

Further investigation: CT guided biopsy and HPE.

Management: Treatment usually consists of aggressive en bloc resection with a wide margin. Supplementary neoadjuvant chemotherapy and radiotherapy is especially useful in reducing the local recurrence rate. Limb-sparing surgery is usually possible.

4.153 MUSCULOSKELETAL SYSTEM

Case No. 153

Clinical history: 5 years old female young child with multiple soft tissue swelling on scalp, pyrexia of unknown origin, gait difficulties and painful limp.

Radiological techniques and observation: Figures 4.153.1–4.153.2 are plain radiographs of skull frontal and lateral views showing multiple well-defined punched out osteolytic lesions with scalloped edges (geographic skull) in bilateral frontal bones. The lesions have a characteristic bevelled edge giving hole within hole appearance.

Figure 4.153.3 is CT skull axial section in bone window showing multiple osteolytic lesions causing full thickness bone destruction seen in bilateral frontal bones involving both the inner and outer tables of skull with outer tables being affected more than the inner table associated with soft tissue component giving the characteristic bevelled edge appearance.

Interpretation: A: 5 years old female, lesion in frontal bone on both sides; C: Well-defined multiple punched out lytic lesions; B: Bevelled edges appearance; D: Langerhans cell histiocytosis.

Principal diagnosis: Langerhans cell histiocytosis (LCH).

Management: Excision and curettage, intralesional steroid injection, chemotherapy, radiofrequency ablation. Patient to be referred to orthopaedic surgeon.

Discussion:

Classification of Langerhans cell histiocytosis spectrum:

1. **Letterer-Siwe disease:** It is a disseminated multiorgan disease. Typically affects young children/infants less than one-year old and has fulminant course with poor prognosis.

2. **Hand-Schüller-Christian disease:** Usually has multiple lesions confined to one location (usually bone). Typically affects children and has intermediate prognosis.

3. **Eosinophilic granuloma (EG):** Lesions are typically confined to one organ system with 70% bone involvement. Typically affects children and has best prognosis.

Information has been collected in various studies which show that bone involvement occurs in approximately 78% of patients with LCH and often includes the skull (49%), hip/pelvic bone (23%), upper leg bone (17%) and ribs (8%). Skin LCH is seen in as many as 50% of patients. Lung lesions are seen in 20 to 40% of patients, while 30% of patients have lymph node involvement.

LCH in the skin, bones, lymph nodes or pituitary gland usually gets better with treatment and is called “low-risk.” Some patients have involvement in the spleen, liver and bone marrow. This is called “high-risk disease” and may be more difficult to treat. Some patients may develop long-term side effects such as diabetes insipidus, stunted growth, loss of teeth, bone defects, hearing loss, or neurologic problems; while other patients remain without side effects. In a minority of cases, the disease can be life-threatening. Treatment of low-risk LCH in children: Steroid therapy, chemotherapy given by mouth or vein, chemotherapy applied to the skin, Photodynamic therapy with psoralen and ultraviolet A (PUVA) therapy, UVB radiation therapy, surgery, low dose radiotherapy, targeted therapy, immunotherapy. Treatment of high-risk LCH in children: Chemotherapy and steroid therapy, targeted therapy, a liver transplant for patients with severe liver damage.

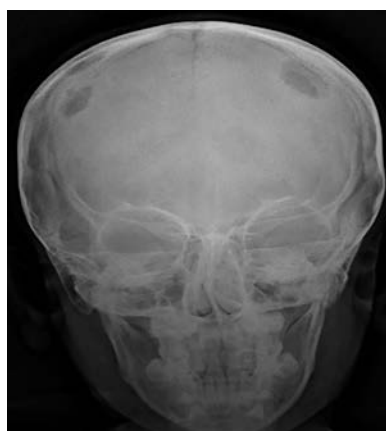


Fig. 4.153.1



Fig. 4.153.2

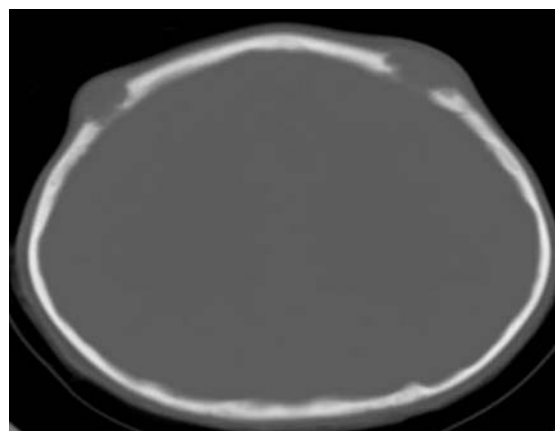


Fig. 4.153.3

Table 4.153.1: Differential diagnosis for pediatric lytic bone lesion

Neuroblastoma metastasis: Neuroblastomas are tumors of neuroblastic origin. Although they may occur anywhere along the sympathetic chain, the vast majority arise from the adrenal gland. Whole brain radiotherapy to be given if cerebral or leptomeningeal metastases are present, Focal radiotherapy for single/symptomatic lesions, Chemotherapy for systemic disease. Surgery reserved for larger symptomatic lesions and has a role in diagnosis, when the lesion is solitary or diagnosis not established.

Thickened bone, the so-called “hair-on-end/ sunburst” periosteal reaction, lytic defects, and separation of sutures. Neuroblastoma often metastasises to the skull base and orbits in the late stages of the disease. Both LCH and metastatic neuroblastoma can involve the posterolateral part of the orbit.

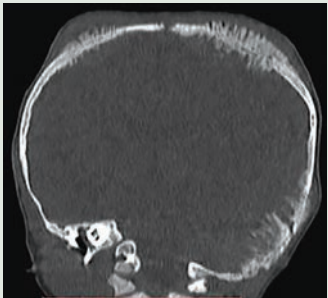


Fig. 4.153.4: Neuroblastoma metastasis

Leukemia of the skull are hematologic malignancies where there is proliferation of hematopoietic cells at an undifferentiated or partially differentiated stage of maturation. Multiple lytic lesions of the skull can occur in a case of leukemia. Treatment options include chemotherapy, radiotherapy and bone marrow transplantation.

Skull lymphoma: One of the most significant radiological findings is a metaphyseal radiolucent band. Subperiosteal new bone growth and osteolytic lesions of the medullary cavity and cortex are other radiographic findings. Combined modality of treatment consisting of surgery, systemic chemotherapy and field radiation therapy is considered as optimum treatment for primary skull lymphomas.

Axial T1-weighted magnetic resonance imaging (MRI) scan after intravenous injection of gadopentetate showed a solid enhancing mass in the right frontal skull with expansion and destruction both of the inner and outer tables of the calvarium. The right frontal lobe was posteriorly displaced by the mass. Local dural involvement by the tumor is evident.

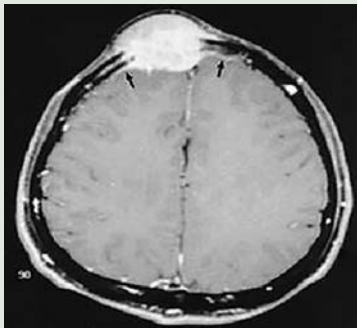


Fig. 4.153.5: Skull lymphoma

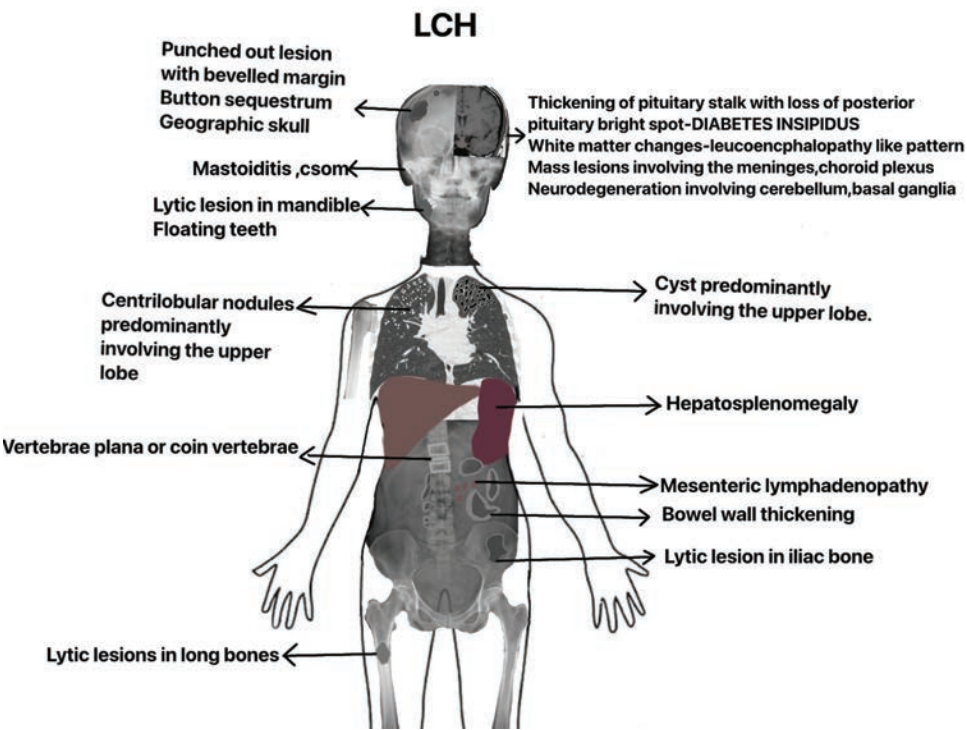


Fig. 4.153.6: Whole body illustration showing LCH findings

| | |
|--|---|
| Kikuchi-Fujimoto disease , also known as subacute necrotizing lymphadenitis or subacute necrotizing histiocytosis, is an idiopathic disease characterized usually by cervical lymph node enlargement (80%). It typically affects young women. | Imaging findings are non-specific and demonstrate primarily cervical nodal enlargement. Homogenous nodal enlargement (83%), perinodal infiltration (80%), central nodal necrotic change (16%). It usually runs a benign course that is self-limiting with most lymph nodes returning to normal size within the first six months of diagnosis. |
| Kimura disease , also known as eosinophilic hyperplastic lymphogranuloma, is a rare benign inflammatory disease that characteristically manifests as enlargement of cervical lymph nodes and salivary glands. Kimura disease typically affects males (80%) between 20 and 40 years of age (80% of cases). | CT: Demonstrates nonspecific appearances of markedly enlarged cervical nodes +/- parotid and submandibular glands, intense enhancement of nodes and heterogenous enhancement of salivary glands. MRI: T1: Hypointense or isointense compared with salivary tissue, T2: Typically, hyperintense compared to salivary gland tissue and variable according to degree fibrosis, T1 C+ (Gd): Usually homogeneous enhancement. Treatment options include conservative management, radiotherapy, steroid and oxyphenbutazone, resection and cyclosporine. |
| Rosai-Dorfman disease/sinus histiocytosis with massive lymphadenopathy is benign idiopathic proliferative disease that involves phagocytic histiocytes. The disease predominantly occurs in young adults with a mean age of 21 years. Rosai-Dorfman disease usually follows a benign and self-limiting course with treatment largely targeted at controlling local manifestations (surgical intervention). | Due to the wide disease spectrum, radiographic features can be variable. Nodal involvement is appreciated as lymphadenopathy on plain film and cross-sectional imaging. CT: Central nervous system—hyperattenuating meningeal-based mass showing contrast enhancement, parenchymal edema surrounding the lesion may be present. MRI: Central nervous system meningeal-based masses. T1: Isointense to grey matter, T2: Hypointense to grey matter, T1 C+ (Gd): Homogeneous enhancement. Often shows increased uptake with Gallium scanning and increased metabolism with FDG-PET. |
| Erdheim-Chester disease is a rare non-Langerhans cell, non-familial multisystemic histiocytosis, with widespread manifestations and of highly variable severity. The most common presenting symptom is bone pain. Slight male predominance. Patients may also present with focal neurological signs, exophthalmos, retroperitoneal fibrosis, diabetes insipidus, and dyspnoea due to extra-skeletal involvement of these systems. | Skeletal involvement: Bilateral, symmetric metaphyseal and diaphyseal sclerosis, increased uptake on Tc-MDP bone scan, cortical thickening. Lung involvement: Interstitial edema pattern with cardiomegaly and pleural effusions. Hairly kidney sign: Irregular symmetrical infiltrates of bilateral perirenal and posterior pararenal spaces. Coated aorta sign: periaortic soft tissue. Retro-orbital tissue with retrograde extension along the optic nerve to the hypothalamus. Intracranial dural accumulations mimicking meningioma. |

Non-Langerhan cell histiocytosis: Kikuchi-Fujimoto disease, Kimura disease, Rosai-Dorfman disease and Erdheim-Chester disease (ECD).

Button sequestrum: The radiological definition of a bony sequestrum refers to an image of calcification within a lucent lesion, completely separated from the surrounding

bone and without referring to the histological nature and vascular status of the calcified tissue. When the sequestrum is small and surrounded by lucent rim it is known as a button sequestrum. These are usually seen in the calvarium. The main conditions that may present with a bony sequestrum are osteomyelitis and skeletal



Fig. 4.153.7: Lytic lesions in bilateral iliac bones

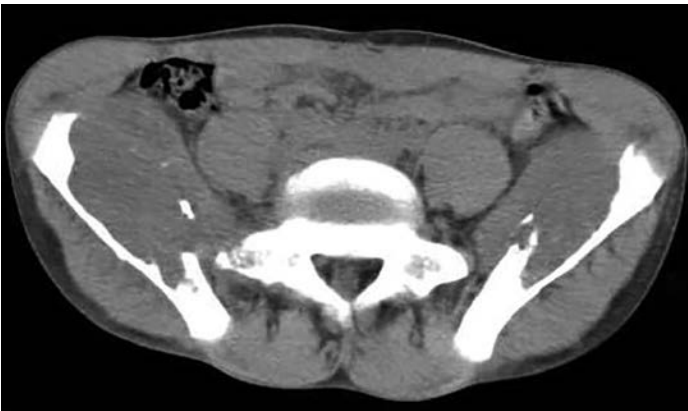


Fig. 4.153.8: Lytic lesions in bilateral iliac bones



Fig. 4.153.9: Button sequestrum

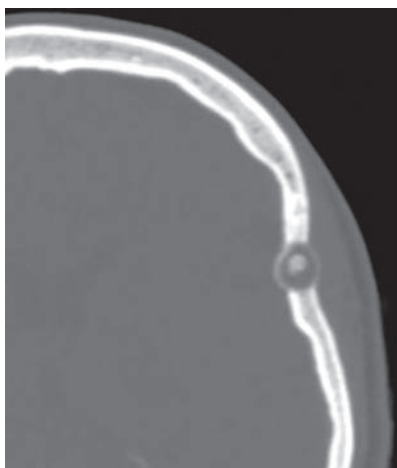


Fig. 4.153.10: Button sequestrum

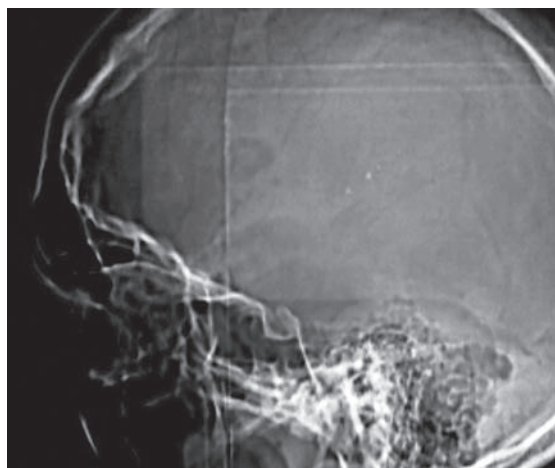


Fig. 4.153.11: Button sequestrum

tuberculosis. Eosinophilic granuloma, lymphoma and malignant fibrous histiocytoma (which include fibrosarcoma and desmoids) can also present with a bony

sequestrum. Some primary bone tumors such as osteoid osteomas can mimic a bony sequestrum.



Fig. 4.153.12: Diaphyseal aclasis

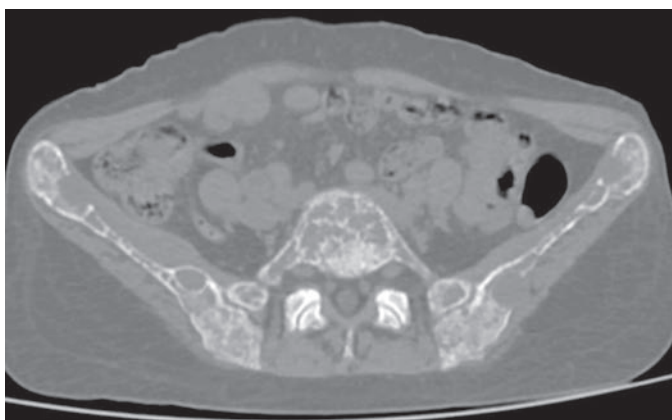


Fig. 4.153.13: Brown's tumour



Fig. 4.153.14: Multiple fibrous dysplasia

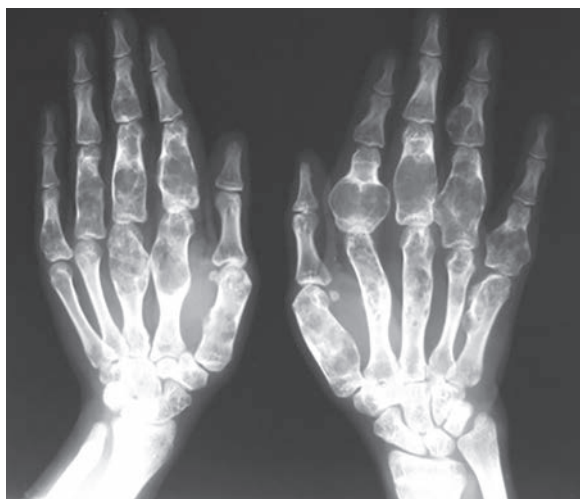


Fig. 4.153.15: Enchondromatosis



Fig. 4.153.16: Multiple non-ossifying fibroma (Jaffe-Campanacci syndrome)

4.154 MUSCULOSKELETAL SYSTEM

Case No. 154

Clinical history: 45 years old female patient with swelling over scalp for 3 months.

Radiographic techniques and observation: Figures 4.154.1 and 4.154.2 are AP and lateral radiograph of skull showing an ill-defined large lytic lesion in the right parieto-temporo-occipital bone with adjacent soft tissue component. The lesion appears to involve both inner and outer table of skull. No evidence of any other lytic lesions. Figures 4.154.3 to 4.154.5 are CT brain plain and contrast in bone and soft tissue window selected sections showing an ill-defined lytic lesion with hyperdense soft tissue component in right parietal bone. Intracranial

extension causing mass effect noted on the right parietal lobe. With contrast, intense enhancement with central areas of necrosis noted. No evidence of any invasion of dural venous sinuses.

Interpretation: A: 45-year-old female, lesion in right parietal bone; C: Ill defined intensely enhancing lytic lesion; B: Irregular destruction of both outer and inner table of skull and large soft tissue component without any foci of calcification; D: Calvarial metastasis.

Patient is a known case of follicular carcinoma of thyroid with bilateral lobes of thyroid appearing enlarged and replaced by ill-defined heterogeneously enhancing mass lesion with coarse calcifications.



Fig. 4.154.1



Fig. 4.154.2

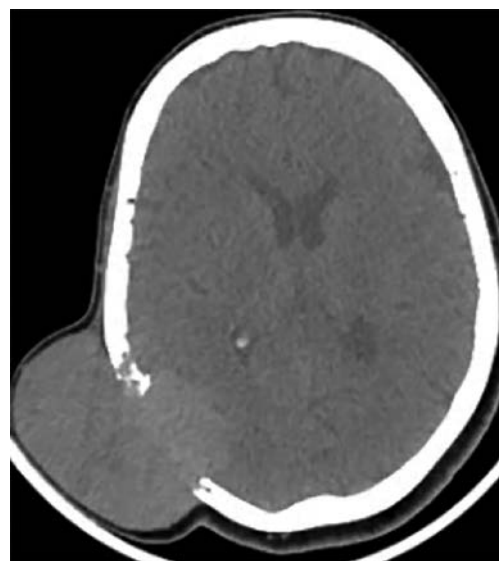


Fig. 4.154.3

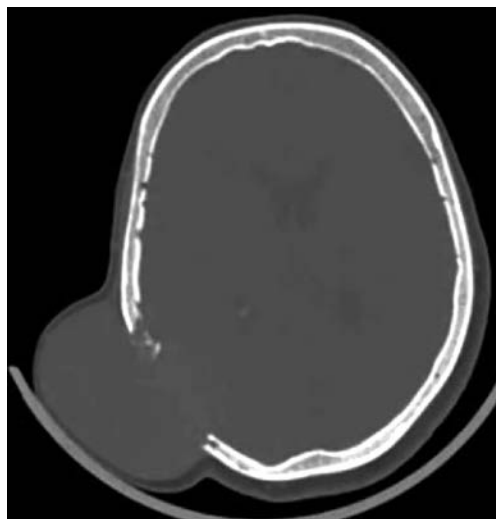


Fig. 4.154.4

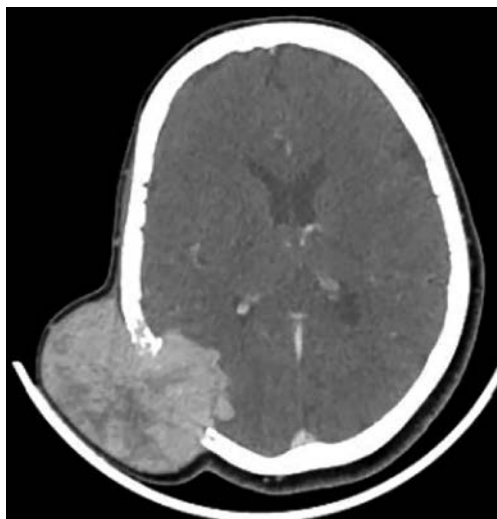


Fig. 4.154.5

Table 4.154.1: Pearls in skeletal metastasis

| |
|---|
| Skeletal metastasis |
| Commonly involve axial skeleton—skull, spine and pelvis |
| No periosteal reaction |
| Little or no soft tissue component |
| Frequently occur where red marrow is found |

Table 4.154.2: Primary based on the type of bone metastasis

| | |
|-----------------------|--|
| Skull metastases | Regardless of primary, usually lytic in appearance |
| Purely lytic | RCC and thyroid |
| Mixed lytic sclerotic | Lung and breast |
| Purely blastic | Prostate, medulloblastoma and bronchial carcinoid |

Principal diagnosis: Calvarial metastases.

Differential diagnosis: In adults,

1. Intra-diploic and anaplastic meningioma—lytic lesion with sclerosis.
2. Lymphoma.
3. Plasmacytoma.
4. Hemangiopericytoma or solitary fibrous tumor.
5. Brown's tumor—multiple, small, salt and pepper skull.
6. Hemangioma—spoke wheel or sunburst pattern of calcifications.
7. Skull vault osteomyelitis—sequestrum.
8. Osteoporosis circumscripta—large lytic lesion with more extensive outer table changes.
9. Multiple myeloma—multiple small punched out lesions of skull.
10. Intradiploic epidermoid—scalloped border with sclerotic rim.

In children,

1. Eosinophilic granuloma—with beveled edges and button sequestrum.
2. Neuroblastoma metastases—sutural lytic lesion.
3. Atretic cephalocele—inside out beveled edges.
4. Dorsal dermal sinus—outside in beveled edges (also in bullet injuries)
5. Luckenschadel skull—Lacunar skull or craniolacunae seen in Chiari II malformations, dysplasia of membranous skull vault. Inner table more affected than the outer with “finger-shaped pits”. Large defects are called “craniofenestrae”.
6. Growing fracture or lepto-meningeal cyst.

Further investigations: Biopsy—if metastases, then primary work up; MRI brain—to look for parenchymal extension; whole body PET/PET-CT for distant metastasis.

Table 4.154.3: Characteristics of skeletal metastasis

| | | | |
|--|---|--|---|
| Specific primary tumor: Bone metastasis | | | |
| Osteolytic bone metastases: Neuroblastoma (in childhood); lung cancer (in adult male); breast cancer (in adult female), thyroid cancer, kidney, colon | Osteoblastic bone metastases: Prostate, breast, lymphoma, malignant carcinoid, medulloblastoma, mucinous adenocarcinoma of GI tract, TCC of bladder, pancreas, neuroblastoma | | Expansile bubbly bone metastases: Kidney, thyroid |
| Skeletal metastases in children: 1. Neuroblastoma (most often) 2. Lymphoma 3. Rhabdomyosarcoma 4. Ewing sarcoma 5. Retinoblastoma 6. Hepatoma | Acral metastasis: Lung, breast, GIT | Permeative bone metastasis: Burkitt lymphoma, mycosis fungoides | Calcifying bone metastases: Breast Osteosarcoma Testicular Thyroid Ovary Mucinous adenocarcinoma of GI tract |
| “Soap bubble” and septated: Renal cell carcinoma | “Flow void sign” —seen in MRI at the lesion core or margin; indicates osseous metastases from RCC | | Distal to elbows and knees —50% from lung and breast |
| Diffuse sclerotic multiple round well circumscribed: Prostate and breast | Cookie bite metastasis: Seen in lung cancer | | Mixed bone metastases: Seen in CA breast, prostate, lymphoma |
| Skeletal metastases in adult: Colon, breast, lung, carcinoid, kidney, thyroid, prostate | | | |
| Isolated lesser trochanter fractures: Pathological until proven otherwise. In elderly patients, most common causes include metastasis, myeloma and lymphoma | | | |



Fig. 4.154.6 Anaplastic meningioma



Fig. 4.154.7: Lymphoma

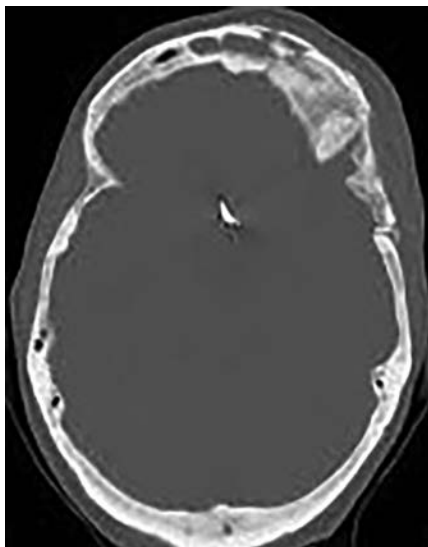


Fig. 4.154.8: Osteomyelitis

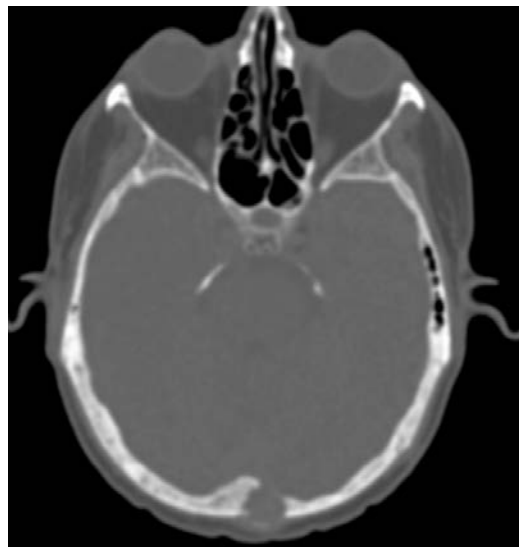


Fig. 4.154.9: Brown's tumor

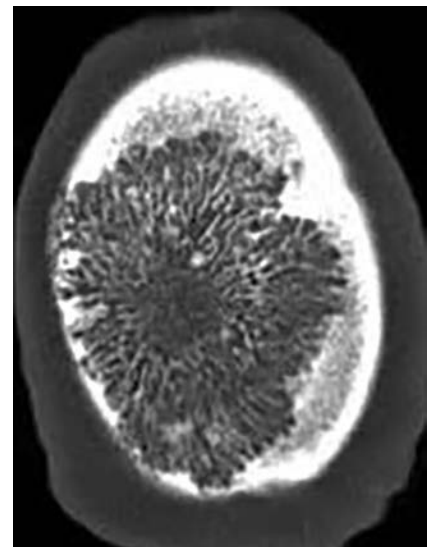


Fig. 4.154.10: Hemangioma

Management: Chemoradiotherapy.

Discussion: Metastases are the most common malignant bone tumors. Skeleton is the third most common site of cancer metastases after lung and liver. Bone scan is highly sensitive.

Primary tumors most frequently encountered as calvarial metastases: Breast (70% of all bone mets in women), lung, melanoma, prostate (60% of all bone mets in men), follicular carcinoma of thyroid, RCC, lymphoma, leukemia, multiple myeloma and intra-hepatic cholangiocarcinoma.

4.155 MUSCULOSKELETAL SYSTEM

Case No. 155

Clinical history: A 35-year-old male presented with painless swelling in anterolateral aspect of right arm for the past five years. The swelling is progressively increasing in size.

Radiological techniques and observations: Figures 4.155.1 to 4.155.3 are MRI of right arm with shoulder joint in T1, T2 and T1 post contrast coronal sections show a large well-defined complex lesion in the intra muscular plane at the anterolateral aspect of right arm near shoulder joint. The lesion shows T1 signal intensity isointense to muscle and T2 hyperintensity with post contrast T1 heterogenous enhancement. No evidence of infiltration into the underlying muscles. No bony involvement is seen. No evidence of ipsilateral axillary lymph nodes.

Interpretation: A: 35-year-old male, lesion in the intra muscular plane at the anterolateral aspect of right arm near shoulder joint; C: Large well-defined lesion with signal intensity isointense to muscle in T1 and hyperintensity in T2; B: Post-contrast T1 heterogenous enhancement; D: Synovial sarcoma.

Principal diagnosis: Synovial sarcoma.

Brief discussion: Synovial sarcomas are relatively common intermediate-to-high grade malignant soft tissue tumors accounting for 2.5–10% of all soft tissue sarcomas. They typically present in adolescents and young adults (15–40 years of age) with mild male predilection (M: F = 1.2:1). The presentation is most often with a slowly-enlarging soft tissue mass which may have been noted for some years and gives a false impression of a benign process. It derives its name

from the fact that microscopically it resembles normal synovium. However, it stains for epithelial markers (e.g. epithelial membrane antigen and cytokeratin), which synovium does not. Additionally, it has been found in many locations that do not normally have synovium. The most common location for these tumours is within the soft tissues adjacent to large joints, e.g. knee and popliteal fossa. While these tumours arise near joints, it is rare for them to arise from the joint itself and despite their name, they do not arise from synovial structures, e.g. joints, tendon sheaths and bursae. Location: Extremities: 80–95%, lower limb: 60–70%, upper limb: 15–25%, from soft tissues: 90–95%, from joint: 5–10%. It is one of the (less common) causes of cannonball metastases to the lung.

Radiographic features: A soft tissue mass near but not in a joint in a young patient (15–40 years old), particularly if dystrophic calcification is present, are very suggestive. Plain radiograph: May be normal unless the mass is large or contains dystrophic calcifications, which are found in up to 30% of cases. Direct bony invasion is seen in ~30% (range 11–50%) of cases, with aggressive bone features (permeative, geographic, or moth-eaten appearances).

Ultrasound: Non-specific findings, with a heterogeneous predominantly hypoechoic mass.

CT: CT is non-specific, similar to ultrasound. It appears as a soft tissue mass of heterogeneous density and enhancement.

MRI is the modality of choice to stage the tumor locally, although again imaging findings are not pathognomonic. T1: iso- (slightly hyper-) intense to muscle and heterogeneous; T2- mostly hyperintense. The markedly heterogeneous appearance of synovial cell sarcomas on fluid-sensitive sequences results in

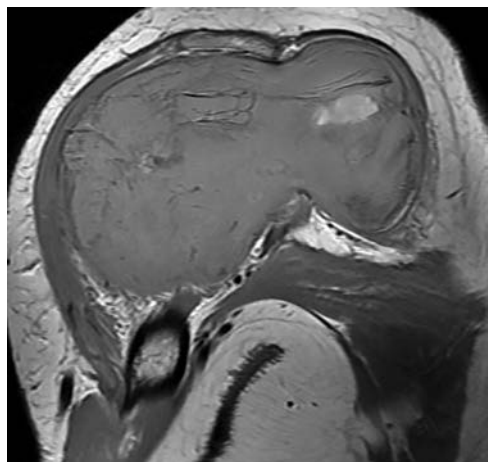


Fig. 4.155.1

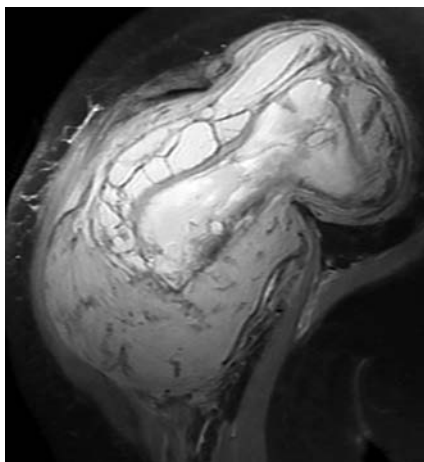


Fig. 4.155.2

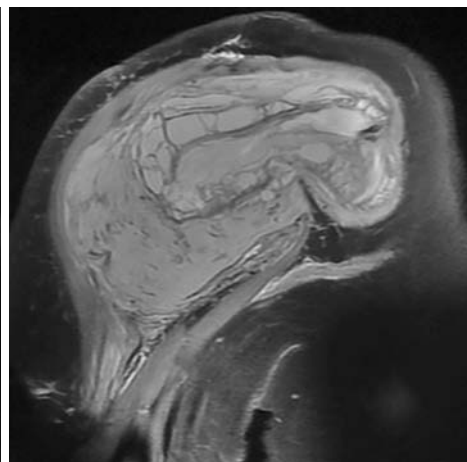


Fig. 4.155.3

Differential diagnosis

Myxoid liposarcomas: Typically found in adults (40–60 years) and are rare in children. They are usually seen in the extremities (75%), most commonly the thigh, and are less commonly seen in the retroperitoneum, groin or elsewhere. Contains lipoblasts. Surgical excision if symptomatic.

Radiographic; Nonspecific soft tissue mass with density greater than fat. USG- Complex hypoechoic mass. Internal vascularity on Doppler sonography. CT: Well defined mass with attenuation higher than fat but lower than muscle. Calcification uncommon. MRI: Low signal on T1WI. High signal on T2WI, Heterogeneous to homogeneous enhancement. More intense enhancement associated with worse prognosis. Lesions with round cell components have more variable appearance.

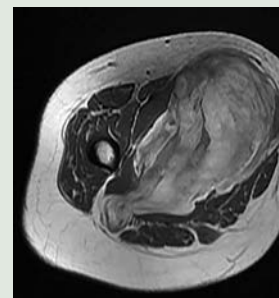


Fig. 4.155.4: Myxoid liposarcomas

Nodular fasciitis: Rapidly growing painful mass in middle aged patient. Found adherent to fascia. The lesion is more common in Upper extremity > thigh > head/neck > chest wall, back. Most common in volar aspect of forearm. Surgical excision if symptomatic.

CT shows nonspecific mass of soft tissue density. Myxoid lesions: ↓ attenuation than muscle. MRI: T1WI: Similar intensity to skeletal muscle. T2WI: Intermediate to high signal intensity. Mild surrounding edema. Enhancement varies with content of lesion. Ossification and calcification rare (ossifying fasciitis). Extension of mass along fascia suggests diagnosis.

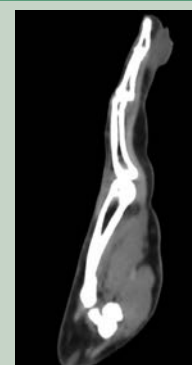


Fig. 4.155.5: Nodular fasciitis

Leiomyosarcoma: Malignant neoplasm arising from smooth muscle cell. Arises in skin, soft tissue, blood vessel. It occurs most commonly in thigh. Age: Most common in middle-aged adults or elderly. Treatment include surgical excision with wide margins. Complete excision difficult with retroperitoneal tumors. Adjuvant chemotherapy or radiation therapy may be needed.

Radiographs may be normal or show soft tissue mass. Moderately vascular or hyper vascular tumor on Doppler US or angiography. CT: Nonspecific soft tissue mass ± calcification. Low-attenuation regions may reflect necrosis, hemorrhage, or cystic change. MR: Nonspecific soft tissue mass with deceptively encapsulated appearance. T1WI: Homogeneous to heterogeneous, hypointense to slightly hyperintense signal. T2WI: Heterogeneously hyperintense to muscle. May contain fluid-fluid levels from hemorrhage. Intense, heterogeneous enhancement.

Intramuscular myxoma: Benign, soft tissue neoplasm with prominent myxoid stroma. Usually occurs in intramuscular plane (82%) and has a predilection for large muscles affecting thigh (51%), buttocks (7%), shoulder girdle/upper arm (9%). Mazabraud syndrome – polyostotic fibrous dysplasia + intramuscular myxoma.

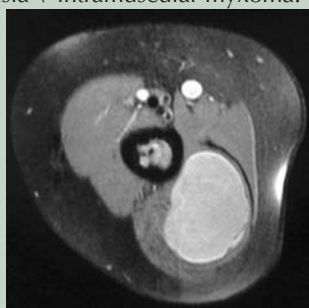


Fig. 4.155.6: Intramuscular myxoma

Radiograph: Usually normal (55%). Focal area of decreased density in soft tissues (45%). USG: Well-circumscribed mass. Heterogeneously hypoechoic to near anechoic. Small anechoic cystic areas in 85%. Bright rim sign of increased echogenicity around lesion corresponding to fat surrounding rim. CT: Attenuation of mass is between fluid and muscle. Mild diffuse enhancement or peripheral and septal enhancement in 50%. MRI: Homogeneous to mildly heterogeneous ± septa ± cystic foci. Low to intermediate signal intensity on T1WI. MR Characteristic rim of fat, especially around superior and inferior poles of lesion may represent atrophy of adjacent muscle. High signal intensity on fluid-sensitive sequences. High signal surrounding lesion from leakage of myxomatous tissue is common. Often flame-shaped or brush-like, along longitudinal muscle fascicles. Cystic areas in 50%. Mild to moderate enhancement. Enhancement pattern—diffuse or shows thick peripheral and septal pattern.

Alveolar rhabdomyosarcomas: Most common soft tissue tumor in children. Age: Predominantly infants to adolescents; most < 5 years of age → Children to young adults with male predominance. Combination of surgery, chemotherapy, and radiotherapy based on patient's risk of recurrence.

Radiograph: Permeative bone invasion in approximately 1/4 ± periosteal reaction. Bone metastases lytic or mixed sclerotic and lytic. USG: Heterogeneous echogenicity ± prominent vascularity on Doppler. CT: Circumscribed to infiltrative soft tissue mass. Heterogeneously enhances ± necrosis and/or hemorrhage. MRI: T1—low to intermediate intensity, isointense to muscle. T2—hyperintense. Heterogeneous enhancement dependent on vascularity and hemorrhage/necrosis. High-flow vessels, especially alveolar type. Bone scan: Useful for detection of bone invasion and bone marrow metastases. PET: F-18 FDG-avid tumors.

Aggressive fibromatosis: True neoplasm that arises from the fascial and musculo-aponeurotic coverings. Mean age at presentation is ~40 with supraclavicular fossae and neck being the most common locations. Recurrence common.

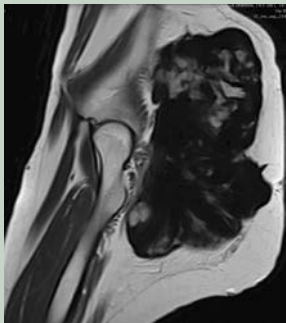


Fig. 4.155.7: Aggressive fibromatosis T2 hypointense

Poorly margined and seen infiltrating the surrounding tissues. The lack of metastasis can help distinguish aggressive fibromatosis from a fibrosarcoma. MRI-T1 homogeneously isointense or mildly hyperintense; high heterogeneous signal in T2/STIR; typically enhances avidly in T1 C.

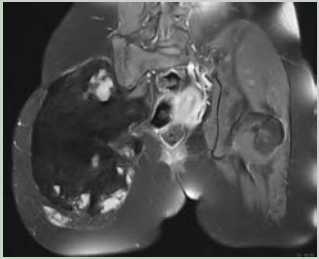


Fig. 4.155.8: Aggressive fibromatosis (post-contrast)

Angiosarcoma: Malignant endothelial neoplasm with exceptionally poor prognosis. Location: Majority involve skin and subcutis. Deep muscles of lower extremities are more commonly affected than arm, trunk and head. Age: All ages; peak incidence in 7th decade: Rare in childhood, M > F (2:1).

CT: Nodular, infiltrative soft tissue mass. Attenuation is similar to muscle. MRI: Isointense to hyperintense (due to hemorrhage) relative to skeletal muscle on T1WI. Hyperintense to muscle on fluid-sensitive sequences – Hemorrhage may also produce fluid-fluid levels. Superficial lesions show skin thickening with prominent enhancement. Serpiginous enhancing vessels relatively common in periphery of deep lesions. Treatment includes surgical excision often combined with radiotherapy. Adjuvant chemotherapy has evolving role.

Other differential diagnosis: Benign fibrous tumours, soft tissue metastases, myositis ossificans, non-tumoral conditions—hematoma, abscess, bursitis, hemangioma, neurofibroma/ neurofibrosarcoma.

Soft tissue hemangioma with phlebolith



Fig. 4.155.9: Soft tissue hemangioma with phlebolith

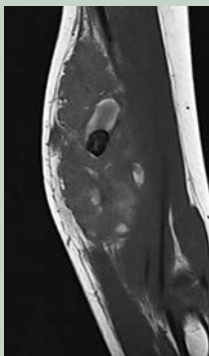


Fig. 4.155.10: Soft tissue hemangioma with phlebolith

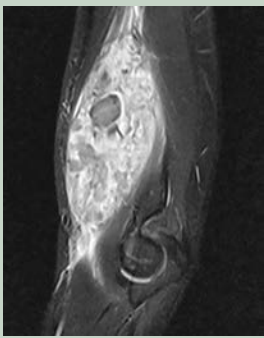
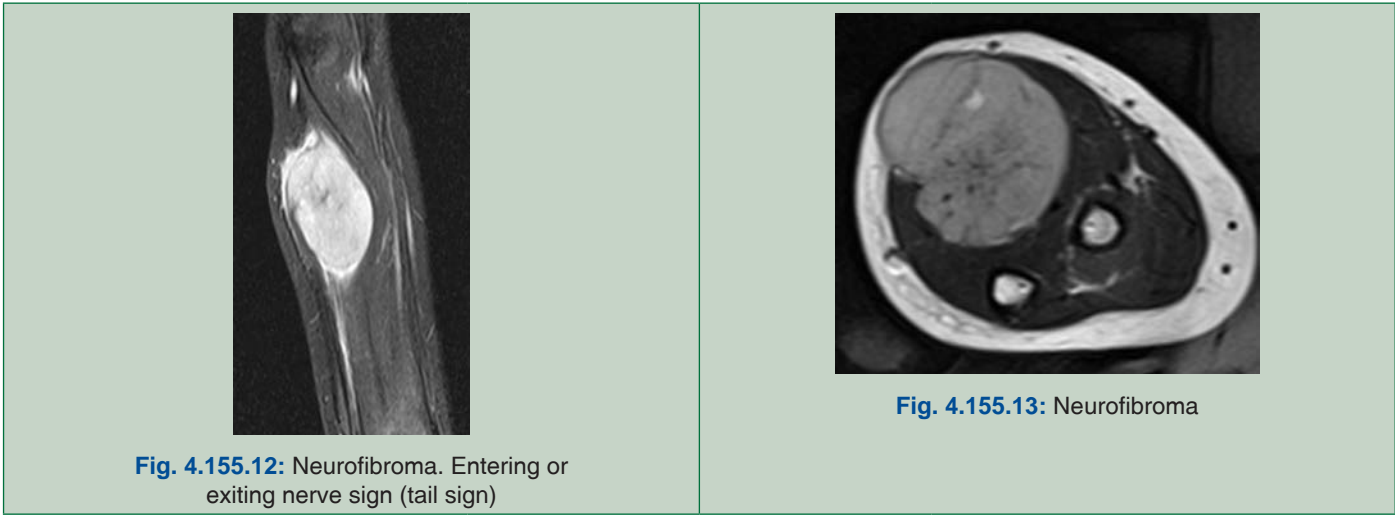


Fig. 4.155.11: Soft tissue hemangioma with phlebolith

Neurofibroma: Target sign: Seen in T2W MRI as central hypointensity (fibrocollagenous core) surrounded by a hyperintense rim (myxomatous tissue).

Fascicular sign: Seen on T2 weighted MRI that suggests a lesion of neurogenic origin. Characterized by multiple small ring-like structures with peripheral hyperintensity representing fascicular bundles within the nerves.



| Table 4.155.1: WHO classification of soft tissue tumors | |
|---|-------------------------------------|
| Adipocytic tumors | Skeletal muscle tumors |
| Fibroblastic/ myofibroblastic tumors | Gastrointestinal stromal tumors |
| Fibrohistiocytic tumors | Chondro-osseous tumors |
| Vascular tumors | Peripheral nerve sheath tumors |
| Pericytic (perivascular) tumors | Tumors of uncertain differentiation |
| Smooth muscle tumors | |

so-called “triple sign” which is due to areas of necrosis and cystic degeneration (very high signal), areas of soft tissue components (relatively high signal) and areas of dystrophic calcifications and fibrotic bands (low signal intensity). Due to (two times present) the high tendency of lesions to bleed, there might be areas of fluid-fluid levels known as “bowl of grapes”. T1 C + (Gd): Enhancement is usually prominent and can be diffuse (40%), heterogeneous (40%) or peripheral (20%). Nuclear medicine: On bone scan, synovial sarcomas typically have heterogeneously increased dynamic and blood pool uptake, with some increase in delayed images, but usually less intense.

Treatment and prognosis: Combination of surgery and usually adjuvant radiotherapy +/- chemotherapy. Radiotherapy is particularly useful in treating tumors where an adequate clear margin cannot be achieved, and ideally, radiotherapy is administered pre-operatively. Overall, 5-year survival is between 36–76%. Both local recurrence (30–50%) and distant metastases are frequent (40–70%), most commonly to the lungs (~80%), bones (~15%), regional lymph nodes (~10%), followed by chest wall/abdomen (~7.5%).

Approach to soft tissue tumors: Differentiating many soft tissue masses as benign vs. malignant with imaging alone can be exceptionally difficult. If a lesion is not pathognomonic for a specific benign entity, then it should be regarded as a potentially malignant mass. Superficial soft tissue masses larger than 5 cm in greatest dimension have a 10% chance of being a sarcoma.

Staging and prognosis: The most commonly utilized staging system is the American Joint Committee on Cancer (AJCC) staging system. Staging is based on histologic grade (three-grade system), primary tumor size and depth, and presence of nodal disease and distant metastases. It does not take into account anatomic site or whether tumor extends outside the compartment of origin.

Patient prognosis is most directly related to the presence of nodal and distant metastatic disease. The sites of soft tissue sarcoma metastatic disease are highly dependent on the tumor type. The presence of nodal metastases indicates stage III disease. Lymph nodes are considered suspicious for tumor involvement by imaging if they are greater than 1 cm in short-axis dimension with obliteration of the fatty hilum, as identified on CT or MR. PET/CT demonstrates increased F18 FDG tracer uptake

Table 4.155.2: Note on benign soft tissue fibrous tumors and their mimics

| <i>Benign fibrous tumours</i> | <i>Infection and inflammation</i> | <i>Vascular mimics</i> |
|---|--|---|
| Nodular and proliferative fasciitis Bizarre parosteal osteochondromatous proliferation Myofibroma/ myofibromatosis Fibromatosis colli Juvenile hyaline fibromatosis Fibroma of tendon sheath Desmoplastic fibroblastoma Calcifying aponeurotic fibroma | Soft tissue abscess Bursitis Synovitis Arthroplasty component wear/particle disease Foreign body granuloma Myositis Denervation hypertrophy AV fistula Diabetic myonecrosis Calcific myonecrosis Morel-Lavallée lesion | Haematoma, Aneurysm, pseudoaneurysm, cystic adventitial disease Other mimics: Myositis ossificans, ganglion/synovial cyst, fat necrosis, amyloid deposition, post-injection fibrosis, hemophilia, Hoffa disease, granuloma annulare, fascial hernia |

Table 4.155.3: Soft tissue and periarticular calcifications

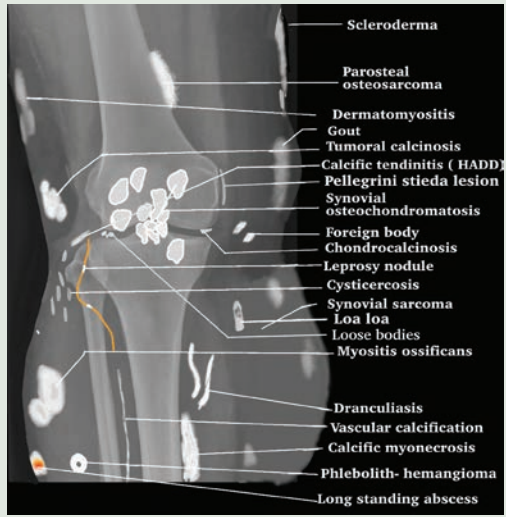
| | |
|--|--|
| Vascular: Hemangioma (press button calcification). Arterial calcification, phleboliths |  |
| Trauma: Myositis ossificans (peripheral calcification), tendinitis, long standing abscess | |
| Metabolic: CPPD, tumoral calcinosis, fluorosis, gout, hyperparathyroidism, chondrocalcinosis—calcification of TFCC, meniscus, ligaments in spine. | |
| Autoimmune: Scleroderma, dermatomyositis, calcinosis cutis | |
| Infection: Cysticercosis, dracunculosis | |
| Neoplasm: Osteosarcoma (central calcification), synovial sarcoma | |

Fig. 4.155.14: Soft tissue and periarticular calcifications

in malignant lymph nodes. Since nodal involvement is uncommon in soft tissue sarcomas, its presence should initiate further work-up for distant metastases. The majority of distant metastases involve the lung. Myxoid liposarcoma has an unusual tendency to

metastasize to other soft tissue sites. Retroperitoneal sarcomas have an increased incidence of metastasis to liver. The presence of distant metastases confers stage IV disease. This has an overall 10 to 20% 5-year survival rate.

4.156 MUSCULOSKELETAL SYSTEM

Case No. 156

Clinical history: 38 years old male with complaints of pain over bilateral hip joint, increasing with weight bearing and movement

Radiological technique and observation: Figure 4.156.1 is frontal radiograph of hip showing diffuse sclerosis of bilateral femoral head with irregularity of the articular surface. Crescent sign noted in left femur. Uniform Joint space maintained with preserved acetabulum (implies no joint disease). No evidence of any lytic lesion/soft tissue swelling. No widening of pubic symphysis. Figures 4.156.2 and 4.156.3 are MRI STIR and T1 coronal views showing a geographic circumscribed lesion with hypointense sclerotic rim in bilateral femoral head with minimal bilateral joint effusion. No joint space narrowing. No evidence of any other lesion noted in the visualized bone.

Interpretation: A: 38 years old male, lesion in bilateral femoral head; C: Diffuse sclerosis with irregularity of the articular surface; MRI showing circumscribed geographic lesion with sclerotic rim; B: Preserved joint space with normal acetabulum; D: AVN of bilateral femoral head.

Principal diagnosis: Avascular necrosis: Stage 2 on right head of femur and stage 3 on the left head of femur (based on modified Ficat and Arlet grading).

Brief discussion: Avascular necrosis

Pathogenesis: Loss of blood supply due to injury/compression of the vessels → 1. Avascular phase → necrosis of the vulnerable anterosuperior aspect of the femoral head → 2. Revascularization phase → deposition and resorption of bone with neovascularization of periphery and center → 3. Repair and remodeling

→ bone deposition and regression of osteoclasts → 4. Deformity. Blood supply to head of femur is by medial and lateral circumflex arteries (branch of profunda femoral artery) and the artery to fovea through the ligament teres (branch from the obturator artery).

General radiological features of AVN: Patchy sclerosis of femoral head; crescentic lucency indicative of fracture; collapse of articular cortex; articular surface fragmentation; 2° osteoarthritis (OA): Joint space narrowing, acetabular subchondral sclerosis, osteophyte.

MRI IN AVN: Subchondral fractures appear as T1 hypointense smooth, concave line (parallel to the articular cartilage) and circumscribes the entire necrotic area. T1 → circumscribed geographic subchondral lesion in the anterosuperior aspect of the femoral head. T2 → Double line sign → outer hypointense line (sclerosis) and inner hyperintense line (zone of hyperemia and granulation).

Radionuclide scan: Bone seeking agent ^{99m}Tc MDP (20–30 mCi) or marrow seeking agent ^{99m}Tc sulfur colloid used. Images are acquired in angiographic, blood pool static and delayed planar phases. Early disease → photopenia in the anterosuperior aspect of the femoral head → pathognomonic of AVN (due to interrupted blood supply). Late → doughnut sign—central photopenia with peripheral increased uptake due to reactive hyperemia, osteoblastic and reparative response.

Treatment: Early diagnosis is needed as there is continuous progression of the osteonecrosis of the hip. Initially with <50% collapse of the femoral head → core decompression can be tried. >50% involvement requires arthroplasty.



Fig. 4.156.1

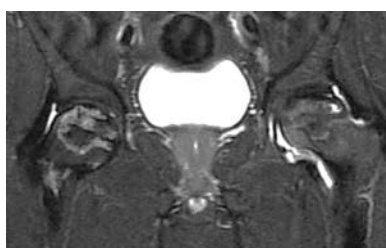


Fig. 4.156.2

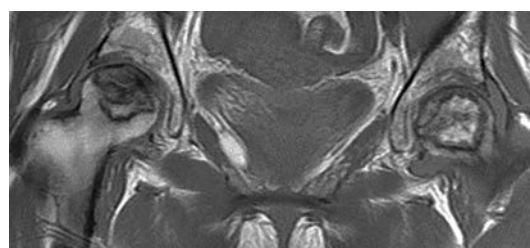


Fig. 4.156.3

Table 4.156.1: Differential diagnosis of avascular necrosis

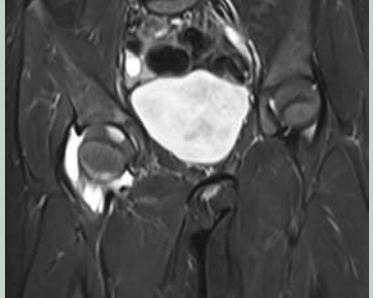
| | | |
|---|--|--|
| <p>Transient bone marrow edema: (transient osteoporosis of hip) Painful bone marrow edema of unknown etiology and self-limiting condition, common in 2nd and 3rd decades, especially in pregnant women and middle-aged men.</p> | <p>X-ray: Osteopenia with cortical thinning and prominent trabeculae within 8 weeks of onset of pain. MRI: Femoral head marrow edema ↓ T1W, ↑ T2W; enhancement with contrast, peak enhancement may be delayed. May show subchondral fractures. Portions of femoral head/neck/greater trochanter may exhibit completely normal signal ± involvement of acetabulum. No changes indicating irreversibility</p> |  <p>Fig. 4.156.4: Transient osteoporosis of bilateral hip joints</p> |
| <p>Stress fractures: Common in long distance runners, osteoporotic females following a trivial trauma.</p> | <p>X-ray: Normal. MRI is the investigation of choice showing T1 and T2 hypointense fracture line, surrounded by a hypointense edema on T1 that is hyperintense on T2 and STIR sequences.</p> |  <p>Fig. 4.156.5: Stress fracture in neck of femur</p> |
| <p>Pseudofractures: Also called cortical infarctions, looser's zones, and milkman lines. Rarefaction zones can range in diameter from a few millimetres to several centimetres, impacting various parts of the skeletal system and are usually symmetrically distributed.</p> | <p>Pseudofractures: When viewed en face, those associated with some malacic disorders may look as small, subperiosteal notches in the cortex or as small, irregularly circular, punched-out zones of decalcification.</p> |  <p>Fig. 4.156.6: Looser's zones</p> |
| <p>Idiopathic chondrolysis of hip: The patient presents with insidious onset of pain around the hip, progressive stiffness and limp. Involvement can be unilateral or bilateral. It is characterized by extensive loss of articular cartilage of the proximal femoral epiphysis and acetabulum with resultant joint space narrowing and restriction of motion.</p> | <p>Radiographic hallmarks include a concentrically narrowed joint space <3 mm without osteophyte formation, accompanied by osteopenia. MRI findings include cartilage loss, more severe centrally and on femoral side; bone remodelling, mild synovial hypertrophy, a little or no joint fluid and widespread marrow edema of femoral head, neck and acetabulum. Geometric or polygonal focal marrow edema centered in the middle one-third of the affected proximal femoral epiphysis on coronal images.</p> |  <p>Fig. 4.156.7: Idiopathic chondrolysis of hip (R)</p> |

Table 4.156.2: Causes of avascular necrosis

| Causes of avascular necrosis (Mnemonic— PLASTIC RAGS) | |
|---|---|
| Pancreatitis, pregnancy | Rheumatoid arthritis, Radiation therapy |
| Legg-Calve-Perthes disease, Lupus erythematosus | Amyloid disease |
| Alcoholism, Atherosclerosis | Gaucher disease |
| Steroids | Sickle cell disease |
| Trauma | |
| Idiopathic, Infection | |
| Caisson disease, Collagen disease (SLE) | |

Table 4.156.3: Classification of avascular necrosis

| FICAT and ARLET classification | | Steinberg staging | |
|--------------------------------|---|-------------------|---|
| Stage | Radiological findings | Stage | Radiological findings |
| I | Plain radiograph, MRI and scintigraphy—normal | 0 | Normal radiograph, MRI and bone scan |
| IIA | Sclerotic and cystic lesion | I | Normal radiograph; abnormal bone scan and/or MRI |
| IIB | Subchondral collapse (crescent sign) and/or subchondral aliasing | II | Cystic and sclerotic radiographic changes |
| III | Irregular femoral contour | III | Subchondral lucency or crescent sign |
| IV | Collapse of femoral head, acetabular involvement and articular destruction (osteoarthritis) | IV | Flattening of femoral head, with depression graded into Mild < 2 mm Moderate 2–4 mm Severe >4 mm |
| | | V | Joint space narrowing with or without acetabular involvement |
| | | VI | Advanced degenerative changes |

Crescent sign: In radiograph, refers to curvilinear lucent subchondral line due to subchondral fracture. In MRI, the subchondral fracture cleft may be filled with fluid.

Table 4.156.4: Avascular necrosis and bone infarct

| | |
|---|---|
| Avascular necrosis: Death of bone and marrow elements secondary to the loss of blood supply. This term is used for the lesions located in the subchondral region of the bones. | Bone infarct: Death of the bone and marrow elements secondary to the loss of blood supply occurring in the metaphyseal and diaphyseal region away from the subchondral region. |
|---|---|

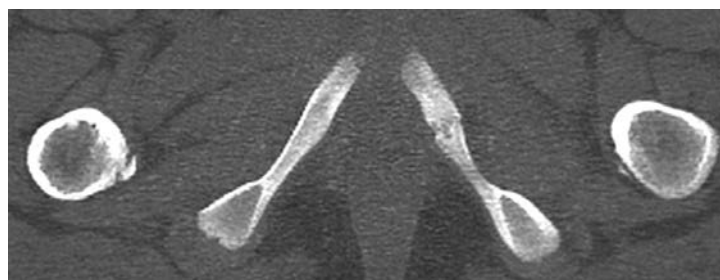
**Fig. 4.156.8:** Legg-Calve-Perthes disease**Fig. 4.156.9:** Kienbock's disease**Fig. 4.156.10:** van Neck-Odelberg disease

Table 4.156.5: Osteonecrosis in other sites

| Name | Important features | Location |
|---|---|---|
| Blount's disease >6 years | Enlarged and deformed medial tibial condyle, metaphyseal irregularity with posteromedial beak | AVN of medial tibial condyle |
| Calvé-Kümmel-Verneuil disease 2–15 years | Uniform collapse of vertebral body into thin disc with increased density. Spares neural arch. Normal intervertebral disc space with intervertebral vacuum cleft (pathognomonic) | AVN Vertebral body also known as vertebral osteochondrosis/ vertebra plana |
| Freiberg disease 10–18 years M: F = 1:3 | Increased density with widened metatarso-phalangeal joint. Late-sclerosis with flattening, fragmentation and cortical thinning | AVN of head of 2nd (3rd/4th) metatarsal. |
| Keinbock's disease 20–40 years | Increased density, altered shape and collapse of lunate bone. Associated with negative ulnar variance | AVN of lunate |
| Kohler's disease 3–10 years | Irregular outline with fragmentation, increased density with maintained joint space. | AVN of tarsal scaphoid/ navicular bone |
| Legg-Calve-Perthes disease 2–12 years M: F= 5:1 | Epiphysis smaller than the opposite side. Widened joint space, demineralisation of bone, crescent sign-subchondral fracture. CT-loss of asterisk sign; MRI-double line sign and joint incongruity. | Idiopathic AVN of femoral head In adults idiopathic AVN– Chandler's disease |
| Preiser's disease | Sclerosed scaphoid bone with collapse in late stages. | Non-traumatic AVN of scaphoid |
| Sinding-Larsen-Johansson disease 10–14 years | Chronic traction injury of immature osteotendinous junction affecting the proximal end of patellar tendon. Dystrophic calcification/ossification may occur. MRI: High T2/STIR signal intensity. | Traction tendinitis of proximal patellar tendon. Immature osteotendinous junction |
| Jumper's knee Adult counterpart of Sinding-Larsen-Johansson disease | Chronic injury of the proximal and posterior fibres of the patellar tendon at the origin site (the inferior pole of the patella). | Traction tendinitis of proximal patellar tendon. |
| Osgood-Schlatter disease | X-ray: Ossification and thickening in the inferior patellar ligament at tibial tubercle. MRI: Bone marrow edema adjacent to tibial tubercle. Inferior patellar tendon and adjacent soft tissues show thickening and edematous changes. | Traction apophysitis of patellar ligament insertion on tibial tubercle. |
| Sever's disease | May show oedematous changes within the calcaneal apophysis, possibly extending into the adjacent calcaneal tuberosity. | Calcaneal apophysitis |
| Iselin's disease | X-ray: Obliquely oriented bony fleck at base of 5th metatarsal. MRI: T2/STIR hyperintensity around the base of 5th metatarsal due to bone marrow edema. | Apophysitis of the base of 5th metatarsal |
| van Neck-Odelberg disease | X-ray: Enlarged unilateral ischiopubic synchondroses. MRI: T2 hypointensity with adjacent edema as T2 and STIR hyperintensity. | Hyperostosis of the ischiopubic synchondrosis |
| Panner disease | MRI: T1/ T2 hypointensity in the capitellum | Osteochondrosis of the capitellum |
| SONK (Spontaneous osteonecrosis of knee) Elderly women with no risk factors for osteonecrosis | It is the insufficiency fracture in the knee. X-ray: Flattening of medial femoral condyle, subchondral radiolucent focus. MRI: Subchondral bone plate fracture, focal subchondral area of low signal intensity subjacent to the subchondral bone plate representing local ischemia. | Occurs in the knee joint. Aka Subchondral insufficiency fracture of the knee (SIF/SIFK) |
| Osteochondritis Dissecans More common in atheletes, gymnastics and in families with history of epiphyseal dysplasias. | Aseptic separation of the osteochondral fragment with gradual fragmentation of the articular surface. X-Ray- lucent region in early stages followed by mixed lytic and sclerotic regions with intra-articular loose bodies. MRI: T1 variable and T2 high signal line demarcating fragment from the bone with T2 hypointense loose bodies. | Occur in medial femoral condyle, capitellum, talus and glenoid |
| Scheuermann disease | Vertebral endplate irregularity due to disk invagination, intervertebral disk space narrowing, more pronounced anteriorly. The condition is associated with Limbus vertebrae, Scoliosis (~25%), Schmorl nodes, spondylolisthesis. | Vertebral epiphysitis results in kyphosis of the thoracic or thoracolumbar spine |

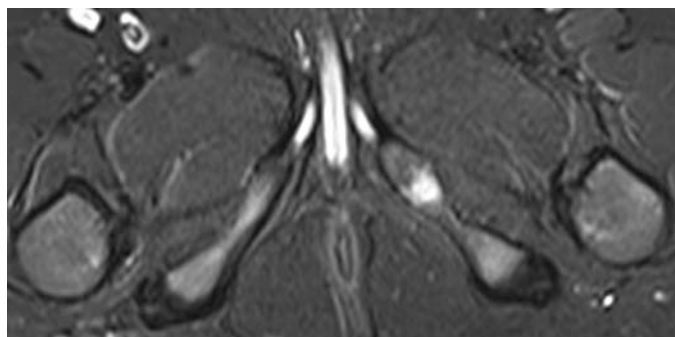


Fig. 4.156.11: van Neck-Odelberg disease



Fig. 4.156.12: Osgood-Schlatter disease



Fig. 4.156.13: Freiberg disease



Fig. 4.156.14:
Osteochondritis dessicans



Fig. 4.156.15: Blount's disease

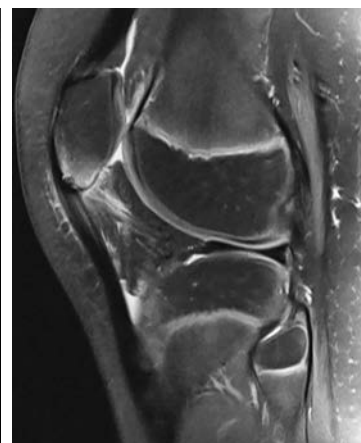


Fig. 4.156.16: Jumper's knee

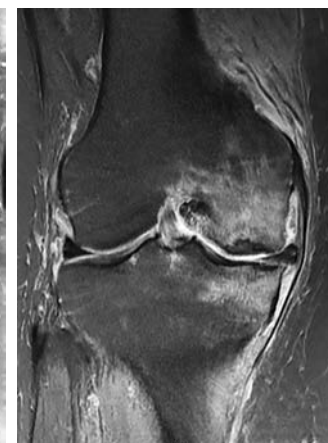


Fig. 4.156.17: SONK
(spontaneous osteonecrosis
of knee)



Fig. 4.156.18: Sinding-Larsen-Johansson disease

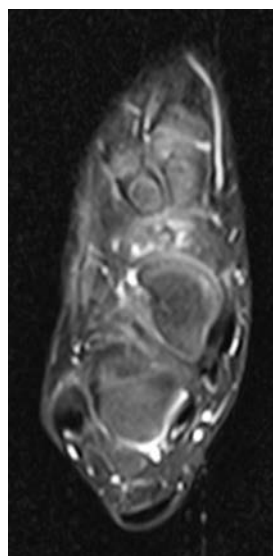


Fig. 4.156.19: Kohler's
disease

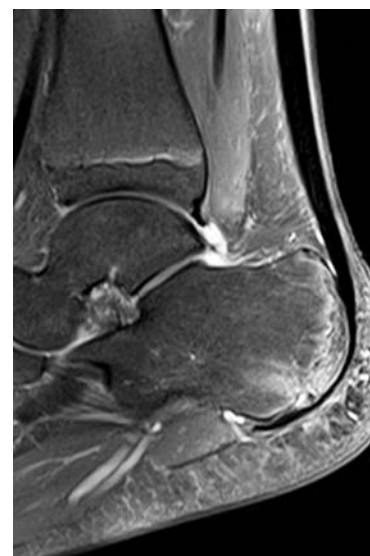


Fig. 4.156.20: Sever's disease

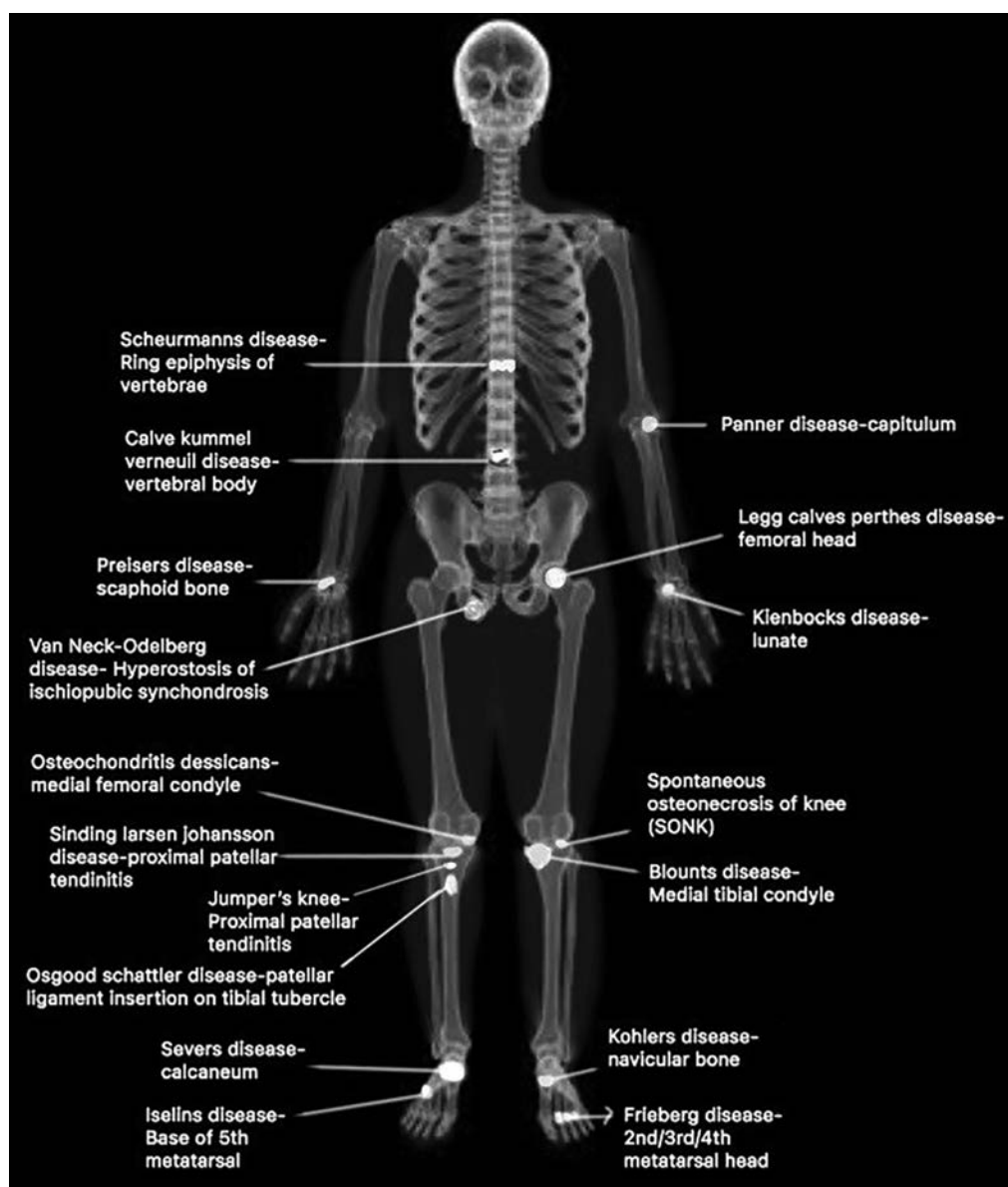


Fig. 4.156.21: Whole body illustration of avascular necrosis



Fig. 4.156.22: Scheuermann's disease

4.157 MUSCULOSKELETAL SYSTEM

Case No. 157

Clinical history: 54-year-old female patient presented with complaints of pain in both hands.

Radiological techniques and observations: Figures 4.157.1 to 4.157.4 are radiograph of both hands AP and oblique view. There is diffuse cartilage loss, with joint space narrowing in the distal interphalangeal (DIP) joints, proximal interphalangeal (PIP) joints and first carpometacarpal (CMC) joint with subchondral erosions, typically central in location producing the classic “gull wing” appearance. Joint ankylosis is noted. There is absence of marginal erosions/fusiform soft-tissue swelling/osteopenia.

Interpretation: A–54-year female patient with pain in both hands; C–Cartilage loss, with joint space narrowing in the distal interphalangeal (DIP) joints, proximal interphalangeal (PIP) joints and first carpometacarpal (CMC); B–Gull wing shaped central subchondral erosions with joint ankylosis without evidence of marginal erosions/osteopenia; D–Erosive osteoarthritis.

Principal diagnosis: Erosive osteoarthritis

Management: The report needs to be highlighted to the referring clinician immediately.

Discussion**Types of arthritis:**

Degenerative: Osteoarthritis

Neuropathic joint

Crystalline arthritis: Gout, calcium pyrophosphate dihydrate (CPPD) crystal deposition disease, hydroxyapatite deposition disease (HADD).

Inflammatory-seropositive- Rheumatoid; **Seronegative-** ankylosing spondylitis, psoriatic arthritis, enteropathic arthritis, Reiter's (Reactive) arthritis.

Connective tissue disorders: SLE, Scleroderma, Sjögren's syndrome, dermatomyositis and polymyositis, rheumatic fever (Jaccoud's arthropathy), mixed connective tissue disease (MCTD).

Infectious: Septic arthritis

Hemorrhagic: Hemophilic arthropathy

Miscellaneous: Diffuse idiopathic skeletal hyperostosis, PVNS, synoviochondrometaplasia.

Note: Both psoriatic and erosive arthritis has gull wing appearance, but psoriatic arthritis has additional features of pencil in cup deformity, involvement of SI joints, skin and DIP, central erosion, acral osteolysis.

Chondrocalcinosis: CPPD crystal deposition disease, haemochromatosis, gout, hyperparathyroidism, Ochronosis, Wilson's disease.



Fig. 4.157.1



Fig. 4.157.2



Fig. 4.157.3



Fig. 4.157.4

Table 4.157.1: Pearls on non-erosive osteoarthritis, rheumatoid arthritis and psoriatic arthritis

| | |
|----------------------------|--|
| Non-erosive osteoarthritis | Distribution and degenerative changes is similar to erosive osteoarthritis, but no erosions are seen |
| Rheumatoid arthritis | Different joint distribution- proximal joints |
| Psoriatic arthritis | 1st carpometacarpal joint, scaphotrapezium and scaphotrapezoid joints are not involved (these joint involvement is typical for osteoarthritis) |

Table 4.157.2: Differential diagnosis for arthritis

Degenerative non-erosive osteoarthritis: Seen predominantly in weight bearing joints. The most affected joint is the knee. In the foot, the first MTP joint is the most commonly afflicted. Asymmetric joint space narrowing, marginal osteophytes, subchondral cyst formation (geodes), loose bodies formation, subchondral marrow edema (visible as T1 hypointensity; T2/STIR hyperintensity), and subchondral sclerosis (T1/T1 hypointensity) are all common symptoms. Heberden nodes and Bouchard nodes are examples of eponymous osteophytes.



Fig. 4.157.5: Degenerative non-erosive osteoarthritis



Fig. 4.157.6: Degenerative non-erosive osteoarthritis

Neuropathic Joint (Refer to case 158)

Rheumatoid arthritis: Bilaterally symmetric. There is a predilection for: PIP and MCP joints (especially 2nd and 3rd MCP), ulnar styloid, triquetrum. As a rule, the DIP joints are spared. No ankylosis, No proliferative changes.

Late changes include subchondral cyst formation: The destruction of cartilage presses synovial fluid into the bone. Subluxation causes ulnar deviation of the MCP joints, boutonniere and swan neck deformities, hitchhiker's thumb deformity, carpal instability: scapholunate dissociation, ulnar translocation, ankylosis, scallop sign: erosion of the ulnar aspect of the distal radius which may be predictive of extensor tendon rupture (Vaughan-Jackson syndrome)



Fig. 4.157.7: Rheumatoid arthritis

Ankylosing spondylitis (Refer to case 63)

Table 4.157.2: Differential diagnosis for arthritis (Contd.)

Psoriatic arthritis: The combination of erosion and bone proliferation in a distal distribution is the characteristic (e.g. interphalangeal more than metacarpophalangeal joints, Hands>Feet)

The imaging findings include: Enthesitis and marginal bone erosions are prevalent, but not pathognomonic; “pencil-in-cup” deformities are common, but not pathognomonic; joint subluxation or interphalangeal ankylosis can occur. The bone around the diseased joint takes on an “fuzzy” appearance as a result of irregular bone proliferation. Periostitis can take the form of a new bone periosteal layer or an uneven thickening of the cortex itself. Dactylitis: This might manifest as a “sausage digit,” which refers to an entire digit’s soft tissue enlargement. An ultrasound examination of a sausage digit reveals synovitis and tenosynovitis beneath the surface. Ivory phalanx: The distal phalanx of the great toe is usually involved. Sacroilitis show asymmetric involvement. Acro-osteolysis; Arthritis mutilans is a severe form of psoriatic or rheumatoid arthritis characterised by bone resorption and subsequent soft tissue collapse, resulting in telescoping fingers.

**Fig. 4.157.8: Psoriatic arthritis**

Enteropathic arthritis: Refers to arthritis associated with inflammatory bowel disease (IBD). It can also be rarely triggered by enteritis due to *Salmonella*, *Shigella* or *Yersinia*. Axial skeletal involvement is seen predominantly with 15–20% of patients with IBD exhibiting peripheral arthritis more frequently seen with Crohn’s disease. There is asymmetric sacroiliac joint involvement with bone edema progressing to erosion, joint space loss to joint fusion.

Reactive arthritis: Formerly known as Reiter syndrome (urethritis, arthritis and conjunctivitis) but not all patients with reactive arthritis have Reiter syndrome. Extra-articular infection (GIT—*yersinia*, *salmonella*, *shigella*, *E. coli*, and GUT infection—*chlamydia*) causes a sterile inflammatory arthritis that develops 2 to 4 weeks after infection. Small and large joints of the lower limb (metatarsophalangeal joints >> calcaneus > ankle > knee) are commonly involved. Asymmetrical joint involvement, soft tissue swelling, joint space narrowing, proliferative marginal erosions, and sesamoid enlargement can all resemble psoriatic arthritis. New bone development at the entheses of the feet characterises this condition.

Gout: It is a crystal arthropathy due to monosodium urate crystals deposits in and around the joints. Seen >40 years of age. M:F = 20:1. Monoarticular red, inflamed, swollen joint. Treatment: NSAID, Steroids, newer cytokine blocking agents in refractory cases.

Usually affects small joints in hands and foot. Plain radiograph shows “punched-out” erosions with sclerotic margins: Rat bite erosions—seen in a marginal and juxta-articular distribution, with overhanging edges. Joint effusion is the earliest sign. No periarticular osteopenia. Tophi: Pathognomonic; Olecranon and prepatellar bursitis. Periarticular soft tissue swelling in tophi around the joints; Chondrocalcinosis (5%); joint space is lost only in late stages of disease. MRI-T1: Low signal intensity nodular lesions T2: Low/inhomogeneously mixed signal intensity.

**Fig. 4.157.9: Gout**

Calcium pyrophosphate dihydrate disease (CPPD): Also known as pyrophosphate arthropathy or pseudogout, is defined by the co-occurrence of arthritis with evidence of CPPD deposition within the articular cartilage, menisci or ligaments resulting in synovitis. It is the most common crystalline arthropathy, seen at 5th decade of life, equally affecting men and women. It is usually asymptomatic; however, acute arthritis can cause pain, swelling and restricted movement. It can be idiopathic, hereditary or secondary to hemochromatosis, hypothyroidism, ochronosis, hyperparathyroidism, hypomagnesaemia, etc. It can be monoarticular or polyarticular. Treatment includes anti-inflammatory drugs.

Symmetric in distribution and involve non-weight bearing joints or, in the hands, mainly involve the intercarpal and MCP (2nd and 3rd preferentially) joints, wrist joint (mainly radiocarpal and scapholunate joints). A stepladder pattern of joint narrowing is classically described in which the narrowing is progressively less severe from the radiocarpal joint to the midcarpal joint; Also affects patellofemoral joint, shoulder joint, elbow joint. Chondrocalcinosis can occur at knee: Medial meniscus and patellofemoral joint, wrist: triangular fibrocartilage complex and lunotriquetral ligaments, pubic symphysis, spine, chronic retro-odontoid pseudotumor, intervertebral disc.

Crowned dens syndrome: Acute pain and systemic inflammatory syndrome resulting from crystal deposition in the cruciform and alar ligaments surrounding the dens.

Contd.

Table 4.157.2: Differential diagnosis for arthritis (Contd.)

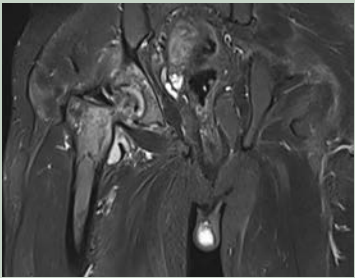
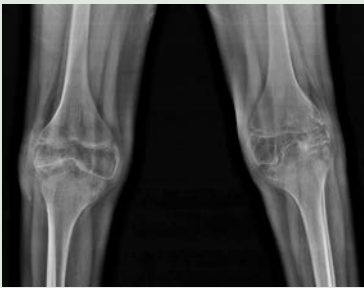
| | | |
|---|---|---|
| Septic arthritis: It is caused by intra-articular infection. Symptoms include painful joint, fever and purulent synovial fluid. <i>Staphylococcus aureus</i> is the most commonly isolated organism. Most commonly affected joints include shoulder, hip and knee. In IV drug abusers, sternoclavicular and sacroiliac joints are frequently affected. Principle treatment includes prompt drainage of purulent fluid and appropriate antibiotics. | Radiograph and CT: Usually normal in very early stage of the disease; joint effusion; narrowing of joint space due to cartilage destruction; subchondral bone destruction; juxta-articular sclerosis and ankylosis if left untreated. USG—joint effusion; increased peri-synovial vascularity. MRI T1: hypointensity within subchondral bone; peri-synovial edema with synovial enhancement. |  |
| Hemophilic arthropathy (Refer to case 160) |  | |
| Pigmented villonodular synovitis (Refer to case 160) | | |
| For spondyloarthropathies, refer to case 63 | | |

Fig. 4.157.10: Septic arthritis

Fig. 4.157.11: Hemophilic arthropathy

Table 4.157.3: Types of erosions

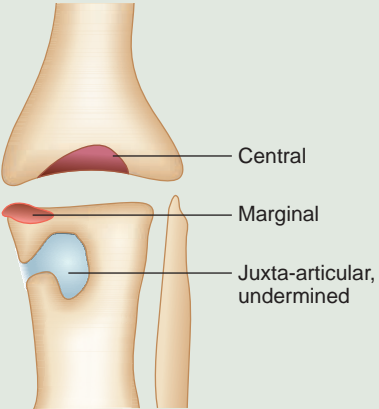
| | | | |
|-----------------|---|----------------------|---|
| Central | Occur into bone normally covered by articular cartilage | Erosive OA |  |
| Marginal | Involving the edge of joint line | Rheumatoid arthritis | |
| Juxta-articular | Occur away from the joint | Gout | |

Fig. 4.157.12: Types of erosions

Features of Arthritis in X-ray hand

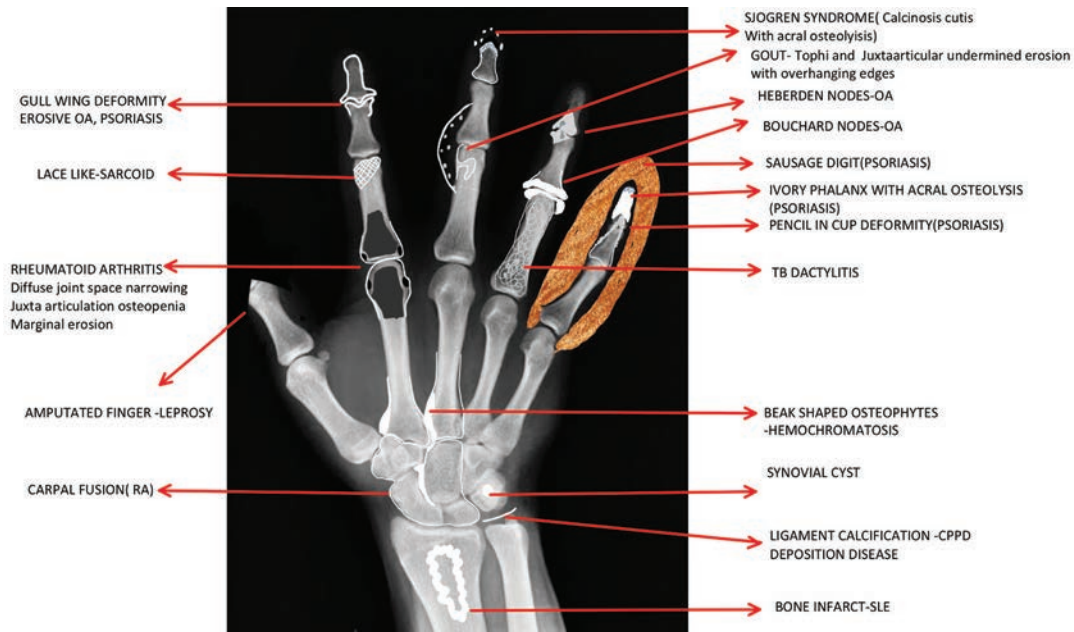


Fig. 4.157.13: Features of arthritis in X-ray hand



Fig. 4.157.14: Distribution of arthritis in X-ray hand

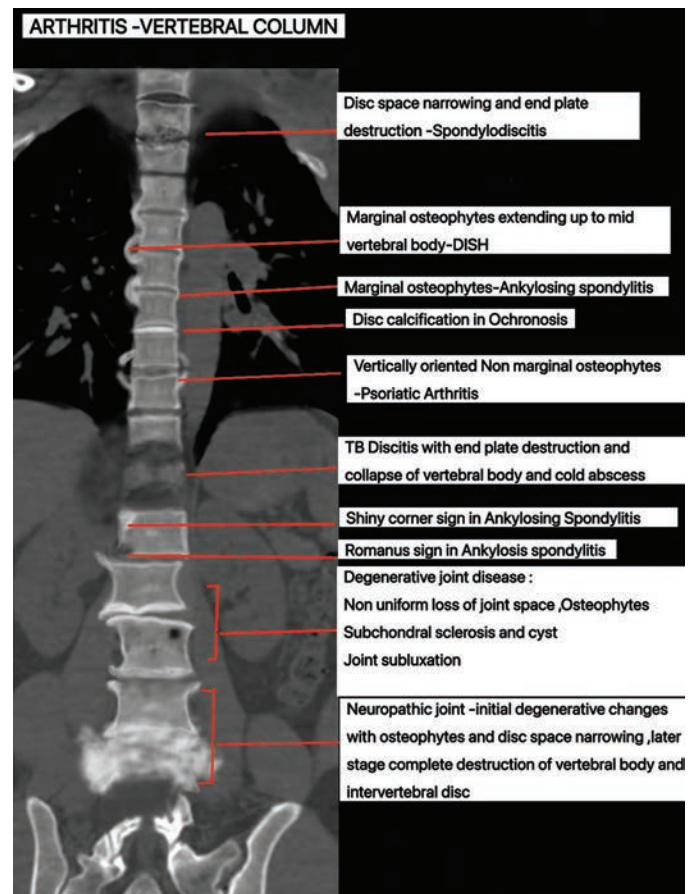


Fig. 4.157.15: Features of arthritis in spine

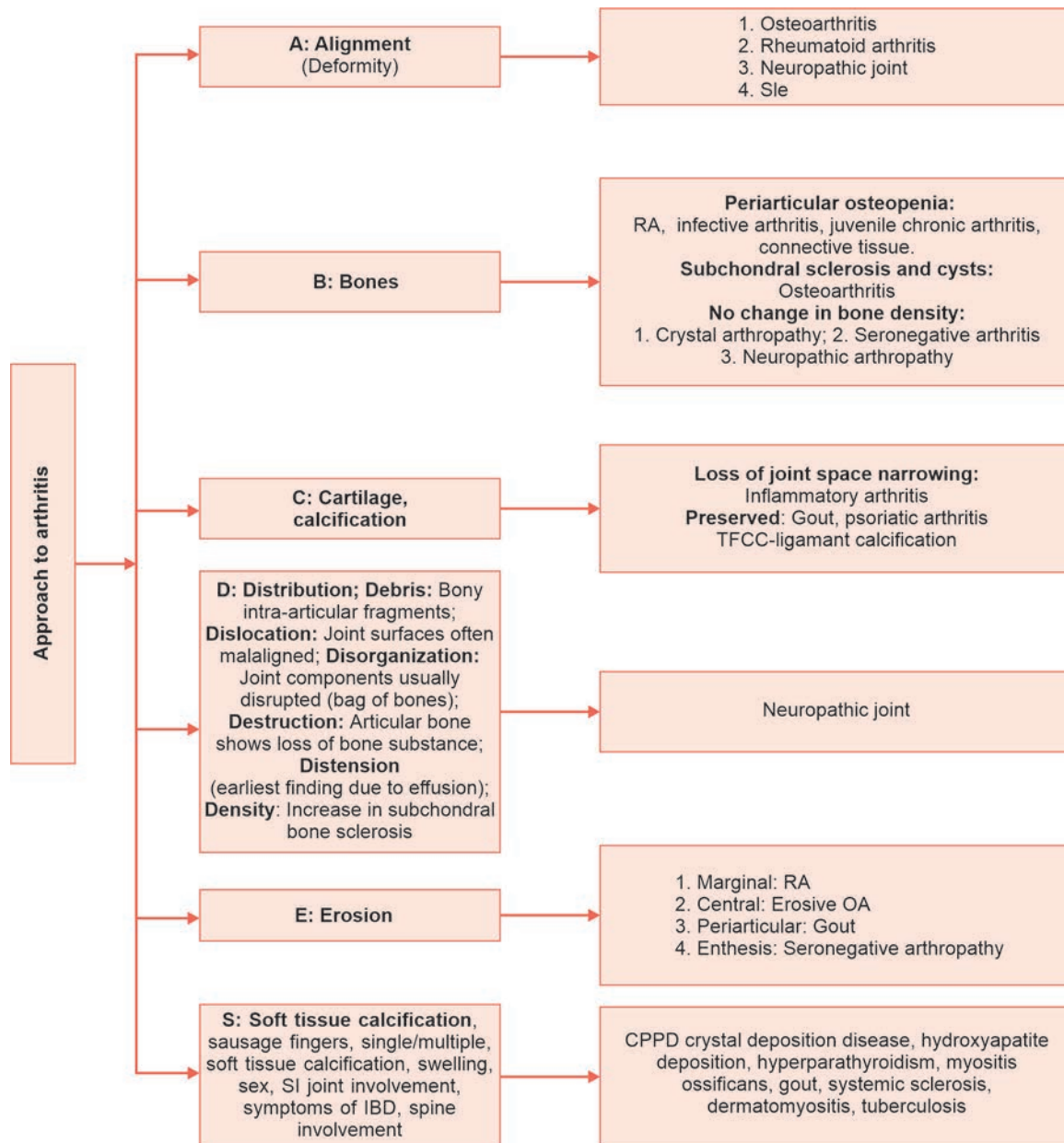


Fig. 4.157.16: Approach to arthritis: ABCDES

4.158 MUSCULOSKELETAL SYSTEM

Case No. 158

Clinical history: A 65-year-old diabetic female on insulin presented with complaints of swelling and pain over foot for 6 months with no history of trauma.

Radiological technique and observation: Figures 4.158.1 to 4.158.5 are frontal and lateral radiograph of foot, CT axial section in bone window and MRI foot sagittal T1 and STIR respectively. Radiograph and

CT show destruction, deformity and resorption of proximal tarsal bones and distal tibia, characterized by subchondral osteopenia and sclerosis, joint space narrowing, cortical irregularities and loose bodies. Disorganization of tarsal and subtalar joints noted with soft tissue swelling. MRI shows altered signal intensity involving distal tibia and proximal tarsal bones with degeneration of subtalar joint, joint effusion and soft tissue edema.



Fig. 4.158.1



Fig. 4.158.2



Fig. 4.158.3

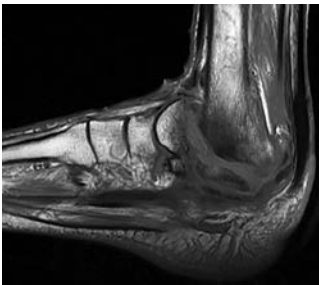


Fig. 4.158.4

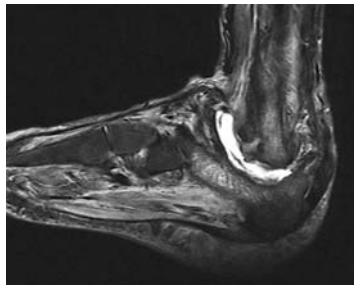


Fig. 4.158.5

Table 4.158.1: Differential diagnosis for neuropathic joint

Osteoarthritis (Refer to case 157)

Gout (Refer to case 157)

Osteomyelitis with septic arthritis: Diabetic patients are more prone for osteomyelitis with or without neuropathic joint. Presence of bone marrow edema with collection and enhancing walls in the presence of clinical signs are more in favor of osteomyelitis. Forefoot and hindfoot predominantly affected.

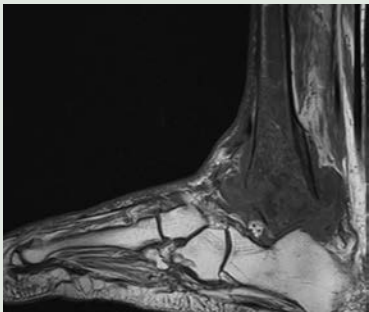


Fig. 4.158.6: Osteomyelitis—ankle joint

Table 4.158.2: Difference between infection and neuropathic joint

| Imaging features of Lisfranc joint | Infection | Neuropathic joint |
|------------------------------------|---|---|
| Demineralization | + (Later stages) | + |
| Bone destruction | + (Later stages) | + |
| Periosteal reaction | + (Later stages) | + |
| Marrow edema | Diffuse marrow edema | Subarticular marrow edema. |
| Secondary signs | Abscess—bright on STIR, hypointense on T1W with ring-like enhancement on contrast. Skin defect/ulcer/sinus is usually seen. | Enhancement is seen at subchondral region. Subcutaneous plane is uninvolved unless superimposed infection. No skin defects. |

| Table 4.158.3: Manifestations of neuropathic joint | | |
|--|--|--|
| Spine | Usually lumbar region, with large osteophytes, prominent sclerosis, advanced discopathy, severe subluxations, and bony fragmentation | <div>Two basic types of neuropathic joint:</div> <ul style="list-style-type: none">• Hypertrophic• Atrophic <div>Hypertrophic: Classic type in which bone production is the dominant feature. Usually predominates in weight-bearing joints such as the lumbar spine, hips, knees, ankle, and tarsus</div> <div>6 Ds:</div> <div>Distension: Earliest finding owing to effusion.</div> <div>Density: Increase in subchondral bone sclerosis.</div> <div>Debris: Bony intra-articular fragments.</div> <div>Dislocation: Joint surfaces often malaligned.</div> <div>Disorganization: Joint components usually disrupted (bag of bones).</div> <div>Destruction: Articular bone shows loss of bone substance.</div> <div>Atrophic: May follow hypertrophic phase or occur as an isolated finding, and is especially more common in the shoulder, hip, and foot. Articular ends of bone may appear surgically amputated or tapered like a licked candy stick</div> |
| Knee | Hypertrophic features—sclerosis, debris, destruction and dislocation. | |
| Foot | Hypertrophic, especially in subtalar joints. | |
| Forefoot | Atrophic, especially in metatarsophalangeal joint region. | |




Fig. 4.158.7: Neuropathic joint involving right shoulder




Fig. 4.158.8: Neuropathic joint involving right shoulder


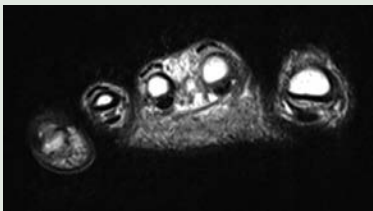



Fig. 4.158.9: Neuropathic joint involving knee

| Table 4.158.4: Other foot lesions | | |
|--|---|--|
| <div>Morton neuroma: It is one of the common causes of forefoot pain and more common in middle to elderly aged females. It is misnomer, as it is not a neoplastic condition. Its exact cause is unknown. The common theories proposed suggest that it results of mechanical compression of intermetatarsal/interdigital plantar nerve against transverse metatarsal ligament. Clinical features include forefoot pain radiating from midfoot to toe, more commonly involving the 3rd web space. The pain increases with activity. Different names are used for compression of intermetatarsal nerve at different web spaces (1st web space—Heuter neuroma, 4th metatarsal space—Iselin neuroma)</div> | <div>Ultrasound—Well defined round to ovoid hypoechoic lesion, in intermetatarsal space, between hyperechoic metatarsal heads which is usually non-compressible is suggestive of Morton neuroma.</div> <div>MRI—Usually dumbbell/ovoid-shaped soft tissue mass, confluent iso to low signal on T1, low to intermediate signal on T2, with variable enhancement on post-contrast images.</div> | <div><p>Fig. 4.158.10: Morton neuroma of 3rd web space</p></div> <div><p>Fig. 4.158.11: Morton neuroma</p></div> |

(Contd.)

Table 4.158.4: Other foot lesions (Contd.)

Sesamoiditis: It is inflammation of sesamoids usually resulting from repetitive stress on the sesamoids. Hallux sesamoids (medial–tibial; lateral–fibular) are ovoid-shaped ossicles embedded within the substance of medial and lateral slips of flexor hallucis brevis muscle. The sesamoids are the commonly injured osseous structure in the first metatarsophalangeal joint area (medial >lateral), as they overlie and shield the first metatarsal head and proximal phalanx. It presents as non-specific metatarsal pain, with restriction of movements at first metatarsophalangeal joint.

Plain radiograph—done to exclude other bony causes of pain around the first metatarsophalangeal joint. Axial view of sesamoid is usually done which provides good view of both the sesamoids. Chronic sesamoiditis may cause sclerosis and fragmentation of sesamoids. **MRI**—may reveal bone marrow edema as low signal or normal signal changes on T1 and high signal intensity on T2/STIR with soft tissue enhancement. Usually associated with reactive changes in adjacent soft tissues—like tendinitis, synovitis, bursitis.



Fig. 4.158.12: Sesamoiditis/chronic AVN



Fig. 4.158.13: Sesamoiditis

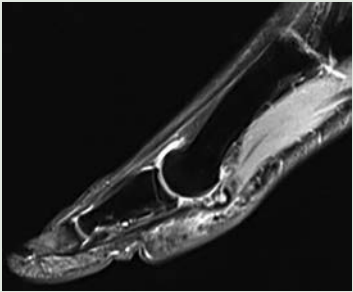


Fig. 4.158.14: Sesamoiditis

Xanthoma Achilles: Xanthomas are non-neoplastic lesions characterized by the local collection of lipid-laden macrophages, giant cells, and other inflammatory cells secondary to the deposition of cholesterol in tissue. The most commonly affected tendons include extensor tendons of hand, Achilles’ tendon and patellar tendons. Associated with hyperlipidemia, occurring more commonly in third decade of life. Cerebrotendinous xanthomatosis is a disorder characterised by hypercholesterolemia, early cataract formation, atherosclerosis, tendon xanthoma, ataxia and intellectual disability. Clinical features: Depends on the size—small lesions may be asymptomatic while larger lesions may present as cosmetically disfiguring mass with pain, irritation and impairment of ambulation.

Radiographic features: Abnormal thickening of Achilles’ tendon, non-calcified soft tissue masses which are usually bilateral and symmetrical. **USG:** Thickening of Achilles’ tendon with an AP dimension >7 mm in males and >6 mm in females, uniform thickening and loss of normal appearance of tendon with focal hypoechoic lesions. **MRI**—thickening of tendon with abnormal morphology and altered signal intensity—loss of normal ventral margin concavity of tendon, heterogeneous signal intensity on T1 and T2 with hypointense (normal tendon fibres) intercalated with hyperintense areas (inflammatory infiltrate), resulting in a diffuse “stippled” or reticulated appearance.

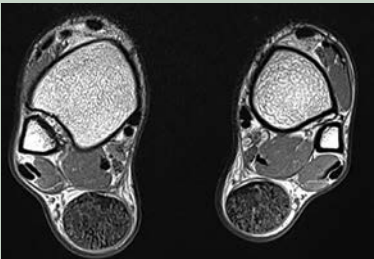


Fig. 4.158.15: Xanthoma Achilles



Fig. 4.158.16: Xanthoma Achilles

(Contd.)

Table 4.158.4: Other foot lesions (Contd.)

Maduramycosis: It is a chronic granulomatous infection, commonly affecting the feet, hands, back and gluteal region usually caused by eumycetoma (*Madurella mycetomatis*) or actinomycetes (*Nocardia*, *actinomadura*, *streptomyces*). First described in 1842, in Madurai, India and named after the same. Farmers who go barefoot in dry, dusty situations are more likely to develop it. Minor damage permits bacteria from the earth to infiltrate the skin and create discharge granulomas, which eventually affect and destroy the underlying bones. Early diagnosis of Madura foot and prevention of deformity/remodelling can be achieved with a typical clinical history and clear radiological indications. Culture is the gold standard for confirming diagnosis.

X-ray—includes features of chronic osteomyelitis, with soft tissue involvement and sclerosis, cavitation, cortical erosion and destruction of underlying bones. **MRI:** Useful for visualising soft tissue involvement and bone destruction. Dot in a circle sign: Small circular hyperintensities (representing granulation tissue) are surrounded by a low signal intensity rim (representing fibrous septa), with hypointense fungal hyphae foci (showing fungus susceptibility loss) in the centre. This can also be seen on ultrasonography. Actinomycetoma more often present with soft tissue micro abscesses, bony periosteal reaction and reactive sclerosis, while eumycetoma frequently present as soft tissue macro abscesses with bone cavitation. Differential diagnosis: Chronic bacterial osteomyelitis, tuberculosis

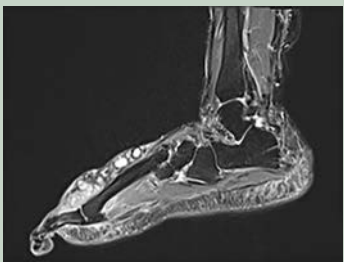


Fig. 4.158.17: Maduramycosis



Fig. 4.158.18: Maduramycosis

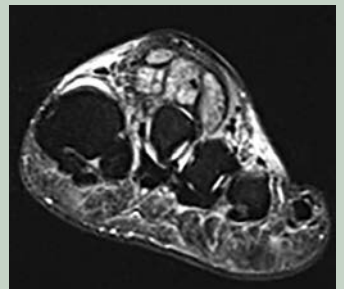


Fig. 4.158.19: Maduramycosis



Fig. 4.158.20: Midtharsal neuropathic joint in diabetes mellitus

Interpretation: A: 65-years-old diabetic female, lesion in ankle; B: Altered density with destruction and disorganization of proximal tarsal and subtalar joints, loose bodies, joint effusion and subcutaneous edema. C: No evidence of cutaneous defect; D: Neuropathic joint.

Principal diagnosis: Neuropathic joint

Brief discussion: Neuropathic joint

Causes: Alcoholism, amyloidosis, Charcot-Marie-Tooth disease, diabetes mellitus, leprosy, yaws, multiple sclerosis, neurosyphilis, syringomyelia, trauma.

Location: Lisfranc joint (60%), metatarsophalangeal joint (30%), tibiotalar joint (10%).

4.159 MUSCULOSKELETAL SYSTEM

Case No. 159

Clinical history: A 20-year-old male patient with restricted movement of bilateral lower limbs.

Radiological techniques and observations: Figures 4.159.1 to 4.159.3 are scannogram, limited coronal and axial CT sections show tiny innumerable calcifications of varying sizes located both intra-articularly and extra-articularly appearing to form a conglomerate mass that invades the muscle in posterior aspect of left distal femur. Mild erosive changes are noted around the knee joint. No evidence of any joint effusion/hematoma/fractures in the visualised bones. STIR Figures 4.159.4 to 4.159.5 are MRI limited sagittal section T1 and T2 weighted images reveal similar but not identical sized foci of variable signal intensity, majority of which are T1 hypointense and STIR hyperintense. Several of these lesions contain central dark signal void. Visualised bones and ligaments appear to be normal. Mild joint effusion noted.

Interpretation: A: 20 years old male with lesion in left knee; C: Periarticular and intraarticular calcification; B: variable MR intensities in T1 and STIR; D: Synovial osteochondromatosis.

Principal diagnosis: Synovial osteochondromatosis.

Differential diagnosis for peri-articular/ intra-articular calcification: Myositis ossificans, post-surgical dystrophic calcification or heterotopic bone formation, calcific tendinitis or bursitis, charcot joint, calcinosis cutis, fibrodysplasia ossificans progressive, gout, CPPD, HADD, calcific periarthritis (fingers and toes), tuberculous arthritis, scleroderma, hyperparathyroidism, hypoparathyroidism, renal osteodystrophy, hypervitaminosis D, milk alkali syndrome, calcinosis circumscripta and tumoralis, sarcoidosis, thermal injury, paralysis, dermatomyositis, polymyositis, ochronosis, Ehlers-Danlos syndrome, Werner's syndrome (adult

progeria), synovial sarcoma, caries sicca (healed tuberculous arthritis).

Rice bodies: Multiple little intra-articular loose entities resembling polished white rice grains macroscopically. Synovial fluid, bursae, and tendon sheaths are all places where they can be found. Patients may be asymptomatic or experience symptoms such as tenderness, effusion, or locking. They are commonly found in rheumatoid arthritis. They can also be seen in tuberculous arthritis, juvenile idiopathic arthritis, chronic synovitis/bursitis. In MRI, they appear T1 and T2 hypointense with non-enhancement.

Brief discussion about the condition: Synovial osteochondromatosis is also known as Reichel syndrome. It is a benign monoarticular disorder characterised by hyaline cartilaginous bodies proliferating in sub synovial region, detaching as a collection of chondral bodies in a joint/bursae/tendon sheaths, with about 70–95 percent of these bodies mineralizing and possibly ossifying. It is usually a self-limiting process, but it can recur locally and rarely progress to malignancy. Because the clinical presentation is non-specific and laboratory testing are not available, imaging plays a critical role in diagnosis and therapy. Because pathology might mimic chondrosarcoma, MRI characteristics are critical for accurate diagnosis. Present in 30 to 50 years and male predilection. Surgical excision is done for treatment. Recurrence rate: 10–12%.

Types: Primary (unknown etiology); secondary (due to trauma/osteoarthritis/neuropathic arthropathy).

Primary synovial chondromatosis: It can be seen in any joint, tendon or bursa but preferentially affects large joints such as the knee, hip, elbow or shoulder. Males are affected more (M: F = 2:1), most commonly in the third to fifth decades.



Fig. 4.159.1



Fig. 4.159.2

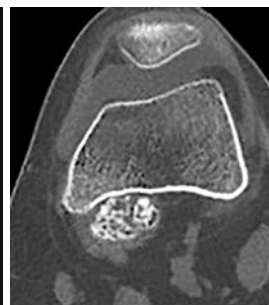


Fig. 4.159.3

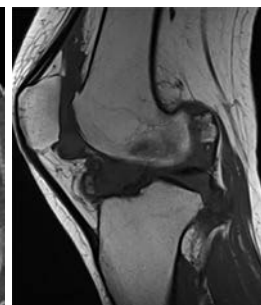


Fig. 4.159.4

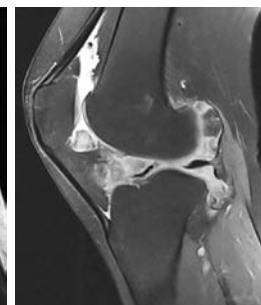



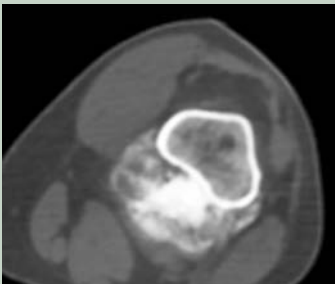


Fig. 4.159.5

Table 4.159.1: Differential diagnosis for periarticular calcification

| | | |
|---|---|--|
| <p>Hyperparathyroidism (Refer to case 145) It is the most frequent cause of a periarticular calcified mass is chronic renal failure. Serum calcium is raised and phosphorus is low or normal in primary type. Calcium is low and phosphorus is increased in secondary hyperparathyroidism.</p> | <p>Resorption of bone is essential radiographic finding. Generalised osteopenia, salt and pepper skull, brown tumours, fragile fractures are other findings. Metastatic soft tissue calcification (more common in secondary type) in periarticular location is also seen. Bone scan—superscan—intense skeletal uptake with no renal uptake.</p> |  <p>Fig. 4.159.6: Hyperparathyroidism</p> |
| <p>Vitamin D toxicity: Hypercalcemia and hypercalciuria are present. Associated with Williams syndrome (idiopathic infantile hypercalcemia), vitamin D supplementation for rickets and overfortification.</p> | <p>Generalised osteopenia. Metaphyseal bands—alternating bands of lucency and sclerosis seen in metaphysis. Metastatic calcification is commonly found in viscera, falx calcification and tentorium.</p> | |
| <p>Myositis ossificans: Location—common in areas prone to trauma—most commonly antecubital fossa/anterolateral thigh.</p> | <p>It is a composed of heterotopic bone and cartilage formation located within muscle. Here, mineralisation progresses from periphery to centre.</p> |  <p>Fig. 4.159.7: Myositis ossificans</p> |
| <p>Tumoral calcinosis: Hereditary metabolic disorder of phosphate regulation with hyperphosphatemia and normal calcium levels. Painless lumps adjacent to joints. Most commonly involved joint is hip, then shoulder/elbow/ foot /wrist.</p> | <p>Plain radiograph: Amorphous and multilobulated (“cloud-like”) calcification located in a periarticular distribution. CT (active phase): Multiple small cystic areas with peripheral mineralisation, sedimentation phenomenon (fluid calcium levels); CT (inactive phase)—solid lobules of calcification. MR (active phase): Bright periphery secondary to foreign body reaction and edema in adjacent tissues. MR (inactive phase): Low signal with a little oedema.</p> | |
| | |  <p>Fig. 4.159.8: Heterotopic ossification</p>  <p>Fig. 4.159.9: Paraosteal osteosarcoma</p> |

(Contd.)

Table 4.159.1: Differential diagnosis for periarticular calcification (Contd.)

Calcinosis cutis: Two patterns of distribution. Calcinosis cutis universalis: Diffuse involvement of skin, subcutaneous tissues, muscles and tendons. Most common in females less than 20 years of age. Localised form of calcinosis universalis is called calcinosis cutis circumscripta (most common in hands and feet-finger and toe tips).

The term calcinosis universalis refers to diffuse, sheet-like deposition of calcium involving the muscles, subcutaneous tissues, and fascial planes. Calcinosis universalis is most commonly with connective tissue disorders unlike tumoral calcinosis, it is plaque or sheet like rather than mass-like.



Fig. 4.159.10: Calcinosis cutis

Fibrodysplasia ossificans progressive (Munchmeyer disease): Rare inherited disease characterized by progressive fibrosis and ossification of muscles, tendons, fascia, ligaments and aponeurosis of multiple sites.

Charcot joint (Refer to case 158)
Progressive degenerative or destructive joint disorder in patient with abnormal pain sensation and proprioception.

Imaging findings are typically described as 6Ds which include increased bone density, joint distension dislocation (effusion), bony debris, cartilage destruction and joint disorganisation.



Fig. 4.159.11: Charcot joint

Synovial sarcoma (Refer to case 155): Periarticular soft tissue mass with calcification

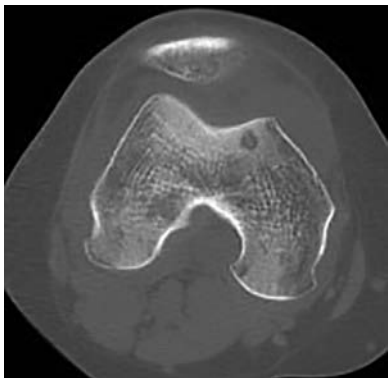


Fig. 4.159.12: Rheumatoid arthritis

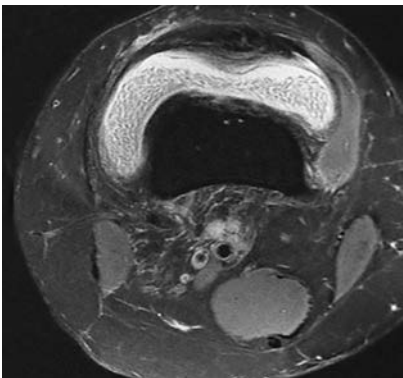


Fig. 4.159.13: Rheumatoid arthritis synovial hyperplasia with rice bodies

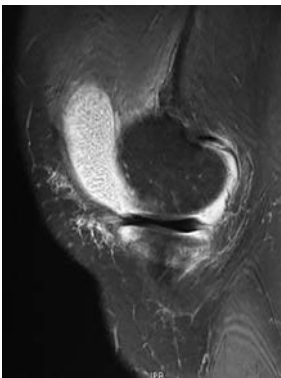


Fig. 4.159.14: Rheumatoid arthritis

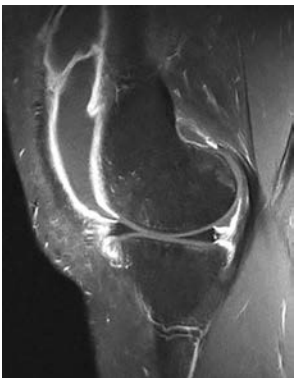


Fig. 4.159.15: Rheumatoid arthritis

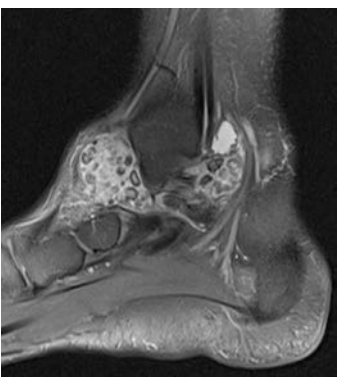
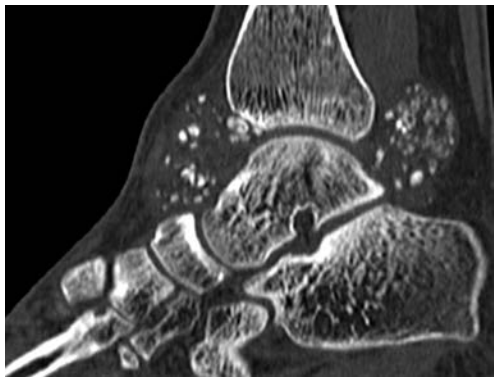


Fig. 4.159.16–4.159.18: Synovial osteochondromatosis

Table 4.159.2: Imaging findings in primary synovial chondromatosis

| Phase | Pathology | MRI features |
|-----------------------|--|--|
| First (initial) | Active formation of hyaline cartilaginous bodies within the synovium with no loose intra-articular bodies. | Radiographs may be unremarkable. MRI images demonstrate hyperintense T2 signal intra-articular masses which correspond to T1-weighted intermediate to hypointense masses without areas of internal signal void. The synovial masses will enhance intensely following IV contrast. |
| Second (transitional) | Combination of both synovial cartilaginous proliferation and shedding of intra-articular loose bodies. | Synovial bodies are characteristically hyperintense on T2 and low to intermediate signal on T1 with central signal void from calcification or central fat and a low signal rim variably depending on the degree of mineralization. They demonstrate mild enhancement with a peripheral and septal pattern. |
| Third (inactive) | Complete shedding of numerous intra-articular cartilaginous bodies and no active synovial proliferation. | Varying degrees of mineralization characterized by central fat signal intensity with a dark rim from calcification. |

Imaging: CT depends on degree of calcification of cartilaginous bodies. An important negative finding in primary synovial osteochondromatosis is that adjacent bone is normal, which shows ring and arc calcification. The appearance of synovial proliferation, loose bodies, and the extent of calcification or ossification on MRI varies and relies on the relative prevalence of synovial proliferation, loose bodies development, and the extent of calcification or ossification. The most common pattern is one of largely unmineralized nodules with T1 intermediate to low signal and T2 high signal, which are typical chondroid signal features. Mineralization occurs in focal areas of signal void within these nodules. Blooming will be visible in gradient echo (GE). Three phases of synovial chondromatosis have been described. Depending on the phase of disease at the time of imaging, it can have a varied MRI appearance but with characteristic and specific diagnostic features. Nodules are uniform in size, multiple, small and can associated with widening of joint space from accumulation of loose bodies.

Secondary synovial chondromatosis: It is more common than the primary form and presents in the setting of chronic pathology of the joint either secondary to a mechanical or an arthritic process leading to formation of loose chondral bodies. It is more commonly seen in the knee, hip or shoulder in the setting of osteoarthritis, trauma, inflammation, osteonecrosis or neuropathy and found in patients who are older than patients with primary disease. The loose bodies arise from loose hyaline cartilage implanting in synovium and inducing synovial metaplasia. The subsequent metaplastic chondral bodies that accumulate in the joint tend to be fewer in number and more variable and larger in size suggesting various times of origin. Several concentric rings of calcification may be seen in secondary synovial bodies as opposed to the more typical 'ring and arc' pattern of chondroid calcification seen in primary synovial chondromatosis. Nodules are larger size, lesser number, non uniform size and shape in secondary synovial osteochondromatosis.

4.160 MUSCULOSKELETAL SYSTEM

Case No.160

Clinical history: A 40-year-old woman with clinical history of knee joint swelling, pain and occasionally joint dysfunction for past 12 months.

Radiological techniques and observation: Figure 4.160.1 is lateral radiograph of the knee showing an ill-defined area of soft tissue opacity that replaced the normal Hoffa fat pad. No evidence of calcifications, no evidence of bone erosions/osteopenia/extra-articular extension.

With these plain radiograph findings possible differentials for soft tissue masses in knee joint without calcification include localised pigmented villonodular synovitis, synovial chondromatosis (non-ossified), chronic synovitis, hemophilic arthropathy and Gout.

Figure 4.160.3 is transverse sonogram of the knee revealing the hypoechoic intra-articular soft tissue mass. No evidence of post-acoustic enhancement. No extra-capsular extension. Figure 4.160.5 is sagittal

proton-density images revealing the localized intermediate signal intensity soft-tissue mass. Sagittal proton-density weighted fat-suppressed images (Fig. 4.160.2) show overall increased signal intensity of the intra-articular soft tissue mass. Figure 4.160.4 T1-weighted fat-suppressed post-contrast images (Fig. 4.160.6) showing prominent diffuse heterogenous enhancement. The gradient-echo image also shows focal hypointense areas, findings that represent the blooming artefact from hemosiderin probably.

Interpretation: A: 40 years old women, lesion in knee; C: Solitary intra articular nodular mass in knee that has post-contrast enhancement and blooms in GRE sequences representing hemorrhage; B: No extra-articular extension and no bone erosion; D: PVNS.

Principal diagnosis: Localized intra-articular pigmented villonodular synovitis (PVNS).

Other synovial diseases include infective synovitis, reactive synovitis, lipoma arborescens, synovial sarcoma



Fig. 4.160.1



Fig. 4.160.2

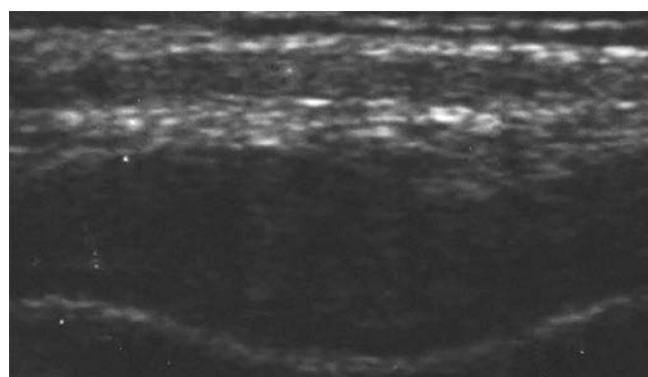


Fig. 4.160.3



Fig. 4.160.4



Fig. 4.160.5



Fig. 4.160.6

Table 4.160.1: Differential diagnosis for PVNS

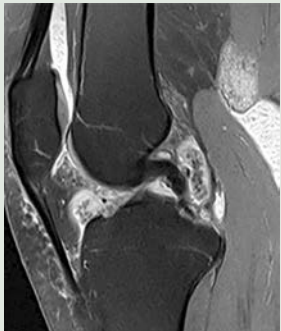
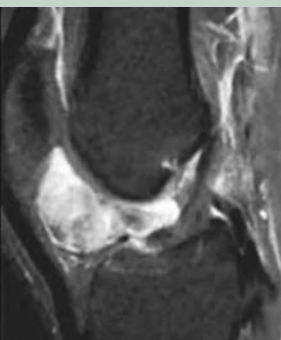
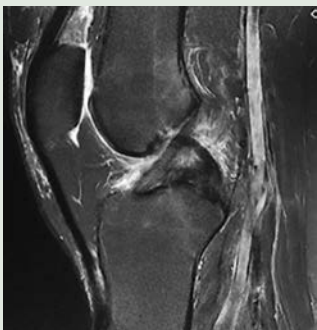

| | | |
|---|---|---|
| Synovial chondromatosis (non-ossified) (Refer to case 159). | Loose bodies are perceived as distinct entities, frequently following the signal of bone or cartilage visible on radiographs, making diagnosis differentiation simple. PVNS can be confused with a conglomerate low signal mass in synovial chondromatosis that is not seen on a radiograph. With GRE imaging, synovialchondromatosis does not bloom. |  |
| Intra-articular nodular synovitis: Commonly seen in young males, knee at infrapatellar fat pad. Less hemosiderin present than PVNS. It may cause mechanical derangement of the knee. | Nodular lesions, similar to nodular form of PVNS. Generally smaller effusion than PVNS. Blooming is less than PVNS. Post-contrast enhancement is seen. |  |
| Gout (Refer to case 157). | Plain radiograph shows “punched-out” erosions with sclerotic margins in a marginal and juxta-articular distribution, with overhanging edges, also known as rat bite erosions. Juxta-articular location (if present) makes gout more likely than PVNS. MRI T1: Low signal intensity nodular lesions T2: Low/inhomogeneously mixed signal intensity |  |
| Amyloid arthropathy: Results from the extracellular deposition of the fibrous protein amyloid within the skeletal system. | Plain radiograph shows juxta-articular soft tissue swelling. Mild periarticular osteoporosis, juxta-articular and subchondral cystic lesions (geodes), usually with well-defined sclerotic margins. Joint space is usually normal. T1/T2 hypointensity articular and juxta-articular mass, similar to gout. Contrast enhancement seen, but there is no blooming with GRE. | |
| Hemophilic arthropathy: Familial (X-linked, so found only in males). | Similar to PVNS, effusion with low signal synovial proliferation on T1 and T2. Contrast enhancement seen in proliferative synovium. Blooms on GRE, adjacent bone erosions seen. Overgrowth of epiphyses/metaphyses should be used to distinguish hemophilic arthropathy from PVNS. |  |

Fig. 4.160.7: Synovial chondromatosis**Fig. 4.160.8:** Intra-articular nodular synovitis**Fig. 4.160.9:** Gout**Fig. 4.160.10:** Hemophilic arthropathy

(Contd.)

Table 4.160.1: Differential diagnosis for PVNS (Contd.)


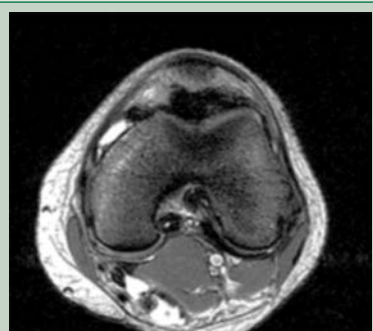
| | | |
|--|--|--|
| Synovial hemangiomas: Benign vascular malformations, rarely occurs in joint. It is considered a subtype of soft tissue hemangiomas. | MRI shows markedly T2 hyperintense background and low-signal-intensity linear structures within lesion; likely from fibrous septa or vascular channels. Fluid-fluid levels may be present. |  |
| Siderotic synovitis: It is characterized by rusty synovial pigmentation and hyperplasia, without the foam cells and multinucleated large cells found in PVNS. The synovium may proliferate in a focused or widespread manner. | MRI findings are same as that of PVNS. It shows blooming on gradient sequence. On PD sequence, it appears hyperintense. |  |
| Cyclops lesion: The cyclops lesion, also known as localized anterior arthrofibrosis, is a painful anterior knee mass that arises as a complication of anterior cruciate ligament (ACL) reconstruction. | At MR imaging, a soft-tissue mass is seen anteriorly or anterolaterally in the intercondylar notch near the tibial insertion of the reconstructed anterior cruciate ligament. | |

Fig. 4.160.11: Synovial hemangiomas**Fig. 4.160.12:** Siderotic synovitis

(refer to case 155), synovial cyst, synovial vascular malformation, CPPD (refer to case 157).

Brief discussion: Pigmented villonodular synovitis is due to monoarticular hemorrhagic proliferation of synovium. Occurs in joint, bursa, tendon sheath. PVNS has diffuse articular form and it is a giant cell tumor in localized, extra-articular form. Clinical presentation: Painful swollen joint, insidious onset with limited range of motion. Sharp, sudden increase of pain if nodule is torsed. Nearly always monoarticular. Location: Single focus involves joints, bursae, tendon sheaths; Rare reports of multifocal occurrence. PVNS (intra-articular): 80% occurs in knee; then ankle > hip > shoulder > elbow.

Imaging: Radiograph: Intra-articular PVNS shows large effusion rarely, after repeated bleeding, may appear dense. Cartilage preserved until late in process: Cartilage narrowing only with secondary degenerative changes. Osteophytes generally present at late stage

- Erosion occurs in 50%
- Large, well-marginated subchondral cyst

- Very rarely and late, may show dystrophic calcification
- Large effusion with or without associated erosions and subchondral cysts.

CT findings: Nonspecific, but may be suggestive if subchondral cysts are large. Effusion, soft tissue mass. May have increased attenuation related to hemosiderin deposits. Synovium enhances post-contrast. Well-defined erosions with sclerotic margins.

MR: Effusion with synovial proliferation, low signal on all sequences, and usually blooms on gradient-echo MR. Protocol advice: Gradient-echo imaging shows blooming phenomenon of hemosiderin-laden nodules in most cases. Post-contrast imaging shows moderate to intense inhomogeneous enhancement—may increase conspicuity for evaluation of extent of lesion, but not required for diagnosis.

Giant cell tumor of tendon sheath: Involves hand and wrist (65–89%) and volar aspect of digits—foot and ankle. **Size:** Begins as small focal mass attached to synovium. May enlarge to involve entire joint, lining entire

Table 4.160.2: Other synovial disease

Infective synovitis: Patients often present with a painful joint, fever, and purulent synovial fluid. *Staph. aureus* is the most commonly isolated agent. Imaging: In the early stages of the disease, X-rays may be normal. Hyperemia can cause juxta-articular osteoporosis, which can be visible as a joint effusion. In the acute phase, the joint space narrows due to cartilage loss. On both sides of a joint, the subchondral bone is destroyed. CT shows synovial thickening with fat fluid level in joint. T1 low signal within subchondral bone. T2 hyper due to perisynovial edema. Post-T1 C+ (Gd) shows synovial enhancement.

Lipoma arborescens: It is rare, can be intra-articular or extra-articular, common in men, predominantly in 5th–6th decade. Clinical presentation is of unilateral painful joint swelling and limitation of motion. Commonest sites of involvement are suprapatellar recess of the knee, followed by shoulder, wrist, elbow, hip and sub-deltoid bursa. Various theories are lipomatous synovial proliferation with replacement of sub-synovial tissue by mature fat cells, non-specific synovial reaction to inflammation or trauma and idiopathic. Treatment is synovectomy with uncommon recurrence rates. Synovial linings of the joints and bursae are involved with frond like depositions of fatty tissue. MRI is the modality of choice for diagnosis. A typical appearance is of a fat-containing frond-like synovial mass (Broccoli sign), usually outlined by concurrent joint effusion. The lesion follows the signal intensity of fat on all sequences, T1-high signal and will saturate on fat suppressed sequences.



Fig. 4.160.13: Lipoma arborescens

Synovial vascular malformation: Can be capillary, venous, arterio-venous, and lymphatic or mixed form. It can be present at birth and can grow slowly. It is usually seen in children and young adults. Clinical presentation is pain and swelling. Commonest site of involvement is knee (60%), followed by elbow (30%), wrist and ankles. Treatment is surgical excision and arthroscopic excision. Complication is recurrent hemarthrosis. The ultrasonography of the knee will depict hypoechoic lesions and they will have multiple cystic spaces and vascular channels. Well-defined lobulated PDW hyperintense and T1 hypointense lesion with irregular frond-like borders in the Hoffa’s fat pad of the knee with PDW hypointense foci within, suggestive of phleboliths.

Synovial cyst: It is an extra-articular fluid collection with equal gender distribution, seen at 4–7 years of age and another peak at 3rd–7th decade. They are cysts lined by synovium and contain synovial fluid within. Popliteal region is the commonest site of involvement, followed by hip, shoulder, wrist, elbow, etc. It can be asymptomatic or clinical presentation can be non-specific symptoms with soft tissue mass. It resolves spontaneously by 10–20 months in children, else aspiration and surgical excision are other treatment options. Complications include rupture, compartment syndrome, secondary hemorrhage and infection. The USG of the knee will show a well-defined anechoic lesion with posterior acoustic enhancement and internal septations in extra-articular location. MRI findings include PDW/SPAIR hyperintense and T1W hypointense well-defined lobulated cystic lesion adjacent to the knee joint.



Figs 4.160.14 to 4.160.17: PVNS

synovial surface. **Morphology:** May be focal nodular mass. May be diffuse, with villonodular proliferation of entire synovium and in all potential joint recesses. In knee, can extend down popliteus tendon sheath and into posterolateral compartment, coronary recess,

meniscomfemoral recess, popliteal fossa, intercondylar notch, and even along collateral ligaments.

Imaging: Soft tissue mass generally on volar side of finger, pressure erosions of underlying bone, rare dystrophic calcification.

4.161 MUSCULOSKELETAL SYSTEM

Case No. 161

Clinical history: 25-years-old male patient came with complaints of new onset seizure and right shoulder pain with limited range of movements.

Radiological techniques and observation: Figure 4.161.1 is frontal radiograph of right shoulder AP view showing irregularity of glenoid rim and articular surface of humeral head. Humerus appears internally rotated with increased space between humeral head and glenoid. Loss of half-moon overlap noted between humeral head and the glenoid. Figure 4.161.2 is axial radiograph of right shoulder joint showing impaction changes and bony loss in anteromedial part of head of humerus.

Interpretation: A—25 years old male with right shoulder pain; C—internally rotated humerus, increased glenohumeral distance, loss of half-moon overlap between the humeral head and the glenoid; B—reverse Hill-Sachs lesion; D—posterior dislocation of shoulder.

Principal diagnosis: Posterior dislocation of right shoulder.

Treatment: Urgent referral to the orthopedic department for closed reduction.

Discussion:

Shoulder radiograph protocol: Depend on the age of the patient, and whether the indication is trauma or non-traumatic.

Shoulder radiograph—approach: (1) Soft tissue: Examine all soft tissue structures for any signs of related or incidental soft tissue. (2) Cortex: The cortex should be smooth (humeral head, glenoid fossa, clavicle, body of scapula). Keep an eye out for fracture fragments and keep the ribs in mind. (3) Alignment and joints: Articular surfaces of the glenohumeral joint should be parallel. In any other view, the humeral head should be on the glenoid. Consider anterior shoulder dislocation if the humeral head is under the coracoid process. Consider a humeral head or glenoid fracture if there is a joint effusion. (4) The inferior margins of the distal clavicle and the acromion should line up at the acromioclavicular joint. If there is a line up/step formation, think ACL injury. Acromioclavicular (AC) distance >8 mm indicate AC ligament rupture. Coracoclavicular (CC) distance >13 mm indicate CC ligament rupture.

Review areas in shoulder radiograph are ribs, lung (e.g. pneumothorax, Pancoast tumor) and any bony/soft tissue regions included in the projection.



Fig. 4.161.1



Fig. 4.161.2

| Table 4.161.1: Shoulder radiograph protocol | | |
|---|--|--------------------------|
| Trauma | Non-trauma | Pediatric |
| Shoulder-AP (external rotation) | Shoulder-AP (external rotation) | Shoulder-AP |
| Scapula-lateral (Y view) | Shoulder-AP (oblique with internal rotation): Grashey view | Scapula-lateral (Y view) |
| | Shoulder-lateral (Neer view) | |
| | Shoulder-axial | |

Table 4.161.2: Radiographic shoulder joint views

| | | |
|--|---|---|
| AP view: Glenohumeral joint in the anatomical position is seen, showing the humeral head superimposing the glenoid of the scapula, shows clavicle, AC joint, superior ribs, scapula, SC joint and proximal humerus. | Lateral or scapular Y view: The degree and direction of any suspected dislocation can be seen in an orthogonal image of the AP shoulder and a profile view of the scapula. | AP shoulder external rotation: Greater tubercle of the proximal humerus is seen |
| Outlet (NEER) view: Special projection demonstrating the coracoacromial arch, often utilized in the investigation of speculated shoulder impingement similar to lateral view, with slight caudal tube angulation. | AP glenoid or Grashey view: The view prevents overlapping of the humeral head over the glenoid. This view is also known as the true AP. | AP shoulder internal rotation: Lesser tubercle of the proximal humerus is seen; ideal view for identifying Hill-Sachs lesion |
| Stryker view: Displays the articular surfaces of the glenoid and humerus; orthogonal view to the AP shoulder | | |

Table 4.161.3: Functional anatomy of shoulder joint

| <i>Static stabilizers</i> | <i>Dynamic stabilizers</i> |
|--|---|
| Articular congruent within the joint (bony glenoid, glenoid labrum and humeral articular surface) Glenohumeral ligaments Joint capsule | Rotator cuff muscles and tendon Long head of biceps tendon Scapular rotator muscles |
| <i>Anterior complex</i> | <i>Posterior complex</i> |
| Supraspinatus muscle and tendon Subscapularis muscle and tendon Rotator cuff interval Anterior capsule and synovial membrane Glenohumeral ligaments Anterior labrum and osseous glenoid | Infraspinatus muscle and tendon Teres minor muscle and tendon Posterior capsule and synovial membrane Posterior labrum and osseous glenoid |

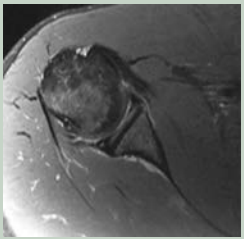
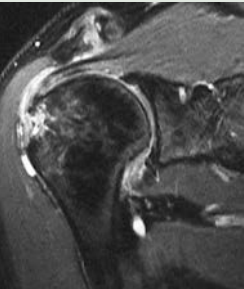
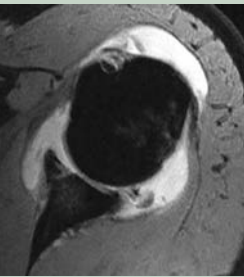
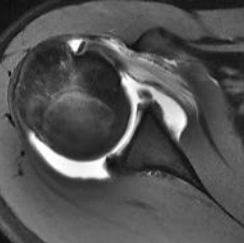
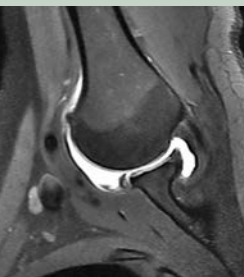
Table 4.161.4: Anterior shoulder dislocation

| <i>Mechanism</i> | <i>Radiological diagnosis</i> |
|---|--|
| Combination of extension, abduction and external rotation with posteriorly directed force applied to the arm. Direct posterior blow to shoulder. | Humeral head and outline of glenoid are incongruent. Medially displaced humeral head and overlies the glenoid on AP view. Anteriorly displaced humeral head on axial and Y-scapular views. |

Glenoid Bone Loss Assessment

1. **Pico method**, is based on CT scanning of both shoulders to provide oblique sagittal images of the healthy and the affected glenoid surfaces. By drawing two identical circumferential areas on the inferior parts of both glenoids, it is possible to measure the missing part of the circle in the affected glenoid and express that area as the size of the defect. The calculating formula was: $a - b/a \times 100$, where surface b refers to the size of the missing part of the circle in the affected glenoid and surface a refers to the size of the circle in the healthy glenoid.

2. **Best fit circle method:** Best fit circle placed along the inferior and posterior margins of Glenoid. A horizontal line is placed within the centre of the circle and extended from posterior to the anterior margin of the circle. This line represents the estimated diameter of intact glenoid (D). A second horizontal line is placed at the same level between the anterior margin of the circle and anterior margin of glenoid, this line represents the amount of anterior glenoid bone loss (d). Glenoid track is calculated as follows: Glenoid track = $(0.83 \times D) - d$, where D is the diameter

| Table 4.161.5: Associated pathologies with shoulder joint dislocation | | |
|---|--|--|
| Associated pathologies | Radiological features | Image |
| Hill-Sachs lesion (70–100%): Due to impaction injury of dislocated soft cancellous bone of the humeral head on the hard-compact bone of anterior glenoid rim. It is located in the first 18 mm of proximal humeral head or the level of coracoid process on MRI. | Compression fracture and bony loss involving posterosuperior humeral head Grading: Ratio of defect to articular surface. Grade 1(<25%)—closed or open reduction. Medium (25–50%)—repaired with fixation over defect. Grade 3(>50%)—hemiarthroplasty. |  Fig. 4.161.3: Hill-Sachs lesion |
| Greater tuberosity fracture (15–35%): Surgical fixation if there is displaced fracture. | Located at the insertion of supraspinatus and infraspinatus tendon. |  Fig. 4.161.4: Greater tuberosity fracture |
| Glenoid fracture (bony Bankart lesion): Instability is proportionate with size of the glenoid bone defect. | Combination of anteroinferior labral–ligamentous complex avulsion with an associated glenoid rim fracture. |  Fig. 4.161.5: Bony Bankart lesion |
| Soft tissue Bankart lesion (70–80%): Avulsion of anterior inferior glenoid labral ligamentous complex with disruption of periosteum | Conventional MRI: Attenuated or absent anteroinferior labrum. Increased signal intensity on gradient echo or proton density fat saturated fast spin echo sequence due to degeneration. Arthrographic MRI: Contrast is seen between labrum and glenoid margin on T1 W fat saturated sequence. |  Fig. 4.161.6: Soft tissue Bankart lesion |
| Perthes lesion: It is a Bankart lesion variant seen in acute instability patients, where torn anteroinferior part of labrum is attached to glenoid rim by intact periosteum. | MRI: Joint fluid extends underneath the torn labrum, filling the space between the elevated periosteum and the scapula. The abduction external rotation sequence of the MRI increases tension on the inferior glenohumeral ligament (IGHL) and hence exaggerate the pathology. |  Fig. 4.161.7: Perthes lesion |

(Contd.)

Table 4.161.5: Associated pathologies with shoulder joint dislocation (Contd.)

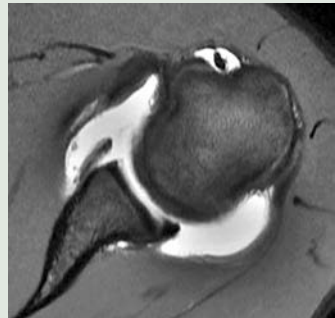
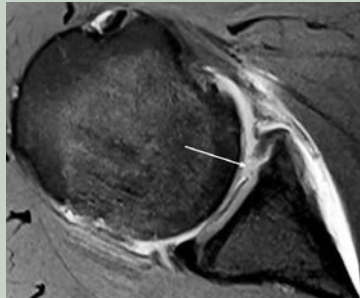
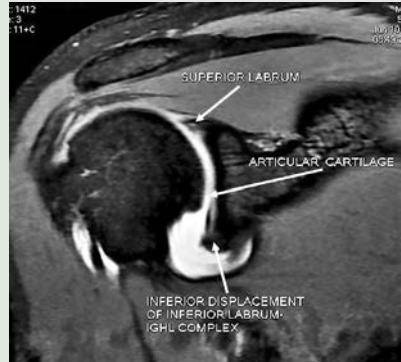
| Associated pathologies | Radiological features | Image |
|--|---|---|
| Anterior labroligamentous periosteal sleeve avulsion (ALPSA): Bankart lesion variant, seen in chronic recurrent shoulder dislocation. Medial displacement and inferior shifting of torn anteroinferior labroligamentous complex with intact periosteum along scapular neck. | MRI: Similar features of Perthes lesion except ALPSA demonstrates intact anterior scapular periosteum which allows medially displace and inferiorly rotate labroligamentous structures on scapular neck. |  |
| Glenolabral articular disruption (GLAD): Bankart lesion variant. Superficial anteroinferior labral tear and chondral injury of the adjacent glenoid articular cartilage. | Bankart lesion features seen along with chondral defect (best seen on PD sequence) Arthrographic MRI: Distends joint and allows detection of loose bodies which can occur from a detached articular fragment. |  |
| Superior labral anterior posterior (SLAP) tear: Injury of superior aspect of glenoid labrum which occurs at the biceps anchor. Type V lesion is often associated with anterior shoulder dislocation. | Conventional MRI: Tracking of fluid along the tear noted. Arthrographic MRI: Better demonstrates the extent of tear due to distension of the shoulder joint. |  |

Fig. 4.161.8: Anterior labroligamentous periosteal sleeve avulsion**Fig. 4.161.9:** Glenolabral articular disruption**Fig. 4.161.10:** Superior labral anterior posterior (SLAP) tear

of intact glenoid in mm, d is the amount of glenoid bone loss in mm. Hill-Sachs interval = Hill-Sachs defect + bone bridge between the rotator cuff attachment and lateral aspect of Hill-Sachs defect. On track (non-engaging): Hill-Sachs interval < glenoid track.




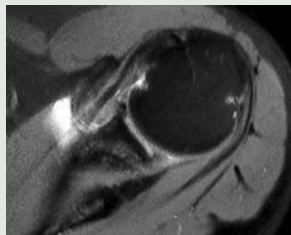

Off track (engaging): Hill-Sachs interval > glenoid track

3. In case of unilateral dislocation, **maximum glenoid width, glenoid width-to-length ratio and the cross-sectional area**, these parameters are compared with opposite normal side to arrive a better conclusion. Glenoid width to length ratio ≥ 0.7 is normal.

4. Anterior glenoid line length to show the degree of flattening. Normal <5 mm.

Glenoid version can be useful in diagnosing glenoid dysplasia, which cause recurrent shoulder dislocation. Glenoid version angle measurement. A line drawn along the long axis of scapula to the center of glenoid, another line drawn between anterior and posterior margins of glenoid, angle between these two lines calculated.

Normal 0 to 7 degrees, >7 degrees indicate retroversion, associated with posterior glenohumeral instability and posterior labral tear.

| Table 4.161.6: Posterior dislocation | | |
|--|--|---|
| Mechanism | Radiological diagnosis | |
| Adduction, flexion and internal rotation combined with axial loading force applied to the arm. Direct impact to the anterior aspect of shoulder. Convulsion and electrocution. Posterior dislocations may even go unnoticed, especially in elderly patients. | Light bulb sign: Fixed internal rotation of the humeral head which takes on a rounded appearance. Trough line sign: Dense vertical line in the medial humeral head due to impaction of the humeral head. Loss of normal half moon overlap sign , in which the glenoid fossa appears vacant due to the lateral displacement of the humeral head (vacant glenoid sign). Rim sign: Widened glenohumeral joint >6 mm. Maloney's arc disruption . | |
| Signs of posterior dislocation of shoulder | | |
| Light bulb sign/tennis racket sign | Trough line sign | Loss of normal half moon overlap sign |
|  |  |  |
| Fig. 4.161.11: Light bulb sign/tennis racket sign | Fig. 4.161.12: Trough line sign | Fig. 4.161.13: Loss of normal half moon overlap sign |
| Associated pathologies | Radiological features | Image |
| Reverse Hill-Sachs lesion: Anteromedial aspect of the humeral head impaction fracture subsequently, resulting in posterior shoulder dislocation. It has surgical importance as it helps to prevent avascular necrosis. | Loss of normal convexity and a wedge defect in the anteromedial aspect of the humeral head. |  |
| | | Fig. 4.161.14: Reverse Hill-Sachs lesion |
| Reverse Bankart lesion: The detachment of posteroinferior labrum with avulsion of posterior capsular periosteum. This leads to laxity of posterior band of the inferior glenohumeral ligament with posterior displacement of the humeral head. Retraction of IGHL altering the morphology of the axillary recess from “U” shape to “J” shape. | Posteroinferior labrum detachment, avulsion of posterior scapular periosteum with posterior glenoid rim fracture | |
| Humeral avulsion of the glenohumeral ligament (HAGL): Avulsion of IGHL from humeral insertion site. Bony humeral avulsion of the glenohumeral ligament (BHAGL) is said, if there is an associated bony fracture fragment. | Fluid is seen between the infraspinatus muscle and the scapula suggesting an associated capsular tear. |  |
| | | Fig. 4.161.15: Humeral avulsion of the glenohumeral ligament |

(Contd.)

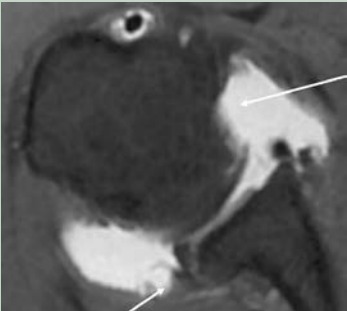
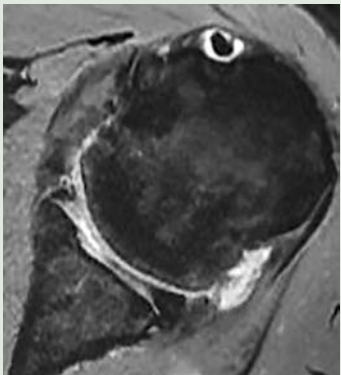
| Table 4.161.6: Posterior dislocation (Contd.) | | |
|--|--|--|
| Mechanism | Radiological diagnosis | |
| Posterior labrocapsular periosteal sleeve avulsion (or POLPSA) lesion: Occurs when trauma causes the posterior scapular periosteum and posterior labrum of the glenohumeral joint to strip off leading to a redundant recess. | MRI: May show fluid extending between the posterior labrum and the glenoid, with stripping of the subjacent periosteal attachment. |  |
| Bennett lesion: An extra-articular posterior capsule avulsive injury caused by traction of the IGHL | Crescentic mineralization is seen adjacent to the posterior inferior osseous glenoid and posterior glenoid sclerosis. Better seen on CT. Usually missed by arthroscopy as it is extra-articular. |  |

Fig. 4.161.16: Posterior labrocapsular periosteal sleeve avulsion

Fig. 4.161.17: Bennett lesion

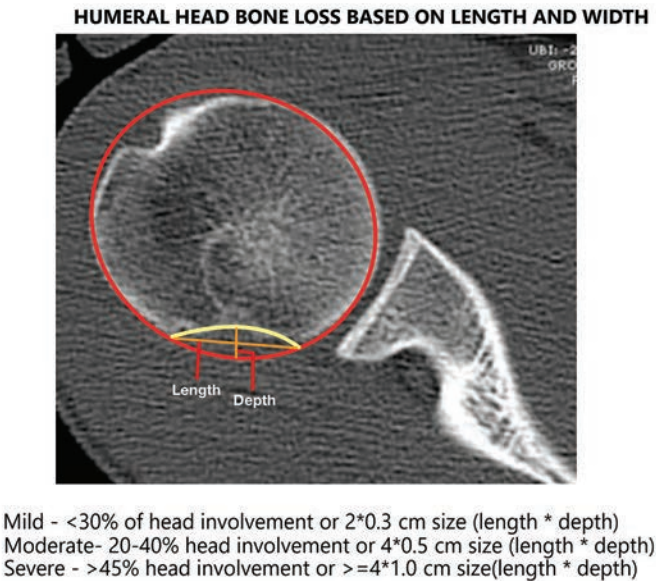
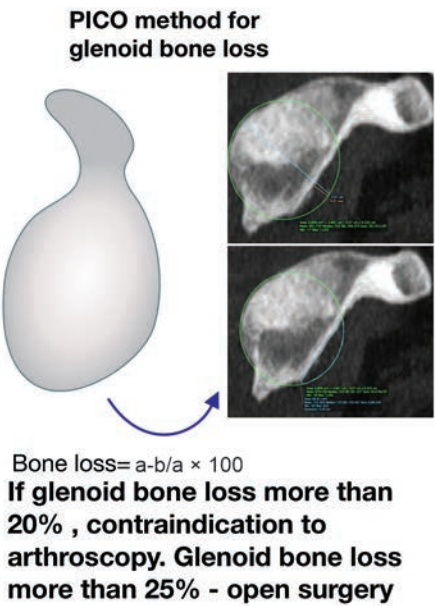


Fig. 4.161.18: Quantitative assessment of Hill-Sachs and bony Bankart lesion

Table 4.161.7: Inferior shoulder dislocation

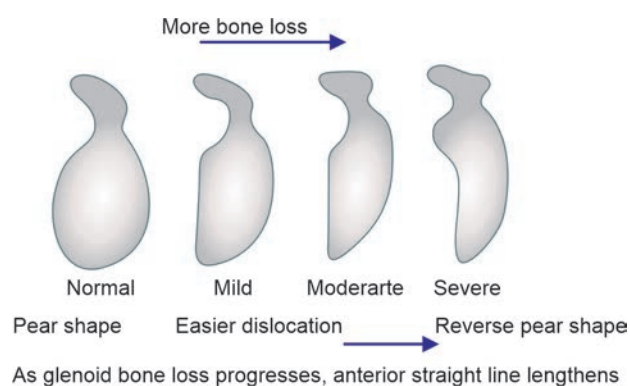
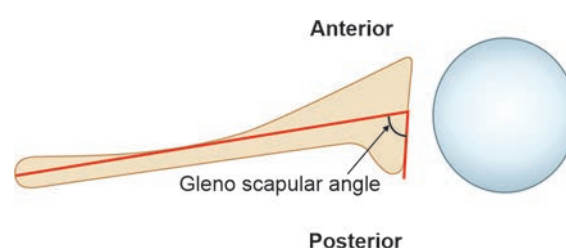
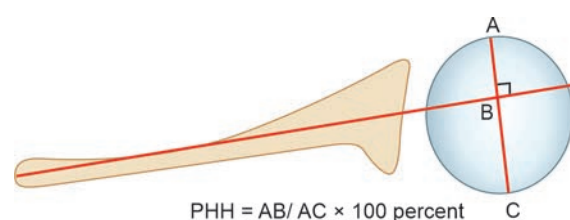
| Mechanism | Radiological diagnosis |
|---|---|
| With the arm hyperabducted, direct axial loading is performed. With extended elbow and pronated forearm, direct loading force is applied on fully abducted arm. | With the arm in significant abduction, the humeral head is displaced immediately below and somewhat medial to the glenoid fossa (luxatio erecta). |

Table 4.161.8: Classification schemes in humeral head bone loss associated with anterior glenohumeral instability (Bigliani et al,1998 and Rowe et al, 1984)

| | |
|----------|--|
| Mild | <30% of head involvement or 2×0.3 cm size (length \times depth) |
| Moderate | 20–40% head involvement or 4×0.5 cm size (length \times depth) |
| Severe | >45% head involvement or $\geq 4 \times 1.0$ cm size (length \times depth) |

Table 4.161.9: Types of glenoid rim lesion

| | |
|----------|--|
| Type I | Displaced avulsion fracture with attached capsule |
| Type II | Medially displaced fragment malunited to the glenoid rim |
| Type III | Erosion of the glenoid rim |
| III A | Erosion of the glenoid rim with <25% bone loss |
| III B | Erosion of the glenoid rim with >25% bone loss |
| Type IV | Erosion of the glenoid rim with greater than 25% deficiency combined with stretched IGHL |

**Fig. 4.161.19:** Qualitative assessment of glenoid bone loss**Fig. 4.161.20:** Diagrammatic representation of glenoid version angle measurement**Fig. 4.161.21:** Diagrammatic representation of percentage of humeral head subluxation in relation to scapular line**Table 4.161.10: Walter's grades of glenohumeral instability**

| | | |
|---|--------------------|--|
| 1 | Normal glenoid | Less than a 5-degree difference in retroversion compared with that on the normal, contralateral side |
| 2 | Minimum deformity | More than a 5-degree difference in retroversion compared with that on the normal side, with no posterior subluxation of the humeral head |
| 3 | Moderate deformity | Posterior subluxation of the humeral head, defined as less than 35 per cent of the head anterior to the bisecting line |
| 4 | Severe deformity | A false glenoid |
| 5 | Severe deformity | Severe flattening of the humeral head and glenoid, with progressive or complete posterior dislocation of the head |
| 6 | Severe deformity | Dislocation of the glenohumeral joint in infancy |
| 7 | Severe deformity | Growth arrest in proximal aspect of the humerus |

| Table 4.161.11: Walch classification system (Glenoid morphology) | | |
|--|--|---|
| Type A | Symmetric arthritis with no posterior part of humeral head subluxation. | |
| | A1 | Minor central wear or erosion |
| | A2 | Severe or major central wear or erosion |
| Type B | Asymmetric arthritis with posterior subluxation of the humeral head. | |
| | B1 | Posterior joint space narrowing, subchondral sclerosis, and osteophytes, without glenoid erosion. |
| | B2 | Biconcave glenoid appearance due to posterior part of glenoid erosion |
| Type C | Glenoid retroversion >25 degrees (dysplastic origin) regardless of glenoid erosion or the location of the humeral head with regard to the glenoid. | |

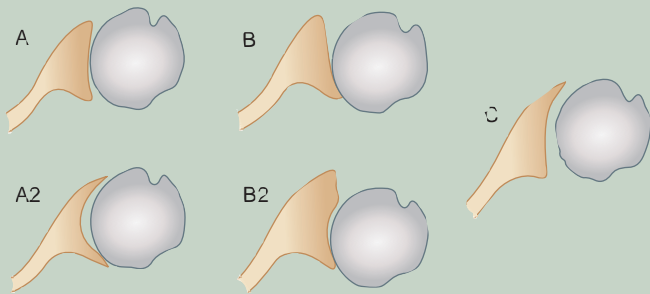


Fig. 4.161.22: Walch classification system

Table 4.161.12: Types of SLAP tears

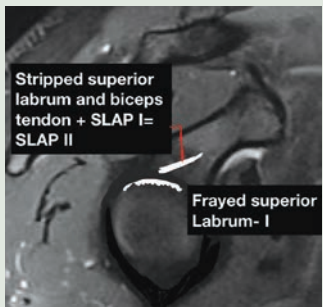


Fig. 4.161.23: SLAP I, II



Fig. 4.161.24: SLAP III, IV



Fig. 4.161.25: SLAP V, VI



Fig. 4.161.26: SLAP VII, VIII

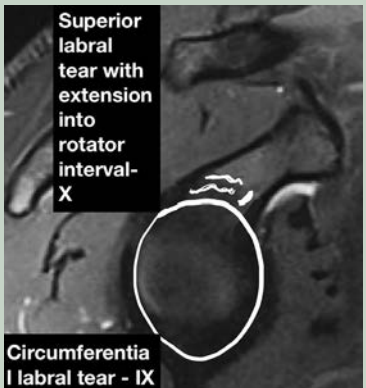


Fig. 4.161.27: SLAP IX, X

4.162 MUSCULOSKELETAL SYSTEM

Case No. 162

Clinical history: A 25-year-old male, history of fall with outstretched hand followed by pain and swelling over the right wrist joint.

Radiological techniques and observation: Figure 4.162.1 is AP radiograph showing triangular-shaped lunate seen overlying the capitate bone. Proximal carpal row alignment is disrupted. Second and third Gilula’s arc disrupted. Normal pronator quadratus fat pad seen. Normal capitate ring seen. Carpometacarpal alignment (M line) appears normal. Figure 4.162.2 is lateral radiograph showing lunate bone displaced anteriorly with loss of longitudinal axial alignment of 3rd metacarpal, capitate, lunate and distal radius.



Fig. 4.162.1



Fig. 4.162.2

Table 4.162.1: Differential diagnosis of lunate dislocation


| | | |
|---|--|---|
| Perilunate dislocation: Stage 2 sequential lesser arc injury, trans scaphoid perilunate dislocation, commonly associated with scaphoid fracture. Treatment is prompt open reduction with ligamentous repair | Lunate articulate with distal radius, line drawn through the distal radius and lunate fails to intersect capitate, capitate displaced dorsally, capitate not sitting within the articular cup of the lunate. Reduced scapholunate angle and increased in capitulunate angle. |  |
|---|--|---|

Fig. 4.162.3: Perilunate dislocation

| | |
|---|--|
| Midcarpal dislocation: Stage 3 sequential lesser arc injury. | Dorsal dislocation of capitate from the lunate and volar subluxation of the lunate from the radius |
|---|--|

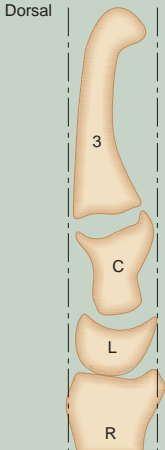
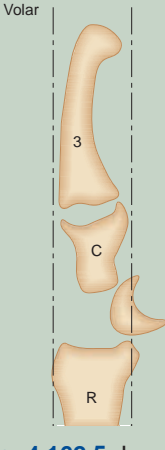
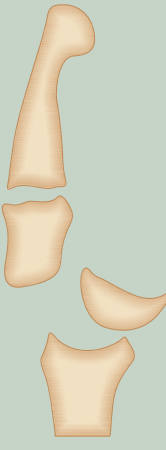
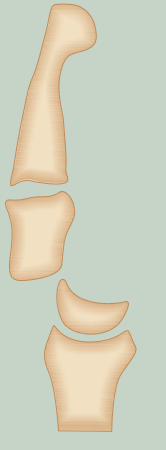
| Normal | Lunate dislocation | Midcarpal dislocation | Perilunate dislocation |
|---|---|--|---|
|  |  |  |  |
| Fig. 4.162.4: Normal | Fig. 4.162.5: Lunate dislocation | Fig. 4.162.6: Midcarpal dislocation | Fig. 4.162.7: Perilunate dislocation |

Table 4.162.2: Vulnerable zone of wrist divides into lesser and greater arc

| | | |
|----|-------------|--|
| 1. | Lesser arc | Outlines the dislocation zone—purely ligamentous |
| 2. | Greater arc | Outlines the fracture—dislocation zone |

Interpretation: A: 25 years old male with FOOSH injury; C: Lunate bone displaced anteriorly; B: Second and third Gilula's arc disrupted. Longitudinal alignment of distal radius, capitate and 3rd metacarpal is maintained with anteriorly displaced lunate; D: Right lunate dislocation.

Provisional diagnosis: Right lunate dislocation.

Management: Emergency reduction and surgical repair of disrupted ligaments is required to prevent long-term joint dysfunction.

Discussion: Lunate dislocation typically occurs in young adults with high energy trauma resulting in loading of dorsiflexed wrist. Patient presents with wrist pain following a fall, volar wrist swelling, acute carpal tunnel syndrome due to compression of median nerve. There is injury of all perilunate ligaments, most significantly dorsal radio lunate ligament. Anteroposterior radiograph shows disruption of normal smooth line between the proximal articular surface of hamate and capitate, increased radiolunate space and lunate overlaps the capitate and has a triangular or piece of pie appearance. Lateral radiograph shows volar displaced and angulation of lunate bone, spilled tea cup appearance and lunate does not articulate with capitate and radius. Treatment is immediate reduction and surgical repair of disrupted ligament. High risk of future degenerative arthritis and joint instability most commonly occur.

Dorsal intercalated segment instability (DISI): It occurs mainly after the disruption of the scapholunate ligament

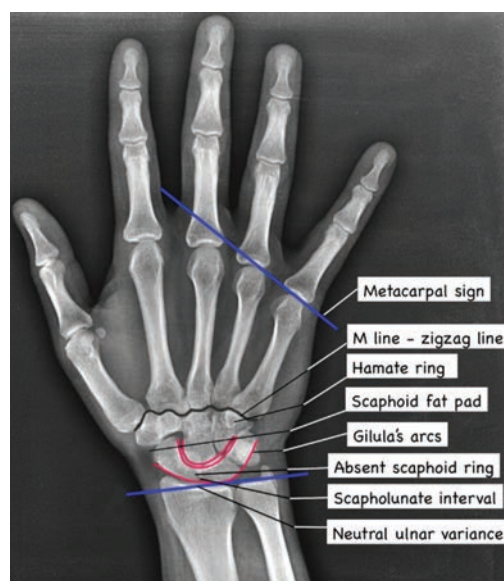


Fig. 4.162.8: Normal Gilula arcs in wrist

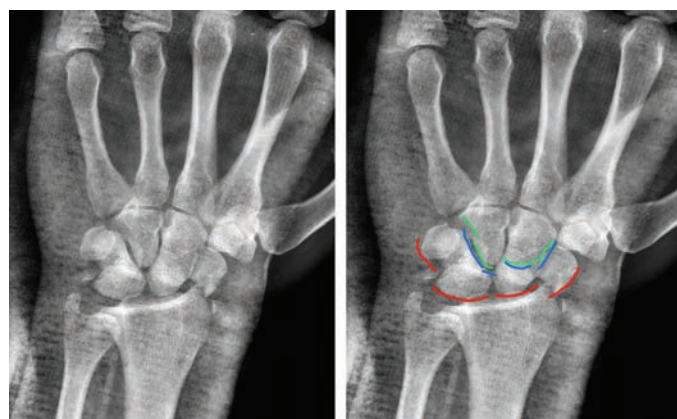


Fig. 4.162.9: Disrupted Gilula arcs in wrist in lunate dislocation on the lateral radiograph with the wrist in neutral position. DISI will show dorsal tilt of the lunate with

Table 4.162.3: Sequential stages of lesser arc injuries

| Stages | Dissociation | Dislocation | Injury of ligaments |
|---------|----------------------------|---|---|
| Stage 1 | Scapholunate dissociation | Rotary subluxation of scaphoid. Terry Thomas sign positive | Radioscaphoid, palmar radiocapitate and scapholunate ligament |
| Stage 2 | Capitolunate failure | Perilunate dislocation (dislocation of capitate) | In addition, radiocapitate ligament |
| Stage 3 | Triquetro lunate failure | Midcarpal dislocation (dorsal dislocation of capitate with subluxation of lunate) | In addition, volar and dorsal radiotriquetral and lunotriquetral ligament |
| Stage 4 | Complete lunate disruption | Lunate dislocation | In addition, dorsal radiocarpal ligament |

Table 4.162.4: Gilula has identified three smooth arcs outlining the proximal and distal rows

| | |
|-------|---|
| Arc 1 | Joins the proximal surface of the scaphoid, the lunate and the triquetrum |
| Arc 2 | Outlines the distal concavities of the same bone |
| Arc 3 | Formed by the proximal convexities of the capitate and the hamate |

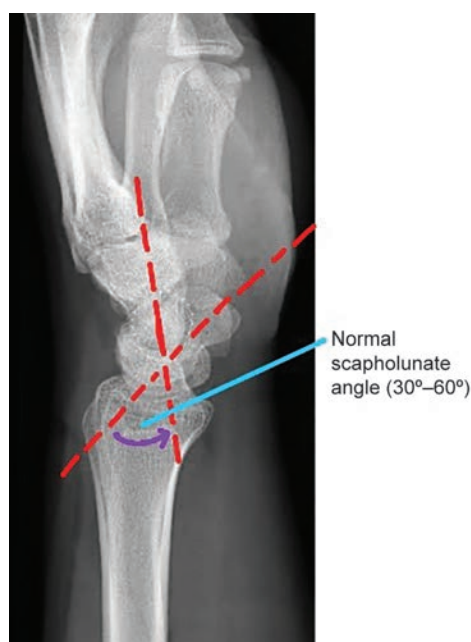


Fig. 4.162.10: Normal scapholunate angle

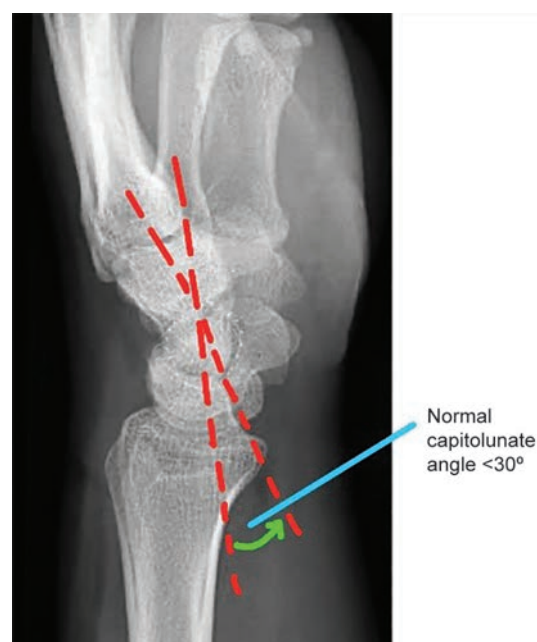


Fig. 4.162.11: Normal capitulate angle

scapholunate angle $>60^\circ$ (a sign of scapholunate ligament dissociation) and capitulate angle $>30^\circ$ (the capitate is displaced posteriorly compared to the distal radius).

VISI-volar intercalated segmental instability: Disruption of radiocarpal ligaments on the ulnar side of wrist. The main ligaments involved in this instability are ulnar half of the volar arcuate ligament and lunotriquetral ligament. Lateral radiograph of wrist shows scapholunate angle $<30^\circ$ and capitulate angle $>30^\circ$. Main treatment is early reduction and casting with K wires.

Scaphoid fat pad: A little triangular or linear radiolucent collection of fat close to the radial aspect of the scaphoid is the typical scaphoid fat pad. The radial collateral ligament of the wrist, which runs from the radial styloid to the ulnar portion of the scaphoid, forms the ulnar boundary. The extensor pollicis brevis and abductor pollicis longus tendon sheaths, which start in the dorsal forearm and insert on the base of the first metacarpal and proximal phalanx of the thumb, respectively, form the radial margin. The scaphoid fat pad's radiolucency is normal. It is not always obvious in children.

Obliteration/lateral displacement of the normal scaphoid fat pad is the scaphoid fat pad or stripe sign. A scaphoid fracture is the most common cause of a positive sign, however, it can also be caused by a radial styloid or proximal first metacarpal fracture. It is better visualised in the posteroanterior and oblique views of wrist.

Pronator quadratus fat pad sign: On lateral wrist radiographs, the pronator fat pad normally appears as a thin radiolucent triangle, with its base attached to the palmar surface of the distal radius.

The pronator quadratus sign an indirect sign of distal forearm trauma. Obliteration or displacement of the fat plane indicates distal radius or ulna fracture. Other causes for positive pronator quadratus sign are muscle strain or haematoma, inflammatory conditions, infectious conditions like osteomyelitis and cellulitis, septic arthritis of wrist.

Scapholunate dissociation: Also known as rotary subluxation of the scaphoid, refers to an abnormal orientation of the scaphoid relative to the lunate. The typical pattern of scapholunate dissociation consists of relative flexion of the scaphoid and relative extension of the lunate. Radiological appearance: Terry Thomas sign—widening of the scapholunate interval >4 mm on PA view, increase scapholunate angle to greater than 60° , signet ring sign—ringed appearance of scaphoid.

Fracture of the hook of the hamate (hamulus): The eye sign: dense, oval, cortical ring shadow that is normally seen over the hamate on the dorsovolar projections. The eye of the hamate is actually hook of the hamate seen on end. Absence of eye or indistinct outline of the cortical shadow or presence of sclerosis suggests the diagnosis of hamulus fracture.

Carpometacarpal dislocation: Without fractures they are rare because these joints are supported by carpometacarpal and intermetacarpal ligament. On frontal projection, normally wavy W appearance of the CMC joints to all fingers and the thumb. Disruption of W and loss of joint margin results in possibility of major injury in that region.

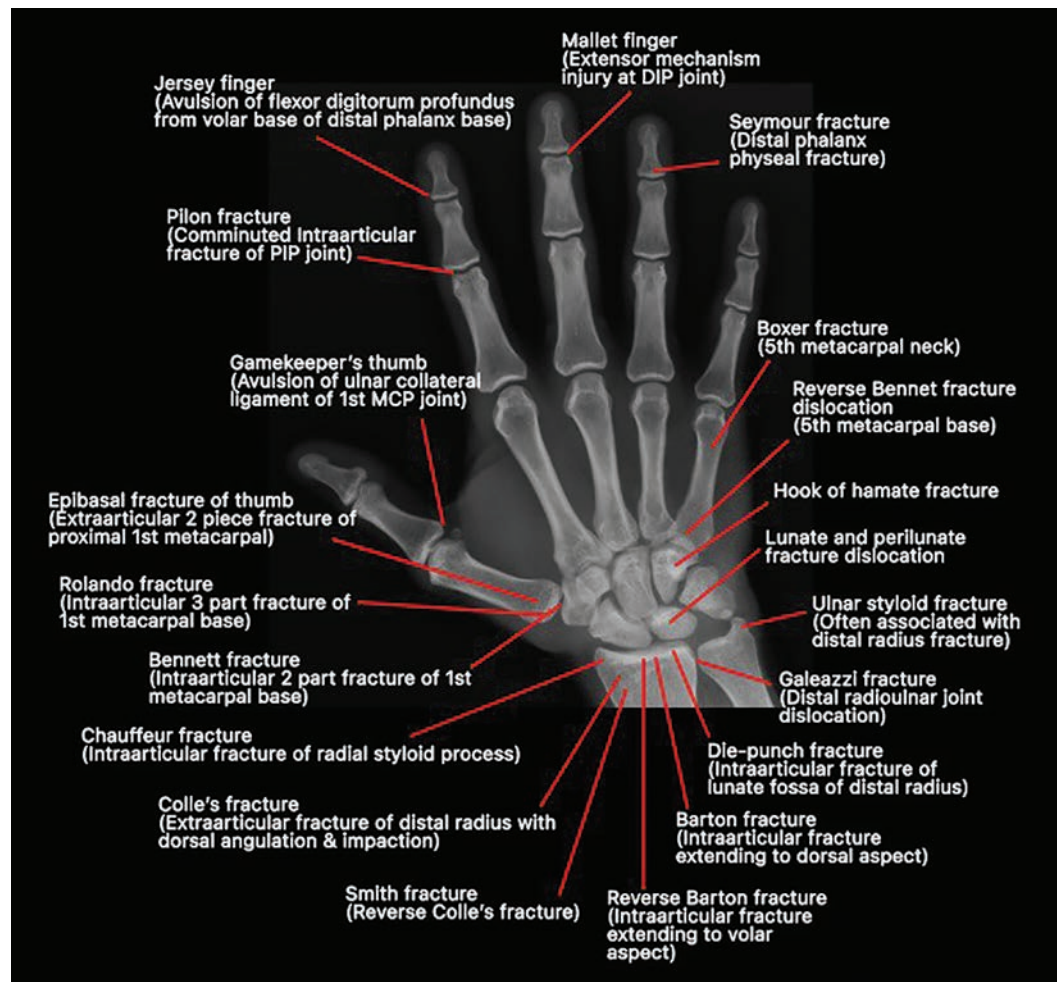


Fig. 4.162.12: Eponymous fractures in hand radiograph

4.163 MUSCULOSKELETAL SYSTEM

Case No. 163

Clinical history: A 40-years-old-male with alleged history of road traffic accident two weeks ago, now presented with right knee joint pain, mild restriction of movement and swelling.

Radiological techniques and observation: Figures 4.163.1 and 4.163.2 are plain radiograph images of right knee in AP and lateral view showing transverse fracture involving the tibial eminence with no displacement of fracture fragment. Distal femur, proximal fibula and patella appear normal. No significant joint effusion noted. Soft tissue appears normal.

Figures 4.163.3A and B are CT of right knee joint in bone window in coronal and sagittal view revealing the bony fracture in the anterior tibia spine. Visualised distal femur, patella appears normal. Figures 4.163.5 to 4.163.6 are MRI right knee joint in sagittal T2, STIR sagittal and coronal section showing diffuse bony contusion of lateral tibial condyle. Undisplaced fracture line seen extending to articular surface of lateral tibial condyle. Avulsion and

anterior elevation of tibial attachment of anterior cruciate ligament noted with secondary ligamentous laxity. Areas of contusion involving the anterior roots of both medial and lateral menisci with mild suprapatellar effusion noted.

Interpretation: A: 40 years old male with history of injury in ankle joint; C: Avulsion and anterior elevation of tibial attachment of anterior cruciate ligament with secondary ligamentous laxity; B: Fracture in the anterior tibial spine and bony contusion of lateral tibial condyle at the site of attachment of ACL; D: ACL avulsion injury.

Principal diagnosis: Anterior cruciate ligament avulsion fracture Meyers and McKeever classification type III.

Management: This patient is referred to orthopaedic department. Since this is type III avulsion fracture managed surgically by open reduction and internal fixation or arthroscopic reduction and internal fixation.

Discussion: Anterior cruciate ligament (ACL) avulsion fracture or tibial eminence avulsion fracture typically involves separation of the tibial attachment of the ACL



Fig. 4.163.1



Fig. 4.163.2



Fig. 4.163.3A and B

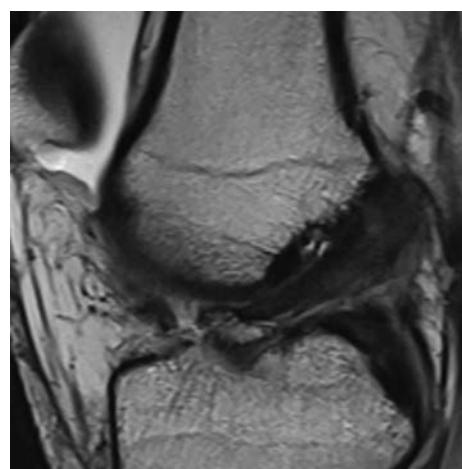


Fig. 4.163.4

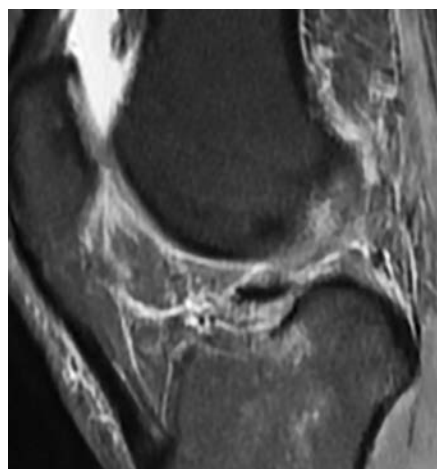


Fig. 4.163.5

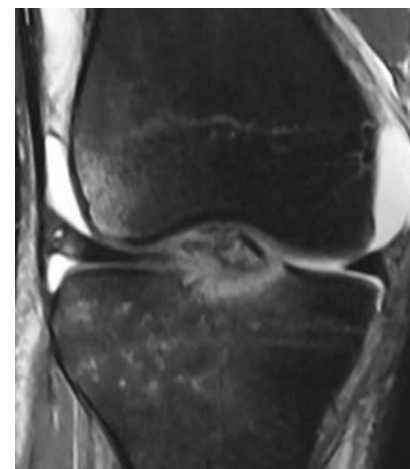
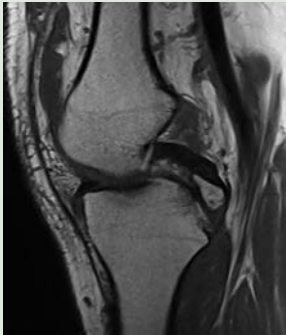




Fig. 4.163.6

Table 4.163.1: Knee joint bony avulsion fractures

| | | |
|---|---|--|
| <p>PCL avulsion fracture: Isolated PCL disruption most often manifests as avulsion at the tibial insertion (40–55 percent), rather than at the femoral origin or as a mid-substance rupture. The PCL can be injured in a variety of ways, including a direct hit to the front tibia when the knee is flexed or hyperextension.</p> | <p>Posterior tibial articular surface will show focal discontinuity on the lateral view. At MRI, a discrete bone fragment is noted attached to an otherwise intact PCL and separated from the remainder of the tibia. Associated with disruption of the medial and lateral collateral ligament complexes, medial and lateral meniscal tears, and focal bone contusions of the anterior tibia and lateral femoral condyle.</p> |  <p>Fig. 4.163.7: PCL avulsion fracture</p> |
| <p>Conjoined ACL and PCL avulsion fracture: Very rare and is attributed to a fracture that extends from anterior to posterior tibial plateau.</p> | <p>ACL and PCL fibres are intact but the knee is unstable. MRI clearly demonstrates the fracture line and the insertion point of ACL and PCL.</p> | |
| <p>Segond fracture: Cortical avulsion of tibial insertion site of middle 1/3rd of lateral capsular ligament.</p> | <p>Plain radiograph shows elliptic fragment of bone parallel to the tibia, just distal to the lateral tibial plateau. MRI demonstrates marrow edema along the lateral tibial rim and association with ACL and meniscal tears.</p> |  <p>Fig. 4.163.8: Segond fracture</p> |
| <p>Reverse Segond fracture: Similar to the Segond fracture except that it is located on the opposite side of the knee, arising from the medial aspect of the proximal tibia.</p> | <p>Elliptic bone fragment will be seen arising from the medial aspect of the proximal tibia associated with PCL and medial meniscus tears.</p> | |
| <p>Arcuate complex avulsion fracture: Consists of the lateral (fibular) collateral ligament, biceps femoris tendon, popliteus muscle and tendon, popliteal meniscal and popliteal fibular ligaments, oblique popliteal, arcuate, and fabellofibular ligaments and lateral gastrocnemius muscle.</p> | <p>On radiography the avulsed elliptic piece of bone fragment arising from the fibular styloid process. MRI to confirm the exact origin of the fracture fragment, either by direct visualization or identification of marrow edema in the head of the fibula and adjacent soft-tissue swelling</p> | |
| <p>Biceps femoris tendon avulsion fracture: Unlike the arcuate complex, which inserts on the fibular styloid process, the conjoined tendon is formed by the biceps femoris and lateral collateral ligament that attaches to the lateral margin of the fibular head.</p> | <p>The biceps femoris tendon avulsion fracture presents as an bone fragment from the fibular head. Avulsion of the biceps femoris tendon insertion will be seen on MRI. Disruption of the lateral collateral ligament, Segond fracture, and injury to the popliteal musculotendinous unit are all attributed to this condition.</p> | |
| <p>Pellegrini-Stieda lesion: Ossification of the femoral epicondylar or proximal attachment of medial collateral ligament (MCL) is thought to be the result of chronic trauma.</p> | <p>Areas of ossification may demonstrate marrow fat signal intensity or may be hypointense if sclerotic. Calcification has low-signal-intensity on T1- and T2-W images. Grade III MCL tears may also be associated with avulsed cortical fragments from the attachment site at the femoral epicondyle.</p> |  <p>Fig. 4.163.9: Pellegrini-Stieda lesion</p> |

(Contd.)

Table 4.163.1: Knee joint bony avulsion fractures (Contd.)

Sinding-Larsen-Johansson syndrome
Chronic traction injury of the immature osteotendinous junction of patellar tendon as it inserts into the inferior pole of the patella. **Patellar sleeve avulsion:** Cartilaginous injury to the lower pole of the patella. **Jumper's knee** is a chronic insertional injury of the posterior and proximal fibers of the patellar tendon at the site of its origin at the inferior pole of the patella.

MRI is useful in differentiating Sinding-Larsen-Johansson syndrome from patellar sleeve avulsion, as only a bone avulsion at the proximal patellar insertion is identified in the former entity while the latter demonstrates extensive cartilaginous injury in addition to the osseous deformity.



Fig. 4.163.10: Sinding-Larsen-Johansson syndrome

Osgood-Schlatter disease: Chronic avulsion injury, due to repetitive microtrauma and traction on tibial tubercle by the patellar tendon. Radiograph may be normal or reveal fragmentation anterior to the tibial tubercle, soft-tissue swelling, and obliteration of the inferior angle of the infrapatellar fat pad.

MRI: Patellar tendon enlargement with increased signal intensity at its distal insertion on both T1- and T2-weighted images, a distended deep infrapatellar bursa, marrow edema within the proximal tibia adjacent to the tuberosity and thickened cartilage anterior to the tibial tubercle.

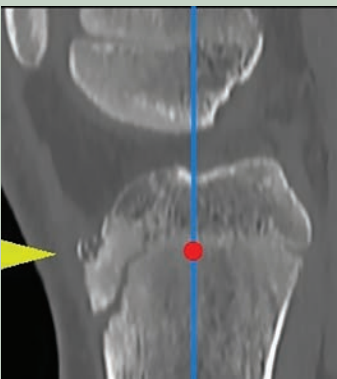


Fig. 4.163.11: Osgood-Schlatter disease

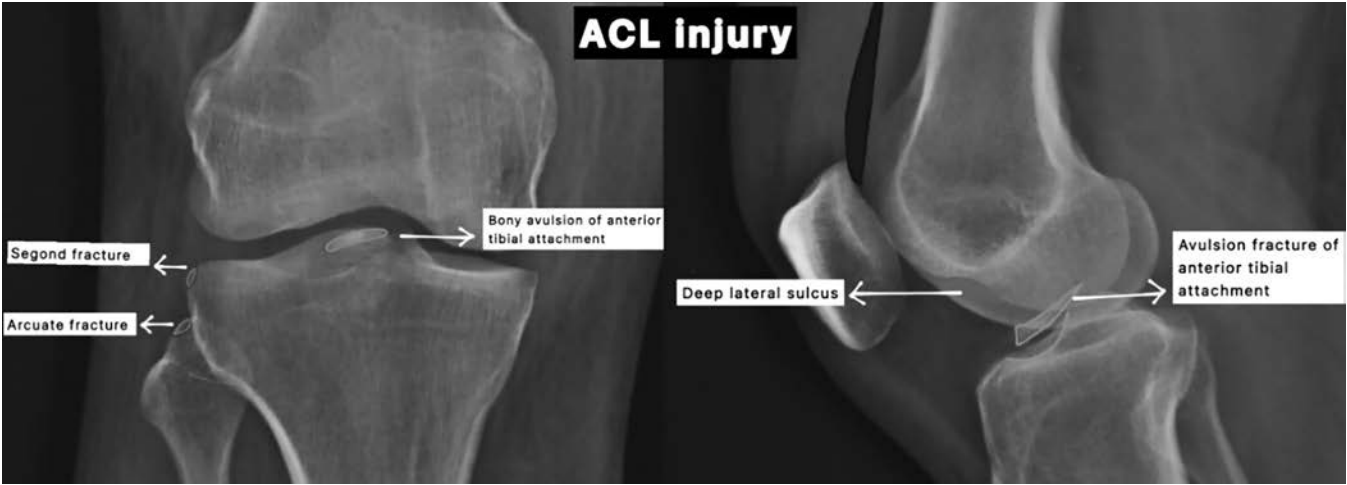







Fig. 4.163.12: Radiograph signs of ACL avulsion fracture

to variable degrees. Separation at the femoral attachment is rare. Children are more affected than adults. This could be owing to the relative softness of incompletely ossified bone in comparison to ligamentous fibres, or to the relative elastic property of ligaments in children. They are frequently caused by a direct impact over the distal end of the femur with the knee flexed or by forceful hyperextension of the knee.

Radiograph signs of ACL avulsion fracture: **Lateral femoral notch sign (deep lateral sulcus sign)** a depression on the lateral femoral condyle at the terminal sulcus, a junction between the weight-bearing tibial articular surface and the patellar articular surface of the femoral condyle. **Anterior tibial translocation sign or anterior drawer sign** is seen in cases of complete rupture of the ACL and refers to anterior translocation of the

Table 4.163.2: Meyers and McKeever classification of ACL avulsion fracture

| | | | | |
|---|---|---|---|---|
|  |  |  |  |  |
| Fig. 4.163.13: Type 1 ACL avulsion fracture | Fig. 4.163.14: Type 2 ACL avulsion fracture | Fig. 4.163.15: Type 3a ACL avulsion fracture | Fig. 4.163.16: Type 3b ACL avulsion fracture | Fig. 4.163.17: Type 4 ACL avulsion fracture |
| Type 1 | Type 2 | Type 3a | Type 3b | Type 4 |
| Minimally/nondisplaced fragment | Anterior elevation of the fragment | Complete separation of the fragment, involves small portion of eminence | Complete separation of the fragment, involves the majority of the eminence | Comminuted avulsion and rotation of the fracture fragment |

tibia to the femur of >7 mm. **Second fracture** involves the lateral aspect of the tibial plateau (~75% of cases). **Arcuate fracture:** Avulsion fracture of proximal fibula at the site of insertion of arcuate ligament complex.

Joint Effusion

Management: Treatment of tibial spine fractures depends on type of fracture, entrapment of soft tissues at fracture site and associated knee injuries. Type 1 and 2 fractures are treated with long leg cast immobilization for a period of 4–6 weeks, for type 3 and 4 open reduction and internal fixation to arthroscopic reduction and internal fixation.

Avulsion injuries: They occur where the joint capsule, ligament, tendon or muscle attachment site is pulled off from the bone, usually taking a fragment of cortical bone, e.g. greater tuberosity—insertion of rotator cuff, lesser tuberosity—insertion of subscapularis, coracoclavicular avulsion, medial epicondyle—apophyseal avulsion in children, coronoid process, biceps tubercle of radius, olecranon process, volar plate avulsion injury, mallet finger, iliac crest avulsion, anterior superior iliac spine avulsion, anterior inferior iliac spine avulsion, ischial tuberosity avulsion, anterior cruciate ligament avulsion, posterior tibial plateau/intercondylar area in posterior cruciate ligament, patellar tendon avulsion, tibial tuberosity avulsion, medial collateral ligament avulsion, calcaneal tuberosity avulsion fracture, 5th metatarsal property avulsion.

Patterns of bone contusion in knee joint: Can give clues for the mechanism and associated injuries. Five classic bone contusion patterns have been described:

Pivot-shift injury—valgus stress to flexed and externally rotated knee, Contusion pattern: Posterolateral tibial plateau and mid-part of lateral femoral condyle, associated with anterior cruciate ligament (ACL) tears, *See also:* Contrecoup injury of the knee.

Dashboard injury: Anterior force to tibia in a flexed knee (e.g. knees against dashboard in motor vehicle collision, or fall onto flexed knee), Contusion pattern: Anterior tibia +/- posterior patella associated with posterior cruciate ligament (PCL) tear.

Clip injury—valgus stress to flexed knee, contusion pattern: Lateral femoral condyle and lateral tibial plateau +/- medial femoral condyle from medial collateral ligament (MCL) avulsive stress, associated with MCL injuries.

Hyperextension injury—direct force to anterior tibia with foot planted, contusion pattern: “kissing contusions” of anterior tibial plateau and anterior femoral condyle, associated with ACL, PCL, meniscal injuries, and in severe cases knee dislocation.

Lateral patellar dislocation—twisting injury to flexed knee, anterolateral lateral femoral condyle and inferomedial patella, associated with medial patellar retinaculum +/- medial patellofemoral ligament injury +/- medial patellotibial ligament injuries.

Celery stalk sign: The celery stalk sign is a term given to the appearance of the anterior cruciate ligament which has undergone mucoid degeneration and has been likened to that of a celery stalk. Its low signal longitudinal fibres are separated from each other by higher signal mucinous material, best appreciated on T2 weighted images.

Table 4.163.3: Common avulsion fractures

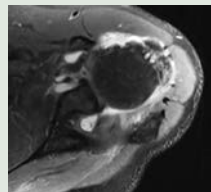


| | | |
|--|---|---|
| Iliotibial band avulsion: The iliotibial band represents the distal extension of the superficial and deep layers of the fascia lata and tensor fascia lata. | The superficial layer consists of primary tendinous component and inserts onto the Gerdy tubercle along the anterolateral tibia, while its deep layer inserts on the intermuscular septum of the distal femur. Iliotibial band is avulsed and retraction from its distal insertion site on the Gerdy tubercle. Accompanying ACL injury is a common finding. | |
| Hamstring avulsion: Very common in athletes, the injury involves avulsion of the apophysis causing a small fragment of bone to detach. | Tendinous without bone involvement. The most common pattern being the conjoint tendon (of semitendinosus and biceps femoris) fully detaching with a partial or full-thickness injury of semimembranosus | |
| Greater tuberosity avulsion: Full-thickness rotator cuff tear, complete cuff tear, vertical tear with a connection from joint to the bursa, not involving the whole breadth of the tendon, partial-thickness rotator cuff tear. Plain radiograph—decreased acromiohumeral interval, Humeral subluxation superiorly may be seen in chronic tears, may show features of subacromial impingement | MRI-hyperintense signal area within the tendon on T2W, fat-suppressed, and GRE sequences, matches to fluid signal. MR arthrography helps in easy detection of rotator cuff tears, especially full-thickness tears. |  |
| Bennett fracture is a fracture of the base of the thumb resulting from forced abduction of the 1st metacarpal. It is defined as an intra-articular two-part fracture of the base of the first metacarpal bone. | Two-piece fracture of the base of the thumb metacarpal, intra-articular extension, dorsolateral displacement, small fragment of 1st metacarpal, attached to anterior oblique ligament, continues to articulate with trapezium. |  |
| Patella avulsion fracture: Direct trauma to patella/forceful sudden contraction of the quadriceps muscles in the context of a sports injury. | Transverse fracture of mid patella is most common. Others fractures are, comminuted fracture, vertical fracture (least common) osteochondral defect usually from medial facet |  |

Fig. 4.163.18: Greater tuberosity avulsion**Fig. 4.163.19:** Bennett fracture**Fig. 4.163.20:** Patella avulsion fracture

Sesamoid bones are ossification foci within tendons that can be observed as they travel across joints. They can also form in ligaments and have a diameter of a few millimetres. Their purpose, is to change the direction of

the tendon and modulate pressure, minimising friction. Patella, fabella, cyamella, os peroneum, and hallux sesamoid are other examples.

Table 4.163.4: Difference between fabella and cyamella

| <i>Fabella</i> | <i>Cyamella</i> |
|--|--|
| <ul style="list-style-type: none"> Small sesamoid bones are seen within the lateral head of gastrocnemius muscle in 10–30% of individuals. Bipartite or tripartite, differential diagnostic—loose body or osteophyte. Fabella syndrome: Friction of the fabella on the posterolateral femoral condyle causing posterolateral knee pain, conservative treatment /excision in refractory cases. | <ul style="list-style-type: none"> Also called fabella distalis/popliteal fabella, a sesamoid bone of the popliteus tendon which cause of posterolateral knee pain, swelling and locking. Differential diagnostic—loose body, fabella, heterotopic ossification. |

4.164 MUSCULOSKELETAL SYSTEM

Case No. 164

Clinical history: A 58-year-old male patient with pain in the knee for 2 months and no history of trauma.

Radiological techniques and observations: Figures 4.164.1 and 4.164.2 are the proton density weighted MR images in coronal and sagittal sections showing hyperintensity in the posterior horn of medial meniscus, parallel to the tibial plateau. Involvement of superior articular surface is noted. The visualised skeleton shows osteoarthritic changes. Minimal joint effusion noted. No evidence of parameniscal cyst. The anterior horn of medial meniscus, lateral meniscus and cruciate ligaments appear normal. Collateral ligaments appear normal. Surrounding muscles show no significant altered intensity. Bone marrow shows no evidence of altered intensity.

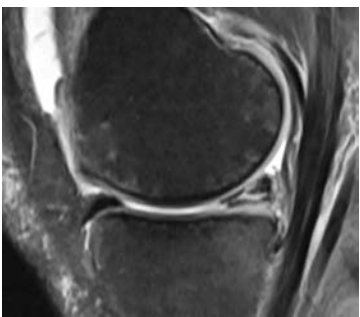


Fig. 4.164.1

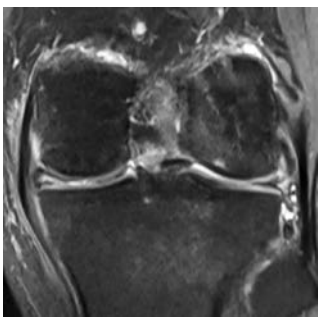
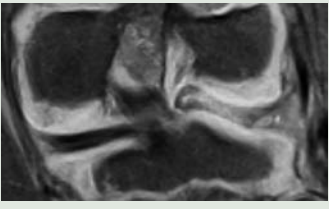

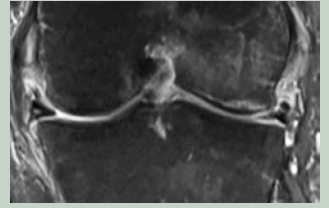
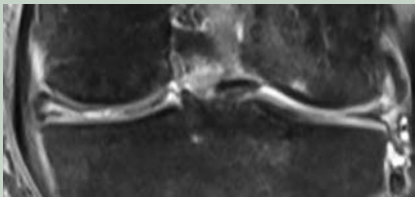

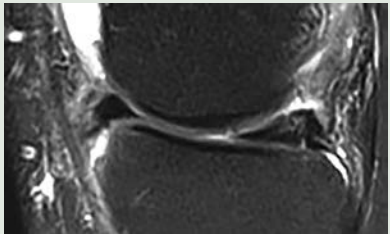

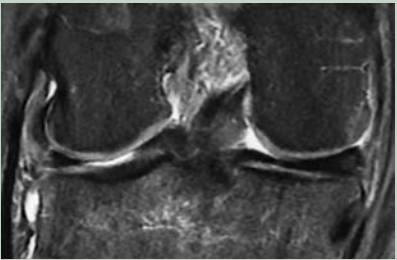
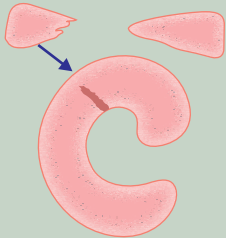


Fig. 4.164.2

Interpretation: A: 55 years old male with knee pain; C: Medial meniscus showing PD hyperintense signal parallel to the tibial surface with involvement of superior articular surface; B: Minimal joint effusion noted with osteoarthritic changes. No evidence of parameniscal cyst; D: Medial meniscus horizontal tear.



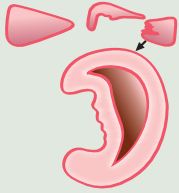
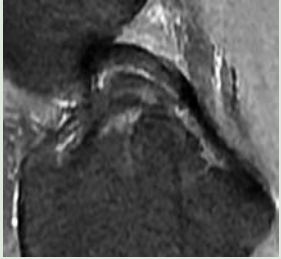
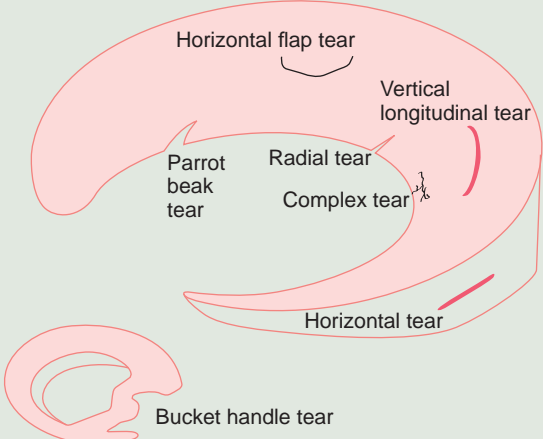
Table 4.164.1: Differential diagnosis of meniscal tear

| | | |
|---|--|--|
| Meniscal degeneration: Internal disruption of normal meniscal architecture ± mucinous degeneration without extension to articular surface. Seen in older adults. Conservatively managed. Meniscal contusion: Similar appearance seen in trauma patients. | MRI: T1 and PD show globular or linear signal located within substance of meniscus, No extension of this signal to articular surface of meniscus/free edge irregularity. Intrameniscal signal usually decreases on T2WI. |  Fig. 4.164.3: Meniscal degeneration  Fig. 4.164.4: Meniscal degeneration |
| Normal meniscal vascular pedicle: Due to the presence of vessels near the posterior horn of medial meniscus and is limited to peripheral 1/3 of meniscus | T2/PD hyperintense signal involving the posterior horn of medial meniscus. |  Fig. 4.164.5: Normal meniscal vascular pedicle |
| Postoperative change: Previous meniscal repair or previous partial or complete meniscal resection (meniscectomy) or meniscal allograft. Truncation or decreased size of meniscus or micrometallic artifact in knee joint from previous surgery. | Residual globular or linear signal within meniscus which may extend to surgical border even in absence of residual or recurrent tear. This is due to: (1) Debridement of meniscus beyond margin of macroscopic tear; (2) Surgical margin extends to underlying meniscal degeneration, which contains abnormal signal; (3) Fibrovascular healing response at site of resection may also have elevated signal extending to surface; (4) High signal extending to surface at site of surgery may persist for 1 year following meniscal repair | |
| Meniscal ossicle: Ossification within meniscus of knee. | Generally, follows normal marrow signal on all sequences and is surrounded by meniscal tissue. | |

| Table 4.164.2: Meniscal tear classification | | |
|---|---|--|
| Type of tear | Imaging features | Image |
| <p>Horizontal tear: It runs parallel to the tibial plateau, involves either one of the articular surfaces or the central free edge, and extends toward the periphery, dividing the meniscus into superior and inferior halves. These tears are seen >40 years without an inciting trauma and are more common in the setting of underlying degenerative joint disease.</p> | <p>Horizontally line of high signal intensity that contacting the meniscal surface or free edge with adjacent osteoarthritic changes. Parameniscal cyst formation is related with complete horizontal tears extending to the periphery.</p> |  <p>Fig. 4.164.6: Horizontal tear in medial meniscus</p>  <p>Fig. 4.164.7: Horizontal tear in medial meniscus with parameniscal cyst</p> |
| <p>Longitudinal (vertical) tear: Longitudinal tear run perpendicular to the tibial plateau and parallel to the long axis of the meniscus, dividing the meniscus into central and peripheral halves. They frequently occur in younger patients after significant knee trauma.</p> | <p>Vertical line of high signal intensity that contacts with one or both articular surfaces.</p> |  <p>Fig. 4.164.8: Vertical tear in posterior horn of medial meniscus</p>  <p>Fig. 4.164.9: Vertical tear in posterior horn of medial meniscus</p> |
| <p>Radial tear: It runs perpendicular to both the tibial plateau and long axis of the meniscus, transecting the longitudinal collagen bundles as it extends from free edge towards the periphery. Radial tears commonly involve the posterior horn of the MM or the junction of the anterior horn and body of the LM</p> | <p>On axial MR images, these tears appear as clefts oriented perpendicular to the free edge. Various imaging signs can be seen with a radial tear, including the "truncated triangle," "cleft," "marching cleft," and "ghost meniscus" signs.</p> |  <p>Fig. 4.164.10 Radial tear</p>  <p>Fig. 4.164.11: Radial tear</p> |

(Contd.)

Table 4.164.2: Meniscal tear classification (Contd.)

| | | |
|---|--|---|
| <p>Complex tear comprises horizontal, radial, and longitudinal components (any two or all three)</p> | <p>Fragmented meniscus with the tear extending in more than one plane.</p>  <p>Fig. 4.164.12: Complex tear</p> |  <p>Fig. 4.164.13: Complex tear</p> |
| <p>Displaced tear includes free fragments, displaced flap tears, and bucket-handle tears. Small free fragments and flaps can be missed at arthroscopy. So, identification of small fragments before surgery is important, as meniscal flap retention results in persistent pain and potential knee locking. Seen more frequently in MM.</p> <p>Bucket handle tear is a longitudinal tear along with central migration of the inner handle fragment.</p> | <p>Absent bow tie, intercondylar notch fragment, a double PCL (can occur only in the presence of intact ACL), a double anterior horn or flipped meniscus, and a disproportionally small posterior horn.</p>  <p>Fig. 4.164.14: Bucket handle tear</p> |  <p>Fig. 4.164.15: Bucket handle tear with double PCL sign</p> |
| <p>Menisci bucket handle tear: Double PCL sign, absent bow tie sign, floating meniscus, fragment in notch sign, flipped meniscus sign, double anterior horn sign/double delta sign.</p> | | |
|  <p>Fig. 4.164.16: Tears in meniscus</p> | | |

Diagnosis: Medial meniscus horizontal tear.

Management: Arthroscopy guided suturing of medial meniscus.

Discussion: The use of proton-density (PD)-weighted sequences has been favoured over T2W sequences for meniscal tear detection. It is hypothesized that the hydrogen nuclei within a tear are bound to macromolecules, which gives them a shorter T2 relaxation time. The menisci are seen on MRI as wedge-shaped

low signal (black) structures in all pulse sequences. Risk for meniscal tears increases with age and presence of degenerative bone disease. MR criteria for menisci tear are: (1) Meniscal distortion in the absence of prior surgery; (2) Increased intra-substance signal intensity unequivocally contacting the articular surface. If these 2 features should be seen in two or more consecutive images, they fulfil "two-slice-touch" rule and it can be reported as a meniscal tear. Tears are more common in the posterior horn of the meniscus, medial more than lateral.

4.165 GASTROINTESTINAL TRACT

Case No. 165

Clinical history: Two days old term male baby presented with abdominal distension and failed to pass meconium.

Radiological techniques and observation: Supine abdominal film (Fig. 4.165.1) demonstrates numerous dilated large bowel loops most likely sigmoid colon and descending colon, with fecal material and absence of gas shadow in rectum.

Figures 4.165.2 and 4.165.3 are Barium enema in AP and lateral film demonstrating a reduced calibre of rectum (the rectum is smaller than the sigmoid colon) with a saw-tooth appearance of the wall. Abrupt transition point is seen at the junction between the rectum and sigmoid colon.

Abnormal rectosigmoid ratio <1 .

Interpretation: A: Term male baby with abdominal distension, failed to pass meconium, C: Dilated bowel loops most likely sigmoid colon and descending colon, with absence of gas shadow in rectum, B: Rectosigmoid ratio <1 on barium enema. Normally, rectum is the most distensible part of bowel (normal rectosigmoid ratio is >1). D: Hirschsprung's disease—short segment.

Principal diagnosis is Hirschsprung's disease—short segment.

Management: This child is referred to multidisciplinary Pediatric surgical team for rectal biopsy to confirm the diagnosis. Surgical treatment is by removal of the affected portion of the colon.

Discussion: Hirschsprung's disease/congenital megacolon.

It occurs with an incidence of $\sim 1:4500$ live births and demonstrates an overall 4:1 male-to-female ratio. The primary abnormality is failure of the normal craniocaudal migration of vagal neural crest cells between weeks 5 and 12 of gestation. This results in distal absence of ganglion cells in the myenteric (Auerbach) plexus and submucosal (Meissner) plexus of the bowel wall. The aganglionic segment begins at the anal sphincter and extends proximally for a varying length of the colon. It is continuous, the presence of "skip" lesions being extremely rare. The physiology of the disease is more complex than pure aganglionosis. Abnormalities of both adrenergic and cholinergic fibers can be demonstrated, and function of the internal anal sphincter is also abnormal. Associated with Down's syndrome in 10% cases.

Classification: Short segment disease (70% cases): Involves the rectum and distal sigmoid colon. Long segment disease (25%): Extends to the splenic flexure or transverse colon. Total colonic aganglionosis (Zuelzer-Wilson syndrome) (5%): The entire colon is involved with occasional extension into the small bowel. Total colonic disease demonstrates a strong familial tendency.

Ultrashort segment disease: This remains a controversial entity in which the abnormality is limited to the anal sphincter. A manometric and clinical diagnosis, there are no abnormal radiologic or histologic findings.



Fig. 4.165.1


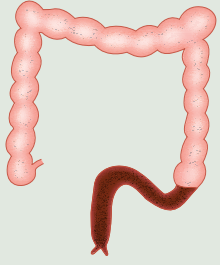
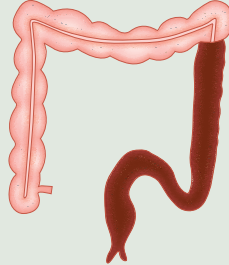





Fig. 4.165.2



Fig. 4.165.3

Table 4.165.1: Differential diagnosis for narrowed large bowel in pediatrics

| | | | |
|---|--|--|---|
|  <p>Fig. 4.165.4: Normal</p> |  <p>Fig. 4.165.5: Short segment Hirschsprung's disease</p> |  <p>Fig. 4.165.6: Left microcolon</p> |  <p>Fig. 4.165.7: Microcolon</p> |
| <p>Normal rectosigmoid ratio >1 (normally rectum is the most distensible part of bowel)</p> <ul style="list-style-type: none">• Habitual constipation-dilated large bowel with fecal material.  <p>Fig. 4.165.8: Habitual constipation</p> | <p>Abnormal rectosigmoid ratio <1</p> <p>Ultra short segment Hirschsprung's disease</p> <ul style="list-style-type: none">• Short segment Hirschsprung's disease  <p>Fig. 4.165.9: Short segment Hirschsprung's disease</p> | <p>Left Microcolon</p> <ul style="list-style-type: none">• Left colon syndrome / meconium plug syndrome• Long segment Hirschsprung's disease | <p>Microcolon</p> <ul style="list-style-type: none">• Total colonic aganglionosis• Meconium ileus• Colonic atresia• Ileal atresia• Megacystis-microcolon-intestinal hypoperistalsis syndrome |

Radiologic scoring system for evaluation of suspicious Hirschsprung's disease (HD): A checklist was used to evaluate the items proposed by contrast enema (CE), based on six subscales, including: 1) Transitional zone, 2) Rectosigmoid index (RSI), 3) Irregular contractions in aganglionic region, 4) Cobblestone appearance, 5) Filling defect due to fecaloid materials and 6) Lack of meconium defecation during the first 48 hours after birth. For subscales 1 and 2, if they were positive, we would consider scoring = 2, and, if they were negative, we would consider scoring = 0. For the other subscales, the positive results had scoring = 1 and negative results had score = 0. Furthermore, the patients were evaluated based on scoring system, as follows: High (5–8), and

low (0–4). Scoring system of CE is an useful diagnostic method in HD. If a patient's score is high, that patient is highly suspicious to HD and reversely, when one's score is low, the patient presents a reduced probability to be diagnosed with HD. Although the intestinal biopsy is the diagnostic gold standard, the first diagnostic method is contrast enema.

Management: Surgical treatment is by removal of the affected portion of the colon. Where this is successful, the prognosis is good. However, in 3–4% of cases, colonic perforation complicates the presentation and this and its sequelae significantly increase both mortality and morbidity. Mortality rates can be as high as 30% due to enterocolitis.

Table 4.165.2: Differential diagnosis for microcolon


| Conditions | Radiological findings | Image |
|---|--|---|
| Left colon syndrome: Meconium plug syndrome refers to a functional colonic obstruction in a newborn due to an obstructing meconium plug. | Associated with maternal Diabetes, Hirschsprung's disease and cystic fibrosis. Contrast enema may demonstrate a small caliber to the left colon with multiple filling defects within due to retained meconium. The rectum is usually normal in size, unlike Hirschsprung disease. Enema can be both diagnostic as well as therapeutic. It is usually transient and affects the left colon with meconium plugging the bowel distal to this segment. Long segment Hirschsprung's disease. | |
| Meconium ileus: Meconium becomes inspissated and obstructs the distal ileum. The initial presentation of 10 to 15% of cystic fibrosis association with partial pancreatic aplasia or stenosis of the pancreatic ducts. | Plain radiography: Non-specific and may show dilated bowel loops proximal to the impaction. Contrast enema will show a microcolon involving the entire large bowel and may show impacted meconium pellets filling defects, particularly in the right colon or in the distal ileum. Low GI obstruction with abdominal distension, failure to pass meconium, and sometimes vomiting within the first 48 hours of life. | |
| Ileal atresia: Significant stenosis or complete absence of a portion of the ileum. Associates with chromosomal abnormalities and cystic fibrosis in 25%. | Antenatal USG shows polyhydramnios and dilated proximal bowel segments. Abdominal radiograph will show air in the dilated loops of proximal bowel. Enema shows microcolon. | |
| Colonic atresia: Less than 10% of all intestinal atresias. Current belief that atresia of the colon is caused by vascular accidents <i>in utero</i> . | Type I, an obstructing intraluminal membrane is present, which may show the pathognomonic "wind sock" sign on contrast enema. In types II and III, the proximal and distal ends of the affected area are completely separate or connected by a cord-like remnant of bowel, with abrupt termination of the opacified colon. | |
| Habitual constipation | Barium enema showed impacted stool filling the sigmoid colon and rectum. |  |
| Megacystis-microcolon-intestinal hypoperistalsis syndrome: Characterized by functional intestinal obstruction, dilated small intestine, microcolon, malrotation, and a massively enlarged bladder with or without megaureter and hydronephrosis but without lower urinary tract obstruction. | Antenatal USG shows massively distended bladder (megacystis), combined with a normal or increased amount of amniotic fluid. Mild bilateral hydronephrosis and isolated dilated stomach, or both, are often present. Structural anomalies of the abdominal wall such as omphalocele, hydrometrocolpos, and segmental colonic dilatation can be additional features. | |
| Anorectal malformations (ARMs) are a complex group of congenital anomalies involving the distal anus and rectum, as well as the urinary and genital tracts. Most ARMs result from abnormal development of the urorectal septum in early fetal life. | Low: Anal stenosis, anocutaneous fistula Intermediate: Anal agenesis without fistula or with rectourethral bulbar fistula. High: Rectal atresia, anorectal agenesis without fistula or with rectourethral prostatic fistula. | |

Fig. 4.165.10: Habitual constipation

Table 4.165.3: Causes of intra-abdominal mass lesions, calcifications and delayed meconium passage in infants

| <i>Causes of a neonatal intra-abdominal mass lesion</i> | <i>Causes of neonatal intra-abdominal calcifications</i> | <i>Causes of delayed passage of meconium in infants</i> |
|---|---|--|
| Complicated meconium ileus Dilated bowel proximal to an obstruction Mesenteric or duplication cyst Abscess Genitourinary causes Hydronephrosis Renal cystic disease Mesoblastic nephroma Wilms' tumor Adrenal haemorrhage Neuroblastoma Retroperitoneal teratoma Ovarian cyst Hydrometrocolpos Haemangio-endothelioma Hepatoblastoma Choledochal, hepatic, or splenic cysts | Complicated meconium ileus Intraluminal calcifications Low obstruction Anorectal malformations with a fistula to the urinary tract Adrenal haemorrhage Neuroblastoma Wolman's disease Hepatobiliary disease Haemangio-endothelioma Hepatoblastoma TORCH infections Duplication and mesenteric cysts Nephrocalcinosis Intravascular thrombus Teratomas | Ileal atresia Meconium ileus Functional immaturity of the colon Colon atresia Anorectal malformations Hirschsprung's disease Megacystis–microcolon–intestinal hypoperistalsis syndrome Extrinsic compression of the distal bowel by a mass lesion Mesenteric cyst Enteric duplication cyst Paralytic ileus, sepsis, drugs, and metabolic upset |

Table 4.165.4: Difference between necrotising enterocolitis and Hirschsprung's disease

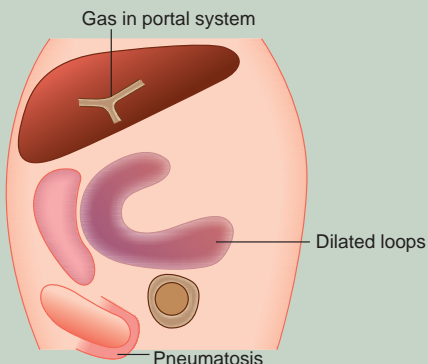
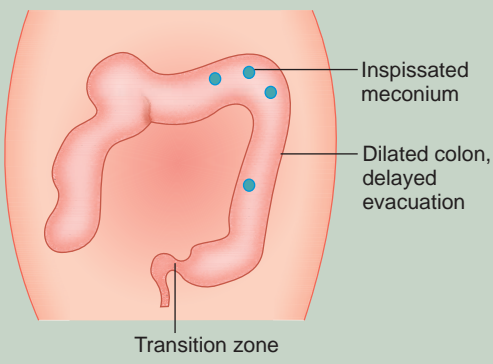
| <i>Necrotising enterocolitis</i> | <i>Hirschsprung's disease</i> |
|---|---|
| Premature infants, develops most often within 2–6 days after birth | Male: Female = 6:1 80% present in first 6 weeks of life |
| Small bowel dilatation: Adynamic ileus, pneumatosis intestinalis (80%), Gas in portal vein Pneumoperitoneum (20%) Barium contraindicated (use water soluble contrast). | Bowel gas pattern of distal colon obstruction, Barium enema normal in 30%, Transition zone between normal and stenotic colonic segment, Rectum: Sigmoid diameter ratio (N: 1.0) is abnormal (<1.0), Saw-tooth appearance of colon on contrast enema, significant barium retention after 24 hr, Transition zone in rectosigmoid–80% |
|  <p>Fig. 4.165.11: Necrotising enterocolitis</p> |  <p>Fig. 4.165.12: Hirschsprung's disease</p> |

Table 4.165.5: Pearls on Meckel diverticulum

Meckel diverticulum: Meckel diverticulum is a congenital intestinal diverticulum due to fibrous degeneration of the umbilical end of the omphalomesenteric (vitelline) duct that occurs around the distal ileum. It is considered the most common structural congenital anomaly of the gastrointestinal tract.

Tc-99m Pertechnetate scan is the diagnostic imaging modality of choice to detect ectopic gastric mucosa (sensitivity 95%). Rule of '2's: Occurs in 2% of population (most common congenital GI abnormality), complications within 2 years of age, located within 2 feet from ileocaecal valve, Length: 2 inches, 20% patients have complications, haemorrhage from peptic ulceration (gastric mucosa) inflammation, ulcers and obstruction.

4.166 GASTROINTESTINAL TRACT

Case No. 166

Clinical history: 65 years old gentlemen presenting with complaints of dyspepsia and loss of weight for 3 months.

Radiological technique and observation: Figures 4.166.1 and 4.166.2 are barium meal spot film showing persistent narrowing with mucosal irregularity along the greater curvature, the distal body and antrum of stomach. Food particles are seen in the fundus and proximal body of stomach. Pyloric channel appears normal. Passage of contrast into duodenum and jejunum with persistence of contrast in distal part of stomach noted. No evidence of lytic lesion in visualized thoracic vertebra.

Figure 4.166.3 is CT contrast portal venous phase showing heterogeneously enhancing partially circumferential irregular mass in the distal body and gastric antrum. Adjacent perigastric fat stranding noted. Multiple enlarged lymph nodes noted along the common hepatic artery and suprapyloric region. No evidence of para-aortic lymphadenopathy. Liver shows numerous hypovascular lesions. No evidence of bony, adrenal, lung metastasis. Both kidneys appear contracted with multiple cortical cysts.

Interpretation: A: 65 years old male, lesion in distal body and gastric antrum; C: Heterogeneously enhancing circumferential irregular mass; B: Multiple enlarged lymph nodes along the Common hepatic artery and suprapyloric region perigastric nodal and numerous peripherally enhancing liver lesions. D: Carcinoma stomach with nodal and liver metastasis.

Principal diagnosis: Carcinoma stomach involving distal body and antrum with perigastric nodal and liver metastasis.

Differential diagnoses for increased gastric wall thickening

- Gastric lymphoma
- Gastric metastases
- Gastric stromal tumor (GIST)
- Gastritis
- MALToma
- Peptic ulcer disease
- Ménétrier disease
- Pancreatitis

Further management: Endoscopic ultrasound and scopy guided biopsy for disease confirmation and staging. MRI scan and PET scan for staging of disease.

Treatment: Decided by multidisciplinary tumor board consisting of surgeon, oncologist, radiologist and radiotherapist. Surgery: Subtotal or total gastrectomy depending on the staging.

Radiotherapy, chemotherapy for inoperable cases.

Discussion: Normal thickness of distended stomach fundus, body and antrum <5 mm; esophagogastric junction <10 mm. Risk factors for carcinoma stomach: Pernicious anemia, adenomatous polyps, chronic atrophic gastritis, post billroth surgery due to bile reflux. Common location of carcinoma stomach: Fundus/cardia–40%, antrum 30%, body–30%.

Staging: T1—limited to mucosa, submucosa (5-year survival 85%), T2—muscle, serosa involved (5-year survival 50%), T3—penetration through serosa, T4—invades adjacent organs.

Gastric outlet obstruction (GOO)—barium meal criteria: Presence of excessive fasting gastric juice—

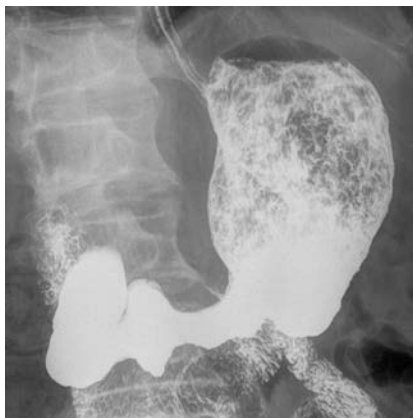


Fig. 4.166.1



Fig. 4.166.2



Fig. 4.166.3

the blobs of barium sink through a layer of fluid and come to rest at the bottom of greater curvature giving a saucer-like appearance. Excessive peristalsis—in compensated phase 2–3 giant peristalsis waves intent both lesser and

greater curvature. In phase of failing compensation—the peristaltic waves gradually disappears after a variable period (1–3 hours) leaving an atonic stomach. Large atonic stomach—seen in both GOO and functional

Table 4.166.1: Difference between gastric carcinoma and gastric lymphoma

| | <i>Gastric carcinoma</i> | <i>Gastric lymphoma</i> |
|----------------------------|-------------------------------|---|
| Wall thickness | <4 cm | >4 cm |
| Peri-gastric fat stranding | Present | Absent |
| Luminal narrowing | Yes | No |
| Gastric outlet obstruction | Present | Absent (aneurysmal dilatation) |
| Lymph nodal involvement | Above the level of renal hila | Bulky and extends below the level of renal hila |
| Trans-pyloric extension | Less likely (5–25%) | Common (40%) |

Table 4.166.2: Numbering of regional lymph nodes of stomach according to classification of Japanese Research Society for Gastric Cancer (JRS GC) 1997

| | | |
|----|--|---|
| 1 | Right paracardial lymph nodes | Perigastric lymph nodes (1 to 6) |
| 2 | Left paracardial lymph nodes | |
| 3 | Lesser curvature lymph nodes | |
| 4 | Greater curvature lymph nodes | |
| 5 | Suprapyloric lymph nodes | |
| 6 | Infrapyloric lymph nodes | |
| 7 | Lymph nodes along the trunk of left gastric artery | Second tier/metastatic lymph nodes (7–9 and 11) |
| 8 | Lymph nodes along the common hepatic artery | |
| 9 | Lymph nodes along coeliac artery | |
| 11 | Lymph nodes along splenic artery | |

Table 4.166.3: Differential diagnosis for carcinoma stomach

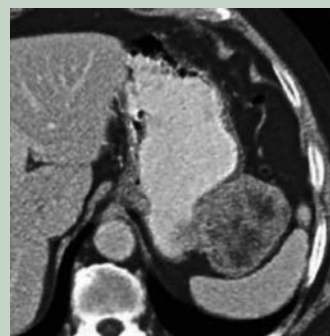
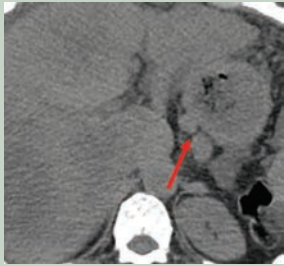


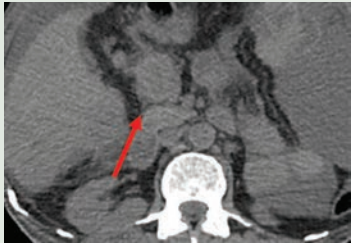
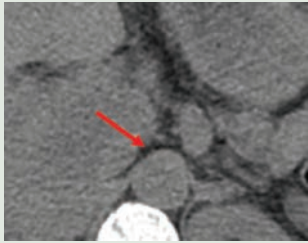
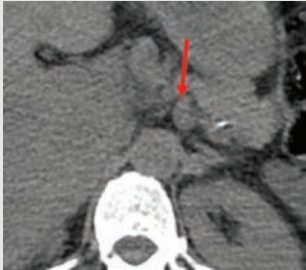
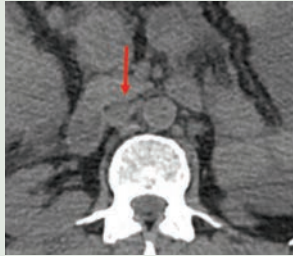
| <i>Differential diagnosis</i> | <i>Radiological features</i> | <i>Imaging</i> |
|--|---|---|
| Gastric lymphoma | Refer to case 167 | |
| Gastric metastases Most common primary sites are colon, malignant melanoma, breast, lung and pancreas. | Can be focal masses (e.g., melanoma) or diffuse, even linitis plastica appearance (e.g., breast cancer) Wall thickening is soft tissue density. Barium study—Bull’s-eye or “target” lesions: Centrally ulcerated submucosal masses in melanoma metastasis. Lobular breast cancer: Linitis plastica or “leather bottle” appearance | |
| Gastric GIST Submucosal tumor of gastrointestinal (GI) tract derived from interstitial cells of Cajal. | Large, lobulated submucosal mass ± cavitation It can present as intramural (50%), exogastric (35%), endogastric (15%) mass. Ulcerations are common in larger masses. Stomach is most common site (2/3 of cases). Treatment: Surgery with en bloc resection, tyrosine kinase inhibitor chemotherapy (imatinib) for metastatic disease |  |

Fig. 4.166.4: Gastric GIST

(Contd.)

Table 4.166.3: Differential diagnosis for carcinoma stomach (Contd.)

| | | |
|---|--|--|
| 10 | Splenic hilar lymph nodes | Third tier / Metastatic lymph nodes (10, 12–20, 110, 111 and 112) |
| 12 | Hepatoduodenal lymph nodes along the proper hepatic artery and bile duct | |
| 13 | Lymph nodes on the posterosurface of head of pancreas | |
| 14 | Lymph nodes along the SMV | |
| 15 | Lymph nodes along the middle colic vessels | |
| 16 | Para-aortic lymph nodes | |
| 17 and 18 | Peripancreatic lymph nodes | |
| 19 | Infra-diaphragmatic lymph nodes along subphrenic vessels | |
| 20 | Paraesophageal region in the diaphragmatic esophageal hiatus | |
| 110, 111, 112 | Lower thorax lymph nodes in paraesophageal, supradiaphragmatic and posterior mediastinal region. | |
|  <p>Fig. 4.166.5: Lesser curvature adenopathy</p> | |  <p>Fig. 4.166.6: Greater curvature lymph nodes</p> |
|  <p>Fig. 4.166.7: Suprapyloric node</p> | | |
|  <p>Fig. 4.166.8: Infrapyloric regional nodes</p> | |  <p>Fig. 4.166.9: Left gastric artery node</p> |
| Lymph nodes on the posterior surface of head of pancreas and along the SMV | | Para-aortic and middle colic adenopathy |
|  <p>Fig. 4.166.10: Lymph nodes on the posterior surface of head of pancreas and along the SMV</p> | |  <p>Fig. 4.166.11: Para-aortic and middle colic adenopathy</p> |

stasis. But in functional stasis barium flows freely through pylorus if the patient correctly postured. The large stomach is more common with benign than with malignant lesions. Delay in emptying: Retention of more than 50% of contrast after 4–6 hours film. Abnormal mobility of the pylorus—where the obstruction beyond the pylorus as in cicatrization of duodenal cap, the pyloric canal shows abnormal mobility.

Krukenberg tumor (“signet ring” subtype of metastatic tumor to the ovary). The colon and stomach are the most common primary tumors to result in ovarian metastases, followed by the breast, lung, and contralateral ovary; pancreatic carcinoma; cholangiocarcinoma/gallbladder carcinoma. They can show low or high signal intensity on T2-W. Other features: Bilateral complex masses with hypointense solid components (dense stromal reaction);

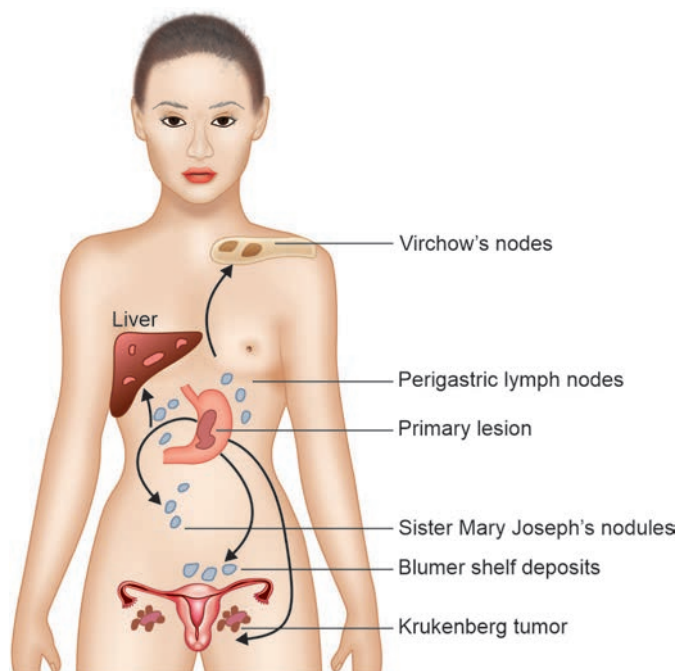
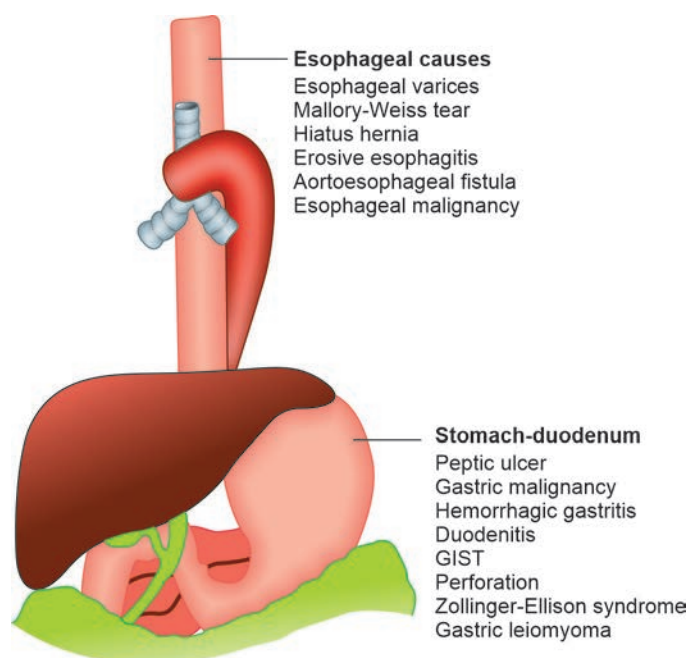


Fig. 4.166.12: Nodal involvement in gastric carcinoma



Other causes

NSAID abuse, visceral artery aneurysms
anticoagulant and fibrinolytic medications, trauma, arteriovenous malformation, pancreatitis, hemobilia
Mesenteric venous thrombosis, pseudoxanthoma elasticum. Dieulafoy's lesion, Osler-Weber-Rendu disease
Coagulation disorders: DIC, Vasculitis: Henoch-Schönlein purpura

Fig. 4.166.13: Causes of hematemesis

internal hyperintensity (mucin) on T1 and T2 weighted MR images.

Sister Mary Joseph nodule: Metastatic lesion involving the umbilicus. The most common cause—intra-abdominal adenocarcinoma. Seen as a solid subcutaneous/dermal nodule/focal umbilical thickening, generally in the context of widespread malignancy. Periumbilical area has a rich vascular, and lymphatic supply and is a point of convergence for multiple peritoneal folds (ligamentum teres, medial umbilical ligaments, median umbilical ligament).

4.167 GASTROINTESTINAL TRACT

Case No. 167

Clinical history: 54-year-old male, complaints of dyspepsia.

Radiological techniques and observation: Figure 4.167.1 is plain radiograph abdomen (AP) and Fig. 4.167.2 is barium meal follow through (spot film—oblique view). Narrow lumen with reduced capacity of the stomach is noted in the plain radiograph. Liver and spleen shadow appears normal. Bilateral psoas shadow appears normal. Visualised skeleton and soft tissue appear normal. On barium meal, gastric fundus appears normal. The mucosa of body and antrum is irregular, distorted, i.e. thickened or nodular. Leather-flask shaped stomach with lack of distensibility is noted. The narrowing of the stomach should be compared with other images of barium meal or dynamic imaging for its persistence. Entry of contrast into the small bowel noted.

Figures 4.167.3 and 4.167.4 are contrast enhanced (IV) axial sections of abdomen showing diffuse thickening of the fundus, body and antrum of stomach. Luminal narrowing of the stomach is noted. Suspicious loss of fat plane between the lesion and the head of pancreas noted. No evidence of adjacent bulky lymph nodes. Visualised liver, spleen and pancreas appears normal.

Interpretation: A: 54 years old male, lesion in fundus, body and antrum of stomach; C: Diffuse thickening, narrow lumen with reduced capacity of the stomach, B: Loss of fat plane between the lesion and the head of pancreas; D: Linitis Plastica.

Principal diagnosis: The principal diagnosis is linitis plastica, possibly adenocarcinoma of stomach.

Differential diagnosis: The cause of linitis plastica includes the following differential diagnoses:

Neoplastic: (1) Gastric carcinoma, (2) Lymphoma, (3) Metastases—particularly breast. (4) Local invasion—

pancreatic carcinoma. Inflammatory: Corrosives—can cause rigid stricture of antrum extending up to the pylorus. Radiotherapy—can cause rigid stricture of antrum with some deformity. Mucosal folds may be thickened or effaced. Large antral ulcers can also occur. Granulomatous: Crohn's disease, TB. Eosinophilic enteritis—commonly involves gastric antrum (causing narrowing and nodules) in addition to small bowel, eosinophil count is elevated. Occasionally spares the mucosa, so needs full thickness biopsy for confirmation. Diffuse gastric diverticula (rare); sarcoidosis, gastric amyloidosis.

Treatment: The patient can be further managed by Endoscopic biopsy; Staging work up to be done. Depending upon the staging surgical treatment/chemotherapy can be undergone with follow-up.

Brief discussion about the condition: Linitis plastica/ Brinton's disease (also called leather bottle stomach).

Linitis plastica is a descriptive term for a tumor of the stomach, usually a carcinoma, which is diffusely infiltrating with considerable fibrosis. Radiographically this usually appears as a narrowed, rigid stomach. It is important to realize that as the infiltration is submucosal, gastric biopsies are frequently negative.

Thick stomach folds/wall: Thickness greater than 1 cm. CT assessment of non-distended stomach remains limited, but CT after gas or water distension is often useful.

Inflammatory: (1) Gastritis—localized or generalized fold thickening \pm inflammatory nodules (< 1 cm, mostly in the antrum), erosions and coarse areae gastricae. (2) Zollinger-Ellison syndrome—suspect if postbulbar ulcers. Ulceration in both first and second parts of duodenum is suggestive, but ulceration distal to this is virtually diagnostic. Thick folds and small bowel dilatation may occur in response to excess acidity. Due to



Fig. 4.167.1

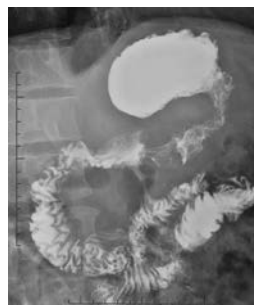


Fig. 4.167.2



Fig. 4.167.3



Fig. 4.167.4

| Table 4.167.1: Distinction between benign and malignant ulcer in barium studies | | |
|---|--|---|
| Character | Benign ulcer | Malignant ulcer |
| Location | Lesser curvature at junction of corpus, antrum within 7 cm from pylorus | Anywhere. Fundal ulcer above the level of cardia, along greater curvature are usually malignant |
| Ulcer size | Usually less than 2 cm | Usually more than 2 cm |
| Projection | Outside lumen | Inside lumen |
| Floor | Smooth | Nodular ulcer floor |
| Crater | Round, ovoid | Irregular |
| Haudek niche | Projecting outside | Not projecting beyond expected margin of stomach |
| Notch (on opposite wall due to fibrosis) | Present | Absent |
| Ulcer collar | Present | Absent |
| Hampton's line | Present | Absent |
| Carmen meniscus sign | Absent | Present |
| Ulcer mound | Smooth | Rolled edge |
| Radiating folds | Symmetric | Nodular, clubbed, fused |
| Areae gastricae | Preserved | Destroyed |
| Mass lesion | No mass | Associated with larger irregular mass |
| Prognosis | Complete heal in 50% by 3 weeks 100% in 6–8 weeks, slower to heal in older patient | Partial healing may occur |

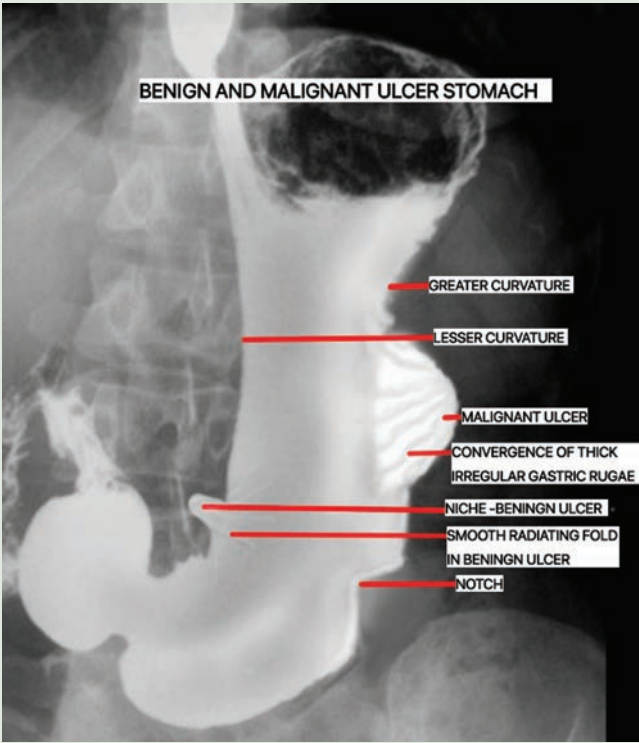


Fig. 4.167.5: Benign and malignant ulcer stomach

Ulcer crater: Collection of barium on dependent surface which usually projects beyond anticipated wall of stomach in profile
Hampton's line: 1 mm thin straight line at neck of ulcer in profile view representing thin rim of undermined gastric mucosa
Ulcer collar: Smooth, thick, lucent band at neck of ulcer in profile view representing thicker rim of edematous gastric wall
Ulcer mound: Smooth, sharply delineated tissue mass surrounding a benign ulcer

Table 4.167.2: Calcification of gastric mucosa

Calcification of gastric mucosa occurs in Mucinous adenocarcinoma of stomach, in which there may be calcified metastatic lymph nodes. Other causes include: Chronic renal failure, drugs (antacids, antihypertensives), hyperparathyroidism, and hypercalcaemia related to malignancy.



Fig. 4.167.6: Multiple calcified lymph nodes in mucinous adenocarcinoma of stomach



Fig. 4.167.7: Calcification of gastric mucosa

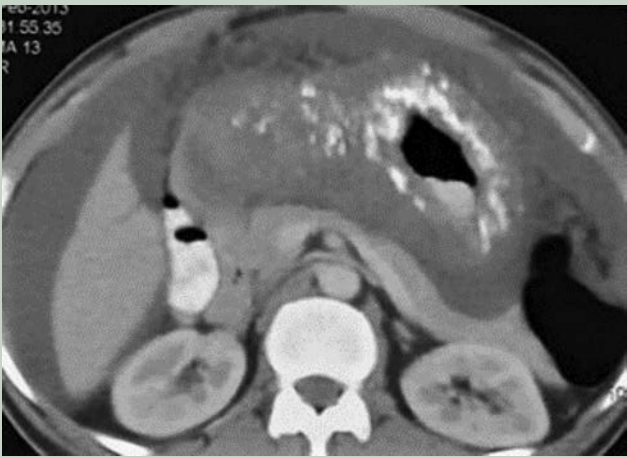


Fig. 4.167.8: Calcification of gastric mucosa in mucinous adenocarcinoma

gastrinoma of non-beta cells of pancreas (no calcification, moderately vascular). 50% malignant—metastases to liver (10% of gastrinomas may be ectopic—usually in medial wall of the duodenum). 3. Pancreatitis (acute). 4. Crohn's disease—mild thickening of folds with aphthoid ulceration may occur in up to 40% of Crohn's disease. Infiltrative/neoplastic. 5. Lymphoma usually non-Hodgkin's lymphoma, may be primary or secondary. 6. Carcinoma—irregular folds with rigid wall. 7. Pseudolymphoma—benign reactive lymphoid hyperplasia. 70% have an ulcer near the centre of the area affected. 8. Eosinophilic gastroenteritis. Others: Menetrier's disease—huge, smooth folds, especially greater curve. Rarely extend into antrum. No rigidity or ulcers. 'Weep' protein sufficient to cause hypoproteinaemia (effusions, oedema, thick folds in small bowel). 9. Varices—occur in fundus and usually associated with oesophageal varices.

Stomach masses and filling defects: Primary malignant neoplasms

1. **Carcinoma**—most polypoidal carcinomas are 1–4 cm in diameter. (Any polyp >2 cm in diameter must be considered to be malignant). Endoscopic US accurate

in local staging for early disease. CT superior for more advanced disease.

2. **Lymphoma**—1–5% of gastric malignancy. Usually non-Hodgkin's. May be ulcerative, infiltrative and/or polypoid. Often cannot be distinguished from carcinoma, but extension across the pylorus is suggestive of a lymphoma. MALT lymphoma is strongly associated with *Helicobacter pylori* infection. CT—marked hypopattenuating wall thickening; mean 3–5 cm. Whole stomach involved in 50%. Most (not all) have adjacent lymphadenopathy.
3. **GIST** (up to 30% are malignant)—commonest in stomach but also small bowel, colon and mesentery. Variable size and malignant potential. Cell-surface marker (c-KIT) detectable by immunohistochemistry. Large tumors hyperenhancing and often heterogeneous on CT/MRI. Ulceration and fistulation common. 50% have metastasis at presentation (liver, peritoneum). May enlarge with treatment: Reduced enhancement suggests response. Features suggestive of malignancy—size >5 cm, gastric location, metastasis, heterogenous enhancement with cystic/necrotic changes.

Table 4.167.3: Normal bowel wall thickness

| | | | |
|-----------|--------|--------|--------|
| Esophagus | 3 mm | Ileum | 1–2 mm |
| Stomach | 2–5 mm | Cecum | <4 mm |
| Duodenum | <3 mm | Colon | 2–4 mm |
| Jejunum | 1–3 mm | Rectum | <5 mm |

4. **Polyps**—It can be hyperplastic, adenomatous, hamartomatus (refer to case no 4.168).

Extrinsic indentation (refer to case no 4.169) 1. Pancreatic tumor/pseudocyst. 2. Splenomegaly/hepatomegaly. 3. Retroperitoneal tumors.

Others

1. Nissen fundoplication may mimic a distorted mass in the fundus.
2. Bezoar—‘mass’ may be mobile. Tricho—(hair) or phyto—(vegetable matter).
3. Lymphoid hyperplasia—innumerable, 1–3 mm diameter, round nodules in the antrum or antrum and body. Association with *H. pylori* gastritis.
4. Pancreatic ‘rest’—ectopic pancreatic tissue causes a small filling defect, usually on the inferior wall of the antrum, and resembles a submucosal tumor. Central ‘blob’ of barium (‘bull’s-eye’ or target lesion) in 50%.

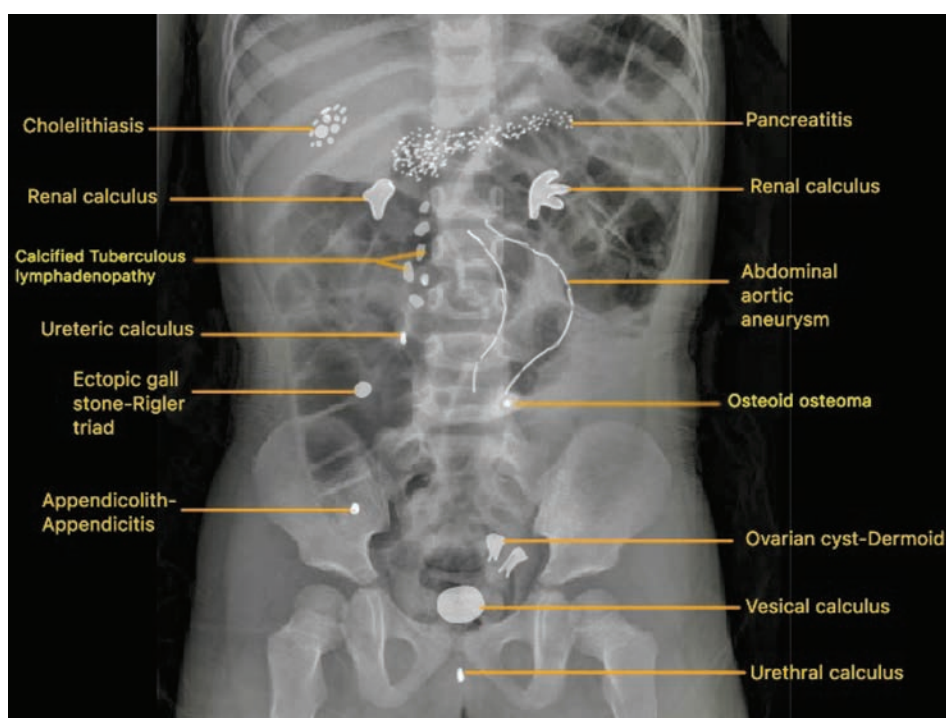
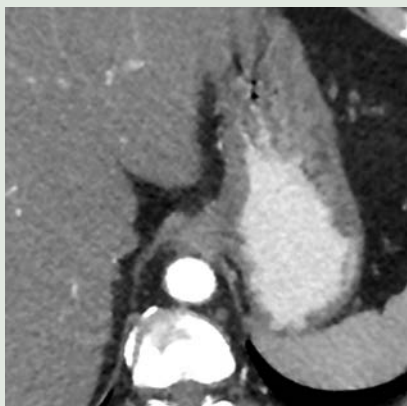
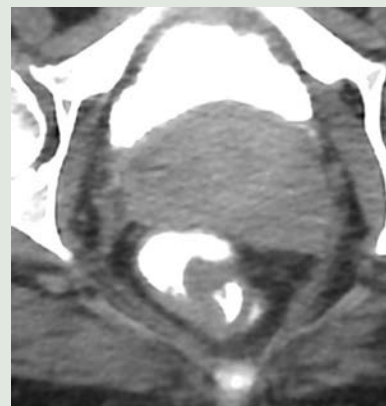


Fig. 4.167.9: Approach to radio-opacity in plain abdomen radiograph

Table 4.167.4: Normal structures that mimic thickening**Fig. 4.167.10:** Oesophagogastric junction**Fig. 4.167.11:** Ileocecal junction**Fig. 4.167.12:** Large bowel contraction

4.168 GASTROINTESTINAL TRACT

Case No. 168

Clinical history: 50-year-old female patient with vomiting for 2 days and colicky lower abdominal pain.

Radiological technique and observation: Figures 4.168.1 to 4.168.3 are contrast enhanced CT axial sections of abdomen showing intussusception involving ileal loops. At the lead point there is a polyp. Other visualized small bowel loops in the left side also shows a sessile polyp which shows enhancement on contrast and appears hyperintense on Figure 4.168.4, which is T2 weighted MRI image. No free fluid seen in the given sections.

Interpretation: A—50 years old female, lesion in ileal loops, C—intussusception of ileal loops, B—lead point is polyp, D—multiple polyps of small bowel with ileoileal intussusception.

Principal diagnosis: Multiple polyps of small bowel with ileoileal intussusception.

Further investigations: Small bowel follow through or MR enterography/capsule endoscopy.

Management: Biopsy may be taken from the polyps, if histology shows increased risk of malignancy, then resection may be done. In case of obstruction, resection anastomosis may be done.

Discussion

Gastric polyps (Fig. 4.168.4)

1. **Hyperplastic**—accounts for 80–90% of gastric polyps. Usually multiple, small (<1 cm in diameter) and occur randomly throughout stomach but predominantly affect body and fundus. Associated with chronic gastritis. Rarely can be very large (3–10 cm).
2. **Adenomatous**—usually solitary, 1–4 cm in diameter, sessile and occur in antrum. High incidence of malignant transformation, particularly if >2 cm in size and carcinomas elsewhere in stomach (because of dysplastic epithelium). Associated with pernicious anaemia.
3. **Hamartomatous**—characteristically multiple, small and relatively spare the antrum. Occur in 30% of Peutz-Jeghers syndrome, 40% of familial polyposis coli and Gardner's syndrome.
Submucosal neoplasms: Smooth, well-defined filling defect, with a re-entry angle.
1. **Leiomyoma**—many previously diagnosed would now be classified as GIST. Can be very large with a substantial exogastric component. Central ulceration and massive haematemesis may occur.
2. **Lipoma**—can change shape with position of patient and may be relatively mobile on palpation.



Fig. 4.168.1



Fig. 4.168.2



Fig. 4.168.3

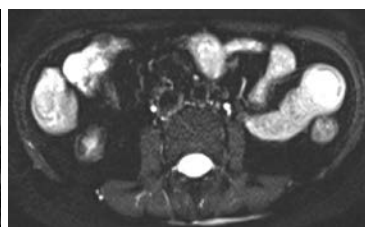


Fig. 4.168.4

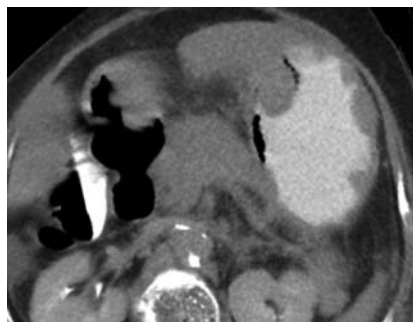


Fig. 4.168.5: Gastric polyp



Fig. 4.168.6: Peutz-Jeghers syndrome

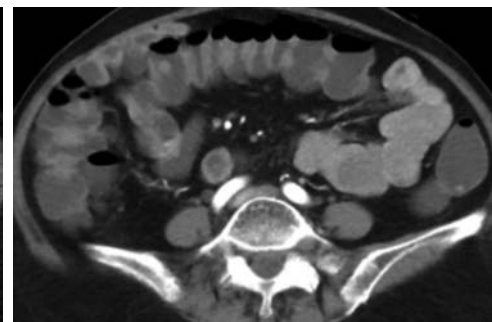


Fig. 4.168.7: Peutz-Jeghers syndrome

Table 4.168.1: Imaging in large bowel polyps

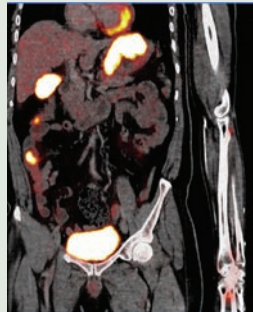


Fig. 4.168.8: Malignant melanoma left hand with stomach, gall bladder and ileal metastasis



Fig. 4.168.9: Barium enema shows multiple polyps in the descending colon

Polyp with diverticulosis

Double contrast barium enema images show multiple polyps with diverticulosis in the descending colon. Polyps show characteristic bowler hat sign with axis pointing towards the bowel lumen. Multiple diverticula are also noted. Their axis points away from the lumen.



Fig. 4.168.10: Polyp with diverticulosis

Multiple colon polyps in familial adenomatous polyposis. Rectal contrast coronal reconstructed CT image: Multiple polyps are seen in the transverse colon with irregular wall thickening causing luminal narrowing in the hepatic flexure—colon carcinoma.

Gardner syndrome is a variant of FAP. In addition to colon polyps, patients also have: Osteomas, desmoid tumors, papillary carcinoma of thyroid gland and epidermoid cysts.

Turcot syndrome is another variant of FAP where patients also have gliomas and medulloblastomas.

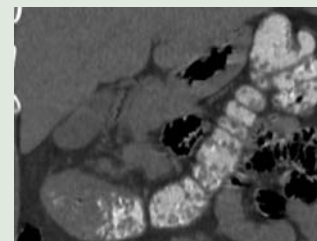


Fig. 4.168.11: Multiple colon polyps in familial adenomatous polyposis

Solitary sessile rectal polyp

It is associated with risk of malignancy when the size is greater than 10 mm and if it is of villous histology.

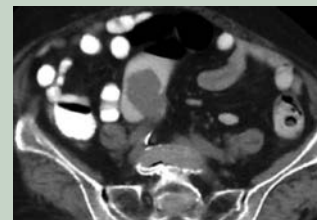


Fig. 4.168.12: Solitary sessile rectal polyp

Sigmoid colon polyp with intussusception

Multiplanar reconstructed image of CT of pelvis with rectal contrast shows sigmoid intussusception with polyp as lead point.



Fig. 4.168.13: Sigmoid colon polyp with intussusception

Table 4.168.2: Histology in adenomatous polyps and percentage of chance of malignant transformation

| Histologic type | <1 cm | 1–2 cm | >2 cm |
|-----------------|-------|--------|-------|
| Tubular | 1.0 | 10.2 | 34.7 |
| Tubulovillous | 3.9 | 7.4 | 45.8 |
| Villous | 9.5 | 10.3 | 52.5 |

Adapted from Muto T, Bussey HJR, Morson BC: The evolution of cancer of the colon and rectum. Cancer. 1975 Dec;36(6):2251–70.

Table 4.168.3: ACR C-RADS categories of colonic findings and management recommendations

| | |
|----|--|
| C0 | Inadequate study/awaiting prior comparisons inadequate prep: Cannot exclude lesions ≥ 10 mm owing to presence of fluid/feces inadequate insufflation: One or more colonic segments collapsed on both views awaiting prior colon studies for comparison |
| C1 | Normal colon or benign lesion; continue routine screening no visible abnormalities of the colon no polyp ≥ 6 mm lipoma or inverted diverticulum non-neoplastic findings – e.g., colonic diverticula |
| C2 | Intermediate polyp or indeterminate finding: Surveillance or colonoscopy recommended intermediate polyp 6–9 mm, <3 in number; indeterminate findings, cannot exclude polyp ≥ 6 mm in technically adequate exam |
| C3 | Polyp, possibly advanced adenoma: Follow-up colonoscopy recommended polyp ≥ 10 mm ≥ 3 polyps, each 6–9 mm |
| C4 | Colonic mass, likely malignant: Surgical consultation recommended lesion compromises bowel lumen, demonstrates extracolonic invasion |

Table 4.168.4: Difference between polyp and diverticulum

| Polyp | Diverticulum |
|---|---|
| Bowler's hat sign—dome towards the bowel axis | Dome points away from the lumen |
| Meniscus sign—inner margin well defined, fades outwards | Outer margin well defined, fades inward |
| Filling defect in barium pool | Protrusion out of lumen/fluid level. |
| Mexican hat sign, stalk sign | |

3. **Neurofibroma**—leiomyomas and lipomas are more common, even in patients with generalized neurofibromatosis.
4. **Metastases**—frequently ulcerate: 'Bull's-eye' lesion. Usually melanoma, but bronchus, breast, lymphoma, Kaposi's sarcoma and any adenocarcinoma may metastasize to stomach. Breast primary often produces a scirrhous reaction, indistinguishable from linitis plastica.

Small Bowel Polyps: Peutz-Jeghers Syndrome

Multiple hamartomatous polyps are seen in the small bowel. They can also have gastric polyps. Colonic polyps if present are usually adenomatous. Characteristic oral and perioral pigmentation may be seen ((Figs 4.168.6 and 4.168.7).

Polypoid sessile tumor: Small plaque-like growth.

Often presents with intussusception with or without enlarged mesenteric nodes; perivascular invasion. \pm metastases, liver, peritoneal surfaces, ovaries.

Risk factors: Celiac and Crohn disease, polyposis syndromes increase risk of SB carcinoma.

Inflammatory polyps may be seen in ulcerative colitis in acute stage. They are usually pseudopolyps which are islands of normal mucosa with denuded surrounding mucosa.

Histologic type: Hyperplastic, adenomatous, and hamartomatous. There are no reliable radiographic findings to distinguish adenomatous polyps from the other types. Hyperplastic polyps are generally small (<1 cm diameter), and these small lesions are believed not to have malignant potential.

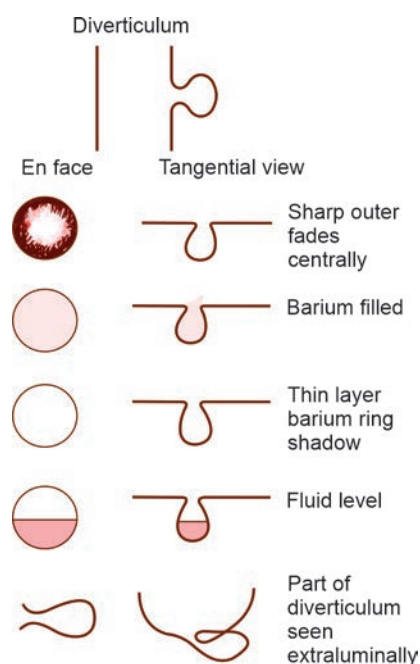


Fig. 4.168.14: Diverticulum

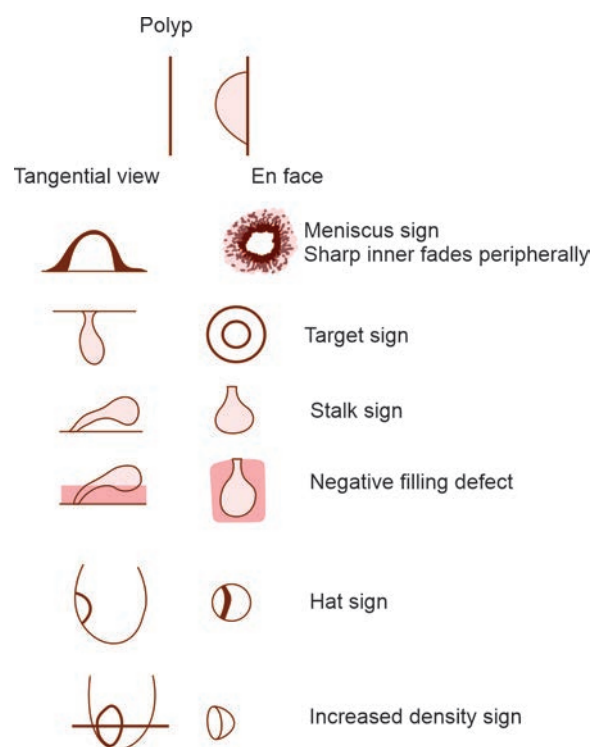


Fig. 4.168.15: Polyp

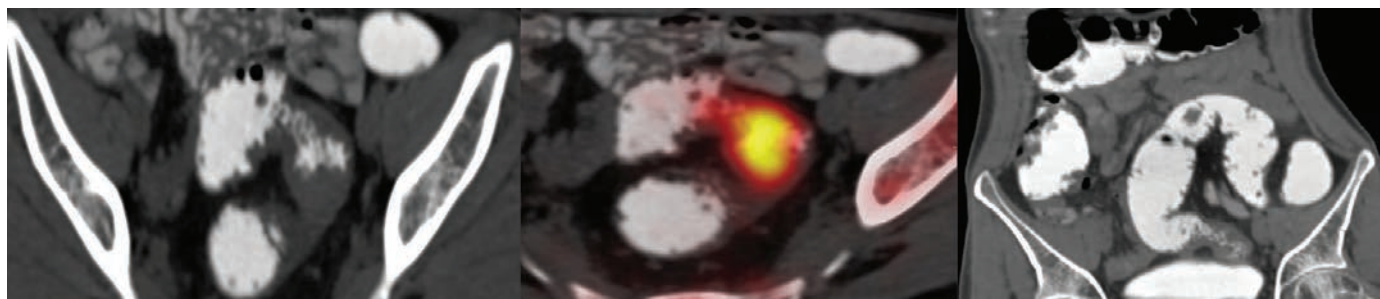


Fig. 4.168.16: FAP with malignant transformation

Adenomatous polyps can be further classified into three histologic subtypes: Tubular, tubulovillous, and villous adenomas.

The majority of adenocarcinomas of the colon arise from pre-existing adenomas. Polyps with a higher percentage of villous features are at a higher risk for malignant transformation than are tubular adenomas.

Polyp diameter is also a key factor in assessing the risk of malignancy in an adenomatous polyp because the larger the polyp, the higher the risk.

Pedunculated polyps with stalk greater than 2 cm are more than 90% benign.

Malignant potential of colorectal adenomas increases with increasing size of polyp.

4.169 GASTROINTESTINAL TRACT

Case No 169

Clinical history: 58-year-old male presented with hematemesis, abdominal distension and abdominal pain with occupational history of working in paint industry.

Radiological technique and observations: Figure 4.169.1 is barium meal image in right anterior oblique projection that shows filling of contrast in stomach, duodenum up to the duodeno-jejunal flexure. There is smooth indentation on the lesser curvature of the stomach due to extrinsic compression, causing luminal narrowing. No evidence of mucosal irregularity, ulceration, filling defect and outpouchings noted.

With these findings, the possible causes include, lesser sac lesion (pseudocyst), left lobe of liver lesion, GIST from stomach, lymphoma from stomach, body of the pancreas lesion, large retroperitoneal mass and lymph node enlargement. Plain CT-axial and contrast enhanced CT-axial images of the upper abdomen, maximum intensity projection, reformatted images of abdominal aortic angiogram—sagittal and coronal sections has been provided.

Figures 4.169.2 is plain CT-axial section showing well-defined soft tissue dense lesion with central ill-defined areas of hypodensities noted within. The predominant part of the lesion is in the lesser sac. The lesion displaces the stomach anterolaterally narrowing its lumen. However, the fat plane between the lesion and stomach is maintained. Superiorly the lesion extends to involve the left lobe of liver, with the fat plane between the lesion and liver being obliterated. The fat plane between the lesion and the pancreas is lost. Figures 4.169.3 to 4.169.5 are contrast images showing intense vascularity with multiple tortuous vessels indicating neovascularity in the periphery of the lesion with central areas of necrosis. In angiogram, the predominant blood supply to the lesion comes from the common hepatic artery.

There is no evidence of enlarged porta hepatis/perigastric/peripancreatic/para-aortic lymph nodes

noted. No evidence of any vascular invasion noted. No evidence of calcification/cystic components noted. No other lesions in the liver/visualized bones.

Interpretation: A—58 years old male working in paint industry, lesion in retroperitoneum, C—well defined soft tissue dense lesion with central ill-defined areas of hypodensities, B—intense vascularity and necrosis of the lesion indicate malignant vascular neoplasm arising from the retroperitoneum, D—angiosarcoma.

Principal diagnosis: Angiosarcoma

Further investigations and management: Local and locoregional staging with MRI and systemic staging with PET. Based on the staging, USG guided biopsy for confirmation/surgical resection/systemic or hepatic arterial chemotherapy: Antiangiogenic therapy.

Discussion:

Angiosarcoma: Angiosarcomas are malignant sarcomas of vascular endothelial cell origin. Endothelial cells make up the lining of vessels. Angiosarcomas can occur in any region of the body, although they are most commonly located in the skin, breast, liver, and deep tissue.

Etiology

- Environmental carcinogens (polyvinyl chloride, arsenicals, thorotrast)
- **Drugs:** Cyclophosphamide, anabolic steroids, diethylstilbestrol, oral contraceptives
- Post-radiation (median latency: 74 months)
- Neurofibromatosis type 1

CT: 3 patterns

- Multifocal hypervascular masses in liver ± spleen, other organs. May have peripheral and delayed enhancement that simulates hemangiomas
- Single or multiple hepatic masses with variable necrosis
- Diffuse infiltration of liver (micronodular)
Often metastatic to nodes, lungs, bones



Fig. 4.169.1



Fig. 4.169.2



Fig. 4.169.3

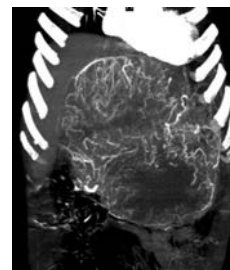


Fig. 4.169.4

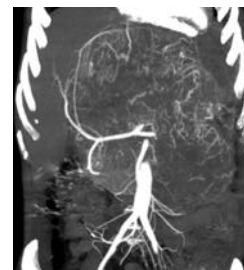

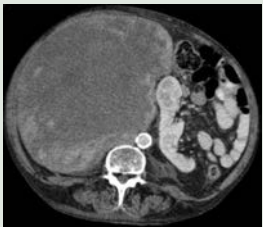
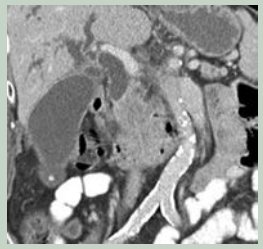
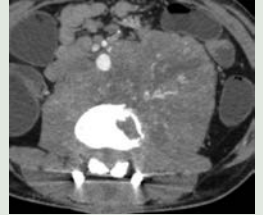
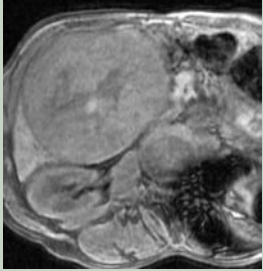


Fig. 4.169.5

Table 4.169.1: Differential diagnosis of lesion in the gastrohepatic space

| Condition/demography/treatment | Radiological findings | Image |
|---|--|--|
| Gastrointestinal stromal tumor: Submucosal tumor of gastrointestinal (GI) tract derived from interstitial cells of Cajal. About 50–70% of GISTs occur in stomach; 33% in small bowel; 5–15% rectocolon; and only 1–5% in esophagus. Treatment includes surgery with en bloc resection and tyrosine kinase inhibitor chemotherapy (imatinib) | Rounded, exophytic, submucosal gastric mass. Ulcerations are common in larger masses. Necrotic center of tumor may fill with barium. Hypo- or hypervascular, well-circumscribed, submucosal mass on arterial phase images; ulceration and necrosis are common |  Fig. 4.169.6: Gastrointestinal stromal tumor |
| Pleomorphic liposarcoma: Retroperitoneal tumor in adults between 50 and 60 years of age and originates from retroperitoneal smooth muscle tissue, from the vascular wall, or from embryonic remnants of the Wolffian ducts | Pleomorphic liposarcoma is an aggressive, heterogeneous tumor that is the least common liposarcoma subtype, characterized on imaging by areas of necrosis and the absence of adipose components, making it indistinguishable from other solid retroperitoneal tumors |  Fig. 4.169.7: Pleomorphic liposarcoma |
| Pancreatic mass: Pancreatic ductal adenocarcinoma makes up the vast majority (~90%) of all pancreatic neoplasms and remains a disease with a very poor prognosis and high morbidity. 80% of cases occurs after the age of 60. | Typically ductal adenocarcinomas appear as poorly defined masses with extensive surrounding desmoplastic reaction. Double duct sign may be seen. If the tumor surrounds a vessel by more than 180 degrees, then it is deemed T4 disease and is unresectable |  Fig. 4.169.8: Pancreatic ductal adenocarcinoma |
| Lymphoma: Lymphoma is the most common malignant retroperitoneal neoplasm, as well as being the most common small round cell tumor. The treatment consists of chemotherapy combined with radiotherapy or immunotherapy. | Typically presents as a para-aortic or pelvic mass, involving the adjacent structures, with a homogeneous and hypovascular aspect. FDG avidity depends on factors such as the histological characteristics, grade, and proliferation of the tumor |  Fig. 4.169.9: Lymphoma |
| Exophytic hepatocellular CA: Hepatocellular carcinoma (HCC) is the most common primary malignancy of the liver. However, exophytic HCC is a rare entity (0.3 to 3% of all HCCs). It is strongly associated with cirrhosis, from both alcohol and viral etiologies. HCC constitutes approximately 5% of all cancers partly due to the high endemic rates of hepatitis B infection | Its characteristic enhancement pattern: Early arterial enhancement with early “washout.” Rim enhancement on delayed post-contrast images causing a capsule appearance is considered relatively specific for HCC. Propensity to invade vascular structures, most commonly the portal vein, but also the hepatic veins, IVC, and right atrium. |  Fig. 4.169.10: Hepatocellular carcinoma |

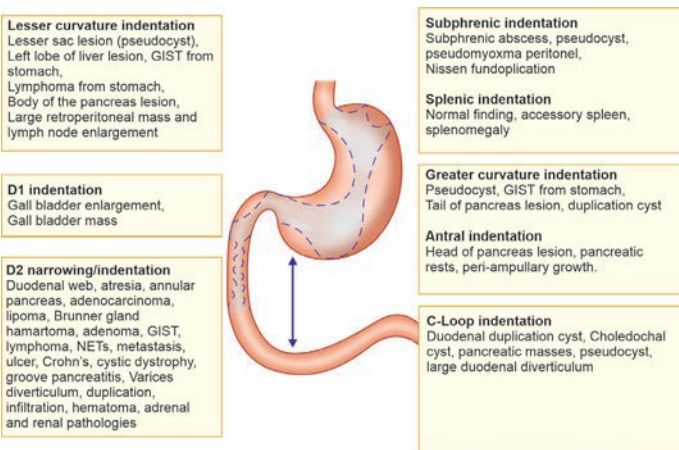


Fig. 4.169.11: Indentations of various lesions on stomach and duodenum

MRI: To evaluate tumor response to preoperative radiation or chemotherapy.

A nonspecific mass with signal intensity similar to that of muscle on T1 and very high signal intensity on T2. Hypointensity on both images may suggest organized hemorrhagic focus. MRI is capable of detecting the vascular channels and spaces that suggest the diagnosis of a vascular lesion.

Table 4.169.2: Approach to origin of the tumors

1. **Beak sign:** When a mass deforms the edge of an adjacent organ into a “beak” shape, it is likely that the mass arises from that organ (beak sign). On the other hand, an adjacent organ with dull edges suggests that the tumor compresses the organ but does not arise from it

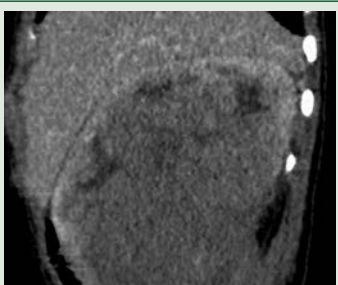
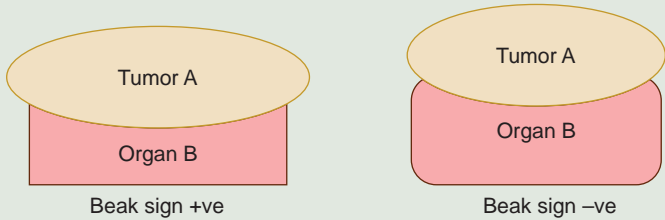


Fig. 4.169.12: Beak sign +ve for kidney

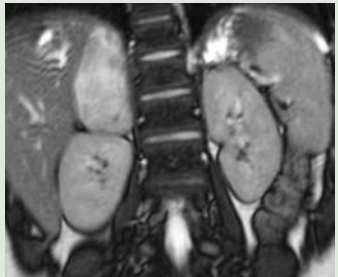


Fig. 4.169.13: Beak sign –ve for kidney

2. **Phantom organ sign:** When a mass arise from a organ, sometimes it becomes undetectable. This is known as the phantom organ sign. For example, in this image, the left adrenal gland is not visualized and a mass is seen in the region, which is possibly arising from the left adrenal gland.



Fig. 4.169.14: Phantom organ sign showing renal tumor

(Contd.)

Table 4.169.2: Approach to origin of the tumors (Contd.)

3. Embedded organ sign: Tubular organs: When a tumor compresses an adjacent plastic organ (e.g. gastrointestinal tract, inferior vena cava) that is not the organ of origin, the organ is deformed into a crescent shape. In contrast, when part of an organ appears to be embedded in the tumor, the tumor is in close contact with the organ and the contact surface is typically sclerotic with desmoplastic reaction. Occasionally, the contact surface becomes ulcerative. When the embedded organ sign is present, it is likely that the tumor originates from the involved organ

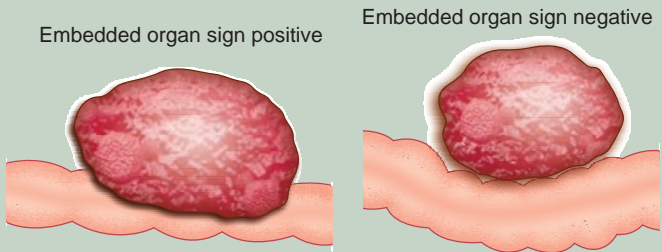


Fig. 4.169.15: Embedded organ sign +ve



Fig. 4.169.16: Embedded organ sign –ve for stomach

4. Prominent feeding artery sign: Feeding artery to the lesion arises from the organ of origin. Exophytic liver mass (hepatic artery/portal vein), meningioma (middle meningeal artery) Glioma (MCA)

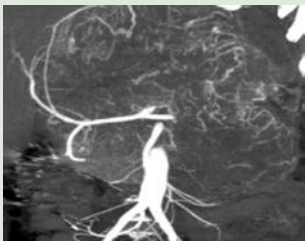


Fig. 4.169.17: Prominent feeding artery sign from SMA for angiosarcoma

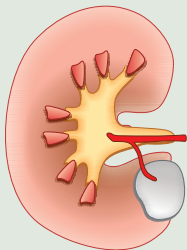


Fig. 4.169.18: Prominent feeding artery sign from renal artery for RCC

Beak sign with feeding artery sign

5. Draining vein sign: This is particularly of use in identifying the vascular neoplasms, such as the AVM and dural AV fistulas. The main drainage vessels of hepatocellular carcinoma (HCC) change from hepatic veins to hepatic sinusoids to portal veins during multistep hepatocarcinogenesis. The right ovarian vein drains into the inferior vena cava and the left ovarian vein into the left renal vein in most individuals. (ovarian vein sign)

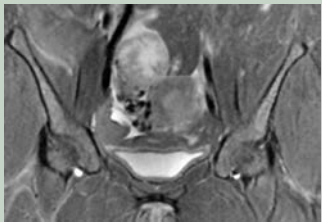


Fig. 4.169.19: Draining vein sign

6. Displacement of the organs: The displacements of the adjacent organs give clue, on particularly where the 'tumor is arising'. On radiographs, central radio-opacity with displacement of the bowel loops peripherally indicates that the lesion is intraperitoneal, whereas the anterior displacement of the bowel loops in the lateral radiograph indicates that the lesion is retroperitoneal.

Kidney is displaced inferolaterally by neuroblastoma. Splenic lesions displace the splenic flexure, whereas the liver lesions displace the hepatic flexure inferiorly.

IVC is lifted up in right adrenal and retroperitoneal lesions, whereas splenic vein is in left adrenal and retroperitoneal lesions. Enlarged right adrenal pushes IVC anteriorly while Left adrenal pushes splenic vein anteriorly. Kidneys are displaced up to midline or opposite side anteriorly indicates retroperitoneal mass.

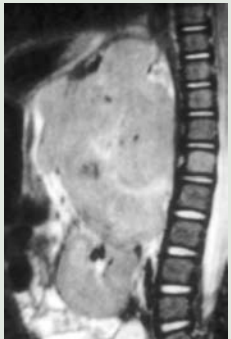


Fig. 4.169.20: Organ displacement sign: Kidney is displaced inferolaterally by neuroblastoma

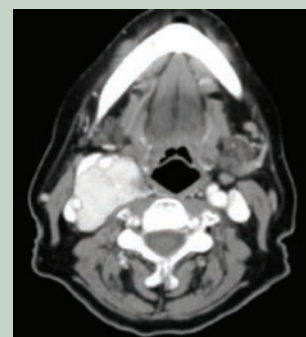
(Contd.)

Table 4.169.2: Approach to origin of the tumors (Contd.)

7. Intendation of adjacent organs: The lesions intending the lesser curvature, greater curvature, D1 and the C- loop of duodenum, gives clue to diagnosis regarding the organ of origin and has been discussed in the previous section.

**Fig. 4.169.21:** Indentation of lesser curvature of stomach

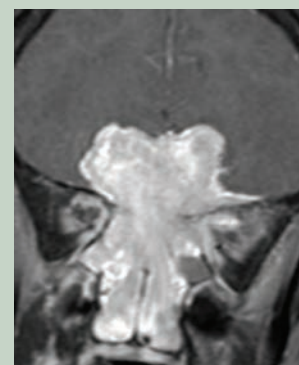
8. Displacement of fat pads: Obliteration of peritoneal fat pad by ascites. One of the diagnostic criteria for diagnosis of chest wall invasion of lung carcinoma is infiltration of extrapleural fat pad. The displacement of the parapharyngeal fat pads and the carotid vessels by neck lesions help to narrow the organ of origin.

**Fig. 4.169.22:** Fat pad displacement sign: PPS fat displaced anteromedially in carotid body tumor

9. Broad base: The broad base of the tumor, gives clue regarding the origin of the tumor. For example, meningioma has broad base towards the dura, the mediastinal mass has broad base towards the mediastinum, the pleural-based lesions have positive extrapleural sign.

**Fig. 4.169.23:** Broad base sign—mediastinal mass with broad base to mediastinum

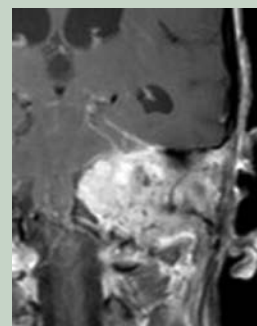
10. Shape of the lesions: The various shapes of the lesions give clue to diagnosis, as exemplified by popcorn shape—hamartoma
Tubular—hydrosalpinx
Oval/round—ovarian lesion
Dumbbell shaped—neurofibroma, esthesioneuroblastoma.
Sandwich shape—lymphoma
Coat hanger—exostosis
Figure of 8—pituitary macroadenoma, etc.

**Fig. 4.169.24:** Shape of lesion—dumbbell-shaped esthesioneuroblastoma

(Contd.)

Table 4.169.2: Approach to origin of the tumors (Contd.)

11. **Vector of growth:** The course of the structures from which the tumour arises, can be traced down which indicates the 'vector of growth' of the tumour, e.g. glomus jugulare grows superolaterally towards the middle ear. Mandibular schwannomas grow along its course causing widening of the foramen ovale. Lower cranial nerve tumors grow towards the brainstem while meningioma grows along the meninges.

**Fig. 4.169.25:** Vector of growth—glomus jugulare growing towards middle ear

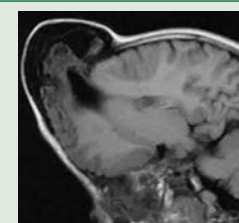
12. **Cleft sign:** The CSF cleft between the tumor and the brain, indicates that the tumour arises from the extra-axial location. The presence of cleavage between the lesion and the bone indicates that the lesion is of parosteal origin rather than periosteal.

**Fig. 4.169.26:** CSF cleft sign—meningioma

13. **Distal changes:** Lesions (nerve sheath tumors) affecting the cranial nerves especially vagus and hypoglossal nerve cause ipsilateral vocal cord palsy and atrophy of the ipsilateral side of tongue respectively. Denervation changes such as edema usually occur, in case of brachial plexus injury.

**Fig. 4.169.27:** Distal changes seen as left hemitongue fatty atrophy in hypoglossal nerve palsy due to left side tumor

14. **Bony defect/widening:** Lesions affecting the brain especially, meningocele, encephalocele and atretic cephalocele cause clefts in the brain, whereas extramedullary nerve sheath tumours of the spine cause widening of the neural foramen. Lesions arising from the cranial nerves cause widening of the corresponding foramen. For example, maxillary nerve lesions cause widening of the rotundum.

**Fig. 4.169.28:** Atretic cephalocele showing bony defect

15. **Regional lymphadenopathy:** The regional lymph nodes drainage for pelvic malignancies occurs in particular pattern toward the origin of tumor. The perivesical, internal and external iliac nodes are the regional nodes for bladder, cervix and endometrium. In addition, the common iliac nodes are regional for cervix and endometrium.

**Fig. 4.169.29:** Regional lymphadenopathy

16. **Characteristics of metastasis:** Cystic metastasis—GIST, calcifying metastasis—mucinous adenocarcinoma, hypervascular metastasis—renal cell carcinoma, follicular thyroid carcinoma, neuroendocrine tumor.

4.170 GASTROINTESTINAL TRACT

Case No. 170

Clinical history: 44-year-old male with complaints of vague abdominal pain.

Radiological techniques and observations: Figure 4.170.1 is double contrast barium meal spot film showing a large ill-defined filling defect with mucosal irregularity in the fundus and upper part of the body of stomach along the greater curvature. Extraluminal soft tissue opacity noted lateral to the filling defect, with no calcification within it. The margins appear irregular. The superior margin makes obtuse angle with gastric wall and the inferior margin makes right angle with the gastric wall. Small central barium-filled crater noted within the mass. No other lesions or filling defects in the stomach. Antropyloric region appears normal. Visualised vertebra appears normal.

Figures 4.170.2 to 4.170.4 are CECT abdomen axial and sagittal images showing a large well-defined, heterogeneously enhancing solid mass lesion in the wall of the fundus and the proximal body of the stomach along the greater curvature. Areas of low attenuation and a few specs of calcification seen within the lesion. The smaller intraluminal component makes obtuse angles with the stomach wall, and shows small mucosal irregularity. The larger extraluminal component extends laterally up to the lateral abdominal wall-internal intercostal muscle, posteriorly indents the anterior surface spleen and limited superiorly by the diaphragm. No evidence of fat within the lesion. Visualised sections of liver and spleen show no mass lesion. No perigastric lymph node enlargement. Visualised bones and soft tissue appear normal.

Interpretation: A: 55-year-old male, lesion in the gastric wall along the greater curvature, C: Large well defined, heterogeneously enhancing solid mass (embedded organ sign positive) has both intra- and extraluminal

components, with areas of necrosis and a few flecks of calcification, B: Mucosal irregularity with ulceration, D: Malignant GIST.

Principal diagnosis: Malignant gastrointestinal stromal tumor.

Management: Biopsy to confirm the diagnosis. Patient to be referred to the surgical gastroenterology department for further evaluation and to discuss with pathology department for planning the management based on its neoplastic potential. Imatinib (competitively binds to ATP binding site of tyrosine kinase, leading to cell death by apoptosis; areas of apoptosis appear as cystic spaces on CT or MRI) shows good response. PET is a sensitive modality for follow-up, superior to CT in predicting early response to imatinib. Hypermetabolic (FDG-avid) foci indicate viable tumor—for both primary tumor and metastases.

Discussion: Gastrointestinal stromal tumor (GIST) is the most common mesenchymal neoplasm of the gastrointestinal tract. GIST is defined by its expression of KIT (CD117), a tyrosine kinase growth factor receptor. The expression of KIT is important to distinguish GIST from other mesenchymal neoplasms such as leiomyoma, leiomyosarcoma, schwannoma and neurofibroma. Pharmacologically targeting this receptor with a KIT tyrosine kinase inhibitor (STI-571, imatinib), has been shown to be of clinical usefulness. In the stomach, small intestine, colon, and anorectum, GIST accounts for almost all mesenchymal tumors, because leiomyomas and leiomyosarcomas in these sites are very rare. GIST most frequently occurs in the stomach (70% of cases), followed by the small intestine (20–30%), anorectum, colon and oesophagus. Imaging features: Exophytic masses of stomach or small bowel that may ulcerate; obstruction is rare despite of its large size. Heterogeneous contrast enhancement is seen. Crescent-shaped necrosis



Fig. 4.170.1



Fig. 4.170.2



Fig. 4.170.3



Fig. 4.170.4

Table 4.170.1: Differential diagnosis for GIST




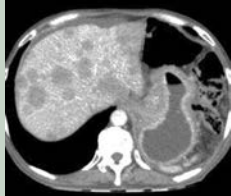
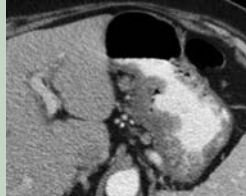
| | | |
|---|--|---|
| Gastrointestinal stromal tumour (GIST) Age >45 years. No gender predilection. Most common mesenchymal tumor of GI tract. Excellent prognosis for completely resected benign lesions. | Mass is hypo/hypervascular and shows variable enhancement. Metastasizes to liver, lungs, peritoneal cavity. Barium meal shows smooth rounded filling defect. Bowel obstruction is nil, mass rarely circumferential. Lymphadenopathy is rare. |  <p>Fig. 4.170.5: GIST</p> |
| Lymphoma: Diffuse wall thickening/ exophytic mass without bowel obstruction. Mesenteric and retroperitoneal adenopathy is common, and multiple. | Nodular fold thickening on barium studies with no evidence of obstruction. Lymphadenopathy is common, and multiple. May be indistinguishable from GIST, but lymphoma is rarely hypervascular, unlike GIST. |  <p>Fig. 4.170.6: Lymphoma</p> |
| Sarcoma: Sarcomas are rare in stomach. Histologically are classified as fibro-, myo-, lympho- and myxosarcoma. Common in 4th decade. | Bulky mass. Liposarcomas contain fat. Primary location in mesentery aids in differentiation. Bowel obstruction is common, unlike GIST. Secondary invasion of bowel may mimic GIST. |  <p>Fig. 4.170.7: Sarcoma</p> |
| Exophytic gastric carcinoma: Bulky and exophytic mass. Lymphadenopathy and evidence of distant metastases may be present. | Hypodense mass less vascular than GIST. Focal thickening of adjacent gastric wall differentiates from GIST. Gastric outlet obstruction present when circumferential. Heterogeneous on CECT. |  <p>Fig. 4.170.8: Exophytic gastric carcinoma</p> |

Table 4.170.2: Imaging in GIST

| | |
|--|--|
| Grading and classification 4 tumor subtypes Benign spindle cell GIST Malignant spindle cell GIST Benign epithelial GIST Malignant epithelial GIST | Features of malignant GIST 1. Invasion 2. Size >5 cm 3. Evidence of metastases 4. HPE: High mitotic rate, high nuclear grade and high cellularity |
| Torricelli-Bernoulli sign: It denotes nondependent air trapped in a necrotic ulcer in a gastrointestinal tumor seen on axial CT or MRI. Occasionally, a vertical stream of bubbles can be seen from the orifice of the ulcer. |  <p>Fig. 4.170.9: Malignant GIST</p> |

(Torricelli-Bernoulli sign) in large GIST noted. 30% show aneurysm dilatation of enteric bowel. Liver is the most common site of metastases, followed by mesentery.

Mesenteric metastases are smooth and multiple. Lymphadenopathy is not common; if lymphadenopathy is present, consider alternate diagnosis of lymphoma.

Table 4.170.3: Assessing response after treatment in GIST–CHOI response criteria

| | |
|---|---|
| Complete response Disappearance of all target lesions | Progressive disease $\geq 10\%$ increase in sum of longest diameters (SLD) of lesions; does not meet the criteria for partial response by virtue of tumor attenuation, new intratumoral nodules, or, an increase in the size of the existing intratumoral nodules |
| Partial response $\geq 10\%$ decrease tumor size at computed tomography (CT); or $\geq 15\%$ decrease in tumor attenuation at computed tomography (CT); or no new lesions | Stable disease None of the above |

Table 4.170.4: Differential diagnosis for bull's-eye (target) lesion in the stomach

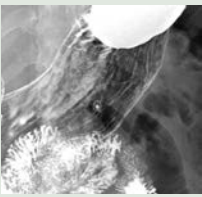
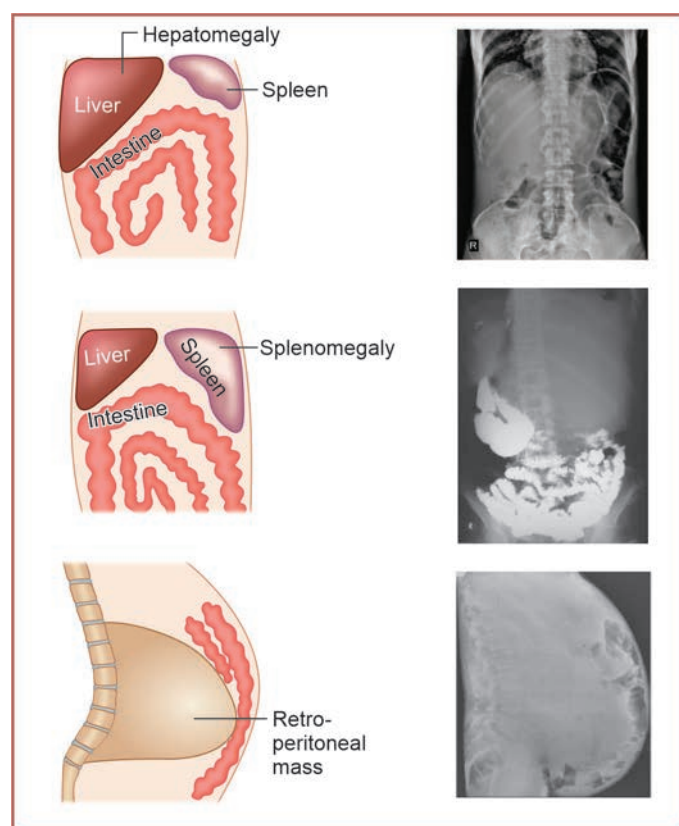
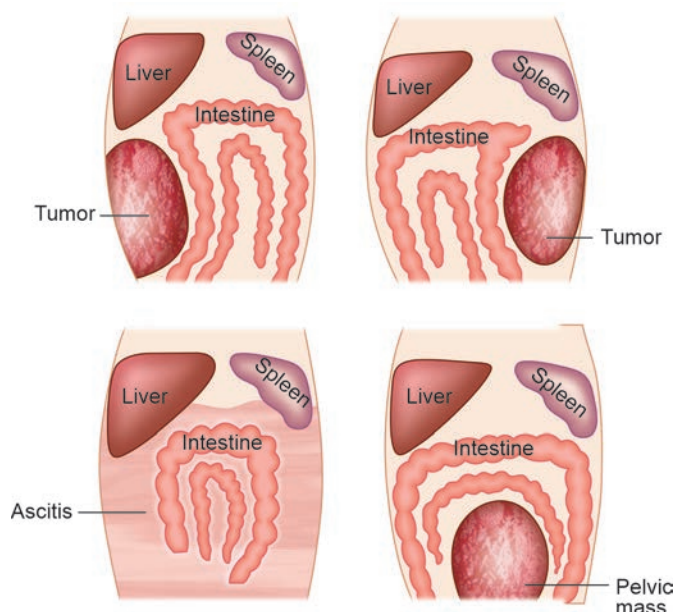
| | |
|---|---|
| 1. Submucosal metastases may be multiple. Melanoma (commonest), lymphoma, carcinoma (breast, bronchus, pancreas) and carcinoid. |  |
| 2. Leiomyoma | |
| 3. Pancreatic 'rest'—ectopic pancreatic tissue: Usually on inferior wall of antrum. A central 'blob' of barium is seen in 50%—collects in primitive duct remnant. Can also occur in duodenum, jejunum, Meckel's diverticulum, liver, gallbladder and spleen. | |
| 4. Neurofibroma may be multiple. | |

Fig. 4.170.10**Fig. 4.170.11:** Bowel displacement patterns in hepatomegaly, splenomegaly and retroperitoneal mass**Fig. 4.170.12:** Bowel displacement patterns in tumors, ascites and pelvic mass

type 1—often multiple small GISTs. 3. Carney-Stratakis syndrome: Familial paraganglioma and gastric stromal sarcoma.

Choi response criteria: The use of the size of the tumor as only criteria during evaluation for response to chemotherapy has some limitations, especially for tumors such as gastrointestinal stromal tumor (GIST). The Choi response criteria for GIST proposed that tumor attenuation could provide an additional measure of response to imatinib therapy.

Associated abnormalities: 1. Carney triad: Malignant epithelial gastric GIST, pulmonary chondroma and Extra-adrenal paraganglioma. 2. Neurofibromatosis

4.171 GASTROINTESTINAL TRACT

Case No. 171

Clinical history: A 21-year-old female patient, who came with a history of vomiting, abdominal pain and abdominal distension for 4 days.

Radiological techniques and observation: Figures 4.171.1 to 4.171.4 are scanogram, coronal reformatted and limited axial sections of IV contrast enhanced computed tomography images respectively.

Scanogram shows multiple dilated air-filled bowel loops, predominantly in the central and left upper quadrants of the abdomen. There is no evidence of any free air. There is no abnormal soft tissue density or gas shadow displacing bowel loops. There are no abnormal calcifications. The bones appear normal. Features are suggestive of small bowel obstruction. Provided CT shows dilated jejunal loops (>3 cm), with multiple air fluid levels. The ileal and large bowel loops are collapsed. There is a transition point noted in the jejunum. There is no obvious extraluminal mass or lymphadenopathy at the transition point. There is no intraperitoneal free air. There is no intraperitoneal free fluid. There is no portal vein gas. There is no hernia. There is no rectal gas. There is no linear gas within the bowel wall. The SMA, SMV and coeliac axis are all normally opacified. The small bowel wall including the obstructed loops appear to enhance normally.

With these imaging findings, the possibilities include: 1) Small bowel obstruction, 2) Paralytic ileus—not likely due to the history, the presence of a transition point, the collapsed large bowel with the absence of rectal gas. Further differentiation can also be made by the visualization of peristaltic movement on ultrasound in mechanical obstruction (however, this can be misleading, as there may be absence of peristaltic movement late in mechanical obstruction, where the bowel goes for atonic paralysis after repeated contraction.)

Interpretation: A—21 years old female patient, B—circumferential wall thickening of small bowel loops with narrowing noted at the region of the transition point, C—small bowel feces sign is seen, D—acute small bowel obstruction.

The principal diagnosis is acute small bowel obstruction.

Management: The management of acute intestinal obstruction is emergency laparotomy. However, in some cases of low grade/intermittent obstruction, conservative management may be considered.

Conventional abdominal radiography is the preferred initial radiologic examination. Results of this technique are usually diagnostic in most cases; but can be equivocal or normal, nonspecific, or misleading in a minority. If the findings on plain radiographs are those of an unequivocal SBO pattern and a high-grade partial or complete SBO is suspected, immediate surgical evaluation should be performed.

However, if surgery is not imminently planned or other treatment options are being considered, assessment of the severity and cause of the obstruction with cross-sectional studies becomes a priority. Multidetector CT is the preferred additional imaging modality, since it has a good sensitivity for high-grade and complete SBO. In settings in which CT is unavailable, sonography can serve as a useful substitute.

Findings at plain abdominal radiography: Plain abdominal radiograph may show

1. Multiple air-fluid levels (arrows).
2. Width of >2.5 cm.
3. There is a differential vertical height of more than 2 cm between corresponding air-fluid levels in the same bowel loop (circled area).
4. Distention of the small bowel diameter to more than 2.5 cm and a small bowel-colon diameter ratio of greater than 0.5.



Fig. 4.171.1



Fig. 4.171.2



Fig. 4.171.3

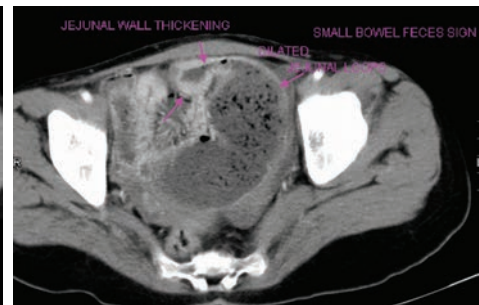


Fig. 4.171.4

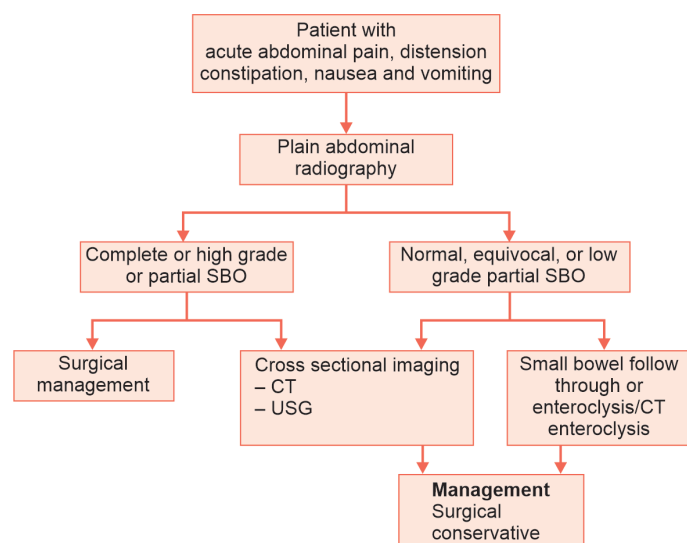


Fig. 4.171.5: Imaging protocol in small bowel obstruction

Findings at sonography:

1. Lumen of the fluid-filled small bowel loops is dilated to more than 3 cm
2. The length of the segment is more than 10 cm
3. Peristalsis of the dilated segment is increased, as shown by the to-and-fro or whirling motion of the bowel contents.
4. The level of the obstruction is determined by means of the location of the bowel loops and the pattern of the valvulae conniventes.

Role of CT in small bowel obstruction

CT criteria for obstruction: These are the presence of dilated small bowel loops (diameter >2.5 cm from outer wall to outer wall) proximally to normal-caliber or collapsed loops distally. When CT findings are equivocal for the presence of obstruction after positive oral contrast material has been given, it is often helpful

to perform delayed scanning to assess the passage of contrast material. A complete obstruction is considered to be present when there is no passage of contrast medium beyond the point of obstruction on delayed scans obtained at 3–24 hours.

Severity of obstruction: The presence of high-grade versus incomplete obstruction can be determined by the degree of distal collapse, proximal bowel dilatation, and the presence of the “small bowel feces” sign in cases where no positive oral contrast material has been given. In a high-grade obstruction, there is a 50% difference in caliber between the proximal dilated bowel and the distal collapsed bowel.

The transition point is determined by identifying a caliber change between the dilated proximal and collapsed distal small bowel loops.

SBO can be divided into two types: Simple and closed-loop obstructions. Simple obstruction of the bowel is considered when the bowel is occluded at one or several points along its course. Closed-loop obstructions are diagnosed when a bowel loop of variable length is occluded at two adjacent points along its course. The occlusion can be partial or complete. At CT, the findings of a closed-loop obstruction reveal a characteristic fixed radial distribution of several dilated, usually fluid-filled bowel loops with stretched and prominent mesenteric vessels converging toward the point of torsion (spoke wheel). The configuration can be U-shaped or C-shaped, depending on the orientation of the closed loop. Because of the presence of constrictions of two adjacent bowel segments and the intervening mesentery, a narrow pedicle can be formed, leading to torsion of the loops and producing a small bowel volvulus. Signs and role of CT scan: Feces sign, beak sign, whirlpool sign, spoke wheel sign, cocoon sign, enhancement pattern of bowel.

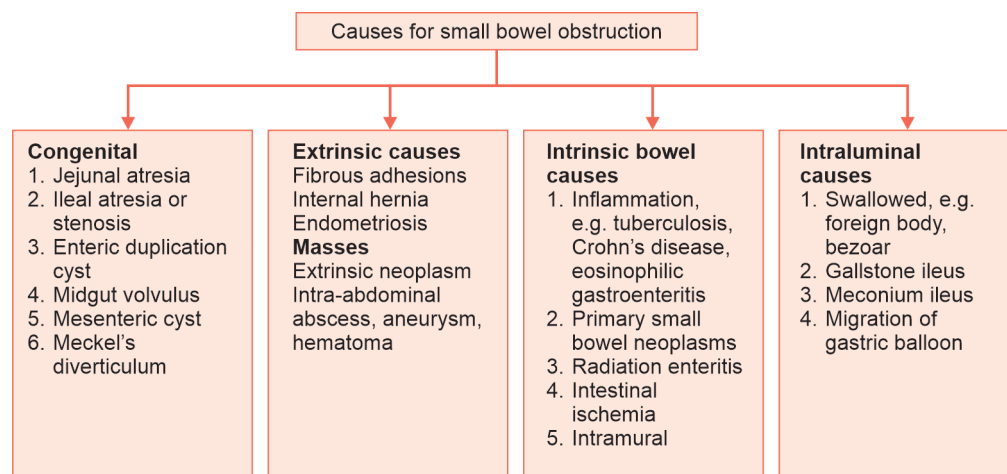


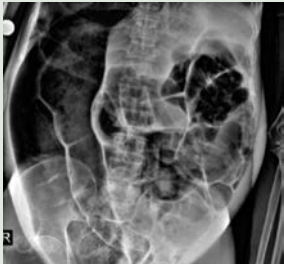
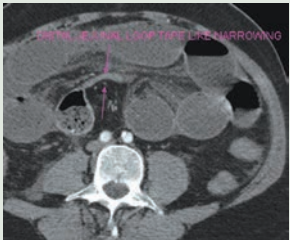



Fig. 4.171.6: Causes of small bowel obstruction

| Table 4.171.1: Difference between small bowel obstruction, large bowel obstruction and paralytic ileus | | | |
|--|--|---|--|
| | Small bowel obstruction | Large bowel obstruction | Paralytic ileus |
| Valvulae conniventes | Present | Absent | Present |
| No of loops | Many | Few | Many |
| Distribution of loops | Central | Peripheral | Both |
| Haustra | Absent | Present: Indentation on wall | Present |
| Diameter | 3-5 cm | 5 cm+ | > 3 cm |
| Radius of curvature | Small | Large | Small and large |
| Solid faeces | Absent | Present | Absent |
| Transition point | Present | Present | Absent |
| Rectal shadow | Absent | Absent | Present |
| Image |  Fig. 4.171.7: Small bowel obstruction |  Fig. 4.171.8: Large bowel obstruction |  Fig. 4.171.9: Paralytic ileus |

| Table 4.171.2: Checklist for small bowel obstruction | |
|--|--|
| <p>X-ray: Small bowel vs large bowel obstruction, Bowel wall gas (ischemia), portal vein gas (ischemia), CBD gas (gallstones), hernia sac (hernial obstruction), Ectopic gall stone (gall stone obstruction), Mass sign / fat halo sign (intussusception), worms in bowel loops and more than 3 air fluid levels.</p> <p>CT: Feces sign, beak sign; indicate adhesion, whirlpool sign; indicate intussusception, cocoon sign—focal clumping of bowel loops, enhancement pattern of bowel, SMA-SMV axis, bowel wall gas. Spoke wheel sign, small bowel feces sign—to know the transition point.</p> |  Fig. 4.171.10: Small bowel obstruction |
| <p>Closed loop obstruction: Occurs when a loop of bowel twists on its own mesentery, leading to two transition points with a high risk of ischemic complications and perforation. Emergent surgical intervention is warranted.</p> |  Fig. 4.171.11: Closed-loop obstruction |
| <p>Hernia obstruction: An inguinal hernia may be obstructed by a narrow neck of the hernial sac. Risk of strangulation is increased. X-ray shows bowel gas in the region of the groin or scrotum with dilated small bowel loops.</p> | |

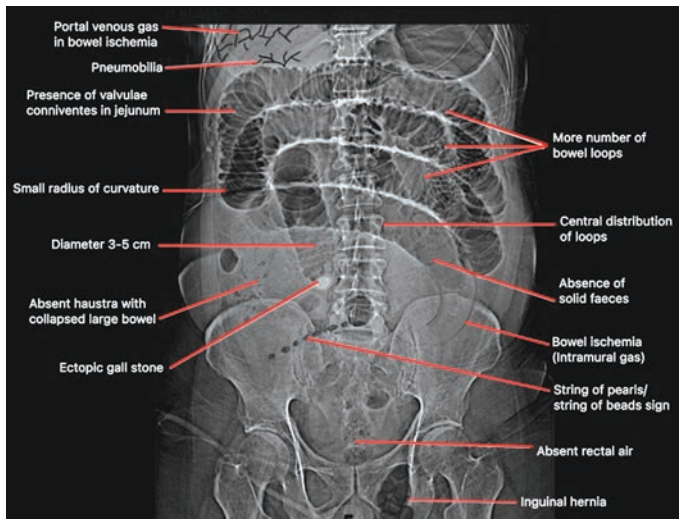


Fig. 4.171.12: Small bowel obstruction

Positive vs neutral oral contrast: Neutral (water attenuation) contrast agents such as mannitol are preferred for most small bowel indications because they allow greater conspicuity of small bowel pathology, when IV contrast agent is given. The indications for positive (iodine based) contrast agents are when the suspected pathology is known to be an intraluminal filling defect (e.g., polyposis syndrome), or when serosal metastases are suspected, or when IV contrast is contraindicated. By the use of positive bowel contrast agent, possibly highlighted are intra-abdominal abscess, enteric fistula or leak, extraluminal tumor, hematomas. Possibly obscured are bowel wall nonenhancement, bowel wall hyperenhancement, CT angiogram reformation, active gastrointestinal bleeding.

Role of MRI: No ionizing radiation, can be used in pregnant and paediatric patients, avoids artifacts due to residual barium in CT, helpful in identifying the cause of obstruction.

Signs of pneumoperitoneum RUQ gas (best place to look for small collections)

1. Single large area of hyperlucency over liver
2. Doge’s cap sign—triangular collection of gas in Morison’s pouch (hepatorenal space)
3. Outline of falciform ligament—long vertical line to the right of the midline extending from ligamentum teres notch to umbilicus; most common structure outlined.
4. Ligamentum teres sign—air outlining fissure of ligamentum teres hepatis (posterior free edge of falciform ligament) seen as vertically oriented sharply defined slit-like/oval area of hyperlucency between 10th and 12th rib within 2.5–4 cm of right vertebral border.
5. Ligamentum teres notch—inverted V-shaped area of hyperlucency along undersurface of liver.
6. Saddle bag/mustache/Cupola sign—gas trapped below central tendon of diaphragm.
7. Abdominal distension, no gastric air fluid level
8. Football sign—large pneumoperitoneum outlining entire abdominal cavity
9. Double wall sign/Rigler sign/bas-relief sign—air outlining the luminal + serosal surface of the bowel wall with patient in supine position (usually requires >1000 ml of free intraperitoneal gas + intraperitoneal fluid). Rigler’s triad consists of three findings seen in gallstone ileus: Pneumobilia, small bowel obstruction and ectopic calcified gallstone, usually in the right iliac fossa.
10. Telltale triangle sign—triangular air pocket between three loops of bowel
11. Outline of ligaments of anterior inferior abdominal wall
12. Inverted V sign—outline of both lateral and umbilical ligaments

Table 4.171.3: Radiographs in small bowel obstruction



Fig. 4.171.13: Small bowel obstruction: Erect image



Fig. 4.171.14: Small bowel obstruction: Supine image

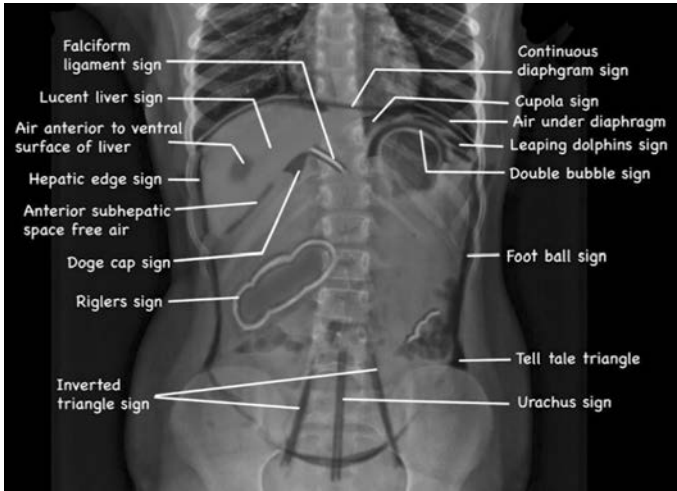


Fig. 4.171.15: Signs of pneumoperitoneum

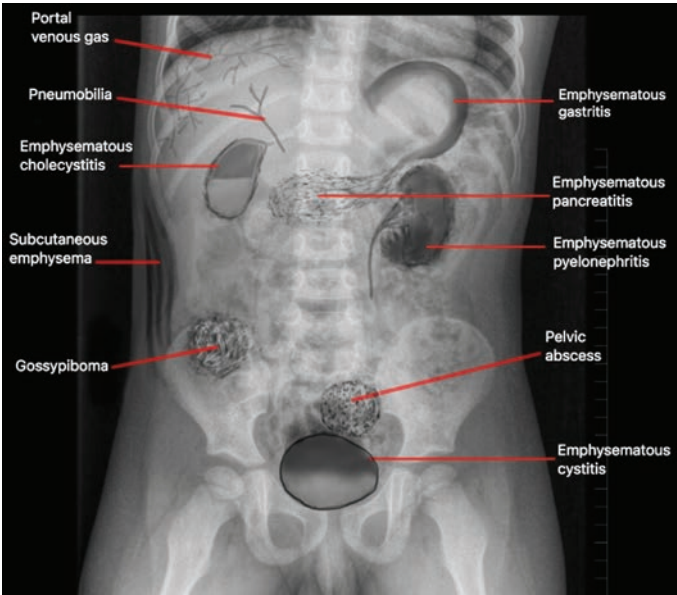


Fig. 4.171.16: Approach to radiolucency in plain abdomen radiograph

- 13. Outline of medial umbilical ligaments
 - 14. Urachus sign—outline of middle umbilical ligament
- Conditions simulating pneumoperitoneum: Intestine between liver and diaphragm—Chilaiditi's syndrome, subphrenic abscess, curvilinear atelectasis in the lung,

subdiaphragmatic fat, diaphragmatic irregularity, cysts in pneumatosis intestinalis.

| Table 4.171.4: Major clinical and CT findings of bowel ischemia | | | |
|---|--|---|---|
| Features | Arterial ischemia | Venous ischemia | Nonocclusive ischemia |
| Incidence | 60–70% | 5–10% | 20–30% |
| Clinical risk factors | Cardiovascular disease: Atrial fibrillation, postmyocardial infarction, aortic injury, atherosclerosis, septic emboli, systemic vasculitis | Bowel strangulation, hypercoagulable state, portal hypertension, venous trauma, infection | Hypotension, heart failure, recent surgery or trauma, medications, including recreational |
| Clinical presentation | Acute or chronic | Acute or chronic | Acute or chronic |
| Vasculature | Arterial filling defect, severe arterial narrowing, dissection, aneurysm | Venous filling defect, often with enlarged venous diameter | Nonspecific |
| Bowel wall thickness | May be thin acutely but may be thickened and involved with hematoma, edema, or inflammation | Thickened and edematous | Generally thickened |
| Bowel wall enhancement | Variable; diminished or non-enhancement in regions of pale ischemia; hyperenhancement in areas of reperfusion | Diminished enhancement of mucosa and serosa, target appearance | Diminished enhancement |
| Mesentery/fat | Mesenteric fat stranding with free fluid associated with territory of ischemia | Mesenteric fat stranding with free fluid associated with territory of ischemia | Mesenteric fat stranding with free fluid associated with territory of ischemia |

(Contd.)

Table 4.171.4: Major clinical and CT findings of bowel ischemia (Contd.)


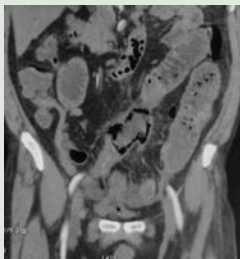
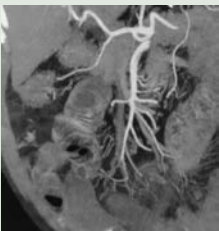
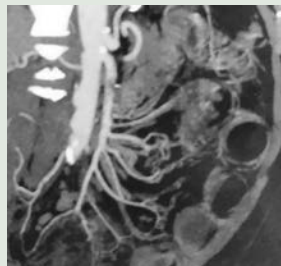

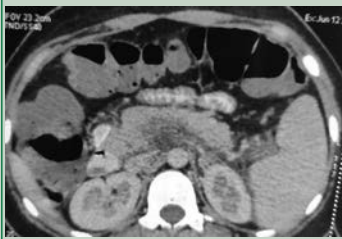
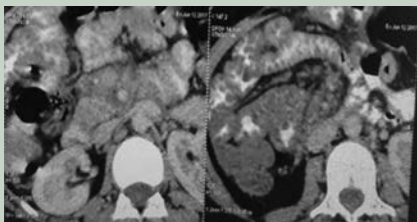
| Features | Arterial ischemia | Venous ischemia | | Nonocclusive ischemia |
|--|--|---|--|--|
| SMA thrombosis with small bowel ischemia |  Fig. 4.171.17: SMA thrombosis with small bowel ischemia |  Fig. 4.171.18: SMA thrombosis with small bowel ischemia |  Fig. 4.171.19: SMA thrombosis with small bowel ischemia |  Fig. 4.171.20: SMA thrombosis with small bowel ischemia |
| SMV thrombosis with small bowel ischemia |  Fig. 4.171.21: SMV thrombosis with small bowel ischemia |  Fig. 4.171.22: SMV thrombosis with small bowel ischemia | |  Fig. 4.171.23: SMV thrombosis with small bowel ischemia |

Table 4.171.5: Infantile form of hypertrophic pyloric stenosis

Infantile form of hypertrophic pyloric stenosis—USG findings: Pyloric volume >1.4 cm³: Most criteria independent of contracted or relaxed state. Pyloric length (mm) + 3.64 x muscle thickness (mm) >25. Pyloric muscle wall thickness >3 mm. Pyloric transverse diameter >13 mm with pyloric channel closed. Elongated pyloric canal >17 mm in length. “Target sign”: Hypoechoic ring of hypertrophied pyloric muscle round echogenic mucosa centrally on cross-section. “Cervix sign”: Indentation of muscle mass on fluid-filled antrum on longitudinal section. “Antral nipple sign”: Redundant pyloric channel mucosa protruding into gastric antrum. Exaggerated peristaltic waves. Delayed gastric emptying of fluid into duodenum

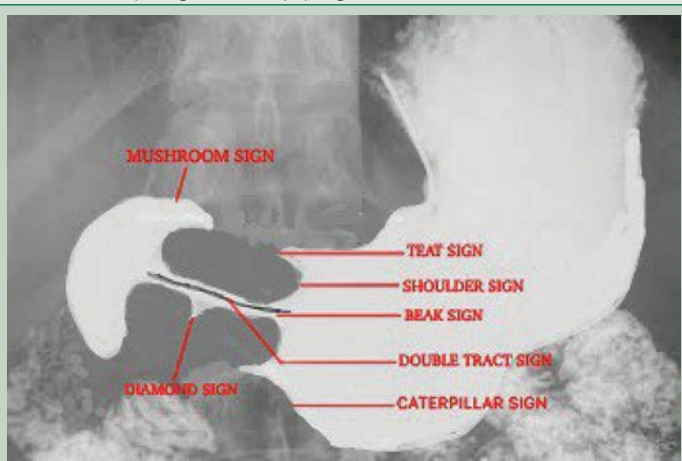


Fig. 4.171.24: Infantile form of hypertrophic pyloric stenosis

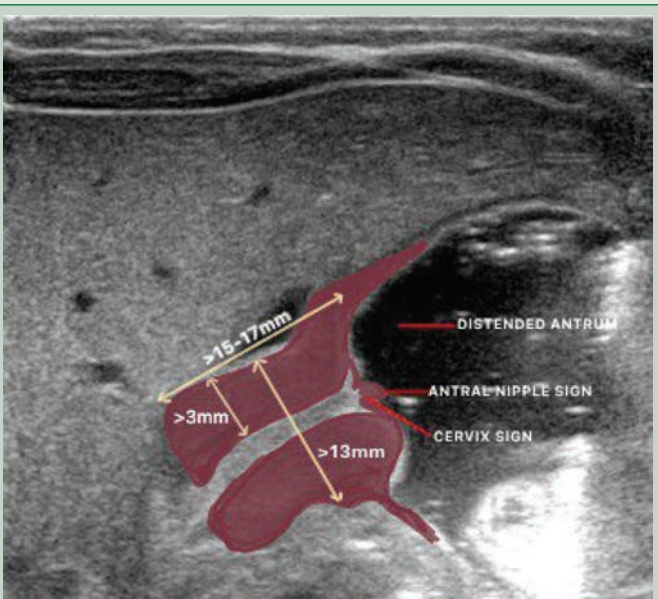
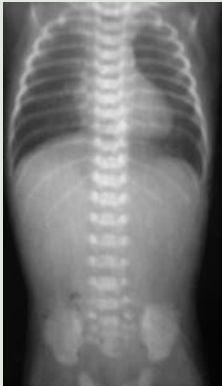
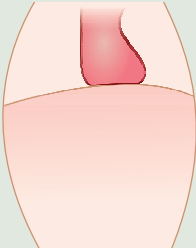

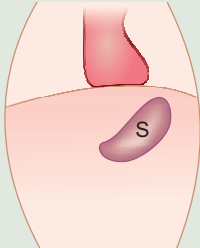

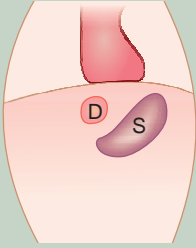
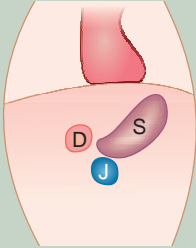
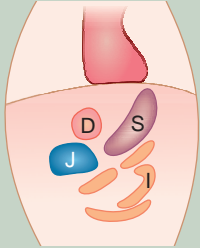
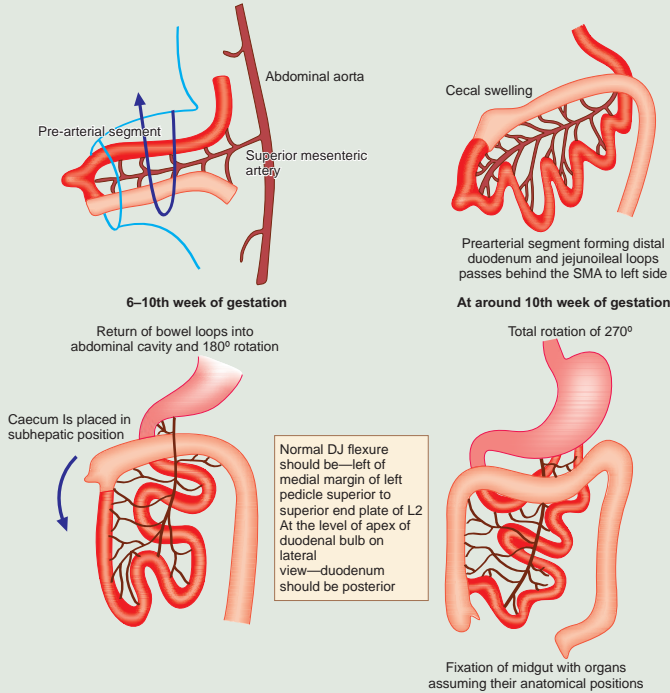
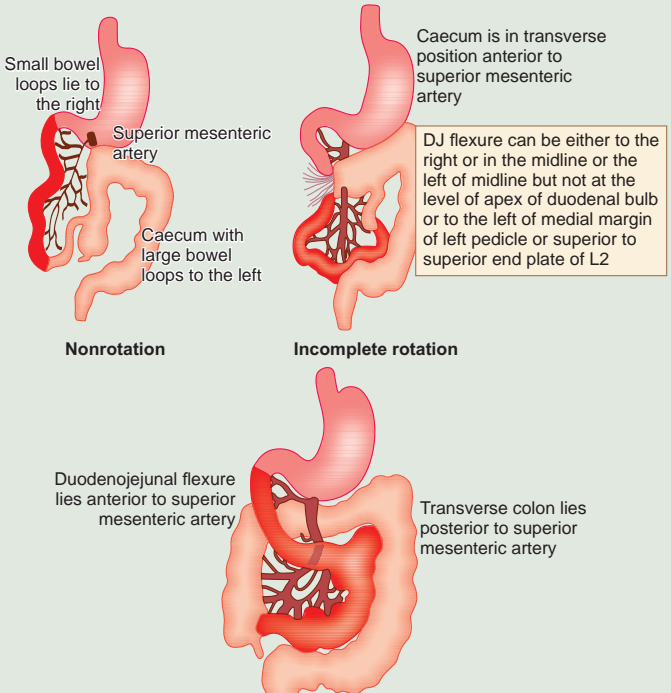


Fig. 4.171.25: Infantile form of hypertrophic pyloric stenosis

Table 4.171.6: Approach to neonate with vomiting

| | | | |
|---|--|--|--|
|  |  |  |  |
| Fig. 4.171.26: Absent bubble: oesophageal atresia | Fig. 4.171.27: Absent bubble: Oesophageal atresia | Fig. 4.171.28: Congenital hypertrophic pyloric stenosis | Fig. 4.171.29: Prominent single bubble |
|  |  |  |  |
| Fig. 4.171.30: Duodenal atresia/ web | Fig. 4.171.31: Double bubble | Fig. 4.171.32: Triple bubble— jejunal atresia | Fig. 4.171.33: Multiple bubbles—ileal atresia/small bowel obstruction |
|  | |  | |
| Fig. 4.171.34: Normal midgut rotation | | Fig. 4.171.35: Midgut rotation abnormalities | |

4.172 GASTROINTESTINAL TRACT

Case No. 172

Clinical history: A 70-year-old male with bleeding per rectum and weight loss for three months.

Radiological technique and observations: Rectal MR images have been provided.

Figures 4.172.1 to 4.172.3 are T2 fat sat, T2 axial and sagittal images of pelvis respectively showing diffuse circumferential thickening in the rectum about 6 cm from anal verge with linear nodular extension beyond the serosa into the perirectal fat. There is infiltration of mesorectal fascia with multiple enlarged mesorectal lymph nodes. There is no evidence of extramural vascular invasion. Fat plane between the lesion and urinary bladder maintained. Visualised skeleton shows no altered signal intensity.

Interpretation: A—70 years old male, lesion in rectum, C—diffuse circumferential thickening with enhancement, B—linear nodular extension beyond the serosa and mesorectal fat infiltration, D—rectal carcinoma

Principal diagnosis: Rectal carcinoma stage III

Treatment: The treatment is based on the clinical or cTNM staging, which is based on the results of imaging and endoscopy. Low risk tumors: T1, T2 and borderline T3 without suspicious nodes can directly undergo surgery. Intermediate risk tumors: T3 with >5 mm invasion or tumors with 1–3 suspicious nodes—will be treated with short-term radiotherapy preoperatively.

High risk tumors—T3 with involved mesorectal fascia (MRF) or T4 tumors or tumors with 4 or more suspicious nodes will receive neoadjuvant chemotherapy and long term radiation therapy and will be restaged to determine whether total mesorectal excision is possible.

Discussion: Epidemiology—rectal cancer is generally considered a disease of the elderly, but the incidence of cases in patients under the age of 50 is 0.01% national screening average.

Clinical presentation: Patients often present with altered bowel habit or rectal bleeding.

Imaging features: Transrectal ultrasonography: Best for local invasion, pelvic nodes (81% accuracy). Normal layers = gut signature (see GI anatomy); hypoechoic mass disrupting rectal wall; no interruption of hyperechoic submucosa implies tumor confined to mucosa and submucosa; no interruption of hyperechoic serosa implies tumor confined to rectal wall; break in outermost hyperechoic layer implies tumor penetrates into perirectal fat; irregular serrated outer border of muscularis propria (pseudopodia through serosa).

Hypoechoic perirectal lymph nodes indicate tumor involvement. MRI may be performed for diagnosis and/or locoregional staging and helps evaluate which patients may benefit from neoadjuvant therapy and for evaluating poor prognostic factors, helps surgical planning. **CT, MR:** Asymmetric mural thickening with irregular surface. **Extracolonic tumor extension:** Irregular external (serosal) margin of rectum, strands of soft tissue extending from serosal surface into perirectal fat. Loss of tissue fat planes between rectum and surrounding muscles and organs. Metastasis to lymph nodes at external iliac and para-aortic chain, inguinal, retroperitoneum, **PET/CT:** Excellent for staging and recurrence.

TNM Stage: The treatment of a patient with rectal cancer depends on the TNM stage and whether the mesorectal fascia (MRF) is involved.



Fig. 4.172.1

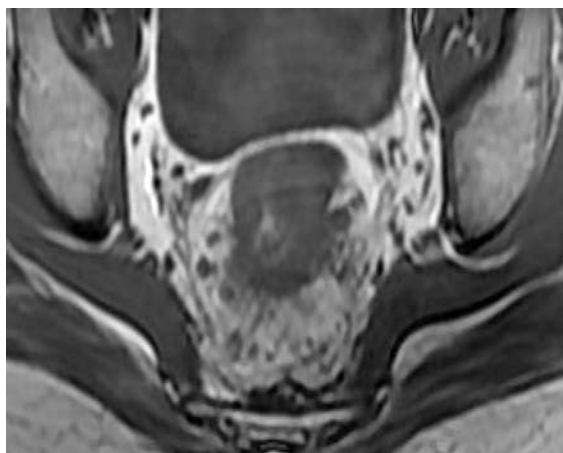


Fig. 4.172.2

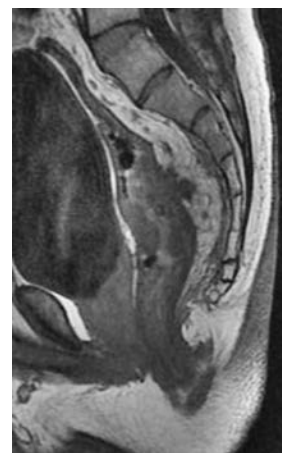
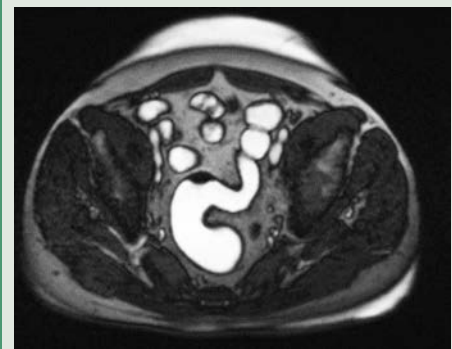
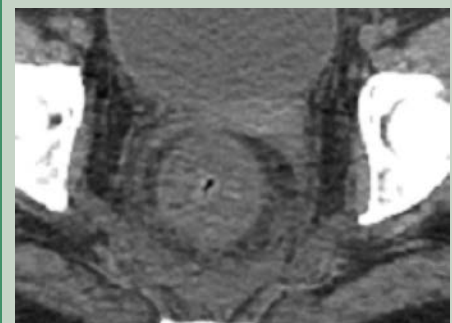


Fig. 4.172.3

Table 4.172.1: Differential diagnosis for rectal carcinoma

| | |
|--|---|
| <p>Benign colon polyps</p> <p>Adenomatous colonic polyp is most common benign colonic tumor</p> <p>Types tubular adenoma (75%), tubulovillous adenoma (15%), villous adenoma (10%)</p> <p>Treatment: Polypectomy or total procto-colectomy when a person has a severe condition or cancer</p> | <p>Imaging features:</p> <p>DCBE: Sensitivity of DCBE, <10 mm 80%, >10 mm 90%</p> <p>Benign polyp: Sessile flat/round polyp</p> <p>Malignant polyp: Pendulated polyp stalk >2 cm in length, irregular lobulated surface, broad base, retraction of colonic wall (dimpling/puckering at base of tumor), lace-like/reticular surface pattern, e.g. villous adenoma</p> <p>Bowler's hat sign—dome towards the bowel axis. Meniscus sign: Inner margin well defined, fades outwards.</p> |
| Diverticulitis—refer to case 181 | |
| <p>Ulcerative colitis (UC) is an inflammatory bowel disease (IBD) that not only predominantly affects the colon, but also has extraintestinal manifestations.</p> <p>Total colectomy is curative of both the intestinal symptoms and of the potential risk of colorectal carcinoma. Medical therapy is able to control the colonic disease.</p> | <p>Plain radiograph shows evidence of mural thickening with thumb printing.</p> <p>Fluoroscopy shows mucosal inflammation leads to a granular appearance to the surface of the bowel, button-shaped ulcers, pseudopolyp, the bowel becomes featureless with the loss of normal haustral markings, luminal narrowing and bowel shortening—lead pipe sign.</p> <p>CT shows the inflamed and thickened bowel has a target appearance due to concentric rings of varying attenuation, also known as mural stratification. MRI shows The median wall thickness in ulcerative colitis ranges from 4.7 to 9.8 mm. Enhancement of the mucosa with an absent or decreased enhancement of the submucosa produces a low SI stripe—the so-called submucosal stripe.</p> |
| Carcinoid tumors (refer to case 175) | |
| <p>Rectal lymphoma 3% of all gastric malignancies. NHL > Hodgkin lymphoma. Primary rectal lymphoma 10%, (arises from lymphatic tissue in lamina propria mucosae), Secondary 90% diffuse infiltrating disease.</p> | <p>Imaging features:</p> <p>Bowel wall thickening: 1–7 cm</p> <p>Ulcerating and homogeneous mass.</p> <p>Aneurysmal (or pseudoaneurysmal) dilatation (30%) occurs due to the replacement of muscularis by tumor or infiltration of myenteric nerve plexus.</p> <p>Large bulky-Lymphadenopathy.</p> |
| <p>Proctitis refers to inflammation of the lining of the rectum (rectal mucosa) it may be acute or chronic.</p> <p>Etiology—infective proctitis, ischemic proctitis, radiation proctitis, fecal impaction—stercoral proctitis</p> | <p>CT shows diffuse thickening of the rectum with presacral fat stranding.</p> |

**Fig. 4.172.4:** Ulcerative colitis**Fig. 4.172.5:** Proctitis

Endometriosis is defined as the presence of functional endometrial glands and stroma-like lesions outside the uterus most common in young women, most common location is ovary treatment: Medical danazol (a synthetic androgen), suppresses estrogen, GRH analogs, oral contraceptive pill, surgery—laparoscopic (adhesiolysis, partial cystectomy, uterosacral ligament excision)

Imaging features:

USG shows hypoechoic solid lesion, irregular shape and indistinct margins, bright foci, cystic areas. **“Kissing ovaries”** due to adhesions causing proximity of ovaries to uterus and negative uterine sliding sign

CT shows complex adnexal mass, peritoneal plaques. MR-T1WI: Endometriotic plaque. Intermediate SI nodule, isointense to muscle \pm high SI foci indicative of hemorrhage in ectopic endometrial glands. T2WI: Endometriotic plaque \downarrow SI nodule reflecting muscular hyperplasia and fibrosis. T1WI C+ shows delayed enhancement. Increased \uparrow DWI, \downarrow ADC compared to myometrium or small bowel wall.



Fig. 4.172.6: Endometriosis

Mucinous cystadenocarcinoma of rectum is a distinct form of colorectal cancer found in 10–15% of patients.

CT shows eccentric bowel-wall thickening, more frequent presence of intratumoral calcification, heterogeneous contrast enhancement more areas with hypoattenuation, solid portion of mucinous carcinoma may show less enhancement than that of nonmucinous carcinoma can produce cystic or calcified hepatic metastases.

Solitary rectal ulcer syndrome (SRUS) is a benign disorder characterized by the presence of an abnormality of the rectum in persons who have a chronic history of straining during defecation. Treatment: Behavioral and dietary modifications. Barium enema may be normal or non-specific, consisting of thickened valves of Houston, nodularity, rectal stricture, circular narrowing of distal rectum.

Malignant melanoma of rectum primary anorectal melanoma is rare, comprising less than 1% of all melanomas.

CT/MRI findings: Polypoid or fungating intraluminal mass expanding the rectal lumen, an exophytic mass with compression of the parent rectal lumen, rectal wall thickening more than 1 cm. Infiltration within the perirectal space and perirectal lymphadenopathy noted.



Fig. 4.172.7: Rectal GIST



Fig. 4.172.8: Rectal hemangioma



Fig. 4.172.9: Rectal hemangioma



Fig. 4.172.10: Rectal hemangioma

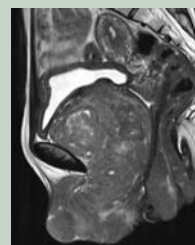


Fig. 4.172.11: Anal canal, urethral and vaginal leiomyomatosis

T-staging: T1 and T2 tumors are limited to the bowel wall.

T3 tumors grow through the bowel wall and infiltrate the mesorectal fat.

They are further differentiated in T3a: <1 mm extension beyond muscularis propria, T3b: 1–5 mm extension beyond muscularis propria, T3c: 5–15 mm extension beyond muscularis propria, T3d: >15 mm, T3 MRF+

tumor within 1 mm of MRF; MRF—no tumor within 1 mm of MRF.

The N-stage is based on the number of suspicious lymph nodes: N0—no suspicious nodes, N1—1–3 suspicious nodes, N2— ≥ 4 suspicious nodes

Risk of recurrence: 5% for T1, 10% for T2, 33% for T1N1 + T2N1, 25% for T3, 66% for T3N1, 50% for T4.

Table 4.172.2: Reporting format for rectal carcinoma

| S. no. | MR rectal tumour | Findings |
|--------|--|--|
| 1. | Clinical information | |
| 2. | Image quality | [Adequate Suboptimal Non-diagnostic] |
| 3. | Tumor location Tumor location from anal verge: Distance of lowest extent of tumor from anal verge: Distance of lowest extent of tumor from top of anal sphincter: Relationship to anterior peritoneal reflection: | [Low (0–5.0 cm) Mid (5.1–10.0 cm) High (10.1–15.0 cm)] [] cm [] cm [Above At or straddles Below Not able to assess] |
| 4. | Tumor characteristics Circumferential extent and location: Craniocaudal extent: | [] cm [No Yes] |
| 5. | T-category For low rectal tumors (0–5 cm) only: Is the lower extent of the tumor at or below the top border of the puborectalis? | [T1 or T2 T2 / early T3 T3 T3 / possible T4* T4*] [No Yes*] |
| 6. | Distance to the mesorectal fascia and extramural depth of invasion Shortest distance of the definitive tumor border to the mesorectal fascia: [] mm [Measured* Unable to estimate Not applicable (involving the peritonealized portion of the rectum or T4a)] Extramural depth of invasion (EMD) at this level: Any tumor spiculations closer to the mesorectal fascia? Any other component of the tumor closer to the mesorectal fascia: *If yes, please specify distance and location: | [] [Record 0 mm for T1 and T2 tumors] [No Yes*] [No Yes*] [] mm |
| 7. | Extramural vascular invasion (EMVI) | [Absent Equivocal Present] |
| 8. | Mesorectal lymph nodes and/or tumor deposits *If yes: Shortest distance of any suspicious mesorectal lymph node or tumour deposit to mesorectal fascia | [No Yes*] (suspicious = irregular border, mixed signal intensity and/or ≥8 mm) [] mm |
| 9. | Extramesorectal lymph nodes | If present, specify location: [None] |
| 10. | Impression | |

Table 4.172.3: MRI-based tumor regression grade (mrTRG)



| Grade | Response | MERCURY (2012) | MERCURY (2016) | | ESGAR (2016) |
|---------|-------------------|--|--|---|---|
| mrTRG 1 | Complete response | No evidence of tumor SI or fibrosis only | Linear/crescentic 1–2 mm scar in mucosa or submucosa only |  | Completely normalized rectal wall |
| mrTRG 2 | Good response | Dense hypointense fibrosis with minimal residual tumor | No obvious residual tumor, signifying minimal residual disease or no tumor | → | Fibrotic wall thickening without clear mass |
| mrTRG 3 | Moderate response | >50% fibrosis/mucin and visible tumor with intermediate SI | >50% fibrosis/mucin and visible tumor with intermediate SI |  | Residual mass (and/or focal high SI on DWI) |
| mrTRG 4 | Slight response | Little areas of fibrosis/mucin, but mostly tumor | Little areas of fibrosis/mucin, but mostly tumor | → | |
| mrTRG 5 | No response | Intermediate SI, same appearances as original tumor/tumor regrowth | Intermediate SI, same appearances as original tumor/tumor regrowth | | |

Table 4.172.4: Imaging findings indicating complete resolution

| Imaging modality | Imaging findings indicating complete resolution |
|----------------------------------|---|
| T2-weighted imaging | Complete normalization of rectal wall Dense fibrotic lesion with low SI similar to pelvic muscle without intermediate tumor SI |
| DWI | No evidence of diffusion restriction within tumor |
| T2 SI or DWI selective volumetry | No viable tumor portion which shows lower SI than cut-off value |

Staging accuracy: Digital rectal examination: ~83%; limited to lesions within 10 cm of anal verge; CT: ~72%, better for more extensive regional spread; 25–73% for lymph node involvement; MR: ~84% with tendency for overstaging. Transrectal ultrasound: ~77% with tendency for overstaging; limited to nonstenotic lesions <14 cm from anal verge; 50–83% sensitivity for involved lymph nodes. PET: 97% sensitive for recurrence.

Narrowing in rectosigmoid /anterior rectal narrowing in barium:

1. Rectal carcinoma
2. Rectal polyp
3. Adult Hirschsprung disease
4. Solitary rectal ulcer
5. Endometriosis
6. Peritoneal metastasis

7. Radiation proctitis

8. Schistosomiasis

Imaging in post-chemoradiation treatment (CRT) in rectal carcinoma: MRI is generally accepted as the first-choice method for evaluating treatment response after CRT. Post-CRT MRI should be performed 6–8 weeks after the termination of CRT, and immediately before surgery. Information about whether the distal level of a tumor is located above or below the level of the mesorectal end (approximately upper end of intersphincteric plane) 1 cm above the anorectal junction is important for determining the salvage of anal sphincter.

MERCURY: Magnetic Resonance Imaging and Rectal Cancer European Equivalence Study.

ESGAR: European Society of Gastrointestinal and Abdominal Radiology.

4.173 GASTROINTESTINAL TRACT

Case No. 173

Clinical history: A 50-year-old female came with complaints of abdominal pain, abdominal distension and obstipation for past 3 days.

Radiological techniques and observation: Scanogram, and limited axial sections of computed tomography images are provided.

Figure 4.173.1 is scanogram showing multiple dilated air-filled bowel loops involving small and large bowel. There is no evidence of any intra-abdominal free air/intramural air/portal venous/biliary gas. No bowel loops seen in inguinal region. There is no abnormal soft tissue density displacing bowel loops. There are no abnormal calcifications. The bones appear normal. Caecum not dilated significantly indicating incompetent ileocecal valve. Rectal gas shadow is not visualized. Dilated large bowel loops seen up to left colon suggestive of large bowel obstruction. Figures 4.173.2 and 4.173.3 are selective axial CT abdomen showing short segment circumferential thickening of sigmoid colon causing narrowing of lumen and proximal dilatation of large bowel and small bowel loops with multiple air fluid levels. There is no obvious extraluminal mass or lymphadenopathy at the transition point. There is no intraperitoneal free air/free fluid.

Interpretation: A: 50 years old female, C: Short segment circumferential thickening of sigmoid colon with dilatation of large bowel and small bowel loops, B: Proximal dilatation of large bowel and small bowel loops with multiple air fluid levels, D: Sigmoid colon growth with large bowel obstruction.

Principal diagnosis: Sigmoid colon growth with large bowel obstruction.

Management: If obstruction persists, emergency laparotomy to be considered. If patient is stable, he is referred to multidisciplinary team for histopathological diagnosis/staging/management.

Investigation: Rectal/IV contrast followed by colonoscopic biopsy.

Differential diagnosis: 1) Adynamic ileus, 2) Colonic pseudo-obstruction, 3) Toxic megacolon, 4) Ischemic colitis.

Discussion: The classic clinical features of bowel obstruction are: Colicky abdominal pain, vomiting, abdominal distension and absolute constipation. Absolute constipation and pain are more prominent early on in large bowel obstruction while vomiting is the predominant early feature of small bowel obstruction.

Plain radiograph findings suggestive of LBO: Colonic distension: Gaseous distension secondary to gas-producing organisms in feces, collapsed distal colon: very few or no air-fluid levels are found in the large bowel because water is reabsorbed, small bowel dilatation, which depends on duration of obstruction, incompetence of the ileocecal valve, rectum has a little or no air. In advanced cases, one may see the stigmata of an ischaemic colon: Intramural gas (pneumatosis coli), portal venous gas, free intra-abdominal gas (pneumoperitoneum).

The CT findings suggestive of mechanical LBO are: A caliber of greater than 6 cm (9 cm in the cecum) should be considered dilated. In colonic obstruction, the cecum is most distensible. If the ileocecal valve is incompetent, dilated small-bowel loops may accompany a large bowel



Fig. 4.173.1



Fig. 4.173.2

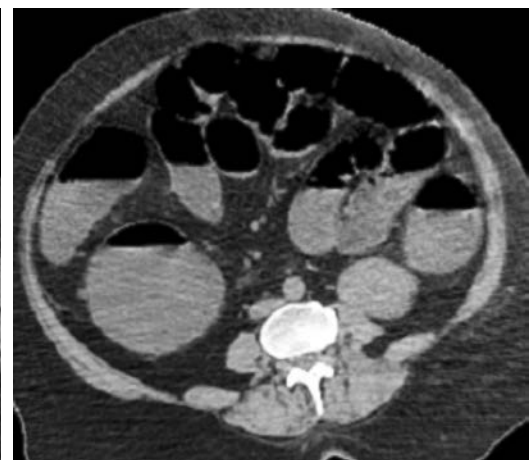


Fig. 4.173.3

| Table 4.173.1: Causes of large bowel obstruction | |
|--|---|
| Category | Causes of large bowel obstruction |
| Neoplastic | Colonic carcinoma Extracolonic tumors (peritoneal carcinomatosis, local invasion and lymphadenopathy) |
| Non-neoplastic | Diverticulitis, volvulus, inflammatory bowel disease, intussusception, enterolith, fecal impaction, endometriosis |
| Mimickers | Colonic pseudo-obstruction (Ogilvie syndrome), toxic megacolon, adynamic ileus |

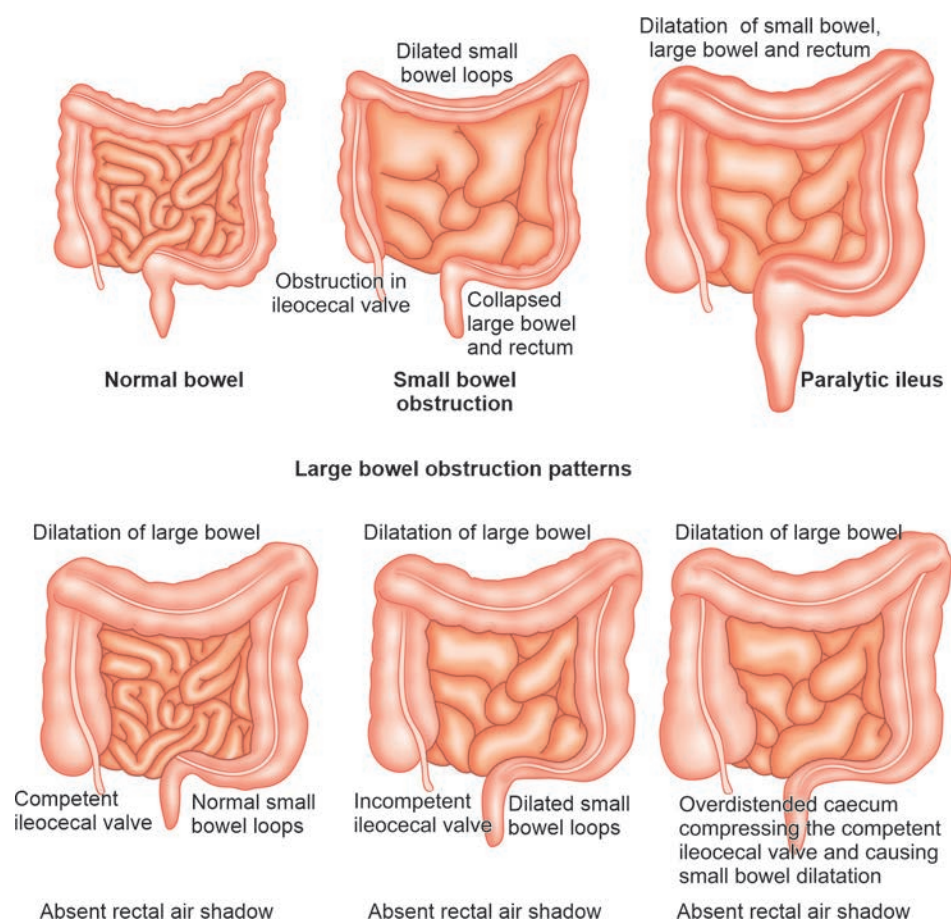


Fig. 4.173.4: Small bowel and large bowel obstruction patterns

obstruction. The large bowel will be distended with a thinned out, stretched wall but should enhance (unless ischaemic).

Colorectal carcinoma: Most common cancer of GI tract.
Risk factors: Personal history of colonic adenoma/carcinoma. 93% of colorectal carcinomas arise from adenomatous polyp. Family history of benign/malignant colorectal tumors in first-degree relatives (3–5 times risk). Personal history of ovarian/endometrial/breast cancer. Dysplasia of colon within flat mucosa. Inflammatory bowel disease. Prominent lymphoid follicular pattern. Pelvic irradiation. Ureterosigmoidostomy.

Environmental risk factors: Low fiber diet, increased ingestion of fat and animal protein, obesity and asbestos worker.

- Genetic risk factors (6% of colorectal carcinomas)**
- a. Familial adenomatous polyposis syndrome: Familial polyposis, Gardner syndrome, Turcot syndrome
Age: Approximately at 40 years
 - b. Certain hamartomatous polyposis syndromes: Peutz-Jeghers syndrome, juvenile polyposis, Cowden disease.
 - c. Hereditary nonpolyposis colon cancer syndrome/ Lynch syndrome.

Table 4.173.2: Differential diagnosis for large bowel obstructions


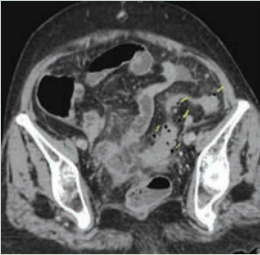

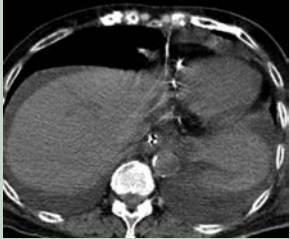


| | | |
|---|---|--|
| <p>Neoplasm: Colorectal carcinoma is the most common cause of large bowel obstruction. Over two-thirds of obstructing colorectal cancers are distal to the splenic flexure, with the sigmoid colon being the most common location due to its relatively narrow diameter and contact with fecal contents.</p> | <p>Asymmetric mural thickening and enhancing short-segment of the colon that narrows its lumen. It is frequently associated with pericolic fat infiltration and lymphadenopathy.</p> |  <p>Fig. 4.173.5: Colorectal carcinoma with bladder invasion</p> |
| <p>Diverticulitis: Obstruction in patients with diverticulitis can be caused by several mechanisms including: Compression by intramural or extramural abscesses, Adherence of small bowel loops to an inflammatory focus, pericolic fibrosis, or a pelvic colon angulated by adhesions.</p> | <p>Visualization of wall thickening of the colon, mucosal hyperenhancement, stranding of mesosigmoid fat, free fluid and engorgement of mesenteric vessels. Complicated diverticulitis is associated with abscess and/or pneumoperitoneum. DD—epiploic appendagitis</p> |  <p>Fig. 4.173.6: Diverticulitis</p> |
| <p>Intussusception: Adult intussusception is relatively rare with only 5% of all intussusceptions. It is often secondary to mural lesions, being the most frequent cause of the colorectal cancer or benign lesions, such as adenomatous polyps or lipomas.</p> | <p>Target appearance (intraluminal soft tissue mass and eccentric fat density), reniform pattern (a bilobed density with peripheral high density attenuation and low attenuation centrally), and sausage pattern (alternating areas of high and low attenuation related to the bowel wall, mesenteric fat and fluid, intraluminal fluid, contrast, or air)</p> |  <p>Fig. 4.173.7: Intussusception</p> |
| <p>Enterolith: An enterolith is a mineral concentration or calculus usually formed inside a diverticulum.</p> | <p>Enteroliths have been found in association with Crohn's disease, tuberculosis, blind loop syndrome, congenital or acquired diverticulum of the small bowel, and intestinal stricture.</p> | |
| <p>Colonic pseudo-obstruction (Ogilvie syndrome): Acute pseudo-obstruction caused by the alteration of sympathetic innervation of the colon.</p> | <p>Abdominal radiograph shows nonspecific diffuse colonic dilatation. MDCT is the definitive modality and shows extensive proximal colonic dilatation with an intermediate transitional zone at or adjacent to the splenic flexure and without any structural obstructing lesions.</p> | |
|  <p>Fig. 4.173.8: Ogilvie's syndrome</p> |  <p>Fig. 4.173.9: Ogilvie's syndrome</p> |  <p>Fig. 4.173.10: Rectal contrast in Ogilvie's syndrome</p> |
| <p>Toxic megacolon: It is most commonly considered a complication of inflammatory bowel disease, specifically ulcerative colitis, but occasionally Crohn's disease.</p> | <p>Typical features seen on plain film include ahaustral dilatation of the transverse colon >6 cm ranging up to 15 cm with absent residual fecal matter (active colitis) and ulcer with mucosal island. MDCT: Diffuse colonic wall thickening, thickened haustra with alternating bands of high and low density ("accordion sign"), multilayered appearance caused by different densities of edematous submucosa, hyperemic mucosa ("target sign"), and pericolic stranding. In addition, detecting colonic dilatation (>6 cm) is indicative of developing toxic megacolon</p> | |

Table 4.173.3: Difference between polyps and diverticulum

| <i>Polyps</i> | <i>Diverticulum</i> |
|---|---|
| Bowler's hat sign—dome towards the bowel axis. | Dome points away from the lumen |
| Meniscus sign—inner margin well defined, fades outwards | Outer margin well defined, fades inwards |
| Filling defects in barium pool | Protrusions out of the lumen/ fluid level |
| Mexican hat sign, stalk sign | |

Table 4.173.4: Colonic and pericolonic changes on CT

| | | |
|---------------------------|---------------------------------|--|
| Wall thickening | >3 mm | Neoplasia, colitis, diverticulitis, ischaemia |
| Wall attenuation | Target sign without enhancement | Fat in ulcerative colitis Gas in pneumatosis coli |
| | Target sign with enhancement | Acute Crohn's disease or ulcerative colitis Ischaemic colitis Pseudomembranous colitis |
| | Homogeneous with enhancement | Neoplasia Chronic Crohn's disease Radiation enteritis |
| Pericolonic lymph nodes | Enlarged | Reactive or malignant infiltration |
| | Increased attenuation | Kaposi's sarcoma |
| | Decreased central attenuation | TB Mucinous carcinoma |
| Mesenteric stranding | Inflammatory | Diverticulitis, colitis, necrosis |
| Fibro-fatty proliferation | Colon | Crohn's disease |
| | Rectum | Ulcerative colitis |

Screening recommendations (American Cancer Society):

(a) For persons >50 years of age: Annual fecal occult-blood test and sigmoidoscopy/BE every 3–5 years, (b) for first-degree relatives of patients with colon cancer screening should start at age 40.

Location: Rectosigmoid: 55%, cecum and ascending colon: ~20%, ileocecal valve: 2%, transverse colon: ~10% and descending colon: ~5%.

Presentation: Right-sided tumors are commonly polypoid lesions with chronic bleeding and intussusception.

Left-sided tumors commonly present as annular strictures with obstruction.

Radiographic features:

Barium enema: "Apple core lesion"—circumferential narrowing of bowel lumen, overhanging border and mucosal destruction.

"Saddle lesion"—growth characteristics between polypoid mass and annular constricting lesion.

CT: Is the modality most used for staging colorectal carcinoma.

CT staging

Stage 1—intramural polypoid mass.

Stage 2—thickening of bowel wall.

Stage 3—slight invasion of surrounding tissues.

Stage 4—massive invasion of surrounding tissue and adjacent organs/distant metastases.

Staging of colorectal cancer (modified Dukes/Astler-Coller classification)

A—limited to mucosa

B—involvement of muscularis propria

B1—extension into muscularis propria

B2—extension through muscularis propria into serosa/mesenteric fat (35%)

C—lymph node metastases (50%)

C1—B1 + regional lymph nodal metastasis

C2—B2 + regional lymph nodal metastasis

C3—B3 + regional lymph nodal metastasis

D—distant metastases

Treatment and prognosis: Treatment involves local control with resection in almost all cases. Adjuvant chemotherapy is reserved for stage III disease. Overall, 5-year survival rate is 40–50%, with the stage at operation the single most important factor affecting prognosis. Duke A: 80–90%, Duke B: 70%, Duke C: 33%, Duke D: 5%

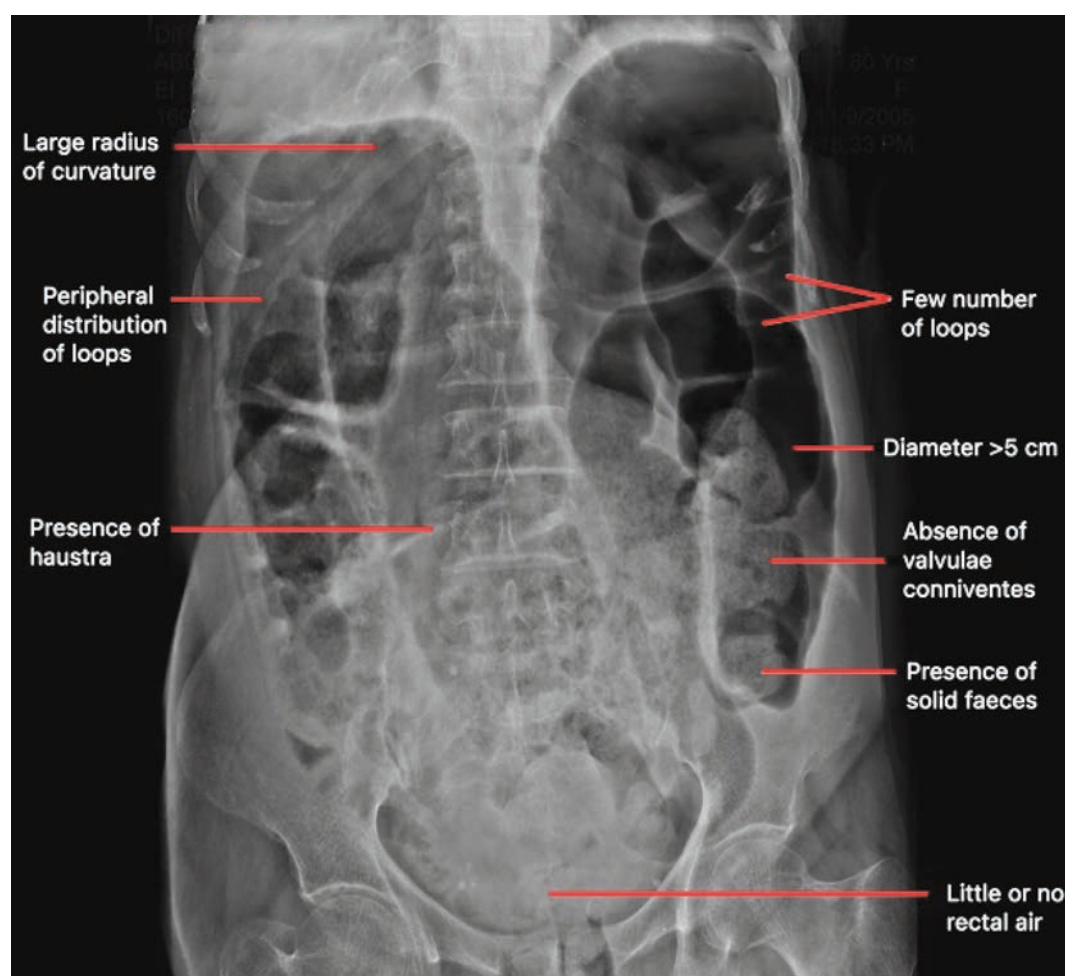


Fig. 4.173.11: Large bowel obstruction—imaging features

Recurrence: Local recurrence at the line of anastomosis: Tend to occur within two years of diagnosis (80%).

The tumor marker CEA is routinely used for detecting postoperative early recurrence and metastatic disease

(especially liver disease). It is also used for monitoring response to treatment of metastatic disease.

Higher levels of CEA are associated with: Higher grade tumors, higher stage disease and visceral metastases (especially liver metastases).

4.174 GASTROINTESTINAL TRACT

Case No. 174

Clinical history: A 75-year-old male with c/o acute abdomen with intense abdominal pain and obstipation.

Radiological techniques and observation: Figure 4.174.1 plain frontal radiograph of abdomen: Markedly dilated loop of large bowel with a coffee-bean shape (omega sign). Sigmoid colon noted arising from the pelvis, with its apex above D10 and point of convergence in the left sacroiliac joint. The interposed loops produce the white-stripe sign.

Visualised bones appear normal. Dilated ahaustral bowel loop indenting the liver producing the liver overlap sign.

Radiographic features are consistent with sigmoid volvulus.

Further investigation like CT was advised to narrow down the diagnosis and to look for associated complications.

Figures 4.174.2 to 4.174.5 show CT abdomen limited axial sections and coronal reformatted images in soft tissue window revealing sigmoid colon dilatation with multiple air-fluid levels and the whirl sign, which represents twisted colon and mesentery. CT images show the whirl sign and the classic beak sign at the level of the twist, which is located in the region of left iliac fossa.

Interpretations: A: 70 years old male, C: Dilated large bowel loops arising from the pelvis in the left iliac fossa with the apex at right upper quadrant rising above the level of D10 vertebra, B: Classical whirl and beak signs. No free air in the peritoneum. D: Sigmoid volvulus.

Principal diagnosis: Sigmoid volvulus.

Differential diagnosis: Sigmoid volvulus and ceacal volvulus.

Management: Patient is referred to surgical gastroenterologist. Rectal tube insertion is successful in treating 90% of cases. Occasionally patients suffer from recurrent sigmoid volvulus, for which a surgeon may consider sigmoid colectomy (surgical fixation of the sigmoid colon), or in the surgically unfit, a percutaneous endoscopic colostomy (PEC) might be performed. The mortality rate is 20–25%. The most serious complication is bowel ischemia.

Discussion

Radiological signs in sigmoid volvulus: Plain radiograph: Abdominal radiographs will show a large, dilated loop of the colon, often with a few gas-fluid levels. Specific signs include: Coffee bean sign, Frimann-Dahl sign—three dense lines converge towards the site of obstruction, Northern exposure sign, left flank overlap sign, ahaustral margin, pelvic overlap sign, air-fluid ratio >2:1, apex of the most distended sigmoid above D10 vertebra and point of convergence at S2, absent rectal gas. Fluoroscopy: Although now uncommonly performed, a water-soluble contrast enema exquisitely demonstrates this condition, with the appearances described as the beak sign (or bird beak sign). CT: Large gas-filled loop lacking haustra, forming a closed-loop obstruction. Whirl sign: Twisting of the mesentery and mesenteric vessels. Bird's beak sign: If rectal contrast has been administered. X-marks-the-spot sign: crossing loops of bowel at the site of the transition. Split wall sign: Mesenteric fat seen indenting or invaginating the wall of the bowel. The liver overlap sign can be seen in sigmoid volvulus wherein the sigmoid loop is seen, usually on an abdominal radiograph, ascending to the right upper quadrant and projecting over the liver shadow.



Fig. 4.174.1

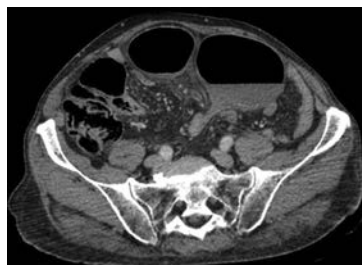


Fig. 4.174.2

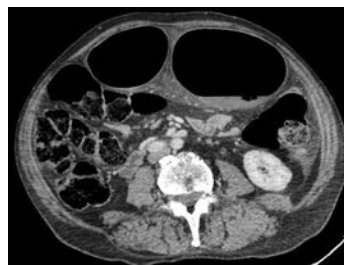


Fig. 4.174.3

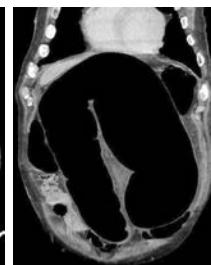


Fig. 4.174.4



Fig. 4.174.5

Table 4.174.1: Differential diagnosis for GI volvulus

| | |
|---|--|
| Gastric volvulus Organo-axial volvulus more common in adults (2/3 of cases) commonly occurs in the setting of para-esophageal hernia or trauma. | Stomach is rotated along its long axis (along the line drawn between the cardia and the pylorus). Antrum rotates antero-superiorly and fundus rotates posteroinferiorly. Complete ($>180^\circ$) present with obstruction or ischemia. Incomplete rotation ($<180^\circ$) also called organo-axial position of the stomach, usually asymptomatic. Mirror image of normal anatomy can occur with reversal of the greater and lesser curves. |
| Mesentero-axial volvulus less common in adults, but is more common than organo-axial volvulus in the pediatric population (59% of gastric volvulus) | Rotation around short axis from the lesser to greater curvature (i.e. perpendicular to the cardiopyloric line), usually incomplete, $<180^\circ$ displacement of antrum above gastro-esophageal junction; stomach appears upside-down with the antrum and pylorus superior to the fundus and proximal body. coincides with the axis of mesenteric attachment and is associated with severe obstruction and strangulation. |



Fig. 4.174.6: Gastric volvulus with wandering spleen



Fig. 4.174.7: Gastric volvulus with wandering spleen



Fig. 4.174.8: Gastric volvulus with wandering spleen

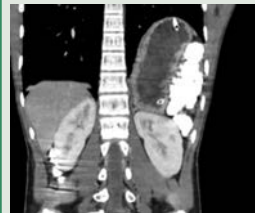


Fig. 4.174.9: Gastric volvulus with wandering spleen

Midgut volvulus is a complication of malrotated small bowel.

It may result in proximal bowel obstruction with resultant ischemia if not treated prompt. Fluoroscopy shows corkscrew sign, tapering of beaking of the bowel in complete obstruction, malrotated bowel configuration. USG: Clockwise whirlpool sign, abnormal superior mesenteric vessels inverted SMA/SMV relationship

Midgut volvulus with duplication cyst



Fig. 4.174.10: Midgut volvulus with duplication cyst

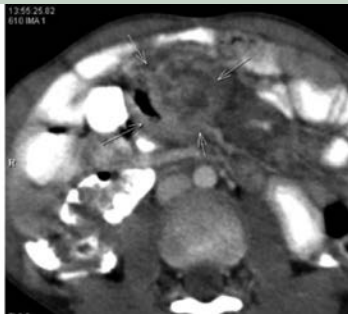


Fig. 4.174.11: Midgut volvulus with duplication cyst

Ultrasound of midgut volvulus



Fig. 4.174.12: Ultrasound of midgut volvulus

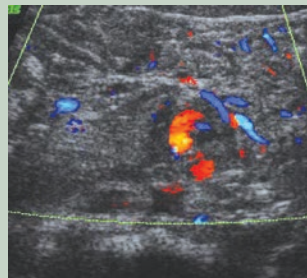


Fig. 4.174.13: Ultrasound of midgut volvulus

Table 4.174.2: Difference between internal hernia and midgut volvulus

| Internal hernia | Midgut volvulus |
|--|---|
| <p>Internal hernias are protrusions of the viscera through the peritoneum or mesentery but remaining within the abdominal cavity.</p> <p>Internal hernias have a low incidence of <1% and represent a relatively small amount of presentations, left and right paraduodenal hernias (most common; represent ~55% of internal hernias, lesser sac hernia, pericaecal hernia, sigmoid mesocolon hernias, intersigmoid hernia, transmesosigmoid hernia, intramesosigmoid hernia, small bowel mesentery internal hernia, transmesenteric hernia, intramesenteric hernia, transomental hernia, supramesic hernia, pelvic internal hernia, broad ligament hernia, falciform ligament hernia, internal hernia due to gastric bypass surgery.</p> <p>CT: The appearance depends on the particular internal hernia. Common features include: Encapsulation of distended bowel loops within an abnormal location, arrangement or crowding of small-bowel loops within a hernial sac, evidence of obstruction with segmental dilatation and stasis, mesenteric vessel abnormalities, engorgement, crowding, twisting, stretching of mesenteric vessels. Fluoroscopy: The appearances on barium studies vary depending on the type and site of the internal hernia, clustering of small bowel loops, distended bowel proximal to the site of obstruction, abnormal site or displacement of normal parts of the gastrointestinal tract.</p> <p>Treatment: In the event that an obstructed internal hernia leads to the development of gangrenous bowel, the gangrenous part has to be resected. In some cases, patients have to undergo emergency surgery for hernia.</p> | <p>Midgut volvulus is a complication of malrotated bowel. It may result in proximal bowel obstruction with resultant ischemia if prompt treatment is not instigated.</p> <p>A midgut volvulus of malrotated bowel can potentially occur at any age but in approximately 75% of cases occur within a month of birth. Most of these are within the first week, with 90% occurring within 1 year.</p> <p>Plain radiograph: Double bubble sign. Fluoroscopy: Corkscrew sign, tapering or beaking of the bowel in complete obstruction, malrotated bowel configuration.</p> <p>Ultrasonogram: Clockwise whirlpool sign, abnormal superior mesenteric vessels, inverted SMA/SMV relationship, solitary hyperdynamic pulsating SMA, truncated SMA, inapparent SMV, abnormal bowel, dilated duodenum proximal to the obstruction, thickened wall of small bowel distal to the obstruction, dilated fluid-filled loops of small bowel, free intra-abdominal fluid.</p> <p>CT: Whirlpool sign of twisted mesentery, malrotated bowel configuration, inverted SMA/SMV relationship bowel obstruction, free fluid/free gas in advanced cases.</p> <p>Treatment: Urgent surgical repair (Ladd procedure) is required to prevent ischemia or to resect infarcted bowel loops. If resection is performed stomas are usually created. Additionally, the Ladd bands are divided and the mesenteric pedicle widened.</p> |



Fig. 4.174.14: Internal hernia

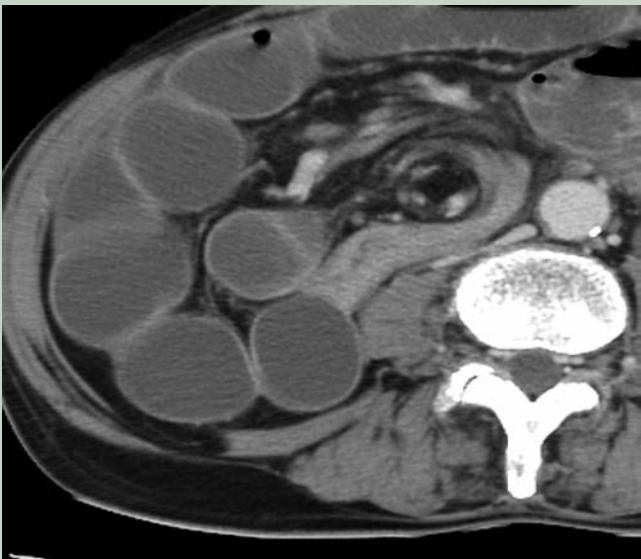

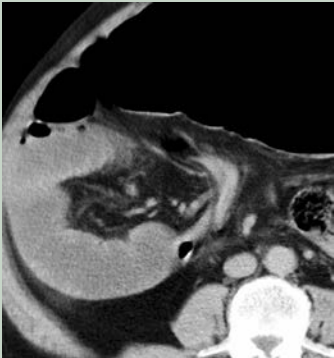


Fig. 4.174.15: Midgut volvulus

| Table 4.174.3: Difference between sigmoid volvulus and ceacal volvulus | |
|---|---|
| <i>Sigmoid volvulus</i> | <i>Ceacal volvulus</i> |
| More common around 70 years of age. | More common around 50 years of age. |
| Presents with constipation, abdominal bloating, nausea and/or vomiting. | Presents with colicky abdominal pain, vomiting, and abdominal distension. |
| Can only move upwards and usually goes to the right upper quadrant with twisting of its mesentric axis located in left iliac fossa. | Can go anywhere and can even be located in the pelvis with twisting of its mesentric axis located in right iliac fossa. |
| Coffee bean shaped | Cecum is kidney shaped with marked distension |
| Associated with large bowel dilatation | Associated with small bowel dilatation |
| Haustral pattern lost. | Colonic haustral pattern maintained. |
| Few air-fluid levels seen. | One air-fluid level seen. |
| Rectal tube insertion, endoscopic detorsion, sigmoid colopexy, percutaneous endoscopic colostomy (PEC). | Right hemicolectomy, cecostomy, cecopexy. |
|  |  |
| Fig. 4.174.16: Sigmoid volvulus | Fig. 4.174.17: Ceacal volvulus |

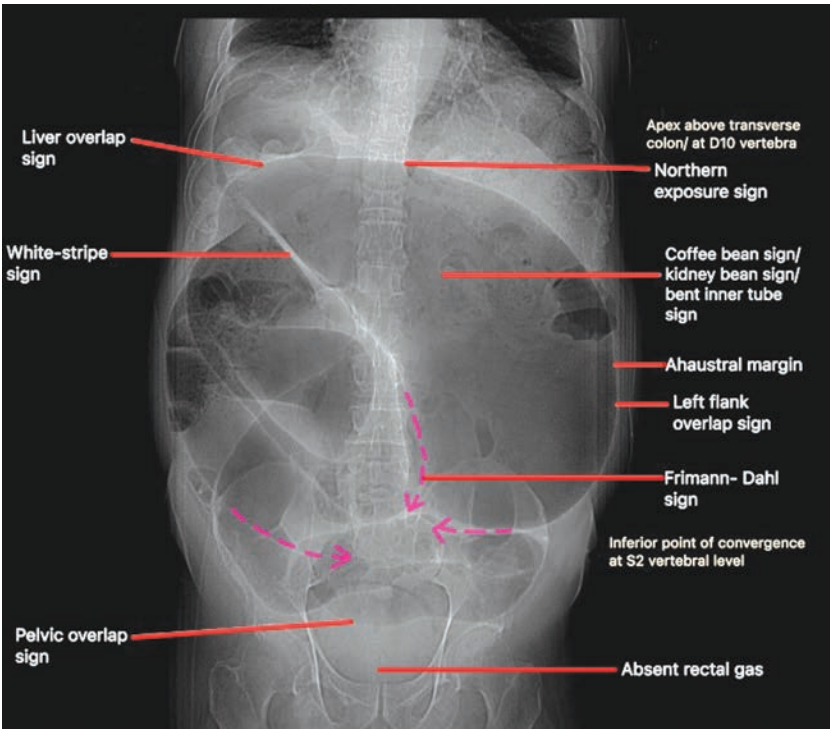


Fig. 4.174.18: Radiograph in sigmoid volvulus

4.175 GASTROINTESTINAL TRACT

Case No. 175

Clinical history: A 63-year-old man with abdominal pain and vomiting 3 weeks and also with skin lesions.

Radiological techniques and observation: Figures 4.175.1 to 4.175.5 show multiple ill-defined lesions are seen in both lobes of liver predominantly in right lobe which show enhancement in arterial phase (Fig. 4.175.3) and washout in venous phase (Fig. 4.175.4) indicating the lesions are hypervascular.

There is a well-defined rounded lesion in the mesentery with spiculated margins and showing heterogeneous enhancement and surrounding minimal fat stranding with eccentric soft tissue dense bowel wall thickening in adjacent ileal loops. No evidence of any other lymphadenopathy/mesenteric lesion. Other visualized abdominal organs appear normal. There is right pleural effusion. Visualized bones appear osteoporotic.

Interpretations: A—63 years old male, lesions in mesentery, C—well defined enhancing solid mass lesions with, B—spiculated margins associated with eccentric small bowel thickening and multiple enhancing lesions in liver, D—small bowel carcinoid with mesenteric deposits and hypervascular liver metastasis.

Principal diagnosis: Small bowel carcinoid with mesenteric deposits and hypervascular liver metastasis. Skin lesions and vomiting may be because of carcinoid syndrome.

Management: Next line of management is biopsy and confirmation of diagnosis.

Nuclear medicine: Gallium 68 Dotatate PET/CT is done for low grade tumors (well differentiated). FDG-PET is preferable for high grade tumors (undifferentiated). SPECT CT-Indium-111 Octreotide scan, Iodine-123-MIBG scan (Figs 4.175.6 to 4.175.8).

Treatment: Multidisciplinary approach by medical and surgical gastroenterologist. For distal small bowel tumors: Surgical resection of bowel and mesentery often with right hemicolectomy. For hepatic metastases: Palliative surgery of primary tumor.

Chemoembolization; radiofrequency ablation; Somatostatin analogue: Octreotide may relieve symptoms, Chemotherapy has no role, except in bone metastases.

Discussion: Carcinoid is the most common primary small bowel tumor: 35–40%. Location: Predominantly distal ileum Neuroendocrine cells of gut are called enteroendocrine cells /APUD cells which on receiving input from nerves release hormones which are of three types—EC cells, D cells, L cells.

Enterochromaffin cells also known as Kulchitsky cells (70%) are most abundant enteroendocrine cells which are located in gastric antrum, duodenum, jejunum, ileum, appendix, colon and rectum which secrete serotonin.

Carcinoid tumors are a type of neuroendocrine tumor that can occur in a number of locations. Arise from endocrine amine precursor uptake and decarboxylation (APUD) cells that can be found throughout the gastrointestinal tract as well as other organ. Locations: Gastrointestinal tract carcinoid (60–85% of all carcinoids), small bowel (40% of GIT carcinoids), mostly terminal ileum, rectum (22.5%), colon (15%), appendix (10%), stomach (7.5%), pancreas (7.5%). Carcinoid tumours of lung (25% of all carcinoids): Bronchial carcinoid, peripheral pulmonary carcinoid tumors, primary hepatic carcinoid, ovarian carcinoid (accounts for 0.5% of carcinoid tumors and 0.3% of ovarian tumors), thymic carcinoid tumor elaborates excessive amounts of vasoactive substances like neuropeptides ACTH, histamine, bradykinin, kallikrein, prostaglandin, substance P, neurokinin-A, serotonin = 5-hydroxytryptamine. Carcinoid syndrome (in 7% of small bowel carcinoids, most commonly in ileal carcinoids): Carcinoid syndrome has a higher morbidity and mortality than does the tumor itself.

When the metabolic pathway to 5-HIAA (in liver) is by-passed, excess 5-HIAA (5-hydroxyindoleacetic acid) is excreted in urine: (a) With metastases to liver/retroperitoneal nodes, (b) with primary pulmonary/ovarian carcinoids.



Fig. 4.175.1

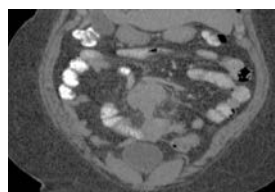


Fig. 4.175.2



Fig. 4.175.3



Fig. 4.175.4

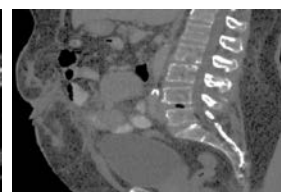


Fig. 4.175.5

| Table 4.175.1: Differential diagnosis for mesenteric lesions | |
|---|---|
| 1. Non-Hodgkin lymphoma | Large discrete/confluent lymph nodes in advanced cases. Lack of fat halo and lymphadenopathy outside of mesentery favors lymphoma. Treated mesenteric lymphoma can look identical to mesenteritis (with chronic misty mesentery). |
| 2. Sclerosing mesenteritis Encasement of mesenteric vessels (especially portomesenteric veins) with resultant collaterals Mesenteric vessels and nodes have halo of spared fat (fat ring or fat halo sign) in acute mesenteritis | Discrete fibrotic soft tissue mass with desmoplastic reaction “Stellate” appearance with calcification within mass encasement of mesenteric vessels (especially portomesenteric veins) with resultant collaterals |
| 3. Desmoid tumour: Benign proliferation of fibrous tissue that usually presents as discrete solid mass (isodense to muscle) | Soft tissue dense mass lesion which displaces but does not usually encase mesenteric vessels associated with Gardner syndrome or prior surgery |
| Others: 4. Peritoneal metastasis 5. GIST—usually have areas of necrosis 6. Small bowel adenocarcinoma (asymmetric thickening and narrowing of small bowel but metastasis are not hypervascular) 7. Hepatocellular carcinoma with mesenteric metastasis (no cirrhotic background of liver). | |

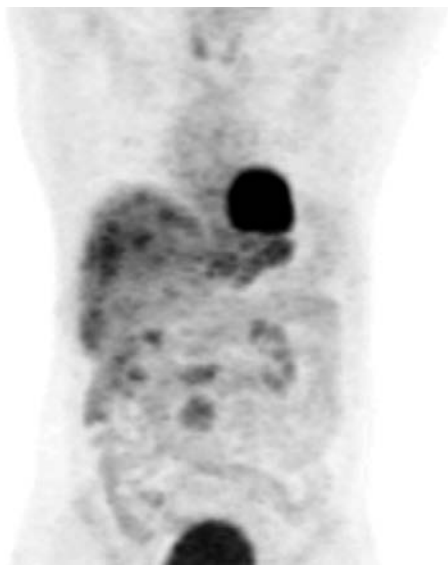


Fig. 4.175.6: Gallium-68-Dotatate PET images, showing avid uptake in carcinoid mass and liver, confirming the diagnosis of carcinoid tumor with multiple liver metastasis

Recurrent diarrhea (70%), asthmatic wheezing from bronchospasm (15%) caused by tachykinin and bradykinin, nausea and vomiting, fever, hypotension (vasomotor instability), right-sided endocardial fibroelastosis (35%) resulting in tricuspid regurgitation, pulmonary valve stenosis, right heart failure. Skin changes: Cutaneous facial flushing + sweating (rare). Desquamative skin lesions (5%).

Rule of 1/3: 1/3 occur in small bowel, 1/3 have metastases, 1/3 are multiple, 1/3 have a second malignancy, 1/3 have carcinoid syndrome.

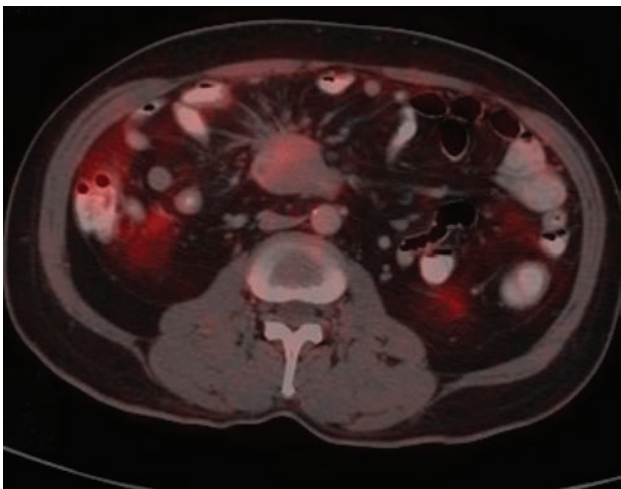


Fig. 4.175.7: Gallium-68-Dotatate PET images, showing avid uptake in carcinoid mesenteric mass

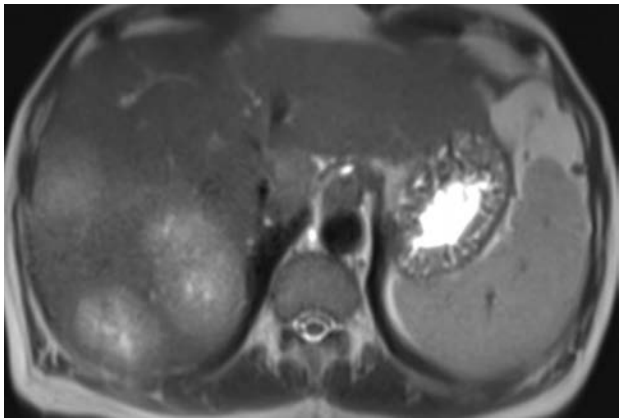


Fig. 4.175.8: Multiple primary neuroendocrine neoplasms of liver

| Table 4.175.2: Neuroendocrine cell tumours | |
|--|---|
| Cells of origin | Tumours |
| Enterochromaffin cells/Kulchitsky cells: APUD cells (type of neuroendocrine cells seen in bowel/bronchi) | Neuroendocrine tumor of GIT like carcinoid tumour |
| Non-chromaffin cells (parasympathetic ganglia) | Carotid body tumour, glomus jugulare, glomus jugulotympanicum |
| Neural crest cells of adrenal medulla, sympathetic ganglion | Neuroblastoma |
| Chromaffin cells (pheochromocytes are neuroendocrine cells) of adrenal medulla | Pheochromocytoma |
| Chromaffin cells of sympathetic ganglia | Extra-adrenal paraganglioma (organ of Zuckerkandel) |
| Duodenal G cell | Gastrinoma |
| Pancreatic islet cells | Pancreatic neuroendocrine tumors—insulinoma |
| Interstitial cell of Cajal | Gastrointestinal stromal tumor |

Metastases: On average 40% have metastases at time of presentation to mesenteric lymph nodes, liver (in 90% of patients with carcinoid syndrome), lung, bone (osteoblastic), peritoneum.

Causes for hypervascular liver metastasis: Carcinoid, choriocarcinoma, melanoma, renal cell carcinoma, thyroid carcinoma, leiomyosarcoma, lung carcinoma, breast CA, hepatocellular carcinoma.

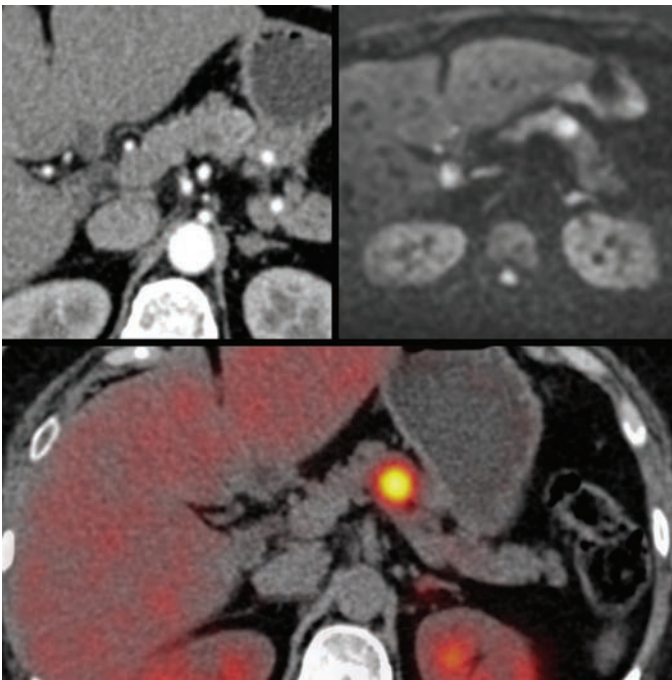


Fig. 4.175.9: Neuroendocrine tumor of pancreas

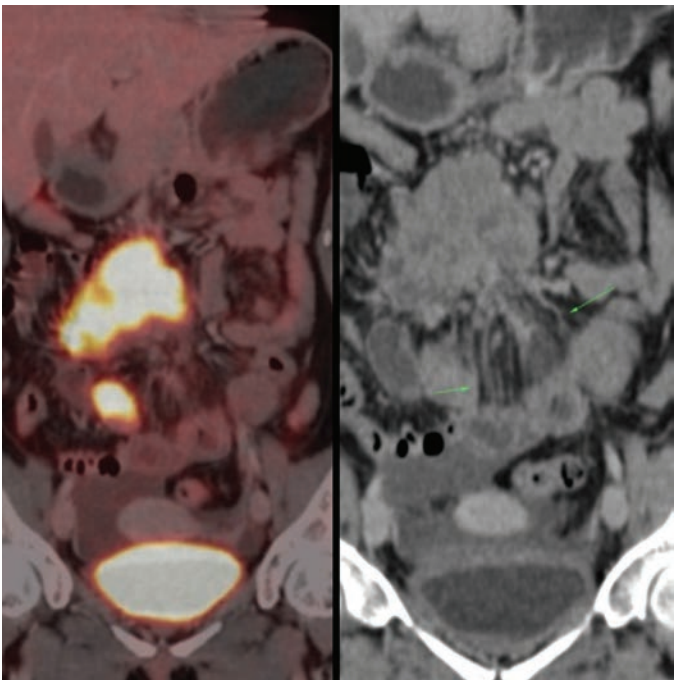


Fig. 4.175.10: Inflammatory myofibroblastic tumor mimicking carcinoid

4.176 GASTROINTESTINAL TRACT

Case No 176

Clinical history: A 50-year-old male presented with the complaints of dull aching lower abdominal pain, with loss of weight and loss of appetite for the past 3 months.

Radiological observation and techniques: CECT abdomen and pelvis with oral contrast in limited axial and coronal sections. Figures 4.176.1 and 4.176.2 show abnormal wall thickening involving the mid-ileum in the hypogastric region with maximum thickness of 2.6 cm, for length of about ~12 cm. There is luminal dilatation of the involved segment. No evidence of bowel obstruction. There is significant periserosal fat stranding which extends up to the serosal surface of the sigmoid colon. No intramural infiltration. Multiple enlarged lymph nodes along inferior mesenteric vessels, largest measuring about 18 × 14 mm.

Interpretation: A: 50 years old male with lesion in mid-ileum, C: Abnormal wall thickening of the mid ileum in the hypogastric region, B: Enlarged mesenteric and retroperitoneal lymph nodes, D: Lymphoma/adenocarcinoma with lymph nodal metastasis.

Principal diagnosis: Lymphoma/adenocarcinoma with lymph nodal metastasis.

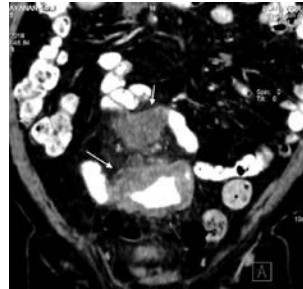


Fig. 4.176.1

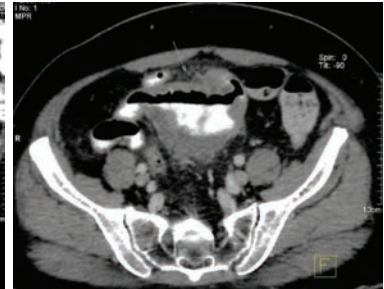


Fig. 4.176.2

Further management: FNAC from the nodal lesions to confirm the metastasis. Surgical resection and anastomosis.

Brief discussion about small bowel adenocarcinoma: Most commonly occurs in duodenum, followed by jejunum and ileum.

- Infiltrating tumor: “Apple core” or annular lesion
 - Short, well-demarcated, circumferential narrowing
 - Irregular lumen, overhanging edges, ± ulceration
 - Narrow, rigid stricture with prestenotic dilatation
- Polypoid sessile tumor: Small plaque-like growth

Risk factors: Celiac and Crohn disease, polyposis syndromes.

Table 4.176.1: Differential diagnosis for small bowel thickening


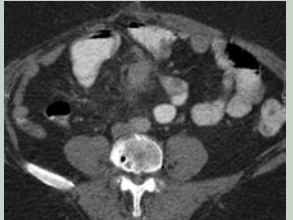
| | | |
|---|---|---|
| 1. Lymphoma-risk factors: Celiac disease, Crohn’s disease, postchemotherapy, SLE, immunocompromised state, Extra-intestinal lymphoma. Location: Terminal ileum | Imaging features: Thick walled (1–7 cm) infiltrating mass. Aneurysmal (or pseudoaneurysmal) dilatation (30%): Occurs due to the replacement of muscularis by tumor or infiltration of myenteric nerve plexus. Enhancement: Homogeneous, associated features: Splenomegaly, mesenteric and retroperitoneal lymphadenopathy, DD: Large adenocarcinoma |  |
| 2. Carcinoid: Location distal ileum, appendix associations—carcinoid syndrome, liver metastasis | Imaging features: Transmural hypervascular mass, mesenteric mass with calcification, desmoplastic reaction, bowel wall thickening Enhancement: Hypervascular DD: Sclerosing mesenteritis |  |
| 3. GIST: Location—stomach more than small bowel | Imaging features: Well-defined exophytic mass. Associations: Hypervascular liver metastasis, mesenteric metastasis in recurrent disease. DD: Lymphoma | |

Fig. 4.176.3: Lymphoma

Fig. 4.176.4: Carcinoid

(Contd.)

Table 4.176.1: Differential diagnosis for small bowel thickening (Contd.)

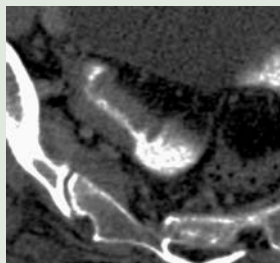
4. Tuberculosis-multifocal thickening with narrowing

Fig. 4.176.5: Tuberculosis

Circumferential wall thickening (1–2 cm). Multiple site; involvement with skip lesions usually less than 4. Mural stratification will be absent.

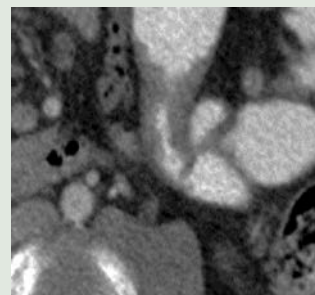


Fig. 4.176.6: Tuberculosis

5. Small bowel polyps: Peutz-Jeghers syndrome

Fig. 4.176.7: Small bowel polyps



Fig. 4.176.8: Polyp with intussusception

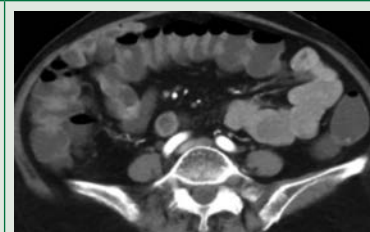


Fig. 4.176.9: Small bowel polyps

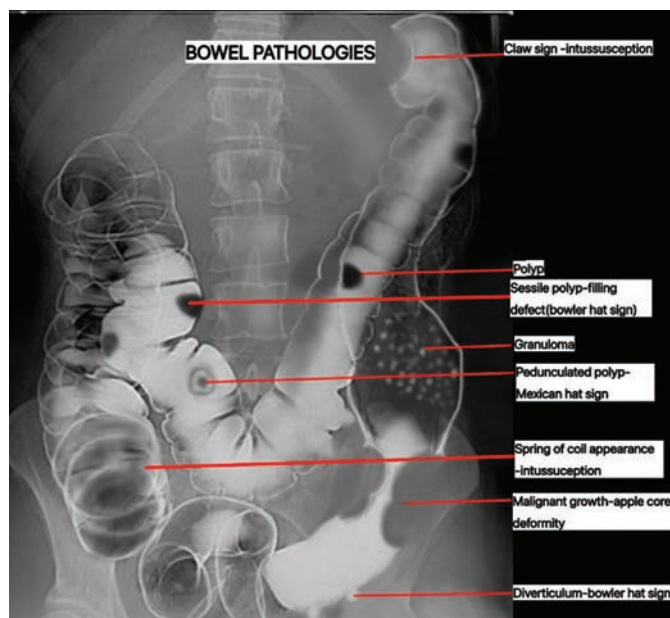


Fig. 4.176.10: Bowel pathologies

CT findings: Annular, ulcerative lesion or discrete nodular mass, circumferential thickened wall \pm mesenteric invasion, soft tissue mass \pm luminal narrowing and obstruction.

Often presents with intussusception \pm enlarged mesenteric nodes; perivascular invasion. Tumor shows moderate enhancement on CECT \pm metastases: Liver, peritoneal surfaces, ovaries

Complications: Small bowel obstruction, intussusception, GI bleed, perforation (rarely) and metastases.

Treatment: Surgical resection (localized), chemotherapy (spread)

Small bowel tumors classification:

- **Benign:** Leiomyoma/leiomyoma of the jejunum, adenoma, lipoma, hemangioma, polyposis syndromes
- **Malignant:** Adenocarcinoma, carcinoid, malignant GIST, lymphoma, metastases.

4.177 GASTROINTESTINAL TRACT

Case No. 177

Clinical history: A 24-year-old male came with complaints of loose stools and pain in the right iliac fossa.

Figure 4.177.1 USG in RIF shows a thickened terminal ileum near the ileocaecal junction with minimal surrounding inflammatory changes. No evidence of adjacent collection/mesenteric lymph nodes. Figures 4.177.2 and 4.177.3 CECT abdomen of 24 years old male patient in axial and coronal view shows uniform enhancement of the bowel loops with thickening in the ileocaecal junction giving a water target appearance, adjacent minimal fat stranding and prominent mesenteric vessels (comb sign). No evidence of mesenteric lymph nodes. No free fluid noted in the pelvis. No evidence of peritoneal thickening. No evidence of collection/abscess. No evidence of inter-bowel loop fistula. Sacroiliac joint appears normal. No evidence of perianal fistula. No evidence of dilated bowel loops. No evidence of ischaemia. No evidence of pneumoperitoneum.

Figures 4.177.4 and 4.177.5 are plain MRI in STIR coronal and T1 post-contrast enhanced MRI in axial view shows diffuse short segment thickening of the distal ileum with prominent vasa recta giving appearance of the comb. No evidence of adjacent lymph nodes or collection or abscess. Sacroiliac joint appears normal. No free fluid noted in the pelvis. No evidence of dilated small and large bowel loops.

Interpretation: A—24 years male, C—thick-walled small bowel loop adjacent to the caecum—terminal ileum, B—perimesenteric fat stranding consistent with inflammation and target pattern of enhancement in the terminal ileum and ileocaecal junction with prominent mesenteric vessels (comb sign). D—Crohn's disease.

Principal diagnosis: Crohn's disease

Differential diagnosis: 1. Ileocaecal TB, 2. Amoebic colitis, 3. Ulcerative colitis, 4. Diverticulitis

Treatment: Refer to gastroenterologist for further management: Steroids and aminosalicic acid.

Discussion: A chronic relapsing immune mediated inflammatory disorder, that results from a dysregulated immune response to luminal antigens in genetically susceptible individuals. Patients present with acute abdomen, anemia, weight loss and altered bowel habits. Transmural inflammation of the bowel wall occurs predominantly in the small intestine especially ileocaecal junction (almost >75% cases) > large bowel > isolated gastroduodenal and jejunal (more common in pediatric age group).

Barium features in Crohn's disease: 1. Aphthoid ulcers: Pooling of contrast in ulcer crater with peripheral lucency due to musosal edema. 2. Fissure ulcer: Tracking of ulcer through the wall of intestine forming an abscess and fistula. 3. Fistula: Fistulae pass to adjacent loops of ileum, caecum, sigmoid colon or urinary bladder and occasionally to the skin or vagina. 4. Longitudinal ulcer: Along the mesenteric border of the ileum. 5. Cobblestone appearance: Caused by a combination of longitudinal and transverse ulceration, separating intact portions of mucosa.

CT findings: Diffuse mural thickening of the bowel wall showing homogeneous or target enhancement or mural stratification (in active lesions). Multiple skip lesions present. Mesenteric changes include fat stranding, hypervascularity (comb sign) and fibrofatty proliferation of the mesenteric fat.

MRI: Bowel wall thickening (mild: 3–5 mm, moderate 5–7 mm and severe >7 mm) with enhancement showing homogenous or target or mural stratification, skip lesions, creeping fat, mesenteric hypervascularity (comb sign) and lead pipe colon due to loss of haustration (common in ulcerative colitis).

Complications: 1. Stenosis, 2. Fistula, 3. Abscess, 4. Ascites (hypoproteinemia)

Treatment: Corticosteroids, 5-ASA preparations, immunomodulation (e.g. azathioprine, ciclosporin, methotrexate).

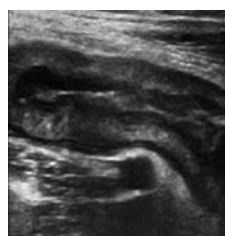


Fig. 4.177.1

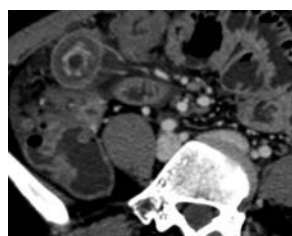


Fig. 4.177.2: Radiologic features in Crohn's disease

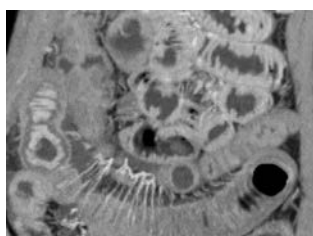


Fig. 4.177.3

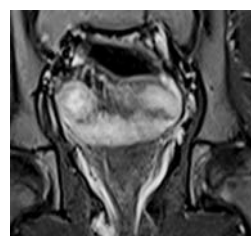


Fig. 4.177.4

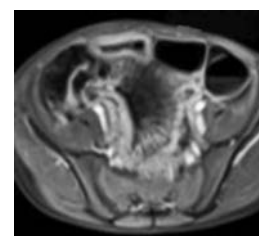


Fig. 4.177.5

Table 4.177.1: Differential diagnosis for Crohn's disease



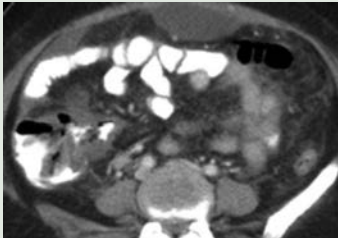
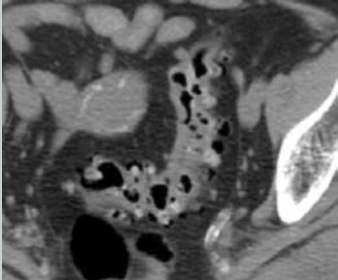
| | | |
|---|---|--|
| <p>Ulcerative colitis Chronic idiopathic diffuse inflammatory disease primarily involving colorectal mucosa. 15–40 years, M = F.</p> <p>Location Rectum only—30% Rectum and distal colon—40% Pancolitis—30% Terminal ileum in only minor cases.</p> <p>Treatment: 1. Medical—steroids, azathioprine, sulfasalazine. 2. Surgical—total/proctocolectomy.</p> | <p>Barium enema: Acute 1. Colorectal narrowing, 2. Fine granular mucosa, 3. Flask shaped/collar button ulcers, 4. Thickened transverse fold due to submucosal edema.</p> <p>Chronic 1. Short, less redundant colon, 2. Lead pipe/wind pipe colon, 3. Complete loss of transverse folds, 4. Benign /malignant strictures</p> <p>CECT: 1. Enhancing inner mucosa, non enhancing submucosa and enhancing muscularis/serosa—target/halo sign 2. Enhancing pseudopolyps. 3. Perirectal fibrofatty proliferation</p> |  <p>Fig. 4.177.6: Ulcerative colitis</p>  <p>Fig. 4.177.7: Ulcerative colitis</p> |
| <p>Ileocaecal TB Ileocaecal junction involved in 90% of cases due to more lymphoid tissues.</p> | <p>Barium features 1. Sterling sign—rapid emptying of narrowed terminal ileum. 2. Fleischner sign—inverted umbrella sign—Wide gaping patulous ileocaecal valve. 3. pulled up caecum 4. String sign—diffuse circumferential thickening causing thin flow of barium through the lumen.</p> <p>CT: Diffuse circumferential thickening of ileal wall, multiple mesenteric lymph nodes which are necrotic and non-enhancing. Ascites/sclerosing encapsulating peritonitis.</p> | |
| <p>Amoebic colitis Causative organism: <i>Entamoeba histolytica</i>. Presents with c/o diarrhea, perianal ulceration.</p> | <p>CT—mucosal edema with enhancing mucosa. Multiple ulcerations and skip lesions noted. “Typically” spares ileum in contrast to Crohn’s) and mainly involves the rectum and the caecum. Co-existing liver abscess and ascites may be present.</p> |  <p>Fig. 4.177.8: Amoebic colitis</p> |
| <p>Diverticulitis Intramural and pericolonic infectious/inflammatory process resulting from perforation of colonic diverticula.</p> | <p>Multiple colonic diverticula and colonic wall thickening With inflammation of pericolonic fat (stranding) Thickened base of sigmoid mesocolon, Engorged mesocolic blood vessels. “Microperforation”: Small bubbles of pericolonic gas. In more complicated diverticulitis: More extensive extraluminal collections of gas and fluid, free intraperitoneal spread of gas or fluid, fistulas to skin or hollow viscera and infectious thrombophlebitis.</p> |  <p>Fig. 4.177.9: Colonic diverticula</p> |

Table 4.177.2: Barium features in Crohn's disease


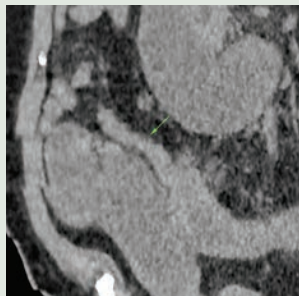

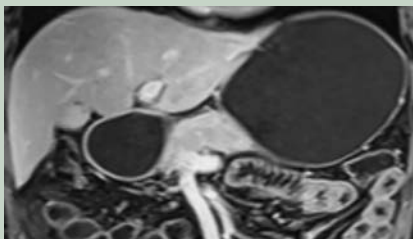
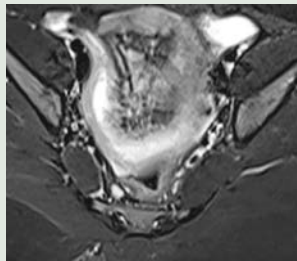

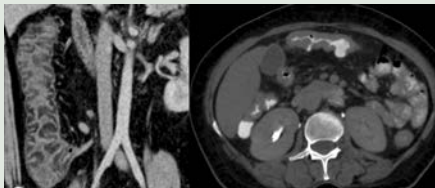
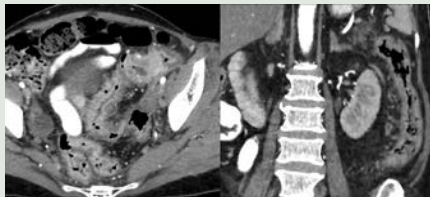
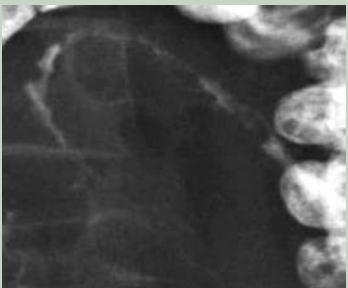

| | |
|--|---|
|  |  |
| <p>Fig. 4.177.10: Pseudo-Billroth 1 sign</p> | <p>Fig. 4.177.11: String sign</p> |
|  |  |
| <p>Fig. 4.177.12: Omega sign</p> | <p>Fig. 4.177.13: MR enterography in Crohn's disease</p> |
|  |  |
| <p>Fig. 4.177.15: Interloop fistula</p> | <p>Fig. 4.177.14: Aphthous ulcer and cobblestone appearance</p> |
|  |  |
| <p>Fig. 4.177.16: Pseudomembranous colitis</p> | <p>Fig. 4.177.17: Ulcerative colitis</p> |

Table 4.177.3: Difference between Crohn's disease and ulcerative colitis

| <i>Crohn's disease</i> | <i>Ulcerative colitis</i> |
|--|--|
| 70–80% small bowel involvement (terminal ileum) | 95% involves rectum (starts from rectum and ascends continuously), small bowel in reflux ileitis |
| Skip lesions + | Lesion in contiguity |
| Aphthous ulcers + | Collar button ulcers + |
| Irregular serosal surface | Smooth serosal surface |
| Peri anal fistula/enteroenteric fistula/sinuses/abscess/strictures/fissuring ulcers are more common | Perianal fistula/sinuses/abscess/strictures rare |
| Malignant transformation rare | More common |
| Trans mural inflammation more common (causes 10–12 mm thickening) | Superficial mucosal involvement (causing thickening of 5–8 mm) giving granular appearance. |
| Barium-string sign of Kantour, cobblestone mucosa, antimesenteric sacculations and creeping mesenteric fat separating the bowel loops and skip lesions | Barium: Lead pipe colon due to loss of haustration, granular mucosa. |

(Contd.)

Table 4.177.3: Difference between Crohn's disease and ulcerative colitis (Contd.)

| Crohn's disease | Ulcerative colitis |
|---|---|
|  |  |
| Fig. 4.177.18: String sign of Kantour | Fig. 4.177.19: Lead pipe colon |

Enhancement patterns of bowel mucosa in Crohn's disease

| | | |
|---|---|---|
|  |  |  |
| Fig. 4.177.20: Homogeneous (active inflammation) | Fig. 4.177.21: Mucosal enhancement | Fig. 4.177.22: Layered enhancement (long standing/chronic) |

Table 4.177.4: MEGS score (MR enterography score) helps in assessing the disease activity, severity and prognosis of inflammatory bowel disease (Crohn's)

| MR enterography features (0–3) | | | | |
|---|--------|---------------------------------|-----------------|----------------------------|
| Bowel wall thickness, mural T2 signal intensity, perimural T2 signal intensity (mesenteric edema), T1 enhancement, mural enhancement pattern, loss of haustral folds (for colon only) | | | | |
| Multiplication factor: Length of the diseased portion in segment(cm) | | | | |
| Extraluminal factors: 5 points each: Enlarged lymph nodes (≥ 10 mm in short axis diameter), vascular engorgement of the vasa recta (comb sign), abscess, fistula | | | | |
| Features | 0 | 1 | 2 | 3 |
| Bowel wall thickness in mm | 1–3 | >3 –5 | >5 –7 | >7 |
| Mural T2 signal intensity | Normal | Mild | Moderate | Marked |
| T2 perimural edema | Normal | Increase in signal but no fluid | Small fluid rim | Large fluid rim (>2 mm) |
| T1 enhancement of bowel wall | Normal | Mild | Moderate | Marked |
| Enhancement pattern | Normal | Homogeneous | Mucosal | Layered |
| Nodes | Nil | <1 cm | 1 node >1 cm | >3 nodes >1 cm |

Summation of scoring of each involved segments give the total score, maximum total score 296. Other scoring system used MaRIA (magnetic resonance index of activity)

CT enteroclysis: Patient in prone position, naso-jejunal intubation done using Bilbao-Dotter tube with side holes, with/without end holes. Two litres iso-osmotic water solution with PEG polyethylene glycol (80–120 ml/min), 1 mg IV glucagon (to reduce bowel motility) and IV contrast administration. Used to study the bowel pathology with adequate distention of the bowel.

CT enterography: Oral administration of neutral or negative contrast agent 1.5 to 2 litres over 30–45 min. Glucagon 1 mg IV and IV contrast administration. Image

taken in enteric phase for better visualisation of bowel wall thickening and pericolic inflammatory changes.

MR enteroclysis: Similar technique to the CT enteroclysis. Various contrast agents used are:

1. Positive—hyper on both T1 and T2 sequences (gadolinium chelates, ferrous ammonium citrate, manganese and food—blueberry juice, milk, green tea)
2. Negative—hypo on both T1 and T2 sequences (superparamagnetic substances like SPIO, BaSO₄)

Table 4.177.5: Patterns of bowel wall enhancement


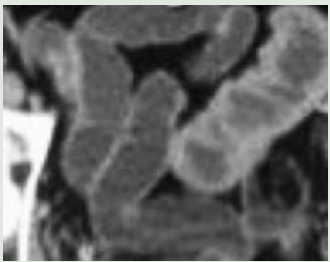

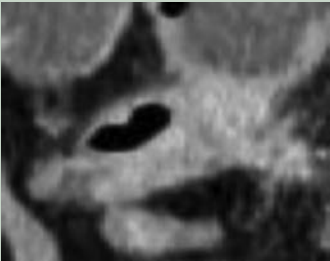

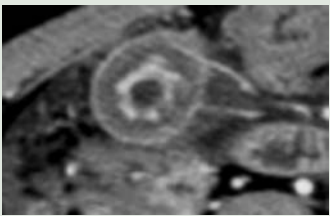

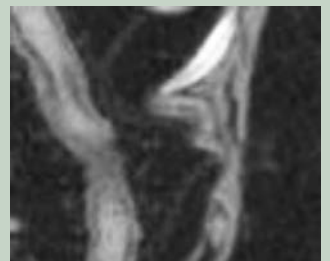

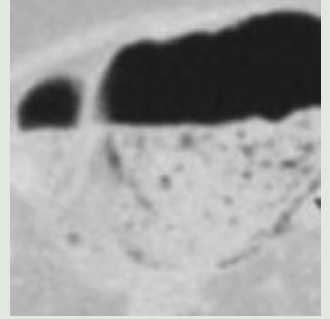
| | | |
|--|---|--|
| White attenuation a. Acute inflammatory bowel disease (due to vasodilatation with acute hyperemia) b. Shock bowel (injury to intramural vessels) c. Reperfusion after ischaemia d. Hemorrhage |  <p>Fig. 4.177.23: White attenuation</p> |  <p>Fig. 4.177.24: Bright enhancement of bowel wall—white attenuation</p> |
| Gray attenuation—no bowel stratification but thick poorly enhancing bowel wall a. Chronic Crohn's disease b. Ischemia c. Neoplasm |  <p>Fig. 4.177.25: Gray attenuation</p> |  <p>Fig. 4.177.26: Gray attenuation</p> |
| Water target attenuation: a. Portal hypertension b. Infection (Salmonella, Shigella, <i>E. coli</i> , CMV, AIDS) c. Acute ulcerative colitis and acute Crohn's disease d. Typhlitis e. Ischaemia |  <p>Fig. 4.177.27: Water target attenuation</p> |  <p>Fig. 4.177.28: Water target attenuation—enhancing mucosa and muscularis propria with edematous submucosa</p> |
| Fat target attenuation: a. Chronic ulcerative colitis b. Chronic Crohn's disease c. Obesity Enhancing mucosa and muscularis propria with submucosal fat |  <p>Fig. 4.177.29: Fat target attenuation</p> |  <p>Fig. 4.177.30: Fat target attenuation</p> |
| Gas attenuation/pneumatosis: a. Ischaemia b. Infection c. Trauma d. Connective tissue diseases e. IBD, COPD, obstruction |  <p>Fig. 4.177.31: Gas attenuation</p> |  <p>Fig. 4.177.32: Gas attenuation</p> |

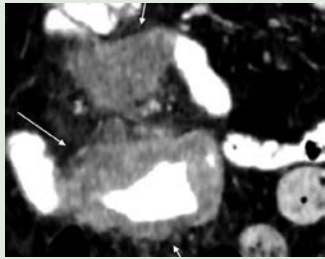
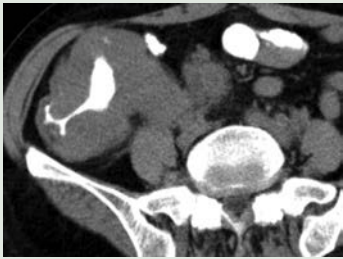
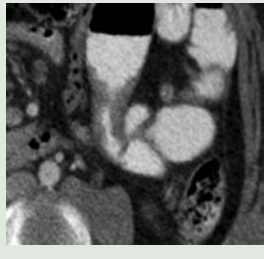
Table 4.177.6: Difference between ileocecal tuberculosis and Crohn's disease

| | | | |
|---|---|--|--|
| <i>Ileocaecal TB</i> | | <i>Crohn's disease</i> | |
| Circumferential wall thickening (1–2 cm) of the cecum and terminal ileum (cecum > terminal ileum) associated with asymmetric thickening of the ileocecal valve and medial wall of the cecum (short segment) | | Symmetrical bowel wall thickening. Long segment Thickening on the ileal side, transmural involvement. | |
| Multiple site involvement with skipped lesion may be seen <4 usually and shows homogeneous attenuation | | Multiple site involvements and skip lesions common. | |
| Mural stratification not seen | | Mural stratification seen | |
| Concentric stricture, enteroliths seen, peri anal fistula and mesenteric abscess is rare. | | Eccentric strictures with pseudo sacculations, peri anal fistula and mesenteric abscess seen. | |
| Adjacent mesenteric lymphadenopathy with central areas of low attenuation (necrotic) | | Regional mesenteric nodes measuring 3-8 mm | |
| Omental caking and peritoneal thickening is seen. | | Enlarged mesenteric vascular bundles in the involved mesentery known as the comb sign. | |
| Fibrofatty proliferation of the mesentery: Uncommon | | Fibrofatty proliferation of the mesentery known as 'creeping fat. | |
| Collection or ascites seen | | Less common | |
| Solid organ involvement seen | | Uncommon | |
| Pulled up cecum due to predominant cecal involvement | | | |
| Length of involvement of small bowel | | | |
| <i>Focal <5 cm</i> | <i>5–10 cm</i> | <i>Segmental 10–30</i> | <i>Diffuse</i> |
| Adenocarcinoma | Diverticulitis Crohn's disease Ischemia | Ischemia, sub-mucosal hemorrhage, radiation, infection, Crohn's disease, lymphoma | Infectious enterocolitis Ulcerative colitis Edema from low protein or cirrhosis SLE |

Table 4.177.7: Small bowel thickness (normal: 3–5 mm)

| <i>Crohn's disease</i> | <i>Pseudomembranous colitis</i> | <i>Ischemia (venous)</i> | <i>Carcinoma/lymphoma</i> | <i>TB</i> | <i>Ulcerative colitis/infection/radiation</i> |
|------------------------|---------------------------------|--------------------------|---------------------------|-----------|---|
| 9–11 mm | 8–10 mm | 7–9 mm | 15–20 mm | 10–20 mm | 7–8 mm |

Table 4.177.8: Diffuse wall thickening without mural stratification

| | | |
|---|--|---|
|  |  |  |
| Fig. 4.177.33: Adenocarcinoma | Fig. 4.177.34: Lymphoma | Fig. 4.177.35: TB |

3. Biphase—hypo on T1 and hyper on T2 (water, methyl cellulose, mannitol)

4

Fat halo sign: Fat suppression is routinely used to differentiate between mural fat depositions and mural edema. Fat depositions are a result of chronic bowel

inflammation, but not typical of active disease. These fat depositions can be diffuse but can also present as a layered pattern. The CT equivalent for this pattern is the fat halo sign.

4.178 GASTROINTESTINAL TRACT

Case No. 178

Clinical history: A 15-year-old boy with history of abdominal pain, loss of weight, loss of appetite, easy fatigability and evening rise of temperature for past five months.

Radiological techniques and observation: Figure 4.178.1 shows ultrasound abdomen image that reveals thickening of the terminal ileum and caecum.

Figures 4.178.2 and 4.178.3 show CECT of abdomen and pelvis with IV and oral contrast study in axial sections demonstrate diffuse circumferential thickening of the terminal ileum with wall enhancement and dilatation of the proximal ileal loops. Caecum appears thickened and contracted. Asymmetric thickening in the region of the ileocaecal wall is seen. Thin and smooth peritoneal

thickening with enhancement is seen. Appendix appears dilated with wall enhancement. No appendicolith and periappendiceal collection. No significant obstruction of the proximal small bowel loops.

Figures 4.178.4 and 4.178.5 show multiple peripherally enhancing necrotic nodes with central low attenuation is noted in right iliac, mesenteric, para-aortic and periportal region.

Figures 4.178.6 and 4.178.7 show coronal reconstructed CECT images demonstrating the thickened terminal ileum. Contracted caecum with thickening is noted and it appears to be slightly elevated from its position and ileocaecal angle is widened. Multiple peripherally enhancing necrotic nodes are noted. No evidence of focal/multiple lesions in liver, spleen, pancreas and kidney. No evidence of skeletal lesions.

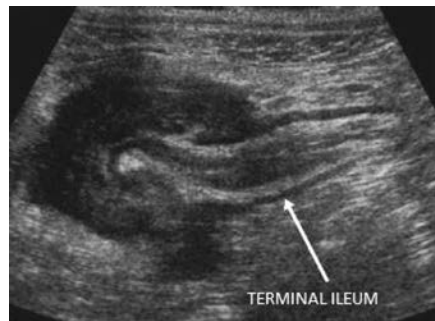


Fig. 4.178.1



Fig. 4.178.2



Fig. 4.178.3



Fig. 4.178.4



Fig. 4.178.5


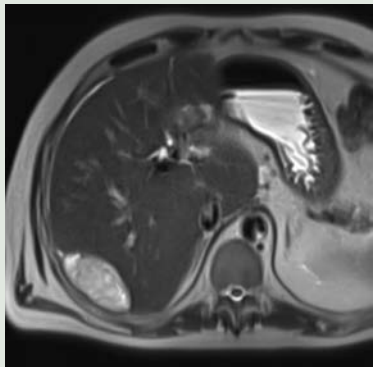

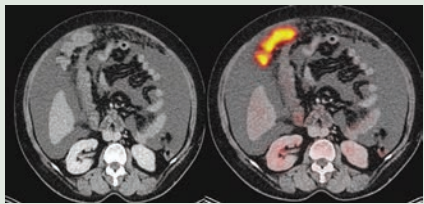


Fig. 4.178.6



Fig. 4.178.7

Table 4.178.1: Differential diagnosis for abdominal tuberculosis

| Differentials | Imaging features | |
|---|--|--|
| <p>Omental metastasis/peritoneal carcinomatosis: Isolated peritoneal metastases are usually asymptomatic. Abdominal distention due to malignant ascites. Intraperitoneal seeding and direct invasion is the most common cause. Peritoneal metastases are not locally treated. Complications do however frequently require treatment for palliation like bypass enterostomies for bowel obstruction and repeated ascitic drainage for malignant ascites.</p> | <p>USG shows ascites that may be anechoic or have low-level echoes. Nodules are of intermediate echogenicity, hypoechoic compared to the peritoneum, infiltration of the omentum results in hyper-echogenicity. CT may help in differentiating tuberculous peritonitis from peritoneal carcinomatosis. The differentiating features are: Nodularity and irregular thickening in parietal peritoneum in case of peritoneal carcinomatosis. Evidence of primary malignancy also supports the diagnosis. Ascites, omental caking, discrete mesenteric nodules are seen in both. Calcified lymph nodes and smooth peritoneal thickening are seen in TB. MRI can be very sensitive, probably more so than CT (85–90%).</p> |  <p>Fig. 4.178.8: Peritoneal carcinomatosis</p> |
| <p>Pseudomyxoma peritonei refers to syndrome of progressive intraperitoneal accumulation of mucinous ascites related to a mucin-producing neoplasm. It is most commonly caused by a mucinous tumor of the ovary, appendix, rarely from colon. Treatment is surgical debulking, followed by infusion of intraperitoneal chemotherapy.</p> | <p>X-ray shows ascites with centrally displaced small bowel loops. CT shows loculated collections of fluid which accumulate along peritoneal surfaces, with scalloped appearance of coated abdominal organs and omental caking. Scattered (curvilinear or punctate) calcifications. USG shows echogenic peritoneal masses or ascites with echogenic particles which do not move.</p> |  <p>Fig. 4.178.9: Pseudomyxoma peritonei</p> |
| <p>Primary peritoneal mesothelioma: An uncommon primary tumor of the peritoneal lining. It shares same features with but less common than its pleural counterpart. Older males (most common age group is 50 to 70 years). History of exposure to asbestos, although prior radiation exposure, exposure to thorium, talc. Dry-painful type with a little to no ascites. Wet type shows abdominal distension with ascites and widespread nodules without a predominant mass, mixed type present with both pain and ascites</p> | <p>Variable sonographic appearances, from sheet-like hypoechoic to echogenic masses with omental thickening and ascites. CT shows nodular, irregular peritoneal and omental thickening, progressing to omental caking. concurrent pleural involvement with calcified pleural plaques. In advanced cases there may be encasement of the intra-peritoneal structures.</p> <p>Besides encasement of the bowel and the liver, also encasement of the mesentery might be observed.</p> |  <p>Fig. 4.178.10: Primary peritoneal mesothelioma</p> |
| <p>Primary peritoneal serous carcinoma</p> <p>This tumor is also one of the primary peritoneal malignancies. It occurs exclusively in women.</p> <p>This tumor is histologically identical to malignant ovarian surface epithelial tumors. It was once thought to be very rare, but now almost one-third of tumors previously diagnosed as ovarian cancer is diagnosed as primary peritoneal serous carcinoma.</p> | <p>Ovaries are normal or</p> <p>Involvement of extraovarian sites is greater than that of the ovarian surface or if ovaries are involved, yet disease is confined to the surface epithelium. There is ascites and omental involvement.</p> |  <p>Fig. 4.178.11: Primary peritoneal serous carcinoma</p> |

(Contd.)

Table 4.178.1: Differential diagnosis for abdominal tuberculosis (Contd.)

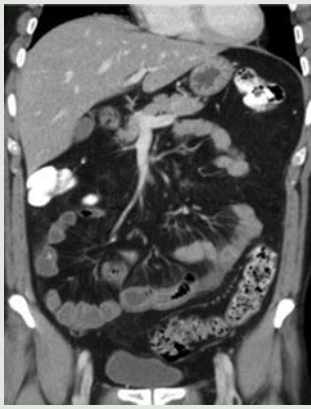
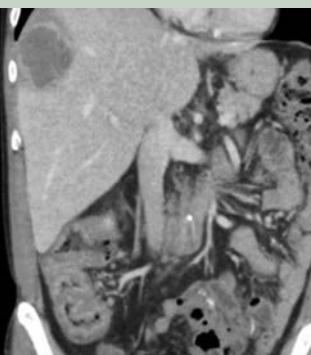

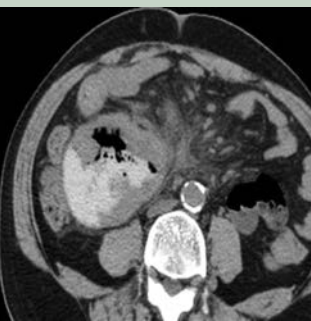
| | | |
|--|---|---|
| <p>Crohn's disease: More terminal ileal involvement compared with tuberculosis, which has more pronounced cecal involvement. Less/no ascites. Symmetrical bowel wall thickening.</p> | <p>CT shows symmetrical small bowel wall thickening involving long segment commonly seen in distal ileum. Mural stratification seen. Fibrofatty proliferation of mesentery results in creeping fat sign. Vascular engorgement results in comb sign. Skip lesions commonly seen. Less or no ascites. Eccentric stricture with pseudo-sacculation. String sign seen in barium series studies.</p> |  |
| <p>Amoebic colitis: It is a type of infectious colitis, caused by protozoan <i>Entamoeba histolytica</i>. Amoebic colitis presents with abdominal pain and dysentery. Antiparasitic therapy for amoebic colitis requires confirmation with laboratory investigation, including a fecal exam.</p> | <p>It shows appearances of infectious colitis on CT are variable and nonspecific amoebic colitis may present with ulceration and skip lesions, mimicking Crohn's disease. Collar button or aphthous ulcers are seen. Larger lesions mimic like a tumor, any part of the colon may be involved, but typically the cecum and rectum are more severely affected and a coexisting liver abscess may be seen. Ileum is usually spared; helps to differentiate it from Crohn's or tuberculosis, which typically involve the terminal ileum.</p> |  |
| <p>Carcinoma caecum: Clinical presentation may be similar to acute appendicitis due to local infiltration and micro-perforation resulting in secondary caecal inflammation.</p> | <p>CT helps in differentiating, there is focal bowel wall thickening (less than 5 cm of extension) which is typically asymmetrical and eccentric. These may have homogeneous contrast enhancement due to infiltration of a tumor mass, or heterogeneous areas of low attenuation from ischaemia and necrosis. Eccentric cecal wall thickening, evidence of metastatic disease are the key features.</p> |  |
| <p>Small bowel lymphoma: Despite the extensive involvement, small bowel obstruction is uncommon because of lack of desmoplastic reaction (lack of stricturing) and perforation is rare. Aneurysmal dilatation occurs due to the replacement of muscularis by tumor or infiltration of myenteric nerve plexus. Less frequently, the disease may manifest as a solid mass lesion (polypoidal/eccentric)</p> | <p>Typically, small-bowel lymphoma involves a single loop of bowel, with 5–20 cm of its length and bowel wall thickening usually ranges from 1–7 cm. Aneurysmal (or pseudoaneurysmal) dilatation (30%). Regional lymph node enlargement in approximately 50% of cases. Lymph node appears discrete and enlarged para-aortic nodes show sandwich sign in CT. The presence of extensive retroperitoneal lymphadenopathy and splenomegaly favours lymphoma, whereas adjacent fat infiltration supports adenocarcinoma.</p> |  |

Fig. 4.178.12: Crohn's disease**Fig. 4.178.13:** Amoebic colitis**Fig. 4.178.14:** Carcinoma caecum**Fig. 4.178.15:** Small bowel lymphoma

Interpretation: A: 15-year-old boy with lesion in terminal ileum, C: Wall thickening with loss of ileo-caecal angle and elevated cecum. B: Peritoneal thickening and ascites with omental nodes. Multiple peripherally enhancing nodes in mesentery, para-aortic regions that represent necrotic nodes. D: Ileo-caecal tuberculosis.

Principal diagnosis: Ileo-caecal tuberculosis with mesenteric, para-aortic and peri-portal necrotic lymph nodes with peritoneal thickening and ascites. Crohn's disease is unlikely as there are no skip lesions, no fistula is visualized. No pseudo-sacculation or comb sign.

Differential diagnosis for ileo-caecal thickening

1. Crohn's disease
2. Amoebic colitis/typhlitis
3. Carcinoma caecum/colon
4. Actinomyces
5. Lymphoma
6. Reactive thickening
7. Ulcerative colitis

Differentials for mesenteric lymphadenopathy

1. Metastases or lymphoma
2. Whipple disease
3. *Mycobacterium avium*—intracellular infection

Differentials for peritoneal thickening

1. Nontuberculous infectious peritonitis
2. Peritoneal/omental metastases
3. Pseudomyxoma peritonei
4. Lymphoma
5. Primary peritoneal mesothelioma
6. Primary peritoneal serous carcinoma
7. Omental infarct

Discussion: Gastrointestinal tuberculosis: Ileocecal region affected in 90% of cases. Common site due to presence of lymph tissue and stasis of bowel contents in that location. Cecum and terminal ileum are usually contracted (cone-shaped cecum) with asymmetric wall thickening of ileocecal valve and medial cecum. Regional lymphadenopathy with central caseation. Involvement of stomach and proximal small bowel is rare. In stomach, it affects antrum and distal body, often simulating peptic ulcer disease. In duodenum there is wall thickening and luminal narrowing.

Tuberculous peritonitis: Three imaging patterns which are wet, dry, and fibrotic fixed. Wet type shows large amount of free or loculated ascites. Higher than water density due to protein/cellular content. Complex ascites with septations or fibrinous strands. Dry type shows mesenteric and omental thickening, fibrous adhesions, and caseous nodules. In fibrotic fixed discrete masses in omentum with matted loops of bowel with loculated ascites. CT is 69% sensitive for TB peritonitis. Difficult to distinguish from carcinomatosis. Carcinomatosis more likely to demonstrate discrete implants or omental caking.

Intestinal cocoon: Encapsulating peritoneal sclerosis is a rare benign cause of acute or subacute small bowel obstruction. It is characterized by total or partial encasement of the small bowel within a thick fibrocollagenous membrane. Can occur at any age, ranging from 2-day neonate to 82 years.

It occurs secondarily due to tuberculosis, continuous ambulatory peritoneal dialysis (prevalence ~0.7%), peritoneovenous or ventriculoperitoneal shunts, treatment with praziquantel, rarely in sarcoidosis and post-

Table 4.178.2: Barium signs of abdominal tuberculosis

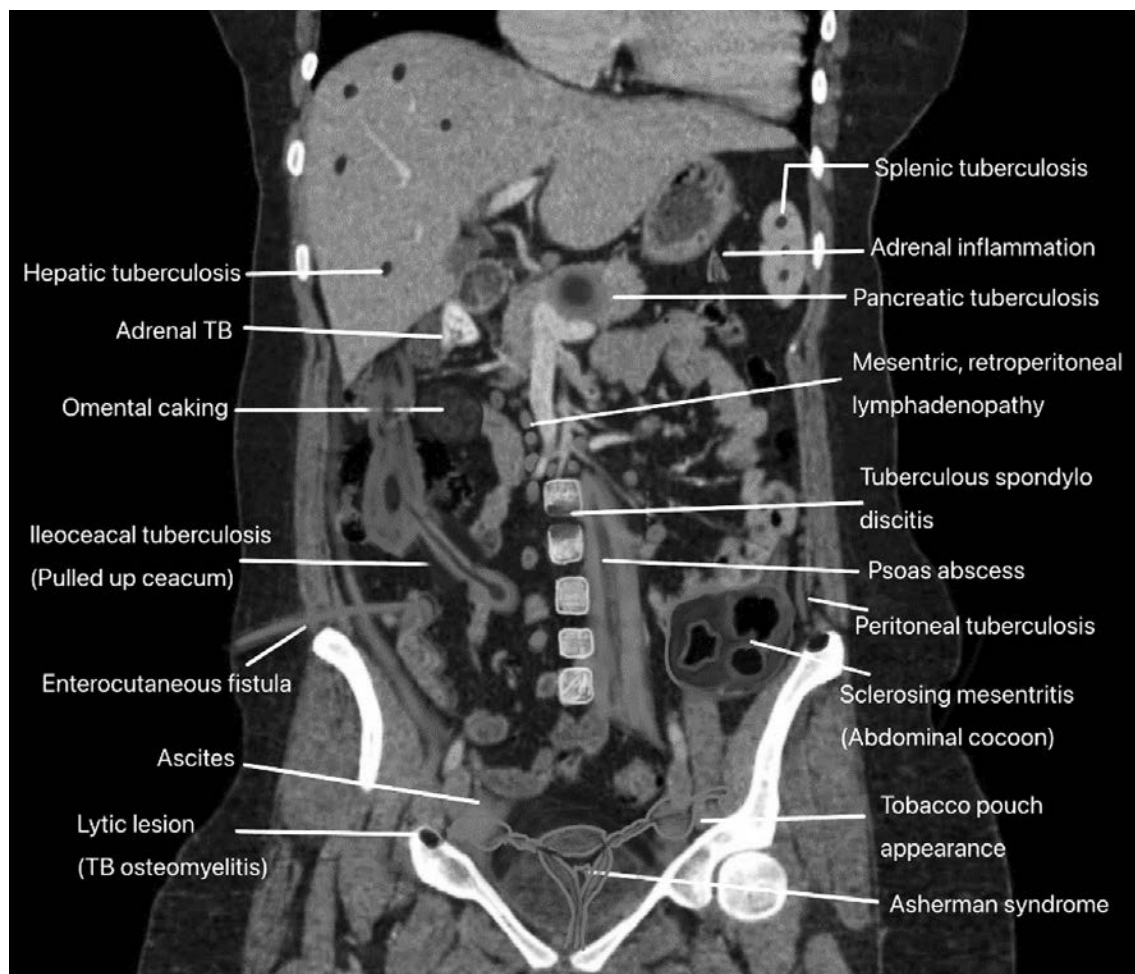
| String sign of Kantor | Pulled-up caecum | Fleischner sign | Gooseneck deformity | Sterling sign |
|--|--|--|---|---|
| String-like appearance of contrast filled bowel loops due to severe narrowing of bowel loops. Especially the distal ileum. Crohn's disease, ileocecal TB, colon cancer | Caecum appears conical in shape and shrunken and pulled up due to fibrotic changes in mesocolon seen in Ileo-cecal tuberculosis. | Thickening of the ileo-caecal valve lips and/or wide gaping of the valve, with narrowing of the terminal ileum. Inverted umbrella sign | Loss of normal ileo-caecal angle and dilated terminal ileum appears as suspended and hanging from a retracted, shortened caecum | Conical and shrunken cecum, widely open ileocecal valves, narrowing terminal ileum, rapid emptying of diseased segment. Represents acute inflammation superimposed on a chronically involved segment of the ileum, caecum or ascending colon. Also seen in Crohn's disease. |

Table 4.178.3: Gastrointestinal TB

| | |
|--|---|
| Etiology: <ul style="list-style-type: none"> • Swallowing of infected sputum in active pulmonary TB • Ingestion of contagious milk • Hematogeneous spread • Direct extension from adjacent organs | Age 20-40 years MC location: <ul style="list-style-type: none"> • <i>M. tuberculosis</i>—ileo-cecal region • <i>M avium-intracellulare</i> (MAI)—jejunum • Ileocaecal region is the most common site. |
| The affinity of tubercle bacillus for <ul style="list-style-type: none"> • Lymphoid tissue • Areas of physiologic stasis • Increased rate of fluid and electrolyte absorption • Minimal digestive activity | Types: <ul style="list-style-type: none"> • Ulcerative: MC 60% • Hypertrophic: 10% • Ulcerohypertrophic |

liver transplantation. Plain radiography there is gas-fluid levels similar to those in patients with any other cause of small-bowel obstruction the wall of the “cocoon” may calcify. Ultrasound findings are clumped bowel loops trilaminar hyperechoic membrane, hypoechoic bowel wall and hyperechoic bowel contents. Ascites may be present. CT imaging findings may include enhancing peritoneum,

thickened >2 mm, signs of small intestinal obstruction fixation of intestinal loops, ascites or localized fluid collections (especially interbowel), bowel wall thickening, peritoneal or mural calcification, calcified and/or reactive adenopathy. MRI will demonstrate the same features as CT, although it may better discriminate between thickened bowel and the peritoneal membrane than CT.

**Fig. 4.178.16:** Features of abdominal tuberculosis

Lymphadenopathy (tuberculous lymphadenitis): Mesenteric and peripancreatic lymph nodes most commonly involved. Lymphadenopathy can range from increased number of normal-sized nodes to massively enlarged conglomerate nodal masses. Multiple groups often affected simultaneously. Enlarged, necrotic nodes with hypoattenuating centers and hyperattenuating enhancing rims on CT which is characteristic of caseating necrosis. Normal mesenteric lymph nodes are less than 5 mm in diameter abnormal >6 mm in its short axis/ Group of 3 or more lymph nodes of any size clustered in 1 location.

Hepatosplenic tuberculosis: Micronodular pattern: Innumerable 0.5–2.0 mm nodules may or may not be discretely visualized (most often hypodense on CT and hyperechoic on US). May simply appear as hepatomegaly on CT. Macronodular pattern: CT findings in acute are hypoattenuating nodules with ill-defined enhancing margins. Chronic stage, the tuberculomas often calcify. TB and histoplasmosis are most common causes of calcified granulomas. MRI: T1WI: Hypointense, minimally enhancing, honeycomb lesions. T2WI: Hyperintense with less intense rim relative to surrounding liver. Rim enhancement on post-gadolinium images.

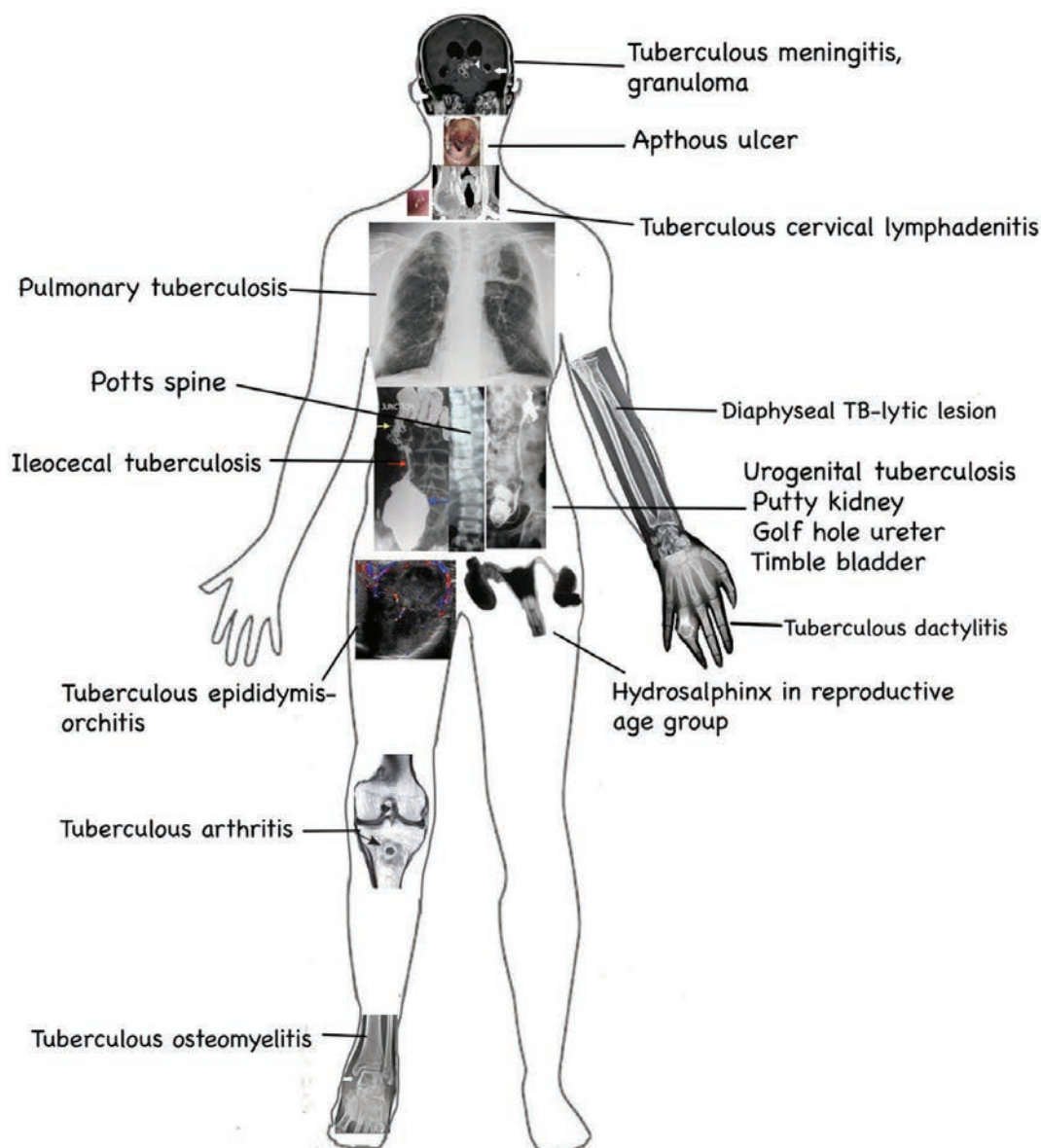


Fig. 4.178.17: Manifestations of tuberculosis

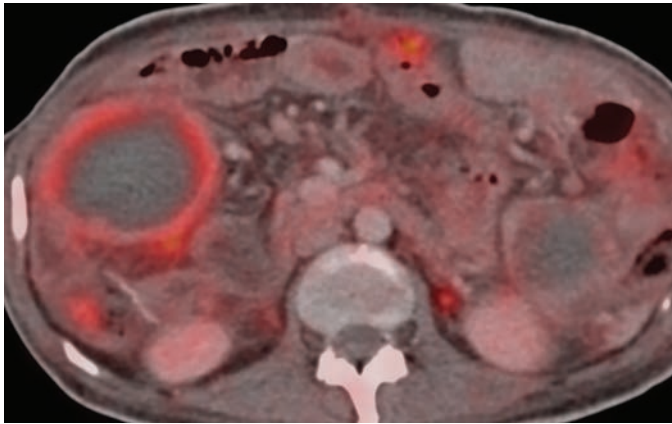


Fig. 4.178.18: Growing teratoma with gliomatosis peritonei

Adrenal tuberculosis: Unilateral (10%) or bilateral (90%); Acute: Enlarged adrenals (often appear as discrete centrally necrotic adrenal masses); Chronic: Small adrenals with dots of calcification and low signal on all MR sequences. May cause adrenal insufficiency (most common cause in developing countries).

Further management: CT chest is performed to look for any primary lung infection. USG KUB and IVP to assess the status of genitourinary tract. Surgery for emergent presentations like obstruction and impending perforation of bowel loops. 6–9 months course of multidrug antituberculous chemotherapy. Most commonly used drugs include rifampin, isoniazid, pyrazinamide, and ethambutol. Exact drug regimen may vary based on resistance patterns.

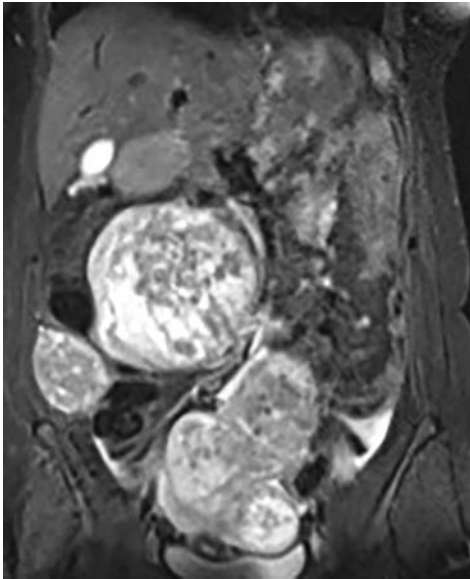


Fig. 4.178.19: Peritoneal leiomyomatosis from benign uterine leiomyoma

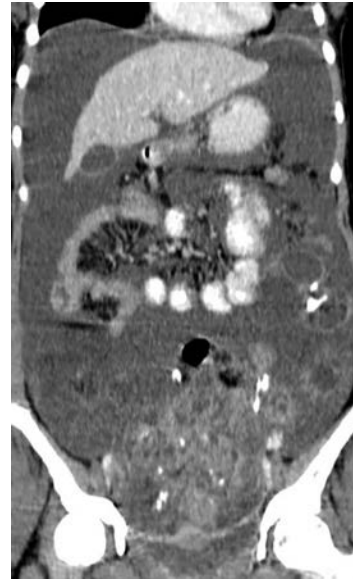


Fig. 4.178.20: Multiple peritoneal GIST

4.179 GENERAL ABDOMEN INCLUDING ABDOMINAL WALL, PERITONEUM

Case No. 179

Clinical history: A 36-year-old woman with previous history of LSCS presented with right lower abdominal pain on and off \times 6 months.

Radiological techniques and observation: Figure 4.179.1 is MRI pelvis sagittal T2-weighted image showing lesion within the intramuscular plane along the scar site, in lower anterior abdominal wall with isointense signal compared with muscle and cystic areas. Figures 4.179.2 and 4.179.3 are axial T1 and T1C with fat suppression show isointense signal compared with muscle and small foci of high signal intensity, indicative of haemorrhage. There was no evidence of intrapelvic endometriosis in the ovaries or cul-de-sac. Uterus appears normal.

Interpretation: A: 36 years old women, C: Well-defined solid lesion in lower anterior abdominal wall in intramuscular plane along the scar site and small foci of hemorrhage in a female, B: Isointense signal compared with muscle on MRI, D: Scar endometriosis.

Principal diagnosis: Scar endometriosis.

Management: Patient is referred to gynaecologist for excision which is the treatment of choice.

Discussion: Endometriosis is defined as the presence of ectopic endometrial glands and stroma in locations outside the uterus. Theories have been proposed to explain the ectopic glands include: (1) The retrograde menstruation theory where retrograde transport of endometrial cells during menstruation mediates the spread of endometrial tissue to the peritoneal cavity. (2) The coelomic metaplasia theory suggests that there is metaplasia of cells lining the peritoneum into functional endometrial tissue, (3) the lymphovascular metastasis theory proposes that dissemination through pelvic veins and lymphatics leads to endometrial cells in distant sites such as the lungs or lymph nodes. (4) The stem cell theory proposes that extrauterine endometrial stem cells contribute to the pathogenesis of endometriosis. Locations—Ovaries, pelvic cul-de-sac, uterine ligaments, uterine serosal surface, and fallopian tubes. Less common sites—rectosigmoid serosa, urinary bladder, ureter, and previous surgical sites, such as cesarean scars.

Management: Surgical excision with negative margins is the treatment of choice in abdominal wall endometriosis. Medical therapies, which may include oral contraceptives, danazol, leuprolide, and progestogen, may provide temporary relief; however, symptoms usually return after cessation of treatment.

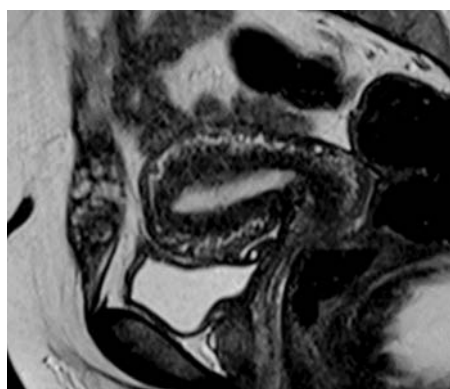


Fig. 4.179.1

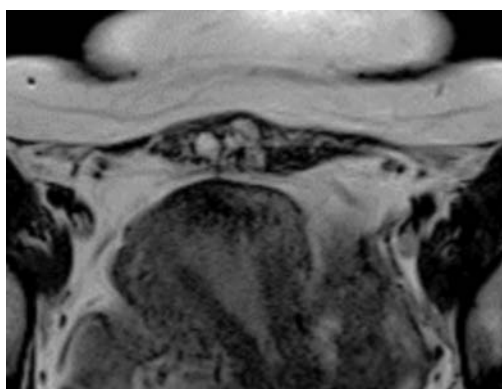


Fig. 4.179.2

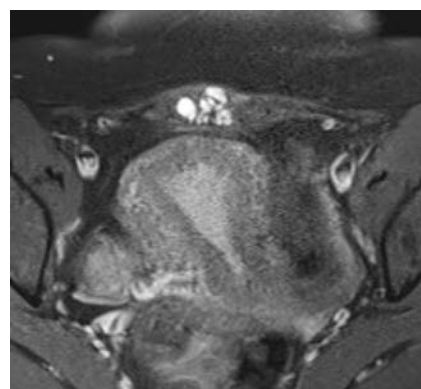


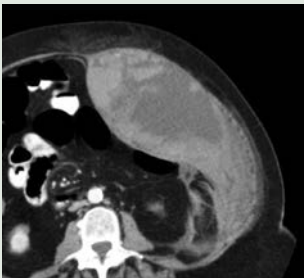
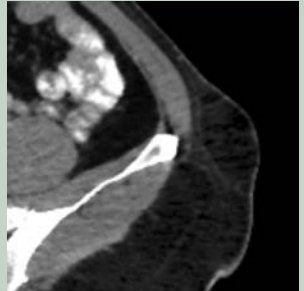
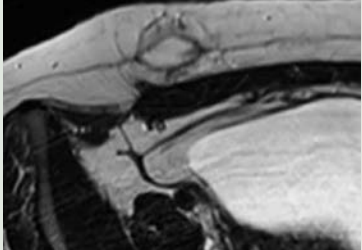
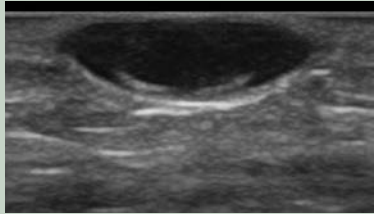
Fig. 4.179.3

Table 4.179.1: Differential diagnosis for anterior abdominal wall mass

| | |
|--|---|
| <p>Desmoid tumors: Characterized by fibroblastic proliferation, without evidence of inflammation. Association with previous surgery, trauma, estrogen therapy, familial adenomatous polyposis and Gardner syndrome.</p> | <p>Well-circumscribed masses/more aggressive with ill-defined margins, homogeneously or focally hyperattenuating when compared to soft tissue on the non-contrast scan. T1: Low signal intensity, T2: low signal intensity, T1 C+ (Gd): May show homogeneous, inhomogeneous, or no significant enhancement. Contains abundant spindle cells with a few areas of collagen.</p> |
|--|---|

(Contd.)

Table 4.179.1: Differential diagnosis for anterior abdominal wall mass (Contd.)

| | | |
|--|---|--|
| <p>Anterior abdominal-wall hematomas: Occur in the rectus abdominis muscle and result from damage to the superior or inferior epigastric arteries or direct tear of the rectus muscle. Causes: Trauma, surgical intervention, blood dyscrasias, and anticoagulant therapy</p> | <p>CT: Well-defined hyperdense mass. CECT: Active contrast extravasation MRI depends on the stage of the haemorrhage.</p> |  <p>Fig. 4.179.4: Anterior abdominal wall hematoma</p> |
| <p>Abdominal-wall lipomas: Most common soft tissue tumor, contains matured adipocytes, soft painless well circumscribed masses commonly in trunk or proximal extremities.</p> | <p>Fat-density lesion with a thin capsule in subcutaneous plane. Speck of calcification may be seen.</p> |  <p>Fig. 4.179.5: Abdominal wall lipoma</p> |
| <p>Epidermoid cysts: They are usually, congenital but can be acquired after traumatic or surgical implantation of epidermal elements. Peripheral enhancement and occasionally, peripheral calcification can be present</p> | <p>Well-defined round or ovoid lesions of high signal intensity on T2W MRI and low signal intensity on T1W images. In many cases, low signal components on T2W and high signal contents on T1W may be found to reflect the keratinized debris within these cysts.</p> |  <p>Fig. 4.179.6: Epidermoid cyst</p> |
| <p>Neurofibromas: Cutaneous manifestations of NF range from small pedunculated dermal neurofibromas to large diffuse and plexiform neurofibromas.</p> | <p>CT: Homogeneously hypoattenuating due to myxoid and mucinous stroma. T1W-I: Low signal intensity, T2W: Heterogeneously high signal intensity. Mild-to-moderate contrast enhancement. "Target sign" (hyperintense periphery and hypointense center) and "split fat sign" (rim of fat around tumor) may be seen.</p> |  <p>Fig. 4.179.7: Neurofibroma</p> |
| <p>Abdominal-wall vascular malformation and hemangioma: More commonly seen in children and young adults</p> | <p>Present as lobulated masses with infiltrative features, a lack of respect for fascial planes, and involvement of multiple tissue types, such as muscle and subcutaneous fat. Phleboliths are often seen</p> | |
| <p>Metastases: Common tumor that metastasize to the abdominal wall include melanoma, breast, stomach, colon, ovary, cervix, pancreas, kidney, bladder, and lung.</p> | <p>The metastases present as well-defined lesions with heterogeneous or peripheral enhancement. Metastasis to the surgical wound or laparoscopy trocar site and needle-tract seeding in radiofrequency ablation (RFA) also leads to abdominal-wall metastases</p> | |
| <p>Dermatofibrosarcoma: Protuberans: Spindle-cell tumor that typically arises in the dermis.</p> | <p>Characterized microscopically by fibroblasts, with a prominent storiform pattern. CT: Nodular heterogeneously enhancing mass arising from the skin and extending into the subcutaneous tissues</p> | |

(Contd.)

Table 4.179.1: Differential diagnosis for anterior abdominal wall mass (Contd.)

| | |
|--|---|
| Subcutaneous Leiomyomas: Rare tumours and have a higher incidence in patients with AIDS (Fig. 4.179.7). | Commonly seen in children and young adults, and present as tender subcutaneous nodules. Well-circumscribed single or clustered masses, and are typically iso- to mildly hyperintense on T1W and heterogeneous high signal intensity on T2W. |
| Lymphoma: Diffuse systemic lymphoma and involvement of the abdominal wall. | CT: Well-defined slightly hyperdense mass lesion showing homogeneous contrast enhancement |

Abdominal wall hernia (4–5%): Congenital or acquired, inguinal hernias are common (75%), femoral (15%) and umbilical (8%).

Types of abdominal wall hernias

1. Groin hernias: Inguinal hernias—indirect inguinal hernia, direct inguinal hernia, combined (pantaloon) hernia—femoral hernia
2. Pelvic hernias: Obturator hernia, sciatic hernia, gluteal hernia
3. Anterior abdominal wall hernias: Umbilical hernia, paraumbilical hernia, epigastric hernia, spigelian hernia (weakness between the muscle fibres of the abdominal wall)
4. Posterior abdominal wall hernia: Superior lumbar hernia, inferior lumbar hernia

Content as omentum: Omentocoele, intestine—enterocoele; more commonly small bowel but may be large intestine or appendix.

A portion of the circumference of the intestine—Richter’s hernia, Meckel’s diverticulum—Littre’s hernia.

The lateral crescent sign an easily detectable sign of an early direct inguinal hernia, which represents the laterally displaced and compressed inguinal canal, including its fat and contents. This sign may be less useful in cases of extremely large hernias, which may compress the inguinal canal to such a thin sliver that it may not be readily detectable at CT.

US imaging has an advantage over CT in the ability to evaluate standing patients. Doppler signals in the contents and presence or absence of peristalsis in the herniated bowel loop may be detected. CT helps to determine the shape, location and complications of abdominal wall hernias.

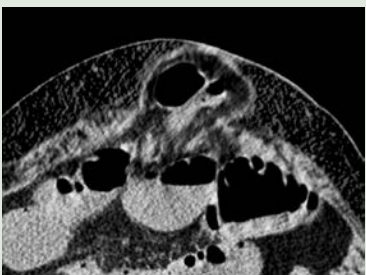


Fig. 4.179.8: Abdominal wall hernia

Umbilical granuloma/abscess: The urachus is a vestigial remnant of two embryonic structures: The cloaca, and the allantois. USG: Echoic collection in a midline cavity within the anterior abdominal wall. CT: Infected urachal sinus shows heterogeneous collection with calculus and gas formation communicating with the umbilicus. The tubular urachus normally involutes before birth, remaining as a fibrous cord between the transversalis fascia anteriorly and the peritoneum posteriorly and attaches the umbilicus to the bladder dome.

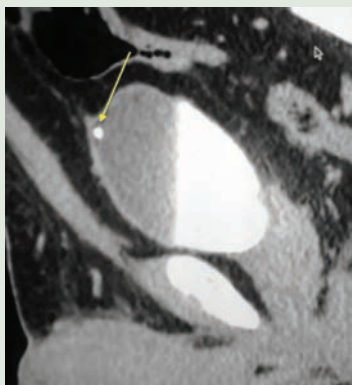


Fig. 4.179.9: Urachal remnant calcification

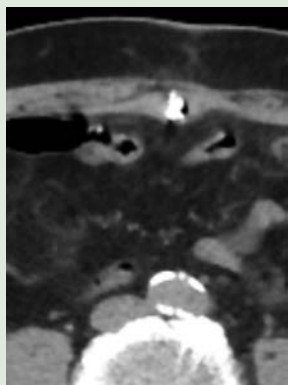


Fig. 4.179.10: Umbilical sinus with granuloma

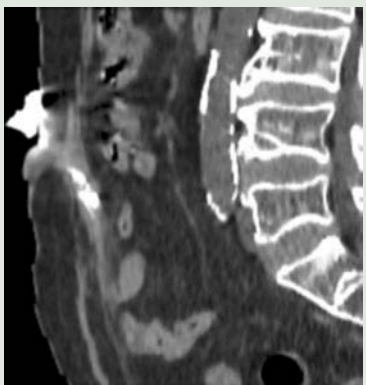


Fig. 4.179.11: Umbilical sinus

Table 4.179.1: Differential diagnosis for anterior abdominal wall mass (Contd.)

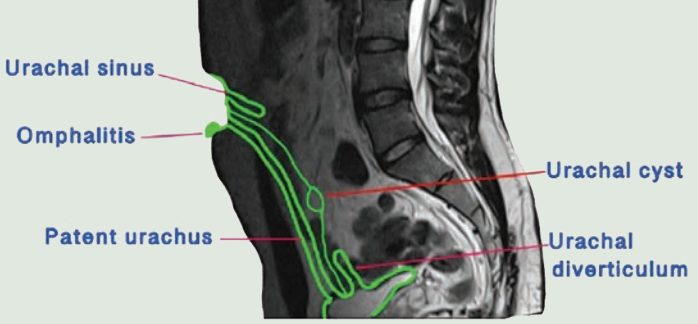


Fig. 4.179.12: Urachal anomalies

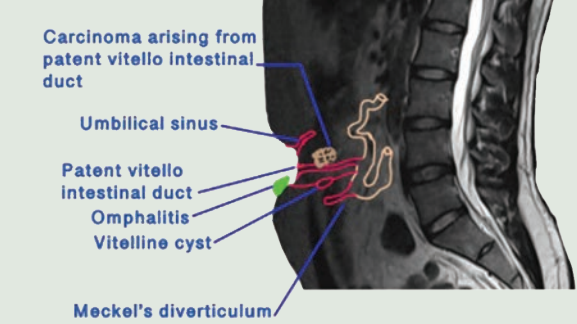


Fig. 4.179.13: Vitellointestinal duct anomalies

4.179.1 Sister Mary Joseph's nodule (Refer to case no. 166)

Others: Anterior abdominal wall abscesses, foreign body granulomas, post-surgical abscess

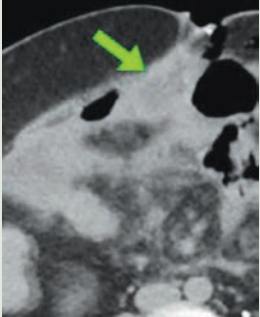


Fig. 4.179.14: Anterior abdominal wall abscess

4.180 GENERAL ABDOMEN INCLUDING ABDOMINAL WALL, PERITONEUM

Case No. 180

Clinical history: A 55-year-old male came with complaints of abdominal pain for the past 20 days. No history of fever/vomiting. Pain was not subsided with analgesic and smooth muscle relaxants. Past history: Patient has undergone appendectomy a month back and immediate postoperative period was uneventful.

Radiological techniques and observation:

Observations: Figure 4.180.1 (scanogram) shows well-defined radio-opacity with mottled gas pattern in the right iliac fossa. Dilated small bowel loops with fluid level seen, visualized psoas shadow appears normal, properitoneal fat plane appears normal. Liver and spleen shadow appears normal and visualized skeleton appears normal. Figures 4.180.2 to 4.180.6 are plain and contrast CT abdomen axial, coronal sections showing a well-circumscribed thick-walled intraperitoneal lesion in the right iliac fossa below anterior abdominal wall, adjacent to the ascending colon and postoperative changes noted in the anterior abdominal wall: The lesion shows multiple intralesional airpockets which is spongiform in

appearance, surrounding minimal fat stranding noted and in the given sections small and large bowel loops are seen separately. No evidence significant free fluid in the peritoneum. Visualized vertebra and bowel loops appear normal.

Interpretations: A: 55 years old male, C: Well-defined intraperitoneal lesion with B: Mottled gas pattern and internal airpockets showing spongiform appearance in the right iliac fossa, D: Gossypiboma with ileus/bowel obstruction.

Provisional diagnosis: With history of post-appendectomy and the imaging pattern, most probably diagnosis is gossypiboma.

Further management: The findings are discussed with surgery department and advised for surgical removal.

Brief discussion about gossypiboma: It is also known as cottonballoma, textiloma or gauzeoma. Sponge-like hypodense lesion simulating faecal matter outside the bowel with surrounding soft tissue thickening and inflammatory reaction in a postoperative patient denotes retained surgical gauze.



Fig. 4.180.1



Fig. 4.180.2



Fig. 4.180.3



Fig. 4.180.4

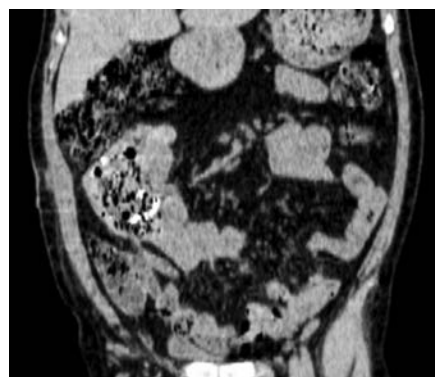


Fig. 4.180.5

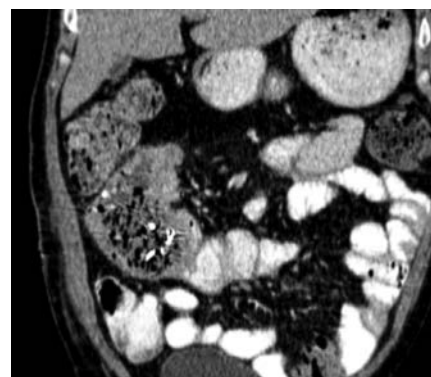


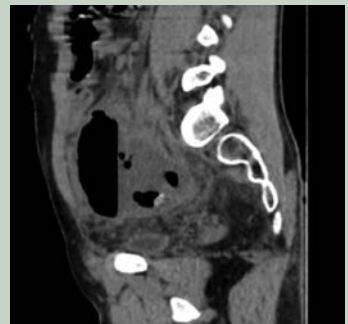

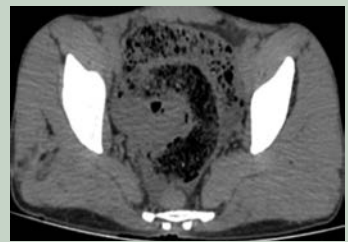




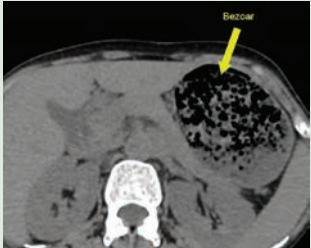
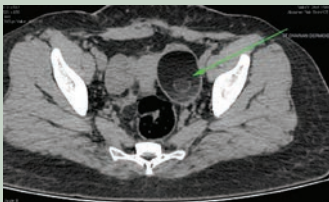
Fig. 4.180.6

Table 4.180.1: Differential diagnosis for textiloma

| | | |
|--|--|--|
| <p>1. Faeculoma: Mass of faeces most frequently noted in the rectum and sigmoid colon, that is much harder than a faecal impaction due to coprostasis.</p> | <p>CT: Spotted appearance on CT but has a recognizable colonic wall and lacks thick well-defined capsule.</p> |  <p>Fig. 4.180.7: Faeculoma</p> |
| <p>2. Abdominal/pelvic abscess with air pockets: Emphysematous cholecystitis, gastritis, pancreatitis, pyelonephritis, pyelitis, cystitis, gas gangrene of the uterus, and Fournier gangrene are various causes for abscess with airpockets. Emphysematous infections of the abdomen and pelvis represent potentially life-threatening conditions that require aggressive medical and often surgical management.</p> | <p>Abdominal radiography may demonstrate mottled gas pattern.</p> <p>Ultrasonography (US) may demonstrate highly echogenic reflectors with low-level posterior shadowing and reverberation artifact ("dirty" shadowing).</p> <p>CT is both highly sensitive and specific in the detection of abnormal gas showing hypodense collection with internal air pockets and well suited to reliable depiction of the anatomic location and extent of the gas</p> |  <p>Fig. 4.180.8: Pelvic abscess with air pockets</p>  <p>Fig. 4.180.9: Pelvic abscess with air pockets</p> |
| <p>3. Infected pancreatic pseudocyst: Pseudocysts are fluid collections diagnosed 4 weeks after acute episode of interstitial pancreatitis. If uncomplicated, they are called simple pseudocysts. Complications such as haemorrhage, infection can develop in pseudocyst.</p> | <p>Uncomplicated pancreatic pseudocysts appear homogeneous with fluid component only. If there is solid component with mottled gas pattern, infection by gas forming organisms should be considered.</p> |  <p>Fig. 4.180.10: Infected pancreatic pseudocyst</p> |
| <p>4. Small bowel faeces sign: It is the result of delayed intestinal transit and is believed to be caused by incompletely digested food, bacterial overgrowth, or increased water absorption of the distal small-bowel contents due to obstruction, combination of small bowel faeces sign and moderate to severe bowel dilatation is fairly suggestive of obstruction, particularly when associated with distal bowel collapse.</p> | <p>CT images will show presence of particulate feculent material mingled with gas bubbles in the lumen of the small intestine.</p> |  <p>Fig. 4.180.11: Small bowel faeces sign</p> |
| <p>5. Bezoar: Accumulation of indigestible contents within the gastrointestinal tract. CT demonstrates mass with mottled appearance due to air trapped within it obstructing segment of bowels.</p> | | |

(Contd.)

Table 4.180.1: Differential diagnosis for textiloma (Contd.)

| | | |
|--|---|--|
|  <p>Fig. 4.180.12: Plain CT abdomen showing bezoar in stomach</p> |  <p>Fig. 4.180.13: Oral contrast showing bezoar in stomach</p> |  <p>Fig. 4.180.14: Bezoar in stomach</p> |
| <p>Ovarian dermoid: Slow growing tumors contains skin elements including squamous epithelium and dermal appendages such as sebaceous and sweat glands and hairs. USG: Cystic adnexal mass with some mural components.</p> | <p>CT: Areas of low attenuation due to fat, fat-fluid level, calcification, Rokitansky protuberance and tuft of hairs. MR imaging with fat suppression and chemical shifting can confirm the presence of fat, enhancement helps to identify solid invasive components.</p> |  <p>Fig. 4.180.15: Ovarian dermoid</p> |

More broadly retained foreign object (RFO) is the technical term for surgical complication resulting from foreign material such as surgical sponge, accidentally left inside foreign material.

Two types of foreign body reaction occur in patient with retained sponges, the first type is an inflammatory reaction with formation of abscess that usually leads to early detection, the second type is an aseptic reaction to cotton material and development of granuloma, which can lead to long asymptomatic periods.

Gossypiboma—Latin words—*gossypium*, i.e. cotton, *boma*—tumor.

Imaging Findings

Plain radiograph: Surgical sponges contain radiopaque material that facilitates detection by standard abdominal radiography. This imaging method not useful when the gauze does not contain radiopaque material or the material disintegrates over time.

Ultrasound: Ultrasound features are divided into three types:

- An echogenic area with intense posterior acoustic shadow.

- A well-defined cystic mass containing distinct internal hyperechogenic wavy stripped structures.
- Nonspecific pattern with a hypoechogenic or complex mass.

CT: Well-circumscribed mass with thick wall, with or without gas, calcification. The internal structure may appear whirl-like/spongiform due to the presence of gas trapped within the mesh of sponges.

CECT: Enhancement of the wall after injection of contrast medium. In long standing cases, it becomes difficult to differentiate gossypiboma from abscess because of the presence of air bubbles, calcification of the cavity wall as well as contrast enhancement of the rim can be seen in both conditions.

MRI: T1: Hypointense and enhancement will be seen with gadolinium contrast.

T2: A soft tissue intense well-circumscribed mass with whorled internal configuration—low signal represents gauze fibres.

Capsule dark on both T1 and T2.

Complications: Abscess, peritonitis, intestinal obstruction, fistula, erosion into gastrointestinal tract.

Treatment: Surgical removal of gossypiboma.

4.181 GENERAL ABDOMEN INCLUDING ABDOMINAL WALL, PERITONEUM

Case No. 181

Clinical history: A 29-year-old male patient, presenting with abdominal pain.

Radiological techniques and observation: Axial CT sections and coronal reformation of abdomen of a 29-year-old male.

Figures 4.181.1 to 4.181.3 show an ill-defined heterogeneous mass-like lesion noted in the left lumbar region with hazy fat stranding noted within the surrounding omentum. There are regions of fat density within the mass. There appears to be a swirling pattern of vessels leading to the mass. There is no free fluid. There is no central dot sign. The bowel appears normal. There is no reactive wall thickening. The bones appear normal. The solid organs appear normal. The appendix appears normal. There is no evidence of diverticulosis. There is no peripancreatic fat stranding. There is no peritoneal

thickening, there is clinical correlation with the point of maximum tenderness.

Interpretation: A: 29 years old male, lesion in omentum
C: There are regions of fat density within the mass. There appears to be a swirling pattern of vessels leading to the mass. B: There is no central dot sign. D: Omental infarct.

The principal diagnosis is an omental infarct. The next step is to perform a CECT abdomen.

Management: Usually conservative.

Discussion: Intraperitoneal focal fat infarction: IFFI is an umbrella term for various conditions with overlapping clinical features, imaging findings, and prognosis. The common underlying pathology in these conditions is fat necrosis. The conditions grouped under IFFI are: Omental infarction, epiploic appendagitis, diverticulitis, encapsulated fat necrosis.



Fig. 4.181.1

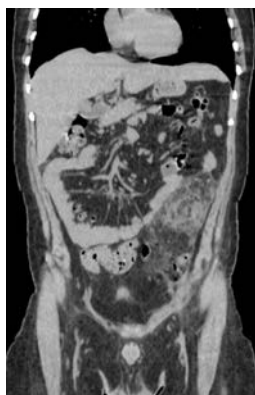


Fig. 4.181.2

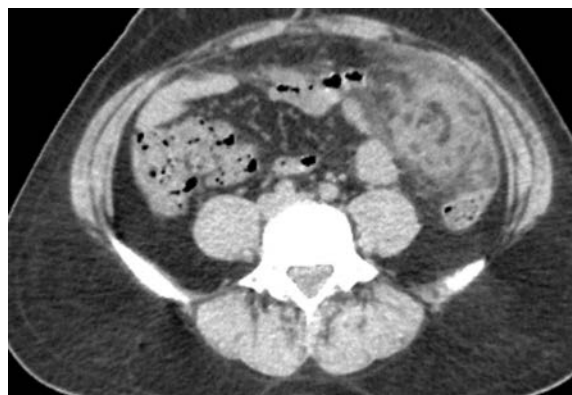


Fig. 4.181.3

Table 4.181.1: Differential diagnosis for omental infarct

Diverticulitis is intramural and pericolic infectious/inflammatory process resulting from perforation of colonic diverticula.

Imaging features: Ultrasound shows thickened bowel wall (>4 mm) and surrounding fat stranding with characterized bowel outpouching. CT shows segmental thickening of bowel wall with multiple colonic diverticula and pericolic fat stranding, engorged mesocolic blood vessels and "microperforation" Small bubbles of pericolic gas. Treatment for localized disease (stage I and II) conservative management with IV antibiotics and rehydration, surgical treatment required for multiple repeated attacks.

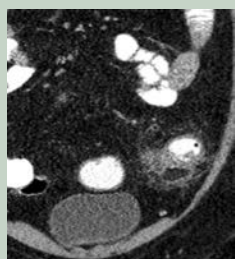


Fig. 4.181.4: Diverticulitis



Fig. 4.181.5: Diverticulitis

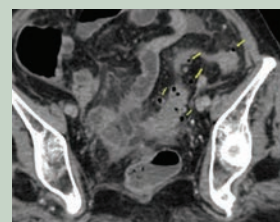


Fig. 4.181.6: Diverticulitis

(Contd.)

Table 4.181.1: Differential diagnosis for omental infarct (Contd.)

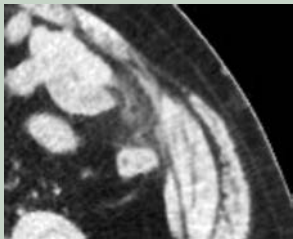
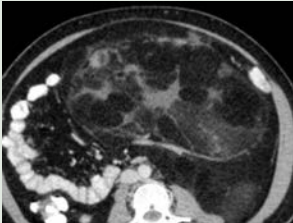
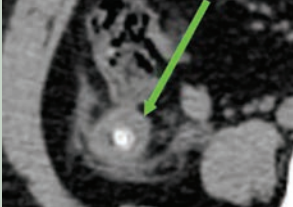
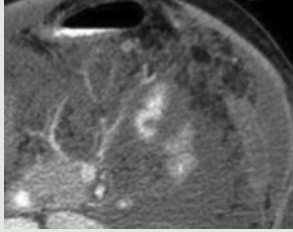
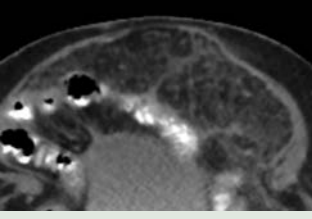
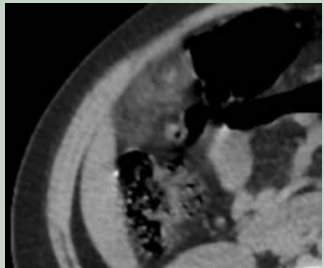
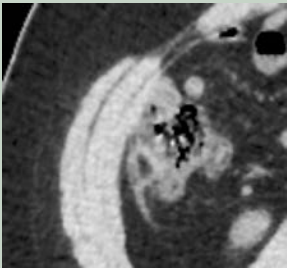
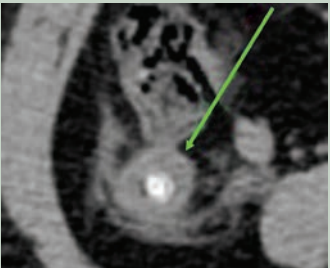

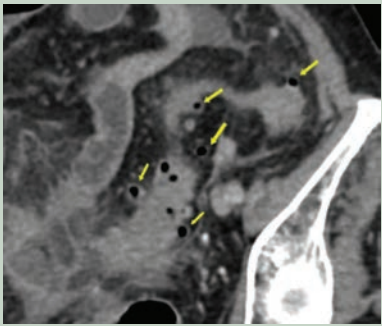
| | | |
|--|--|---|
| <p>Epiploic appendagitis: Ischemic process involving an appendix epiploica of the colon. Common in obese women.</p> | <p>USG: Rounded, non-compressible, hyperechoic mass, without internal vascularity, and surrounded by a subtle hypoechoic line.</p> <p>CT: Fat-density ovoid structure adjacent to the colon, usually 1.5–3.5 cm in diameter with thin high-density rim, and central hyperdense dot sign (representing the thrombosed vascular pedicle)</p> |  <p>Fig. 4.181.7: Epiploic appendagitis</p> |
| <p>Liposarcoma: Clinical presentation and change in size over time help differentiate from mass-like omental infarct.</p> | <p>There is inhomogeneous attenuation within the mass, with evidence of regions of both fat and soft-tissue attenuation. There is poor definition of adjacent structures with evidence of infiltration or invasion. Calcification may be present.</p> |  <p>Fig. 4.181.8: Liposarcoma</p> |
| <p>Acute appendicitis: Clinically mimics omental infarction of the right iliac fossa</p> | <p>Dilated appendix with wall thickening, hyperemia, periappendiceal fat stranding, inflammation, and free fluid.</p> <p>US: Non-compressible appendix on graded compression.</p> <p>Fluid collection, abscess or ectopic gas indicate perforation. Appendicolith may be seen.</p> |  <p>Fig. 4.181.9: Acute appendicitis</p> |
| <p>Pancreatitis with extraperitoneal fat necrosis</p> | <p>Peripancreatic fat stranding with enlargement of the pancreas. Surrounding fluid collections may be noted. Vascular compromise should be ruled out.</p> |  <p>Fig. 4.181.10: Pancreatitis with extraperitoneal fat necrosis</p> |
| <p>Encapsulated fat necrosis</p> <p>Encapsulated fat necrosis is thought to result from a traumatic or ischemic insult.</p> | <p>USG: Well defined, hyperechoic mass with hyperechoic rim.</p> <p>CT: Well-defined encapsulated region of fat attenuation. No surrounding inflammation noted with normal surrounding viscera. Calcification is absent.</p> | |
| <p>Peritoneal carcinomatosis: Usual sites of primary malignancy are ovarian and gastrointestinal.</p> | <p>Range of appearances, but usually soft tissue nodules or diffuse stranding and thickening of the omentum (early). It is usually multifocal.</p> |  <p>Fig. 4.181.11: Peritoneal carcinomatosis</p> |
| <p>Sclerosing mesenteritis—refer to case 175</p> | | |

Table 4.181.2: Differential diagnosis for peritoneal masses

| <i>Cystic</i> | <i>Solid</i> |
|---|--|
| Common <ul style="list-style-type: none"> • Mucinous carcinomatosis • Abscess • Pseudocyst | Common <ul style="list-style-type: none"> • Peritoneal metastases • Metastatic lymphadenopathy • NHL |
| Uncommon <ul style="list-style-type: none"> • Pseudomyxoma peritonei • Mesenteric cyst • TB | Uncommon <ul style="list-style-type: none"> • Carcinoid • Mesothelioma • Sclerosing mesenteritis • Mesenteric fibromatosis • Primary peritoneal serous carcinoma |
| Rare <ul style="list-style-type: none"> • Peritoneal inclusion cyst • Echinococcal cyst | Rare <ul style="list-style-type: none"> • Inflammatory pseudotumor • Soft tissue sarcoma • Desmoplastic round cell tumor |

Table 4.181.3: Differential diagnosis for right iliac fossa lesions with acute pain

| <i>Right iliac fossa lesions</i> | <i>Omental infarct</i> | <i>Epiploic appendagitis</i> | <i>Appendicitis</i> |
|----------------------------------|---|---|---|
| Image |  |  |  |
| | Fig. 4.181.12: Omental infarct | Fig. 4.181.13: Epiploic appendagitis | Fig. 4.181.14: Appendicitis |
| Pathology | A focal area of necrosis within the greater omentum | Ischemic process involving the appendix epiploica of the colon | Inflammation of the appendix due to obstruction of its opening. |
| Epidemiology | Healthy patients, such as marathoners, due to low omental blood flow | Usually occurs in obese females at 20–50 age. | Usually occurs in young adults with increased fibre in diet. |
| Location | Usually right lower quadrant. Centered in the omentum. | Right or left lower quadrant. Left more common. Almost immediately adjacent to colon. | Right lower quadrant |
| USG | Focal ill-defined area of increased echogenicity in the omental fat. Usually more than 5 cm in size. | Rounded non-compressible hyper-echoic mass. Usually 2–3 cm in size. | Aperistaltic blind ending non-compressible tube diameter >6 mm |
| CT | Focal area of fat stranding with swirling of omental vessels in omental torsion. Hyperdense peripheral halo may be present. | Fat density ovoid structure adjacent to colon with a hyperattenuating high density rim. Central hyperdense dot. | Enlarged appendix with peri-appendiceal fat stranding. Faecolith may be present. |
| MR | T1, T2 hyperintense mass with fat suppression. Low signal to surrounding fat. | T1 high signal mass, less signal intensity to normal fat, hypointense rim. Fat suppression + | Enlarged T2 hyperintense appendix, reduced signal intensity in the surrounding fat |

| Table 4.181.4: Differential diagnosis for left iliac fossa lesions with acute pain | | |
|--|---|--|
| Left iliac fossa lesions | Epiploic appendagitis | Diverticulitis |
| Image | <div></div> <p>Fig. 4.181.15: Epiploic appendagitis</p> | <div></div> <p>Fig. 4.181.16: Diverticulitis</p> |
| Pathology | Ischemic process involving the appendix epiploica of the colon | Inflammatory process due to obstruction of neck of diverticulæ from the colon formed by increased intraluminal pressure. |
| Epidemiology | Usually occurs in obese females at 20–50 age. | Elderly male, with low dietary fibre. |
| Location | Right or left lower quadrant. Left more common. | Left most common due to high pressure in sigmoid colon. |
| USG | Rounded non-compressible hyperechoic mass. | Bright bowel outpouching showing some acoustic shadowing. Thickened bowel. |
| CT | Fat density ovoid structure adjacent to colon with a hyperattenuating high density rim. Central hyperdense dot. | Pericolic stranding, disproportionate to segmental bowel wall thickening. Enhancement of inner and outer layers of bowel wall. Fistula or abscess formation may be seen. |
| MR | T1 high signal mass, less signal intensity to normal fat, hypointense rim. Fat suppression + | T2 hyperintense bowel wall with increased intensity in the surrounding fat. |

4.182 GENERAL ABDOMEN INCLUDING ABDOMINAL WALL, PERITONEUM

Case No. 182

Clinical history: 70-year-old female patient with history of CA ovary post-hysterectomy and bilateral salpingo-oophorectomy, presented with distension of abdomen for 1 month.

Radiological techniques and observation: Figures 4.182.1 to 4.182.4—CECT abdomen with oral contrast shows significant fat stranding and nodular thickening in the omentum, thickening and enhancement of peritoneal reflections, stranding and thickening of the omentum, stranding and distortion of the small bowel mesentery and moderate free fluid in peritoneal spaces.

There is a complex mass in the pelvis.

Interpretation: A—70-year-old female, known case of CA ovary with lesion in peritoneum, C—thickening

of the peritoneal reflections, B—moderate ascites, D—peritoneal carcinomatosis.

It indicates involvement of peritoneum. Moderate ascites indicate increased severity. Pelvic mass denotes local recurrence/metastatic deposits.

Principal diagnosis: Known case of CA ovary—post-surgical status with peritoneal carcinomatosis

Management

PET uptake study—to look for local metabolic activity. USG guided ascitic fluid tapping and cytological analysis done for presence of metastatic cells.

Treatment and prognosis: Treatment options are cytoreductive surgery, hyperthermic intraperitoneal chemotherapy (HIPEC), and intraperitoneal chemotherapy. Poor prognosis, increase of CA ovary with peritoneal metastasis and ascites.



Fig. 4.182.1

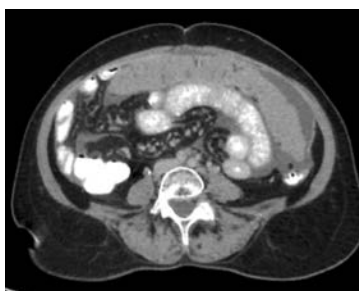


Fig. 4.182.2

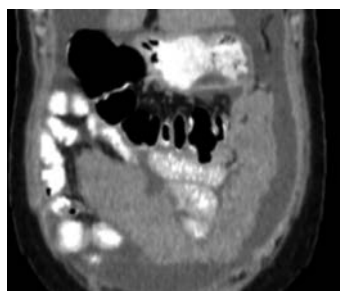


Fig. 4.182.3



Fig. 4.182.4

Table 4.182.1: Differential diagnosis for peritoneal lesions

| | |
|---|---|
| Peritoneal lymphomatosis most commonly metastases from a primary (e.g. non-Hodgkin lymphoma) elsewhere involving mesentery and omentum occurring mostly in children <15 years and in adult | CT: The appearance of peritoneal lymphomatosis may overlap with carcinomatosis and sarcomatosis, however, bulky homogeneous masses or smooth peritoneal soft tissue thickening, ascites, diffuse lymphadenopathy, in addition to imaging features of variable extranodal lymphomatous involvement are contributory findings. Treatment involves combination chemotherapy consisting of rituximab, cyclophosphamide, vincristine and prednisolone. |
| Pseudomyxoma peritonei: More common in females during the fourth or fifth decade of life. It is characterized by loculated collections of fluid which accumulate along peritoneal surfaces, classically resulting in a scalloped appearance of coated abdominal organs and omental caking. Treatment—cytoreductive surgery, systemic chemotherapy and hyperthermic intraperitoneal chemotherapy. | CT: Simple or loculated low attenuation fluid throughout intraperitoneal spaces, omentum, and mesentery 14 scalloping of visceral surfaces, particularly the liver often with scattered (curvilinear or punctate) calcifications, tends to remain localized to peritoneal cavity—thoracic and nodal lesions metastases uncommon. |

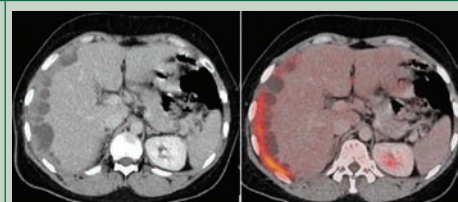




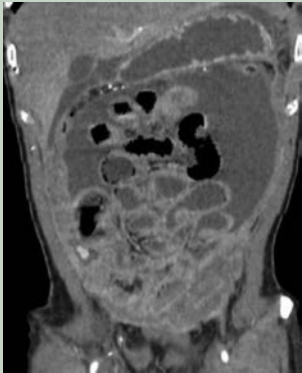

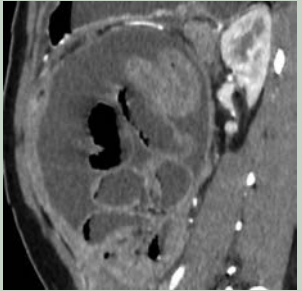
Fig. 4.182.5: Pseudomyxoma peritonei

MRI

T1: Low signal
T2: High signal
T1 C may show enhancement.

(Contd.)

Table 4.182.1: Differential diagnosis for peritoneal lesions (Contd.)

| | | |
|--|---|--|
| <p>Peritoneal mesothelioma Seen in middle aged male (50 to 70 years). Very similar to peritoneal carcinomatosis, but usually no primary neoplasm is known. Treatment options include cytoreductive surgery, peritonectomy and intraperitoneal chemotherapy. However, the prognosis is very poor, with death usually within one year.</p> | <p>Ultrasound: Variable sonographic appearances, from sheet-like hypoechoic to echogenic masses, omental thickening and ascites. CT solid, heterogeneous, enhancing soft tissue mass presence of calcified pleural plaques, indicative of asbestos exposure. Gallium scan: Diffuse uptake throughout the peritoneal cavity.</p> |  <p>Fig. 4.182.6: Peritoneal mesothelioma MRI: Peritoneal masses and nodules demonstrate T1: Low-intermediate signal T2: High signal, C+ (Gd): Shows enhancement</p> |
| <p>Peritoneal tuberculosis: Occurs in age group 25 to 55 years. M:F-1:1. The abdomen is the most common site of extrapulmonary tuberculosis, with peritoneal disease being the commonest form within the abdomen. Treatment: Antitubercular multi-drug regimen.</p> | <p>CT: Nodular or symmetrical thickening of the peritoneum and mesentery showing abnormal peritoneal or mesenteric enhancement, ascites, enlarged hypodense lymph nodes (low attenuation lymphadenopathy due to necrosis).</p> |  <p>Fig. 4.182.7: Peritoneal tuberculosis with hypoattenuating lymphadenopathy</p> |
| <p>Sclerosing peritonitis characterized by total or partial encasement of the small bowel within a thick fibrocollagenous membrane. Presentation is non-specific and patients may present with vomiting, abdominal pain and/or a subacute bowel obstruction.</p>  <p>Fig. 4.182.8: Sclerosing peritonitis</p> | <p>Plain radiograph: Gas-fluid levels similar to those in patients with any other cause of small-bowel obstruction, the wall of the "cocoon" may calcify. Ultrasound: Clumped bowel loops, trilaminar appearance of a hyperechoic membrane, hypoechoic bowel wall and hyperechoic bowel contents with ascites may be present. CT: Enhancing peritoneum, thickened >2 mm, signs of small intestinal obstruction fixation of intestinal loops, ascites or localized interbowel fluid collections, bowel wall thickening, peritoneal or mural calcification, calcified and/or reactive adenopathy.</p> |  <p>Fig. 4.182.9: Sclerosing peritonitis</p>  <p>Fig. 4.182.10: Sclerosing peritonitis MRI may better discriminate between thickened bowel and the peritoneal membrane than CT.</p> |
| <p>Gliomatosis peritonei is a rare complication of ovarian teratomas characterized by peritoneal implants of glial tissue.</p> | <p>MRI: Peritoneal nodules most common in pouch of Douglas, demonstrating T1: Low-intermediate signal T2: High signal, C+ (Gd): Shows enhancement. As cases of malignant evolution have been described up to 7 years from original surgical clearance of teratoma, imaging follow-up should occur annually for at least 5–7 years.</p> | |

(Contd.)

Table 4.182.1: Differential diagnosis for peritoneal lesions (Contd.)

| | |
|--|--|
| Leiomyomatosis peritonealis disseminata: Characterized by multiple vascular leiomyomas growing along the sub-mesothelial tissues of the abdominopelvic peritoneum. | CT: Show homogeneous or heterogeneous attenuation with a variable enhancement pattern similar to that of uterine leiomyomas. MRI may show multiple masses with signal intensity similar to that of skeletal muscle and smooth muscle on both T1WI and T2WI. Homogeneous enhancement following the administration of contrast material. |
| Growing teratoma syndrome is a rare complication after treatment for metastatic non-seminomatous germ cell tumors. Characterized by an increasing metastatic lesion with normal biomarker levels. | The enlarging tumor consists of mature tissues from all 3 germ layers, thus representing a mature teratoma, that presumably arises from differentiated cells that are refractory to chemotherapy or radiation. For diagnosis of the growing teratoma syndrome, which is characterized by an increase in size and a decrease in the density of the lesion, giving the mass a cystic appearance on MRI/CT. MRI promises to be the optimal follow-up modality. |

Table 4.182.2: Imaging of peritoneal metastasis

| | |
|--|--|
| Ultrasound: Malignant ascites may be anechoic or have low-level echoes. Nodules are of intermediate echogenicity, hypoechoic compared to the peritoneum. Infiltration of the omentum results in hyperechogenicity. | MRI: Typically, omental and mesenteric masses are of low T1-weighted and mixed T2-weighted signal intensity compared with surrounding soft tissues. Small subcentimetre deposits (in the absence of ascites) are best visualized using fat-suppressed T2-weighted and fat-suppressed T1-weighted delayed postcontrast imaging. |
| CT: Thickening and enhancement of peritoneal reflections (especially if nodular), soft tissue nodules, stranding and thickening of the omentum (omental cake), stranding and distortion of the small bowel mesentery, ascites, nodular with the non-calcified component are typical and nodal calcification. Peritoneal nodules can often mimic unopacified small bowel loops. Accurate assessment for peritoneal carcinomatosis requires adequate bowel opacification and the intravenous administration of contrast material. | PET: Avid 18F-FDG uptake within well-circumscribed nodules, to diffuse uptake over peritoneal and serosal surfaces. |

Table 4.182.3: Solid tumors of the peritoneum, omentum and mesentery in children

| <i>Tumour</i> | <i>Distribution</i> | <i>Ascites</i> | <i>Calcification</i> | <i>Invasion</i> | <i>Other features</i> |
|---|------------------------------|---------------------|--------------------------|--|---|
| Inflammatory myofibroblastic tumor | Focal | No | Minority, central dense | Rare | Well defined |
| Castleman disease | Focal Satellite nodules + | No | 10–30% varied arborizing | Rare | Peripheral vessels, intense enhancement |
| Mesenteric/desmoid tumour fibromatosis (desmoplastic small round cell tumour) | Focal | No | No | Frequent Encases bowel, SMA | Associated with FAP |
| DSRCT 90% male | Diffuse | Common, not massive | 30% | Peritoneal nodular thickening, omental caking, metastasis common | Dominant mass is retrovesical, omental, or peritoneal |
| Burkitt lymphoma | Diffuse | 25% | Uncommon before therapy | Bowel wall involvement and SMA encasement – common, | Right lower quadrant mass, masses of kidneys, ovaries and breasts |
| Rhabdomyosarcoma | Diffuse | All | No | Primary tumour may invade, omental caking + | Primary tumor in bladder, prostate or retro-peritoneum |

| Table 4.182.4: Classification of peritoneal spaces | |
|---|--|
| Two main peritoneal spaces—supramesocolic compartment and infra-mesocolic compartment is divided by transverse colon, root of which extends across the infra-ampullary segment of descending duodenum, the pancreatic head and along the lower edge of pancreatic body and tail. | |
| Right supramesocolic space has 3 subspaces. <ul style="list-style-type: none">• Right subphrenic space• Right subhepatic space (anterior and posterior: Morrison’s pouch)• Lesser sac (smaller superior and larger inferior recess) | Left supramesocolic space —4 subspaces <ul style="list-style-type: none">• Anterior left perihepatic space• Posterior left perihepatic space (gastrohepatic recess)• Anterior left subphrenic space (perisplenic)• Posterior left subphrenic space |
| Inframesocolic compartment —divided into 2 unequal spaces <ul style="list-style-type: none">• Right inframesocolic space• Left inframesocolic space• Paracolic gutters (right and left) | Pelvic peritoneal spaces <ul style="list-style-type: none">• Right and left paravesical space• Rectovesical pouch (male)• Uterovesical and deeper rectouterine pouch of Douglas (women)• Broad ligament |
| Peritoneal reflections: 8 ligaments, 2 omenta and 4 mesenteries | 8 ligaments —formed by two peritoneal folds that enclose and support a structure within peritoneal cavity <ul style="list-style-type: none">• Right and left coronary ligaments• Gastrosplenic ligament• Falciform ligament• Phrenicocolic ligament• Splenorenal ligament• Hepatoduodenal ligament• Duodenocolic ligament |
| 2 Omenta —peritoneal ligament that joins stomach to another structure—lesser omentum (gastrohepatic ligament) and greater omentum (gastrosplenic ligament) 4 Mesenteries —two peritoneal folds that attach bowel to retroperitoneum—small bowel mesentery, transverse mesocolon, sigmoid mesocolon, mesoappendix | |

Discussion: Peritoneum are a relatively common location for metastases, particularly from tumors of the abdomen and pelvis, that generally imply a poor prognosis, often with a significant impact on palliation. The epidemiology of patients with peritoneal metastases mirrors that of affected patients.

Peritoneal Anatomy

The peritoneum or peritoneal cavity is a large complex serous membrane that forms a closed sac within the abdominal cavity. It is a potential space between the

parietal peritoneum lining the abdominal wall and the visceral peritoneum enveloping the abdominal organs. In females, this closed sac is perforated by the lateral ends of the fallopian tubes.

Gross anatomy: The free surface of the peritoneum has a layer of flattened mesothelial cells which secrete a thin film of serous fluid. The peritoneal reflections forming peritoneal ligaments, mesenteries and omenta, potential peritoneal spaces and the natural flow of peritoneal fluid determine the route of spread of intraperitoneal fluid and disease processes within the peritoneal cavity.

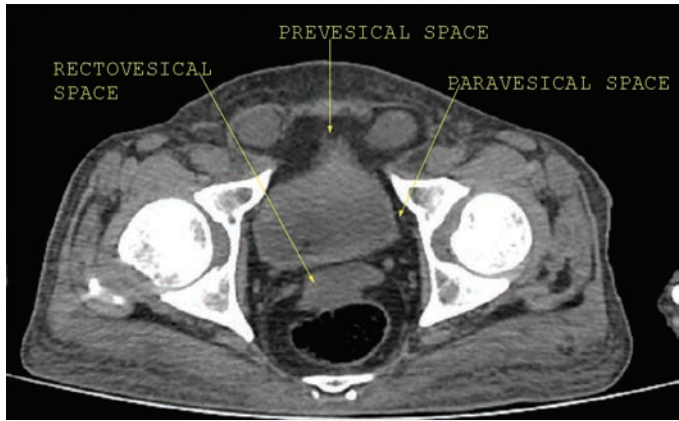


Fig. 4.182.11: Anatomy of peritoneal spaces

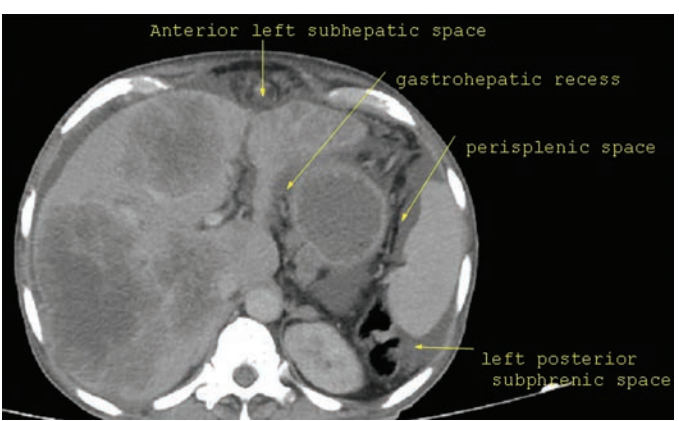


Fig. 4.182.12: Anatomy of peritoneal spaces

| Table 4.182.5: Solid peritoneal lesions | | | |
|--|--|---|---|
| Nodular or irregular thickening | Smooth thickening | Neoplasms | Fibroinflammatory and infiltrative processes |
| <ol style="list-style-type: none"> 1. Metastatic peritoneal carcinomatosis 2. Primary peritoneal carcinoma 3. Lymphomatosis 4. Malignant mesothelioma 5. Tuberculous peritonitis 6. Leiomyomatosis peritonealis disseminata 7. Gliomatosis peritonei | <ol style="list-style-type: none"> 1. Acute peritonitis 2. Diffuse peritoneal malignancy 3. Portal hypertension 4. Tuberculous peritonitis 5. Sclerosing encapsulating peritonitis 6. SLE peritonitis 7. Familial Mediterranean fever 8. Sarcoidosis | <ol style="list-style-type: none"> 1. Metastasis 2. GIST 3. Solitary fibrous tumor 4. Desmoplastic small round cell tumor 5. Malignant mesothelioma 6. Sarcomas 7. Benign mesenchymal tumors 8. Ectopic gastrinoma 9. Extramedullary plasmacytoma | <ol style="list-style-type: none"> 1. Desmoid tumor 2. Retractable mesenteritis 3. Inflammatory pseudotumor 4. Actinomycosis 5. Amyloidoma <p>Others: Haematoma splenosis/ wandering splenunculus, endometriosis, dropped gallstone, peritoneal loose body, parasitic leiomyoma, foreign body granuloma, osseous metaplasia</p> |
| Cystic peritoneal lesions | | Fat-containing peritoneal lesions | |
| <ol style="list-style-type: none"> 1. Loculated fluid collection/abscess 2. Pseudocyst 3. Cystic metastasis 4. Pseudomyxoma peritonei 5. Lymphangioma 6. Enteric duplication cyst 7. Enteric/mesothelial cyst 8. Benign multicystic mesothelioma 9. Peritoneal inclusion cyst 10. Omphalomesenteric duct cyst 11. Hydatid cyst 12. Cystic change in a solid lesion | | <ol style="list-style-type: none"> 1. Fat necrosis—omental infarct, epiploic appendagitis, acute pancreatitis, encapsulated fat necrosis, idiopathic nodular panniculitis 2. Mesenteric panniculitis 3. Postsurgical omental flaps 4. Pseudolipoma of Glisson's capsule 5. Liposarcoma 6. Lipoma 7. Hibernoma 8. Fat-containing metastases 9. Fatty mesenteric lymph nodes 10. Extramedullary haematopoiesis 11. Haemangioma/lymphangioma 12. Hydatid cyst 13. Failed renal transplant | |

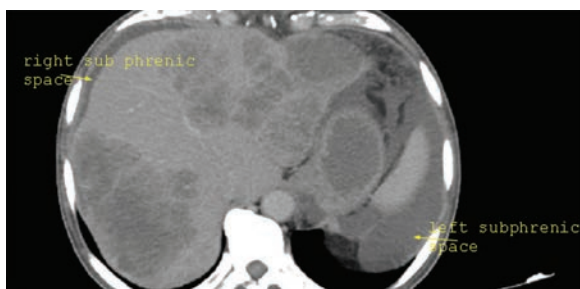


Fig. 4.182.13: Anatomy of peritoneal spaces



Fig. 4.182.14: Anatomy of peritoneal spaces

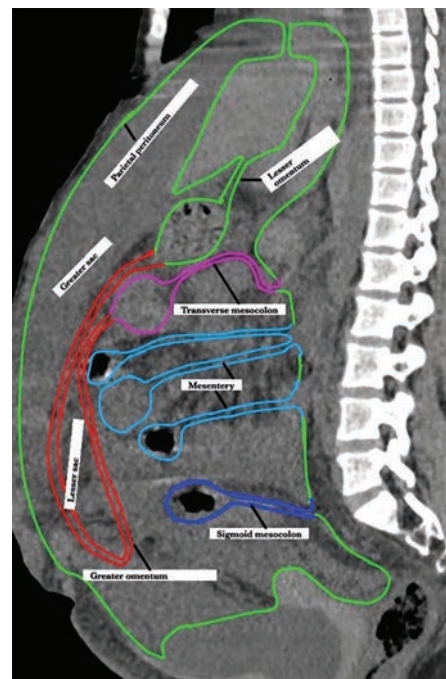


Fig. 4.182.15: Sagittal anatomy of peritoneal spaces

4.183 GENERAL ABDOMEN INCLUDING ABDOMINAL WALL, PERITONEUM

Case No. 183

Clinical history: A 55-year-old male with complaints of diffuse abdominal pain since 2 months.

Radiological techniques and observation: Nonenhanced CT (Fig. 4.183.1), coronal sections and contrast enhanced CT axial (Fig. 4.183.2) show a well-circumscribed solitary homogeneously enhancing isodense mass noted in the mesentery displacing the small bowel loops without causing obstructive features. There is no evidence of mesenteric/retroperitoneal lymphadenopathy. There is no evidence of calcification/desmoplastic reaction. There is no evidence of stranding/induration in mesentery and omentum.



Fig. 4.183.1

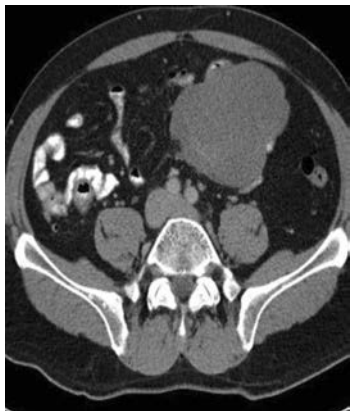
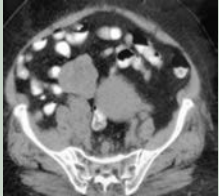
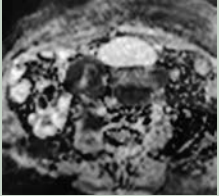

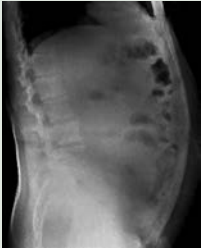
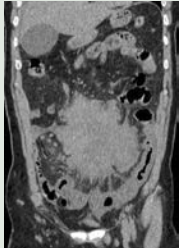
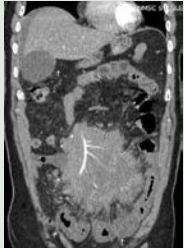
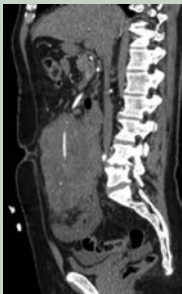
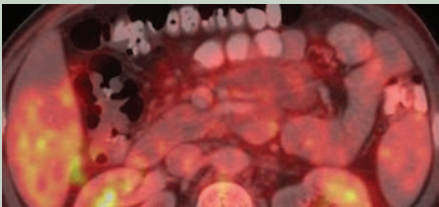
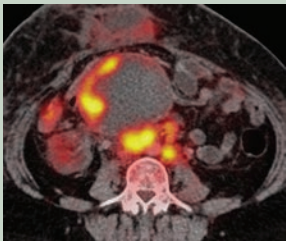


Fig. 4.183.2

Table 4.183.1: Differential diagnosis for mesenteric mass

| | | |
|---|--|---|
| Lymphoma: Third most common form of malignancy in children. More common in developed nations. Prognosis depends on the histological subtype and grade. | Discrete/confluent—envelops but rarely obstructs bowel/vessels Associated paraortic, periaortic, mesenteric, aortocaval and iliac lymphadenopathy (>6 mm short axis. 3 or more nodes clustered in a location). Calcifies post-treatment | Homogenous contrast enhancement. Rarely peripheral enhancement. Bright on diffusion. |
|  |  |  |
| Fig. 4.183.3: Lymphoma | Fig. 4.183.4: Lymphoma | Fig. 4.183.5: Lymphoma |
|  |  |  |
| Fig. 4.183.6: Lymphoma | Fig. 4.183.7: Lymphoma | Fig. 4.183.8: Lymphoma |
|  |  |  |
| Fig. 4.183.9: Lymphoma | Fig. 4.183.10: Lymphoma | Fig. 4.183.11: Lymphoma |

(Contd.)

Table 4.183.1: Differential diagnosis for mesenteric mass (Contd.)




| | | |
|--|--|---|
| Carcinoid tumour: Refer to case 175 | | |
| Exophytic small bowel tumors Occurs after 40 years. Surgical en bloc resection, adjuvant chemo with Imatinib (GIST), Choi response criteria to assess response to treatment for GIST. | GIST/small bowel adenocarcinoma can extend into mesentery and appear similar to desmoid. Homogeneous contrast enhancement/central necrosis with peripheral enhancement |  Fig. 4.183.12: Exophytic small bowel tumor (GIST) |
| Sclerosing mesenteritis/mesenteric panniculitis Immunosuppressant therapy: Tamoxifen + Prednisolone. Surgical excision difficult may be used for palliative treatment to relieve bowel obstruction Fat ring/Fat halo sign -ring of normal fat around vessels and lymph nodes. Pseudocapsule sign <3 mm fibrotic rim around the mass. | Chronic nonspecific inflammation of small bowel mesenteric adipose tissue. Rarely slowly progressive. Retractable/fibrosing mesenteritis has a dominant fibrotic component. Located at mesenteric root. No displacement of bowel. Mesenteric vascular envelop (halo). Hypointense on T2 and T1 |  Fig. 4.183.13: Sclerosing mesenteritis DD for misty mesentery 1. Mesenteric panniculitis 2. Mesenteric lymphoma 3. Cirrhosis 4. Adjacent inflammation: Appendicitis, IBD. 5. Mesenteric venous thrombosis. |
| Mesenteric metastasis | Multiple, less well defined, associated with stranding and induration in mesentery. Primary CA breast, lung, pancreas, GIT, bladder |  Fig. 4.183.14: Mesenteric metastasis |
| Kaposi sarcoma Associated with HHV 8. Th 201 and Ga 67 scintigraphy for further evaluation | Lymphadenopathy around mesenteric root and periphery of mesentery with greatly enlarged nodes 3–5 cm. Conglomerate, concomitant small bowel nodules in a patient with AIDS | |
| Aggressive fibromatosis 14–75 years. Small bowel mesentery most common site. Increased rate of recurrence. | Locally aggressive benign proliferative process, may occur sporadically or with FAP. Homogeneous soft tissue attenuating on CT. Hypoattenuating if myxoid stroma is present. Variable contrast enhancement. Low T1, heterogeneous T2 signal. | |
| Other DDs are vascular, neural tumors, mesenteric tear, hematoma, lymphadenitis, neurofibroma, vascular tumors—hemangioma, histiocytoma, lipoma, liposarcoma and inflammatory myofibroblastic tumor. | | |

Table 4.183.2: Causes of mesenteric fat stranding

| | |
|--|--|
| 1. Focal Local inflammation Mesenteric panniculitis Mesenteric ischemia Mesenteric contusion/tear Lymphoma | 2. Diffuse Generalized edema due to cardiac/renal/hepatic failure Diffuse peritonitis, e.g. due to perforation Acute pancreatitis Main SMV/portal vein occlusion Sarcoidosis, amyloidosis, familial Mediterranean fever Erdheim-Chester disease |
|--|--|

Interpretation: A: 55 years old male, C: Well-defined solid homogeneous enhancing mesenteric mass, B: Displacing adjacent bowel with no calcification, desmoplastic reaction or associated lymphadenopathy, D: Mesenteric desmoid.

Principal diagnosis: Mesenteric desmoid.

Discussion: Desmoid—benign locally aggressive nonencapsulated mesenchymal neoplasm of connective/fibrous tissue. Presenting as small bowel mesentery/abdominal wall mass arising at site of scarring from prior surgery. Can be intra/extra abdominal. Associated with Gardner/familial adenomatous polyposis. Intra-abdominal desmoid may involve bowel loops, bladder wall, ribs, pelvic bone, multiple skull and mandible osteomas, epidermoid cysts and abnormal dentition. Most cases occur between 20–40 years of age. Tends to more aggressive in younger patients. Increased incidence in women of childbearing age. **USG:** Homogeneously hypoechoic masses. Maybe lobulated and may show vascularity on Doppler. **CT:** Usually well circumscribed. Relatively homogeneous or focally hyperattenuating when compared to soft tissue. Shows enhancement with contrast. Low signal intensity on T1 and T2. High signal intensity on T2 suggests active growth. (DD: Lymphoma T2 hypointense lesion with low ADC value).

Management: Poor prognostic features include size >10 cm, multiplicity and aggressive features (bowel loop involvement, encasement of mesenteric vessels and ureter). Stable asymptomatic desmoids can be followed up with serial imaging. Symptomatic desmoids should be surgically resected. Surgical resection can, however, lead to significant morbidity such as bowel ischemia, shortgut syndrome, obstruction and fistula. Conservative management for desmoids that are unresectable—systemic therapy with cytotoxic agents. Radiation is more effective for extra-abdominal desmoids.

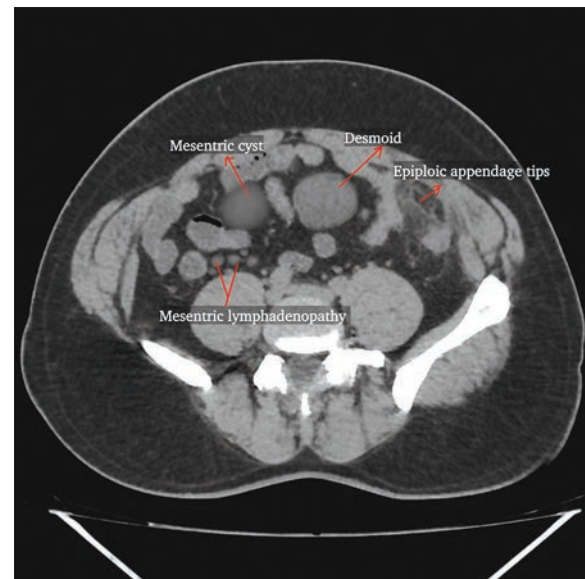


Fig. 4.183.15: Pathologies in mesentery

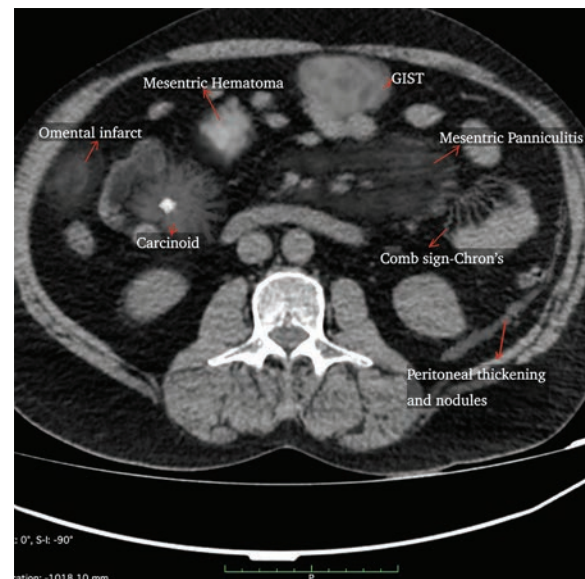


Fig. 4.183.16: Pathologies in mesentery

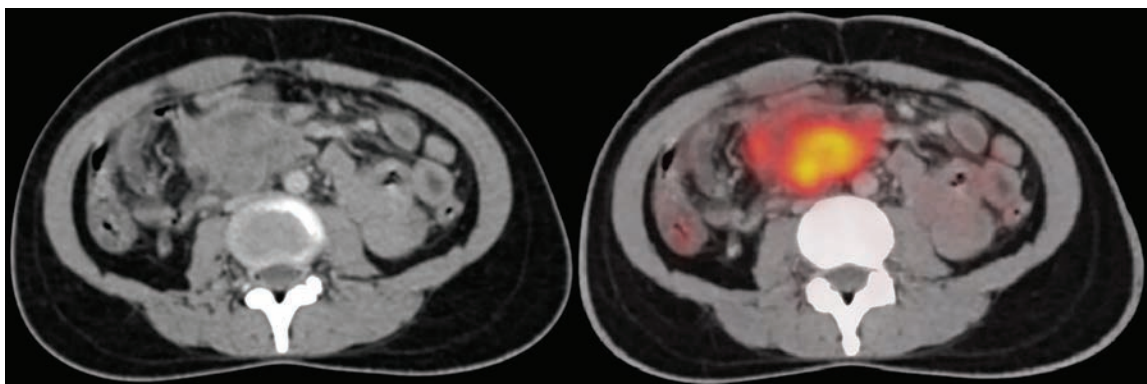


Fig. 4.183.17: Inflammatory myofibroblastic tumour

4.184 GENERAL ABDOMEN INCLUDING ABDOMINAL WALL, PERITONEUM

Case No. 184

Clinical history: 39-year-old female came with complaints of abdominal distension for the past 1 month and abdominal pain for the past 1 week.

Radiological imaging and observation: Plain CT abdomen with oral contrast (Figures 4.184.1 and 4.184.3) given axial, coronal section shows a well-defined thin-walled large cystic lesion with thin-septation noted in close proximity to 2nd part of duodenum, abutting the



Fig. 4.184.1



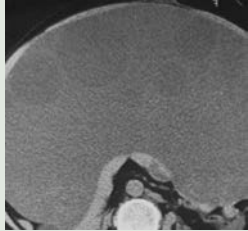

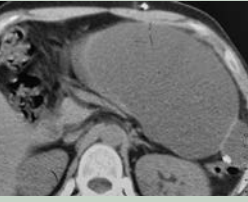
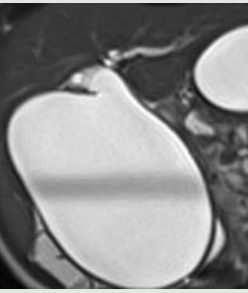
Fig. 4.184.2



Fig. 4.184.3

| Table 4.184.1: Types of mesenteric cyst | | | |
|--|--|--|---|
| Diagnosis | Description | MC location | Imaging features |
| Lymphangioma MC type | Abnormal lymphatic channel that fail to connect properly with lymphatic system—intimate relation to bowel noted | Mesentery | USG: Multiseptated mass with lobules that may be anechoic/ contain internal echoes/ fluid-fluid level by debris CT: Cystic mass with HU of fluid, septation enhance MRI: Serous contents; hypointense on T1 weighted, hyperintense on T2. |
| Nonpancreatic pseudocyst | Residual of old hematoma or infection | Omentum | USG: Anechoic with a thick wall/ may contain internal echoes CT: Cystic lesion with thick wall and internal debris, wall may/may not enhance on contrast |
| Enteric cyst —present less than 1 year with cyclical vomiting, poor feeding, a palpable mass on examination | It is a cyst with the wall that has all three layers of bowel wall. The cyst may/may not communicate with bowel wall | Anywhere in mesentery from oral cavity to rectum | USG: Anechoic with a thick wall composed of multiple layers, resembling a normal bowel wall—gut signature CT and MR imaging: Cystic mass with a thick wall that enhances after contrast material is injected. Contents are usually serous |
| Enteric duplication cyst | Are lined with gastrointestinal mucosa | Mesentery and omentum | USG: A hypoechoic cystic mass is seen occasionally with septations. CT: Fluid-filled mass, without a discernible wall, with low attenuation on CT scans, MRI—low signal intensity on T1-weighted images |
| Mesothelial cyst | Incomplete fusion of mesothelial layers of omentum | Small bowel, mesentery, mesocolon | USG: An anechoic mass with acoustic enhancement is seen CT: A fluid-filled mass with no discernible wall and no internal septations. |

Table 4.184.2: Differential diagnosis for mesenteric cyst

| | | |
|--|--|--|
| Hydatid cyst—intraperitoneal Primary intraperitoneal hydatid is rare—result from rupture of concomitant liver cyst Diagnosis confirmed by radiological imaging along with serological test (complement fixation and indirect hemagglutination ELISA) | USG: Multicentric multiloculated cystic lesion in perihepatic space, mesentry/pelvis. Primary peritoneal hydatid is rare, presence of hydatid cyst in liver is seen in most cases CT: Hyperattenuating wall, septations, daughter cyst and calcification |  <p>Fig. 4.184.4: Intraperitoneal hydatid cyst</p> |
| Pancreatic pseudocyst: Common sequelae of acute/chronic pancreatitis and the most common cystic lesion of pancreas. Pseudocyst are fluid-filled oval/round collection with a relatively thick wall. They are multiple, usually located in pancreatic bed, they can found anywhere from groin to mediastinum | USG: Hypoechoic/anechoic collection with dependent low level echoes representing debris CT: Well-circumscribed peripancreatic collection of homogenously low attenuation, usually surrounded by well defined enhancing wall MRI: T1: Hypointense centre with wall enhancement T2: Hyperintense with dependent debris |  <p>Fig. 4.184.5: Pancreatic pseudocyst</p> |
| Peritoneal CSF pseudocyst: Rare complication of ventriculoperitoneal catheter placement | USG: Anechoic lesion with the tip of VP shunt CT: Small/massive loculated cyst-like structure in the peritoneal cavity at the distal tip of VP shunt |  <p>Fig. 4.184.6: Peritoneal CSF pseudocyst</p> |
| Choledochal cyst: Congenital cystic dilations of biliary tree, type 1-dilation of extrahepatic biliary tree is most common and sometimes so big that mimics mesenteric cyst | USG: Dilated cystic lesion in communication with the biliary tree and is separate from gall bladder CT/MRI: Findings are similar, in addition, tells about any intrahepatic disease |  <p>Fig. 4.184.7: Choledochal cyst</p> |
| Cystic neoplasm of ovary: Can be benign/malignant, common in old age > 60 years | USG: Abdominopelvic cystic lesion (ipsilateral ovary not visualised) with thick septation >3 mm, papillary projections, mural nodules, frank solid components, increased vascularity with associated ascites, lymphadenopathy favours malignant cystic lesion | |

inferior surface of liver, compressing IVC, displacing duodenum medially and rest of bowel loops posteriorly and inferiorly, no evidence of calcification/solid component/haemorrhage.

Interpretation: A: 39-year-old female, C: Benign cystic lesion in mesenteric plane, B: No evidence of calcification/solid component/haemorrhage, D: Mesenteric cyst.

Principal diagnosis: Mesenteric cyst.

Management: FNAC followed by complete excision of symptomatic cysts by laparoscopic/open technique (aspiration and injection of sclerosing agents is ineffective).

Brief discussion about the condition: Mesenteric cyst-represent a small portion of abdominal cyst in pediatric population, usually asymptomatic but at times present with abdominal pain.

Etiology: Mesenteric cyst include: Lymphangioma, enteric duplication cyst, enteric cyst, mesothelial cyst, non-pancreatic pseudocyst, cystic spindle cell tumor. Lymphangioma is the most common mesenteric cyst, though often asymptomatic, presents as painful abdominal mass at times. Bowel resection is often necessary to remove a lymphangioma. This feature suggests its aggressive nature and intimate relation to adjacent bowel.

MC location of mesenteric cyst: Right iliac fossa.

Usually no specific radiological features to differentiate various mesenteric cyst. A thin walled cyst in mesentery

is usually given as lymphangioma by imaging, but it needs a histopathological correlation to confirm the diagnosis. Among mesenteric cysts, lymphangiomas—more common, more frequently symptomatic, are larger and require bowel resection

Differential diagnosis: For a cystic lesion in abdomen, differentials to consider include: (1) Intraperitoneal hydatid, (2) Pancreatic pseudocyst, (3) CSFoma, (4) Ovarian cyst/cystic neoplasm of ovary/cystic teratoma (5) Urachal cyst, (6) Hydrometrocolpos, (7) Choledochal cyst, (8) Cystic mesothelioma, (9) Cystic spindle cell tumor, (10) Necrotic lymph node, (11) Peritoneal abscess.

4.185 GENERAL ABDOMEN INCLUDING ABDOMINAL WALL, PERITONEUM

Case No. 185

Clinical history: 32-year-old female patient with jaundice for 2 months. Patient underwent USG abdomen and reported to have dilated biliary tree and main pancreatic duct and hypoechoic collection in right psoas muscle. Drainage of right psoas collection was attempted—no pus or any aspirate obtained upon aspiration by 18 G needle.

Radiological techniques and observation: Figure 4.185.1—NECT axial sections of abdomen in soft tissue and bone window reveals dilated bilateral biliary radicles. Right psoas appears bulky. Left psoas appears normal. Moth eaten lytic lesion noted in body of visualised lumbar vertebrae (possibly L3). No evidence of any focal lesions in liver. Visualised spleen, stomach and bowel appears normal. Additional imaging with CECT is advised.

Figures 4.185.2 to 4.185.4 are CECT abdomen axial sections showing ill-defined heterogeneously enhancing soft tissue density lesion in preaortic and paraortic region involving head of pancreas causing obstruction with proximal dilatation of biliary tree and main pancreatic

duct. Lesion encases aorta, origin of superior mesenteric artery and bilateral renal arteries. Relative hypo-enhancement of right kidney with right hydronephrosis possibly due to right ureteric encasement. Enlarged right psoas muscle with heterogeneous enhancement due to infiltration mimicking the collection/abscess. Visualised spleen, bowel, gall bladder appear normal. No abnormal enhancement in liver parenchyma.

Interpretations: A: 32-year-old female, C: Diffuse infiltrative retroperitoneal mass lesion involving head of pancreas, B: Dilatation of biliary tree and pancreatic duct, encasing aorta, adjacent arteries, right ureter with infiltration of right psoas muscle and lytic lesion in body of lumbar vertebrae, D: Retroperitoneal lymphoma.

Principal diagnosis: Retroperitoneal lymphoma with involvement of head of pancreas, right psoas muscle and lumbar vertebrae.

Differential diagnosis can be classified either intrinsic mass or extrinsic mass. Intrinsic mass: Retroperitoneal sarcomas/neurogenic tumors/germ cell tumors/retroperitoneal metastases/solitary fibrous tumor.

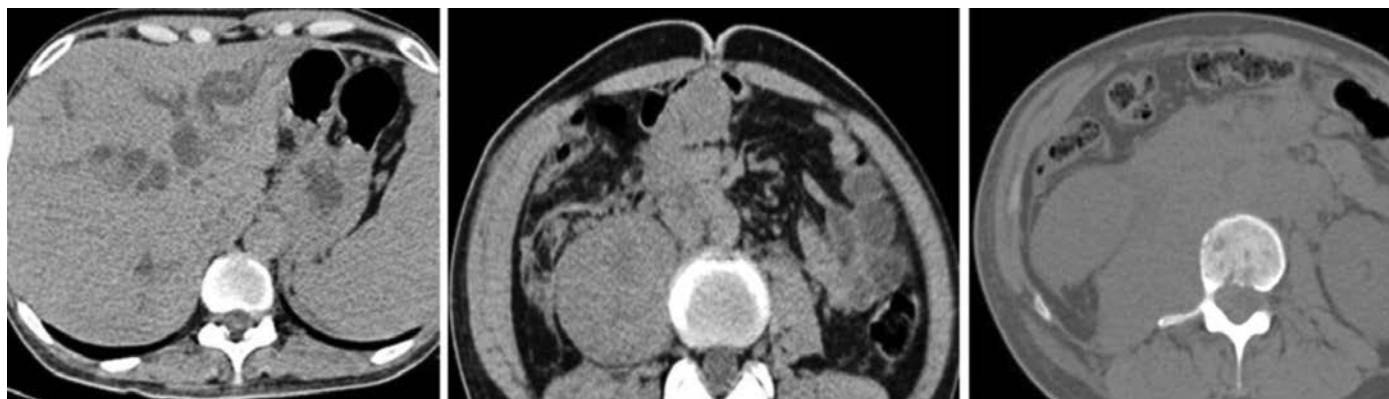





Fig. 4.185.1



Fig. 4.185.2

Fig. 4.185.3

Fig. 4.185.4

| Table 4.185.1: Difference between retroperitoneal sarcoma , neurogenic tumors and retroperitoneal metastases | | |
|--|---|--|
| Retroperitoneal sarcomas | Neurogenic tumors | Retroperitoneal metastases |
|  |  |  |
| Fig. 4.185.5: Retroperitoneal sarcomas | Fig. 4.185.6: Neurogenic tumors | Fig. 4.185.7: Retroperitoneal metastases |
| Age: 40 to 60 years, most malignant tumours of retroperitoneum are mesenchymal in origin. Liposarcoma and leiomyosarcoma account for more than 90 percent cases. | Affects younger population. Paraspinal location with widening of neural foramen. Enhancing retroperitoneal mass in young adult that arise from ganglion cells, parasympathetic system or nerve sheaths. | Most common source is primary pelvic tumour which includes testicular, ovarian, bladder and prostate. Enlarged (para-aortic and iliac nodes >10 mm) architecturally distorted or FDG avid nodes in patients with known malignancy. |
| Liposarcoma Mixed-fatty and solid components. Solid-HU value >+20HU (myxoid tissue) Pseudocystic pattern (HU value between +20 and -20 HU). Displacement of adjacent structures with or without invasion of adjacent structures. CECT-heterogeneous or homogeneous enhancement and lacks prominent vessels. | Ganglioneuroma rare, benign, well-circumscribed oval or lobulated. Ganglioneuroblastoma are malignant, solid to cystic Neuroblastoma: Unencapsulated, irregular, lobulated. Necrosis, haemorrhage and coarse calcifications. Invades adjacent structures | Nodes are not confluent. Mucinous adenocarcinoma metastases may show calcification. |
| Leiomyosarcoma —it can be intravascular (6%), extravascular mass (62%) or mixed (33%). | Paraganglioma: Very avid due to hypervascularity. T2-light bulb sign | CECT: Discrete or confluent nodal mass. Low attenuation nodes can be seen in untreated testicular carcinoma and lymphoma. Bulky retroperitoneal nodes can be seen in seminomas and small clustered nodes in non-seminomatous germ cell tumor. |
| Fibrosarcoma and MFH: Most common soft tissue sarcoma in adults. Rhabdomyosarcomas | Schwannoma: Benign tumor of peripheral nerve sheaths, usually paravertebral—but can arise in any nerve. Neurofibroma: Typically solitary, associated with NF1 | Nuclear medicine: PET is often sensitive and specific than CT alone. However, well-differentiated non-seminomatous germ cell tumors are not very FDG avid. |

Extrinsic mass consists of masses arising from prevertebral/vertebral space, posterior abdominal wall, psoas muscle such as retroperitoneal fibrosis/extramedullary hematopoiesis/Erdheim-Chester disease. If the lesion is cystic, differential diagnosis includes lymphangioma/cystadenoma/cystic mesothelioma/mature teratoma/epidermoid cyst/lymphoceles/hematomas.

Other DDs include fibrosis, lymphoma, liposarcoma, fibrosarcoma, neuroblastoma.

Common clinical and imaging features of all retroperitoneal tumours include: Commonly seen in 5th and 6th decades of life. The tumors are large at time of presentation and involves adjacent structures. Compression of adjacent organs leads to formation of pseudocapsule. Recurrence rates are high. Metastasis to lung, liver, bone and brain.

Management of retroperitoneal lymphoma: Hodgkin's lymphoma—initial chemotherapy or radiation/stem cell transplant for treatment failure or relapse.

Brief discussion about the condition—retroperitoneal lymphoma: Demographics—bimodal in distribution—2 peak incidences (20 to 24 years and 80 to 84 years)

Well-defined homogeneous mass that spreads between adjacent structures without compressing them (encasement of vessels—sandwich sign) favours lymphoma. The aorta and IVC are displaced anteriorly from vertebrae producing floating aorta or CT angiogram sign, whereas irregular plaque-like soft tissue mass encircling the region of aortic bifurcation, involving ureters, pancreas and duodenum without displacing the aorta anteriorly, instead tethering it to the vertebrae favours Erdheim-Chester disease. **Differential diagnosis**

of large retroperitoneal tumor with areas of extensive necrosis, haemorrhage and calcification include—malignant fibrous histiocytoma, leiomyosarcoma and rhabdomyosarcoma. Areas of calcification favours malignant fibrous histiocytoma. Fat containing lesions include lipoma, liposarcoma, teratoma and angiomyolipoma. Fat dense lesion with thick irregular nodular septa and enhancement with contrast favours liposarcoma. Large unilocular or multilocular cystic lesion favours lymphangioma—calcifications being rare.

Ann Arbor staging of lymphoma (both Hodgkin's and Non-Hodgkin's)

Stage I: Single lymph node region/extralymphatic site
Stage II: 2 or more nodal regions on same side of diaphragm.

Stage III: Nodal group involvement above and below diaphragm.

Stage IV: Diffuse involvement of 1 or more extralymphatic sites.

Imaging-CECT: Enlarged nodes (>1 cm in short axis) for mesenteric and para-aortic nodes. Retrocrural nodes enlarged if more than 6 mm in short axis. Treated lymphoma nodes will show calcification. Nodal mass causes displacement of aorta from spine which is unusual for benign pathologies. Confluent soft tissue mantle may surround mesenteric vessels, aorta and IVC.

MRI: T1-low signal adenopathy. Low signal adenopathy may suggest fibrosis from treated disease. DWI-restricted diffusion. PET-Hypermetabolic nodes show avid FDG uptake. Sensitivity of 90 to 95 percent for PET, compared to 80–85 percent for CECT. Allows increased detection of tumor in obscure sites; and changes stage in 30 to 40 percentage of cases. PET is also helpful in distinguishing residual lymphoma vs fibrosis post-radiation. SUV more than ten is predictive of aggressive histology.

Note: Nodes due to NHL typically larger than HL. Nodes are non-contiguous in NHL while contiguous in Hodgkin's lymphoma. Mesenteric adenopathy is more common in NHL (50 percent) as compared to HL (<5 percentage).

RECIST 1.1—Response evaluation criterion in solid tumors (WHO 2009)

Difference in sum of longest diameter of target lesions
A. More than 20% increase/absolute increase of 5 mm progressive disease. B. More than or equal to 30% decrease—partial response. C. Less than 20% increase or more than 30 percent decrease—stable disease. D. Complete disappearance—complete response, E. New lesions—progressive disease.

The Deauville five-point scale (Deauville 5Ps) is an internationally-recommended scale for routine clinical reporting and clinical trials using FDG-PET-CT in the initial staging and assessment of treatment response in Hodgkin lymphoma (HL) and certain types of non-Hodgkin lymphomas (NHL).

Inclusions: FDG-PET/CT for staging and treatment response in both clinical routine and clinical trials using the Deauville 5ps is recommended in Hodgkin lymphoma (HL), diffuse large B cellular lymphoma (DLBCL), marginal zone NHL with an aggressive transformation, FDG-avid nodal lymphomas, essentially all histologic types except: Chronic lymphocytic leukemia (CLL), small lymphocytic lymphoma, lymphoplasmacytic lymphoma/Waldenstrom macroglobulinemia, mycosis fungoides whereas there have been proposed separate criteria for primary extranodal and cutaneous lymphomas, e.g. cutaneous T-cell lymphoma (CTCL), cutaneous B-cell lymphomas (CBCL).

Usage: It is a simple tool based on visual interpretation of FDG uptake. It takes advantage of two reference points of the individual patient, which have demonstrated relatively constant uptake on serial imaging. The two reference organs are the mediastinum (also known as blood pool) and the liver. The scale ranges from 1 to 5, where 1 is the best and 5 is the worst. Each FDG-avid (or previously FDG-avid) lesion is rated independently:

1. No uptake or no residual uptake (when used interim)
2. Slight uptake, but equal to or below blood pool (mediastinum)
3. Uptake above mediastinal, but below or equal to uptake in the liver
4. Uptake slightly to moderately higher than liver
5. Markedly increased uptake or any new lesion (on response evaluation)

X for any lesion not overtly attributable to lymphoma

Assessment of treatment response: Progressive Disease (PD): A Deauville score of 4 to 5 with increasing intensity compared to baseline or any interim scan and/or any new FDG-avid focus consistent with malignant lymphoma; Stable Disease (SD), also called no metabolic response: a Deauville score of 4 or 5 without significant change in FDG uptake from baseline; Partial Response (PR): A Deauville score of 4 or 5, uptake is decreased compared with baseline and absence of structural progression development on CT; Complete Response (CR): Scores 1, 2 or 3 together with the absence of FDG-avid bone marrow lesions are interpreted as complete metabolic response (CR), irrespective of a persistent mass on CT.

Table 4.185.2: Difference between Hodgkin's lymphoma and non-Hodgkin's lymphoma

| | <i>Hodgkin's lymphoma</i> | <i>Non-Hodgkin's lymphoma</i> |
|--|--|--|
| Age | Bimodal: 15 to 35 years and more than 50 years | Increased incidence with advancing age. |
| Site | Essentially a nodal disease (Cervical/mediastinal/paraaortic) Mesenteric nodes and Waldeyer's ring rarely involved | Essentially an extranodal disease (head and neck nodes frequently) Waldeyer's ring and mesenteric nodes commonly involved. |
| Contiguous involvement | Contiguous spread | Non-contiguous spread (skippy spread) |
| Association | Associated with Epstein-Barr virus | May be associated with HIV and autoimmune diseases. |
| General features | Lymph node involvement is usually the only manifestation of disease. | Nodal disease is frequently associated with extranodal sites of tumor (bone marrow >GIT>lung) Involved nodes tend to be bulky |
| Short axis diameter criteria for size enlargement (mm) | Usually short axis more than 10 mm is considered pathological/clustering of small nodes can be abnormal. Exceptions-Jugulodigastric nodes >13 mm/gastrohepatic or portahepatic nodes >8 mm/retrocrural nodes >6 mm/supraclavicular nodes >5 mm/pelvic nodes >8 mm/Any nodes seen at splenic hilum or presacral and perirectal areas are considered unusual. | |
| Neck | Affect 60 to 80% patients at presentation. | Cervical adenopathy—less common, Waldeyer's ring is commonly involved. |
| Abdomen and pelvis | Retroperitoneal nodes are involved in 25 to 35% of patients at presentation Mesenteric nodes are involved in <5% Celiac axis, splenic hilar and porta hepatis nodes are involved in 30%. Diffuse splenic hilar involvement is almost always associated with diffuse splenic infiltration. Nodal spread is contiguous from one lymph node group to another. Nodes are often normal in size or minimally enlarged. | Retroperitoneal nodes are involved in 45–55% of patients at presentation Mesenteric nodes are involved in >50%—Hamburger sign—mesenteric and retroperitoneal nodes compressing a loop of bowel between two large nodal masses. Additional sites like porta hepatis or splenic hilum are more frequently involved than in Hodgkin's disease. Nodal spread is non-contiguous, bulky and more frequently associated with extranodal disease. |
| Thorax | Prevascular and paratracheal (85%) > hilar (28%) and subcarinal (22%) Usually affects >2 nodal groups Paracardiac nodes are important site of recurrence since they are not included in classic mantle radiation field. | Superior mediastinal nodes (35%) > hilar and subcarinal nodes Usually affects only one nodal group in 50% patients. |
| Prognosis | 70 to 80 percentage cure | Highly variable by type—mostly incurable |
| Treatment | Radiation for localised disease and chemotherapy for advanced cases. | Radiation and chemotherapy (CHOP regimen) |

Causes of generalized lymphadenopathy: **Infection:** **Viral:** Infectious mononucleosis, infective hepatitis, AIDS; **Bacterial:** Tuberculosis, brucellosis, secondary syphilis, tularemia; **Protozoal:** Toxoplasmosis; **Fungal:** Histoplasmosis; **Malignant:** Leukaemia,

metastatic carcinoma; **Immunological:** Systemic lupus erythematosus, Felty's syndrome, Still's disease; drug hypersensitivity as hydantoin, hydralazine, allopurinol; **Others:** Sarcoidosis, amyloidosis, lipid storage disease, hyperthyroidism.

4.186 GENERAL ABDOMEN INCLUDING ABDOMINAL WALL, PERITONEUM

Case No. 186

Clinical history : 53-year-old female presented with epigastric pain and dyspnea for 3 months.

Radiological techniques and observation: Contrast enhanced CT in portal venous phase (Figs 4.186.1 to 4.186.7) shows an ill-defined enhancing soft tissue dense tumour along the course of IVC with exophytic paracaval component extending into right atrium. No evidence of uterine lesions. Other findings include multiple collateral, ascites and patent umbilical vein, bilateral kidneys, bilateral adrenal were normal with altered enhancement pattern of the liver was noted. Portal venous system was patent.

Interpretation: A—55-year-old female, C—an ill-defined isodense soft tissue dense lesion along the course of the IVC extending up to the right atrium with heterogeneous enhancement, multiple collaterals, ascites and a patent umbilical vein, B—altered enhancement pattern of the liver with patent portal system, D—leiomyosarcoma.

Principal diagnosis: IVC leiomyosarcoma.

Discussion: Leiomyosarcoma of the inferior vena cava is a rare condition. Leiomyosarcomas originate from smooth muscle cells. These tumors exhibit three main growth patterns: Extraluminal (most common pattern), combined extra- and intraluminal (second most common) and intraluminal. Leiomyosarcoma can develop in any



Fig. 4.186.1



Fig. 4.186.2



Fig. 4.186.3



Fig. 4.186.4



Fig. 4.186.5

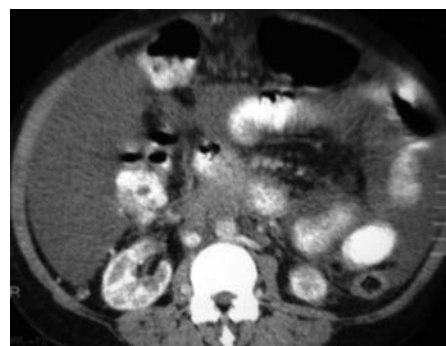


Fig. 4.186.6

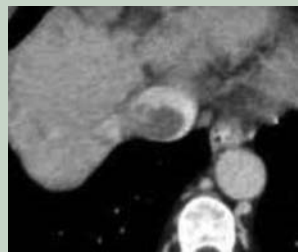
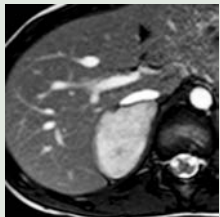



Fig. 4.186.7

vein but is usually found in the inferior vena cava. The tumor is relatively slow growing and tends to expand along the tissue planes of least-resistance rather than invasion of adjacent organs. Depending upon the site of involvement IVC leiomyosarcoma

Upper-segment involvement → from the hepatic vein to the right atrium, middle-segment involvement → the hepatic to renal veins (most common), lower-segment involvement → the infrarenal IVC.

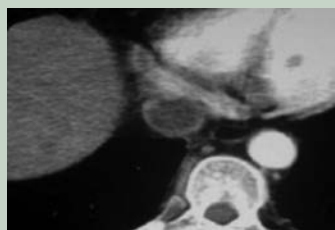
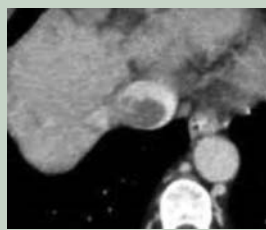
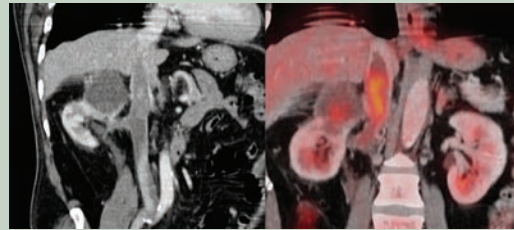
Table 4.186.1: Differential diagnosis for IVC leiomyosarcoma

| Condition | Radiological features | Image |
|--|---|---|
| IVC thrombosis: May be bland thrombus or tumor thrombus. | <p>Acute thrombosis: USG: Hypoechoic thrombus causing distension of vein, partial /no compressibility, no collaterals formation, free edge of thrombus (not adherent to wall), On colour Doppler no flow augmentation with calf muscle squeeze, absence of flow in n case of complete obstruction. CECT: Hypodense thrombus seen as filling defect, can be enhancing in case of tumour thrombus, non-enhancing in bland thrombus.</p> <p>Chronic thrombosis: USG: Hyperechoic thrombus attached to the wall with reduced diameter of vein, non-compressible and multiple collaterals formation.</p> |  <p>Fig. 4.186.8: IVC thrombosis</p> |
| Right adrenal mass | <p>A T2 hyperintense mass is seen in the region of right adrenal gland. IVC is displaced anteriorly and compressed anteroposteriorly.</p> <p>This mass is probably a pheochromocytoma as it is a T2 bright lesion.</p> |  <p>Fig. 4.186.9: Right adrenal mass</p> |
| Right adrenal hemorrhage Commonly seen in trauma. May be associated with vascular tumours, surgery/stress/sepsis—Waterhouse-Friderichsen syndrome. | <p>Hyperdense on non-enhanced CT. MRI appearance depends on stage of hemorrhage.</p> <p>CT shows hyperdense hematoma in the region of right adrenal gland.</p> |  <p>Fig. 4.186.10: Right adrenal hemorrhage</p> |

Other differentials to be considered include other sarcomas such as angiosarcoma, liposarcoma and undifferentiated sarcoma of IVC, renal cell carcinoma with tumor thrombus. Hepatocellular carcinoma with tumour thrombus.

Table 4.186.2 Difference between bland thrombus and tumor thrombus

| Bland thrombus | Tumor thrombus |
|--|---|
| Causes hypercoagulable state, venous stasis, extrinsic compression by lymph node/retroperitoneal fibrosis, vena caval filters, extension of benign tumors like angiomyolipoma, adrenal pheochromocytoma, IVC leiomyomatosis. | Extension of tumor from renal cell carcinoma, hepatocellular carcinoma, adrenocortical carcinoma, Wilms tumor and primary IVC leiomyosarcoma, pancreatic carcinoma and other sarcomas of IVC. |
| IVC narrowed at the site of thrombosis | Expansion of IVC at the level of thrombus |
| No underlying primary tumor | Tumor thrombus shows continuity with the primary |
| No enhancement on arterial phase of post-contrast imaging | Shows enhancement due to neovascularity in arterial phase of contrast imaging |

**Fig. 4.186.11:** Bland thrombus**Fig. 4.186.12:** Tumor thrombus**Fig. 4.186.13:** Tumor thrombus

The tumor may extend into the right side of the heart and, rarely, into the pulmonary artery.

Complications: Metastases to the liver, lungs, and lymph nodes usually occur at late stages of disease, recurrences are common, and subsequent tumors may occasionally exhibit more aggressive histologic characteristics than the original neoplasm.

Imaging: The most typical imaging appearance of these tumors include vein dilatation and an intermediate-attenuation mass with irregular enhancement and total or near-complete vein obstruction. A lobulated, well-defined, and heterogeneous lesion, exhibits signs of hemorrhage and necrosis. The patent blood vessels appear dark on images obtained with spin-echo sequences and presaturation pulses in contrast with the solid tumor. On gradient-echo MR images obtained during breath holding, the patent vessels are hyperintense relative to the less intense tumor. These pulse sequences can be used to create MR angiograms that depict the arterial or venous anatomy that guide surgical planning. Tumor thrombosis may be distinguished from bland thrombosis on the basis of the differences in signal intensity seen on MR images. Tumour is isointense on T1-weighted MR images, and iso- to hyperintense on T2-weighted MR images. Hemorrhagic regions appear as hyperintense areas on T1-weighted images. The tumors usually exhibit marked enhancement.

Treatment: Surgical resection offers the only prospect of cure. Middle and lower IVC → radical excision, in cases with adequate venous collateral pathways, the IVC can be ligated without resulting in appreciable edema in the lower extremities. When the middle third of the IVC is removed, although the right kidney must be resected or autotransplanted to the iliac fossa, the left kidney contains sufficient collateral vessels for patient survival. Tumors in the upper IVC with hepatic vein involvement → no definite surgical therapy, so radiation therapy and

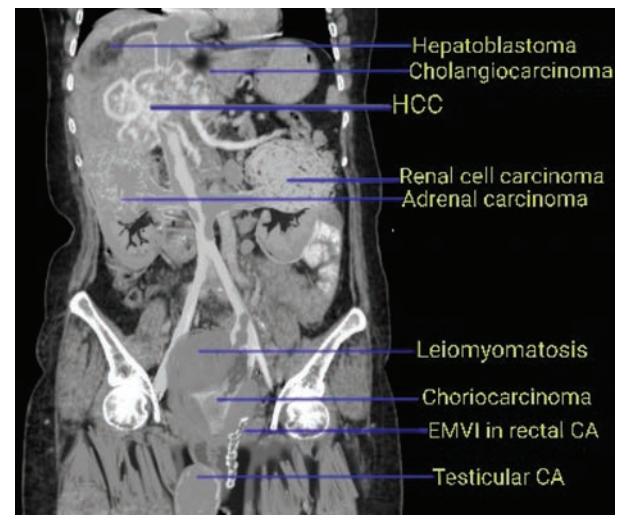


Fig. 4.186.14: Tumors showing venous thrombosis

chemotherapy are often used, but their exact roles have not been well established.

Anterior displacement of IVC caused by: 1. Retroperitoneal liposarcoma, 2. retroperitoneal lymphadenopathy. 3. adrenal and renal lesions. 4. retroperitoneal malignant fibrous histiocytoma, 5. retroperitoneal abscess 5. Psoas collection/abscess.

Masses that extend to IVC are hepatic, renal and adrenal carcinomas.

SVC leiomyosarcoma: The most common SVC malignancy is metastasis. Primary SVC sarcomas are rare tumors, with leiomyosarcoma being the common. Leiomyosarcomas are locally aggressive neoplasms that manifest in patients after middle age and typically metastasize to the lungs and liver. At imaging, they are seen as a well-defined, smooth or lobulated, homogeneously or heterogeneously enhancing mass that expands the parent vessel. Contrast enhancement can help distinguish this entity from bland thrombus.

4.187 GENERAL ABDOMEN INCLUDING ABDOMINAL WALL, PERITONEUM

Case No. 187

Clinical history: A 32-year-old male, presented with complaints of discharge from the perianal region on and off for the past 4 months.

Radiological techniques and observations: MRI pelvis T1 axial, T2 axial fat sat, T2 axial and coronal fat sat MIP images (Figs 4.187.1 to 4.187.6) show a T2 hyperintense fistulous tract approximately measuring 3 cm length in the right perianal region which opens externally in the skin at 7 o'clock position with an adjacent perianal abscess in the subcutaneous plane. The tract extends superiorly, medially and anteriorly and forms a collection at right ischiorectal fossa, just lateral to the anal sphincter, where the tract ramifies into two tracts, the anterior tract continuing anteriorly towards the perineum and ends as a blind ending tract. The posterior tract pierces both the external and the internal anal sphincter and opens internally into the anal canal at 6 o'clock position. The right levator ani muscle is inflamed, but the tract is not seen crossing the levator ani superiorly. The perianal abscess is seen extending like a horseshoe into the right gluteus muscle and into the subcutaneous plane. Any wall thickening in the visualised bowel loops has to be ruled out.

Interpretation: A-32 years old male, C-complex perianal fistula with transsphincteric course, associated with right ischiorectal and right perianal abscesses, B-right levator ani muscle is inflamed, but the tract is not seen crossing the levator ani, D-grade 4 fistula based on St. James University Hospital classification.

Principal diagnosis: Trans-sphincteric perianal fistula with secondary abscesses-grade 4 fistula based on St. James University Hospital classification.

Management: Patient is referred to the surgical department for surgical management. Complete surgical

excision of the fistulous tract (fistulectomy) with the aid of preoperative MR evaluation.

Brief discussion about the condition: Anal fistulae mostly occurs secondary to anal gland infection. Pus from abscess creates a track to the peri-anal skin, through the sphincter muscle usually the longitudinal layer. Thus fistula extends from its internal opening in the anal canal to the skin externally. Fistulae are commonly classified according to the Parks classification based on their relationship to the muscles of the anal sphincter complex (trans-sphincteric, intersphincteric, suprasphincteric or extrasphincteric). MRI is the imaging modality of choice. In fat-suppressed T2-weighted imaging, fistulae appear as high signal against the lower signal sphincter complex and adjacent fat. MRI is especially useful in demonstrating associated abscesses, supralelevator extension and collections, which difficult to detect clinically. Preoperative MRI has been shown to reduce recurrence rates in complex fistulae. Ultrasound has a limited role, tracts within the sphincter and the internal opening can be well demonstrated with endosonography.

'Anal clock': With the patient in the lithotomy position, anterior is 12 o'clock and posterior is 6 o'clock and the transverse anal line (a line drawn from 9 o'clock to 3 o'clock).

Goodsall's rule states that the internal opening of the fistula is dependent on where the fistula is located (i.e. if the internal opening is anterior to the transverse anal line there will be a (usually simple) direct radial fistulous tract. If the internal opening is posterior to the transverse anal line, there will be a tortuous (often more complex) fistulous tract that enters posteriorly in the midline (6 o'clock).

The modified Parks classification (surgical classification) is the most widely used surgical classification for distinguishing four types of fistula. The course of

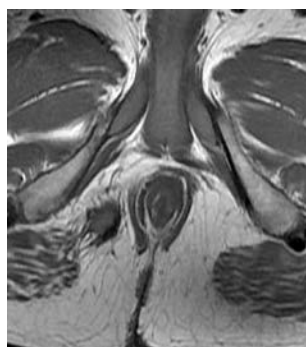


Fig. 4.187.1



Fig. 4.187.2

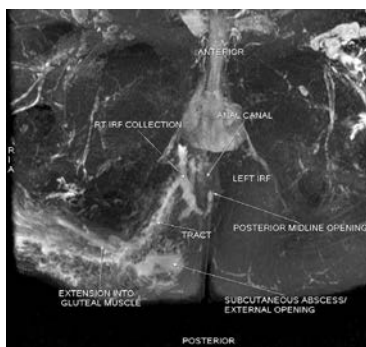


Fig. 4.187.3

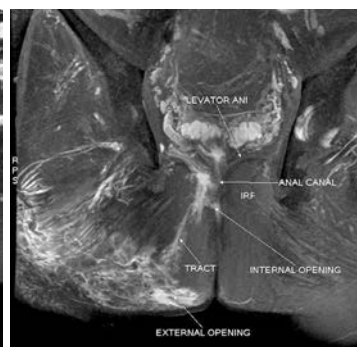


Fig. 4.187.4

Table 4.187.1: Differential diagnosis for perianal fistula

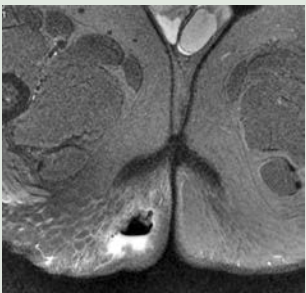

| | | |
|---|---|--|
| Perianal abscess: Often associated with perianal fistulae and are components of grades 2 and 4 fistulae of the St James University Hospital classification. | Associated with diabetes mellitus, Crohn's disease, pelvic infection, trauma, and anorectal cancer/anal cancer +/- radiation therapy. While some abscesses may resolve spontaneously via internal drainage into the anal canal, others may require surgical incision and drainage. |  |
| Pilonidal sinus: Occurs due to skin and subcutaneous tissue infections, occurring at or near the upper part of the natal cleft. The peak age of presentation is 3rd decade. There is an increased male predilection. | USG may show superficial sinus tract and its extent. MRI clearly demonstrates the tract and associated changes/extensions. Fluoroscopy as sinogram, with contrast injected into the cutaneous opening shows the extent of sinus and its morphology. |  |

Fig. 4.187.5: Perianal abscess**Fig. 4.187.6:** Pilonidal sinus**Table 4.187.2: Causes of perianal fistula**

| Primary | Secondary | |
|---|---|---|
| Most common cause—obstruction of anal gland which leads to stasis and infection with abscess and fistula formation. | 1. Iatrogenic—post-surgical complication a. Hemorrhoidal surgery b. Post-ultra low anterior resection c. Hysterectomy d. Post-pelvic radiotherapy | 2. Diverticulitis 3. Inflammatory bowel disease (Crohn's >> UC) 4. Infection (TB, fungal or viral) 5. Childbirth 6. Pelvic malignancies |

Table 4.187.3: St James University Hospital classification

| | |
|---|---|
| Grade 1 | Simple linear inter-sphincteric |
| Grade 2 | Inter-sphincteric with abscess or secondary tract |
| Grade 3 | Trans-sphincteric |
| Grade 4 | Trans-sphincteric with abscess or secondary tract within the ischiorectal fossa |
| Grade 5 | Supralelevator and translevator extension |
| Others (not specifically described in the Parks or St. James classification): Submucosal fistulas are superficial tracts that arise inferiorly from the anal canal and extend to the skin surface without involving the internal or external anal sphincters. They are actually sinus tracts. | |

the fistula and its relationship to the anal sphincters is described in the coronal plane. A. Intersphincteric (~70%): Fistula crosses the intersphincteric space and does not cross the external sphincter. B. Trans-sphincteric (25%): Fistula crosses from the intersphincteric space, through the external sphincter and into the ischiorectal fossa. C. Suprasphincteric (5%): Fistula passes superiorly into the intersphincteric space, and over the top of

the puborectalis muscle then descending through the iliococcygeus muscle into the ischiorectal fossa and then skin. D. Extrasphincteric (1%): Fistula crosses from the perineal skin through the ischiorectal fossa and levator ani muscle complex into the rectum (i.e. it is outside the external anal sphincter).

External anal sphincter composed of skeletal muscle and classically categorized into deep, superficial, and

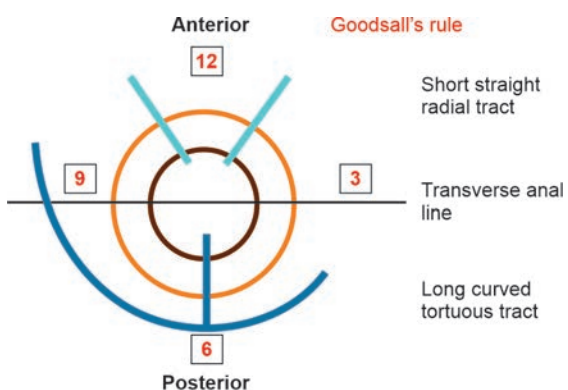


Fig. 4.187.7: Goodsall's rule

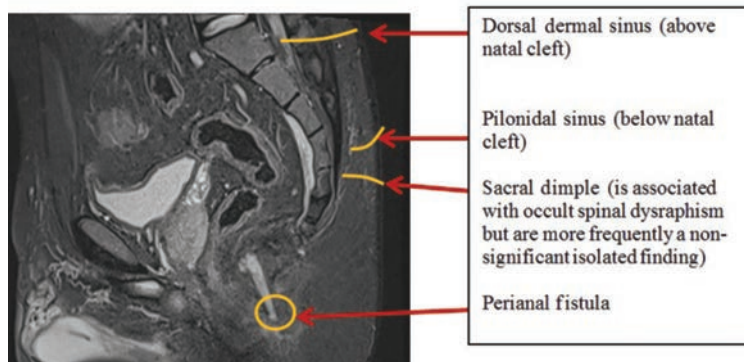


Fig. 4.187.8: Sinus and fistula in pelvis

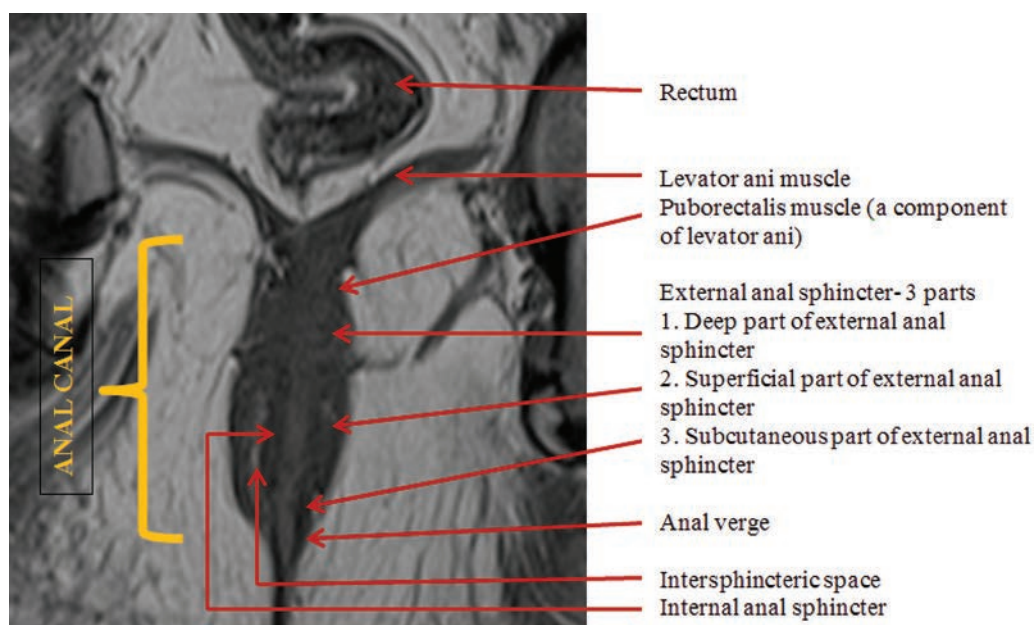


Fig. 4.187.9: Normal anal canal anatomy on coronal MRI

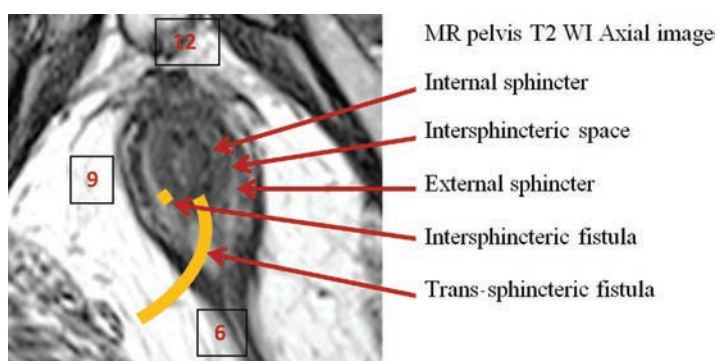


Fig. 4.187.10: Intersphincteric and trans-sphincteric fistula

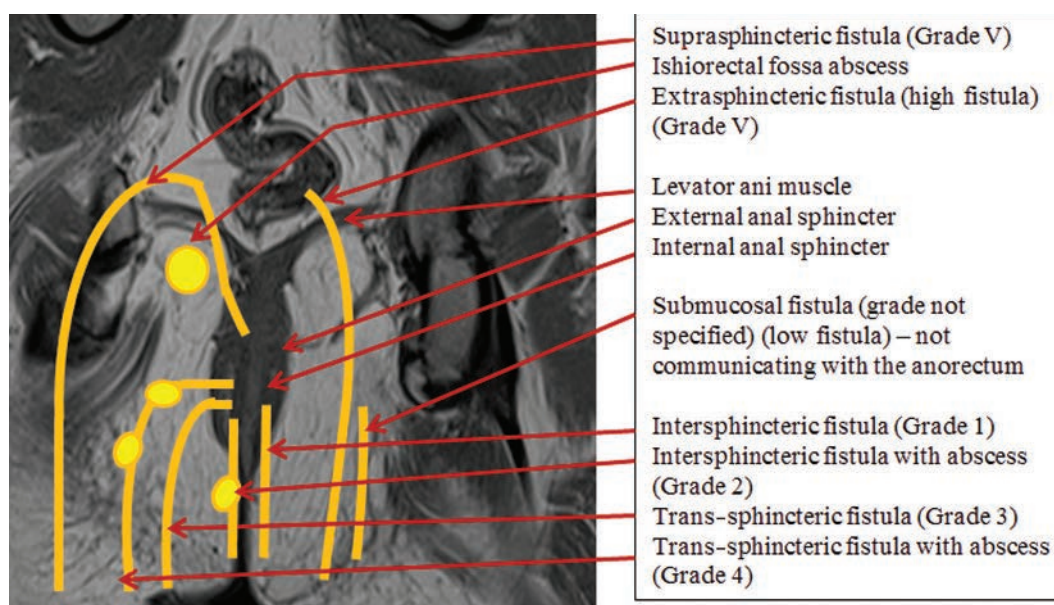


Fig. 4.187.11: Perianal pathologies

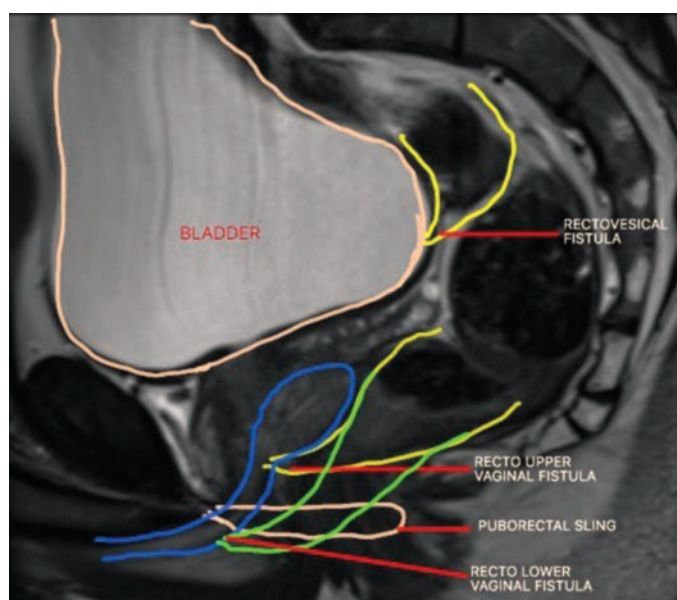


Fig. 4.187.12: Anorectal fistulas

subcutaneous parts: Deep part—circular muscle fibers, blends with puborectalis part of levator ani (posteriorly and laterally), the aforementioned region is called the anorectal ring and is palpable on rectal examination; superficial part—elliptical muscle fibers, attaches from the tip of the coccyx posteriorly to the perineal body anteriorly, only part of the sphincter with bony attachment; subcutaneous part—circular muscle fibers, lower ends curve inwards, lying below the end of the internal sphincter, the intersphincteric groove is palpable on examination.

4.188 HEPATOBILIARY SYSTEM

Case No. 188

Clinical features: 48 years old male patient, who is a chronic alcoholic presenting with complaints of upper GI bleeding 3 episodes in a day.

Radiological imaging techniques and observations: Figure 4.188.1 shows ultrasound of liver, CECT abdomen in triple phase (Figs 4.188.2 to 4.188.4), MRI hASTE (Fig. 4.188.5), T1 fat sat images (Fig. 4.188.6). Liver is shrunk in size with irregular nodular surface. No suspicious arterial phase hyper-enhancing focal lesions identified, splenomegaly noted with spleen measuring 21 cm in length. There is dilatation of the portal, splenic vein as well as presence of gastroesophageal and spleno-renal collaterals. Mesenteric congestion noted. No dilatation of coronary vein/paraumbilical vein. MRI hASTE and T1 fat sat liver shows heterointensity resembling the mosaic architecture and diffuse nodular surface.

Interpretation: A: 48 years old male, liver, C: Shrunk liver with nodular surface with, B: Dilated portosystemic

collaterals and splenomegaly. D: Liver cirrhosis with features of portal hypertension.

Principal diagnosis: Liver cirrhosis with features of portal hypertension with gastroesophageal varices.

Management: Urgent referral to the surgeon for upper GI scopy for gastroesophageal varices.

Treatment: Scopy guided treatment for varices. Medical treatment of portal hypertension.

Role of interventional radiology: BRTO (balloon-occluded retrograde transvenous obliteration) for varices; TIPS (transjugular intrahepatic portosystemic shunt) for portal hypertension.

Cirrhosis is a common endpoint of a wide variety of chronic liver diseases causing hepatocellular necrosis. Causes: Alcohol (60–70%), viral hepatitis (10%)-Hepatitis-B, C, cryptogenic/NASH (non-alcoholic steatohepatitis), biliary diseases (primary sclerosing cholangitis, primary biliary cirrhosis), metabolic cause (Wilson, alpha-1 antitrypsin deficiency), autoimmune

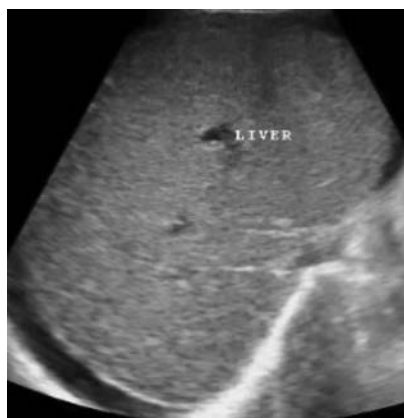


Fig. 4.188.1

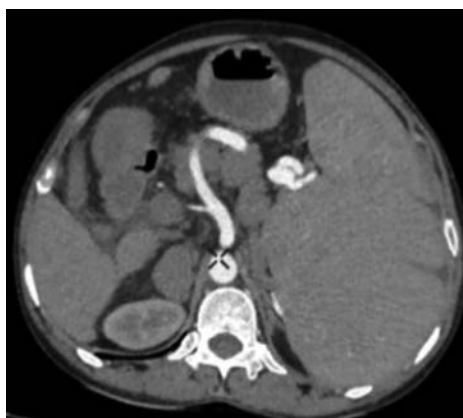


Fig. 4.188.2



Fig. 4.188.3



Fig. 4.188.4

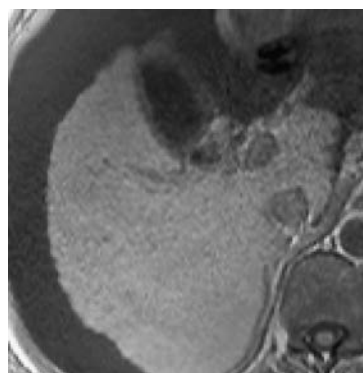


Fig. 4.188.5

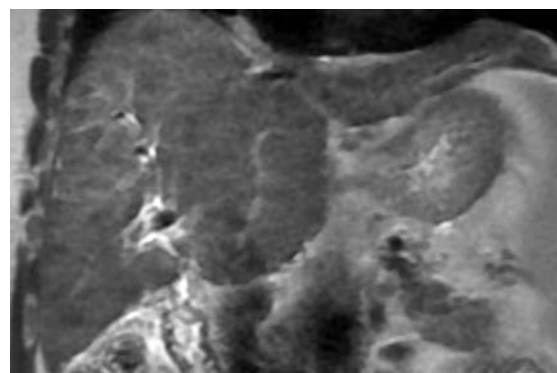


Fig. 4.188.6

Table 4.188.1: Causes of diffuse liver diseases

| <i>Infections</i> | <i>Infiltrative</i> | <i>Vascular</i> | <i>Biliary</i> |
|---|--|---|--|
| Hepatitis Candidiasis Sarcoidosis | Hemochromatosis, fatty liver, Wilson's disease, glycogen storage disease | Budd-Chiari disease, portal vein thrombosis, veno-occlusive disease, intra-hepatic shunts | Cholangitis—primary sclerosing cholangitis |

Table 4.188.2: Doppler measurements in portal vein Doppler

| Portal vein | Size | Diameter on deep inspiration | Mean peak velocity | Direction | Others |
|--|--|--|--------------------|---|---|
| Normal | <13 mm | Increases 70–100% | 15–25 cm/sec | Hepatopetal | Normal |
| Portal hypertension | >13 mm or normal size because of collaterals | Increase <70% indicates portal hypertension | <10 cm/sec | Hepatofugal | Thrombus/ cavernous transformation/ portosystemic collaterals |
| Hepatic vein | | | | | |
| Transmitted cardiac pulsation in normal people | | Absent pulsation in thrombosis and obstruction | | Increased. Pulsation in tricuspid regurgitation | |
| IVC | | | | | |
| Normal | Dilated | | | | |
| <2 cm | >2 cm | | | | |
| Others (normal) | | | | | |
| Splenic vein | | <10 mm | | Hepatopetal flow | |
| Superior mesenteric vein | | <10 mm | | Hepatopetal flow | |
| Coronary vein | | <7 mm | | Hepatopetal flow | |
| Recanalised umbilical vein | | <3 mm | | Hepatopetal flow | |
| Portal hypertension indices | | | | | |
| Portal hypertension index = (hepatic artery RI \times 0.69) \times (Splenic artery RI \times 0.89) | | | | | |
| Normal portal hypertension index | | | <2.08 | | |
| Portal hypertension index in portal hypertension | | | >2.08 | | |
| Hepatic artery RI in portal hypertension | | | >0.8 | | |
| Splenic artery RI in portal hypertension | | | >0.6 | | |

hepatitis, vascular (congestive cardiac failure, Budd-Chiari syndrome) and portal vein thrombosis.

Complications: Portal hypertension and hepatocellular carcinoma.

CT and USG signs of liver cirrhosis: Liver is heterogeneous in appearance. Nodular surface. Widened GB Fossa; Falciform ligament/ligamentum teres widening. Acute: Enlarged liver. Chronic: Shrunken liver. Right lobe atrophy (posterior segments VI and VII), left lobe hypertrophy (segments II, III). Caudate lobe hypertrophy.

Causes of caudate lobe hypertrophy: Cirrhosis; Budd-Chiari; primary sclerosing cholangitis; congenital hepatic fibrosis; cavernous transformation of the portal vein.

Causes of left lobe hypertrophy: Cirrhosis- primary sclerosing cholangitis, primary biliary cirrhosis; right portal vein embolization; lobar hepatectomy of right lobe.

Measurement of caudate lobe hypertrophy: Caudate to right lobe ratio

Image at the level bifurcation of main portal vein

Line 1: Parasagittal line drawn through the right lateral border of portal vein

Line 2: Parasagittal line drawn through the left lateral border of caudate lobe

Line 3: line orthogonal to lines 1 and 2 midway between the portal vein and IVC extended to the right liver edge

Right lobe measurement (RL) is along line 3 from right liver edge to line 1.

Table 4.188.3: Comparison between METAVIR and fibroscan scores

| | Elastogram (kPa) | Elastography (m/s) |
|------------------------|------------------|--------------------|
| F0 = No fibrosis | < 2 | 0.81 to 1.19 |
| F1 = Mild fibrosis | 2.5 to 7 | 1.2 to 1.36 |
| F2 = Moderate fibrosis | 7.5 to 10 | 1.35 to 1.76 |
| F3 = Severe fibrosis | 10 to 14 | 1.77 to 1.99 |
| F4 = Cirrhosis | > 14 | > 2 |

Fibroscan was the first commercially available TE elastography

Table 4.188.4: METAVIR scoring system for chronic HBV and HCV, Brunt score for NASH

| METAVIR scoring | Fibroscan cut-off values |
|-----------------|--|
| F0 | No fibrosis |
| F1 | Mild fibrosis: Portal fibrosis without septa |
| F2 | Moderate fibrosis: Portal fibrosis and a few septa |
| F3 | Severe fibrosis: Numerous septa |
| F4 | Cirrhosis |

Caudate measurement (C) is along line 3 between lines 1 and 2

Caudate: Right lobe ratio: C/RL

Normal: <0.6, Borderline: 0.6–0.65, Abnormal >0.65

Causes of hyperdense liver on CT: Iron: Genetic hemochromatosis, erythropoietic hemochromatosis, transfusion iron overload, Copper: Wilson disease, Iodine: Amiodarone—anti-arrhythmic drug (HU = 95–145), Gold: Colloidal form of gold for rheumatoid therapy, Thorotrast: Alpha emitter with atomic number 90; Thallium: Accidental/suicidal ingestion of rodenticides, other causes acute massive protein deposits, glycogen storage disorder.

Diffusely decreased attenuation: 1. Fatty infiltration—alcohol, obesity, early cirrhosis, parenteral feeding, bypass surgery, malnourishment, cystic fibrosis, steroids, Cushing's syndrome, late pregnancy, carbon tetrachloride exposure, chemotherapy, high-dose tetracycline and glycogen storage disease; 2. Malignant infiltration; 3. Budd-Chiari; 4. Amyloid—no change after intravenous contrast.

Elastography: The noninvasive assessment of tissue mechanical properties such as elasticity, which describes the resistance to deformation of a tissue to an applied stress.

Quantitative elastography: 1. Quantitative US elastography methods include transient

elastography (TE) and acoustic radiation force impulse (ARFI) techniques such as point shear-wave elastography (pSWE) and two-dimensional (2D) shear-wave elastography (SWE). 2. Quantitative MR elastography: Requires external hardware to generate shear waves in the tissue of interest.

Qualitative assessment:

Table 4.188.5: Color coding with respect to fibroscan values

| | |
|------------|---------|
| Dark blue | <6 kPa |
| Light blue | <12 kPa |
| Yellow | <18 kPa |
| Orange | <24 kPa |
| Red | >30 kPa |

MR elastography: New technique quantifying liver stiffness in a similar fashion to US methods.

Angiography: To assess vascular complications such as variceal bleeding and portal hypertensive changes. Hepatic arteriography in cirrhotic liver demonstrates increased tortuosity of intrahepatic branches, so-called 'corkscrew vessels', which reflect lobar shrinkage.

Role of Interventional Radiology

Transjugular intrahepatic portosystemic shunt (TIPS): A TIPS is placed to reduce portal pressure in patients with complications related to portal hypertension. Transjugular intrahepatic portosystemic shunt (TIPS) creates a transhepatic communication between a major intrahepatic portal vein branch (usually the right) and a hepatic vein using a needle system from the jugular vein.

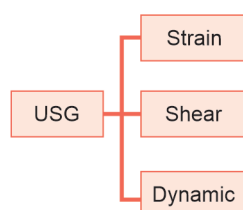
**Fig. 4.188.7:** Types of ultrasound elastography

Table 4.188.6: TIPS-indications, contraindications and Doppler criteria for failed TIPS

| | |
|---|--|
| Indications: <ul style="list-style-type: none"> • Acute variceal bleeding that cannot be successfully controlled with other treatment • Recurrent and refractory variceal bleeding • Refractory ascites • Refractory hepatic hydrothorax • Decompression in hepatic venous outflow obstruction • End stage liver disease awaiting transplant | Absolute contraindications <ol style="list-style-type: none"> 1. Congestive heart failure 2. Multiple hepatic cysts 3. Uncontrolled systemic infection or sepsis 4. Severe hepatic failure 5. Severe hepatic encephalopathy 6. Severe pulmonary hypertension. |
| Doppler criteria for failed TIPS: <ol style="list-style-type: none"> 1. Shunt velocity of <50 cm/sec 2. Increase or decrease in shunt velocity of >50 cm/sec compared to initial post-procedure value 3. Hepatofugal flow in main portal vein | |

Complications

- Obstruction to flow:* Shunt obstruction (38%), hepatic vein stenosis
- Biliary injury
- Stent dislodgment with embolization to right atrium, pulmonary artery, internal jugular vein.
- Vascular injury:* Hepatic artery pseudoaneurysm, arterioportal fistula, intrahepatic/subcapsular hematoma

High risk for variceal bleed in cirrhotic disease are liver stiffness measurement (LSM) >20 kPa, diameter of varices ≥ 4 mm, hepatic venous pressure gradient >10 mmHg. **CT variceal bleeding score** is for predicting the development of variceal bleeding according to their maximum diameter (scores 1–4): (1) Definitely low-risk or no varices; (2) probably low-risk (3) probably high-risk; and (4) definitely high-risk. Score of 4 was assigned if the diameter was definitely >3 mm, a score of 3 if the diameter was between 2 and 3 mm, a score of 2 if the diameter was between 1 and 2 mm and a score of 1 if there is no varices.

DIPS (direct intrahepatic portosystemic shunt) or percutaneous TIPS: Ultrasound guided percutaneous simultaneous puncture of portal vein and inferior vena cava followed by introduction of guidewire through the portal vein.

BRTO (balloon-occluded retrograde transvenous obliteration) for varices

PARTO: Vascular plug assisted retrograde transvenous obliteration.

CARTO: Coil assisted retrograde transvenous obliteration.

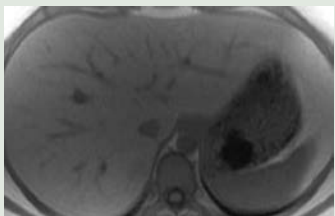
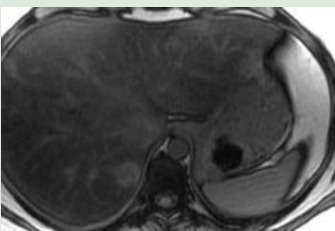
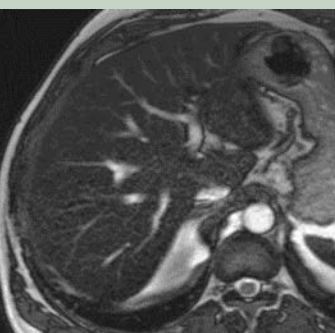
BATO: Balloon occluded antegrade transvenous obliteration.

The classic procedure involves obtaining a systemic venous access and the target shunt catheterized using a selective catheter. Occlusive balloon is inflated to occlude the shunt, then the contrast is injected upstream

of the occlusion to further evaluate variceal anatomy. Significant efferent collateral vessels are embolised. Sclerosant is injected upstream of balloon into the gastric varices itself.

Assessment of fatty liver: The attenuation value in the healthy liver (50–57 HU) on non-contrast enhanced CT, and its reduction by 1.6 HU for each milligram of triglycerides deposited per gram of hepatic tissue. CT criteria for steatosis on non-intravenous contrast scans included the following: Liver attenuation 10 HU less than the spleen attenuation, absolute liver attenuation of less than 40 HU, and liver-to-spleen attenuation ratio less than 1. CT criteria for steatosis with intravenous contrast in the venous phase—liver attenuation 20 HU less than spleen attenuation. The pattern of hepatic fatty changes on CT can be graded as: 0, normal; 1, diffuse, homogeneous; 2, geographic pattern; 3, focal; and 4, focal sparing (pseudotumor, glove pattern, simulating metastasis). The severity of hepatic fatty infiltration on CT is graded as below: Grade 0, normal; grade 1, liver attenuation slightly less than that of the spleen; grade 2, more pronounced difference between the liver and spleen, and the intrahepatic vessels are not visible or show slightly higher attenuation than that of the liver; and grade 3, markedly reduced liver attenuation, with sharp contrast between the liver and intrahepatic vessels. In quantitative evaluations, a hepatic attenuation index is obtained by calculating liver to spleen attenuation ratio with a cut-off value of 0.8 to exclude moderate steatosis. It can also be calculated as hepatic-splenic attenuation difference: A difference of 10 HU between the attenuations of the liver and spleen defines hepatic steatosis (i.e. liver shows attenuation of 10 HU less than spleen). MRS is a fast, safe, noninvasive method for the quantification of hepatic fat content showing an increase in the intensity of the lipid peak. Qualitative assessment of fatty liver in ultrasound is grading it as follows: Grade I: diffusely increased hepatic echogenicity but

Table 4.188.7: Differential diagnosis for diffuse liver diseases

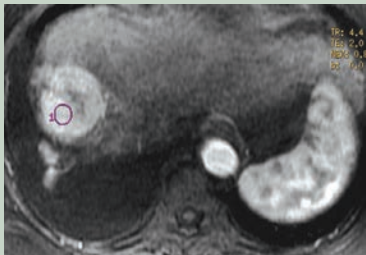
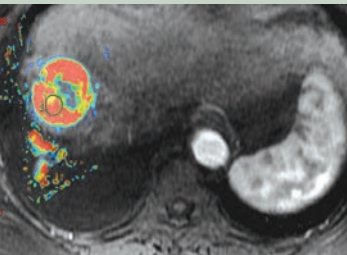
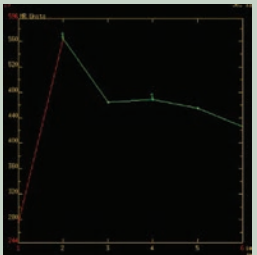
| | | |
|---|---|---|
| <p>Hepatic steatosis 15% of general population, metabolic derangement leading to non-alcoholic steato-hepatitis.(NASH) 5 % may progress to HCC.</p> | <p>USG: Hyperechogenic. Poor definition of posterior liver is seen CT: Density <40 HU, less than spleen by >10 HU. MRI: Mild increased signal on T1 and T2 with loss of signal in opposed phase. Fat quantification can be done in liver using MRI: Chemical shift encoding-proton density fat fraction (PDFF) or using MRS. In colloid scan: Heterogeneous uptake, reversal of liver spleen uptake</p> |  <p>Fig. 4.188.8: Hepatic steatosis (CSI-inphase)</p>  <p>Fig. 4.188.9: Hepatic steatosis (CSI-opposed phase)</p> |
| <p>Haemochromatosis/Iron overload Primary: Hereditary/idiopathic AR, Chromosome 6 Primary: Liver, pancreas, heart, pituitary. Secondary: Hemosiderosis (cirrhosis, ineffective erythropoiesis-hemolytic anemias, parenteral transfusions). Secondary: Liver, spleen, bone marrow</p> | <p>CT demonstrates hepatic iron deposition through an increase in HU value (>75 HU dual energy CT (80+120 kv) can be used to quantify). MRI is the most specific imaging technique—signal loss is seen (hypointense on T2). MR liver iron quantification is a non-invasive means of measuring liver iron concentration in hemochromatosis using 1. T2 relaxometry (in which multiple images are acquired with different TE and transverse magnetization R2 and R2*) 2. Liver to muscle signal intensity ratio.</p> |  <p>Fig. 4.188.10: Haemochromatosis</p> |
| <p>Viral Hepatitis: Hepatitis B and hepatitis C</p> | <p>Imaging findings: Altered echoes, hepatomegaly, periportal edema, diffuse GB wall edema, splenomegaly</p> | |
| <p>Wilson's disease: Autosomal recessive disorder, copper is deposited in the liver, cornea and lenticular nucleus of the brain</p> | <p>Imaging demonstrates the generalised cirrhotic changes Rarely causes a detectable increase in hepatic attenuation on CT On MRI there may be a subtle increased signal on T1W with a decrease on T2W images. There are no specific features on US studies.</p> | |
| <p>Malignant diffuse disease Metastases: Breast HCC (rarely) Lymphoma, leukemia</p> | <p>USG: Heterogeneous echoes Other findings such as vascular thrombosis in HCC may be helpful Biopsy is diagnostic</p> | |
| <p>Budd-Chiari syndrome: Refer to case 188</p> | | |

periportal and diaphragmatic echogenicity is still appreciable. Grade II: Diffusely increased hepatic echogenicity obscuring periportal echogenicity but diaphragmatic echogenicity is still appreciable. Grade III: Diffusely increased hepatic echogenicity obscuring periportal as well as diaphragmatic echogenicity. Hepatorenal index (HRI) can be calculated sonographically or CT to quantify fatty liver. In a normal

liver, HRI is in the range from 1.00 to 1.04. Hepatic steatosis is classified as mild (HRI 1.05–1.24), moderate (1.25–1.64) or severe (1.65).

MR elastography: It is useful in evaluation of liver fibrosis/cirrhosis by assessment of liver stiffness.

A pneumatic driver is used to generate compression waves (of frequency 60 Hz) that are transmitted to the

| Table 4.188.8: MR perfusion for liver | | |
|--|---|--|
| MR perfusion of liver showing enhancing nodule in segment 8 with rapid washout suggestive of hepatocellular carcinoma. | | |
|  |  |  |
| Fig. 4.188.11: Enhancing lesion in segment 8 of liver in case of hepatocellular carcinoma | Fig. 4.188.12: Perfusion color mapping in segment 8 of liver in case of hepatocellular carcinoma | Fig. 4.188.13: Time intensity curve showing increased perfusion in case of hepatocellular carcinoma |

liver through a passive driver placed over the right hypochondrium. GRE magnitude and phase images are obtained in end expiration and processed to get color wave images, gray scale and color elastogram images with superimposed confidence interval maps. The color elastogram images can be used for quantitative estimation of fibrosis. Limitations: Liver stiffness can also be increased in case of acute inflammation, cholestasis, post-prandial state, congestion. Superimposed iron deposition can lead to wave distortion and non-diagnostic study.

CT liver volumetry: Indications—preoperative assessment for living donor liver transplantation, before resection to determine the remnant liver volume. Technique: Bolus tracking, patient position supine with their arms above their head. Scout—from domes of the diaphragm to the pubic symphysis. Scan extends from the right dome of diaphragm down to the lower pole of kidneys. Scan direction is caudocranial. Contrast injection considerations—monitoring slice (region of interest) descending aorta at the level of the carina, threshold 100 HU. Volume: 120–150 ml according to

the donor’s weight (1.5–2 ml/kg) of non-ionic contrast medium using an automatic pump at a flow rate of 4–5 ml/sec. Scan delay—minimal scan delay, respiration phase, inspiration. Dynamic phases—arterial phase: Achieved by contrast agent bolus tracking usually at 15–25 seconds post-injection; portal phase: starts about 40 seconds post-injection. Volumetric assessment is depending upon the degree of hepatic veins opacification allowing better delineation of the virtual hepatectomy plane. Post-processing: The hepatic venous phase is used for CT volumetry, where hepatic veins appear opacified, using 6 or 8 mm slice thickness. The liver boundary is traced to exclude the surrounding structures/organs as well as vessels and hepatic fissures, then we summate the liver area on every single cut. Virtual hepatectomy plane is drawn on each cut on axial images, to the right of the middle hepatic vein in right hemi-hepatectomy and along falciform ligament in left lateral segmentectomy. The volume of all cuts is summed to get the total and lobar volume of the liver. Assume that the mean liver density equals 1 g/ml, i.e. the calculated volumes equal to their respective weights.

4.189 HEPATOBILIARY SYSTEM

Case No. 189

Clinical history: A 30-year-old male patient with right hypochondrial pain and abdominal distension.

Radiological techniques and observations: Contrast enhanced CT limited axial sections and coronal sections (Figure 4.189.1) are provided. Arterial phase shows hepatomegaly, irregular surface of liver with hypertrophy of caudate lobe and left lobe. Multiple perisplenic collaterals are seen. Venous phase shows dysmorphic liver with heterogeneous enhancement of liver parenchyma (similar to nutmeg like appearance seen in cardiac failure). Coronal image shows narrowing of intrahepatic portion of IVC. Gall bladder is not visualised. No evidence of any filling defects in portal vein or any evidence of intrahepatic biliary radicle dilatation. No evidence of any splenomegaly or any evidence of bony lesions.

Interpretation: A: 30 years old male, lesion in liver, C: Hepatomegaly with caudate and left lobe hypertrophy, B: Heterogeneous enhancement of parenchyma in venous phase and narrowing of intrahepatic portion of IVC. D: Budd-Chiari syndrome.

Principal diagnosis: Imaging findings favour diagnosis of Budd-Chiari syndrome.

DSA images of the same patient are provided.

Digital subtraction images (Figs 4.189.2 to 4.189.6) of treatment of the same patient are provided. Images represent IVC venogram, hepatic venogram, hepatic venoplasty and hepatic vein stent placement respectively. IVC venogram shows narrowing of intrahepatic portion of IVC. Hepatic venogram shows decrease in luminal diameter near IVC hepatic veins confluence. Venoplasty (balloon dilatation of vein) is done followed by stent placement since venous angioplasty by itself is usually not sufficient to keep a vein open, presumably because of low intravascular blood pressure compared to arterial system. Therefore, metal stents are usually required for long term patency in venous system. Final image represents normal flow of contrast through IVC post-procedure.

IVC thrombosis: Etiology can be divided as IVC thrombosis in congenitally abnormal IVC and congenitally normal IVC. Congenitally abnormal IVC can be classified as—1. Infrarenal (duplicate IVC, persistent left-sided IVC, preaortic IVC

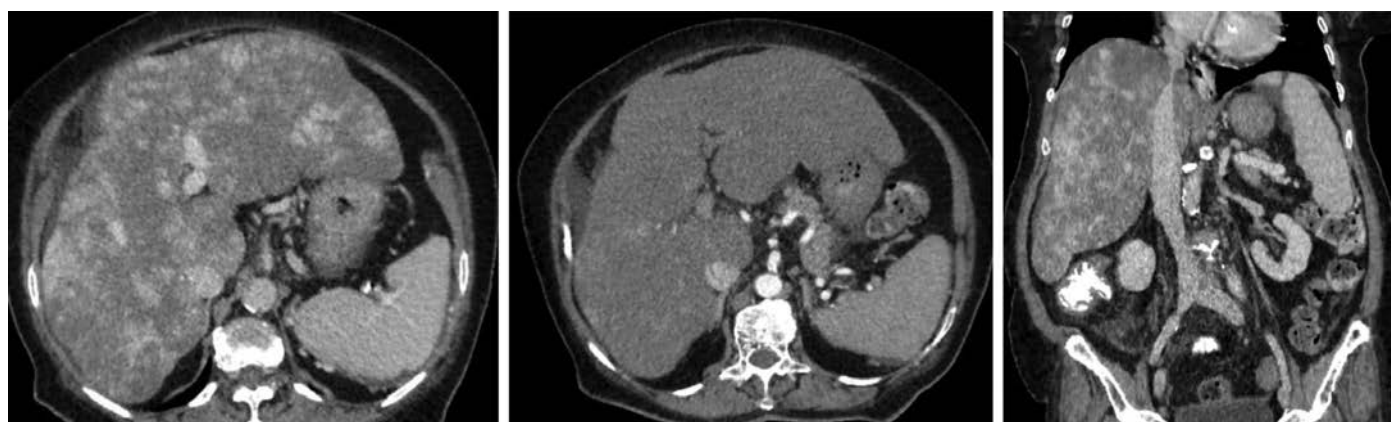


Fig. 4.189.1

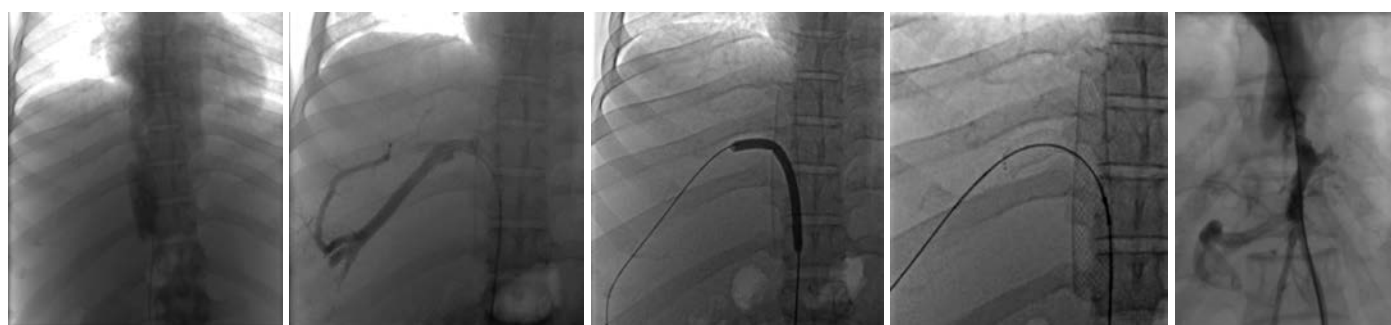


Fig. 4.189.2

Fig. 4.189.3

Fig. 4.189.4

Fig. 4.189.5

Fig. 4.189.6

Table 4.189.1: Pearls on Budd-Chiari syndrome**Budd-Chiari Syndrome**

Type 1: IVC

Type 2: Major hepatic veins

Type 3: Centrilobular veins

MRI: Comma sign; intrahepatic flow voids due to collaterals

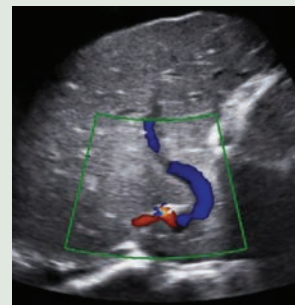
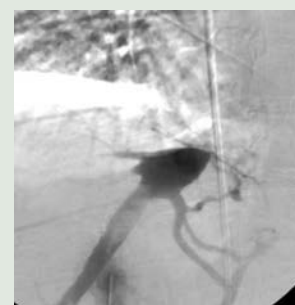
ANGIO: Spider web pattern of collaterals

Colloid scan; heterogeneous uptake with increased uptake in the Caudate lobe.

USG: Caudate lobe hypertrophy, Ascites with GB wall thickening, narrowing/obstruction of IVC, hepatic vein diameter <3 mm/thrombosed collaterals, PV diameter >12 mm/hepatofugal flow/<11 cm/sec, Hepatic artery RI >0.7

CT:

Flip-flop enhancement: Prominent enhancement of central liver around IVC and weakly enhanced periphery followed by enhanced periphery and decreased central enhancement; mottled liver enhancement.

**Fig. 4.189.7:** Doppler showing comma-shaped collaterals**Fig. 4.189.8:** Selective middle hepatic venogram showing hepatic vein and IVC confluence stenosis and multiple collaterals

and absence of infrarenal IVC), 2. Renal (accessory left renal vein, retroaortic and circumaortic left renal vein), 3. Suprarenal (absence of hepatic IVC, congenital caval stenosis and IVC membranes). IVC thrombosis in congenitally normal IVC can be due to prothrombotic states (thrombophilia, malignancy, OCP, smoking, obesity, pregnancy) or abdominal pathologies like renal cell tumor, extrinsic compression of IVC by abdominal masses like fibroids, May-Thurner syndrome (compression of left common iliac vein against lumbar vertebrae by overlying common iliac artery), IVC web or thrombotic occlusion of IVC filters and Budd-Chiari syndrome.

IVC occlusion and collaterals: IVC occlusion can be classified as peripheral/low/distal (below the renal veins), middle (between renal and hepatic veins) and central/upper/proximal (between hepatic vein and right atrium). Strictly peripheral occlusions drain via gonadal collaterals since renal and suprarenal IVC are patent. Left gonadal vein drains into left renal vein and right gonadal veins drains into inferior vena cava. In middle type occlusion, collaterals of IVC between hepatic vein and portal vein become prominent. In proximal type collaterals develop between IVC and SVC via paralumbar or azygous system.

Portacaval collaterals: Four cavoportal collaterals are identified

a. **Caval-superficial-umbilical-portal pathways:**

The vessels mentioned in superficial pathways communicate with recanalized paraumbilical vein that drains to left portal vein. These paraumbilical veins are seen in and around falciform ligament. These paraumbilical veins are divided into three groups. **Superior vein of Sappey:** Drains upper portion of falciform ligaments, it also communicates with superior epigastric veins. **Inferior vein of Sappey:** It drains lower part of falciform ligament, it also communicates with inferior epigastric veins around navel. **Vein of burrow:** It also communicates with inferior epigastric veins around navel; however it does not enter liver directly, it communicates with inferior vein of Sappey, namely **intercalary veins**. All these paraumbilical veins drain venous blood from anterior abdominal wall directly to liver. This flow dilutes the portal perfusion at these sites causing **pseudolesions**. Direction of flow through these paraumbilical veins in portal hypertension and cirrhosis is from portal vein to vena cava while in IVC obstruction it is from vena cava to portal vein.

Table 4.189.2: Common collaterals in IVC obstruction

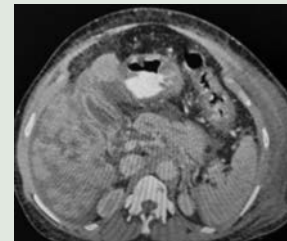
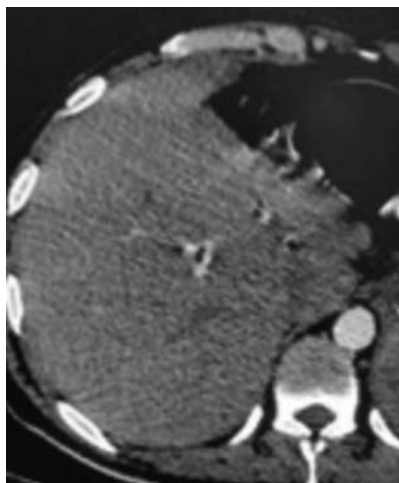
1. Deep pathway: Ascending lumbar veins anastomoses with azygous on right and hemiazygous on left. Azygous vein enters SVC at the level of T4 vertebrae. Accessory hemiazygous and hemiazygous veins joins azygous veins at the level of T8 and T9 respectively.

**Fig. 4.189.9:** Deep pathway in IVC obstruction (prominent lumbar veins)

2. Intermediate pathway: Blood returns through the periuretric plexus, periuterine and periovarian plexus connected to bilateral gonadal veins to drain into IVC ultimately.

**Fig. 4.189.10:** Intermediate pathway in IVC obstruction**Fig. 4.189.11:** Intermediate pathway in IVC obstruction

3. Superficial pathways: Blood flows from external iliac vein to inferior epigastric vein, anastomosing with superior epigastric vein, internal mammary vein and superior vena cava

**Fig. 4.189.12:** Superficial pathway in IVC obstruction**Fig. 4.189.13:** Caval-superficial-umbilical-portal pathways

- b. Caval-mammary-phrenic hepatic capsule portal pathways:** In this pathway blood flows from internal mammary vein (internal thoracic vein) to inferior phrenic vein. Inferior phrenic vein communicates with hepatic capsular veins which in turn drains into intrahepatic portal tributaries.
- c. Caval mesenteric portal pathways:** Venous blood drains from internal iliac vein to hemorrhoidal venous plexus. From there blood ascends through inferior mesenteric vein to portal vein. Pathway is located between superior rectal branches of inferior mesenteric vein and middle and inferior rectal branches of internal iliac veins
- d. Caval renal portal and caval retroperitoneal portal pathways:** Left renal vein can develop communication

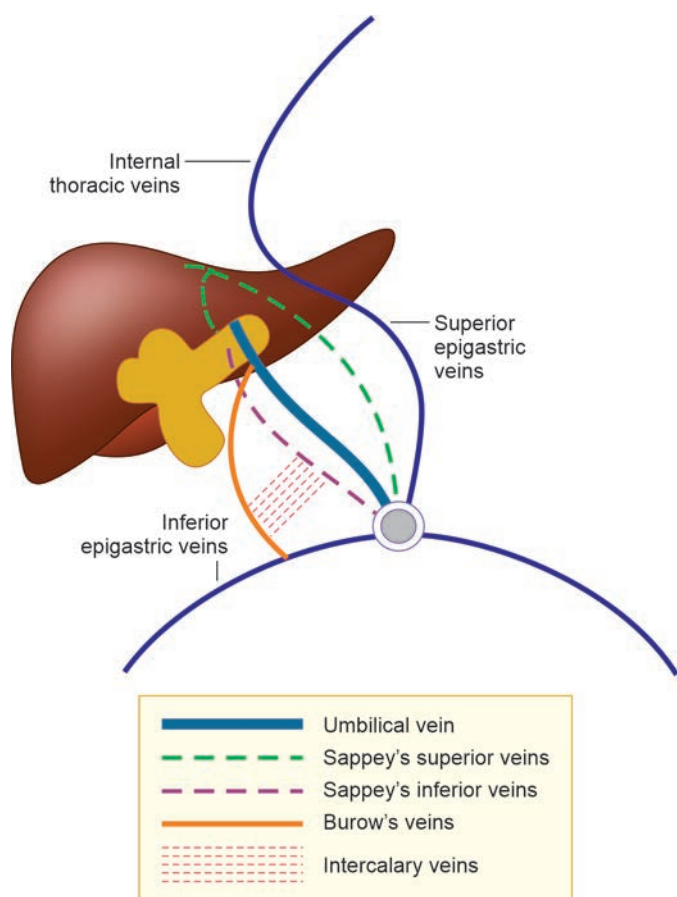


Fig. 4.189.14: Caval-superficial-umbilical-portal pathways

with splenic vein via inferior phrenic vein and epiploic veins of stomach. Other tributaries of portal system such as duodenal jejunal and pancreatic veins may communicate with retroperitoneal branches of renal or lumbar veins. These in turn are tributaries of IVC and azygous system.

IVC occlusion and Doppler imaging: Flow in IVC is slow and varies with respiration and cardiac pulsations. Prominence of caval waveform also depends on degree of hydration of patient. Renal tumors and HCC are two tumors with increased tendency to invade venous channels. Tumor thrombus extension to IVC can be detected by loss of normal cardiac and respiratory periodicity of venous waveform or in some cases tumour thrombus may be visualised as it extends to IVC lumen. In occlusion of IVC reversal of flow may be seen in caudal direction. Intrahepatic comma-shaped collaterals may be seen with bicolor sign. Superficial abdominal wall collaterals may be seen. Flow in the iliac veins may be reversed/redirected to superficial vessels.

Management of Budd-Chiari syndrome: In general, those with less advanced disease can be managed with

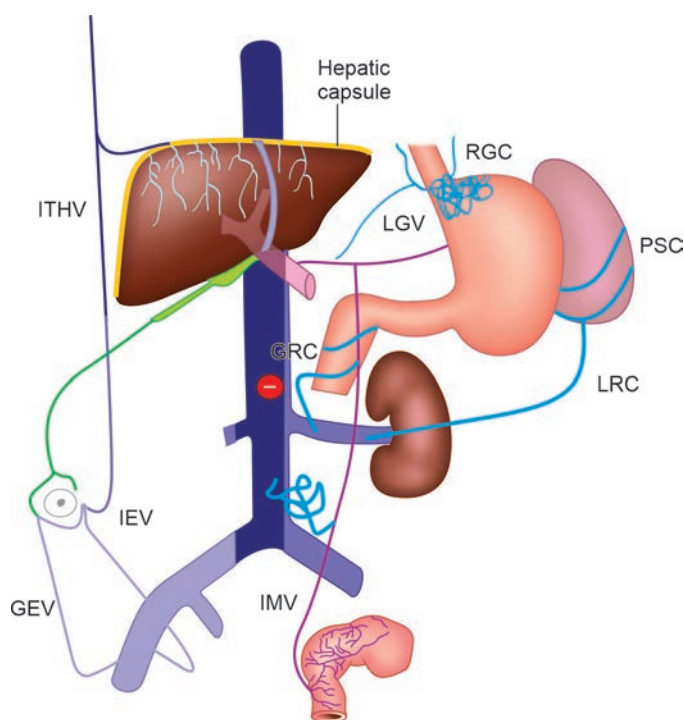



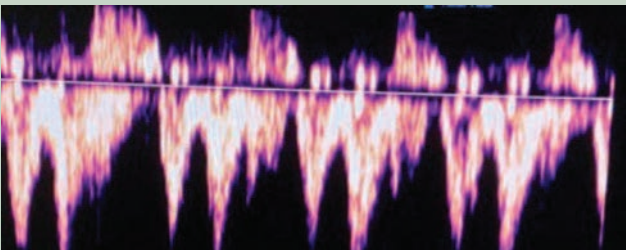

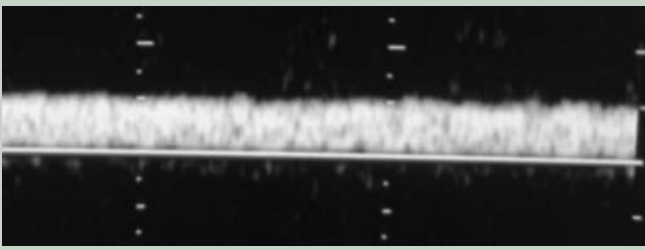
Fig. 4.189.15: Caval mesenteric portal pathways

anticoagulation alone. TIPS is used in patients with an intermediate prognosis and refractory ascites; and those with more severe disease are candidates for liver transplantation. TIPS can be performed as a bridge procedure for liver transplantation in patients with cirrhosis.

Treatment of IVC Occlusion

1. **Anticoagulation and compressive stockings:** Parenteral anticoagulation in acute phase followed by 3 to 6 months of oral anticoagulation is the protocol. Graduated compression stockings (GCS) is recommended to reduce the incidence of post-thrombotic syndrome (due to increased load of thrombus in IVC thrombosis) after acute proximal DVT.
2. **Surgical thrombectomy and systemic thrombolysis:** Many patients with proximal DVT are treated with anticoagulation alone develop disabling post thrombotic syndrome. Therefore, surgical thrombectomy and systemic thrombolysis have been tried as complimentary treatment to anticoagulation in those patients. Iliofemoral thrombectomy is a minimally invasive surgery using Fogarty's catheter, whereas IVC thrombectomy is much more invasive that requires direct caval venotomy. So IVC thrombectomy is limited only to patients with tumor-associated thrombus. Thrombolytic agents

Table 4.189.3: Normal IVC and IVC thrombosis

| Normal IVC Doppler | Loss of phase variation in IVC thrombosis |
|--|--|
|  <p>Fig. 4.189.16: Normal IVC</p>  <p>Fig. 4.189.17: Normal IVC spectral waveform</p> |  <p>Fig. 4.189.18: IVC thrombosis</p>  <p>Fig. 4.189.19: Loss of phase variation in IVC thrombosis</p> |

used are streptokinase and alteplase and these agents significantly reduced the occurrence of post-thrombotic syndrome. However, increased frequency of bleeding problems due to systemic thrombolysis prevented its widespread use.

3. Endovascular treatment of IVC thrombosis:

Localized delivery of thrombolytic agents directly into thrombus is known as CDT-catheter directed thrombolysis was considered as a potentially safer and much more effective alternate to systemic thrombolysis. In cases of chronic thrombosis, CDT is ineffective due to rapid organisation and fibrosis of clot. To overcome this issue pharmacomechanical catheter-directed thrombolysis (PMCT) is introduced. It is defined as mechanical disruption of thrombus followed by pharmacological thrombolysis. This technique reduced the dose of thrombolytic agents and

reduced the duration of hospital stay. Most recently suction thrombectomy with Angiovac system was introduced to treat patients with massive clot burden. It is basically vacuum based device for percutaneous removal of undesirable materials from intravascular system.

4. **Percutaneous treatment modalities:** a) Peripheral infusion catheter directed thrombolysis: Infusion catheters have side holes for uniform slow dispersion of therapeutic agents within the clotted segment. After thrombus is crossed with 0.035 inch guidewire, infusion catheter is advanced to clotted segment, alteplase is infused. b) Ultrasound enhanced CDT-System comprises 5.2F multilumen drug delivery catheter, ultrasound core wire and a controller. Thrombolytic agent is infused and ultrasound energy is turned on simultaneously. Ultrasound waves

Table 4.189.4: Application of HVPG in differential diagnosis of portal hypertension

| Type of portal hypertension | WHVP | FHVP | HVPG |
|-----------------------------|-----------------------------------|-----------|-----------|
| Prehepatic | Normal | Normal | Normal |
| Presinusoidal | Normal | Normal | Normal |
| Sinusoidal | Increased | Normal | Increased |
| Postsinusoidal | Increased | Normal | Increased |
| Posthepatic | | | |
| Budd-Chiari syndrome | Hepatic vein cannot be cannulated | | |
| Heart failure | Increased | Increased | Normal |

accelerate the thrombolysis process by disturbing the fibrin matrix within the thrombus, which exposes more binding sites for thrombolytic agent. c) Angiojet rheolytic thrombectomy. It works on principle of Bernoulli effect. It has three components—dual lumen catheter, pump set and a pump drive unit. Catheter consists of one lumen supplying pressurized saline to distal catheter tip, second lumen incorporating first lumen, guidewire. Pump drive unit generates high pressure pulsatile saline flow that exits the catheter tip through multiple retrograde-directed jets. These jets create a local low pressure zone (Bernoulli effect) for thrombus aspiration and provides driving force for evacuation of thrombus debris.

5. **Angioplasty/stenting and role of prophylactic IVC filters:** Fibrotic transformation of thrombus after 2 weeks of clot formation makes PMCT and CDT less effective and there comes the role of stenting. Large diameter (15 to 30 mm) self-expanding stents (to provide strong radial force) are used in IVC due to dynamic nature of cava diameter within cardiac cycle and respiratory variation. Diagnostic venogram

prior to stent placement allows better evaluation of length and location of narrowing, dominant concern of stent malposition/migration is extension of stent into right atrium resulting in potentially fatal arrhythmias. In case of stenting across ilio-caval bifurcation kissing technique stents are used. In case of external compressions causing IVC obstruction where surgery is contraindicated, stenting of IVC can be done. Major concern related to PMCT in IVC occlusion therapy is development of pulmonary embolism following the procedure. So, in most of cases prophylactic IVC filters are used to prevent embolism.

IVC/hepatic vein pressure measurement: Measurement of hepatic vein pressure serves as an indirect method of measuring portal hypertension.

$$\text{HVPG} = \text{WHVP} - \text{FHVP}$$

FHVP: Free hepatic venous pressure; WHVP: Wedged hepatic venous pressure; HVPG: Hepatic venous pressure gradient. HVPG more than 10 mm Hg indicates portal hypertension. If more than 12 mm Hg, it indicates increased risk of variceal bleed.

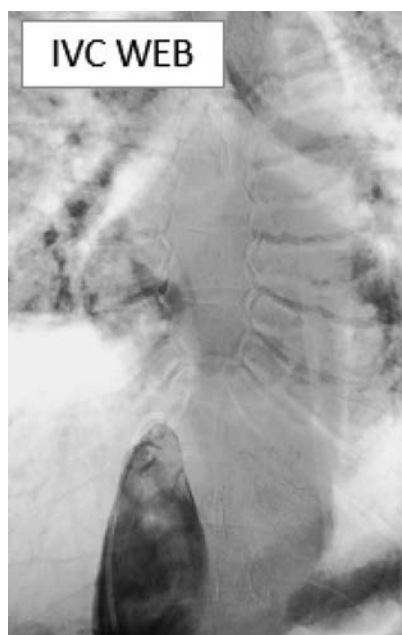


Fig. 4.189.20: IVC web

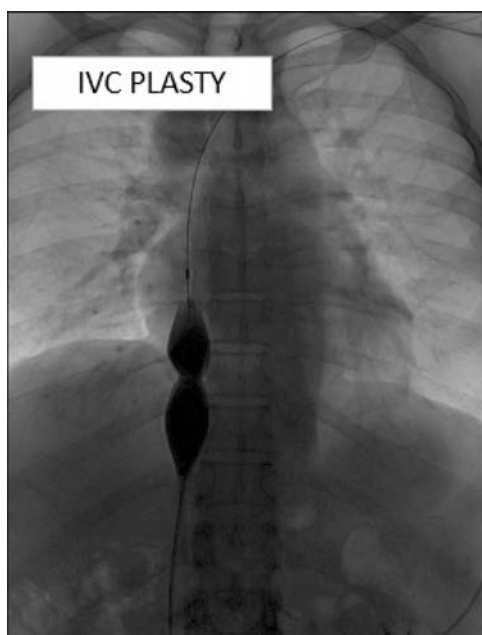


Fig. 4.189.21: IVC plasty



Fig. 4.189.22: Post-angioplasty in IVC

4.190 HEPATOBILIARY SYSTEM

Case No. 190

Clinical history: A 3 months old female presented with mass in the epigastric region for 1 month, gradually increase in size for one month.

Observation: A large well-defined hypoattenuating mass lesion is seen in the left lobe of liver, the mass lesion shows peripheral hyperenhancement on arterial phase and progressive centripetal filling on venous and delayed phase (Figs 4.190.1 to 4.190.4). Liver appears enlarged in size. No e/o portal vein/hepatic vein infiltration, no evidence of portal lymphadenopathy. Rest of the organs appear normal. No e/o tapering of the aorta below the coeliac artery level. No evidence of haemorrhage, calcification and capsular retraction.

Interpretation: A—3-month-old female child, lesion in liver, C—large well defined hypoattenuating mass lesion, the lesion shows, B—peripheral enhancement on arterial phase and progressive centripetal filling on venous and delayed phase. D—infantile hepatic hemangioma

Principal diagnosis: Infantile hepatic haemangioma.

Management: Multidisciplinary approach paediatric surgeon, oncologist—1. Reduction in size with propranolol, 2. Embolization, 3. Surgical segmental resection.

Differential diagnosis: 1. Hepatoblastoma, 2. Neuroblastoma metastasis, 3. Mesenchymal hamartoma, 4. Hepatic angiosarcoma, 5. Undifferentiated embryonal sarcoma, 6. Rhabdoid tumour of the liver, 7. Hepatocellular carcinoma, 8. Fibrolamellar variant of hepatocellular carcinoma, 9. Rhabdomyosarcoma of biliary tree

Discussion: Hepatic haemangioma is divided into: 1. Congenital: It is present since birth, does not proliferate beyond birth, 2. Infantile: Seen a few weeks after life, progressive in size.

Infantile hepatic haemangioma 85% present before 6 month of age, heterogenous, hypervascular liver mass. Associated with hemangioma in other organs and skin.

Infantile hepatic hemangiomas (previously called infantile hemangioendothelioma) occurring in fetuses and neonates and have been identified *in utero* as early as at 16 weeks of intrauterine life. It is the most common liver mass in infants (<6 months). Associations with hypothyroidism, it is due to high levels of type 3—iodothyronine deiodinase activity produced by hepatic hemangiomas and hemangiomas elsewhere in 10% of cases.

Radiographic features: In plain radiograph non-specific findings such as hepatomegaly and liver calcifications, in 15% of the cases, may be seen. Indirect signs of congestive heart failure may be present on a chest radiograph. In USG Infantile hepatic hemangioma show variable sonographic appearance and can be either hypoechoic or hyperechoic or it may display mixed echogenicity with prominent vascular channels. Color Doppler evaluation will show increased flow. In CT, there is typical peripheral enhancement with gradual filling-in. Another finding is a reduction in the aortic calibre (mid-aortic syndrome) distal to the level of the celiac axis because of the important vascular distribution toward the liver. The same thing will cause celiac trunk and hepatic artery hypertrophy. In MRI, multifocal hemangiomas are spherical lesions with homogeneous signal intensity on MRI. Large flow voids are usually present. Typical signal characteristics include: T1: hypointense T2: hyperintense They generally demonstrate the same type of enhancement vascular changes as seen on CT.

Treatment and prognosis: The natural history of infantile hepatic hemangiomas in infancy is a rapid, proliferative growth in the first six months of life, followed by regression and involution.

If the child remains asymptomatic, no treatment may be needed. If symptoms arises high output cardiac failure occur, the first line treatment is propranolol. If medical treatment not works, the lesions may be embolized to control any arteriovenous shunting causing the cardiac failure.

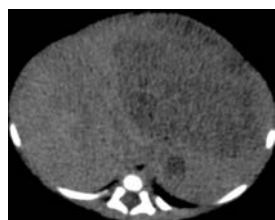


Fig. 4.190.1: Axial noncontrast CT

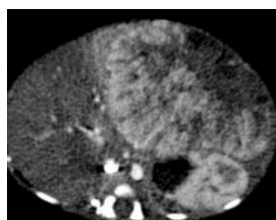


Fig. 4.190.2: CECT—arterial phase

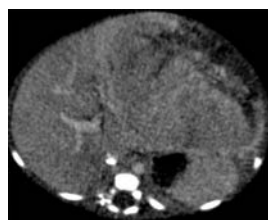


Fig. 4.190.3: CECT axial—portal venous phase

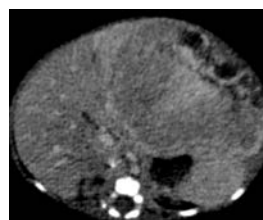


Fig. 4.190.4: CECT axial—equilibrium phase



Fig. 4.190.5: CECT axial—delayed phase

Table 4.190.1: Differential diagnosis for hepatic hemangioma


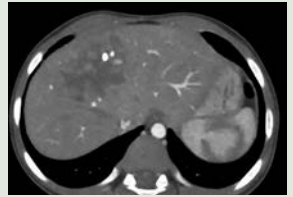
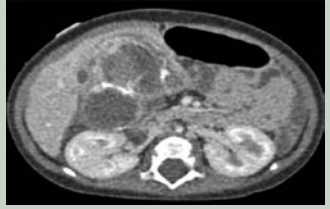
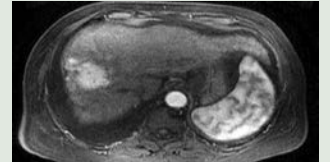
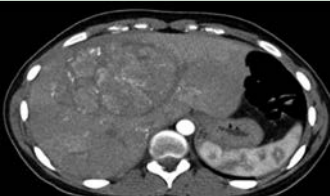

| | | |
|--|---|---|
| <p>Hepatoblastoma: Most common pediatric hepatic tumor. Age: Usually less than 5 years. AFP is elevated more than in HCC.</p> | <p>Heterogeneously enhancing mass (may be multifocal) with tumor thrombus in hepatic veins and IVC. Nodular appearance with areas of hemorrhage and necrosis. May metastasize to the lungs.</p> |  <p>Fig. 4.190.6: Hepatoblastoma</p>  <p>Fig. 4.190.7: Hepatoblastoma</p> |
| <p>Rhabdoid tumor of the liver: It is a very rare tumor, most common in infants less than one year of age, highly aggressive hepatic neoplasm.</p> | <p>Heterogeneously enhancing mass lesion with cystic changes and calcifications, if tumor rupture, peri-tumoral hematoma can occur.</p> |  <p>Fig. 4.190.8: Rhabdoid tumor of the liver</p> |
| <p>Pediatric hepatocellular carcinoma: Age group affected is predominantly more than 5 years peak incidence 15 to 18 years. The second most paediatric hepatic malignancy after hepatoblastoma, serum AFP levels are markedly elevated.</p> | <p>Multiple hyperenhancing mass lesion on arterial phase with rapid washout on portal venous and delayed phase imaging.</p> |  <p>Fig. 4.190.9: Pediatric hepatocellular carcinoma</p> |
| <p>Fibrolamellar variant of hepatocellular carcinoma: Serum alpha fetoprotein is not elevated. More common in adolescent young females</p> | <p>Well-defined variable enhanced mass with nonenhanced central scar and calcification seen</p> |  <p>Fig. 4.190.10: Fibrolamellar variant of hepatocellular carcinoma</p> |
| <p>Rhabdomyosarcoma of biliary tree (embryonal/botryoid type): CBD is the most common location: Median age of presentation is 3 years of age</p> | <p>Present as obstructive jaundice and hepatomegaly, intraductal mass with IHBR dilatation, large tumour can present with cystic areas and mimic choledochal cyst. Portal vein is displaced and no thrombosis</p> |  <p>Fig. 4.190.11: Rhabdomyosarcoma of biliary tree</p> |

Table 4.190.2: Clinical categories of hepatic vascular malformation

| Types | Multifocal | Focal | Diffuse |
|-----------------------|---|---|--|
| Clinical presentation | Manifest in first year of life. Usually asymptomatic, some have CHF | Manifest in perinatal period. Usually symptomatic, may have CHF | Manifest with mass effect. Develop abdominal compartment syndrome or severe hypothyroidism, no CHF |
| GLUT 1 reactivity | GLUT 1 positive | GLUT 1 negative | Not yet established |

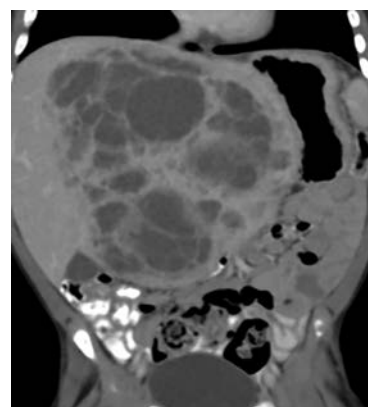
Table 4.190.3: Difference between hepatocellular carcinoma, mesenchymal hamartoma and hepatoblastoma

| Hepatocellular carcinoma | Mesenchymal hamartoma | Hepatoblastoma |
|---|--|--|
| Common malignancy in children over 5 years of age | Well-defined multi-lobulated cystic mass less than 1 year of age | More common in children less than 5 years of age |
| Underlying liver disease | Normal liver | Normal liver |
| Raised AFP level | Normal AFP level | Raised AFP level |

Table 4.190.4: Difference between infantile hepatic hemangioma and mesenchymal hamartoma

| Features | Infantile hepatic hemangioma | Mesenchymal hamartoma |
|-------------|--|--|
| Age and sex | Most common, <1 year of age, female > male, associated with CHF, hypothyroidism and involution | Second most common seen in newborn up to 2 years of age, male > female, right lobe most commonly involved. |
| USG | Multi focal—small and uniform hypoechoic Focal—large, heterogenous with central haemorrhage, necrosis, calcification Diffuse—replaced liver without discrete mass. | Predominantly cystic (multiloculated) with solid areas—echogenic and low level internal echoes |
| Doppler | Hepatic artery and vein enlarged with feeding/draining vessels within and surrounding lesion. Tapering of aorta below coeliac axis origin | Relatively a little blood flow to solid areas and septa. |
| NECT | Well-defined hypodense mass with speckled calcification. | Complex cystic mass, no calcification |
| MRI | T1—hypointense, T2—hyperintense/heterointense, flow void within and surrounding lesion | Solid—T1 and T2 hypointense, cystic—T2 hyperintense, variable in T1 (depends on protein content) |
| Arterial | Intense peripheral nodular or corrugated enhancement and progressive centripetal fill in. | Enhancement of septa and solid areas seen |
| Tc99m | Early uptake with delayed photopenic (sulphur colloid) and delayed tracer accumulation (RBC) | |

Alpha fetoprotein is a glycoprotein, normally elevated during gestation in fetus and mother and after birth with levels falling rapidly up to 6 month of age. First day of life value range from 40000 ng/ml (in term baby) to 1,60000 ng/ml (in preterm baby), AFP value decreased by 50% at 4th week of life. After 2 years of age AFP value reaches adult value of 0–8 ng/ml. Raised in hepatoblastoma and hepatocellular carcinoma.

**Fig. 4.190.12:** Mesenchymal hamartoma

| Table 4.190.5: Classification of liver tumors | | |
|---|--|---|
| | <i>Paediatric</i> | <i>Adult</i> |
| Benign | | |
| Solid | Infantile haemangioma Focal nodular hyperplasia Hepatic adenoma | Hepatocellular adenoma, hepatocellular hyperplasia, focal nodular hyperplasia, lipoma, angiomyolipoma, myelolipoma, leiomyoma, fibroma |
| Cystic | Polycystic liver disease Mesenchymal hamartoma Lymphangioma | Simple hepatic cysts Biliary cystadenoma Bile duct adenoma |
| Multiple | Polycystic liver disease | Simple hepatic cysts Nodular regenerative hyperplasia |
| Malignant | | |
| Solid | Hepatoblastoma Hepatocellular carcinoma (HCC) Embryonal rhabdomyosarcoma | Hepatocellular carcinoma (HCC) Fibrolamellar carcinoma, cholangiocarcinoma, angiosarcoma Epithelioid hemangioendothelioma Leiomyosarcoma, primary lymphoma |
| Cystic | Undifferentiated embryonal sarcoma | Cystadenocarcinoma |
| Multiple | Metastasis, neuroblastoma | Metastasis, multifocal HCC |

4.191 HEPATOBILIARY SYSTEM

Case No. 191

Clinical history: 62-year-old male with history of loss of weight and fullness in right upper quadrant of the abdomen. On examination, liver was palpated below the costal margins.

Radiological techniques and observation: Axial (Figs 4.191.1, 4.191.3) and sagittal sections of CECT abdomen (Fig. 4.191.2) revealed a large mass (10 cm) in the right lobe of liver. The mass had peripheral nodular discontinuous pattern of enhancement equal to the hepatic vasculature in that phase with progressive centripetal filling.

Figure 4.191.4—axial T2-weighted MR image shows the large T2 hyperintense lesion right lobe of liver.

Interpretation: Large heterodense mass lesion (>10 cm) in right lobe of liver showing peripheral nodular discontinuous pattern of enhancement following the hepatic vasculature with centripetal type of filling and pooling of contrast towards the center in delayed images.

Principal diagnosis: Giant cavernous hemangioma. The differential diagnosis is considering delayed centripetal filling from periphery to center: Cavernoma, cholangio carcinoma, sclerosing hemangioma, colonic primary carcinoma with liver metastasis.

Considering central scar: Fibrolamellar variant of HCC, focal nodular hyperplasia.

Examples of central to peripheral centrifugal type of enhancement: Budd-Chiari syndrome, atypical hemangioma.

Examples of flash filling type of enhancement: Small capillary hemangioma (<2 cm), small HCC, hypervascular metastasis (neuroendocrine tumor, melanoma and thyroid Ca).

Further management: Preoperative embolization of the mass then performed the patient was having a

normal celiac vascular anatomy at MR imaging. Pre-embolization angiography of the hepatic artery shows the classic snowy tree or cotton wool appearance of a hemangioma. Then surgical excision is done after embolization if there is recurrence.

Angiography signs of liver lesions: Corkscrew sign: Tortuous hepatic arteries in liver cirrhosis, spoke wheel pattern: Focal nodular hyperplasia (from central to periphery), thread and streak sign—HCC, spider web pattern—intra-hepatic collaterals in Budd-Chiari syndrome.

Discussion: The term giant hemangioma is defined as the lesions larger than 10 cm. Hemangiomas are the most occurring benign tumors of the liver. MR imaging also has high sensitivity (98–100%) and specificity (92–98%) in the diagnosis of hemangiomas.

Age of presentation: Adults. Females more than males, associated with FNH, VHL, Klippel-Trenaunay syndrome.

Histopathology: Large vascular channels with blood.

Plain CT: Usually low density lobulated mass.

CECT: Uniform enhancement if <1 cm. Peripheral nodular enhancement in arterial phase with progressive centripetal filling in of contrast, isodense compared with blood pool in all phases—not seen in >5 cm lesion due to thrombosis.

MRI: Lesions shows low signal intensity on T1-weighted images and markedly high signal intensity on T2-weighted images; markedly hyper with increase in TE, 'light bulb sign' hyper in DWI due to T2 shine through, hypointense internal septa are commonly seen in giant hemangiomas. Many lesions have a central scar, which remains hypointense on contrast-enhanced images. It is not uncommon for giant hemangiomas to have central loculations or clefts of high signal intensity on T2-weighted images.



Fig. 4.191.1



Fig. 4.191.2



Fig. 4.191.3

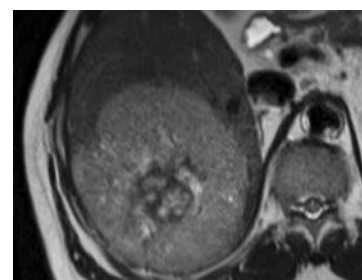


Fig. 4.191.4

Table 4.191.1 Differential diagnosis for giant hemangioma

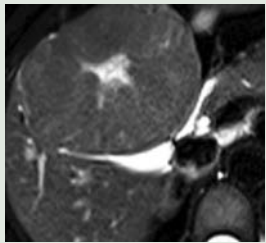
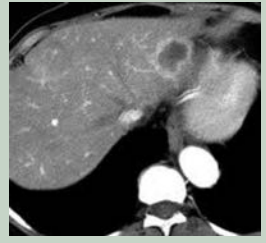
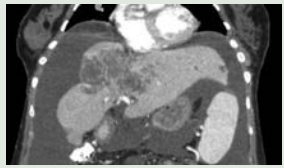
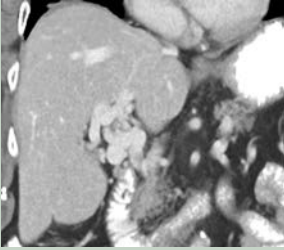
| | | |
|---|---|---|
| <p>Focal nodular hyperplasia (FNH) is a regenerative mass lesion of the liver and the second most common benign liver lesion. Young to middle age with female predilection.</p> <ul style="list-style-type: none"> • Telangiectatic variant: Most common • Mixed hyperplastic and adenomatous variant • Lesions with large cell hepatocellular atypia | <p>NECT: Hypo to isodense CECT: Arterial phase-enhancing lesion with non enhancing central scar Venous phase-washout (isodense to liver) Delayed phase-enhancement of central scar. MRI-T2 hyperintense scar. Central scar can also occur in giant haemangioma, it is differentiated from FNH by delayed post-contrast enhancement of the central scar in FNH. Liver-specific contrast agents (eovist, meglumine) show uptake</p> |  <p>Fig. 4.191.5: Focal nodular hyperplasia</p> |
| <p>Sclerosing/sclerosed hepatic hemangiomas also known as, hyalinised hepatic hemangiomas, are a rare variant of hepatic hemangioma.</p> | <p>T1: Hypointense T2: Variable T2 signal intensity, less than that of a typical hemangioma, increasing sclerosis/fibrosis appears to correspond with increasing T2 hypointensity. Peripheral enhancement is usually a thin rim in late phases. Capsular retraction has been described in some hyalinised /sclerotic hemangiomas.</p> |  <p>Fig. 4.191.6: Sclerosed hepatic hemangiomas</p> |
| <p>Intra-hepatic cholangiocarcinoma: 2nd most common primary liver malignancy. Age: 50–60 years; M>F; abdominal pain, jaundice, weight loss, palpable mass. Usually mass forming type, periductal type occurs as intraparenchymal lesion.</p> | <p>CECT: Early peripheral hilar cholangio carcinoma enhancement and delayed central enhancement in centripetal fashion with dilated intrahepatic biliary radicals. NECT: Capsular retraction due to fibrosis and punctuate calcifications. MRI: T1 hypo and T2 Hyperintense. Enhancement pattern similar to CECT.</p> |  <p>Fig. 4.191.7: Intra-hepatic cholangio-carcinoma</p> |
| <p>Portal cavernoma is a sequelae of portal vein thrombosis and is the replacement of the normal single channel portal vein with numerous tortuous venous channels.</p> <ul style="list-style-type: none"> • Atrophy of the left lateral segment (segments 2 and 3) • Whereas hypertrophy is more common in cirrhosis • Hypertrophy of segment IV, whereas atrophy is more common in cirrhosis • Hypertrophy of the caudate lobe which is also seen in cirrhosis | <p>CECT: Numerous vascular structures in the region of the portal vein, which enhance during the portal venous phase, and not during the arterial phase (distinguishing it from an arteriovenous malformation). Doppler: Cavernous transformation of portal vein, hepatopetal flow and portosystemic collaterals</p> |  <p>Fig. 4.191.8: Portal cavernoma</p> |
| <p>Fibrolamellar variant of HCC: Refer to case 192</p> | | |

Table 4.191.2: MRI approach to liver lesions

| | |
|---|--|
| T1 hyperintense tumors | HCC, dysplastic nodule, hemorrhagic tumors, melanoma Lesions in hemochromatosis liver, thrombosed portal vein |
| T2 hypointense tumors | Regenerating nodules |
| T2 hyperintense lesion (lesion has CSF intensity) | Cystic metastases, T2 light bulb sign—hemangioma, cystadenocarcinoma |
| Capsule | HCC, adenoma |

| Table 4.191.3: Scar tumors in liver | |
|--|--|
| <ul style="list-style-type: none">• Focal nodular hyperplasia• Fibrolamellar carcinoma• Well-differentiated hepatocellular Ca• Hypervascular metastasis• Intrahepatic cholangio Ca | <ul style="list-style-type: none">• Lipoma• Angiolipoma• Hepatocellular adenoma/ carcinoma• Liposarcoma metastasis• Focal fatty change |

Angiogram: Cotton wool/snowy tree appearance.

Nuclear scintigraphy: With Tc 99m RBC shows increased activity in delayed, 1–2 hr. Technetium-99m—labeled red blood cells. Scintigraphy can be used to confirm the diagnosis of a lesion seen at US or CT, but this technique is less sensitive for lesions smaller than 2 cm.

4.192 HEPATOBILIARY SYSTEM

Case No. 192

Clinical history: A 30-year-old female, with complaint of right upper abdominal pain.

Radiological techniques and observation: The figures are six selected axial images (Figs 4.192.1 to 4.192.6) from a CT scan of the liver in plain, arterial and portal venous phases. There is a well-defined hypodense lesion with internal hyperdense areas probably haemorrhage noted in segments 8, 7 and 4A of liver. Following intravenous contrast, the lesion demonstrates heterogeneous enhancement in arterial phase with washout on portal venous phases. Non-cirrhotic liver background noted. No other abnormality is seen in the visualized sections of the abdomen.

Interpretation: A—30 years old female, lesion in liver, C—Well-defined hypodense lesion with internal hyperdense areas probably haemorrhage noted in segments 8, 7 and 4A of liver. Following intravenous contrast, the lesion demonstrates, B—enhancement in arterial phase with washout on portal venous phases. No other abnormality is seen in the visualized portions of the abdomen. D—hepatic adenoma.

Principal diagnosis: With these imaging findings, principal diagnosis of benign hepatic adenoma was made.

Differential diagnosis: Hepatic hemangioma (post-acoustic enhancement due to blood sinusoids), angiolioma, focal nodular hyperplasia.

Management: Surgical excision due to increased risk of haemorrhage and necrosis. Patient referred to surgical gastroenterologist.

Discussion: Hepatic adenoma: Solitary Benign tumour, common in young female on oral contraceptive pills, other risk factors are obesity, metabolic disorders, diabetes mellitus, glycogen storage disorders (multiple and has malignant potential) and anabolic steroids. Commonly located in right lobe (subcapsular) and tendency to bleed, contains macroscopic fat. Calcification is rare, can be seen in areas of necrosis (old hemorrhage). Hepatic adenoma can be of four types: 1. Inflammatory-most common subtype, 2. HNF-1 alpha mutated (occur in female on OCP), 3. Beta catenin mutated (GSD, anabolic steroids), 4. unclassified. Imaging: USG: Usually hyperechoic due to hemorrhage and fat. Color Doppler shows peripheral and intra tumoural vessels. NECT: Heterodense lesion with areas of low (fat) and high attenuation (hemorrhage). CECT: Enhancing in arterial phase (homogeneous/heterogeneous depends on the presence of fat and hemorrhage) and washout in portal



Fig. 4.192.1



Fig. 4.192.2



Fig. 4.192.3



Fig. 4.192.4



Fig. 4.192.5

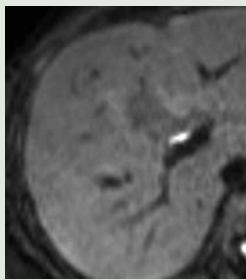
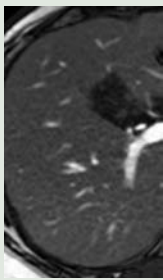
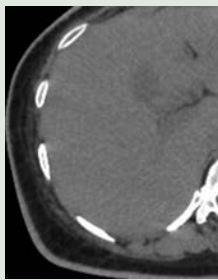
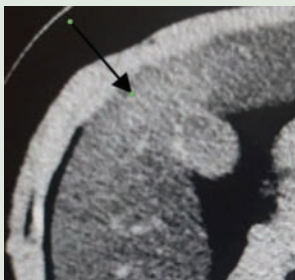


Fig. 4.192.6

Table 4.192.1: Benign and malignant fat containing liver lesions

| <i>Benign fat containing lesions</i> | <i>Malignant fat containing lesions</i> |
|--|---|
| Focal fatty change, hepatic angiomyolipoma, focal nodular hyperplasia, hepatic lipoma, pseudolipoma of the Glisson capsule, xanthomatous lesion of Langerhans cell histiocytosis, hepatic adenoma, hepatic teratoma, hepatic adrenal rest tumor: Can rarely have malignant transformation, postoperative: Pack using omental tissue. | Hepatocellular carcinoma Primary or secondary liposarcoma. |

Table 4.192.2: Difference between focal fat sparing, focal fatty steatosis and focal liver lesion

| Table 4.192.1: Difference between focal fat sparing, focal fatty steatosis and focal liver lesion | | | | |
|--|--|--|--|---|
| <i>Focal fat sparing</i> | | <i>Focal fatty steatosis</i> | <i>Focal liver lesion</i> | |
| Localized absence of increased intracellular hepatic fat, in a liver otherwise fatty in appearance | | Small areas of liver steatosis | Focal areas of hyper or hypoattenuation | |
| Adjacent to the porta hepatis (segment IV) Gallbladder fossa Adjacent to the falciform ligament Subcapsular parenchyma | | Peri-ligamentous, peri-portal distribution of lesions | Can occur anywhere | |
| Absence of distortion of vessels that run through the region | | Presence of non-distorted, traversing blood vessels (third inflow phenomenon) | Distorted vessel + | |
| Absence of mass effect | | Absence of mass effect | Mass effect + | |
| Non-hyperechoic region in the generalised hyperechoic liver | | Hyperechoic region with geographic borders | Well-defined hyper/hypoechoic—depends on type of lesion | |
| Lack of reduced attenuation on pre- and post-contrast than rest of liver. | | Reduced attenuation than rest of liver | Depends on type of lesion | |
| T1-isointense T2-isointense In/out phase—no signal loss in out of phase imaging, hepatic contrast agents—appear bright and better delineated | | T1: Hyperintense T2: Mild hyperintense In/out phase—Signal loss + on out of phase images | Depends on type of lesion | |
|  | |  |  |  |
| Fig. 4.192.7: Focal fatty sparing | | Fig. 4.192.8: Focal fatty steatosis | Fig. 4.192.9: Focal fatty steatosis | Fig. 4.192.10: Focal fatty sparing |

venous and delayed phase, enhancing pseudo capsule seen in delayed phase (helps in differentiating hepatic adenoma from FNH). MRI: Variable intensity on T1 and T2 weighted images. No uptake in hepatobiliary phase. Sulphur colloid: photopenic.

Treatment: Surgical resection, because of the risk of hemorrhage and malignant transformation.

A variety of benign and malignant liver lesions may contain macroscopic and/or intracytoplasmic fat

in sufficient quantities enabling characterization on imaging studies. Most fat containing liver lesions (80%) in patients with cirrhosis are malignant, most of which are hepatocellular carcinoma.

A hyperechoic liver lesion on ultrasound can arise from a number of entities, both benign and malignant. Benign: Hepatic hemangioma, focal nodular hyperplasia, hepatic adenoma. Malignant: Hepatic metastasis, hepatocellular carcinoma and cholangiocarcinoma.

Table 4.192.3: Chemical shift imaging in liver (1.5 TESLA)

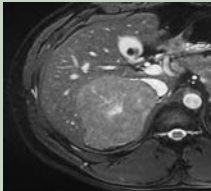
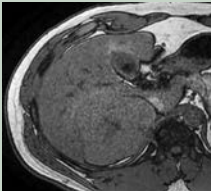

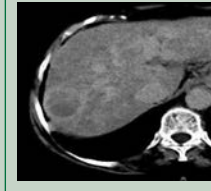

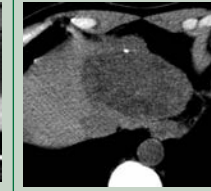
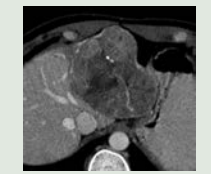
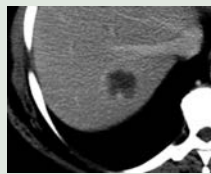
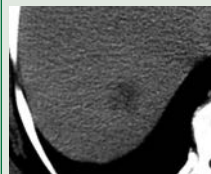
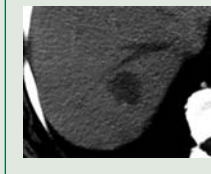
| <i>Inphase</i> | <i>Opposed phase</i> | <i>Inference</i> |
|-----------------------------|---------------------------|--|
| TE: 4.4 msec Water + Fat | TE: 2.2 msec Water–Fat | - |
| Hyperintense | Hyperintense | No significant fat: Normal. |
| Hyperintense | Hypointense | Significant fat (fatty liver, focal fatty lesions) |
| Hypointense | Hyperintense | Iron deposition (hemochromatosis) |

Table 4.192.4: Difference between focal nodular hyperplasia, hepatic adenoma, hepatocellular carcinoma, FLCC and hemangioma

| | <i>Focal nodular hyperplasia</i> | <i>Hepatic adenoma</i> | <i>Hepatocellular carcinoma</i> | <i>FLCC</i> | <i>Hemangioma</i> |
|--|--|--|--|--|--|
| Age/Presentation | 3 to 4th decade, F:M = 8:1, asymptomatic or vague pain. | Women in child bearing age, use of OCPs, steroids, diabetes mellitus, pregnancy and glycogen storage diseases. | 6th to 7th decade, M:F = 2.5:1. In Children >5 years, 44% in macronodular cirrhosis (post-hep B, alcoholic), Carcinogens, inborn errors of metabolism. | Seen in young age (20 to 40 years) No gender predilection. Non cirrhotic liver. | Adult females. Associated with FNH, VHL, Klippel-Trenaunay syndrome. Asymptomatic. |
| Histopathology | Congenital vascular malformation/ Reparative proliferation of hepatocytes with fat, Kupffer cells, biliary ducts with no drainage and absent portal veins. | Hepatocytes arranged in sheets with no intervening bile ducts or portal vein and abnormal Kupffer cells. | Expansive encapsulated pattern, infiltrative pattern. | Well-circumscribed well-differentiated tumor with dense background in which tumor cells separated by sheet like fibrous bands. | Large vascular channels with slow blood. |
| CT | Iso to mild hyper- dense with mass effect. No calcification | Isodense mass with fat (7%), necrosis (40%), hemorrhage (50%) | Hypodense mass/ diffuse infiltrating. | Single large tumors with dense fibrotic bands forming central scar. Calcification (35–65%). | Usually low density lobulated mass. |
| MRI | T1-Iso to Hypo, T2-Iso to hyperintense lesion mass Central scar is T1-hypo and T2-hyperintense Scar is more T2 hyperintense than mass | Variable intensity on T1 and T2 weighted images. | T1 hyperintense, if >1.5 cm and T2 hyper/hypo if well-differentiated. Thin hypointense capsule in T1 and T2 ring sign. | Hypointense central scar on all sequences (T2 hypointense) | T1 hypo, T2 hyperintense lesion showing increasing hyperintensity with increasing TE (light bulb sign), hyperintense in DWI due to T2 shine through. |
| CECT/MRI Early arterial/ angiographic phase (20 sec) | Central nodal artery supplying from the centre to the periphery. | - | Neovascularity and multiple feeding arteries. | Heterogenous enhancement of mass. No enhancement of scar. | - |
| Arterial phase (40 sec) | Hyperenhancing mass except the scar (hypoenhancing central scar) | Hyperenhancing mass | Homogeneous enhancement in <2 cm and heterogeneous in >2 cm lesion | Arterial phase heterogenous enhancement of the mass. Scar—no enhancement. | Uniform enhancement if <1 cm. Peripheral nodular enhancement. |

(Contd.)

Table 4.192.4: Difference between focal nodular hyperplasia, hepatic adenoma, hepatocellular carcinoma, FLCC and hemangioma (Contd.)

| | <i>Focal nodular hyperplasia</i> | <i>Hepatic adenoma</i> | <i>Hepatocellular carcinoma</i> | <i>FLCC</i> | <i>Hemangioma</i> |
|---|---|---|---|---|--|
| Portal venous phase (70 to 80 sec) | Isodense mass and scar | Iso to hypo | Rapid washout, inhomogeneous | Rapid washout except the scar | Progressive centripetal filling in of the contrast to which is similar to blood pool in all phases |
| Equilibrium phase (180 sec) | Hyperenhancement of central scar (delayed washout due to myxomatous tissue) | Hypo with delayed enhancing pseudocapsule | Iso with enhancing capsule. Peripheral washout sign-peripheral early washout. | Hypoenhancing with delayed enhancing scar | |
| Delayed phase (6 to 15 min) | Persistent enhancement of central scar | - | - | Delayed enhancement in 20% cases | Persistence of contrast in the lesion |
| Hepatobiliary phase (MRI) | Lesion enhances in hepatobiliary phase, less than liver parenchymal enhancement | Hypointense | Iso to hypointense | Heterogenous arterial enhancement, iso to hypointense portal venous/delayed phase | Hypointense |
| Sulphur colloid uptake | Normal/increased/decreased (each 33%) | Photopenic (non-functioning Kupffer) with uptake in rim (compressed tissue) | Cold spot | No accumulation of sulfur colloid in the scar | Cold spot |
| Tc HIDA | Normal/increased | Increased | Cold spot/atypical | Normal/Increased | |
| Other characteristics | No true capsule. Central scar present. | Pseudocapsule, increased hemorrhage, necrosis and fat | SPIO (taken up by Kupffer cells) and Gd in late arterial phase improves pick up. Increased uptake with gallium scan | No contrast uptake with liver specific contrast media like eovist | Angio: Cotton wool/snowy tree. With Tc 99m RBC shows increased activity in delayed (1–2 hr image) |
| Treatment | Conservative management | Surgical resection | Partial hepatectomy, TACE, TARE | Partial hepatectomy | Surgical resection: Abdominal pain and size greater than 5 cm |
|  |  |  |  |  |  |
| Fig. 4.192.11: Focal nodular hyperplasia (T2 hyperintense central scar) | Fig. 4.192.12: Focal nodular hyperplasia | Fig. 4.192.13: Hepatic adenoma | Fig. 4.192.14: Hepatocellular carcinoma | Fig. 4.192.15: Hepatocellular carcinoma | Fig. 4.192.16: Fibrolamellar variant of HCC |
|  |  |  |  | | |
| Fig. 4.192.17: Fibrolamellar variant of HCC | Fig. 4.192.18: Hemangioma (venous phase) | Fig. 4.192.19: Hemangioma (delayed phase) | Fig. 4.192.20: Hemangioma (arterial phase) | | |

4.193 HEPATOBILIARY SYSTEM

Case No. 193

Clinical history: 30-years-old female presented with vague abdominal pain for 1 month duration.

Imaging technique and observation: USG abdomen image (Fig. 4.193.1) shows a well-defined slightly hypoechoic lesion from the surrounding liver tissue that causes slight distortion of the outer liver contour. No evidence of post-acoustic enhancement. No evidence of cystic changes. No evidence of calcification. MR abdomen with pre-contrast T2 and T1 weighted image (Figs 4.193.2 to 4.193.3) given.

Axial T2-weighted image shows a large lobulated lesion that is isointense relative to the surrounding liver parenchyma. The central scar has slightly higher signal intensity than the lesion. In axial T1-weighted images the lesion appears isointense with hypo intense central scar.

Interpretation: A—30 years old female, lesion in liver, B—Well defined hypoechoic lesion without posterior enhancement or calcification, C—T2 isointense lesion with hyperintense central scar, D—Focal nodular hyperplasia.

Principal diagnosis: Focal nodular hyperplasia.

Differential diagnosis: Hepatic adenoma, fibrolamellar variant of HCC, hepatic cavernous hemangiomas, hyper vascular metastasis.

Further management: Specific hepatobiliary MR contrast agents (Gadoxetate), specific super-paramagnetic iron oxide-based [e.g., ferucarbotran (Resovist)] and manganese-based [i.e., mangafodipir trisodium (Teslascan)]. Bright, homogeneous enhancement of FNH on arterial phase and prolonged enhancement of entire FNH on hepatobiliary phase (delayed—20 minutes to 2 hours depends on the contrast agent). Hepatobiliary MR contrast media are targeted at the Kupffer cells and hepatocytes, these help to demonstrate the hepatocellular

origin of the lesions. The Kupffer cells show uptake of ferucarbotran and lower the signal intensity of the lesions as well as the surrounding liver on T2- and T2*-weighted images.

Nuclear medicine: Radionuclide scans best demonstrate Kupffer cell activity.

Technetium sulfur colloid (TcSC) shows normal or increased uptake in 60% it is almost pathognomonic.

Tc-HIDA scan (hepatic iminodiacetic acid) shows normal or increased uptake, prolonged enhancement seen in (80%) of cases.

Treatment: Asymptomatic lesion—conservative management. FNH with atypical imaging features—percutaneous guided biopsy and follow-up. Symptomatic patients due to compression of adjacent structures or hepatic capsular stretching—trans-arterial embolization or surgical resection may be considered.

Discussion: Focal nodular hyperplasia (FNH) is the second most common benign liver tumor after hemangioma. FNH is classified into two types: classic (80% of cases) and nonclassic (20%).

Magnetic resonance (MR) imaging has higher sensitivity and specificity for FNH demonstrates intense homogeneous enhancement during the arterial phase of gadolinium-enhanced imaging and enhancement of the central scar during later phases. Various atypical Features of FNH on MRI are: Heterogeneous appearance on both T1- and T2-weighted sequences due to the presence of small hemorrhagic foci, sinusoidal dilatation or fatty infiltration. High protein concentrations, blood degradation products or copper accumulation may result in T1 hyperintensity. An extremely small or undetectable scar on CT (16% to 40%) and MRI (22%) due to obliterative vascular hyperplasia of the central scar. The presence of a pseudo-capsule due to compressed adjacent hepatic parenchyma, FNH rarely shows intra-



Fig. 4.193.1

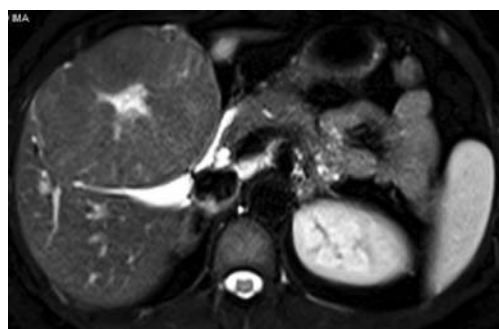


Fig. 4.193.2

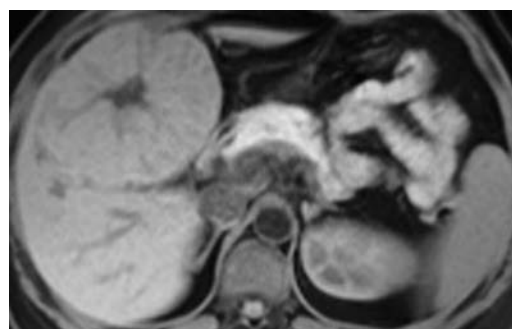


Fig. 4.193.3

Table 4.193.1: Differential diagnosis for focal liver lesion

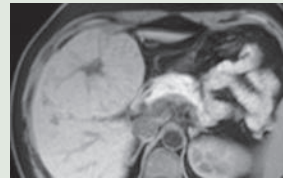
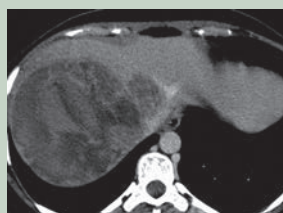



| | | |
|---|--|---|
| Focal nodular hyperplasia: 2nd most common benign tumor, usually in young women. Common location—usually subcapsular and rarely pedunculated. Usually solitary lesion (80%); multiple (20%) | Immediate, intense, homogeneously enhancing lesion on arterial phase followed rapidly by isodensity on venous phase with delayed enhancement of scar. Prolonged enhancement of entire FNH on MR hepatobiliary phase (delayed ~ 20 minutes) |  |
| Hepatic adenoma: Common in young woman in 3rd to 4th decades with increased risk in oral contraceptive and anabolic steroid users. Common location: Subcapsular region of right lobe of liver (75%) and intraparenchymal or pedunculated (10%) | Hypervascular tumor containing fat, hemorrhage and encapsulation Gadoxetate-enhanced MR: Shows no substantial uptake or retention. |  |
| Fibrolamellar hepatocellular carcinoma: Slow-growing tumor that usually arises in normal (noncirrhotic) liver. α -fetoprotein – within normal limits. Most patients present in 2nd–3rd decade of life | Usually large (>12 cm) heterogeneous mass Has “aggressive” features Biliary, vascular, and nodal invasion and metastases (70%) of cases at time of diagnosis, large fibrous scar with calcification Hypointense scar on T2WI |  |
| Cavernous hemangioma Benign tumor having multiple vascular channels lined by single layer of endothelial cells supported by thin fibrous stroma, More common in postmenopausal women: Kasabach-Merritt syndrome: Multiple hemangiomas throughout body with thrombocytopenia | Typical hemangioma—2–10 cm CECT: Arterial phase: Early peripheral, nodular or globular, discontinuous enhancement Portal phase: Progressive centripetal enhancement to uniform filling, still isodense to blood vessels Delayed phase: Persistent complete filling |  |
| Hypervascular metastasis: Most common malignant tumor of liver. Important primary tumors include endocrine (islet cell), carcinoid, melanoma, thyroid, breast and renal carcinomas and pheochromocytoma. Commonly affects older patients. | Hyperdense in late arterial phase images. Hypodense (washout) during portal venous and delayed phases. In MR hepatobiliary phase metastases are conspicuous as hypointense focal agents. While rest of normal liver is brightly enhanced. Treatment: Chemo- or radioembolization |  |

Fig. 4.193.4: Focal nodular hyperplasia**Fig. 4.193.5:** Hepatic adenoma**Fig. 4.193.6:** Fibrolamellar hepatocellular carcinoma**Fig. 4.193.7:** Cavernous hemangioma**Fig. 4.193.8:** Hypervascular metastasis**Table 4.193.2: Characterization of liver lesions using MR hepatobiliary phase**

| Lesion | Hepatobiliary phase |
|---------------------------|--|
| Focal nodular hyperplasia | Iso to hyperintense with prolonged enhancement |
| Hepatic adenoma | Hypointense |
| Hemangioma | Iso/hypointense |
| Metastasis | Defect |
| Cholangiocarcinoma | Cloud appearance |

lesional steatosis. Telangiectatic FNH, an uncommon entity but the most common among non-classic FNHs. Multiple lesions, which are found in 20% of cases and are mostly atypical. Multiple FNH syndrome is defined as consisting of two or more FNHs in combination with hepatic liver hemangioma or vascular malformations or intracranial tumors.

4.194 HEPATOBILIARY SYSTEM

Case No. 194

Clinical history: A 45-year-old diabetic patient came with the history of right upper quadrant pain, high grade fever for the past 4 days.

Radiological techniques and observation: Plain CT axial section of abdomen, Figs 4.194.1 and 4.194.2 show multiple well-defined hypodense lesions in right lobe of liver involving segments 5, 6, 7, 8. Left lobe appears normal. Mild hepatomegaly noted. No evidence of internal components/septations/calcification. No intrahepatic biliary dilation. On contrast administration, the lesions appear hypodense at centre with peripheral rim enhancement, and a thin outer ring of hypoattenuation. No perihepatic collection noted. No perihepatic nodes seen.

Interpretation: Multiple peripherally enhancing well-defined hypodense lesions in right lobe of

liver with hypodense centre and a thin outer ring of hypoattenuation in clinical background of acute upper abdominal pain and fever.

Principal diagnosis: Multiple pyogenic liver abscess

Differential diagnosis: Cystic metastasis, cystic liver disease, hydatid cyst, biliary cystadenoma, hepatic peliosis, hepatic hemangioma.

Discussion: Liver abscess: Pyogenic liver abscess: often multiple. Spread through portal vein, involve both lobes of liver. Causative organism: Gram-negative aerobic and anaerobic: *E. coli*, *Klebsiella pneumonia*, *Bacteroides*. Gram-positive: Anaerobic and microaerophilic streptococci, enterococci. Fungal abscess: Typically seen in the immunocompromised population, multiple <2 cm lesion. Amoebic abscess: Often single (more common in subdiaphragmatic location, segment 7) causative organism: *Entamoeba histolytica*.



Fig. 4.194.1

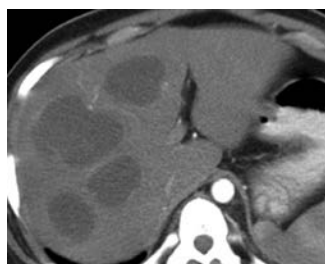


Fig. 4.194.2



Fig. 4.194.3: Cluster sign

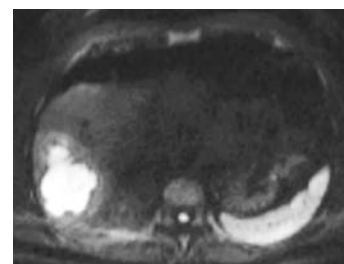


Fig. 4.194.4: Abscess shows diffusion restriction

Table 4.194.1: Difference between pyogenic and amoebic liver abscess

| Content | Pyogenic liver abscess | Amoebic liver abscess |
|----------------------|---|---|
| Age | Mostly older | Mostly younger |
| Presentation | Subacute | Acute |
| Number | Often multiple | Usually single |
| Location | Either lobe of liver | Usually right hepatic lobe subdiaphragmatic in location |
| Predisposing factors | Diabetes, immunocompromised state, diverticulitis, cholangitis, cholecystitis, recent hepatobiliary surgery or trauma | Residence/travel to endemic area, farm/animal exposure, malnutrition immunosuppression, alcohol, associated with cecal/ascending colon wall thickening. |
| Causative organism | Polymicrobial | Single organism |
| | Peripheral rim of enhancement of cyst Green-coloured pus | Thick (3–15 mm) wall that typically enhances Anchovy sauce pus |
| Cluster sign on CT | Positive | Negative |
| Double target sign | +++ | + |
| Biochemical cyst | LFT abnormal | Serology positive |
| Treatment | Antibiotics+ catheter drainage | Amebicidal drugs—metronidazole for 7–10 days |

| Table 4.194.2: Multifocal cystic liver lesions | | | |
|--|--|--|------------------|
| <i>Developmental</i> | <i>Inflammatory</i> | <i>Neoplastic</i> | <i>Trauma</i> |
| Biliary hamartoma | Pyogenic abscess | Cystic metastasis | Bilioma |
| Caroli disease | Amoebic abscess | Cystic HCC (HCC after necrosis/radiotherapy) | Seroma, hematoma |
| Polycystic liver disease | Fungal abscess | Biliary cystadenoma, Biliary intra ductal papillary mucinous neoplasm (B-IPMN) (rarely multifocal) | Vascular |
| Others—melioidosis, pseudomonas | Hydatid cyst Pseudocyst of pancreas | Multiple neuroendocrine tumours | Hepatic peliosis |

| Table 4.194.3: Gharbi ultrasound staging of hydatid cyst in liver with differential diagnosis of cystic liver lesions | |
|--|--|
| Hydatid cyst Infection by <i>Echinococcus</i> species resulting in cyst formation in multiple parts of body MC organism <i>Echinococcus granulosus</i> Well-defined fibrous capsule with parent cyst and multiple daughter cyst <i>Echinococcus multilocularis</i> | Ultrasound: (Gharbi ultrasound staging) 1: Homogeneously hypoechoic cystic thin-walled lesion 2: Septated cystic lesion 3: Cystic lesion with daughter lesion 4: Pseudotumor lesion 5: Calcified lesion CT: Hydatid cyst typically shows fluid attenuation with hyperattenuating cyst wall even without calcification, calcification of cyst wall/ internal septa easily detected on CT. Detachment of laminated membrane can be visualised as linear areas of increased attenuation. Daughter vesicles manifest as round structures located peripherally in mother cyst Mimics slow growing tumor, infiltrates liver and porta hepatis. No well-defined capsule MRI: Low signal intensity rim on T2 weighted MR images—characteristic sign |

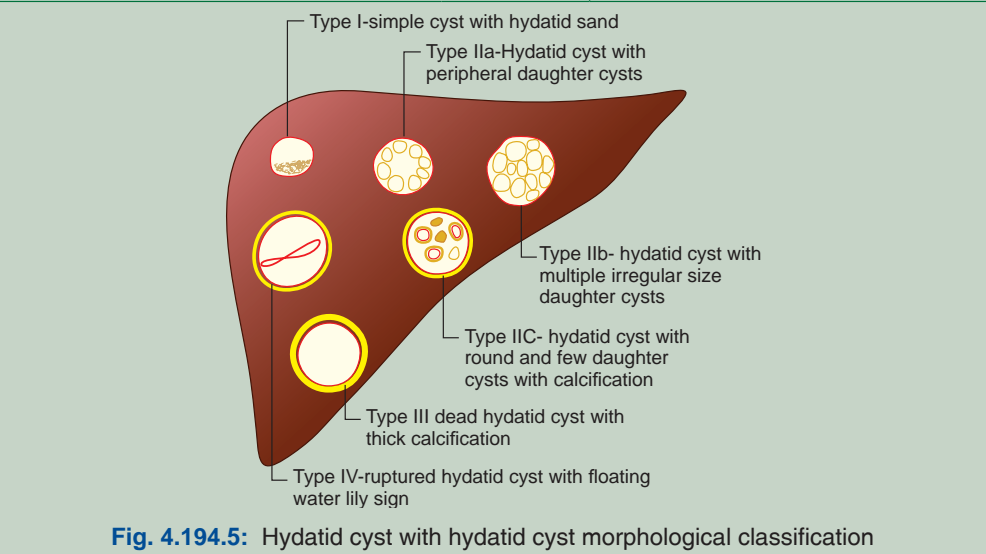


Fig. 4.194.5: Hydatid cyst with hydatid cyst morphological classification

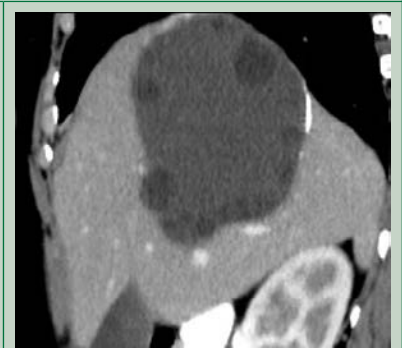


Fig. 4.194.6: Hydatid cyst-liver (CT)

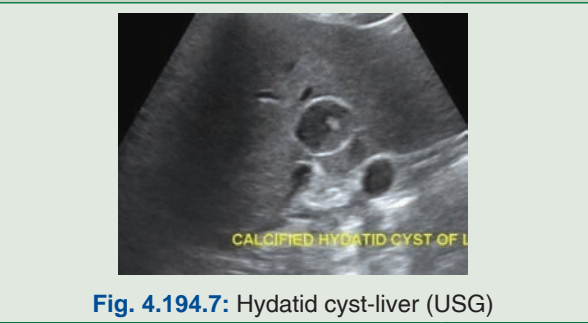


Fig. 4.194.7: Hydatid cyst-liver (USG)

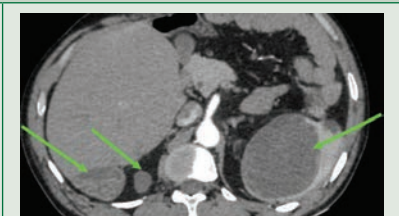


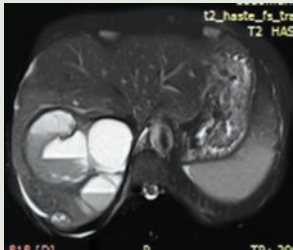
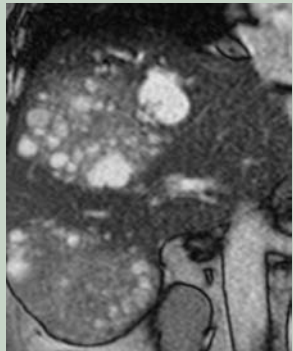


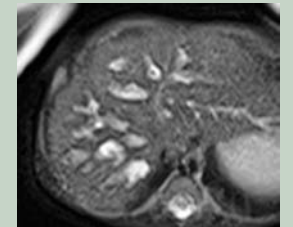
Fig. 4.194.8: Hydatid cyst in spleen and liver



Fig. 4.194.9: Hydatid cyst in brain

Contd.

Table 4.194.3: Gharbi ultrasound staging of hydatid cyst in liver with differential diagnosis of cystic liver lesions (Contd.)

| | | |
|---|---|---|
| <p>Cystic liver metatsasis causes: Neuro-endocrine tumors, gastrointestinal stromal tumor (GIST), lung adenocarcinoma, mucin secreting colorectal carcinoma, ovarian carcinoma, choriocarcinoma, sarcoma, transitional cell carcinoma, adenoid cystic carcinoma.</p> | <p>High mucinous content, rapid growth of the tumor with hemorrhage, necrosis, or cystic degeneration, cystic degeneration after chemotherapy USG: Centrally hypoechoic with thick septations, increased vascularity in Doppler, CT: Centrally hypoattenuating with peripherally enhancing irregular thickened wall MRI: T2—mild to moderate hyperintensity T1+C: Early rim enhancement with washout—peripheral angiogenesis</p> |  <p>Fig. 4.194.10: Cystic liver metatsasis</p> |
| <p>Biliary cystadenocarcinoma: Age: 60–70 years Usually solitary, multilocular cystic lesion, multifocal biliary cystic tumors are rare Bile duct dilation with cystic lesion in left lobe of liver can be predictive of BCAC</p> | <p>USG: Anechoic with thickened irregular wall with papillary projections and mural nodules CT: Multilocular cystic lesions with enhancing walls, fine septations, variable calcification, enhancing mural nodules MRI: Low signal intensity on T1, high on T2, on contrast septa enhance MRCP: Demonstrate communication with the biliary tree, to visualise biliary tree proximal to obstruction</p> |  <p>Fig. 4.194.11: Biliary cystadenocarcinoma</p> |
| <p>Hepatic cyst (polycystic disease) Benign liver lesion with no malignant potential Discovered incidentally, asymptomatic Association: Polycystic liver disease Autosomal dominant polycystic kidney disease von Hippel-Lindau disease</p> | <p>USG: Round/ovoid anechoic well-defined lesion with posterior acoustic enhancement with no internal vascularity on Doppler CT: Hypodense (HU: 0-10), wall usually imperceptible, does not enhance on administration of contrast MRI: T1: Homogeneous low signal intensity T2: Increased signal intensity greater than other T2 hyperintense lesion (hemangioma)</p> |  <p>Fig. 4.194.12: Hepatic cyst (polycystic disease)</p> |
| <p>Caroli's disease (type 5 choledochal cyst)-autosomal recessive disorder Presents with jaundice in few months of life . Congenital disorder comprising of multifocal cystic dilation of segmental intrahepatic bile ducts. Associations: • ARPKD • Medullary sponge kidney Clinical features: Right upper quadrant pain, recurrent cholelithiasis, cholangitis with fever and jaundice</p> | <p>Disease may be diffuse, lobar/ segmental. USG: Dilated intrahepatic bile ducts with intraductal bridging CT: Multiple hypodense rounded areas which are inseparable from the dilated intrahepatic bile ducts. Central dot sign: Enhancing dots within the dilated intrahepatic bile duct representing portal radicles MRI:T1: Multiple hypointense areas noted (dilation of IHBR) T2: Hyperintense T1+C: Enhancement of central portal radicles within the dilated IHBD MRCP: Demonstrates continuity with the biliary tree</p> |  <p>Fig. 4.194.13: Caroli's disease</p>  <p>Fig. 4.194.14: Caroli's disease</p> |

(Contd.)

Table 4.194.3: Gharbi ultrasound staging of hydatid cyst in liver with differential diagnosis of cystic liver lesions (Contd.)

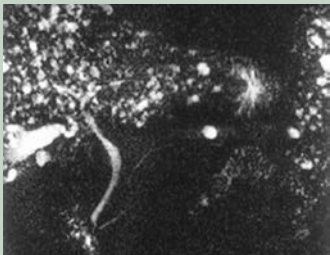
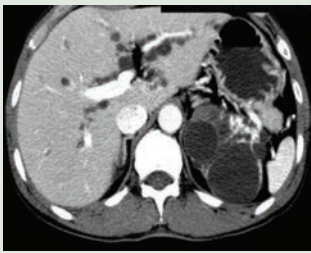
| | | |
|---|---|---|
| <p>Biliary hamartoma: One cause of multiple benign hepatic lesion. Asymptomatic, found incidentally</p> <p>Patho: They are thought to arise from embryonic bile duct remnant that has failed to involute also known as von Meyenburg complexes</p> | <p>Multiple small round irregular lesion with some predilection for subcapsular region</p> <p>CT: Hypodense lesion, no enhancement</p> <p>MRI: T1: Hypointense, no enhancement on contrast</p> <p>T2: Hyperintense</p> |  |
| <p>Peribiliary cyst: Obstruction of the neck of the periductal glands</p> <p>Association: Cirrhosis, portal hypertension, and AD polycystic disease</p> <p>Lesions usually increase in size and number as cirrhosis and portal hypertension progress</p> | <p>Located along the portal tracts in the hilum and adjacent to the large intrahepatic ducts—string of beads</p> <p>CT: Multiple hypodense lesion adjacent to intrahepatic ducts</p> <p>With no enhancement.</p> |  |
| Others—Pseudocyst of pancreas, lymphangioma | | |

Fig. 4.194.15: Biliary hamartoma**Fig. 4.194.16:** Peribiliary cyst**Table 4.194.4: Multifocal solid liver lesions**

| Adult | | Pediatric | |
|--|---|--|---|
| Benign | Malignant | Benign | Malignant |
| 1. Hemangioma 2. Hepatic adenomatosis 3. Regenerative nodules 4. Degenerative nodules | 1. Metastasis 2. Multifocal HCC 3. Lymphoma 4. Hepatic epitheloid hemangioendothelioma | 1. Mesenchymal hamartoma—predominantly cystic (1–10 years) 2. Hemangioma 3. Infantile hemangioendothelioma | 1. Metastasis (neuroblastoma common) 2. HCC (11–18 years) 3. Multifocal hepatoblastoma 20% (1–10 years) |

Cholangitic abscess: Biliary spread of infection.

Risk factors: Diabetes, immunocompromised state, gastrointestinal tract cancers, diverticulitis, cholangitis, cholecystitis, recent hepatobiliary surgery or trauma. More likely to form in the right lobe.

Ultrasound: An anechoic mass with well-defined or indistinct borders increased through transmission, may contain echogenic debris or gas. Abscess by *Klebsiella*—more likely to be solid **CT:** Multiple hypodense lesions cluster sign—Feature of pyogenic abscess, aggregation of multiple low attenuation lesions in localized area to

form solitary large abscess cavity **CECT:** Double target sign. Central low attenuation lesion surrounded by high attenuation inner rim (abscess membrane—contrast enhancement in early phase) and low attenuation outer rim (edema—enhance only on delayed phase) **MRI:** The central portion of the lesion will show low signal intensity on T1- and high signal intensity on T2 peripheral halo of hyperintensity indicating edema may be seen on T2-weighted imaging. DWI: Abscess show diffusion restriction T1 + Contrast: enhancement of capsule.

Table 4.194.5: Differential diagnosis for multifocal liver lesions

Metastasis: MC malignant focal liver tumours
Secondary: Primary = 18:1
Commonly from: Colon, stomach, pancreas, breast, lung
Silent primaries—pancreas, stomach, lung
CT: Most metastasis are hypodense, hypovascular, e.g. lymphoma, pancreas, cervical carcinoma, adenoma of lung, nasopharyngeal carcinoma.
Cystic metastasis (fluid dense): GIST, cystadenocarcinoma ovary, pancreas, mucinous adenoca colon, sarcoma
Calcified metastasis—mucinous adenoca colon, stomach carcinoma
CECT: Metastasis show enhancement less than surrounding liver following contrast, enhancement is peripheral in early phase, portal phase shows central fill in and delayed phase shows wash out
Hyperenhancing (vascular) metastasis seen commonly in carcinoma of thyroid, renal, neuroendocrine tumor

USG: Hyperechoic metastasis—colon, other GIT, vascular metastasis from islet cell tumor, carcinoid, choriocarcinoma, RCC
Hypoechoic metastases: Hypovascular, highly cellular—lymphoma, pancreas, cervical carcinoma, adenocarcinoma of lung, nasopharyngeal ca
Cystic metastasis—commonly with primaries having cystic components, GIST, cystadenocarcinoma ovary, pancreas, mucinous adenocarcinoma colon, sarcoma, melanoma. Calcified metastasis—mucinous adenoca colon, stomach, chondroid/osteoid
Diffuse infiltration—most difficult pattern to appreciate
MRI: Five major morphologic patterns: 1) Doughnut—T1 low signal mass with central region of even lower signal, lesions with necrosis, mucin. 2) central high signal, surrounded by low signal rind, lesions with necrosis. 3) Amorphous heterogeneously hyperintense with featureless contents, outer margins indistinct. 4) Halo—T2 low signal lesion with high signal rim—2 to 10 mm thickness. 5) Light bulb smooth, sharply defined round lesion. T2 contents high signal similar to GB, CSF common in cystic metastasis, carcinoid, islet cell

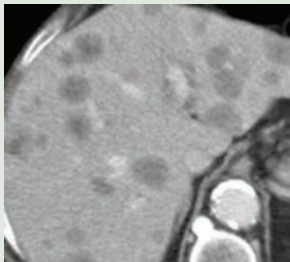


Fig. 4.194.17: Liver metastasis

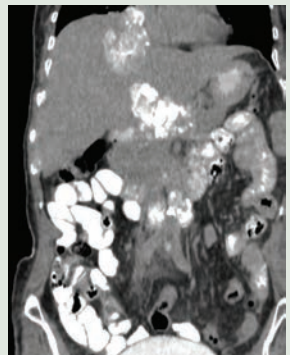


Fig. 4.194.18: Hypervascular liver metastasis

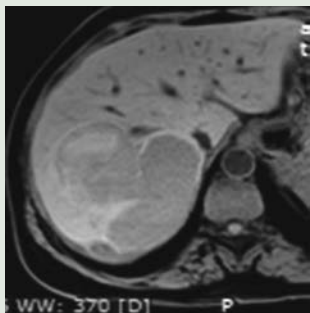


Fig. 4.194.19: Cystic liver metastasis

Liver metastases are typically hypoattenuating on unenhanced CT, enhancing less than surrounding liver following contrast. If there is concomitant hepatic steatosis, then the lesions may be iso- or even slightly hyperattenuating. Enhancement is typically peripheral, and although there may be central filling in, on portal venous phase, the delayed phase will show washout; helpful in distinguishing a metastasis from a hemangioma. Metastasis with a fluid-fluid level on MRI is characteristic of a neuroendocrine tumor metastasis, a large metastasis from any origin that has outgrown its blood supply.

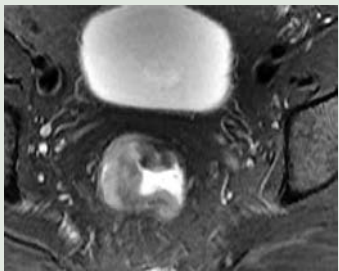


Fig. 4.194.20: Metastasis from carcinoma rectum/colon causing bilobar IHBRD

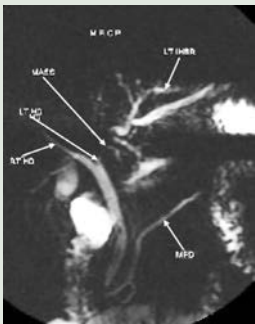


Fig. 4.194.21: Metastasis from carcinoma rectum/colon causing left lobar IHBRD

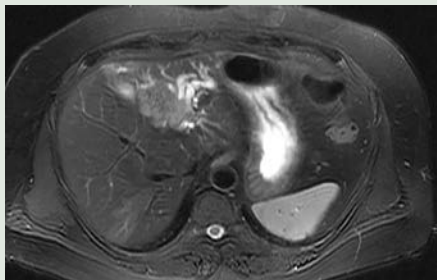


Fig. 4.194.22: Metastasis from carcinoma rectum/colon causing left lobar IHBRD

(Contd.)

Table 4.194.5: Differential diagnosis for multifocal liver lesions (Contd.)

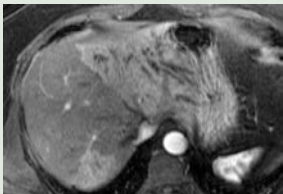

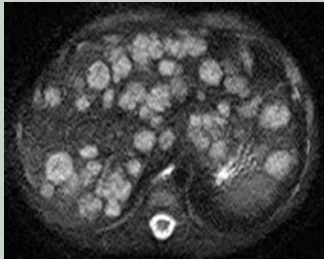
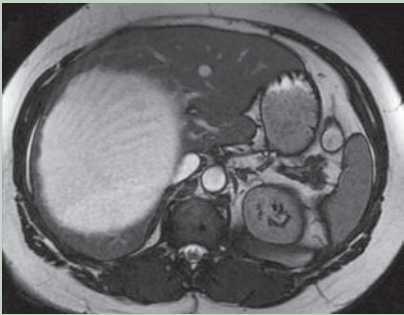
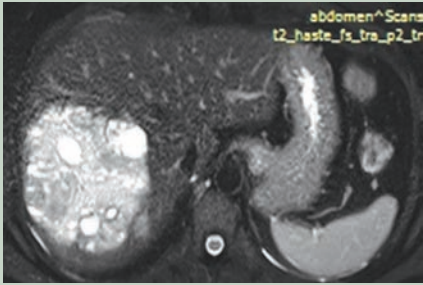
| | | |
|--|--|---|
|  <p>Fig. 4.194.23: Metastasis from carcinoma rectum/colon causing bilobar IHBRD</p> | | |
| <p>Lymphoma: Primary or secondary with HL or NHL (50% of patients). Most are secondary: Nodular, diffuse or miliary forms</p> <p>USG: Multiple well-defined hypoechoic mass, diffuse infiltration cannot be differentiated from normal liver</p> | <p>CT: Multiple well-defined low density masses. Diffuse infiltration may not be differentiated from normal liver. Additional areas involvement—spleen, pancreas, para-aortic, periportal, celiac lymph nodes, kidney</p> <p>MRI: Hypo in T1, hyper in T2 Gd-DTPA—transient peripheral enhancement. Difficult to differentiate from metastases</p> <p>Scintigraphy—gallium citrate will show uptake by lymphoma tissue</p> |  <p>Fig. 4.194.24: Lymphoma</p> |
| <p>Hepatic epithelioid hemangioendothelioma: Malignant hepatic vascular tumour (low to intermediate) Male: female 3:2 incidence 30–40 years. Multiple solid tumor nodules located predominantly in a peripheral location. Cause capsule retraction</p> <p>USG: Appear hypoechoic</p> | <p>CT: Multiple hypoattenuating lesion in both hepatic lobes that coalesce to form larger confluent hypoattenuating region in a peripheral / subcapsular distribution Hepatic or portal vein or their branches terminate within the edge of these lesions (lollipop sign)</p> <p>MRI: T1: Hypointense lesion T1+C: peripheral halo or target type enhancement pattern T2: Heterogenous increased signal</p> | |
| <p>Infantile hepatic hemangioma (hemangioendothelioma)</p> <p>Benign tumors</p> <p>Have substantial arteriovenous shunting that may lead to fatal cardiovascular compromise and hydrops fetalis. Rapid proliferative growth in first 6 months of life followed by regression</p> | <p>Ultrasound: Variable sonographic appearance with either hypo/hyperechoic with prominent vascular channels</p> <p>CT: Typical peripheral enhancement with gradual fill in. Midaortic syndrome—Reduction in aortic calibre distal to celiac axis because of vascular distribution to liver</p> <p>MRI: Homogeneous signal intensity with prominent flow voids T1: Hypointense, T2: Hyperintense</p> |  <p>Fig. 4.194.25: Hemangioendothelioma</p> |
| <p>Neuroblastoma: Most common cause of paediatric liver metastasis, in Stage 4s neuroblastoma diffuse liver involvements seen, stage 4s also called pepper syndrome</p> | <p>Hepatomegaly with altered signal with multiple T2 hyperintense foci interspersed in parenchyma</p> | |

Table 4.194.6: Difference between benign biliary cystadenoma/malignant cystadenocarcinoma and benign biliary intraepithelial neoplasia

| <i>Benign biliary cystadenoma/malignant cystadenocarcinoma</i> | | <i>Benign biliary intraepithelial neoplasia</i> |
|--|--|---|
| Very rare multilocular cystic tumor originating in bile ducts Biliary cystadenoma is a premalignant form of biliary cystadenocarcinoma. (15% chance of cystadenocarcinoma) Female prevalence, age> 30 years USG: Ovoid multiloculated anechoic mass with highly echogenic septations, fluid-fluid level can be seen. CT: Multiloculated mass of near water density with contrast enhancement in wall and internal septa MRI: Locules with variable signal intensity on T1w imaging +T2 W imaging based on protein content No bile duct communication | | It is a rare neoplasm involving the intra- and extrahepatic biliary tract and is characterized by mucin-secreting papillary and/or cystic lesions. Secretions from the bile duct may intermittently impede bile flow, leading to diffuse intra/ extra hepatic bile duct obstruction and dilatation, repeated episodes of cholangitis. Male prevalence Age: 60–70 years resembles pancreatic IPMN bile duct communication Cystadenocarcinoma (30%) USG: Cystic bile duct dilation upstream and downstream of tumor. Well-defined intraluminal echogenic mass can be identified with preservation of bile duct wall CT/MR: Demonstrate bile duct dilatation, any intraductal mass and invasion of mass to surrounding structures and presence of nodes |
| <i>Benign</i> | <i>Malignant</i> | |
| Nodularity absent No thick septation No lymph nodes No metastasis | Nodularity present, enhancing mural nodules present Thick enhancing septation Lymph nodes and distant metastasis Variable calcification noted | |
|  |  | |
| Fig. 4.194.26: Benign biliary cystadenoma | Fig. 4.194.27: Malignant cystadenocarcinoma | |

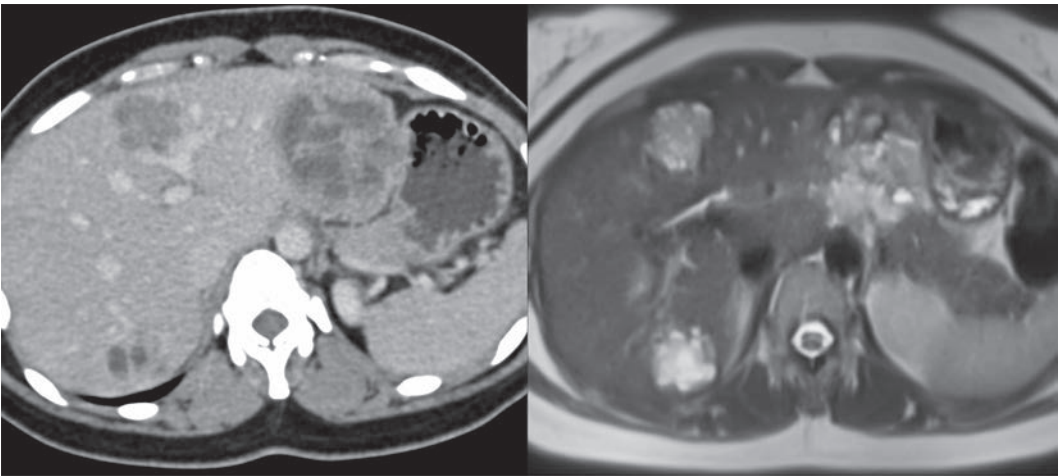


Fig. 4.194.28: Hepatic neuroendocrine tumour

4.195 HEPATOBILIARY SYSTEM

Case No. 195

Clinical history: 43-year-old male patient with vague abdominal pain. Chronic alcoholic.

Radiological techniques and observations: CE MRI abdomen axial (Figs 4.195.1 to 4.195.2), coronal (Fig. 4.195.3) and sagittal (Figs 4.195.4 to 4.195.5) images are shown. Well-defined enhancing lesion measuring $4 \times 3.5 \times 3.3$ cm in segment 4B/3 of left lobe of liver, showing avid enhancement on contrast. Capsular retraction noted. No evidence of calcification, fat density, necrosis or scarring within the lesion. Nodular surface seen in the anterior surface of the liver. Mild caudate lobe hypertrophy. Hepatic veins appear normal. No evidence of intrahepatic biliary radical dilatation. Visualised bowel, stomach, pancreas, spleen are normal. No peritoneal deposits or perihepatic, periportal or para-aortic lymphadenopathy. No evidence of ascites. Visualised bones appear normal.

Interpretation: A: 43-year-old male, lesion in liver, C: A well-defined lesion in segment 4B/3 of liver, B: with minimal capsular retraction showing contrast enhancement, D: HCC in background of cirrhosis.

Principal diagnosis: Hepatocellular carcinoma.

Management: Patient to be immediately referred to the hepatology department for further management. Next serum alpha-feto protein (AFP) has to be done. It was raised in this case, measuring 2200 IU/ml, favouring the diagnosis of hepatocellular carcinoma. Single lesion with no significant co-morbidities can be taken up for tumor resection based upon the Barcelona Clinic Liver Cancer Staging System.

Transarterial Chemoembolization (TACE) is defined as the infusion of a mixture of chemotherapeutic agents with or without iodized oil followed by embolization with particles. The goal of chemoembolization is to expose tumors to high concentrations of a local chemotherapeutic agent in a hypoxic environment with minimal systemic drug bioavailability. The most

common multidrug combination used is mitomycin C, doxorubicin, and cisplatin. Doxorubicin is the most commonly used single-agent regimen worldwide. Regardless of the chemotherapeutic regimen, the drugs are emulsified in Lipiodol, an oily contrast agent that acts as a carrier of the chemotherapeutic agents and accumulates selectively within the neovasculature and extravascular spaces of liver tumors. Embolization of the target vessel after infusion of the Lipiodol chemotherapeutic agent mixture, is done using absorbable gelatin sponge, polyvinyl alcohol particles, and trisacryl gelatin microspheres.

Currently, TACE is recommended for unresectable intermediate stage HCC (BCLC stage B or Child-Pugh class A/B with large or multifocal HCC and no vascular invasion or extrahepatic spread). TACE may also be safely performed in select patients with portal vein thrombosis with no increase in morbidity or mortality. TACE also has an effective role for the palliative treatment of multiple hepatic malignant neoplasms and liver metastases.

TACE procedure is performed with standard endovascular techniques. Review of preoperative imaging is imperative for comprehensive evaluation of possible variant hepatic arterial anatomy, presence of extrahepatic tumoral blood supply, and portal vein patency. Selective angiography of the celiac and superior mesenteric arteries is performed to assess for variant hepatic arterial anatomy with imaging through the portal venous phase to confirm patency of the portal venous system. Various microcatheters are available for subsequent superselective angiography of the intrahepatic arterial vasculature. TACE can be performed from the subsegmental to the lobar level, depending on the type and number of tumors to be treated. Major complications after TACE include liver failure, abscess, cholecystitis, biloma requiring percutaneous drainage, pulmonary arterial oil embolus, gastrointestinal hemorrhage or ulceration from non-target embolization, renal dysfunction, and iatrogenic hepatic artery injury preventing treatment. Follow-up

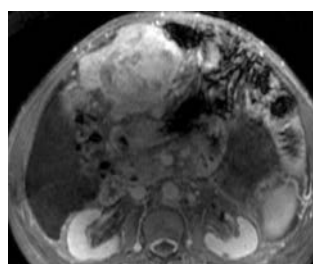


Fig. 4.195.1

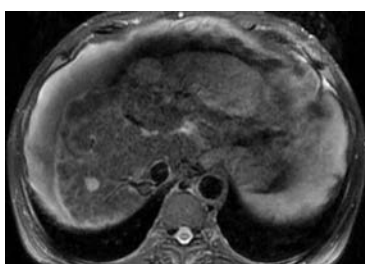


Fig. 4.195.2

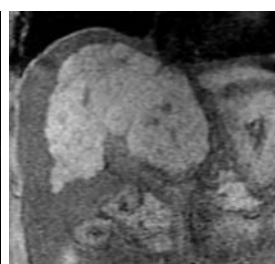


Fig. 4.195.3

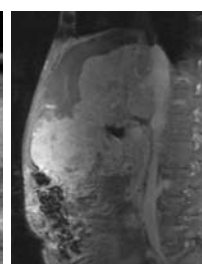


Fig. 4.195.4

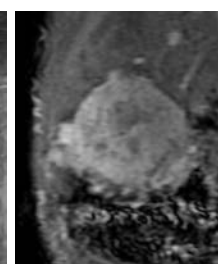
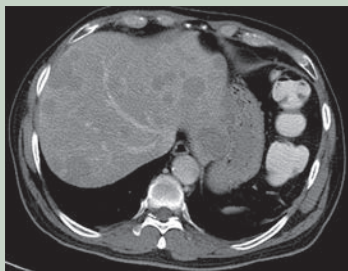


Fig. 4.195.5

Table 4.195.1: Differential diagnosis for delayed contrast enhancement and capsular retraction

| | Imaging features | Image |
|---|--|---|
| Metastases particularly after treatment or with fibrotic tumours (breast/ carcinoid/ lung/ colorectal carcinoma) | Typically hypoattenuating on NECT and enhancing less than surrounding liver in CECT. If there is concomitant hepatic steatosis, then the lesions may be iso- or even slightly hyperattenuating. Enhancement is typically peripheral, and although there may be central filling in, on portal venous phase, the delayed phase will show washout; helpful in distinguishing from a hemangioma. |  |
| Fig. 4.195.6 | | |
| Intrahepatic cholangio-carcinoma: Refer to case 196 | | |
| Sclerosed hemangioma: It is thought that this is the same “solitary necrotic nodule” described by pathologists. | CT features suggestive of sclerosed haemangiomas include geographic outline, capsular retraction, decrease in size over time, and loss of previously seen regions of enhancement. Additional features include the presence of transient hepatic attenuation difference, rim enhancement, and nodular regions of intense enhancement as seen in typical haemangiomas. | |

imaging after TACE is usually performed at 4 to 6 weeks. Assessment of tumor response after TACE is generally based on iodized oil deposition on unenhanced CT and tumor enhancement and size on postcontrast CT or MR images. Chemoembolization with drug-eluting beads is a recent advancement (DEB-TACE).

Brief discussion about the condition: Hepatocellular carcinoma is the second most common cause of cancer death worldwide and occurs most often in patients with risk factors for developing HCC including cirrhosis and chronic hepatitis B. Surveillance programs for HCC in high-risk patients have long been implemented in countries where the incidence of HCC is high.

Liver imaging reporting and data system (LI-RADS): Once a focal hepatic nodule is detected during HCC surveillance with ultrasound (US) or other imaging modalities, a diagnostic imaging test including contrast-enhanced CT, MRI, or contrast-enhanced ultrasound (CEUS) is performed. Malignant lesions previously confirmed with biopsy (e.g. HCC, intrahepatic cholangiocarcinoma) or benign lesions of nonhepatocellular origin (eg, hemangioma) do not require LI-RADS categorization unless there is discordance between imaging and pathology findings or unless there is some other doubt about the diagnosis. Refer to OSCE for further explanation.

Table 4.195.2: The Barcelona Clinic Liver Cancer (BCLC) classification system sorts HCC into one of four categories

| Stage | Management |
|---|--|
| Stage 0 (very early stage) —asymptomatic early tumors, PS 0, Child-Pugh A, solitary lesion measuring less than 2 cm in diameter. | Resection. If portal hypertension/ hyperbilirubinemia, transplant is then recommended if other clinical comorbidities, radiofrequency ablation is then recommended |
| Stage A (early stage) —asymptomatic early tumors, PS 0–2, Child-Pugh A to C, solitary lesion >2 cm or early multifocal disease characterized by up to 3 lesions measuring less than 3 cm | Usually, resection is viable for single lesions if multiple lesions, transplant is then recommended if other clinical comorbidities are present, radiofrequency ablation is then recommended |
| Stage B (intermediate stage) —asymptomatic multifocal disease PS 0 Child-Pugh A to C, multifocal disease: More than one lesion with at least one over 3 cm, or more than 3 lesions regardless of their size | Transarterial chemoembolisation (TACE) |
| Stage C (advanced stage) —symptomatic tumors and invasive and/ or metastatic disease, PS 1-2, Child-Pugh A to C vascular invasion and/ or nodal disease and/ or metastatic disease | Usually palliative: Sorafenib, phase II trial agents, or other palliative treatments |
| Stage D (end-stage disease) terminal stage, PS > 2, Child-Pugh C it is not radiological staging, only clinical | Symptomatic treatment only equivalent to Okuda stage III |

Table 4.195.3: Staging system for HCC

| <i>Okuda staging system: Variables</i> | <i>Staging of HCC based on the number of variables present</i> |
|---|--|
| 1. Disease involving >50% of hepatic parenchyma 2. Ascites 3. Albumin ≤ 3 mg/dl 4. Bilirubin ≥ 3 mg/dl | Stage A: 0 variables Stage B: 1–2 variables Stage C: 3–4 variables Higher stages were correlated with a poorer prognosis. |

Table 4.195.4: Hepatospecific MR contrast agents

| | <i>Mn- DPDP (Mangafodipir trisodium)</i> | <i>Gd- EOB- DTPA Gadoxetate</i> | <i>Gd- BOPTA Gadobenate</i> |
|-------------|--|--|--|
| Uptake | Vitamin B6 receptors on hepatocytes | Anion transporter on hepatocytes | Anion transporter on hepatocytes |
| Excretion | >50% biliary, remainder renal | 50% biliary, 50% renal | 3–5% biliary, 95% renal |
| Trade name | Teslascan | Primovist/ Eovist | Multihance |
| Scan timing | 15 min to several hours | Dynamic imaging as for extracellular Gd; 20 min for hepatocyte phase (hepatobiliary phase) | Dynamic imaging as for extracellular Gd; 60 min for hepatocyte phase (hepatobiliary phase) |

Table 4.195.5: MRI differentiate underlying regenerative, dysplastic nodule from early HCC

| <i>Nodule</i> | <i>Regenerative</i> | <i>Dysplastic</i> | <i>HCC</i> |
|---------------|---------------------|-----------------------------------|---|
| T1W | Iso to hyper | Hyper | Hypo |
| T2W | Hypo to iso | Hypo/hyper | Usually hyper |
| Contrast | No enhancement | Partial Enhancement No washout | Marked enhancement Washout in the portal phase |
| Diffusion | Hypo to iso | Hypo to iso | Hyper |

Table 4.195.6: Difference between benign and malignant nodule

| <i>Features</i> | <i>Benign nodule</i> | <i>Malignant nodule</i> |
|----------------------------|----------------------|-------------------------|
| Size | <20 mm | >20 mm |
| Arterial hyper-enhancement | No | yes |
| Avid SPIO uptake | Yes | No |
| Avid hepatocellular uptake | Yes | No |

Barcelona Clinic Liver Cancer (BCLC) staging system–2016: This system of staging has made criteria for categories of hepatocellular carcinoma for therapeutic management.

The classification has the following variables into account—performance status (PS), Child-Pugh score, radiologic tumor extent, tumor size, multiple tumors, vascular invasion, nodal spread and extrahepatic metastases.

Okuda staging system was an advance on the earlier hepatocellular (HCC) staging classifications, in that it

incorporated both cancer-related variables and liver function related variables to determine prognosis.

CT protocol for focal liver lesions: Plain CT (NECT attenuation value of normal liver parenchyma is between 40–80 HU)

Triple phase CECT abdomen (arterial phase imaging for hypervascular lesions and portal venous phase imaging for hypovascular lesions): 120–150 ml at 3 to 5 ml/sec.

1. 20 second delay. Early arterial at 18–25 seconds and late arterial at 35–45 seconds. Transient hyperattenuation of liver may be present (predominant arterial supply, decreased portal supply).
2. 60–70 second delay portovenous phase (parenchymal phase)
3. 180 sec equilibrium phase
4. 10 to 20 minutes after contrast administration: Delayed contrast phase. Retention of contrast may be observed in cholangiocarcinoma, fibrous tumors, or scars.

| Table 4.195.7: Differential diagnosis for signs in liver imaging | | |
|---|---|---|
| T1 hyperintense lesions HCC Dysplastic nodule Hemorrhagic tumors Melanoma Thrombosed portal vein Lesions in hemochromatosis liver | T2 light bulb sign (lesion has CSF intensity) Hemangioma Cysts Cystic metastases Cystadenocarcinoma CAPSULE HCC, adenoma T2 hyperintense central scar–FNH >>HCC in noncirrhotic liver | Angiogram phase Hepatocellular carcinoma (prominent feeding vessels) FNH (single vessel supplying scar) Arterial phase Peripheral Nodular enhancement: Hemangioma |
| T2 hypointense tumor Regenerating nodules DWI: Restriction–abscess CSI: Fat containing lesion: Hepatic adenoma, fatty liver Iron overload–Hemochromatosis Hepatobiliary phase enhancement: Intrahepatic cholangiocarcinoma, FNH | NECT hyperdense lesions Hepatic adenoma Siderotic nodules Delayed enhancement: Scar | Portal phase washout: HCC and FLC variant of HCC Equilibrium phase: Capsule in HCC Centripetal enhancement: Hemangioma Delayed enhancement: Cholangiocarcinoma |

Liver tumours enhancement pattern

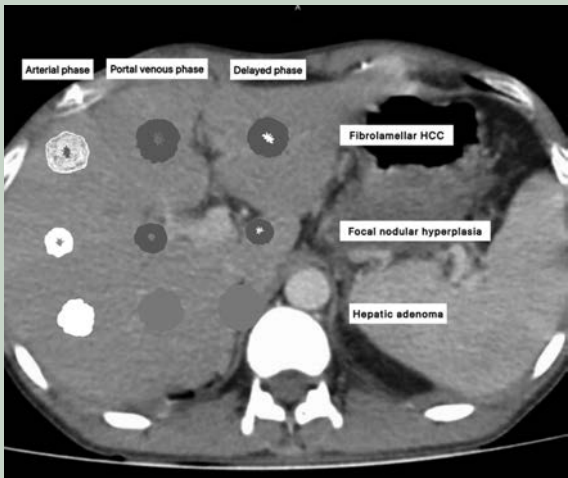


Fig. 4.195.7: Liver tumors and enhancement patterns-1

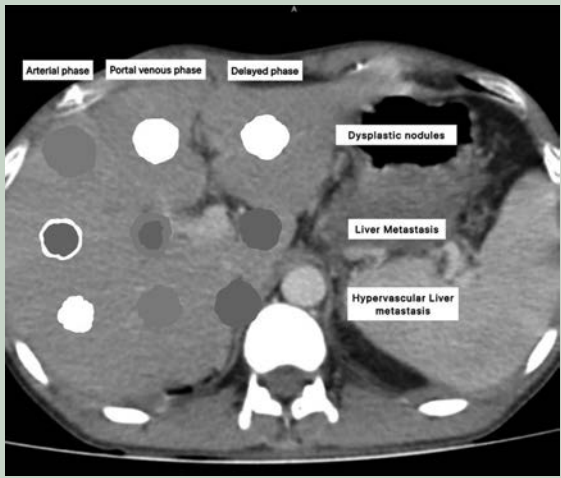


Fig. 4.195.8: Liver tumors and enhancement patterns-2

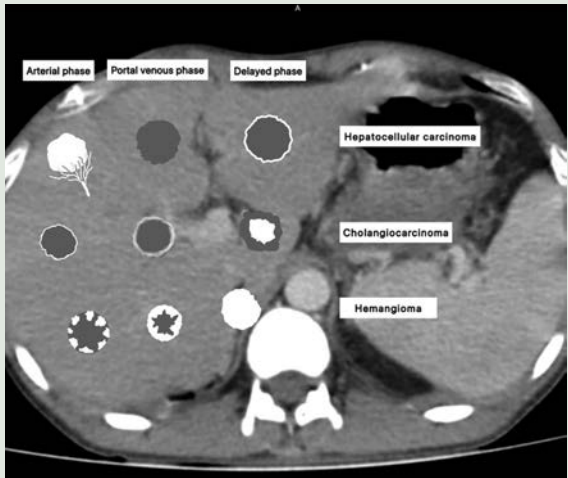


Fig. 4.195.9: Liver tumors and enhancement patterns- 3



Fig. 4.195.10: Liver tumors and enhancement patterns-4

Table 4.195.8: Differential diagnosis for hepatic calcifications

| | |
|---|---|
| <i>Infection</i> (most common cause) <ol style="list-style-type: none"> 1. Old pyogenic/amebic abscess 2. Granulomatous disease: Tuberculosis (48%), histoplasmosis, brucellosis, coccidioidomycosis 3. Echinococcal cyst (in 10–20%) curvilinear I ring calcification 4. CMV, toxoplasmosis, <i>Pneumocystis carinii</i> 5. Schistosomiasis—turtleback/tortoise shell calcifications 6. Cysticercosis, filariasis, paragonimiasis infection, dracunculiasis 7. Syphilitic gumma | <i>Benign tumors</i> <ol style="list-style-type: none"> 1. Congenital cyst 2. Cavernous hemangioma 3. Hepatocellular adenoma 4. Capsule of regenerating nodules 5. Infantile hemangioendothelioma |
| <i>Vascular</i> <ol style="list-style-type: none"> 1. Hepatic artery aneurysm 2. Portal vein thrombosis 3. Hematoma | <i>Primary malignant tumor</i> <ol style="list-style-type: none"> 1. Fibrolamellar carcinoma (calcified in 15–25%) 2. Hepatocellular carcinoma 3. Hepatoblastoma (10–20%) 4. Intrahepatic cholangiocarcinoma (in 18%) 5. Epithelioid hemangioendothelioma 6. Cystadenocarcinoma |
| <i>Biliary</i> <ol style="list-style-type: none"> 1. Intrahepatic calculi 2. Ascariasis, clonorchiasis | <i>Metastatic tumor</i> <ol style="list-style-type: none"> 1. Mucin-producing neoplasm: Carcinoma of colon, breast, stomach 2. Ovarian carcinoma 3. Melanoma, thyroid carcinoma, pleural mesothelioma, chondro and osteosarcoma, carcinoid, leiomyosarcoma, neuroblastoma |

4.196 HEPATOBILIARY SYSTEM

Case No. 196

Clinical history: A 65-year-old male patient came with complaints of yellowish discolouration of urine and pruritis.

Radiological techniques and observations: Ultrasound abdomen, Figs 4.196.1 and 4.196.2 show extensive intrahepatic duct dilatation, more pronounced in the left hepatic lobe. The common bile duct is difficult to visualize. No evidence of portal vein thrombosis.

Further MRCP is required to look for any mass lesion: MRCP haste axial (Figs 4.196.3 and 4.196.4), TRUFISP coronal (Figs 4.196.5 and 4.196.6), MR cholangiogram (Figs 4.196.7 and 4.196.8) images show:

A well defined mass lesion noted in the common hepatic duct at the confluence of right and left hepatic ducts with extension into the right and left hepatic ducts. The gallbladder is contracted. CBD is not dilated. No focal lesions noted in the liver. Periportal lymphadenopathy is present.

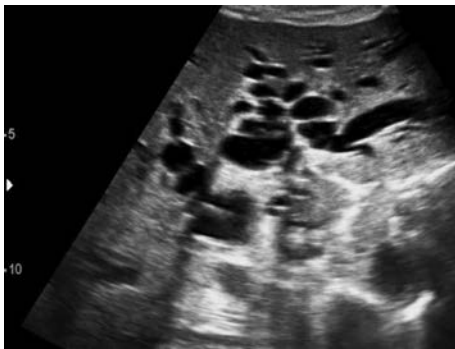


Fig. 4.196.1

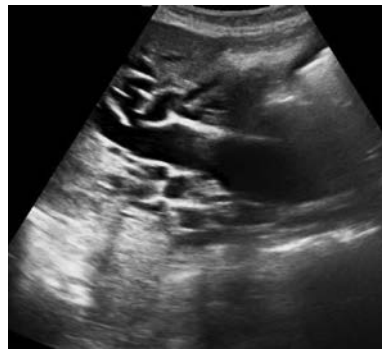


Fig. 4.196.2

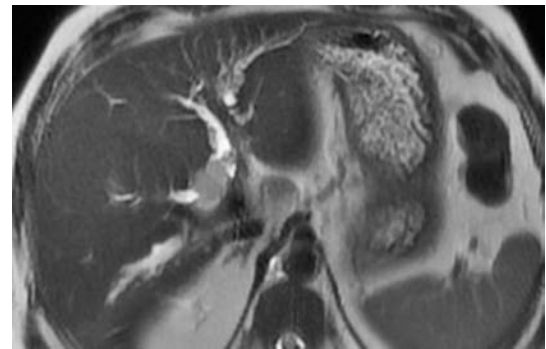


Fig. 4.196.3

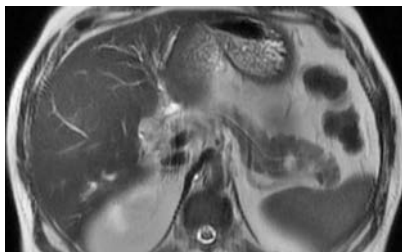


Fig. 4.196.4

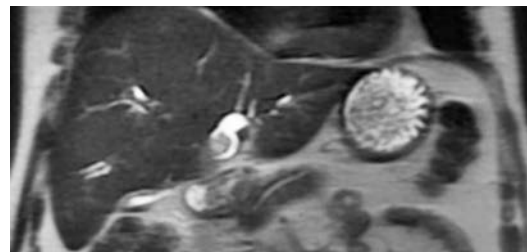


Fig. 4.196.5

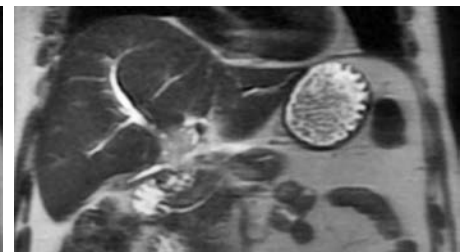


Fig. 4.196.6

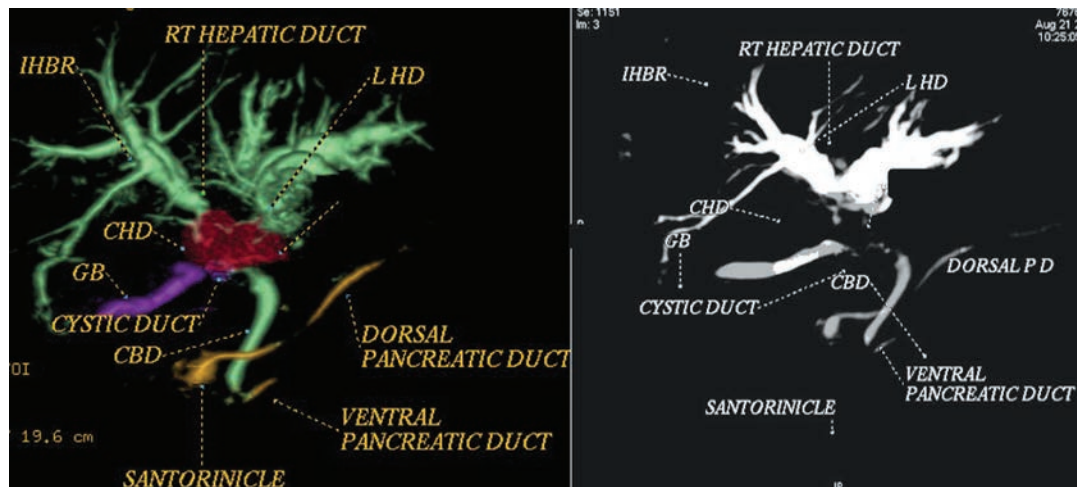


Fig. 4.196.7

Interpretation: A: 65-year-old male, lesion in biliary tract, C: Extensive IHBR, well-defined mass lesion noted in the common hepatic duct at the confluence of right and left hepatic ducts with extension into the right and left hepatic ducts, B: The gallbladder is contracted. CBD is not dilated. Periportal lymphadenopathy is present, D: Klatskin tumor.

Principal diagnosis: Hilar cholangiocarcinoma—Klatskin tumor (Bismuth Corlette Classification Type 4).

Management: Urgent referral to the clinician. Further investigations: PET-CT for systemic staging.

Treatment: The patient is to be discussed in the Multidisciplinary tumour board meeting for further histological diagnosis and treatment. Neoadjuvant chemotherapy/surgery/palliative management will be decided. PTBD external drainage to decompress biliary obstruction.

Discussion: Cholangio-carcinoma—biliary tract cancer is the second most common primary hepatobiliary malignancy after hepatocellular carcinoma. May occur at any part of the biliary tract from the ampulla of Vater to the smallest intrahepatic ductules and the gallbladder. Peak age—6th to 7th decades. More common in males. Clinical features—asymptomatic mass/obstructive jaundice.

Courvoisier's sign states that in the presence of an enlarged gallbladder which is nontender and

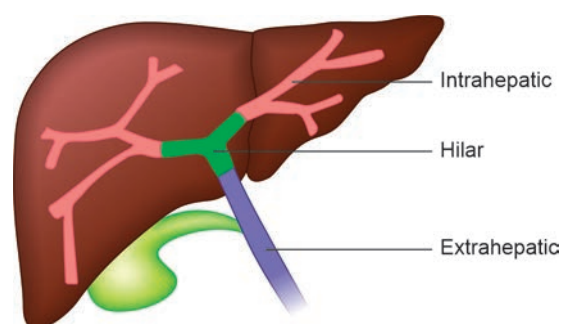


Fig. 4.196.8: Anatomical classification of cholangiocarcinoma

accompanied with mild jaundice, the cause is unlikely to be gallstones. CT-Courvoisier sign: Elevated attenuation (>15 HU) of bile within the gallbladder—common and reliable CT indicator of malignant biliary obstruction.

Risk factors: 1. Liver flukes, 2. Recurrent pyogenic cholangitis, 3. Virus infection (HIV, HBV, HBCV, EBV), 4. Primary sclerosing cholangitis, 5. Toxins (Thorotrast, polyvinyl chloride)

Anatomical classification: Intrahepatic peripheral cholangiocarcinoma, arises peripheral to secondary confluence. Hilar cholangiocarcinoma: Arises from right or left hepatic ducts or from primary biliary confluence. Extrahepatic cholangiocarcinoma.

Morphological classification: Mass forming cholangiocarcinoma, periductal cholangiocarcinoma, intraductal cholangiocarcinoma.

Table 4.196.1: Bismuth-Corlette classification

| Type | Bismuth-Corlette classification of tumors |
|------|---|
| I | Tumor involves the common hepatic duct |
| II | Tumor involves the bifurcation of the common hepatic duct |
| IIIA | Tumor involves the right hepatic duct |
| IIIB | Tumor involves the left hepatic duct |
| IV | Tumor involves the right and left hepatic ducts |

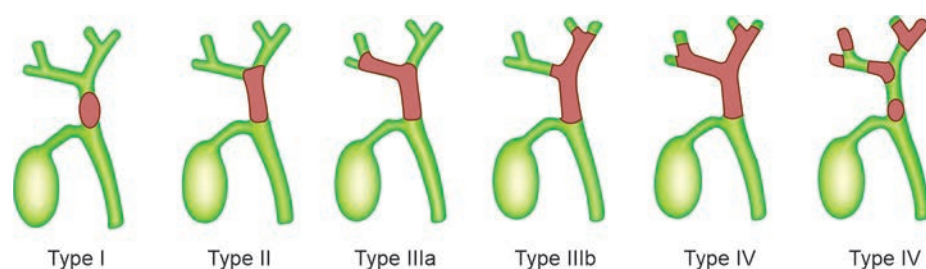
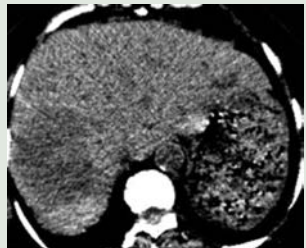
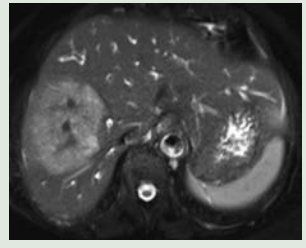
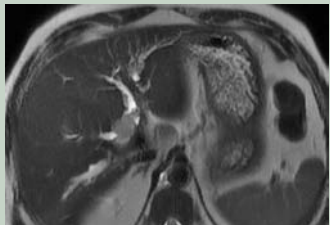
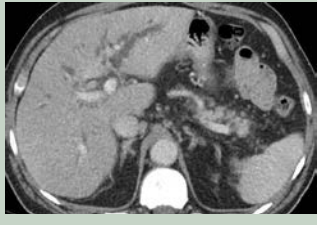


Fig. 4.196.9: Bismuth-Corlette classification of tumors

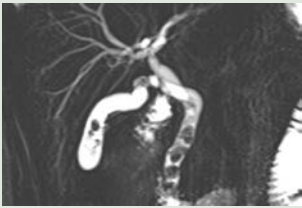
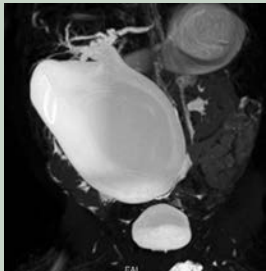
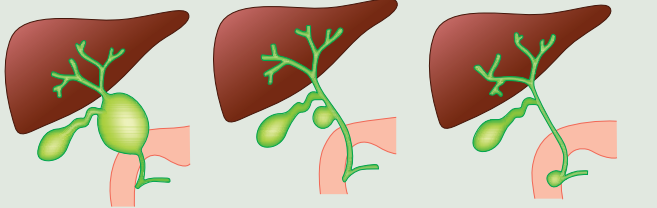
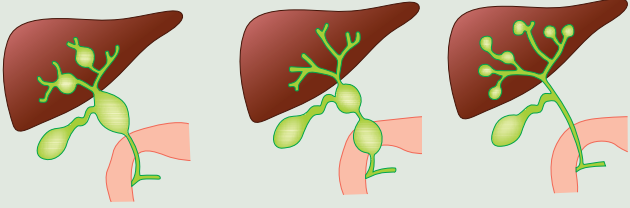
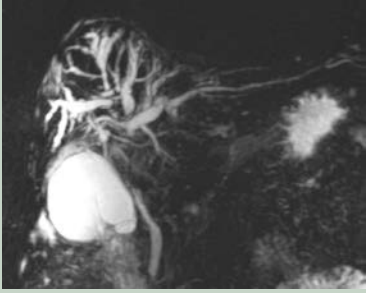
Table 4.196.2: Difference between malignant and benign strictures

| Common bile duct narrowing criteria | Malignant stricture | Benign stricture |
|-------------------------------------|---|--|
| Borders | Irregular | Smooth |
| Margin | Shouldered | Tapered |
| Stricture length | 18+/-7 | 9+/-7 mm |
| Proximal duct diameter | 22+/- 5 | 18+/-5 mm |
| Enhancement arterial phase | 85% | 10% |
| Enhancement portal phase | 95% | 15% |
| | Irregular abrupt narrowing with shouldering. Proximally dilated ducts are elongated and tortuous. Caput medusa appearance | Smooth, gradual tapering of stricture. Proximally dilated ducts are not twisted or elongated. Withered tree appearance |

Table 4.196.3: Growth patterns of cholangiocarcinoma

| | | |
|---|---|--|
| Intrahepatic mass forming Exophytic (peripheral) nodular | USG Homogeneous mass of intermediate echogenicity with peripheral hypoechoic halo. Capsular retraction+ NECT Homogeneous low in attenuation . Capsular retraction + Peripheral intrahepatic duct dilatation CECT Peripheral enhancement and gradual centripetal enhancement Rarely forms tumor thrombus of portal vein MRI/MRCP Appearances similar to CECT |  <p>Fig. 4.196.10: Intrahepatic mass forming cholangiocarcinoma</p>  <p>Fig. 4.196.11: Intrahepatic mass forming cholangiocarcinoma</p> |
| Periductal infiltrating Most common: Hilum (Klatskin) |  <p>Fig. 4.196.12</p> USG Altered calibre bile duct without any mass NECT Duct wall thickening (most commonly at hilum) which is longer with proximal IHBRD CECT Shows contrast enhancement MRI/MRCP Appearances similar to CECT |  <p>Fig. 4.196.13: Periductal (Infiltrating cholangiocarcinoma)</p> |
| Intraductal = Biliary intraductal papillary mucinous neoplasm (IPMN-B) | USG alterations in duct calibre with hyperechoic polypoidal mass lesion NECT duct ectasia with hypoattenuating polypoidal mass CECT shows contrast enhancement MRI/MRCP appearances similar to CECT | |

| Table 4.196.4: Differentiating features of various strictures | |
|---|---|
| Cholangiocarcinoma | Irregular biliary tract with abrupt luminal narrowing |
| Benign stricture | Smoothly narrowed biliary tract |
| Primary sclerosing cholangitis | Multifocal intrahepatic strictures and dilatations |
| Autoimmune cholangitis | Smooth thick wall may have short or long stricture |
| Biliary stones | Round filling defects |

| Table 4.196.5: Cholangiogram appearances of various lesions | |
|---|--|
| Recurrent pyogenic cholangitis More common in left lobe, posterior segments of right lobe. Oriental cholangitis/cholangiohepatitis, intrahepatic pigment stone disease. Chronic Infection by <i>C. sinensis</i> or <i>O. viverrini</i> or ascaris stricture + dilated large ducts + wall thickening + calculus + pruned small ducts + lobe atrophy |  Fig. 4.196.14: Choledocholithiasis—Intra-and/or extrahepatic biliary calculi |
| Choledochal cyst: Congenital segmental aneurysmal dilatation of any portion of bile ducts, most commonly main portion of common duct (CD) |  Fig. 4.196.15: Choledochal cyst |
| Todani classification of choledochal cysts <ul style="list-style-type: none">• Type I: Solitary fusiform-extrahepatic (80–90%); CD• Type II: Extrahepatic supraduodenal diverticulum• Type III: Intraduodenal diverticulum; choledochocele• Type IVa: Fusiform and intrahepatic cysts• Type IVb: Multiple extrahepatic cysts• Type V: Multiple intrahepatic cysts; Caroli disease | |
|  Type I Fusiform dilation of extrahepatic bile duct Type II Saccular outpouchings representing true diverticulum Type III Choledochocele protusion of focally dilated intramural segment of distal CBD into duodenum Fig. 4.196.16 |  Type IVa Dilation of extrahepatic and intrahepatic bile ducts Type IVb Multiple cystic dilation of only extrahepatic bile duct Type V Caroli disease cystic dilation of intrahepatic bile ducts Fig. 4.196.17: Todani classification of choledochal cysts |
| Primary sclerosing cholangitis chronic idiopathic inflammatory process of bile ducts. 70%—male 70%—ulcerative colitis both IHD + EHD |  Fig. 4.196.18: Primary sclerosing cholangitis |

Primary biliary cirrhosis: Chronic progressive cholestatic syndrome of unknown etiology. Females, middle age, Involves small IHBD 90%-Periportal and portocaval lymphadenopathy

Normal EHBD + Dilated IHBD+lance like fibrosis+halo sign in MRI

IG-G4 sclerosing cholangitis: Elevated serum IgG4 level (> 135 mg/dL)

Other organ involvement Pancreas (autoimmune pancreatitis), kidneys, retroperitoneum, salivary glands, or lacrimal glands. Response to steroid therapy. Imaging: Single or multiple bile duct strictures (intrahepatic, extrahepatic, or both), fleeting biliary strictures. continuous long segment duct involvement

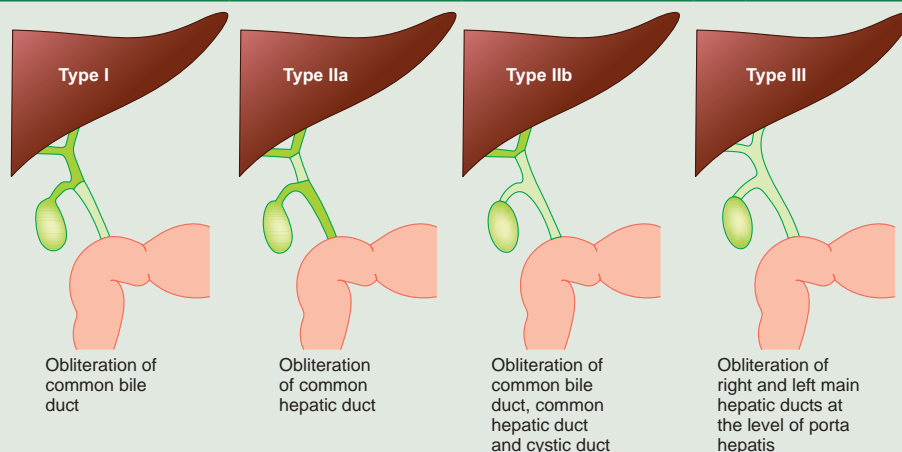


Fig. 4.196.19: Kasai classification of biliary atresia

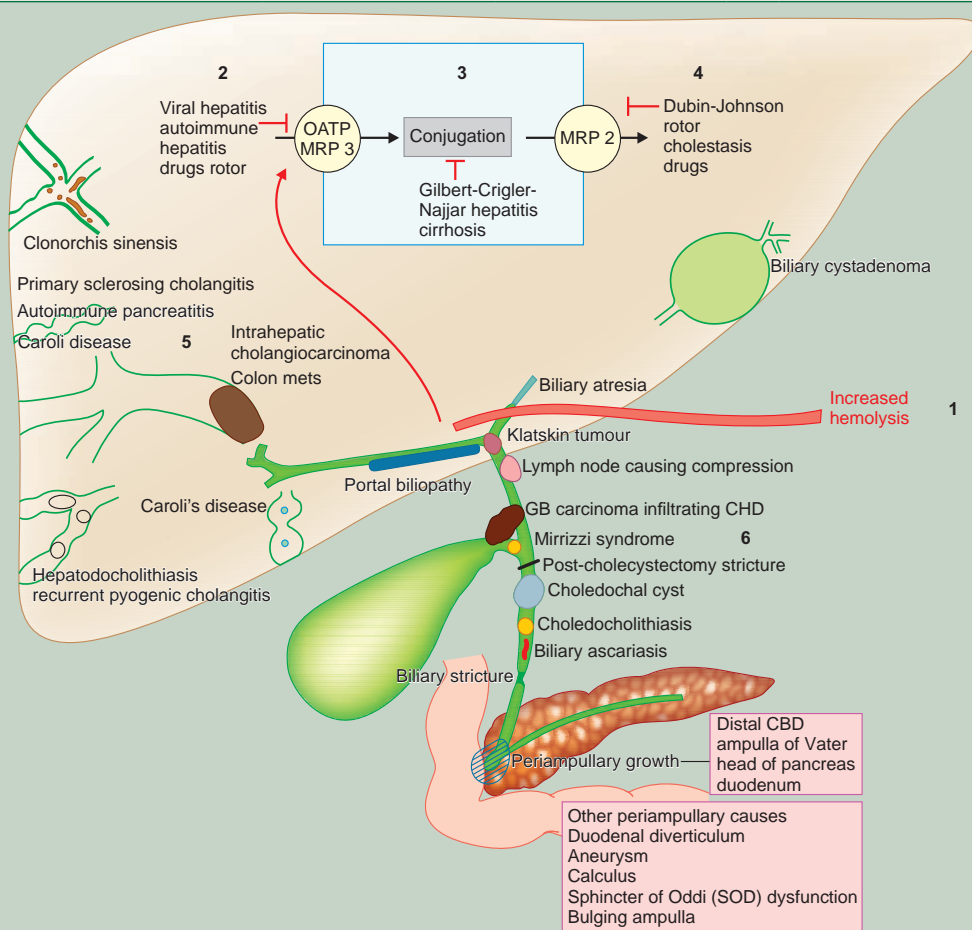


Fig. 4.196.20: Causes for obstructive jaundice

4.197 HEPATOBILIARY SYSTEM

Case No. 197

Clinical history: 54-year-old male presented with complaints of right hypochondrial pain and weight loss for past 6 months.

Radiological techniques and observation: MRI T2 HASTE axial (Fig. 4.197.1) and coronal (Fig. 4.197.2) sequence are provided, showing ill-defined hyperintense mass lesion noted in the body and neck of gall bladder with lesion infiltrating the adjacent liver parenchyma in segment 4B and extending to cystic duct and CBD causing narrowing of CBD. No evidence of infiltration of portal vein/hepatic artery/duodenum. No evidence of nodal enlargement in the porta hepatis/para aortic region noted. No evidence of any other satellite lesion noted. No evidence of free fluid noted. Volume rendering reformatted image, Fig. 4.197.3 shows narrowing of proximal CBD and bilobar IHBR dilatation.

Interpretations: A: 54-year-old male, mass in gallbladder, C: Mass lesion in the body and neck of gall bladder with lesion infiltrating the segments 4b and 5 of liver parenchyma, B: Extending to cystic duct and CBD. MRCP showing narrowing of proximal CBD, D: Carcinoma of gall bladder.

Principal diagnosis: Carcinoma of gallbladder with extension as described above.

Management: This patient is referred to multidisciplinary team for histopathological diagnosis/staging/management. Based on the stage surgical or palliative treatment can be started.

Differential diagnosis: (1) Chronic cholecystitis, (2) metastatic disease to GB, (3) GB polyp, (4) Xantho-

granulomatous cholecystitis, (5) adenomyomatosis, (6) hepatocellular carcinoma, (7) cholangiocarcinoma

Risk factors for gallbladder carcinoma: The presence of gallstones, diffuse mural calcification “porcelain” gallbladder, presence of gallbladder adenomas, an anomalous pancreaticobiliary duct junction and exposure to carcinogenic chemicals.

Types: Adenocarcinomas (85–90%) and can be papillary, tubular, mucinous, or signet cell type; anaplastic; squamous cell or adenosquamous carcinomas

Biomarkers: Elevated serum levels of CA 19-9 and carcinoembryonic antigen.

Radiological features: Ultrasound: Ultrasound findings suggestive of gallbladder cancer include wide polyp base and irregular borders. USG can be useful for differentiating adenomyomatosis from the wall-thickening type of gallbladder cancer by detecting intramural cystic spaces or echogenic foci within the wall.

Doppler imaging can be helpful for differentiating polyp from tumefactive sludge by demonstrating blood flow to the polypoid tumors. CT : CT is superior to ultrasound in assessing lymphadenopathy and spread of the disease into the liver, porta hepatis, or adjacent structures and is useful in predicting which patients will benefit from surgical therapy. MRI : MRI shows prolongation of the T1 and T2 relaxation time in gallbladder carcinoma. These lesions are usually heterogeneously hyperintense on T2-weighted images and hypointense on T1-weighted images compared with liver parenchyma. Ill-defined early enhancement is a typical imaging appearance of gallbladder carcinoma on dynamic gadolinium enhanced

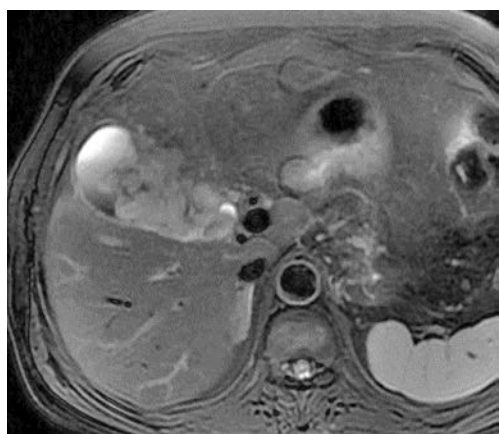


Fig. 4.197.1

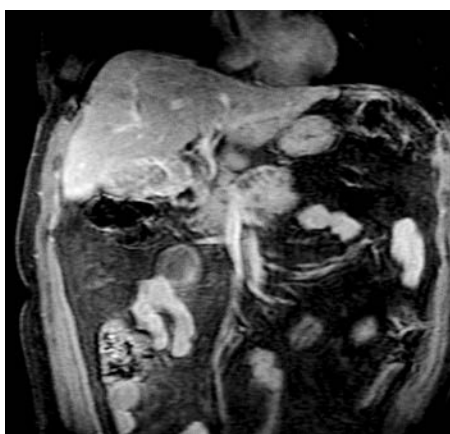


Fig. 4.197.2

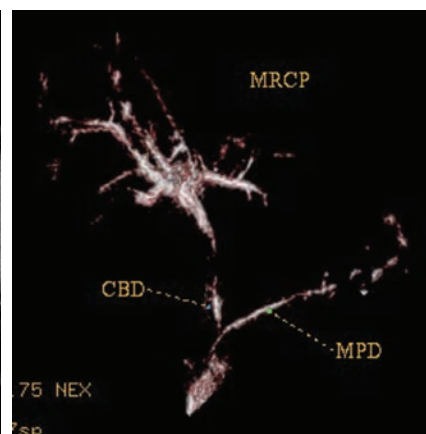


Fig. 4.197.3

Table 4.197.1: Differential diagnosis for gallbladder carcinoma


| | | |
|---|---|---|
| <p>GB polyp: 90% are benign, and the majority are cholesterol polyps.</p> <p>Patients with Peutz-Jeghers have an increased prevalence of adenomas within the gallbladder</p> <p>Risk of malignancy polyp >10 mm (South India), >6 mm (North India)</p> | <p>USG: Non-shadowing polypoid ingrowth into gallbladder lumen, which is usually immobile.</p> <p>CT: Soft tissue attenuation projections into the lumen of the gallbladder and will demonstrate enhancement similar to that of the rest of the gallbladder</p> |  <p>Fig. 4.197.4: GB polyp</p> |
| <p>Chronic cholecystitis: Chronic cholecystitis is associated with gallstones in approximately 95% of cases. Women are more commonly affected. Chronic inflammatory changes cause the gallbladder wall to become thickened and fibrotic, and with increasing fibrosis, the gallbladder eventually becomes shrunken and distorted</p> | <p>Cholelithiasis and gallbladder wall thickening. The gallbladder may appear contracted or distended, and pericholecystic inflammation is usually absent. HIDA scan: Delayed visualization of the gallbladder between 1-4 hours is a reliable sign of chronic cholecystitis.</p> <p>Ejection fraction <35%</p> <p>Acute cholecystitis—GB not visualized in nuclear study.</p> |  <p>Fig. 4.197.5: Chronic cholecystitis</p> |
| <p>Xanthogranulomatous cholecystitis: Most patients present in the sixth or seventh decade. Xanthogranulomatous nodules form in addition to extensive fibrous reaction. The gallbladder often becomes adherent to adjacent organs and may be associated with fistula formation.</p> | <p>The gallbladder wall is often markedly thickened and irregular with loss of normal planes with adjacent structures. An infiltrating mass may be apparent.</p> <p>The presence of intramural nodules is visualized on both sonography and CT.</p> | |
| <p>Cholangiocarcinoma: Malignant tumor from cholangiocytes in the biliary tree.</p> <p>Mean age is 65 years. Typically the presentation is with painless jaundice.</p> <p>Patterns: Mass forming, periductal, intraductal.</p> <p>Cholangiocarcinoma only rarely forms a tumor thrombus. Lobar or segmental hepatic atrophy is usually associated with vascular invasion.</p> <p>DWI/ADC: A peripherally hyperintense “target” appearance on DWI favours cholangiocarcinoma over hepatocellular carcinoma.</p> | <p>Mass-forming: Homogeneously low attenuation on NECT heterogeneous minor peripheral enhancement with gradual centripetal enhancement, capsular retraction, bile ducts distal to the mass are typically dilated.</p> <p>Periductal infiltrating: Duct wall thickening, longer than benign strictures and show enhancement.</p> <p>Intraductal tumors: Alterations in duct caliber, usually duct ectasia with or without a visible mass.</p> |  <p>Fig. 4.197.6: Cholangiocarcinoma</p> |
| <p>Adenomyomatosis: Acquired, hyperplastic lesion of the gallbladder characterized by excessive proliferation of surface epithelium with invaginations into the thickened, hypertrophied muscularis propria.</p> <p>The intramural diverticula formed by epithelial invaginations into the muscularis are referred to as Rokitsky-Aschoff sinuses (RAS)</p> | <p>Diffuse or segmental thickening of the gallbladder wall and anechoic intramural diverticula.</p> <p>A V-shaped reverberation or comet-tail artifact.</p> <p>An additional diagnostic clue is the presence of color Doppler twinkling artifacts in the gallbladder wall that probably result from calcifications or cholesterol depositions</p> | |
| <p>Metastatic disease to gallbladder: Most commonly occurring primary malignant neoplasms are melanoma, breast carcinoma, RCC, gastric, hepatocellular carcinoma and non-Hodgkin lymphoma.</p> | <p>Hypervascular lesions with arterial enhancement and early washout are likely related to melanoma, HCC, or RCC as a primary. Portal venous persistent enhancement is more commonly seen in metastases from gastrointestinal tract adenocarcinomas.</p> | |



Fig. 4.197.7A: Diffuse gallbladder wall thickening

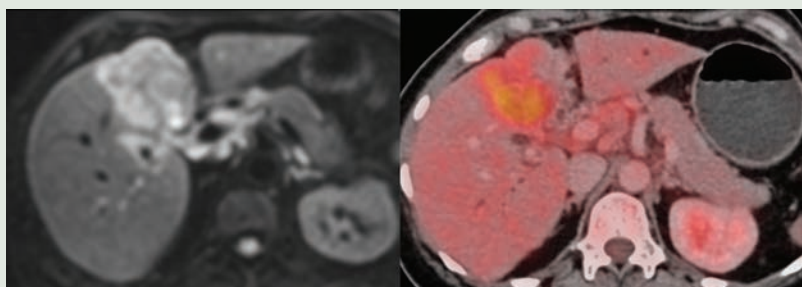


Fig. 4.197.7B: Gallbladder mass with liver segment 4b/5 infiltration

DD for diffuse gallbladder wall thickening: Nonmalignant ascites, hepatitis, serositis, acalculous and calculous cholecystitis, HIV, porcelain GB, intramural gas.

MRI. MR with MRCP offers the potential of evaluating parenchymal, vascular, biliary, and nodal involvement with a single noninvasive examination. In addition, adding diffusion-weighted improves sensitivity for distinguishing gallbladder cancers from benign gallbladder diseases with wall thickening.

Gallbladder malignancies have three major histologic and imaging presentations: Focal or diffuse thickening or irregularity of the gallbladder wall; Polypoid mass originating in the gallbladder wall and projecting into the lumen and a mass obscuring or replacing the gallbladder, often invading the adjacent liver (most common) malignancy manifesting as mural thickening: focal or diffuse irregular thickening of the gallbladder wall is the least common presentation of gallbladder carcinoma and is the most difficult to diagnose, particularly in the early stages. This thickening is best appreciated sonographically (normally 3 mm or less). More advanced gallbladder malignancies can cause marked mural thickening, often with irregular and mixed echogenicity.

Carcinoma manifesting as a polypoid mass: Polypoid carcinomas on ultrasound usually have a homogeneous tissue texture, are fixed to the gallbladder wall at their base and do not cast an acoustic shadow. Most benign polyps are usually small, measuring smaller than 1 cm. If a gallbladder polyp is higher than 1 cm in diameter and is not clearly benign, cholecystectomy should be considered. The polypoid cancer usually enhances homogeneously after administration of contrast medium, and the adjacent gallbladder wall may be thickened. Necrosis or calcification is uncommon.

Carcinoma manifesting as a gallbladder fossa mass: A large mass obscuring or replacing the gallbladder is the most common presentation of gallbladder carcinoma. On USG examination, the mass is often complex, with regions of necrosis, and small amounts of pericholecystic fluid are often present. Gallstones are commonly seen within the illdefined mass, which typically invading

| Table 4.197.2: Stage grouping in AJCC | |
|---------------------------------------|--|
| Stage | Grouping |
| 0 | Tis N0 M0 |
| 1 | T1 N0 M0 |
| 2 | T2 N0 M0 |
| 3 | T1 N1 M0 T2 N1 M0 T3 N0 M0 T3 N1 M0 |
| 4a | T4 N0 M0 T4 N1 M0 |
| 4b | Any T N2 M0 Any T Any N M1 |

the hepatic parenchyma. On CT imaging, infiltrating carcinomas that replace the gallbladder often show irregular contrast enhancement with scattered regions of internal necrosis.

Narrowing of proximal CBD in 4 conditions: Post-cholecystectomy stricture, Mirizzi syndrome/calculus, GB mass extending into cystic duct, cholangiocarcinoma

GB carcinoma pearls: Associated with gallbladder calculus/porcelain GB, GB polyp >1 cm, obstruction of CHD, infiltration of adjacent liver segment 5/4b, irregular focal thickening of GB wall, porta hepatis lymph node/peri-pancreatic lymph nodes involvement, mass replacing GB, duodenal infiltration, omental extension, liver metastases.

AJCC gallbladder carcinoma staging: Primary tumor (T): TX- Primary tumor cannot be assessed, T0- No e/o of primary tumor

Tis Carcinoma *in situ*, T1 tumor invades lamina propria (T1a) or muscle layer (T1b), T2 tumor invades perimuscular connective tissue; no extension beyond serosa or into liver, T3 tumor perforates the serosa (visceral peritoneum) or directly invades one adjacent

| Table 4.197.3: Difference between gallbladder polyp and gallbladder calculus | |
|--|---|
| Gallbladder polyp | GB calculus |
| Enhances on CT | Do not enhance |
| T1 hypointense | T1 bright pigment stones, T1 hypointense–cholesterol stones |
| Thickening on chronic state | No thickening of wall |
| No shadowing on ultrasound. Does not changes with position | Shadowing on ultrasound, changes with position |

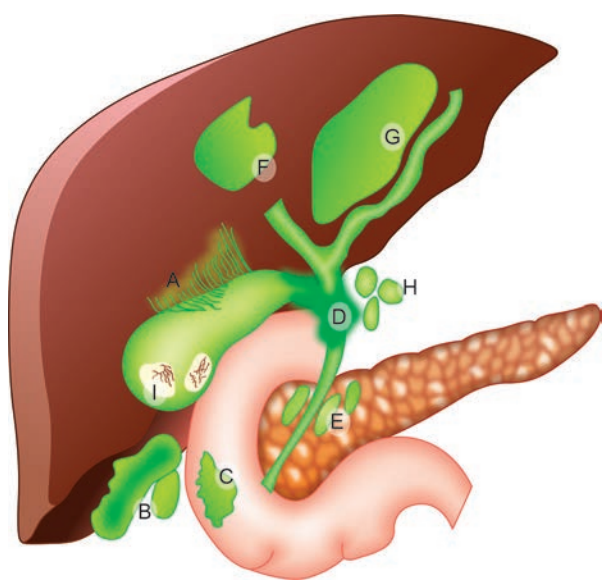


Fig. 4.197.8: Gallbladder carcinoma with extension into liver (A), Subhepatic space (B), Duodenum (C), Extrahepatic bile duct (D), Lymphatic spread (E), (F) Metastasis, (H) Porta hepatis lymph nodes Cholangitic abscess (G), Cholelithiasis (I).

organ, or both (extension 2 cm or less into liver), T4 Tumor extends more than 2 cm into liver, or into two or more adjacent organs (stomach, duodenum, colon, pancreas, omentum, extrahepatic bile ducts, any involvement of liver).

Regional lymph nodes (N): NX Regional lymph nodes cannot be assessed, N0 No regional lymph node metastasis, N1 Metastasis in cystic duct, pericholedochal, or hilar lymph nodes (in the hepatoduodenal ligament), N2 Metastasis in peripancreatic (head only), periduodenal, periportal, celiac, or superior mesenteric lymph nodes.

Distant metastasis (M) : MX Distant metastasis cannot be assessed, M0-No distant metastasis, M1 Distant metastasis.

Treatment and the prognosis: Survival in patients with gallbladder carcinoma is strongly marked by the pathologic stage at presentation. Patients with malignancy limited to the gallbladder mucosa have an excellent prognosis. If there is the direct extension of disease to the muscularis propria, a radical cholecystectomy is necessary. When disease extends through serosa, more radical procedures such as extended cholecystectomy, pancreatoduodenectomy, and major hepatic resection can be performed.

Pattern of GB wall thickening in dengue fever: Uniform echogenic pattern is seen in dengue fever without warning sign; in severe dengue, striated or tram track pattern, asymmetric pattern and honeycombing pattern are obtained.

Comet tail appearance in radiology-thyroid colloid nodule, FNH on ultrasound, adenomyomatosis of gall bladder, GB polyp, asbestosis kidney.

4.198 HEPATOBILIARY SYSTEM

Case No. 198

Clinical history: 26-year-old female, complaints of abdominal pain.

Radiological techniques and observation: MRCP image (Fig. 4.198.3): Angled coronal 2D thick slab fat-suppressed half-Fourier acquisition single-shot turbo spin-echo MR image and T2 haste axial (Fig. 4.198.2) and coronal (Fig. 4.198.1) images show the Dorsal pancreatic duct (Santorini duct) draining separately into the minor papilla. The common bile duct joins the smaller ventral pancreatic duct at a more inferior level and drains into the duodenum through the major papilla.

Interpretation: A: 26 years old female, pancreas, C: Dorsal pancreatic duct (dorsal Santorini duct) draining separately into the minor papilla, B–No irregularity of duct wall, D–Pancreatic divisum

Principal diagnosis: The principal diagnosis is pancreatic divisum.

Differential diagnosis:

1. *Meandering main pancreatic duct:* Meandering main pancreatic duct (MMPD) comprises a reverse Z-type and loop-type of pancreatic ducts.
2. *Ansa pancreatica:* Ansa pancreatica is a rare anatomic variation of the pancreatic ducts. It is a communication between the main pancreatic duct and the accessory pancreatic duct.
3. *Anomalous pancreaticobiliary junction:* Anomalous pancreaticobiliary junction refers to the union of the pancreatic duct and common bile duct outside the duodenal wall.

Treatment: A diagnosis of pancreas divisum does not routinely warrant treatment, especially when incidental and asymptomatic. In symptomatic patients (e.g. recurrent pancreatitis), management options may include: 1. Non-operative treatment +/- pancreatic

enzyme supplements, 2. Minor papillectomy, 3. Minor papilla stenting, 4. Balloon dilatation of any associated stricture.

Brief discussion about the condition: The term dominant dorsal duct syndrome is sometimes used in the literature to reflect the main pancreatic duct draining via the minor papilla does not always have the classical pancreas divisum anatomy.

Pathology: It results from failure of fusion of dorsal and ventral pancreatic anlagen. As a result, the dorsal pancreatic duct drains most of the pancreatic glandular parenchyma via the minor papilla. Although controversial, this variant is considered as a cause of pancreatitis.

Pancreatic divisum can result in a santorinicoele, which is a cystic dilatation of the distal dorsal duct (Santorini duct), immediately proximal to the minor papilla.

Three subtypes are known:

- Type 1 (classic): No connection at all; occurs in the majority of cases: 70%
- Type 2 (absent ventral duct): Minor papilla drains all of pancreas while major papilla drains bile duct; 20–25%
- Type 3 (functional): Filamentous or inadequate connection between dorsal and ventral ducts: 5–6%

Some authors suggest increased sensitivity of secretin MRCP (S-MRCP) in detection sensitivity of pancreas divisum.

Pancreatic duct configurations: The ductal configuration was evaluated as type 1–type 5. At type 1, there was a bifid configuration with dominant duct of Wirsung, at type 2, there was a dominant duct of Santorini without divisum, at type 3, Wirsung duct was seen with absent duct of Santorini. The pancreas divisum is type 4 and 'ansa pancreatica' is type 5.

At the point of embryologic fusion of the ducts of Santorini and Wirsung in the pancreatic neck, the duct may

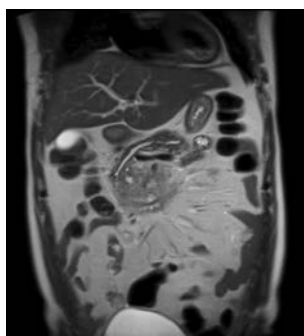


Fig. 4.198.1

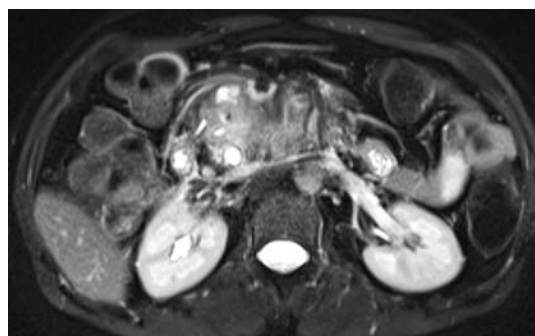


Fig. 4.198.2

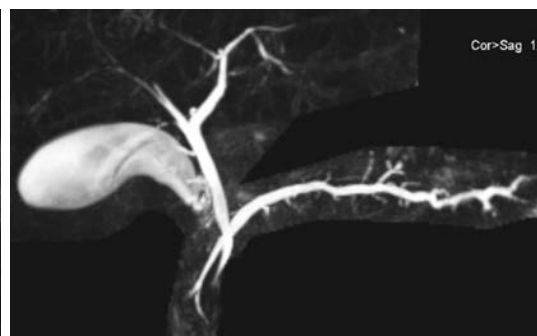


Fig. 4.198.3

Table 4.198.1: Meandering main pancreatic duct and ansa pancreatica

| Meandering main pancreatic duct (MMPD) | Ansa pancreatica |
|---|---|
| The main pancreatic duct (MPD) usually runs smoothly with obtuse-angled curves from the tail and body of the pancreas through the head of the pancreas to the major papilla; in other words, it runs in the antero-posterior, cranio-caudal, and left-right directions. MMPD is defined as the MPD forming a loop or a reverse-Z curve in the head of the pancreas in patients with normal pancreaticobiliary junction. This might be a cause for idiopathic pancreatitis, especially idiopathic recurrent acute pancreatitis (IRAP). | The ansa pancreatica is a rare type of anatomical variation of the pancreatic duct. It is a communication between the main pancreatic duct (of Wirsung) and the accessory pancreatic duct (of Santorini). Recently, the ansa pancreatica has been considered as a predisposing factor in patients with idiopathic acute pancreatitis. The ansa pancreatica arises as a branch duct from the main pancreatic duct. It descends down initially, it then ascends upward forming a loop finally terminating at the minor papilla. This type of pancreatic ductal variation can be identified on ERCP or MRCP studies. |



Fig. 4.198.4: Pancreatic divisum and santorinicele

narrow slightly or demonstrate a loop. These are normal variations and should not be confused with a stricture.

- The pancreatic duct course varies greatly but is most commonly a descending course (50% of cases). When the pancreatic duct is oriented vertically, it may be confused with the extrahepatic bile duct. Other courses include sigmoid, undulating, and loop configurations.
- It is important to be familiar with the various courses of the pancreatic duct and not to mistake them for pathologic conditions such as extrinsic mass-effect from neoplastic lesions.

Pancreatic head configurations: The normal appearance of the pancreatic head is a gentle near-vertical convexity lateral to the superior pancreaticoduodenal artery with three variant (pseudomass) appearances. All three variants show discrete lobulations of normal pancreatic tissue lateral to the anterior superior pancreaticoduodenal artery. In type I variants, the lobule is oriented anteriorly; in type II, posteriorly; and in type III, horizontally.

Anomalous Pancreaticobiliary Junction

An anomalous pancreaticobiliary junction, also known as pancreaticobiliary maljunction, describes the abnormal junction of the pancreatic duct and common bile duct that occurs outside the duodenal wall to form a long common channel (>15 mm).

Associations: The anomalous junction is often associated with a choledochal cyst. The vast majority of patients with Todani type Ia, Ic, and IVa choledochal cysts have an anomalous pancreaticobiliary junction.

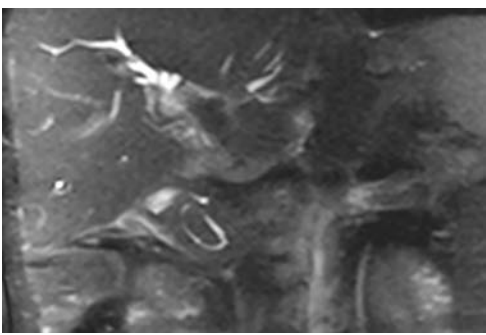


Fig. 4.198.5: Annular pancreas

Classification: The Japanese Study Group on Pancreaticobiliary Maljunction (JSPBM) proposed the following classification: Type A (stenotic type): Dilatation of the common bile duct upstream of a stenotic segment of the distal common bile duct, which joins the common channel. Type B (non-stenotic type): Nonstenotic distal common bile duct smoothly joins the common channel; no localized dilatation of the common channel. Type C (dilated channel type): Narrow distal common bile duct joins dilated common channel. Type D (complex type): Complex maljunction associated with annular pancreas, pancreas divisum, or other complicated duct systems

Treatment and prognosis: The anomaly is associated with a higher risk of acute pancreatitis, cholangitis, and biliary tract carcinoma (cholangiocarcinoma, gallbladder carcinoma). Treatment is surgical correction.

Annular pancreas: Annular pancreas is a morphological anomaly which can cause duodenal obstruction. This condition is important to recognize, as radiologists are

Table 4.198.2: Imaging findings in annular pancreas

| CT | MRI/MRCP |
|--|--|
| Pancreatic tissue is seen to completely or incompletely surround the 2nd part of the duodenum. Associated duodenal narrowing and dilatation of proximal duodenum may also be seen. In adults, it is frequently associated with pancreatitis. | Apart from annular pancreas features, pancreatic ductal anatomy can be well assessed with MR imaging. Annular duct usually joins the main pancreatic duct or accessory duct (duct of Santorini). |

frequently the first to make the diagnosis. common equally in children and adults. identification usually occurs during the 3rd to 6th decade of life. About 25–33% of cases of annular pancreas in adults are asymptomatic and is an incidental finding on imaging. However, it can cause pancreatitis, duodenal obstruction and rarely biliary obstruction in adults. More common symptoms in adults include abdominal pain, post-prandial fullness, vomiting and gastrointestinal bleed from peptic ulcer disease. In children, an annular pancreas may be associated with other congenital anomalies or cause duodenal obstruction.

Embryology: The pancreas is developing from a single dorsal and two ventral buds, which appears as outgrowths of primitive foregut at 5 weeks of gestation. The ventral buds fuse rapidly. In the 7th week of gestation, the duodenum expands, and rotates the ventral bud from right to left, and fuses with the dorsal bud. The ventral bud forms the inferior part of uncinus process and inferior head of pancreas while the dorsal bud gives rise to tail and body of pancreas. Annular pancreas develops due to failure of the ventral bud to rotate with duodenum, causing encasement of duodenum.

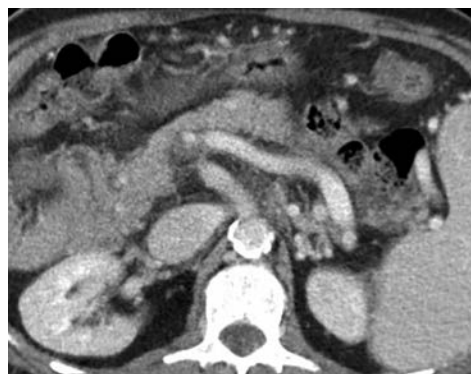
Classification: Annular pancreas can be either complete or incomplete: Complete annular pancreas: Pancreatic parenchyma or annular duct is seen to completely surround the 2nd part of duodenum. Incomplete annular pancreas: annulus does not surround the duodenum completely, giving a 'crocodile jaw' appearance. Associations: Down syndrome/pancreas divisum/pancreatitis/pancreatic cancer/intraductal papillary mucinous neoplasm (IPMN).

Dorsal Pancreatic Agenesis

Agenesis of the dorsal pancreas is an extremely rare congenital pancreatic anomaly. While complete agenesis of the dorsal pancreas is extremely rare, partial agenesis of the dorsal pancreas is thought to be more common.

Clinical presentation: While many patients with this anomaly are asymptomatic, some patients may present with abdominal pain.

Pathology: It is due to an embryological failure of the dorsal pancreatic bud to make the body and tail of the

**Fig. 4.198.6:** Dorsal pancreatic agenesis

pancreas. Partial dorsal pancreatic agenesis may be appreciated as a short, rounded pancreatic head adjacent to the duodenum with absence of the pancreatic neck, body, and tail. With the partial agenesis of the dorsal pancreas, the size of the body of the pancreas varies, there is a remnant of the duct of Santorini, and the minor duodenal papilla is present.

Dorsal pancreatic agenesis: With complete agenesis of the dorsal pancreas, the neck, body, and tail of the pancreas, the duct of Santorini, and the minor duodenal papilla are all absent.

Associations: Hyperglycemia: May be seen in a significant proportion of cases (up to 50%), solid pseudopapillary tumor of the pancreas: Possible association, polysplenia/pancreatitis.

CT: The pancreatic body and tail are hypoplastic or absent to varying degrees with preservation of the pancreatic head.

Accessory pancreas: Ectopic pancreatic tissue, also known as heterotopic pancreatic tissue, refers to the presence of pancreatic tissue in the submucosal, muscularis or subserosal layers of the luminal gastrointestinal tract outside the normal confines of the pancreas and lacking any anatomic or vascular connection with the main pancreas.

Clinical presentation: Most commonly an asymptomatic entity.

Location: Proximal duodenum/gastric antrum including within gastric duplication cysts

Proximal jejunum/Meckel diverticulum/Ileum.

Table 4.198.3: Causes of postbulbar duodenal obstruction classification

| I. Developmental or congenital factors | II. Extrinsic factors (extraduodenal disease) | III. Intrinsic factors (intraduodenal disease) |
|--|--|---|
| A. Occlusion by superior mesenteric artery or "duodenal ileus" B. Obstruction at ligament of Treitz C. Volvulus of jejunum D. Congenital band E. Malrotation of small intestine F. Annular pancreas | A. Abdominal aneurysm B. Pancreatic lesions 1. Benign cyst 2. Islet-cell adenoma 3. Carcinoma C. Enlarged mesenteric nodes D. Retroperitoneal tumors | A. Ulceration 1. Ulcer, second portion of duodenum 2. Marginal ulcer 3. Duodenitis (regional enteritis) B. Neoplasm 1. Benign 2. Malignant a. Carcinoma b. Sarcoma (lymphosarcoma, Hodgkin's sarcoma, reticular cell sarcoma) |
| IV. Unknown, e.g., lupus erythematosus | | |

Barium study: In 45% of the cases of ectopic pancreas discovered on upper gastrointestinal examination, the ectopic pancreatic tissue contains a central small collection of barium, i.e. a central niche or umbilication, indicative of the rudimentary duct's draining orifice. It is this finding that is diagnostic of ectopic pancreatic tissue.

CT: Contrast enhanced CT may show a homogeneously enhancing tissue (similar to normal pancreas) or cystic area (acinar component or pseudocyst).

Treatment and prognosis: Laparoscopic wedge resection is usually successful in removing the ectopic tissue, although its success is dependent on the location.

Modified CT severity index for acute pancreatitis: Scores are usually generated by estimating pancreatic inflammation and the necrosis to give a score out of 10. Pancreatic inflammation: 0: Normal pancreas, 2: intrinsic pancreatic abnormalities with or without inflammatory changes in peripancreatic fat, 4: Pancreatic or peripancreatic fluid collection or peripancreatic fat necrosis. Pancreatic necrosis: 0: None, 2: 30% or less, 4: more than 30%. Extrapancreatic complications: 2: one or more of pleural effusion, ascites, vascular complications, parenchymal complications and/or gastrointestinal involvement. Total score Total points are given out of 10 to determine the grade of pancreatitis and aid treatment: 0–2: Mild; 4–6: Moderate; 8–10: Severe.

The Revised Atlanta classification of acute pancreatitis (2012) is an international multidisciplinary classification of the severity of acute pancreatitis, updating the 1992 Atlanta classification. The classification system is based on local and systemic determinants of severity, with: Local determinants which is related to the presence or absence of the (peri)pancreatic necrosis, sterile or infected systemic determinants related to the presence or absence of organ failure, transient or persistent.

The grading of severity (mild, moderate, severe, and critical) is based on the combinations of these determinants and, discrimination was made between two clinical phases of pancreatitis: a) Early (1st week): in which severity is based on the presence or absence of systemic organ failure. b) Late (>1st week): In which severity is based on the presence of local complication or persistent systemic organ failure. The Atlanta classification makes acute pancreatitis into two basic types: 1) Interstitial edematous pancreatitis (IEP), 2) Necrotizing pancreatitis (NP) which is further subdivided into: a) Parenchymal necrosis, b) Peripancreatic necrosis, c) Combined type (peripancreatic and parenchymal necrosis): Most common. All types of necrotizing pancreatitis may be of sterile or infected; gas formation is the best imaging feature to suggest infection. New term for fluid collections associated with acute pancreatitis is given: 1) Fluid collections associated with interstitial edematous pancreatitis (i.e. minimal or no necrosis). a) Acute peripancreatic fluid collections (APFC) in the first-4 weeks: Non-encapsulated peripancreatic fluid collections; b) Pseudocysts: Develop after 4 weeks; encapsulated peripancreatic or remote fluid collections. 2) Fluid collections associated with necrotizing pancreatitis–a) Acute necrotic collections (ANCs): In the first 4 weeks; non-encapsulated heterogeneous non-liquefied material; b) walled-off (pancreatic) necrosis (WON or WOPN): develop after 4 weeks; encapsulated heterogeneous non-liquefied material. ANCs and WONs are collections that contain both fluid and necrotic material of various amounts (an important point to differentiate them from APFCs and pseudocysts, however, in indeterminate cases follow-up is recommended).

4.199 HEPATOBILIARY SYSTEM

Case No. 199

Clinical history: 68-years-old female with dyspepsia.

Radiological techniques and observation: CT Abdomen plain and contrast, MRI upper abdomen—axial and coronal T2 HASTE, axial T1, diffusion images, ADC map with MRCP.

Figures 4.199.1 to 4.199.3 are CT abdomen images showing a well-defined lobulated hypodense multicystic

lesion in the head of the pancreas with central stellate calcified scar. MPD appears dilated. Figures 4.199.4 to 4.199.15 show T1 hypointense T2 hyperintense multiseptated cystic mass lesion noted in the head of the pancreas, each cyst measuring 10 mm, with multiple thin septa and central hypointense stellate scar. The lesion does not show diffusion restriction. Lesion is compressing and narrowing the main pancreatic duct with upstream dilatation and mild diffuse atrophy of



Fig. 4.199.1



Fig. 4.199.2



Fig. 4.199.3

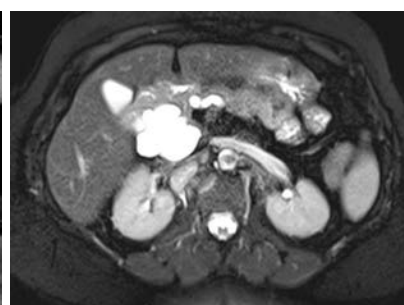


Fig. 4.199.4

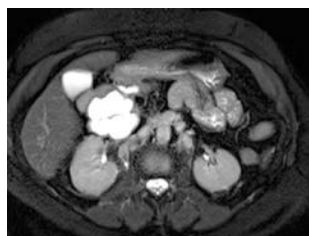


Fig. 4.199.5

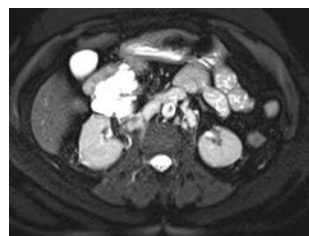


Fig. 4.199.6

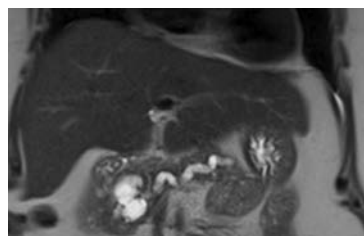


Fig. 4.199.7

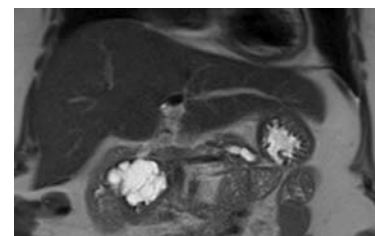


Fig. 4.199.8

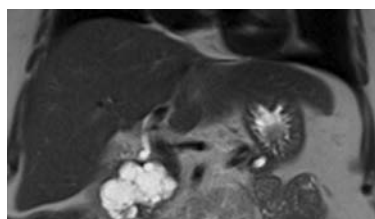


Fig. 4.199.9

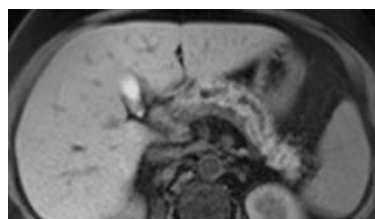


Fig. 4.199.10

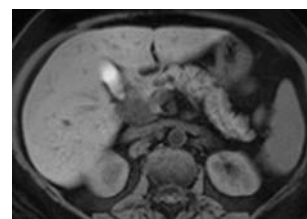


Fig. 4.199.11

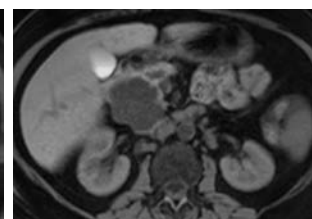


Fig. 4.199.12

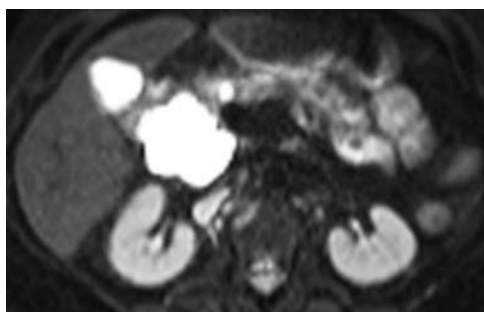


Fig. 4.199.13

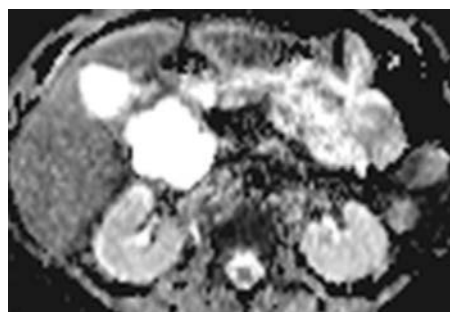


Fig. 4.199.14

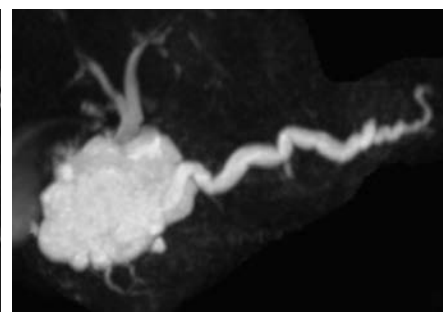


Fig. 4.199.15

Table 4.199.1: Differential diagnosis for serous cystadenoma of the pancreas

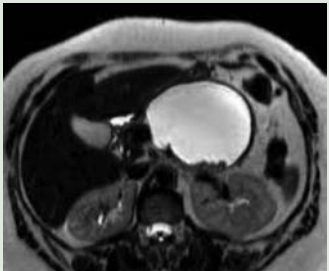
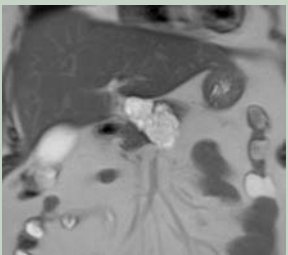
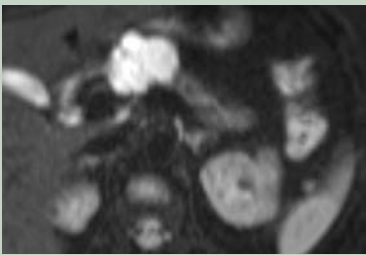
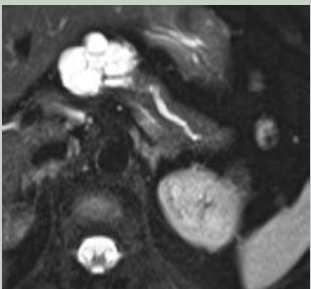
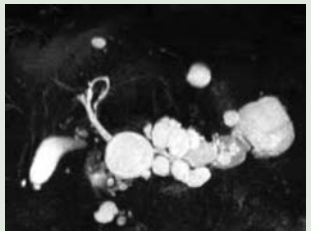

| | | |
|---|--|---|
| Mucinous cystic neoplasm “Mother lesion”—occur in middle aged females. Premalignant or malignant. | Tendency to occur in the tail of pancreas. <6 cysts, relatively large cysts >2 cm, Displacing MPD, Contains ovarian stroma, “Mother” lesion—middle aged females. Endoscopic US with cyst aspiration: Elevated CEA/CA 19-9 in cases of invasive malignancy. |  |
|  |  |  |
| Fig. 4.199.17: Mucinous cystic neoplasm | Fig. 4.199.18: Mucinous cystic neoplasm | Fig. 4.199.19: Mucinous cystic neoplasm |
| Side Branch IPMN Commonly seen in males aged 50–70 years. More common in familial pancreatic cancer, Peutz-Jeghers and familial adenomatous polyposis. | Multiple cystic lesions scattered throughout the pancreas, communication with adjacent MPD is the key to diagnosis, enlargement of cyst in secretin MRCP, ERCP-direct visualization of patulous, bulging, “fish-mouth” ampulla with mucin extruding through. Demonstrates dilatation of MPD or communication of side branch IPMN with MPD. |  |
| Non-syndromic Islet cell tumors 40–60 years Larger at presentation. Symptoms due to mass effect. | Lesions usually >5 cm with frequent cystic/necrotic degeneration. Shows enhancement with contrast. Strong tendency to be malignant (80–100%), may present with metastases. Invasion of portal vein and SMV noted. |  |
| Fig. 4.199.20: Side branch IPMN | Fig. 4.199.21: Non-syndromic Islet cell tumors | |
| Solid and pseudopapillary neoplasm: Rare, slow growing low grade tumor. <35 years old females “daughter lesion” | Can occur anywhere in pancreas, Solid mass with cystic components and internal haemorrhage. No biliary or pancreatic ductal obstruction. | |
| Main branch IPMN (Refer to case 200) | | |
| Other differentials include: Walled-off necrosis (other features of pancreatitis seen), choledochal cyst (fills up in HIDA scan), hydatid cyst (daughter cysts seen), choledochocoele, groove pancreatitis and pancreatic lymphangiomias. | | |

Table 4.199.2: Patterns of cystic pancreatic carcinoma

| | | |
|----------------------------------|--|---|
| Microcystic or honeycomb pattern | Macrocytic or oligocystic variant (<10%) >2 cm cysts. This variant is difficult to distinguish from mucinous cystic tumor. | “Solid” serous adenoma—enhancing septa predominate. |
|----------------------------------|--|---|

Table 4.199.3: Classification of cystic neoplasms of pancreas

| | |
|--|---|
| <i>Epithelial neoplastic</i> | <i>Epithelial non-neoplastic</i> |
| Intraductal papillary neoplasm all types | Lymphoepithelial cyst |
| Mucinous cystic neoplasm | Mucinous non-neoplastic cyst |
| Serous cystic neoplasm | Enterogenous cyst |
| Cystic neuroendocrine tumor | Retention cyst/dysodontogenetic cyst |
| Acinar cell cystadenoma | Peri-ampullary duodenal wall cyst |
| Cystic acinar cell carcinoma | Endometrial cyst |
| Solid pseudopapillary neoplasm | Congenital cyst (in malformation syndromes) |
| Accessory splenic epidermoid cyst | |
| Cystic hamartoma | |
| Cystic teratoma (dermoid cyst) | |
| Cystic ductal adenocarcinoma | |
| Cystic pancreatoblastoma | |
| Cystic metastatic epithelial neoplasm | |
| Others | |
| <i>Non-epithelial neoplastic</i> | <i>Non-epithelial non-neoplastic</i> |
| Benign non-epithelial neoplasm (e.g. lymphangioma) | Pancreatitis associated pseudocyst |
| Malignant non-epithelial neoplasms (e.g. sarcomas) | Parasitic cyst |

Table 4.199.4: Difference between serous and mucinous cystic neoplasm

| | |
|--|---|
| <i>Serous cystic neoplasm</i> | <i>Mucinous cystic neoplasm</i> |
| Mostly benign | Potentially malignant |
| Grandmother lesion | Mother lesion |
| Small cysts <2 cm and >6 in number | Large cysts >2 cm and <6 in number. |
| Sponge-like or honeycomb pattern | |
| Central stellate sunburst calcification (in 33%) | Peripheral amorphous or septal calcification (in 15%) |
| Hypervascular soft tissue component | Hypovascular soft tissue component |
| Involves pancreatic head commonly | Involves pancreatic tail commonly |
| Contains glycogen | Contains mucin |

Table 4.199.5: Risk factors and imaging features in cystic neoplasm of pancreas

| | |
|--|--|
| <i>Risk factors</i> | <i>Imaging features</i> |
| <ul style="list-style-type: none"> Older age Symptomatic patient—pain, pancreatitis. Elevated CEA / CA 19-9 | <ul style="list-style-type: none"> Larger lesions >40 mm Thick enhancing septations, wall thickening Mural nodularity Upstream pancreatic duct dilatation/atrophy |

the rest of the pancreatic parenchyma. Mass is smoothly indenting the adjacent duodenum and IVC without infiltration. SMA, SMV and portal vein appear normal. No evidence of any infiltration of adjacent structures and vessels. Mass smoothly indents and narrows the distal CBD without significant biliary dilatation. Diffuse fatty infiltration of liver noted. A few oval-shaped discrete non-necrotic nodes noted in the peri-portal, porta-caval and para-aortic region—possibly non-neoplastic.

Interpretation: A: Elderly female with multisepted cystic mass lesion in the head of the pancreas, C: With multiple thin septations and central calcified stellate scar causing compression of MPD with, B: Upstream dilatation and mild diffuse atrophy of the rest of the pancreatic parenchyma, D: Serous cystadenoma of the pancreas.

Principal diagnosis: Serous cystadenoma of the pancreas

Further investigations: Endoscopic US with cyst aspiration: Low CEA, CA 19-9, mucin, amylase. No evidence of atypia on cytology. ERCP: To evaluate ampulla and ducts.

Management: Complete surgical excision (large tumors, especially >4 cm with mass effect or patient symptomatology)

Indeterminate lesions without classic imaging appearance: MR or endoscopic ultrasound

Asymptomatic small tumors with classic imaging features: Serial imaging follow-up.

Brief discussion: Cystic neoplasms of pancreas.

Congenital cysts of pancreas: Autosomal dominant polycystic kidney disease, von Hippel-Lindau disease, Beckwith-widemann syndrome, Meckel-Gruber syndrome, cystic fibrosis, lymphoepithelial cysts and true cysts.

Serous cystadenoma: 30% of pancreatic cystic neoplasms, benign lesion.

Age and sex: Females, median age 65 years “grandmother lesion”.

Location: More common in pancreatic head. Growth rate = 4 mm/yr.

Association: Multiple serous cystadenomas in pancreas associated with von Hippel-Lindau disease.

European Evidence-based Guidelines on Pancreatic Cystic Neoplasms

a. *Serous cystic neoplasm:* SCN is a benign lesion. There are no deaths that are due to dissemination/malignant behaviour of an SCN. Specific mortality due to an SCN is nearly zero. Cases reported as ‘malignant’ do not fulfil the WHO criteria for an SCN.

Asymptomatic patients with radiological evidence of an SCN should be followed up for 1 year. After 1 year, symptom-based follow-up is recommended. Only when the diagnosis is uncertain follow-up required. In these cases, a patient should undergo the same follow-up as for a BD-IPMN as given below.

When the diagnosis of SCN is clear, surgery is recommended only in patients with symptoms related to the compression of adjacent organs (i.e., bile duct, stomach, duodenum, portal vein)

The size of about 60% of SCN remains stable. An increase in cyst size is seen in 40% but the rate of growth is slow and new onset of symptoms is very rare.

b. *Mucinous cystic neoplasm:* MCN 40 mm should undergo surgical resection. Resection is also recommended for MCN which are symptomatic or have risk factors (i.e., mural nodule) irrespective of their size. The rate at which the size of an MCN increases should be considered. Some case reports have suggested considerably faster growth of MCN during pregnancy, potentially leading to tumor rupture. Therefore, patients with MCN should be observed closely during pregnancy. It is safe to follow-up presumed MCN that measure <40 mm, in the absence of risk features such as a suspicious mural nodule or symptoms.

For patients with MCN measuring between 30 and 40 mm, clinicians can incorporate other factors such as age, comorbidities, patient’s surgical risk, and patient preference.

For cysts measuring <30 mm, it may be difficult to make a definitive diagnosis of an MCN, and smaller MCN may sometimes be difficult to distinguish other cystic lesions. We therefore recommend similar surveillance for MCN and IPMN measuring <3 cm. MCN measuring <40 mm without a mural nodule or symptoms may undergo surveillance with MRI, EUS, or a combination of both. Surveillance is recommended every 6 months for the first year, then annually if no changes are observed. Patients with an MCN measuring <40 mm and with no concerning features or symptoms should have lifelong surveillance as long as they are fit for surgery. Earlier studies have evaluated features associated with malignant transformation for all mucinous lesions combined. However, IPMNs and MCN may have different rates of growth and malignant transformation and different features predictive of malignancy. To avoid incomplete treatment of invasive carcinoma, a standard oncologic resection (distal pancreatectomy in 90–95% of MCN) with lymph node dissection and splenectomy is indicated for any MCN with imaging features indicating high-grade dysplasia or cancer. MCN without suspect features with a low risk of malignancy can be treated with a non-oncological resection (distal pancreatectomy with splenic preservation with or without preservation of splenic vessels, or PSP). A PSP (parenchyma sparing pancreatectomy) may be considered in selected patients to decrease the long-term risk of diabetes, provided the anatomical location is favourable. PSP are associated with higher early morbidity and longer hospitalisation. A laparoscopic approach is feasible for MCN. Its benefit over an open approach is comparable to other indications.

Other uncommon and undefined cystic tumors of the pancreas: If the diagnosis of a cyst is unclear based on a specific imaging modality, next line of investigation

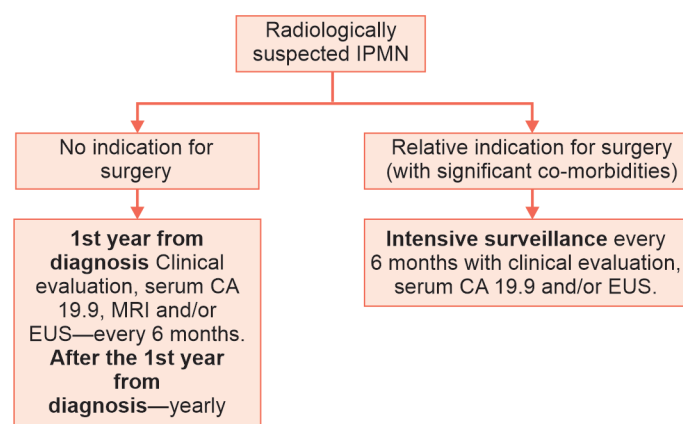


Fig. 4.199.22

is: For a cyst measuring <15 mm, either cross-sectional imaging or EUS alone may be performed. For cysts ≥ 15 mm, or if the diagnosis is unclear, both cross-sectional imaging and EUS should be performed, including EUS-FNA if warranted. The follow-up criteria for small/undefined cyst: Cysts which are of unclear aetiology, have no risk factors for malignancy, and measure <15 mm, should be re-examined after 1 year. If stable for 3 years, follow-up may be extended to every 2 years. Cysts measuring ≥ 15 mm should be followed up every 6 months during the first year and annually thereafter. As an undefined cyst may be mucinous by nature, surveillance is recommended. Most studies report that the risk of malignant transformation of PCN increases with size. This probably also applies to cysts of unclear aetiology. A prospective population-based study found that unidentified cysts are very common (49% when including diameters of ≥ 2 mm), increase in number and size with age of the population (57% of subjects), but have no effect on pancreatic disease-associated mortality over 5 years. Recommendations that include 6-month surveillance intervals may therefore constitute overtreatment in cases where IPMN and MCN have been ruled out. Patients with undefined cysts should undergo lifelong follow-up, unless the patient is unwilling, or unfit to undergo pancreatic surgery. The long-term evolution of PCN is still largely unknown, which also applies to undefined pancreatic cysts. Therefore, no rational term for termination of surveillance can be given. However,

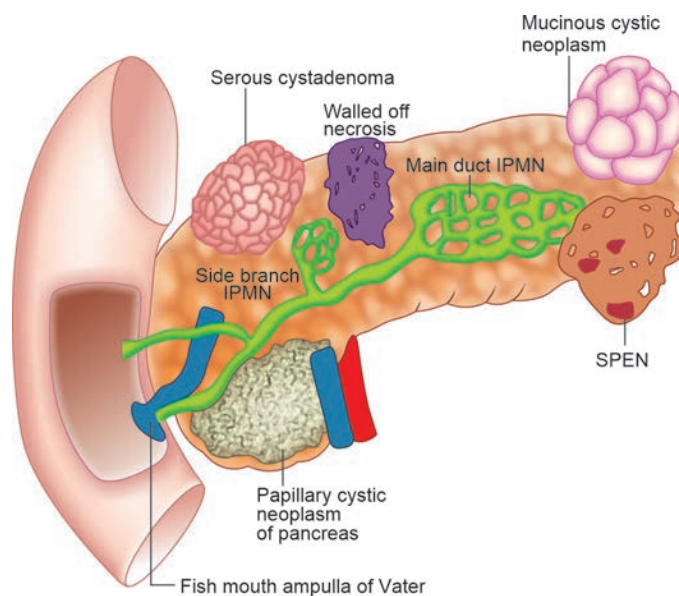


Fig. 4.199.23: Cystic pancreatic neoplasms

recent data suggest that the risk of progression increases over time. To establish diagnosis of cystic pancreatic lesions: Rare cystic pancreatic lesions include hydatid cysts, haemangioma, lymphoepithelial cysts, acinar cell cystadenomas, desmoid cysts, and haemolymphangiomas. Such cysts require a multidisciplinary approach, in an expert pancreatic centre, to determine the optimum management strategy. Surgery may be necessary if the diagnosis remains unclear.

4.200 HEPATOBILIARY SYSTEM

Case No. 200

Clinical history: 61-year-old male presented with complaints of abdominal pain

Radiological technique and observation: Limited section of T1-axial, T2-axial MRI abdomen images Figs 4.200.1 and 4.200.2 are provided. MRI shows a well-defined T1 hypointense/T2 hyperintense cystic lesion in the head of the pancreas. The lesion demonstrates an eccentric mural nodule within. T2 shows communication of the cyst with the side branch of MPD. MPD shows ductal wall thickening. There is narrowing noted at the level of cyst-neck junction. No evidence of side branch/main branch MPD dilatation.

Interpretation: A—61-years-old male, pancreatic head region, C—well-defined cystic lesion, B—cystic lesion shows communication with side branch of MPD and eccentric mural nodule, D—IPMN.

Principal diagnosis: Intraductal papillary mucinous neoplasm—IPMN—side branch type with high risk stigmata.

Further investigation and management: According to the International Consensus Guidelines, the patient has to undergo resection.

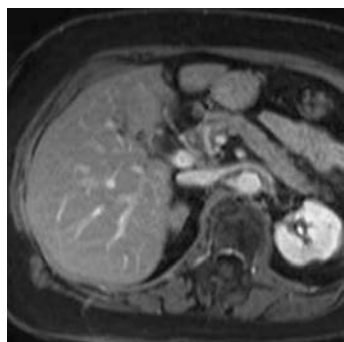


Fig. 4.200.1

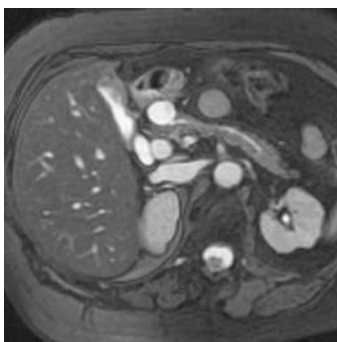


Fig. 4.200.2

International consensus Guidelines (Fukuoka guidelines): High risk stigmata (increased risk of malignancy): Dilated main pancreatic duct ≥ 10 mm, solid enhancing mural nodule (management: complete surgical resection of the lesion).

Worrisome features (moderate risk of malignancy): Branch duct IPMN size ≥ 3 cm, dilated main pancreatic duct of 5–9 mm, non-enhancing mural nodule, thickened enhancing wall, focal stenosis of pancreatic duct with distal parenchymal atrophy (management: Should undergo EUS—presence of suspicious cytology or mural nodularity/main duct involvement on EUS in this subgroup warrants consideration of surgery. If EUS is negative, follow-up with CT/MR based on size (2–3 years for cysts < 1 cm, yearly $\times 2$ years for 1–2 cm, and 3–6 months for > 2 cm)

European evidence based guidelines for IPMN: Absolute indications for Surgery: Positive cytology for malignancy, Enhancing mural nodule > 5 mm, pancreatic duct dilatation > 10 mm

Relative indications: Increased CA19-9, Growth rate > 5 mm per year, Pancreatic duct dilatation 5–10 mm, Enhancing mural nodule < 5 mm, New onset diabetes, acute pancreatitis, patients with significant co-morbidities.

No indication for surgery: Does not fall into any group. Needs clinical evaluation, CA19-9 and MRI every 6 months until 1 year and yearly thereafter.

Intraductal papillary mucinous neoplasm (IPMN): Mucin-producing papillary tumor arising from epithelium of main pancreatic duct (MPD) or duct side branches. Presentation usually between 50 and 70 years with slight male predominance

IPMN can be divided into 3 types: Side branch IPMN: Mucin-producing neoplasm centred in pancreatic duct

Table 4.200.1: Differential diagnosis of cystic lesion of pancreas

| | |
|---|---|
| Walled of necrosis | Common cystic pancreatic neoplasms <ul style="list-style-type: none"> Serous cystadenoma Mucinous cystic neoplasm IPMN |
| Rare cystic pancreatic neoplasms <ul style="list-style-type: none"> Solid pseudopapillary tumor Acinar cell cystadenocarcinoma Lymphangioma Hemangioma Paraganglioma | Solid pancreatic lesions with cystic degeneration <ul style="list-style-type: none"> Pancreatic adenocarcinoma Cystic islet cell tumor (insulinoma, glucagonoma, gastrinoma) Metastasis Cystic teratoma |

Table 4.200.2: Approach to management of cystic lesions of pancreas

| Incidentally detected cystic pancreatic mass | | |
|--|--|--|
| <2 cm | 2–3 cm | >3 cm |
| Single year follow-up in 1 year (MRI) | Imaging characterization | a. Serous cystadenoma—consider resection if >4 cm |
| a. Stable: Benign—no further follow up b. Growth: Do MRI/MRCP | a. Uncharacterized cystic mass—yearly follow-up b. BD-IPMN Follow-up every 6 months for 2 years c. Serous cystadenoma—Followup every 2 years | b. Uncharacterised cystic mass or other cystic neoplasm—cystic aspiration—resect depending on comorbidities and risk |

side branch with normal MPD (risk of malignancy 17%). Main duct IPMN: Mucin-producing neoplasm centered in main pancreatic duct (risk of malignancy 58%). Combined IPMN: Involves both main duct and side branch with malignancy risk similar to main duct IPMN

Imaging: CT: Side branch IPMN: (1) Communication with adjacent MPD is key to diagnosis. (2) Often multiple small cysts scattered throughout pancreas. Main branch IPMN: 1) Markedly dilated, tortuous MPD without evidence of distal obstructing mass and often with “bulging” ampulla. 2) Presence of polypoid enhancing

nodularity within MPD lumen is very suspicious for malignancy

MRI: MR likely superior for identifying small cysts and multifocal disease, visualizing communication between cyst and main duct, and assessing main duct involvement. Superior soft tissue resolution of MR may allow better assessment of subtle mural nodularity.

Endoscopic ultrasound (EUS): Spatial resolution of EUS may help identify suspicious morphologic features (e.g., mural nodularity) not visible. On CT/MR, and can help guide FNA and cyst aspiration. ERCP: “Fish-mouth” ampulla with mucin extruding through ampulla (due to mucin hypersecretion) in main duct IPMN.

Pancreatic protocol: Thin-section, multi-phase technique with

- Pre-contrast images and
- Early arterial phase (CT angiography phase) images of the aorta and the superior mesenteric artery (20–25 after the start of contrast injection)
- Pancreatic phase (40–50 s after the start of contrast injection), and
- Portal venous phase images (70–80 s after the start of contrast injection).

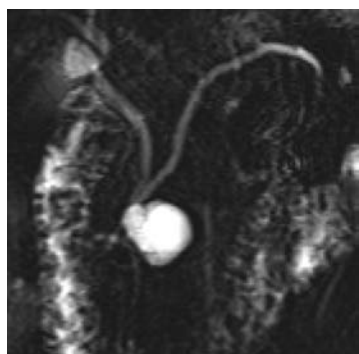


Fig. 4.200.3: Intraductal papillary mucinous neoplasm

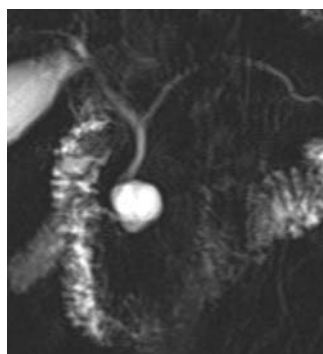


Fig. 4.200.4: Intraductal papillary mucinous neoplasm

Table 4.200.3: Biomarkers for cystic pancreatic lesions

| | <i>Amylase</i> | <i>CEA</i> | <i>CA 19-9</i> | <i>MUCIN</i> |
|--------------------|----------------|------------|----------------|--------------|
| Walled of necrosis | ↑ | ↓ | ↓ | – |
| Serous | ↓ | ↓ | ↓ | – |
| Mucinous | | | | |
| Cystadenoma | ↓ | ↑ | ↓ | + |
| Mucinous | | | | |
| Cystadenocarcinoma | ↓ | ↑ | ↑ | + |
| IPMN | ↑ | ↑ | ↓ | + |

4.201 HEPATOBILIARY SYSTEM

Case No. 201

Clinical history: 55-year-old male with obstructive jaundice.

Radiological techniques: Contrast enhanced CT axial, oblique coronal, oblique sagittal MPR images along the CBD and pancreatic duct and MRCP images provided.

Observations: CECT arterial phase images (Figs 4.201.1 to 4.201.6) show an ill-defined, non enhancing hypodense mass lesion in the head of pancreas. There is no evidence of any calcifications. Bilobar intrahepatic biliary radicles, CBD and MPD appears dilated with abrupt cut-off distally. The lesion appear to infiltrate the wall of adjacent 2nd part of duodenum. Upstream pancreatic parenchymal atrophy noted. Visualized vessels appear normal. MRCP shows dilated bilobar IHBR, CBD and MPD. There is irregular narrowing of distal CBD and MPD with a "rat tail" appearance. The lesion appears hypointense on T2 with infiltration of adjacent duodenal wall. There is no evidence of adjacent vessel involvement.

Interpretation: A: 55 years old male, mass in head of pancreas, C: Non-enhancing mass in the pancreatic head with absent calcifications, T2 hypointense, dilatation of MPD and CBD with, B: Distal irregular "rat tailing" and upstream pancreatic atrophy, D: Pancreatic adenocarcinoma

Principal diagnosis: Pancreatic adenocarcinoma.

Prognosis: Poor

Distance from duodenal lumen to dilated ducts: 14–42 mm (mean 25 mm)

Further investigations:

1. **Tumour markers:**

- Elevated tumour markers: CA 19-9 (most important), CEA, CA 242.
- CA 19-9: Normal range 0–37 U/ml, >37 U/ml is considered abnormal.

2. **Endoscopic US and biopsy:** Hypoechoic mass with minimal internal vascularity, biliary and pancreatic ductal dilatation upstream from tumor. Guides biopsy.

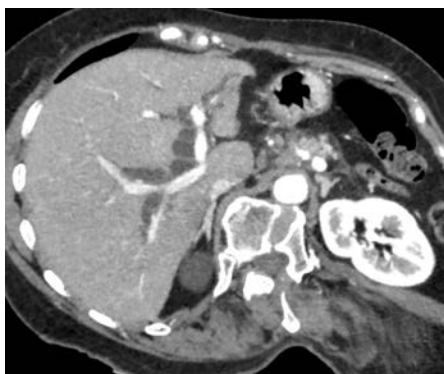


Fig. 4.201.1

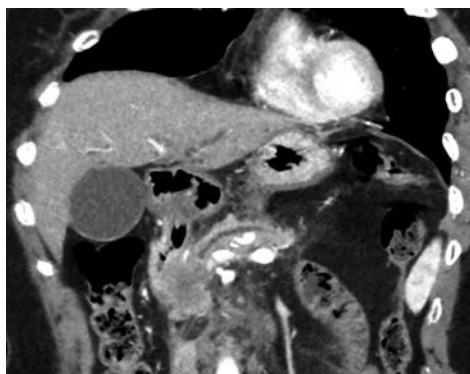


Fig. 4.201.2

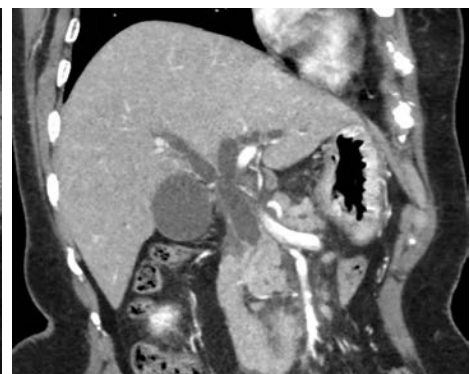


Fig. 4.201.3

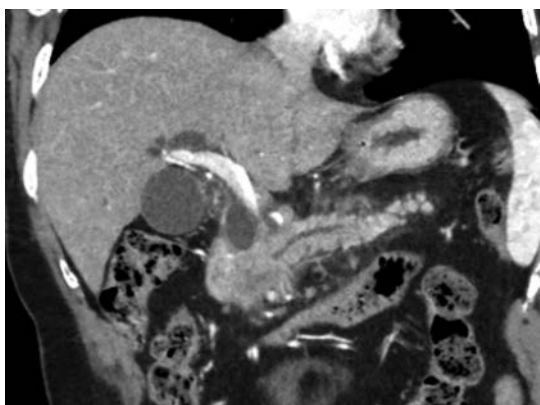


Fig. 4.201.4



Fig. 4.201.5

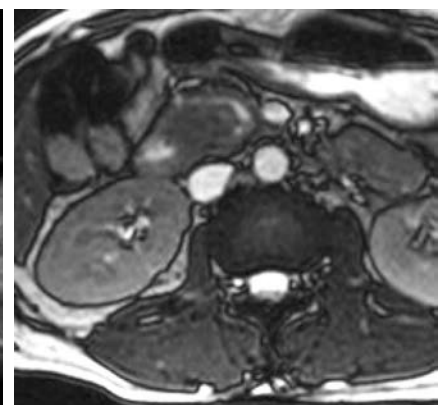


Fig. 4.201.6

Table 4.201.1: Differential diagnosis for pancreatic adenocarcinoma

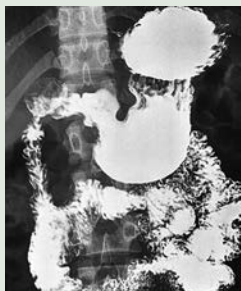
| | | |
|--|--|---|
| 1. Ampullary carcinoma: 6% of peri-ampullary lesions, Median age—65 years, earlier in patients with hereditary polyposis syndromes, M:F = 2:1 | Well-defined lobulated mass centered in ampulla, almost always obstructs common bile duct (CBD), pancreatic duct (PD) obstructed in only 50%, usually does not cause upstream pancreatic atrophy. Shows enhancement in both arterial and venous phases. In MRI, T1 hypo and T2 isointense. |  |
| Prognosis: Good. Distance from duodenal lumen to dilated ducts: 2 to 9 mm (mean 5 mm) | | |
| 2. Distal CBD Cholangio-carcinoma: 20% of all cholangio-carcinomas occur in distal 1/3rd of CBD, | Asymmetric enhancing CBD duct wall thickening or intraductal mass, delayed enhancement noted. Biliary dilatation with abrupt cut-off, MPD may not be dilated with distal non-dilated duct forms “3-segment sign”. | Fig. 4.201.7: Ampullary carcinoma |
| Prognosis: Intermediate | | |
| 3. Duodenal adenocarcinoma Rare, represents <1% of all gastrointestinal neoplasms, 7th decade, slight male predominance. | Presents as gastric outlet obstruction. May manifest as polypoid or fungating, ulcerative and annular constrictive or infiltrating types. Compared with other peri-ampullary masses, dilatation of ducts is only modest. | |
| Prognosis: Good | | |
| 4. Inflammatory mass Middle aged adults, M>F. | Parenchymal calcifications seen, enhancement seen with contrast, “penetrating duct sign”—mass is penetrated by an unobstructed pancreatic duct, beaded duct and ductal calculi seen. | |

Table 4.201.2: WHO 2010 classification of pancreatic neoplasms

| | |
|--|--|
| I. Epithelial <i>Benign tumors:</i> Acinar cell cystadenoma, serous cystadenoma <i>Premalignant lesions:</i> Pancreatic intraepithelial neoplasia, grade 3 (PanIN-3), intraductal papillary mucinous neoplasm (IPMN), intraductal tubulopapillary neoplasm (ITPN), mucinous cystic neoplasm (MCN) <i>Malignant:</i> Ductal adenocarcinoma—adenosquamous carcinoma, mucinous adenocarcinoma, hepatoid carcinoma, medullary carcinoma, signet ring cell carcinoma, acinar cell carcinoma, acinar cell cystadenocarcinoma, IPMN with an associated invasive carcinoma, mixed acinar ductal carcinoma, mixed acinar neuroendocrine carcinoma, mixed acinar neuroendocrine ductal carcinoma, mixed ductal neuroendocrine carcinoma, MCN with an associated invasive carcinoma, pancreatoblastoma, serous cystadenocarcinoma, solid pseudopapillary neoplasm | II. Neuroendocrine neoplasms III. Mature teratoma IV. Mesenchymal tumors V. Lymphomas VI. Secondary tumours |
|--|--|

3. **Barium upper GI study:** Widening of c-loop of duodenum, “Frostberg reverse 3 sign”—Inverted 3 contour to medial part of duodenal sweep and

“Antral padding”—extrinsic indentation by tumor by posteroinferior margin of antrum.

4. **ERCP:** “Double duct sign” with obstruction of MPD and CBD at same level, abrupt cut-off (or) Irregular, nodular, rat-tailed ducts.
5. **PET CT:**
- Not effective for diagnosis of primary tumor.
 - Not helpful to assess vascular invasion or loco-regional staging.
 - To differentiate pancreatic carcinoma from benign lesions, inflammatory lesions and autoimmune pancreatitis.
 - Judging response to treatment.
 - To differentiate post-treatment fibrosis and residual tumor.
 - Useful for distant staging.

Management: Resectable—complete surgical resection with negative surgical margins.

Depends on resectability of tumour under MD Anderson criteria for determination of loco-regional resectability.

Brief discussion

Pancreatic adenocarcinoma: Malignancy arising from ductal epithelium of exocrine pancreas. 95% of pancreatic malignancies.

Age: Median age at onset—71 years, almost always after age 45, Peak: 7th–8th decade, M:F = 1.3:1. Risk factors: Family history, cigarette smoking, alcohol, obesity, diabetes mellitus, chronic pancreatitis, high fat diet. Associations: Hereditary pancreatitis, hereditary breast and ovarian cancer syndrome, Peutz-Jeghers, ataxia telangiectasia, familial colon cancer, Gardner syndrome, and familial aggregation of pancreatic cancer.

Clinical presentation: Jaundice, severe weight loss, epigastric pain radiating to back. Body and tail tumors are asymptomatic. Trousseau syndrome (migratory thrombo-phlebitis) due to tumour induced hypercoagulability. Bleeding varices—result from SMV or splenic vein occlusion.

Imaging: Head (60%), body (20%), diffuse (15%), tail (5%), average size 2–3 cm.

Plain CT: Poorly margined, hypodense mass with tendency to infiltrate posteriorly into retroperitoneum. Tumor virtually never calcifies in absence of treatment.

CECT: Pancreatic adenocarcinoma enhances poorly in pancreatic phase, i.e. hypodense relative to pancreatic parenchyma.

Pancreatic protocol: Precontrast—water as oral contrast, slice thickness 2 mm. To look for calcifications.

Secondary signs: Mass effect, abnormally convex pancreas, double duct sign, atrophy of distal pancreas

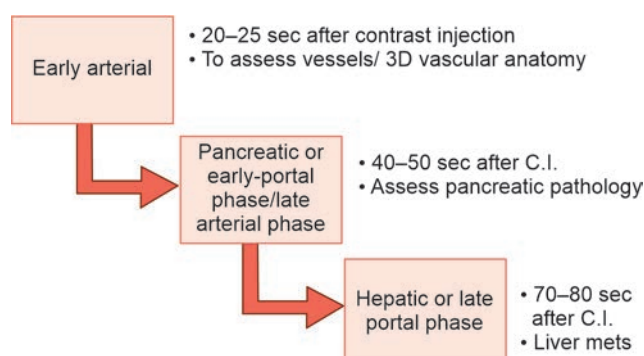


Fig. 4.201.8: CT pancreatic protocol

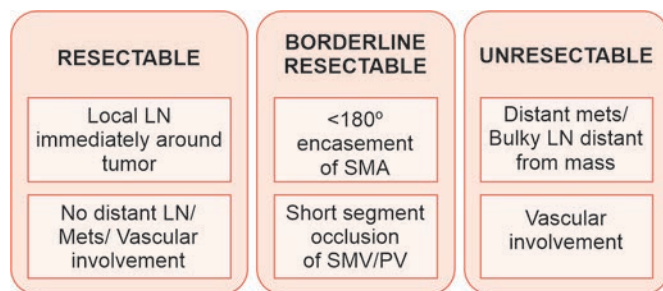


Fig. 4.201.9: Resectability criteria in pancreatic carcinoma

and adjacent soft tissue infiltration into duodenum or stomach.

| Table 4.201.3: Signs of vascular invasion in pancreatic adenocarcinoma | |
|--|-------------------------------|
| Venous invasion | Occlusion/thrombosis/stenosis |
| Arterial invasion | Contact tumor—vessel >180° |

Signs of vascular invasion: Loss of perivascular fat, vessel deformity, thrombosis, collaterals and tear drop sign in SMV. Secondaries: Liver, lymph nodes and peritoneum.

Dilatation of venous posterior pancreaticoduodenal arcade because of superior mesenteric vein invasion.

MD Anderson criteria for determination of locoregional resectability

Extra-pancreatic perineural invasion (EPNI): Pancreatic malignancy has one of the highest incidences of perineural invasion (70–100%) which correlates with a poor prognosis and decreased survival. (preoperative multidetector CT diagnosis of extrapancreatic perineural or duodenal invasion is associated with reduced postoperative survival after pancreaticoduodenectomy for pancreatic adenocarcinoma: Preliminary experience and implications for patient care. Stephanie T. Chang et al. rsna.org)

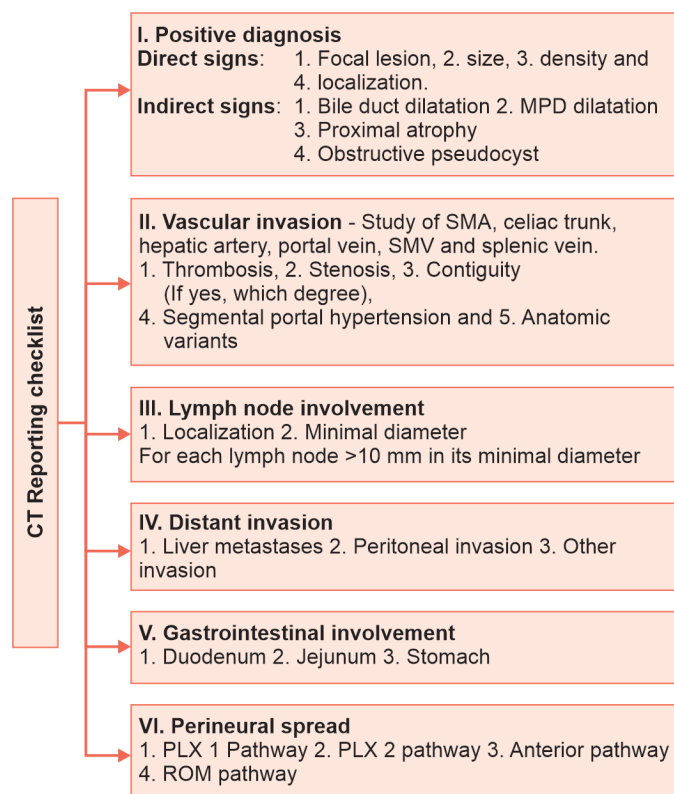
- Not included among conventional criteria.
- Patients with apparently resectable pancreatic ductal adenocarcinoma and MDCT findings of EPNI and/or duodenal invasion have significantly reduced postoperative survival compared with patients without these findings.
- MDCT criteria for EPNI: Extrapancreatic soft-tissue infiltration extending directly from the intrapancreatic tumor along any of the four established pathways for perineural spread. These pathways include
 1. Plexus pancreaticus capitalis 1 (PLX 1) pathway arises from mid-to-upper uncinate process then extends posterior to portal vein (PV) along posterior hepatic plexus to right ganglion of paired celiac ganglia (CG). Typically involved by tumors in the mid-to-upper aspect of the uncinate process.
 2. Plexus pancreaticus capitalis 2 (PLX 2) pathway extends from caudal uncinate process along posterior inferior pancreaticoduodenal artery (PIPDA) and jejunal venous trunk (JT) of superior mesenteric vein to superior mesenteric ganglion (MG). Typically involved by tumors in the caudal aspect of the uncinate process.
 3. Anterior pathway extends along gastroduodenal artery (GDA) and common hepatic artery (CHA) to right celiac ganglion. Typically involved by tumor

Table 4.201.4: Resectability in pancreatic carcinoma

| Vessel | Resectable | Borderline resectable | Locally advanced |
|---|--------------|---|--|
| Superior mesenteric artery | No extension | Tumor abutment affecting less than or equal to 180° of the circumference of the artery, periarterial stranding and tumor points of contact forming a convexity against the vessel improve chances of resection. | Encased (>180° of the circumference of the artery) |
| Celiac trunk Hepatic artery | No extension | Short-segment encasement or abutment of the common hepatic artery (typically at the gastroduodenal origin), surgeon should be prepared for vascular resection or interposition grafting. | Encased and no technical option for reconstruction. |
| Superior mesenteric vein Portal vein | No extension | Short-segment occlusion with suitable vessel condition superiorly and inferiorly, segmental venous occlusion alone without SMA involvement is rare and should be apparent at CT. | Occluded and no technical option for reconstruction. |

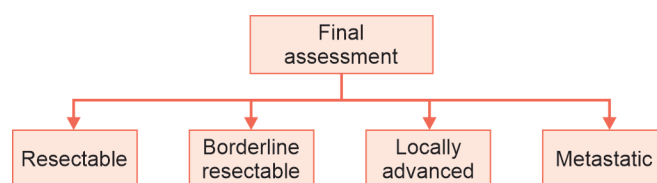
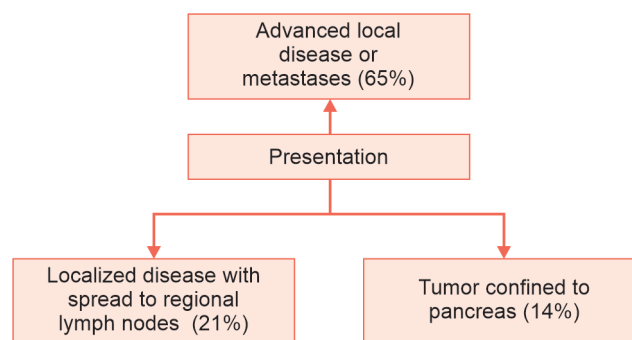
Table 4.201.5: Oncologic resections in pancreatic carcinoma

| | |
|----|---|
| R2 | Presence of macroscopic tumoral residue: Per-operative surgical finding. |
| R1 | Presence of microscopic tumoral residue: Post-operative pathologic finding. |
| R0 | No tumoral residue. |

**Fig. 4.201.10: CT reporting checklist in pancreatic carcinoma**

extending anteriorly from the head and/or neck of the pancreas.

4. Root of mesentery (ROM) pathway extends within small bowel mesentery or transverse mesocolon.

**Fig. 4.201.11: Assessment in pancreatic carcinoma****Fig. 4.201.12: Presentation in pancreatic carcinoma**

Typically involved by carcinomas of the uncinate process that extend along perineural fascicles within either the small bowel mesentery along the superior mesenteric artery or within the transverse mesocolon.

MRI features:

Normal pancreas: Diffusely high signal intensity on T1WI (liver). Parenchyma variable in signal on T2WI. Pancreas enhances avidly and homogeneously on T1WI C+ (hyperintense to liver on arterial phase and isointense on delayed phase).

Pancreatic adenocarcinoma:

- Tumor conspicuous on T1WI, appearing low signal and juxtaposed against high signal pancreatic parenchyma.

Table 4.201.6: TNM staging of pancreatic tumors

| <i>T: Primary tumor</i> | <i>N: Regional lymph nodes</i> | <i>Stages</i> |
|--|---|-----------------------------------|
| Tx: Primary tumor cannot be assessed T0: No evidence of cancer | N0: No regional nodes involved | 0: Tis N0 M0 |
| Tis: Carcinoma <i>in situ</i> includes PanIN-3, IPMN, ITPN and MCN with high grade dysplasia | N1: Metastasis in 1–3 regional lymph nodes | IA: T1 N0 M0 IB: T2 N0 M0 |
| T1: Tumor limited to the pancreas, ≤ 2 cm in greatest dimension | N2: Metastasis in ≥ 4 regional lymph nodes | IIA: T3 N0 M0 IIB: T123 N1 M0, |
| T1a ≤ 0.5 cm | | |
| T1b > 0.5 cm and < 1 cm | | |
| T1c 1–2 cm | M: Distant metastases | III: T123 N2 M0 |
| T2: Tumor limited to the pancreas, > 2 cm and ≤ 4 cm in greatest dimension | M0: No distant metastases | T4, any N, M0 |
| T3: Tumor extends beyond the pancreas, > 4 cm in greatest dimension but does not involve the celiac axis or superior mesenteric artery | M1: Distant metastases | IV: Any T, any N, M1 |
| T4: Tumor involves celiac axis or SMA (unresectable primary tumor) | | |

Table 4.201.7: Pancreatic adenocarcinoma vs neuroendocrine tumor

| <i>Features</i> | <i>Pancreatic adenocarcinoma</i> | <i>Pancreatic neuroendocrine tumor</i> |
|---------------------------------|--|---|
| 1. Calcification | 2% | 20% |
| 2. Necrosis/cystic degeneration | Less | More often |
| 3. Ductal involvement | Often | Uncommon |
| 4. Vascular involvement | Encasement present | Infiltration with tumor thrombus present |
| 5. Enhancement | Pancreatic phase: Vascular but hypodense to adjacent parenchyma | Early arterial phase: Vascular and hyperdense to adjacent parenchyma |

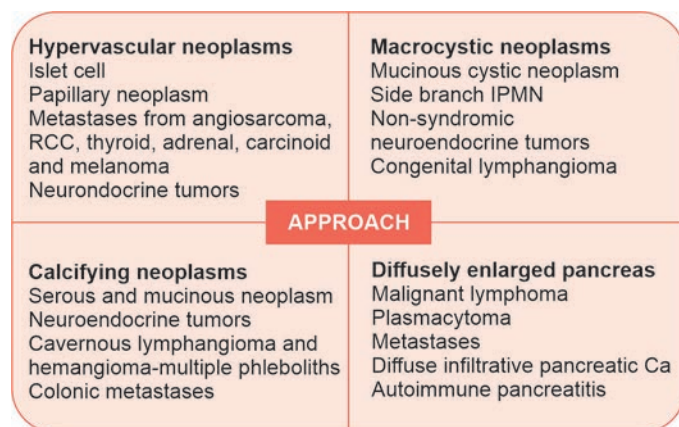
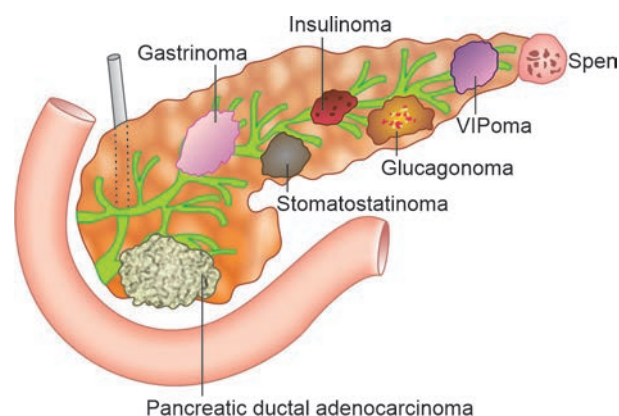
Table 4.201.8: Pancreatic adenocarcinoma vs lymphoma

| <i>Features</i> | <i>Pancreatic lymphoma</i> | <i>Pancreatic adenocarcinoma</i> |
|-----------------------|----------------------------|----------------------------------|
| Ductal dilatation | CBD \gg MPD | MPD \geq CBD |
| Lymph nodes | Infrarenal group | Peripancreatic group |
| Vascular invasion | Less common | More common |
| Intratumoral necrosis | Uncommon | Common |

- Atrophic pancreas upstream from tumor often abnormally low signal on T1WI
 - Conspicuity on T1WI C+.
 - T2WI generally not useful for tumor detection, as tumors often isointense to pancreas.
 - MRCP and T2WI can nicely demonstrate abrupt cutoff and obstruction of pancreatic and common bile ducts.
 - “Four-segment” sign—dilated biliary tree and main pancreatic duct with visualization of distal bile duct and pancreatic duct.
 - Tumors often demonstrate restricted diffusion with lower ADC values than adjacent normal pancreas.
 - MR generally 2nd choice (behind CT) for evaluating vascular involvement.
- Prognosis:**
- Only 15–20% of patients are candidates for surgery at time of presentation
 - 5-year survival rate is ~20% after surgery
 - Survival no better than chemoradiation alone if surgery performed for tumor found to be locally advanced.
 - 5-year survival rate is $< 5\%$ without surgery with median survival of 3.5 months
 - Pancreatic adenocarcinoma vs pancreatic neuroendocrine tumor.

Table 4.201.9: List of paediatric pancreatic and peri-ampullary neoplasms

| Paediatric pancreatic neoplasms | Peri-ampullary neoplasms (arising within 2 cm of the major papilla) |
|--|---|
| <ul style="list-style-type: none"> • Solid pseudopapillary neoplasm • Pancreatoblastoma • Nesidioblastosis • Acinar cell carcinoma • Burkitt lymphoma • Lymphangioma • PNET • Neuroblastoma • Islet cell tumors | <ul style="list-style-type: none"> • Pancreatic carcinoma (85%) • Cholangiocarcinoma of distal common bile duct (6%) • Ampullary tumor (4%) • Duodenal wall tumor (adenocarcinoma, adenoma, carcinoid, smooth muscle tumor) |

**Fig. 4.201.13:** Approach to pancreatic mass**Fig. 4.201.14:** Solid pancreatic neoplasms

Management

- Only potentially curative treatment for resectable tumor is complete surgical resection with negative surgical margins (R0 resection)
- Pancreatico-duodenectomy (Whipple resection) for tumors of pancreatic head/uncinate, distal pancreatectomy for tumors of body/tail, and very rarely total pancreatectomy.
- Chemotherapy and radiation (external beam) utilized for resectable, borderline, and unresectable cancers.
- Gemcitabine and Folfirinox are chemotherapy mainstays.
- Neoadjuvant chemoradiation often utilized prior to surgery in borderline resectable tumors.
- Palliative procedures include endoscopic biliary stenting (for jaundice), enteric stents or diverting gastrojejunostomy (for gastric/duodenal obstruction), and chemical splanchnicectomy or celiac nerve block to palliate abdominal pain.

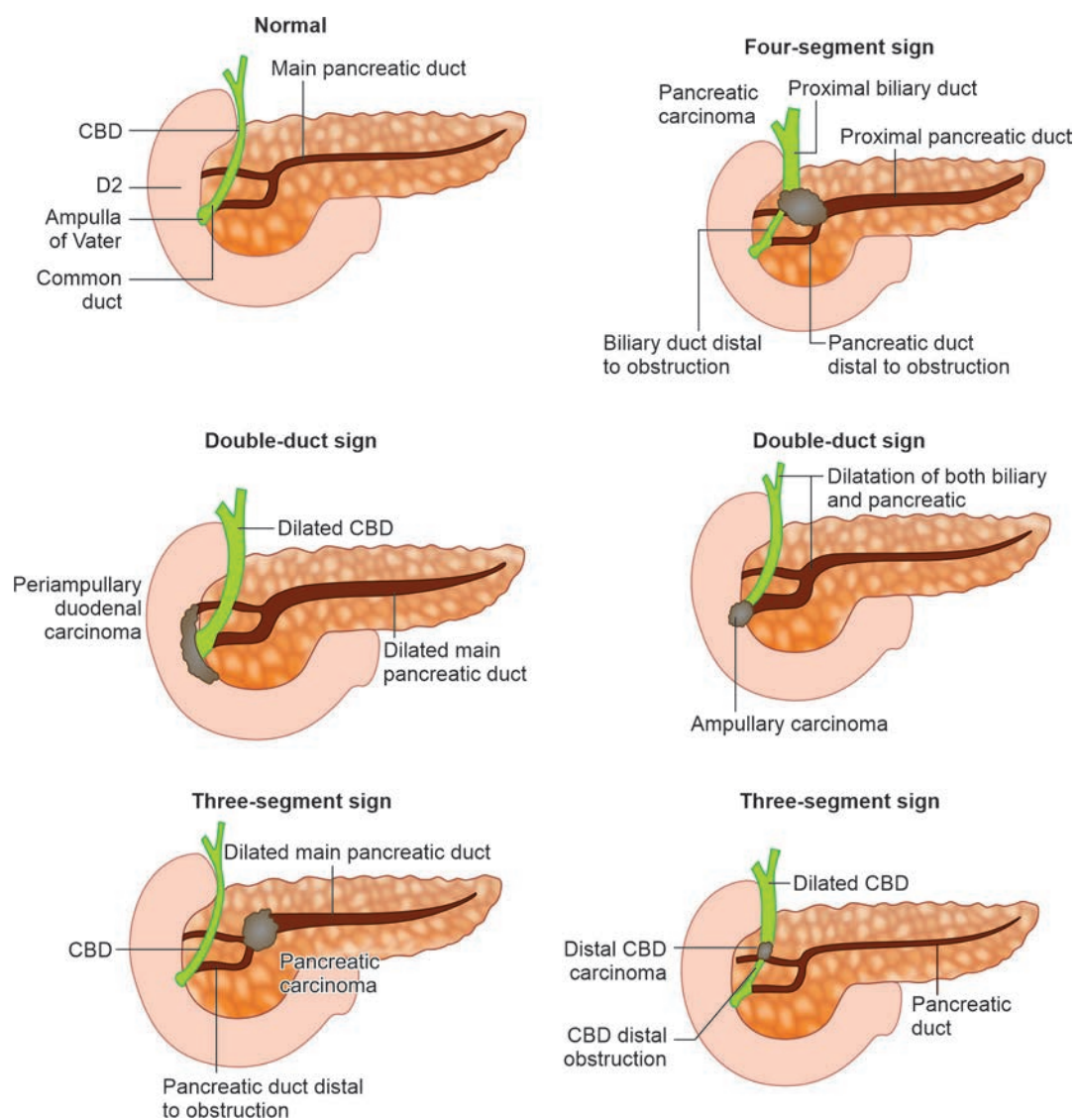


Fig. 4.201.15: MRCP patterns in periamпуляр carcinoma

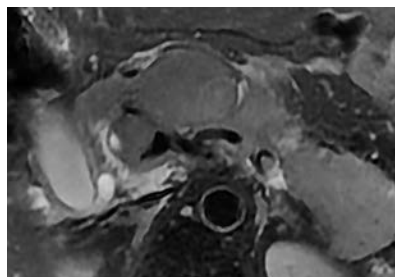


Fig. 4.201.16: Pancreatic lymphoma

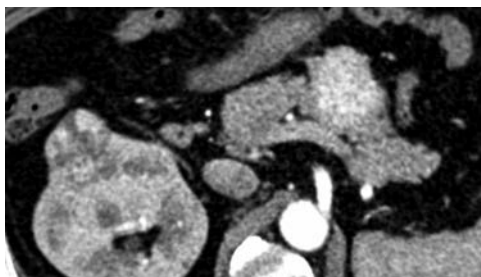


Fig. 4.201.17: Renal cell carcinoma with pancreatic metastasis

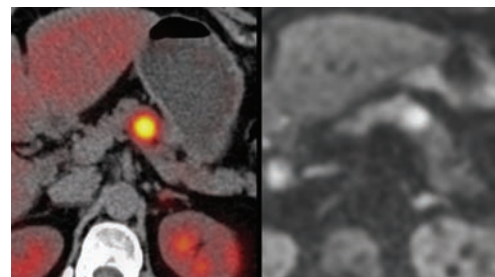


Fig. 4.201.18: Neuroendocrine tumor

4.202 HEPATOBILIARY SYSTEM

Case No. 202

Clinical history: 39-years-old male presented with the complaints of abdominal pain.

Radiological techniques and observation: Contrast enhanced CT abdomen, Figs 4.202.1 and 4.202.2 show well-defined mass lesion in the pancreatic body that shows heterogeneous hyperenhancement without surrounding fat stranding. There is no evidence of vascular invasion in the given sections. Rest of the pancreas appears normal. There are multiple well-defined heterogeneously hyperenhancing lesions noted in the arterial phase in right lobe of liver. Visualized stomach wall appears normal. Visualized spleen appears normal.

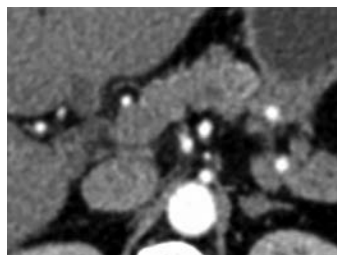


Fig. 4.202.1

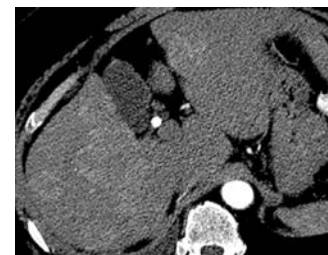


Fig. 4.202.2

Interpretation: A: 39 years old male, mass in body of pancreas, C: Well-defined mass lesion in the pancreatic tail that shows heterogeneous hyperenhancement without surrounding fat stranding. B: Multiple well defined

Table 4.202.1: Differential diagnosis for pancreatic neuroendocrine tumor

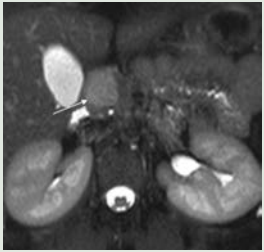
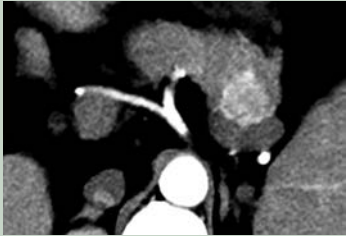
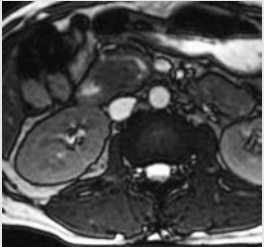
| | | |
|---|---|--|
| <p>1. Insulinoma: Most common NET (50%) Solitary Benign (90%) F>M. Whipple's triad</p> <ul style="list-style-type: none"> • Hypoglycemia • Low fasting glucose • Relief by IV glucose <p>Surgically resected Excellent prognosis</p> | <p>They tend to be hyperattenuating on arterial phase and, therefore, dedicated protocols with arterial or pancreatic phase imaging may aid in better detection. Some may show calcification.</p> |  <p>Fig. 4.202.3: Insulinoma</p> |
| <p>2. Gastrinoma Age: Young adults, 2nd M.c (25%) Multiple, malignant (60%) M>F associated with MEN 1</p> | <p>Located most commonly in the Passaro's triangle. Associated with Zollinger Ellison syndrome. Poor prognosis Smaller tumors-hypervascular tend to be homogenous and well-circumscribe. Larger tumors-may appear heterogeneous and contain areas of cystic or necrotic change, can occasionally manifest as primarily cystic lesions and are distinguishable from other cystic neoplasms by their hypervascular rim.</p> |  <p>Fig. 4.202.4: Gastrinoma</p> |
| <p>3. Glucagonoma: Associated with 4D syndrome (dermatitis, diarrhea, diabetes, DVT), average size—7 to 8 cm, location—tail of pancreas</p> | | |
| <p>4. Nesidioblastosis: Persistent hyper-insulinemic hypoglycemia of Infancy. First few hours –1 year, rare in adults. The cause is unknown.</p> | <p>In adults may be genetically induced as in congenital hyperinsulinsim, or response to metabolic and hormonal changes. Imaging shows enlarged hyperechoic pancreas. Definitive treatment is surgical, but the resection volume remains undefined.</p> | |
| <p>5. Pancreatic adenocarcinoma: Head (60%), body (20%), diffuse (15%), tail (5%) Average size 2–3 cm, poorly marginated, hypodense mass with tendency to infiltrate posteriorly into retroperitoneum</p> | <p>Tumor enhance poorly most conspicuous in portal venous (~70 seconds) and pancreatic (~40 seconds) contrast phases. Tumor virtually never calcifies in absence of treatment</p> |  <p>Fig. 4.202.5: Pancreatic adenocarcinoma</p> |

Table 4.202.2: Imaging in pancreatic neuroendocrine tumor

| CT | MRI | PET/CT | Hepatic venous sampling after arterial stimulation—increased hormone levels in occult tumors |
|---|--|--|--|
| Well-circumscribed, non-infiltrative margins Ca ⁺⁺ common Conspicuous on arterial phase Invasion of PV /SMV | T1 Hypointense T2 Hyperintense DWI help identify tiny occult lesions | Increased FDG uptake Novel tracers: Ga-68 DOTA (well differentiated) F-18 (FDG PET) (poorly differentiated) Indium 111 SPECT (Octreoscan) | Diagnosing microscopic pancreatic neuroendocrine tumor using 68-Ga-DOTATATE PET/CT |

Table 4.202.3: T-staging of pancreatic neuroendocrine tumours AJCC vs ENETS

| Stage | AJCC/UICC 2009 | ENETS 2006 |
|-------|--|--|
| T1 | Pancreatic confined primary tumor <2 cm | Pancreatic confined primary tumor <2 cm |
| T2 | Pancreatic confined primary tumor >2 cm | Pancreatic confined primary tumor 2–4 cms |
| T3 | Pancreatic tumor extending beyond pancreas without major vessel involvement | Pancreatic tumor >4 cm in size OR extending beyond pancreas with invasion limited to duodenum or bile duct |
| T4 | Pancreatic tumor extending to involve major vessels such as celiac or superior mesenteric artery | Pancreatic tumor invading major vessels or invasion of adjacent organs other than duodenum or bile duct |

Table 4.202.4: Staging protocol of pancreatic neuroendocrine tumors, as proposed by the European Neuroendocrine Tumor Society

| T stage | N stage | M stage |
|---|---|---|
| TX: Primary tumor cannot be assessed | NX: Regional lymph nodes cannot be assessed | MX: Distant metastasis cannot be assessed |
| T0: No evidence of primary tumor | NO: No regional lymph node metastasis | MO: No distant metastasis |
| T1: Tumor confined to pancreas, <2 cm | N1: Regional lymph node metastasis | M1: Distant metastasis |
| T2: Tumor confined to pancreas, 2–4 cm | | |
| T3: Tumor confined to pancreas more than 4 cm, or invades bile duct or duodenum | | |
| T4: Tumor invades adjacent organs or major vessels | | |

heterogeneously hyper enhancing lesions noted in the arterial phase in right lobe of liver, D: Pancreatic NET.

Diagnosis: Pancreatic neuroendocrine tumor (NET) with hypervascular liver metastasis.

Differential diagnosis: Hyperenhancing pancreatic masses: Insulinoma, gastrinoma, glucagonoma, nesidioblastosis in children. Hypoenhancing pancreatic mass: Pancreatic adenocarcinoma, pancreatic lymphoma, pancreatic metastasis, pancreatic AVM.

Most tumors are sporadic, but some are associated with familial syndromes such as multiple endocrine neoplasia type 1, von Hippel-Lindau syndrome, and neurofibromatosis type 1.

Further investigation: The use of nuclear medicine imaging such as Indium 111 SPECT (Octreoscan) and new positron emission tomographic techniques.

Treatment: Medical therapy, chemotherapy, surgical debulking, radiofrequency ablation, hepatic artery chemo-

embolization, and radionuclide therapy; however, in patients with MEN1 or VHL syndrome, treatment is controversial because multiple tumors often are present.

Discussion: Arising from pancreatic endocrine cells: APUD cells. Age: 4th–6th decades, MEN1: <30 years. 85% arise in the pancreas while 15% ectopic (duodenum, stomach, lymph nodes and ovary). Classified into functioning and non-functioning tumors. Now, syndromic and non-syndromic. Associations: MEN 1 (Gastrinomas), VHL, NF-1 and tuberous sclerosis.

Syndromic NET: Produce clinical syndrome, small <3 cm/ insulinoma, glucagonoma, gastrinoma, somatostatinoma, VIPoma (vasoactive intestinal polypeptide), carcinoid.

Non-syndromic NET: Symptoms due to mass effect, large at presentation/ectasies.

Much larger (>5 cm) with frequent cystic/necrotic degeneration. Strong tendency to be malignant (80–100%)/cystic NETs more likely to be non-insulin-producing/nonsyndromic.

4.203 HEPATOBILIARY SYSTEM

Case No. 203

Clinical history: 9-year-old child came with the complaints of left upper quadrant pain, nausea, vomiting and abdominal distension.

Radiological techniques and observation: Spot image of the barium meal follow through, CT abdomen imaging has been provided. Figure 4.203.1: Spot image of the barium meal follow through shows well-defined large radioopacity in the left hypochondrium, left iliac region, epigastric region causing displacement and extrinsic compression of greater curvature and fundus of stomach to right with severe luminal narrowing of the fundus of the stomach. The radio-opacity also causes inferior displacement of large bowel loops and splenic flexure. There is free flow of contrast, beyond the point of obstruction. Figures 4.203.2 to 4.203.5: CT abdomen limited axial section shows well-defined hypodense cystic lesion measuring 16×12 cm (fluid dense-HU +10) possibly arising from the spleen causing displacement of the stomach medially. No evidence of internal debris, calcification, septation. Spleen could not be visualised separately.

Interpretation: A: 9-year-old female child with lesion in spleen, C: Barium meal follow showing large radio-opacity causing displacement of greater curvature and of stomach to right and inferior displacement of large bowel loops, splenic flexure—suggest the lesion is arising from spleen. B: On CT the nature of the lesion is cystic and the spleen could not be visualised separately which indicates that the lesion is arising from the spleen, D: Lymphangioma.

Principal diagnosis: Lymphangioma of spleen.

Differential diagnosis: Congenital—Epidermoid cyst = true cyst = congenital cyst. Vascular—Splenic laceration/fracture, hematoma, post-traumatic cyst/cystic degeneration of infarct. Infection/

inflammation: Microabscesses fungal organisms in immune compromised, multiple round hypoechoic/hypoattenuating large lesions + renal involvement, wheel-in-wheel appearance when central hyperechoic portion becomes necrotic + hypoechoic, granulomatous infection, hydatid cyst, intrasplenic pancreatic pseudocyst. Cystic neoplasm—cavernous hemangioma—most common primary neoplasm of spleen; hyperdense lesion, lymphoma, lymphangioma/lymphangiomatosis—multiple septated subcapsular cystic lesions, necrotic metastasis: malignant melanoma (in 50%); breast, lung, ovarian, pancreatic, endometrial, colonic, prostatic, carcinoma; chondrosarcoma.

Discussion: Splenic lymphangiomas are relatively rare benign tumors that correspond to abnormal dilatation of lymphatic channels that can be either congenital or acquired. On imaging, they usually present as lobulated and multiloculated cystic lesions without solid component or significant enhancement. Clinical presentation: Presentation ranges from asymptomatic incidental finding to a large multicentric, symptomatic mass requiring surgical intervention. May occur alone on spleen or as part of a systemic lymphangiomatosis.

Radiographic features: Ultrasound: Appear as well-defined round hypoechoic lesions and may show occasional internal septation and intralocular echogenic debris. Tiny echogenic calcifications may be present. CT: They appear as single or multiple thin-walled low attenuation masses with sharp margins that are typical subcapsular in location. They are hypodense with no enhancement. The presence of curvilinear peripheral mural calcifications suggests the diagnosis of cystic lymphangioma. MRI T1: Hypointense relative to the surrounding viscera. High T1 signal intensity may occur with internal bleeding or large amounts of intracystic proteinaceous content. T2: Multiloculated hyperintense areas that correspond to the dilated lymphatic spaces. The intervening septa appear as hypointense bands,



Fig. 4.203.1

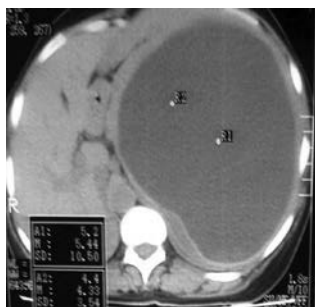


Fig. 4.203.2

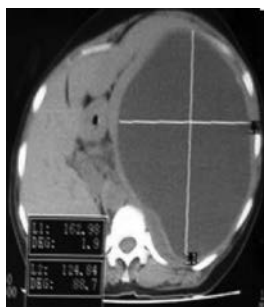


Fig. 4.203.3



Fig. 4.203.4

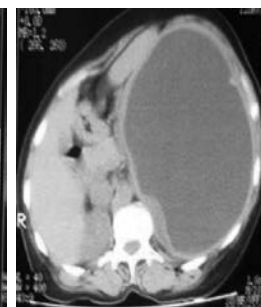
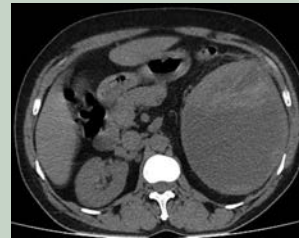

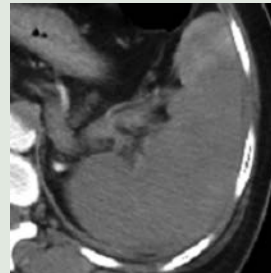


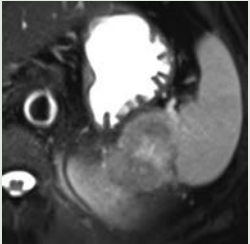
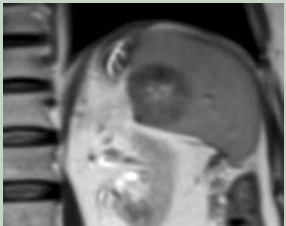
Fig. 4.203.5

corresponding to the presence of fibrous tissue. T1 C+ (Gd): No significant enhancement. Angiography: Multiple well-defined avascular lesions of varying sizes—Swiss cheese appearance.

Table 4.203.1: Differential diagnosis for cystic spleen lesions

| | | |
|---|---|---|
| Fungal microabscess Organism: Fungus (candida most common), M. Tuberculosis and MAI in AIDS patient. Hepatosplenomegaly usually seen. | USG: Multiple round hypoechoic/hypoattenuating “target” lesions often associated with hepatic+renal involvement. CT: Multiple small hypodense lesions seen “wheel-in-wheel” appearance seen when central hyperdense portion become necrotic + hypodense. | |
| Pyogenic splenic abscess Organism: Staphylococci, <i>E.coli</i> and salmonella. Cause: Hematogenous spread; Predisposed: Immunocompromised patients, critically ill patients, HIV patients, endocarditis, drug abuse. Clinical features: Fever, chills, LUQ pain (<50%) | USG: Poorly-demarcated, predominantly hypoechoic with some internal hyperechoic. Septation±, gas ±. NECT: Low attenuation ill-defined lesion within the splenic parenchyma. Solitary and multi-loculated Irregular borders without capsule. Low attenuation nonenhancing complex fluid collection with bulging splenic parenchyma. MRI-T1C: Low signal intensity with peripheral enhancement |  <p>Fig. 4.203.6: Pyogenic splenic abscess</p> |
| Simple true cyst: Epidermoid/true/congenital/epithelial cyst. Contains epithelial lining, developmental in origin | USG: Well defined anechoic mass, some time shows internal echoe. It indicates cholesterol crystal. CT: Large, well-defined unilocular, attenuation value equal to water, walls are thin or imperceptible and do not enhance. MRI: T2 hyperintensity. |  <p>Fig. 4.203.7: Simple true cyst</p> |
| Parasitic cyst (<i>Echinococcus</i>) Prevalence: in <2% of patients with hydatid cyst. Cause: Systemic dissemination, intraperitoneal spread of ruptured liver cyst | USG: Well-defined anechoic cyst, hydatid sand(internal echoes) multiseptate cyst + daughter cyst; water lily sign: cyst, floating membrane, endocyst. NECT: large uni/multilocular well-defined near water density cyst; Hydatid sand: Area of increased density within cyst; Daughter cysts: Decreased cyst than mother cyst; Curvilinear ring-like calcification. CECT: Enhancement of cyst wall with septations. MRI: T1W: Matrix and rim appears hypointense T2W: Mother and daughter cysts—hyperintense, floating membrane hypointense. | |
| Splenic infarct Splenic arterial branches are end arteries with no inter-communication. Causes: Embolic disease (endocarditis, atheromatous plaques, metastatic carcinoma) local thrombosis (sickle cell disease, CML, polycythaemia vera, MF with MM) Vasculitis: PAN | USG: Hypoechoic wedge-shaped or rounded parenchymal defects MRI: Haemorrhagic infarcts: Hyper on T1 and T2WI. Chronic infarcts: Hypo on T1 W and hyper on T2W, finally leads to complete calcification and atrophy of spleen. CECT: segmental wedge-shaped low attenuation area. Axial CECT of global splenic infarction demonstrates peripheral “cortical rim sign”. |  <p>Fig. 4.203.8: Splenic infarct</p> <p>Global: Complete nonenhancement of spleen with or without cortical rim sign. Lack of mass effect and peri-splenic changes suggest infarct.</p> |
| <i>Pneumocystis carinii</i> infection | Splenomegaly with multiple hypoattenuating foci that become progressively calcify either in rim-like or punctate fashion | |
| Sarcoidosis | Most commonly, splenic involvement is manifested by splenomegaly with associated hepatomegaly and lymphadenopathy. MRI-T1W and T2W hypointensity | |

(Contd.)

| Table 4.203.1: Differential diagnosis for cystic spleen lesions (Contd.) | | |
|---|---|---|
| Hemangioma Adults, 35–55 years. Splenic haemangiomas are usually cavernous. Usually found incidentally. Usually small single lesion <4 cm in size. Multiple as a part of generalized angiomatosis (Klippel-Trénaunay-Weber syndrome) CT: Homogeneous, hypodense, solid or cystic masses. Central and punctate or peripheral and curvilinear calcifications noted. Enhance from periphery to center. | Tc-99m labelled RBC scan with SPECT: Early dynamic scan : Focal defect or less uptake. Delayed scans (30–50 mins): Persistent filling. Conventional Angiography. Cotton wool appearance: Pooling of contrast. Typically retain contrast beyond the venous phase. |  Fig. 4.203.9: Hemangioma USG: Well margined predominantly hyperechoic lesion. |
| Splenic metastasis: May be multiple (60%), solitary (61%), nodular and diffuse. Haematogenous spread. Cystic splenic metastasis: Melanoma, breast, ovary and endometrium. | USG: Predominantly hypoechoic CT: Multiple well-defined areas of low attenuation, solid or cystic seen Melanoma: Solid or cystic Ovary, breast and endometrium: Cystic. MRI: T1W: Iso to hypointense; T2W: Hyperintense T1C: Enhancement depends on the primary |  Fig. 4.203.10: Splenic metastasis |

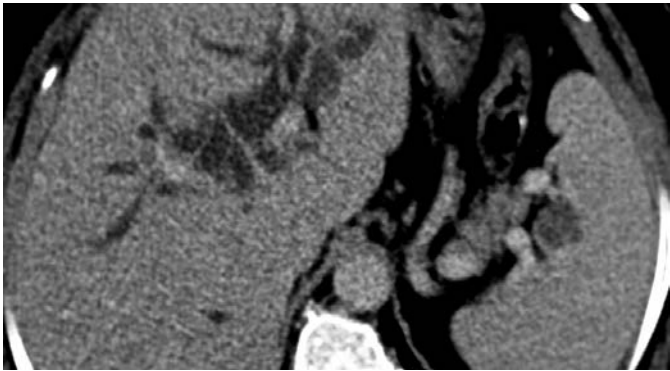


Fig. 4.203.11: Sclerosing angiomatoid transformation (SANT) of spleen

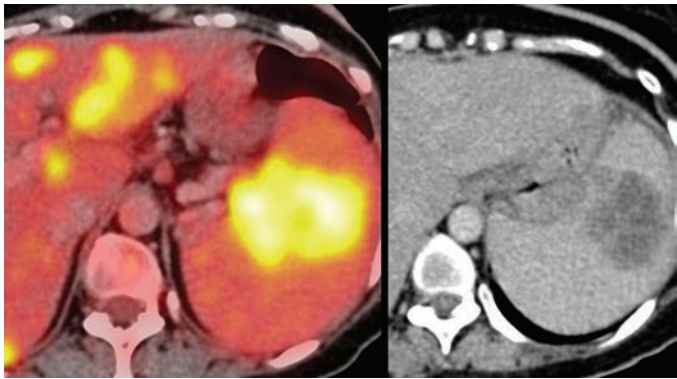


Fig. 4.203.12: Splenic lymphoma

4.204 HEPATOBILIARY SYSTEM

Case No. 204

Clinical history: 45-years-old male with complaints of left upper quadrant pain, weight loss with fever and night sweats.

Radiological technique: CECT abdomen (Figs 4.204.1 and 4.204.2), FDG-PET/CT imaging (Figs 4.204.3 and 4.204.4) has been provided.

Observations: CECT, axial and coronal sections of abdomen has been provided. It shows focal well-defined nonenhancing hypodense lesion on venous phase compared to the surrounding parenchyma in the spleen. Spleen appears enlarged. No other focal lesion noted in splenic parenchyma. No calcification noted within the lesion. 18F-FDG PET imaging shows increased uptake in the spleen. Visualised spine, liver, and lung segments appear normal.

Interpretation: A: 45 years old male, lesion in spleen, C–Focal well-defined hypoenhancing lesion on late venous phase compared to the surrounding parenchyma in the spleen. Splenomegaly present. B: 18F-FDG PET imaging shows increased uptake in the spleen, D: Lymphoma.

Principal diagnosis: Lymphoma of the spleen

Further investigations and management: Patient proceeded with excisional biopsy for histopathological analysis.

Discussion: Splenic lymphoma is most common malignancy to involve the spleen. They commonly secondary, rarely being primary. Patient commonly presents with fever, weight loss, left upper quadrant pain. Radiological feature: Splenomegaly is most

common presentation on imaging, but a normal spleen does not exclude lymphoma involvement. Associated enlarged splenic hilum lymph nodes may be seen either in the primary or secondary forms. The secondary form will show signs of disease involving other organs and systems, particularly nodal disease. USG: The focal disease may manifest as small circumscribed nodules, sometimes referred to as a milliary pattern, or bulky splenic masses and, generally, these are hypoechogenic on ultrasound. A diffuse infiltrative disease is usually only characterized as an enlarged spleen. CT: Post-contrast images: The focal lesions are hypoenhancing compared to the background parenchyma and they are best appreciated in a late venous phase, particularly when the lesions are small. Calcification of the splenic lesions is uncommon but might be seen after treatment. Although uncommon, lesions can rarely demonstrate necrosis or cystic degeneration (usually after treatment). MRI: Single or multifocal disease will present as well-defined masses, T1: Low to iso-intensity compared to the background parenchyma, T2: Low to iso-intensity compared to the background parenchyma. T1 C+: Focal lesions will have a mild or absent enhancement compared to the background parenchyma (hypoenhancing lesions). DWI: Relatively low ADC values inferring diffusion restriction. PET-CT (18F-FDG): PET has become the imaging modality of choice to stage and follow-up of Hodgkin and aggressive forms of NHL disease. Splenic lymphoma can manifest on PET either as a diffusely FDG-avid spleen, in cases of a diffuse infiltrative disease, or as single or multiple FDG-avid focal splenic lesions. Treatment: Chemotherapy for systemic disease. Splenectomy for isolated splenic tumor.



Fig. 4.204.1



Fig. 4.204.2

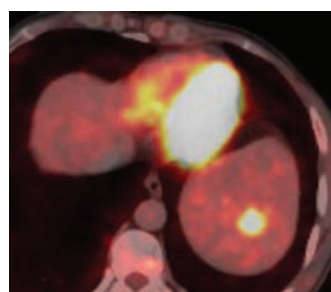


Fig. 4.204.3

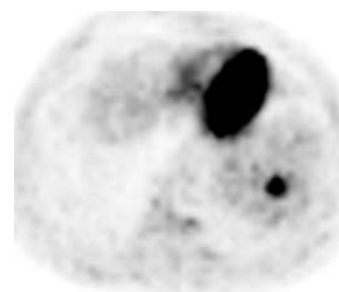


Fig. 4.204.4

Table 4.204.1: Benign and malignant lesions of spleen

| Benign lesion | Malignant lesion |
|--|------------------------------------|
| Hemangioma, hamartoma, littoral cell angioma, peliosis | Angiosarcoma of spleen, metastasis |

Table 4.204.2: Differential diagnosis for solid splenic lesions


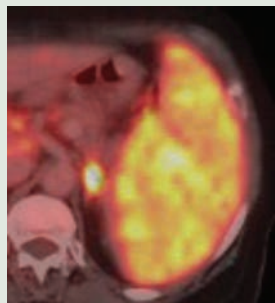
| Condition | Radiological features | Images |
|--|---|---|
| Hemangioma: Most common primary benign neoplasm of spleen. M/C- 35–55 years. Splenic haemangiomas are usually cavernous. Usually small single lesion <4 cm in size. Multiple generalized angiomatosis (Klippel-Trénaunay-Weber syndrome) | USG: Well-marginated predominantly hyperechoic lesion. CT: Homogenous, hypodense, solid or cystic masses. Central and punctate or peripheral and curvilinear calcifications noted. Enhance from periphery to center. MRI-T1C: Peripheral enhancement with progressive central fill-in, with retention of contrast on delayed images. | |
| Splenic peliosis: It is an unusual benign disorder characterized by the presence of irregular cystic blood-filled cavities. | USG: May be seen as an echogenic mass lesion with numerous poorly defined foci of varying hypoechogenicity. NCCT: Typically seen as a hypo-attenuating, multi-loculated lesion with well-defined septae within. CECT: The lesion may show significant enhancement with loss of definition of the lobules and septae. Fluid–fluid levels may also be present. | |
| Splenic hamartoma: Congenital usually solitary. Types: Mixture of red and white pulp, white pulp and red pulp hamartomas asymptomatic. Multiple elsewhere: Tuberous sclerosis, Wiskott-Aldrich syndrome | USG: Well-defined diffuse, heteroechoic mass. CT: Iso / hypodense to spleen. MRI: T1W: Iso intense T2W: Hyperintense, T1C: Diffuse heterogeneous enhancement does not show an increase in signal intensity with increasing TE. Sulfur colloid scintigraphy: Radiotracer uptake is seen. | |
| Littoral cell angiodysplasia: Littoral cell angiodysplasia derives from its cell of origin, the littoral cell, which lines the sinuses of the splenic red pulp. | USG: Splenomegaly, mottled echo texture but no discrete masses. CT: The masses are hypoattenuating compared to normal spleen. They demonstrate progressive homogeneous contrast enhancement, later than normal splenic parenchyma. MRI: The masses are often low in T1 and T2 signal intensity due to hemosiderin. | |
| Splenic metastasis: May be multiple (60%), solitary (61%), nodular and diffuse. Haematogenous spread. Cystic splenic metastasis: Melanoma, breast, ovary and endometrium. | USG: Predominantly hypoechoic lesion. CT: Multiple well-defined areas of low attenuation, solid or cystic seen; Melanoma: Solid or cystic. Ovary, Breast and Endometrium: Cystic. MRI:T1W: Iso to hypointense T2W: Hyperintense T1C: Enhancement depends on the primary. | |
| Angiosarcoma of spleen: Splenic angiosarcoma is considered the most common primary nonhematolymphoid splenic malignancy. USG: Splenomegaly and heterogenous echotexture with increased vascularity. MRI: Nodular hypointense masses on both T1- and T2-weighted images. T1C+: Shows intense and multinodular (heterogeneous) enhancement with focal areas of non-enhancement, likely representing intratumoral hemorrhage and necrosis | CT: Heterogeneously enlarged spleen with cystic and solid component.  |  |

Fig. 4.204.5: Angiosarcoma of spleen**Fig. 4.204.6:** Angiosarcoma of spleen
PET imaging: Increase uptake in the splenic lesion.

4.205 HEPATOBILIARY SYSTEM

Case No. 205

Clinical history: 29-year-old-male child presented with history road traffic accident with multiple fractures.

Radiological techniques and observation: Axial CECT images of abdomen, Figs 4.205.1 to 4.205.5 show irregular areas of hypoattenuation in right lobe liver, GB appears normal, linear non-enhancing area in the upper pole of spleen, with collapsed IVC. Bilateral adrenals are hyperenhancing. There is also hyperenhancement (white attenuation) of the bowel wall. Free fluid noted adjacent to bowel loops. No evidence of extravasation of contrast. No evidence of hyperattenuating fluid noted in the pelvis. Portal vein appears normal. No evidence of pneumoperitoneum. No evidence of bowel wall edema. Pancreas appears normal. Both the kidneys show normal enhancement pattern. No evidence of diaphragmatic injury. Comminuted nondisplaced fracture noted in the left iliac wing, right superior and inferior pubic ramus.

Interpretation: A: 9-year-old male child, lesion in liver
C: Liver/spleen laceration. Bilateral adrenal hyper enhancement (shock/sepsis), pelvic bone fracture,
B: Hyperenhancing bowel: Ischemia/inflammatory bowel disease. Subhepatic fluid: Ascites/hemoperitoneum,
D: Traumatic hypoperfusion complex.

Principal diagnosis: Traumatic hypoperfusion complex.

Discussion: CT hypoperfusion complex also called as shock bowel. Features: Small caliber abdominal aorta: AP diameter <13 mm both 20 mm above and below the renal arteries 2; this occurs in ~30% of patients with hypovolemia, and is not specific; Collapsed inferior vena cava: AP diameter <9 mm in three consecutive segments; i.e. 20 mm both above and below the renal veins; Halo sign—low density (<20 HU) fluid surrounding the IVC—this occurs in ~80% of patients with severe hypovolemia; thickened bowel loops (>3 mm) with enhancing walls and hyperenhancing mucosa—most commonly involves the jejunum—wall thickening is due to submucosal

edema; shock pancreas: Heterogeneous enhancement with peripancreatic fluid (<20 HU); hypoenhancement of the spleen; decreased splenic volume; hypoenhancement of the liver: 25 HU less than the spleen; bilateral adrenal gland hyperenhancement may be a feature mainly in pediatrics; hyperenhancing kidneys; ascites.

Treatment: Appropriate fluid management

Organ injury and grading:

Liver laceration and AAST grading: Refer to OSCE

Spleen laceration and AAST grading: Refer to OSCE

Kidney laceration and AAST (The American Association for the Surgery of Trauma) grading: Refer to OSCE

Pancreatic laceration and AAST (The American Association for the Surgery of Trauma) grading: Refer to OSCE

The terms pancreatic abscess and intrapancreatic pseudocyst are totally abandoned in this new classification.

Radiological signs of bowel injury: Definitive signs—visible bowel wall discontinuity, perforation in blunt trauma, the presence of extra-luminal oral contrast media (if used) or bowel contents; extra-luminal free gas (especially in the absence of pneumothorax/pneumomediastinum) in penetrating trauma, extra-luminal free gas is not specific to bowel perforation; extra-luminal contrast media/bowel contents leak and a wound track extending to bowel is considered the most sensitive; wall thickening/mesenteric contusion is less sensitive Suggestive signs—mural hematoma: discontinuity in the bowel wall with mural thickening (>3–4 mm); may be complete (i.e. perforated) or incomplete moderate/large volume of free fluid without solid organ injury 2–3 intermesenteric fluid forming triangles; abnormal bowel wall enhancement: Decreased due to mesenteric vascular interruption and small bowel ischemia, or increased due to vascular permeability secondary to hypoperfusion; positive seatbelt sign increases the likelihood of traumatic bowel injuries.

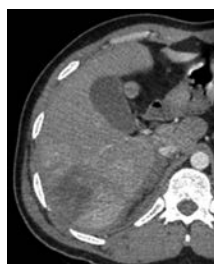


Fig. 4.205.1

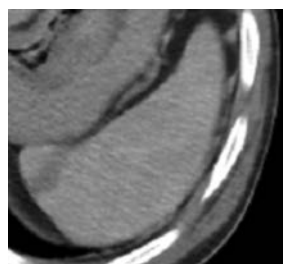


Fig. 4.205.2

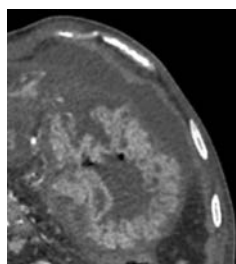


Fig. 4.205.3




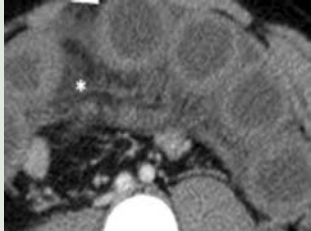

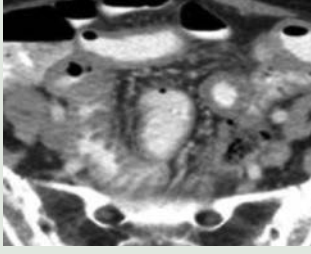


Fig. 4.205.4



Fig. 4.205.5

Table 4.205.1: Differential diagnosis for traumatic hypoperfusion complex: Idiopathic angioedema, vasculitis (e.g. Henoch-Schönlein purpura), inflammatory bowel disease, radiation enteritis

| | | |
|---|---|--|
| Idiopathic angioedema Etiology—unknown | Long segment concentric thickening of the bowel submucosa (most common-jejunum) Mural stratification Straightening of bowel loops | |
|  <p>Fig. 4.205.6: Idiopathic angioedema</p> |  <p>Fig. 4.205.7: Idiopathic angioedema</p> |  <p>Fig. 4.205.8: Idiopathic angioedema</p> |
| Ischemic Bowel Etiology—arterial occlusion, venous occlusion, low flow state, radiation therapy | Features: Bowel wall thickening (common), usually uniform and segmental, rarely localized and mass-like Low-density ring of submucosal edema between enhancing mucosa and serosa (target sign), bowel dilatation | |
| Vasculitis Example – Henoch – Schönlein purpura | Multifocal bowel thickening, lymphadenopathy, mesenteric edema and vascular engorgement. | |
| Radiation enteritis Due to radiation therapy on small bowel and vasculature | Bowel wall thickening and luminal narrowing Small bowel obstruction fistulas between the bowel (especially colon) and the bladder or vagina | |
| | |  <p>Fig. 4.205.9: Ischemic bowel</p>  <p>Fig. 4.205.10: Vasculitis</p>  <p>Fig. 4.205.11: Radiation enteritis</p> |

Radiological signs of mesenteric injury: Definitive signs: Active extravasation of contrast media is indicative of active bleeding and a significant mesenteric injury, intermesenteric free fluid, often forming triangles, beading and termination of mesenteric

vessels, abrupt termination of the mesenteric vessels, accumulation ('pooling') of contrast on multiphase imaging, suggestive signs: mesenteric infiltration: Haziness and fat stranding, mesenteric hematoma, bowel wall thickening.

Table 4.205.2: Goldman classification of urethral injuries

The Goldman classification of urethral injuries is used than AAST urethral grading. It is based on anatomical location of the urethral injury.

Classification

Type I: Stretching of the posterior urethra due to disruption of puboprostatic ligaments, though the urethra is intact

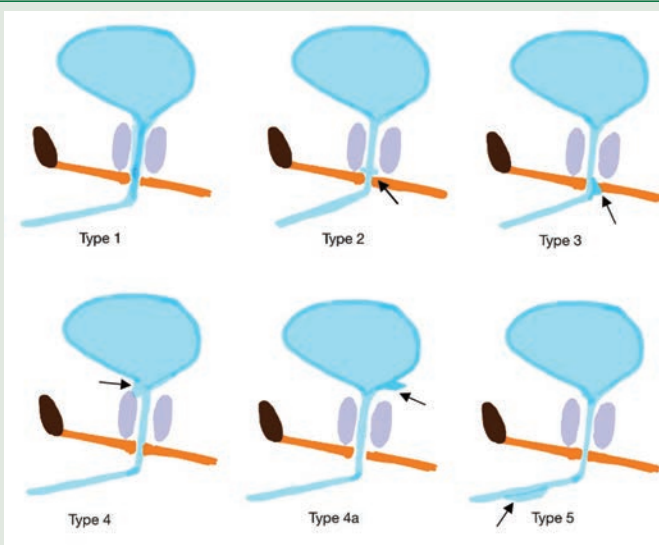
Type II: Posterior urethral injury above urogenital diaphragm

Type III: Injury to the membranous urethra, extending into the proximal bulbous urethra (i.e. with laceration of the urogenital diaphragm)

Type IV: Bladder base injury involving bladder neck extending into the proximal urethra internal sphincter is injured, hence the potential for incontinence

Type IVa: Bladder base injury, not involving bladder neck (cannot be differentiated from type IV radiologically)

Type V: Anterior urethral injury (isolated)

**Fig. 4.205.12:** Goldman classification of urethral injuries

4.206 URINARY AND REPRODUCTIVE SYSTEM

Case No. 206

Clinical history: 1½-year-old male child, brought by the mother with history of lethargy and poor appetite for 1 month, and recent increase in the abdomen size.

Radiological techniques and observations: Abdomen plain radiograph, Fig. 4.206.1 shows large homogenous opacity in the left upper quadrant and the epigastrium, crossing the midline, displacing the splenic flexure of colon, proximal descending colon and transverse colon inferiorly. The medial and inferior margins of the lesion are well defined. Part of the lateral and superior margins of the lesion are not clearly seen. No calcification within the lesion is noted. Vertebral body and intervertebral spaces appear normal. Visualised bones appear normal. No evidence of splaying of ribs. Liver shadow appears normal. Bilateral psoas shadows appear normal.

Differential diagnoses for pediatric left hypochondrial mass:

1. Wilms' tumor
2. Congenital mesoblastic nephroma <3–12 months
3. Nephroblastomatosis
4. Renal clear cell sarcoma
5. Hepatoblastoma (from left lobe)
6. Lymphatic malformation

Ultrasonogram abdomen, Fig. 4.206.2 shows large heteroechoic, predominantly solid left suprarenal mass. The left suprarenal gland is not seen separately, causes substantial mass effect on the anterior aspect of left kidney without appearing to arise from the left renal parenchyma. Further imaging with CECT abdomen is required to characterize the lesion and its extent. CECT abdomen, Fig. 4.206.3 shows large heterogeneously enhancing solid mass in the left suprarenal region, and

the left suprarenal gland is not seen separately (phantom organ sign). The lesion compresses the left kidney posteriorly and laterally, beak sign is negative. The bowel loops are displaced anteriorly and to the right and laterally the mass is seen indenting the spleen. Medially the lesion crosses the midline. It elevates the aorta away from the vertebral column causing encasement and displacement of aorta to the right. The lesion is seen displacing the IVC to the right. Posteriorly the mass is seen eroding the adjacent lumbar vertebra with possible extension in to the left neural foramina. The contact surface of the underlying kidney is smooth. Intralesional calcifications are seen. Hypodense areas noted within the lesion possibly necrosis. Liver and spleen appear normal. No evidence of lymphadenopathy, ascites. Visualised skeleton appears normal.

Interpretation: A: 1½-year-old male child, left suprarenal region, C: Large enhancing mass appearing to arise from the left suprarenal region and causing substantial mass effect on the left kidney without appearing to arise from the left renal parenchyma. B: Calcifications and necrosis are present, and the lesion is seen crossing the midline. D: Neuroblastoma

Principal diagnosis: Neuroblastoma

Management: Patient to be referred to the paediatric surgery department to assess through a multidisciplinary approach. Management depends on the staging of the tumor. Histopathology confirms the diagnosis. I-123 MIBG is used for diagnosis, staging and follow-up imaging. Combination of surgery and chemotherapy is advocated.

Discussion: Neuroblastoma is a malignant tumor of sympathetic chain primitive neural crest cells.



Fig. 4.206.1

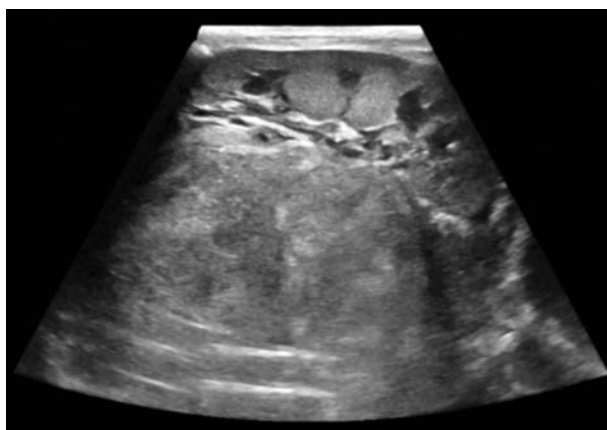


Fig. 4.206.2

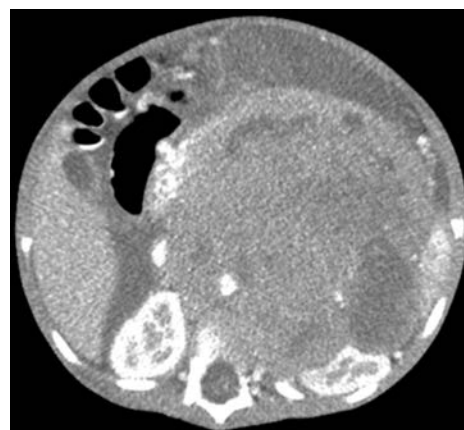

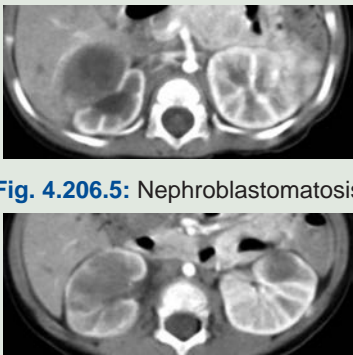
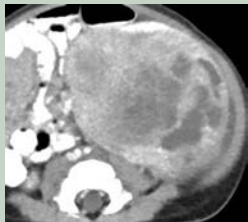
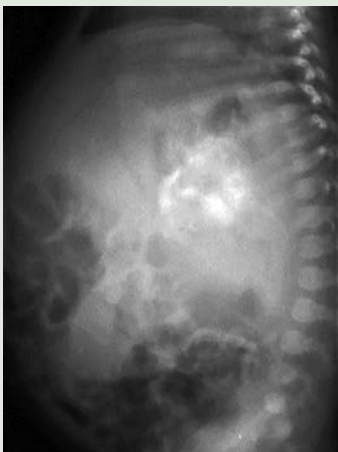


Fig. 4.206.3

| | | |
|---|--|--|
| <p>Wilms tumor: Malignant tumor of primitive metanephric blastema. Most common abdominal tumor in children 1–8 years old.</p> | <p>Ultrasound frequently 1st study performed. CT and MR better characterize tumor and local extent. Large, heterogeneous predominantly hypoechoic (US)/ hypo-enhancing (CT/MR) renal mass. Renal vein and inferior vena cava tumor thrombus. Contralateral kidney may show synchronous tumor or nephrogenic rests. Chest radiograph or CT: Lung metastases in 10–20%.</p> |  <p>Fig. 4.206.4: Wilms tumor</p> |
| <p>Nephroblastomatosis: Persistent metanephric blastema after 34 weeks; 30–40% develop Wilms tumor. Multiple or diffuse nephrogenic rests.</p> | <p>Homogeneous, multifocal ovoid or subcapsular, rind-like renal masses that enhance less than normal kidney. Diffusely homogeneous appearance; (Wilms tumor—heterogeneous). Nephrogenic rests usually < 2 cm in size (Wilms tumor usually >3 cm)</p> |  <p>Fig. 4.206.5: Nephroblastomatosis</p> <p>Fig. 4.206.6: Nephroblastomatosis</p> |
| <p>Mesoblastic nephroma: Hamartomatous renal tumor of young infants. Solitary well-defined renal mass. Classic type usually solid, smaller. Cellular type usually larger with cystic/necrotic/hemorrhagic foci. Usually diagnosed in first 6 months of life. After 3 months Wilms tumor becomes more common.</p> | <p>Prenatal polyhydramnios (70%), rarely hydrops seen. Vascular invasion not seen. Irregularity/discontinuity of margins, infiltration of adjacent soft tissues, surrounding fluid and/or free pelvic fluid suggest tumor rupture. MR shows well-defined oval/round mass, usually solid. Cystic/necrotic/hemorrhagic foci imply more aggressive cellular variant. Irregularity/discontinuity of margins, infiltration of adjacent soft tissues, surrounding fluid and/or free pelvic fluid suggest tumor rupture—more common with cellular type.</p> |  <p>Fig. 4.206.7: Mesoblastic nephroma</p> |
| <p>Teratoma</p> | <p>Shows coarse calcification. Occasionally tooth may be seen. Large masses displace the bowel loops anteriorly. In CT fat density, fat fluid level may be seen.</p> |  <p>Fig. 4.206.8: Teratoma</p> |

Ossifying renal tumour of infancy: Rare tumour. Peak age is 1 to 3 months old infants. Origin is considered to be from intra-lobar nephrogenic rests.

Calcification may resemble staghorn calculus. It is attached to renal papilla and grows into collecting system. Enhances post-contrast. Usually benign with no recurrence reported so far.

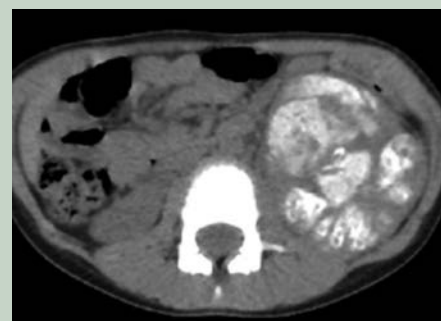


Fig. 4.206.9: Ossifying renal tumour of infancy

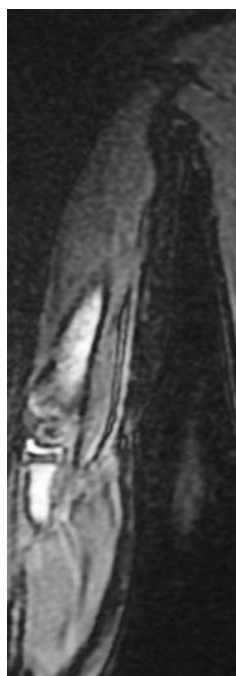


Fig. 4.206.10: Neuroblastoma



Fig. 4.206.11: Neuroblastoma

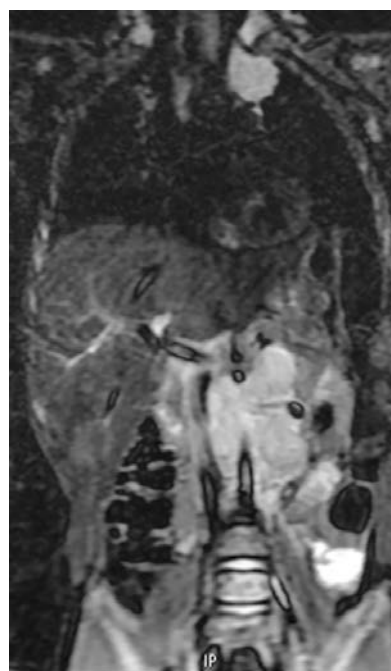


Fig. 4.206.12: Neuroblastoma with bone metastases

Increasing degrees of cellular differentiation/benignity along spectrum: Neuroblastoma (malignant) → ganglioneuroblastoma → ganglioneuroma (benign).

Radiograph shows fine stippled calcification in the region of adrenal gland.

Ultrasound is an excellent 1st-line modality for palpable abdominal mass in child. MR is increasingly used over CT for characterizing tumor and defining extent at diagnosis and follow-up. MIBG remains favoured nuclear medicine study for diagnosis, staging, follow-up.

MIBG scintigraphy: I-123 MIBG is used for diagnosis, staging and follow-up imaging. MIBG is analogous to norepinephrine, therefore, shows avid uptake in catecholamine production process. Increased uptake at any site of active neuroblastoma. Sensitivity, specificity ~90% in neuroblastoma. Evaluates bony cortical and marrow disease. In MIBG-avid tumors, post-therapy evaluation more specific than MR or FDG-PET.

Location anywhere along the sympathetic chain from neck to pelvis:

1. Adrenal (35–48%) 90% adrenal in prenatally detected cases

| Table 4.206.1: Classification for neuroblastoma | |
|--|---|
| International neuroblastoma staging system (INSS) | International neuroblastoma risk group staging system (INRGSS) |
| (Postsurgical staging system) | (Preoperative imaging system) |
| Older system, based on resection, pathology (1988, 1993) Used for risk groups by Children's Oncology Group (COG). | Newer system, more comprehensive, imaging-based system (2009). Utilizes modifying image-defined risk factors Used to stratify as very low, low, intermediate, or high risk in conjunction with age, genetics, histology—may replace COG risk stratification |
| Stage 1—localized disease, completely resected | L1—localized, not involving vital structures |
| Stage 2A—localized; incomplete gross resection; lymph nodes—ve | L2—loco regional tumor with 1 or more imaging-defined risk factors |
| Stage 2B—localized; complete or incomplete resection; ipsilateral lymph nodes +ve; contralateral lymph nodes –ve | |
| Stage 3—unilateral tumor with contralateral +ve lymph nodes or tumor crossing the midline | |
| Stage 4—metastatic disease | M—metastatic disease |
| 4S—<12 months with skin, liver involvement | MS—< 18 months with metastases confined to skin, liver, bone marrow. Better prognosis. Bones (including marrow) must be clear by MIBG to qualify for stage MS/4S (with marrow disease, limited to less than 10% involvement by biopsy). |



Fig. 4.206.13: Right supra-renal neuroblastoma



Fig. 4.206.14: Neuroblastoma with bone metastases

2. Extra-adrenal retroperitoneum (25–35%)
3. Posterior mediastinum (16–20%)
4. Pelvis (2–3%)
5. Neck (1–5%)
6. Metastatic disease with no primary identified (1%).

Neuroblastoma with bone metastases: Large lobulated T2 hyperintense retroperitoneal mass, in the left suprarenal region, encasing and lifting the aorta. The lesion is seen crossing the midline. Posterior mediastinal mass noted. Multiple dorsal and lumbar vertebral metastases and distal left humerus metastasis.

Other accompanying syndromes of neuroblastoma include:


1. Hutchinson syndrome: Skeletal metastases may present with skeletal pain or limping and irritability or proptosis with periorbital and cranial bumps.

2. Pepper syndrome: Hepatomegaly due to extensive liver metastasis
3. Blueberry muffin syndrome: Multiple cutaneous lesions
4. Opsomyoclonus rapid, involuntary conjugate fast eye movements
5. Proptosis and periorbital ecchymoses (“raccoon eyes”): Orbital metastases

The organ of Zuckerkandl comprises a small mass of chromaffin cells derived from neural crest located along the aorta, beginning cranial to the superior mesenteric artery or renal arteries and extending to the level of the aortic bifurcation or just beyond. The highest concentration is typically seen at the origin of the inferior mesenteric artery. They are involved in paraganglioma-extra-adrenal pheochromocytoma and neuroblastoma.

Natural history and prognosis: Cog risk stratification: Low risk (30% of all Neuroblastoma, 70% of neonatal neuroblastoma): 5-year survival > 95% with observation (select cases) or surgery. Spontaneous regression most likely in 1) Newborns with small adrenal lesions 2) Non-MYC amplified infants with localized disease or asymptomatic 4S/MS disease. Intermediate risk (20% of all neuroblastoma): 5-year survival > 90% with surgery + chemotherapy. High risk (50% of all neuroblastoma): 5-year survival of 30–40% with intensive multimodality therapy. May include myeloablative therapy with stem cell rescue, biologic agents.

Table 4.206.2: Difference between neuroblastoma and Wilms tumor

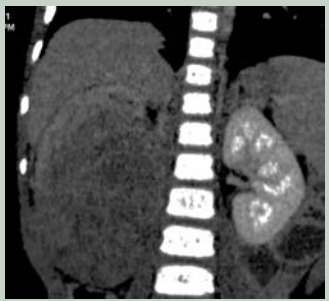
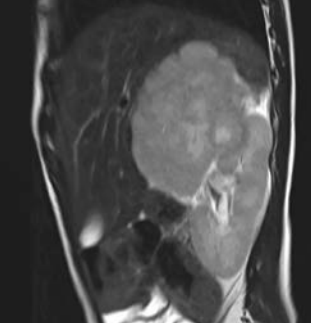
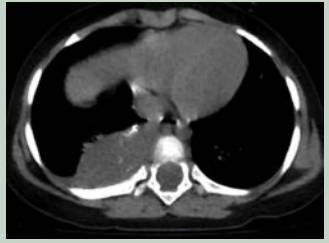

| Feature | Neuroblastoma | Wilms tumor |
|----------------------|--|--|
| Age | <2 years | 2–3 years |
| Origin | Retroperitoneal neural crest. Typically displaces rather than invades kidney | Kidney Claw sign of residual renal parenchyma along tumor |
| Margin | Poorly marginated | Well circumscribed |
| Renal mass effect | External compression Externally displaces the kidney down and out | Intrinsic mass effect Intrinsically displaces urinary collecting system |
| Laterality | Crosses the midline | 10% bilateral, not cross the midline |
| Calcification | Almost always present; punctate calcification | Uncommon <15% |
| Vessel involvement | Frequently encasement and displacement of great vessels Elevates the aorta away from the vertebral column | Displaces adjacent structures without insinuating between them Renal vein invasion in 5–10% IVC invasion |
| Metastasis | Bone (skull metastases are located in the spheno-orbital region), liver. | Para-aortic lymph nodes, lung, liver. |
| Radiograph | Chest radiographs may show a calcified mass. Paravertebral widening in the lower chest may be caused by retrocrural spread. Punctate calcification in paravertebral / suprarenal region. | Calcification is unusual |
| IVP |  <p>Fig. 4.206.15: Neuroblastoma IVP in Fig. 4.206.14 showing displaced left kidney inferiorly and laterally with soft tissue mass in the suprarenal region</p> | Intrinsically displaced urinary collecting system. |
| Ultrasound | Heterogeneous and hypervascularized on colour Doppler. Small echogenic foci within the mass represent calcification. | Mixture of solid hyperechoic masses and relatively cystic areas; often the cystic components predominate. |
| CT | CT of the chest, abdomen and pelvis requires IV bolus of contrast. Low-attenuation areas represent regions of necrosis or haemorrhage | Well-circumscribed heterogeneous partially cystic mass due to focal hemorrhage and necrosis, cyst formation, fat, calcification. Contralateral synchronous tumor, nephrogenic rests |
| MR | Neural foramen extension seen in neuroblastoma. Gadolinium is required to assess the contralateral kidney for nephroblastomatosis or another Wilms' mass | |
| Radionuclide imaging | MIBG and skeletal scintigram are essential for determining distal spreading. 30% of the primary lesions do not take up MIBG. Rare cases, the uptake stops despite the presence of persistent demonstrable disease. 99mTc-MDP bone scintigraphy should be performed in all patients at diagnosis and follow-up. | Non-functioning kidney. Hypo- / iso- / hyperperfusion on radionuclide angiogram. Absent tracer accumulation on delayed static images. Displacement of kidney seen. Distortion of collecting system may be demonstrated. |

(Contd.)

Table 4.206.2: Difference between neuroblastoma and Wilms tumor (Contd.)

| Feature | Neuroblastoma | Wilms tumor |
|---------|---|---|
| |  Fig. 4.206.16: Neuroblastoma |  Fig. 4.206.17: Wilms tumor |

Table 4.206.3: Summary of neuroblastic tumors

| | | |
|---|---|--|
| Neuroblastoma: Typically occur in infants and very young children (mean age of presentation being ~22 months) with 95% of cases diagnosed before the age of 10 years. Occasionally, may be identified antenatally or immediately at birth (congenital neuroblastoma). | Neuroblastoma on ultrasound demonstrates a heterogeneous mass with internal vascularity. On CT, the tumor typically is heterogeneous with calcifications seen in 80–90% of cases. Areas of necrosis are of low attenuation. MRI is superior to all other modalities in assessing the organ of origin, intracranial or intraspinal disease and bone marrow disease. | |
| Ganglioneuroblastoma: They are seen more commonly in children younger than 10 years. There is no definite gender predilection. The tumor contains elements of both malignant neuroblastoma and benign ganglioneuroma. They may be encapsulated. | They are commonly attached to a nerve trunk. Imaging features can be variable and can range from a solid, well-margined, vertically extending paraspinal mass (4–5 vertebral body) with homogeneous enhancement or as an irregular, cystic, poorly-margined, locally-invasive mass with evidence of metastatic disease. Calcification may be seen. |  Fig. 4.206.19: Ganglioneuroblastoma |
| |  Fig. 4.206.18: Ganglioneuroblastoma |  Fig. 4.206.20: Ganglioneuroblastoma |
| Ganglioneuroma: The median age at diagnosis is 7 years, and there is slight female predominance. Ganglioneuromas are usually asymptomatic and often discovered incidentally as they are slow growing and usually endocrinologically inactive. Prognosis is usually excellent, however, local recurrence has been reported. | Lesions are well-defined and can be quite large at presentation. Paravertebral ganglioneuromas frequently extend through the neural foramina to involve the epidural space of the spinal canal. Contrast enhancement in CT/ MR ranges from none to heterogeneous enhancement. Calcification may be present in less than 25% of cases. Associated with multiple endocrine neoplasia type IIb: Particularly with mucosal ganglioneuromas. |  Fig. 4.206.21: Ganglioneuroma |

(Contd.)

Table 4.206.2: Difference between neuroblastoma and Wilms tumor (Contd.)

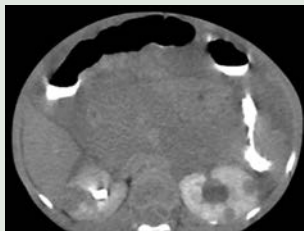
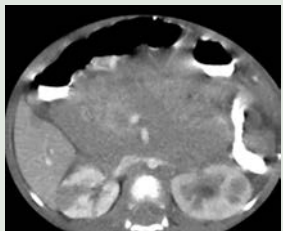

| | | |
|--|---|--|
|  <p>Fig. 4.206.22: Renal lymphoma bilateral kidneys show hypodense lesions that are FDG avid with enlarged paraortic lymph nodes</p> |  <p>Fig. 4.206.23: Renal lymphoma bilateral kidneys show hypodense lesions that are FDG avid with enlarged para-aortic lymph nodes</p> |  <p>Fig. 4.206.24: Renal lymphoma bilateral kidneys show hypodense lesions that are FDG avid with enlarged paraortic lymph nodes</p> |
|--|---|--|

Table 4.206.4: Pediatric renal masses

| <i>Benign lesions</i> | <i>Malignant lesions</i> | <i>Pearls</i> |
|--|---|--|
| Nephroblastomatosis Mesoblastic nephroma Multilocular cystic nephroma Angiomyolipoma Ossifying renal tumor of infancy Metanephric adenoma | Wilms tumour Clear cell sarcoma Rhabdoid tumor Renal cell carcinoma Lymphoma Renal medullary carcinoma | Most common solid mass in newborn—mesoblastic nephroma Most common solid mass in infant with calcification—ossifying tumour of kidney Most common solid mass in a toddler—Wilm's tumor Most common renal mass in toddler with lung metastasis—Wilm's tumor Most common renal mass in toddler with bone metastasis—clear cell sarcoma Most common renal mass in toddler with CNS metastasis—Rhabdoid tumor Most common renal mass in children >5 year—RCC |

Table 4.206.5: Age group for renal neoplasm

| <i>Renal neoplasm</i> | <i>Age range</i> | <i>Peak age</i> |
|---|----------------------------------|-------------------------------|
| Wilms tumor • Unilateral form • Bilateral form | 1–11 years | 3.5 years |
| Nephroblastomatosis | 2 months–2 years | 15 months |
| Renal cell carcinoma | 6 months–60 years | 7–11 years and 50 to 60 years |
| Mesoblastic nephroma | 0–1 year | 1–3 months |
| Multilocular cystic renal tumor • Cystic nephroma • Cystic partially differentiated tumor | Adult female 3 months–4 years | Adult female 1–2 years |
| Clear cell carcinoma | 1–4 years | 2 years |
| Rhabdoid tumor | 6 months–9 years | 6–12 month |
| Angiomyolipoma | 6–41 years | 10 years |
| Renal medullary cell carcinoma | 10–39 years | 20 years |
| Ossifying tumor of infancy | 6 days to 14 months | 1–3 months |
| Metanephric adenoma | 15 months–83 years | None |
| Hodgkin's lymphoma | >10 years | Late teens |

I-131 MIBG therapy, especially for refractory/recurrent disease.

Neuroblastic tumors: Neoplasms of neuroectodermal origin, derived from the primordial neural crest cells

that form the sympathetic nervous system. On a spectrum, from least to most differentiated and thus from aggressive to more quiescent: Neuroblastoma → ganglioneuroblastoma → ganglioneuroma. They

Table 4.206.6: Benign and malignant cystic renal masses

Based on neoplastic potential, cystic renal masses are classified as,

| <i>Benign</i> | <i>Malignant—subtypes of RCC</i> |
|--|--|
| 1. Localized renal cystic disease (previously unilateral polycystic kidney) | Clear cell RCC |
| 2. Mixed epithelial and stromal tumor family: A) Cystic nephroma, B) Mixed epithelial and stromal tumor (MEST) | Multilocular cystic renal neoplasm |
| 3. Multicystic dysplastic kidney | Papillary RCC |
| | Tubulocystic RCC |
| | Acquired cystic disease-associated RCC |

Table 4.206.7: Imaging features of focal cystic renal masses

| <i>Focal cystic renal masses</i> | <i>Imaging features</i> |
|---|---|
| Cystic nephroma: Rare benign tumor that typically occurs in boys younger than 4 years, or women aged 40–60 years. Children often present with a painless abdominal mass, while adults are more likely to present with abdominal pain or hematuria but may be asymptomatic. | Well-circumscribed, encapsulated, multicystic mass with variably enhancing septa. The lesions often herniate into the renal pelvis or proximal ureter. Because of the fibrous composition of the septa and capsule of the lesion, they are hypointense on both T1- and T2W MR images. Cystic nephromas have larger cysts, thinner septa and fewer stromal elements compared with MEST. The presence of enhancing nodular components should suggest renal cell carcinoma or MEST and not cystic nephroma. |
| Mixed epithelial and stromal tumor (MEST): Cystic nephroma and MESTs are part of the same spectrum. MEST also has a marked female predominance and is almost always found in perimenopausal women. These complex cystic and solid masses are characterized histologically by the presence of stromal elements that resemble ovarian stroma and an epithelial component consisting of cysts with an epithelial lining. | Typically, MEST manifests at imaging as an expansile multiloculated cystic mass that may herniate into the renal pelvis. On CT and MRI, MEST appears as a multiloculated cystic lesion with both cystic and enhancing solid components. Delayed enhancement, a capsule, and calcifications may also be present. It may also bulge into the renal pelvis and cause obstructive-symptoms akin to cystic nephroma. |
| Multilocular cystic renal neoplasm (previously multilocular cystic RCC): They comprises 3–6% of renal cell carcinoma. Seen in middle age adult. No gender predilection. It is a low grade tumor with excellent prognosis and no reported cases of metastasis or progression. | At pathology, the lesions have numerous cysts lined by malignant clear cells with fibrous septa that may or may not be vascularized. Multilocular cystic RCC have more loculations and lack nodular and enhancing mural nodules compared with cystic clear cell RCC. |
| Multicystic dysplastic kidney (MCDK): MCDK is the 2nd most common abdominal mass in neonate (after hydronephrosis). Congenital nonfunctional kidney replaced by multiple cysts and dysplastic renal tissue. Cysts may shrink and undergo involution. Probable etiology due to atresia of ureter or ureteropelvic junction (UPJ) during metanephric stage of intrauterine development. Up to 40% of patients with MCDK have contralateral renal abnormality (UPJ obstruction and VUR most common). Unilateral MCDK with abnormal contralateral kidney may develop renal insufficiency. Bilateral MCDK is incompatible with life. Hypertension is seen on complication. Treatment—surgery. | Wide range of noncommunicating cysts size up to 15 cm in length in newborn period; may involute with time, to 1–2 cm. No recognizable normal corticomedullary architecture. Renal shape typically preserved, though cysts may result in lobulated contour. Can be segmental in duplicated kidneys. Often followed with annual US scans to assess growth of contralateral kidney and to confirm involution of MCDK (unusual growth of MCDK should rise the suspicion of Wilms tumor arising in these lesions). CECT shows no parenchymal contrast enhancement, no contrast excretion on delayed images and no hydronephrosis. Usually noted incidentally on MR. MAG3 scintigraphy shows lack of radiotracer uptake or excretion. |
| Unilateral hydronephrosis: Most common cause of abdominal mass in neonate. Cysts are communicating. May have PUJ obstruction. | |

are composed of neuroblasts or ganglion cells and the composition ranges from pure neuroblasts (neuroblastoma) mixture of neuroblasts and ganglion cells (ganglioneuroblastoma) → pure ganglion cells (ganglioneuroma). Occur anywhere in anatomic distribution of sympathoadrenal neuroendocrine

system. Most commonly occur in abdomen, especially adrenal gland, followed by posterior mediastinum. Sex predilection M = F. 85% of cases occur in first 4 years of life. The less differentiated, the earlier the presentation. Thus, neuroblastomas typically occur in infants and very young children (mean age of presentation 22 months),

Table 4.206.8: Summary of renal cystic diseases

| | <i>Autosomal dominant polycystic kidney disease</i> | <i>Tuberous sclerosis</i> | <i>Autosomal recessive polycystic kidney disease</i> | <i>Medullary cystic disease Kidney</i> | <i>Simple cyst</i> |
|---------------------------|---|---|--|--|--------------------|
| Inheritance | Autosomal dominant | Autosomal dominant | Autosomal recessive | None | None |
| Kidney size | Normal or large | Normal or large | Very large >90th centile | Small or large | Normal |
| Laterality | Bilateral unequal | Bilateral | Bilateral equal | Uni- or bilateral | Unilateral |
| Extrarenal manifestations | Cysts in liver spleen pancreas | Cardiac rhabdomyomas, intracranial tubers | Congenital hepatic fibrosis | None | None |
| Cyst size | Visible cysts of variable size | Similar to ADPKD, \pm angiomyolipomas | Generally small | Large then often involute | Variable |
| Diagnosis | US, genetic | US, cardiac echo, cranial MRI | US, IVU, liver biopsy | US, MAG3 | US, IVU |
| Malignancy risk | No | Yes | No | Rare | No |

Table 4.206.9: Old Bosniak classification system of renal cystic masses

| <i>Bosniak category</i> | <i>USG features</i> | <i>Workup</i> |
|---------------------------------|---|-----------------------------|
| Type 1: Simple cyst | Round, anechoic, thin walled, post-acoustic enhancement | None |
| Type 2: Mildly complicated cyst | Thin septation, wall calcification | CT or USG follow-up |
| Type 3: Indeterminate lesion | Multiple septa, internal echoes, mural nodule | Partial nephrectomy; biopsy |
| Type 4: Clearly malignant | Solid mass component | Nephrectomy |

Table 4.206.10: Differential diagnosis for renal cysts based on the location

| <i>Perirenal cysts</i> | <i>Cortical cysts</i> | <i>Medullary cysts</i> | <i>Renal pelvic cysts</i> |
|---|---|--|------------------------------------|
| Lymphocele Urinoma Lymphangioma Perirenal seroma (regresses with time) Atypical renal lymphoma (rare) | Glomerulocystic disease (GCKD) ADPKD, ARPKD Tuberous sclerosis Trisomy 13 Meckel-Gruber Syndrome Obstructive uropathy Post-dialysis | All major cystic diseases of kidney including medullary cystic kidney disease, multicystic dysplastic kidney, congenital and acquired cystic diseases. Pyelocalyceal diverticulum. | Parapelvic cyst Peripelvic cyst |

whereas ganglioneuroblastoma and ganglioneuromas present in older children (mean age of presentation 1–10 years and 6–15 years respectively). Ganglioneuroma may occur *de novo* or may arise from maturing neuroblastomas and ganglioneuroblastoma. They may also arise in neuroblastomas and ganglioneuroblastoma that have been treated with chemotherapy.

Pediatric solid multifocal lesions in bilateral kidney: (1) Lymphoma, (2) Nephroblastomatosis, (3) Bilateral Wilms tumor.

Pediatric solid multifocal lesions in unilateral kidney: Nephroblastomatosis.

Pediatric solid lesions in unilateral kidney: Nephroblastomatosis.

Cystic renal masses: Most of them are benign simple cysts. However, complex cystic lesions, malignant cystic lesions are also seen.

Focal cystic renal masses: It includes cystic nephroma, mixed epithelial and stromal tumor (MEST), multilocular cystic renal cell carcinoma and multicystic dysplastic kidney (MCDK). Because it is difficult to distinguish cystic nephroma and MEST from cystic renal cell carcinoma, most are treated surgically.

Table 4.206.11: Proposed update to the Bosniak classification of cystic renal masses (2019)

| Class | CT | MRI |
|-------|--|---|
| 1 | Well-defined, thin (≤ 2 mm) smooth wall; homogeneous simple fluid (-9 to 20 HU); no septa or calcifications; the wall may enhance | Well-defined, thin (≤ 2 mm) smooth wall; homogeneous simple fluid (signal intensity similar to CSF); no septa or calcifications; the wall may enhance |
| 2 | Six types, all well-defined with thin (≤ 2 mm) smooth walls: 1. Cystic masses with thin (≤ 2 mm) and a few (1–3) septa; septa and wall may enhance; may have calcification of any type 2. Homogeneous hyperattenuating (≥ 70 HU) masses at noncontrast CT 3. Homogeneous nonenhancing masses. 20 HU at renal mass protocol CT, may have calcification of any type 4. Homogeneous masses -9 to 20 HU at noncontrast CT 5. Homogeneous masses 21 to 30 HU at portal venous phase CT 6. Homogeneous low-attenuation masses that are too small to characterize | Three types, all well-defined with thin (≤ 2 mm) smooth walls: 1. Cystic masses with thin (≤ 2 mm) and a few (1–3) enhancing septa; any nonenhancing septa; may have calcification of any type 2. Homogeneous masses markedly hyperintense at T2-weighted imaging (similar to CSF) at noncontrast MRI 3. Homogeneous masses markedly hyperintense at T1-weighted imaging (approximately 32.5 normal parenchymal signal intensity) at noncontrast MRI |
| 2F | Cystic masses with a smooth minimally thickened (3 mm) enhancing wall, or smooth minimal thickening (3 mm) of one or more enhancing septa, or many (≥ 4) smooth thin (≤ 2 mm) enhancing septa | Two types: 1. Cystic masses with a smooth minimally thickened (3 mm) enhancing wall, or smooth minimal thickening (3 mm) of one or more enhancing septa, or many (≥ 4) smooth thin (≤ 2 mm) enhancing septa 2. Cystic masses that are heterogeneously hyperintense at unenhanced fat-saturated T1-weighted imaging |
| 3 | One or more enhancing thick (≥ 4 mm width) or enhancing irregular (displaying ≤ 3 mm obtusely margined convex protrusion(s)) walls or septa | One or more enhancing thick (≥ 4 mm width) or enhancing irregular (displaying ≤ 3 mm obtusely margined convex protrusion(s)) walls or septa |
| 4 | One or more enhancing nodule(s) (≥ 4 mm convex protrusion with obtuse margins, or a convex protrusion of any size that has acute margins) | One or more enhancing nodule(s) (≥ 4 mm convex protrusion with obtuse margins, or a convex protrusion of any size that has acute margins) |

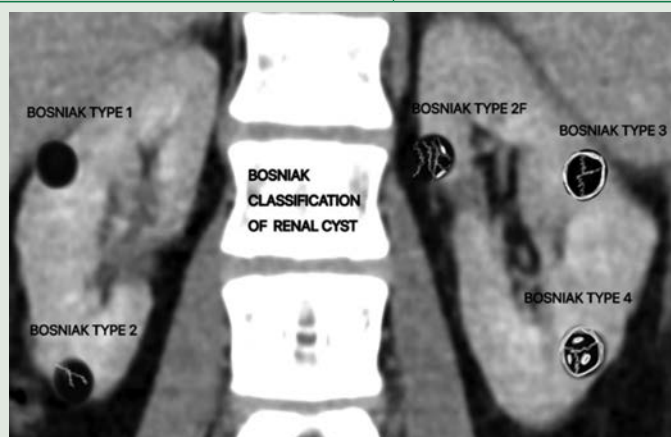
**Fig. 4.206.25:** Bosniak classification of renal cysts

Table 4.206 12 Imaging features of cystic renal diseases

| | <i>X-ray /IVP</i> | <i>Ultrasound</i> | <i>CT</i> | <i>MRI-T1</i> | <i>MRI-T2</i> | <i>Contrast enhancement</i> |
|---------------------------------|--|--|--|---|---|---|
| Acquired cystic kidney disease | None | Small echogenic kidneys with variable sized, well-defined anechoic cysts | Small kidneys with replacement of parenchyma with numerous hypodense cysts variable in size | Small kidneys with cortical and medullary cysts of variable size and signal intensity | Small kidneys with cortical and medullary cysts of variable size and signal intensity | None |
| Medullary cystic kidney disease | None | Cortical thinning with well-defined, anechoic cysts involving medulla and corticomedullary region | Thinned cortex with hypodense cysts involving medulla and corticomedullary region | Thinned cortex with hypointense to intermediate medullary and corticomedullary cysts | Thinned cortex with hyperintense medullary and corticomedullary cysts | None |
| ARPKD | None | Nephromegaly with cortical and medullary anechogenicity with multiple small cortical cysts and loss of cortico-medullary differentiation | Multiple small hypodense cysts at the corticomedullary junction | Hypointense cortex with loss of cortico-medullary junction | Small hyper-intense cortical cysts and normal medulla | None |
| ADPKD | Enlarged renal shadow with filling defects bilaterally | Bilateral progressive nephromegaly with multiple, variable sized, well-defined anechoic cysts within cortex and medulla | Progressive nephromegaly + cysts of variable size, replacing parenchyma +/-Haemorrhage calcification and increased attenuation | Nephromegaly with cysts of variable size and signal intensity | Nephromegaly with cysts of variable size and signal intensity | Parenchymal enhancement without cyst enhancement |
| Simple renal cysts | None | Thin-walled anechoic cysts with well defined posterior walls and posterior acoustic enhancements | Multiple and bilateral sharply margined variable sized cysts measuring -10 to +20 Housefield units | Variable sized hypointense cysts | Variable sized hyperintense cysts | None |
| Lithium nephropathy | None | Normal sized kidneys with increased echogenicity | Normal sized kidneys with numerous small hypodense cysts | Hypointense small cysts not differentiated from renal parenchyma | Numerous 1-2 mm hyperintense cysts | Parenchyma enhances while hypointense nonenhancing cysts. |

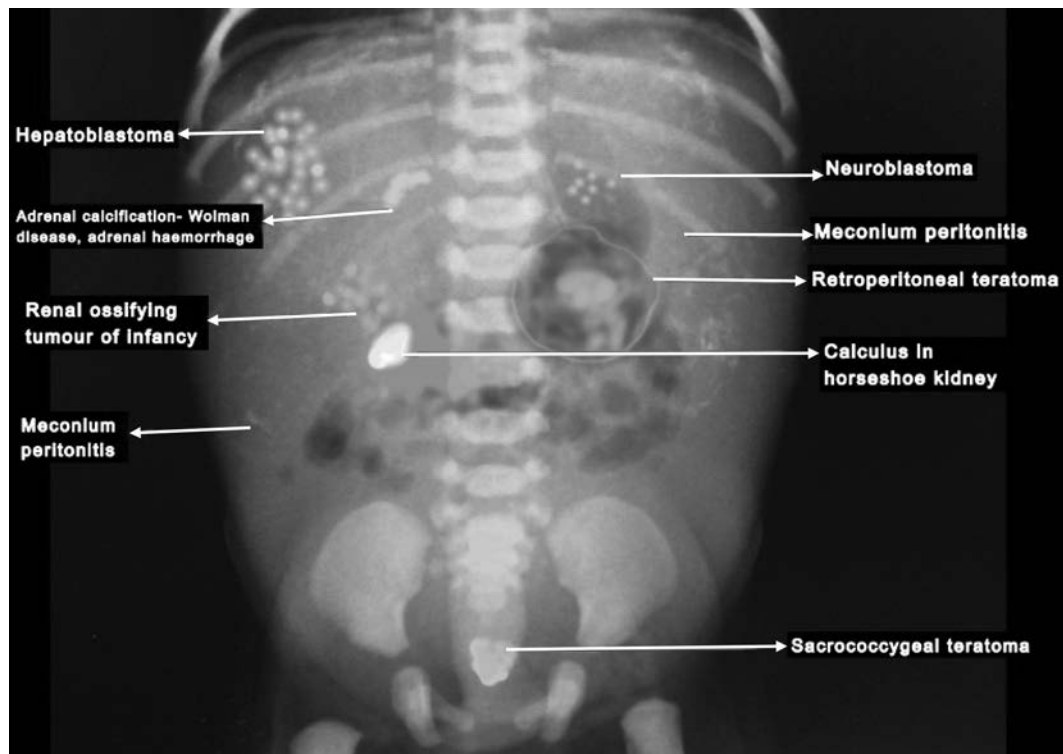


Fig. 4.206.26: Approach to calcifications in pediatric abdomen radiograph

Volume 2

RADIOLOGY Exam Made Easy

A Comprehensive Case Based Approach to Radiologic Examination

Volume 1

RADIOLOGY Exam Made Easy

A Comprehensive Case Based Approach to Radiologic Examination

is an exam preparatory manual which focusses on crystal-clear explanations about various differential diagnoses from all the systems.

Highlights and salient features

- A complete stepwise aid for radiology board examinations
- Ultraprecise structured guidelines for radiology case presentation
- Exam-oriented systematic approach to image interpretation.
- Illustrative system-wise radiological anatomy
- Comprehensive coverage of over 200+ examination cases with an all-inclusive list of possible differential diagnoses
- 70 plus OSCE/CORE exercises explained with high quality images and original illustrations
- High yield viva voce material, including topics like contrast agents, equipment, physics principles
- Emergency radiology—a proactive approach
- An overview of the international certifying examinations such as FICR, MICR, EDIR
- Anatomy, instruments, interventional radiology, nuclear medicine, recent advances topics and more than 2000 images and illustrations.
- The content is derived from standard articles, textbooks, and the Stanley Radiology Museum's famed archives with inputs from experienced faculty—all pieced together in a comprehensive, easy to read format.
- The book provides a concise and handy reference and case based approach for radiology residents appearing for final year examinations. Also provides valuable information that clinical radiologists will find useful in their day-to-day practice.

C Amarnath

is currently Professor and Head, Department of Radiodiagnosis, Government Stanley Medical College, Chennai, Tamil Nadu. He is also the senior consultant at Scans World imaging center, Chennai. He completed his MBBS at Tirunelveli Medical College and Hospital, Tamil Nadu, in 1996, and MD at Barnard Institute of Radiology, Madras Medical College, Chennai, in 2005. Later, he completed his various academic degrees, including DNB, FRCR, FIMSA, FICR, MBA, EDiR, DiICRI, MICR and PhD. He has over 20 years of teaching experience in the field of radiology.

He has to his credit over 50 publications and more than 300 presentations so far, including 15 international presentations. He has contributed chapters in over 8 textbooks, including the *IAN Textbook of Neurology and DeJongs: The Neurological Examination*. He is also on the editorial board of *European Journal of Radiology*. He is the editor of *Comprehensive Textbook of Clinical Radiology and Radiologic Physics: Essentials and Applications*.

He was honored as the "Best Radiology Teacher" by the Iradix website in 2009. Later, he received Prof TS Swaminathan young achiever award in 2014 from TNPY (Tamilnadu and Pondicherry Chapter) chapter of IRIA for his contribution to radiologists' society. He also received the "Dynamic Indian of the Millenium Award" in 2017 from KG Foundation for his notable achievements.

He has played a pivotal role as organizing chairman and secretary in over 25 National and international Radiology conferences and CMEs. He was instrumental in developing the Department of Radiodiagnosis at Govt Stanley Medical College, creating a state-of-the-art conventional and digital Museum and installing 128 slice CT scan, fluoroscopy, MRI, digital mammogram machines, and Biplane DSA lab. He was instrumental in starting multiple courses in the college, including MD, PhD, DRDT, BSc and Msc.

He is the Founder President of the Indian Society of Head and Neck Radiology (ISHNR). After serving as Secretary of TNPY IRIA from 2014–16 and as Secretary-General of National IRIA during 2017–18, he was again elected as the president of TNPY IRIA in 2020 and as the President of National IRIA for the year 2021. He is the youngest ever Radiologist to become the President of Indian Radiological and Imaging Association (IRIA).

Highlights and salient features

- A complete stepwise aid for radiology board examinations
- Ultraprecise structured guidelines for radiology case presentation
- Exam-oriented systematic approach to image interpretation.
- Illustrative system-wise radiological anatomy
- Comprehensive coverage of over 200+ examination cases with an all-inclusive list of possible differential diagnoses
- 70 plus OSCE/CORE exercises explained with high quality images and original illustrations
- High yield viva voce material, including topics like contrast agents, equipment, physics principles
- Emergency radiology—a proactive approach
- An overview of the international certifying examinations such as FICR, MICR, EDIR
- Anatomy, instruments, interventional radiology, nuclear medicine, recent advances topics and more than 2000 images and illustrations.
- The content is derived from standard articles, textbooks, and the Stanley Radiology Museum's famed archives with inputs from experienced faculty—all pieced together in a comprehensive, easy to read format.
- The book provides a concise and handy reference and case based approach for radiology residents appearing for final year examinations. Also provides valuable information that clinical radiologists will find useful in their day-to-day practice.

C Amarnath

MD, DNB, MNAMS, FRCR, FICR, FIMSA, MBA, PhD

is currently Professor and Head, Department of Radiodiagnosis, Government Stanley Medical College, Chennai, Tamil Nadu. He is also the senior consultant at Scans World imaging center, Chennai. He completed his MBBS at Tirunelveli Medical College and Hospital, Tamil Nadu, in 1996, and MD at Barnard Institute of Radiology, Madras Medical College, Chennai, in 2005. Later, he completed his various academic degrees, including DNB, FRCR, FIMSA, FICR, MBA, EDiR, DiICRI, MICR and PhD. He has over 20 years of teaching experience in the field of radiology.

He has to his credit over 50 publications and more than 300 presentations so far, including 15 international presentations. He has contributed chapters in over 8 textbooks, including the *IAN Textbook of Neurology and DeJongs: The Neurological Examination*. He is also on the editorial board of *European Journal of Radiology*. He is the editor of *Comprehensive Textbook of Clinical Radiology and Radiologic Physics: Essentials and Applications*.

He was honored as the "Best Radiology Teacher" by the Iradix website in 2009. Later, he received Prof TS Swaminathan young achiever award in 2014 from TNPY (Tamilnadu and Pondicherry Chapter) chapter of IRIA for his contribution to radiologists' society. He also received the "Dynamic Indian of the Millenium Award" in 2017 from KG Foundation for his notable achievements.

He has played a pivotal role as organizing chairman and secretary in over 25 National and international Radiology conferences and CMEs. He was instrumental in developing the Department of Radiodiagnosis at Govt Stanley Medical College, creating a state-of-the-art conventional and digital Museum and installing 128 slice CT scan, fluoroscopy, MRI, digital mammogram machines, and Biplane DSA lab. He was instrumental in starting multiple courses in the college, including MD, PhD, DRDT, BSc and Msc.

He is the Founder President of the Indian Society of Head and Neck Radiology (ISHNR). After serving as Secretary of TNPY IRIA from 2014–16 and as Secretary-General of National IRIA during 2017–18, he was again elected as the president of TNPY IRIA in 2020 and as the President of National IRIA for the year 2021. He is the youngest ever Radiologist to become the President of Indian Radiological and Imaging Association (IRIA).



Dedicated to Education

CBSPD
CBS Pu
 4819/XI, Prahla
 E-mail: delhi@cb
 New Delhi | Be
 Hyderabad | Jha

Dedicated to Education

CBSPD

CBS Publishers & Distributors Pvt Ltd

4819/XI, Prahla Street, 24 Ansari Road, Daryaganj, New Delhi 110 002, India

E-mail: delhi@cbspd.com, customercare@cbspd.com; Website: www.cbspd.com

New Delhi | Bengaluru | Chennai | Kochi | Kolkata | Lucknow | Mumbai

Hyderabad | Jharkhand | Nagpur | Patna | Pune | Uttarakhand



Scan for
price of this
book and
catalogue